



UNIVERSITÀ DEGLI STUDI DI SALERNO



UNIVERSITÀ DEGLI STUDI DI SALERNO
Dipartimento di Farmacia

PhD Program

in **Drug Discovery and Development**

XXXIV Cycle – Academic year 2021/2022

PhD Thesis in

***Design, synthesis, biological evaluation, and binding
studies of small-molecule modulators of PRMTs
(Protein Arginine Methyltransferases)***

Candidate

Giulia Iannelli

Supervisor(s)

Prof. *Gianluca Sbardella*

Prof. *Sabrina Castellano*

PhD Program Coordinator: Prof. *Gianluca Sbardella*

INDEX

ABBREVIATIONS	VII
ABSTRACT	IX
CHAPTER I.....	1
Introduction	1
1.1. Epigenetics	3
1.1.1. Genomic organization	3
1.2. Methylation: an important epigenetic mark	5
1.3. Protein Arginine Methyltransferases (PRMTs).....	7
1.4. Biological role of PRMTs	10
1.4.1. PRMT1	11
1.4.2. PRMT2.....	13
1.4.3. PRMT3.....	14
1.4.4. PRMT4.....	14
1.4.5. PRMT5.....	16
1.4.6. PRMT6.....	18
1.4.7. PRMT7	19
1.4.8. PRMT8.....	20
1.4.9. PRMT9.....	20
1.5. Chemical probes of PRMTs	21
1.5.1. Non-selective inhibitors	21
1.5.2. Type I pan-selective	22
1.5.3. PRMT3-selective inhibitors.....	26
1.5.4. CARM1 (PRMT4)-selective inhibitors	28
1.5.5. PRMT5-selective inhibitors.....	31
1.5.6. PRMT6-selective inhibitors.....	35
1.5.7. PRMT7-selective inhibitors.....	36
1.6. Aim of this Ph. D. work	37
CHAPTER II.....	39
Deconstruction-Reconstruction and Fragment Growing Approach.....	39
2.1 Background	41
2.2 Previous work: First Reconstruction Step.....	42
2.3 Aim of this Ph. D. project: Design of multisubstrate CARM1 inhibitors	45
2.3.1. AlphaLISA and radioisotope-based studies of activity to PRMTs	47
2.3.2. Selectivity profile of compound 8.....	51
2.3.3. SPR-based studies of binding to PRMT4.....	52

2.3.4.	Structural studies	54
2.3.5.	Assessment of cellular activity and toxicity	57
2.4	Identification of PRMT7 and PRMT9 inhibitors	61
2.5	Conclusions.....	63
2.6	Chemistry.....	65
2.6.1.	Synthesis of 6-amino-4-acetoxy-2-naphthoate 10	66
2.6.2.	Synthesis of compounds 12a – f.....	66
2.6.3.	Synthesis of compounds 1 – 9.....	67
2.6.4.	Synthesis of amino-adenosine derivatives 22 – 25.....	69
CHAPTER III		71
Development of Alkene 1,3-Functionalization Reaction and Design of Ketone-based Compounds as PRMTs Inhibitors		71
3.1.	Alkene 1,3-Functionalization reaction.....	73
3.1.1.	Introduction	73
3.1.2.	Aim of our study.....	76
3.1.3.	Optimization of reaction conditions.....	77
3.1.4.	Results and Discussion.....	78
3.2.	Design of ketone-based compounds	82
3.2.1.	Aim of work	82
3.2.2.	Results.....	83
3.2.3.	Conclusions	85
3.2.4.	Chemistry	85
CHAPTER IV		91
Pro-drug Strategy		91
4.1.	Background.....	93
4.2.	Aim of work.....	95
4.3.	Results	96
4.4.	Conclusions.....	97
4.5.	Chemistry.....	98
4.5.1.	Synthesis of compounds 73 – 75	98
4.5.2.	Synthesis of compound 76	100
4.5.3.	Synthesis of compound 77	101
4.5.4.	Synthesis of compounds 67 – 72	102
CHAPTER V.....		105
Proteolysis-targeting chimera: PROTACTM		105
5.1.	PROTAC approach.....	107
5.2.	Aim of work.....	109
5.3.	Results	111

5.4.	Conclusions.....	111
5.5.	Chemistry.....	112
5.5.1.	Synthesis of compounds 109a – c and 110a – c.....	112
5.5.2.	Synthesis of functionalized protein binders 111a – c.....	113
5.5.3.	Synthesis of compound 116.....	114
5.5.4.	Synthesis of linkers 117a – c.	115
CHAPTER VI		117
Scaffold Replacement Approach		117
6.1.	Aim of work.....	119
6.2.	Results.....	120
6.3.	Conclusions.....	121
6.4.	Chemistry.....	123
6.4.1.	Synthesis of compounds 133 – 135.....	123
6.4.2.	Synthesis of compounds 130a,b, 131a, b and 132a, b.....	125
CHAPTER VII.....		127
Conclusions		127
CHAPTER VIII		131
Materials and Methods.....		131
8.1.	General Information.....	133
8.2.	Synthetic Procedures	134
8.2.1.	Preparation of compounds 1 – 38	134
8.2.2.	Preparation of compounds 39 – 64	165
8.2.3.	Preparation of compounds 67 - 108.....	194
8.2.4.	Preparation of compounds 109 - 129	216
8.2.5.	Preparation of compounds 130 - 153	237
8.3.	Biological Protocols.....	251
8.3.1.	Radioisotope-based filter-binding assay	251
8.3.2.	AlphaLISA	252
8.3.3.	SPR	254
8.3.4.	PAMPA.....	256
8.3.5.	MTT assay.....	257
8.3.6.	Western blot.....	258
8.4.	NMR DATA.....	260
References		321

ABBREVIATIONS

53BP1	p53-binding protein 1	EMCL	Epigenetic Medicinal Chemistry Laboratory
ACN	acetonitrile	ERα	estrogen receptor- α
AcOEt	ethyl acetate	EtOH	ethanol
AcOH	acetic acid	EZH2	enhancer of zeste homolog 2
aDMA -	ω -NG,NG-asymmetric	FAD	flavin adenine dinucleotide
Rme2a	dimethylarginines	FBDD	fragment-based drug discovery
ADP	adenosine diphosphate	FOXMI	forkhead box protein M1
ALPHA	amplified luminescent proximity homogeneous assay	GAPDH	glyceraldehyde-3-phosphate dehydrogenase
ASH1L	absent small and homeotic disks protein 1 homolog	GBM	glioblastoma multiforme cells
BAF	SWI / SNF chromatin remodeling complex	GCN5	general control non-depressible 5
BAH	bromo-adjacent homology	H1	histone 1
BMP	bone morphogenetic protein	H2A	histone 2a
BRCA1	BReast CAncer gene 1	H2B	histone 2b
BRD4	bromodomain-containing protein 4	H3	histone 3
CARM1	coactivator-associated arginine methyltransferase 1	H4	histone 4
CBP	CREB-binding protein	HD	huntington's disease
CDX2	caudal-type homeobox transcription factor 2	HDMs	histones demethylases
CRBN	cereblon	hnRNPUL1	heterogeneous nuclear ribonucleoprotein U like 1 gene
DBU	1,5-diazabicyclo(5.4.0)undec-7-ene	HRR	homologous recombination repair
DCE	dichloroethane	IBX	2-iodoxybenzoic acid
DCM	dichloromethane	ITC	isothermal Titration Calorimetry
DEAD	diethyl azodicarboxylate	JMJ6	jumonji Domain Containing 6
DIBAL-H	diisobutylaluminium hydride	KDM	lysine demethylases
DIPEA	<i>N,N</i> -Diisopropylethylamine	KLF4	kruppel-like factor 4
DMAP	4-Dimethylaminopyridine	LSD	lysine-specific demethylase
DMF	dimethylformamide	MDH1	malate dehydrogenase 1
DNA	deoxyribonucleic Acid	MDM4	mouse double minute 4
DNMT	DNA Methyl Transferase	MeOH	methanol
DOT1L	DOT1-like (disruptor of telomeric silencing 1-like)	MEP50	methylosome protein 50
DPPA	diphenylphosphoryl azide	MHC	major histocompatibility complex
DSBs	DNA double-strand breaks	miRNAs	small single-stranded non-coding RNA molecule
DSF	differential Scanning Fluorimetry	MLL	mixed-lineage leukaemia
EDC	1-ethyl-3-(3-dimethylaminopropyl)carbodiimide		
EGF	epidermal growth factor		

MMA - Rme1	ω -NG-monomethylarginines	PRMT9	protein arginine methyltransferase 9
MRE11	meiotic recombination 11 homolog 1	PROTAC	target protein degradation
mRNA	messenger ribonucleic acid	PTMs	post-translational modifications
MTT	3-(4,5-dimethylthiazol-2-yl)-2,5-diphenyltetrazolium bromide	RBP s	RNA binding proteins
NBS	<i>N</i> -BromoSuccinimide	RNA	ribonucleic acid
NBS1	nijmegen breakage syndrome 1	SAM	S-5'-adenosyl-L-methionine
NCOA2	nuclear receptor coactivator 2	SAP145	spliceosome-associated protein
NFIB	nuclear Factor 1 B-type	SAR	structure–activity relationship
NSCLC	non-small cell lung cancer	SCLC	small-cell lung cancer
p300	E1A-associated protein of 300 kDa	sDMA - Rme2s	ω -NG, N' ^G -symmetric dimethylarginines
PABP1	poly(A)-binding protein 1	SET	suppressor of variegation 3–9 enhancer-of-zeste trithorax
PAD4	peptidyl arginine deiminase 4	SH3	SRC Homology 3 Domain
PAMPA	parallel artificial membrane permeability assay	Smad	small mothers against decapentaplegic
PEG	polyethylene glycol	SOX2	SRY-Box Transcription Factor 2
PH	pleckstrin homology	SPA	scintillation proximity assay
PHD	plant homeodomain	SPR	surface plasmon resonance
PHF1	PHD finger protein 1	SRC-3	steroid receptor coactivator-3
PKMTs	protein lysine methyltransferases	SRSF1	serine/arginine-rich splicing factor 1
PMTs	protein methyltransferases	SUV39H2	suppressor of variegation 3-9 homolog 2, also known as Su(var)3-9 homolog 2
POI	protein of interest	SUV420H1-TV2	suppressor of variegation 4-20 homolog 1, -transcription variant 2
PRMT	protein arginine methyltransferase	TBAF	tetra-n-butylammonium fluoride
PRMT1	protein arginine methyltransferase 1	TEA	triethylamine
PRMT2	protein arginine methyltransferase 2	TFA	trifluoroacetic acid
PRMT3	protein arginine methyltransferase 3	TFAA	trifluoroacetic anhydride
PRMT4	protein arginine methyltransferase 4	TGF-β	transforming growth factor- β
PRMT5	protein arginine methyltransferase 5	THF	tetrahydrofuran
PRMT6	protein arginine methyltransferase 6	TOSMIC	toluenesulphonylmethyl isocyanide
PRMT7	protein arginine methyltransferase 7	TPR	tetratricopeptide repeat
PRMT8	protein arginine methyltransferase 8	UPS	Ubiquitin Proteasome System
		VHL	Von Hippel Lindau

ABSTRACT

The methylation of arginine residues is a common post-translational modification, performed by a family of nine methyltransferases known as PRMTs (Protein Arginine Methyltransferases). Arginine methylation plays a key role in gene regulation due to the ability of the PRMTs to deposit activating or repressive “histone marks”. These modifications correlates PRMTs to several biological processes and their aberrant activity is involved in many pathological conditions like inflammation, neurodegeneration, and cancer. Therefore, PRMTs have been identified as promising therapeutic targets. This Ph. D. project is focused on the design, synthesis, and *in vitro* evaluation of new putative modulators of PRMTs. To this purpose, different approaches have been applied to obtain different classes of compounds. The main strategy exploited a deconstruction–reconstruction and fragment growing approach, starting from naphthalene-based type I PRMT inhibitors, previously identified by us. Herein we report the identification of **EML981**, whose inhibitory activity toward PRMT4 has been supported by biochemical and crystal structure studies. Subsequently, the lower homologous **EML734** has been identified as the first in class dual inhibitor of PRMT7 and PRMT9. Moreover, at the University of Vienna, I have been implicated in the development of a new synthetic methodology defined as “Alkene 1,3-Functionalization”. This procedure has been applied to develop analogues of **EML981** bearing sp³-rich fragments with a view to strengthen the intermolecular interactions with protein target and to increase the *druglikeness* of compound. Concurrently, three side approaches have been investigated. The first reports the pro-drug strategy, applied to promising pyrrole-based compounds previously identified by us. The second approach involves the design, synthesis and biological evaluation of compounds able to induce protein degradation (PROTACs). Finally, the scaffold replacement approach has been applied to inhibitor **EPZ007345**, affording a small library of compounds.

CHAPTER I

Introduction

1.1. Epigenetics

The term epigenetics refers to the complex interactions between the genome and the environment that are involved in development and differentiation in higher organisms.

In 1942, the British embryologist and geneticist Conrad H. Waddington defined epigenetics as “the branch of biology which studies the causal interactions between genes and their products, which bring the phenotype into being”. However, to date, one of the most appropriate definitions of the same concept is the one enunciated in 2007 by Adrian Bird, according to which the epigenetic phenomena are “the structural adaptation of chromosomal regions so as to register, signal or perpetuate altered activity states”.¹ Therefore, epigenetics is concerned with the study of changes in gene expression, which generate heritable phenotypic differences in cells, without altering the nucleotide sequence of DNA. These modifications are fundamental in maintaining cellular identity and regulating processes such as differentiation, development, cell proliferation and genomic integrity.

1.1.1. Genomic organization

In the eukaryotic cells, DNA is compacted in a multi-protein complex called chromatin. The basic element of chromatin is the nucleosome (Figure 1.1) in which histone octamer is surrounded by the 147 bases of DNA for 1.7 laps. Specifically, the histone octamer is composed of a tetramer, containing two copies of both H3 and H4, combined with two H2A/H2B dimers. Histone H1 interacts with the DNA linker located between nucleosomes.²

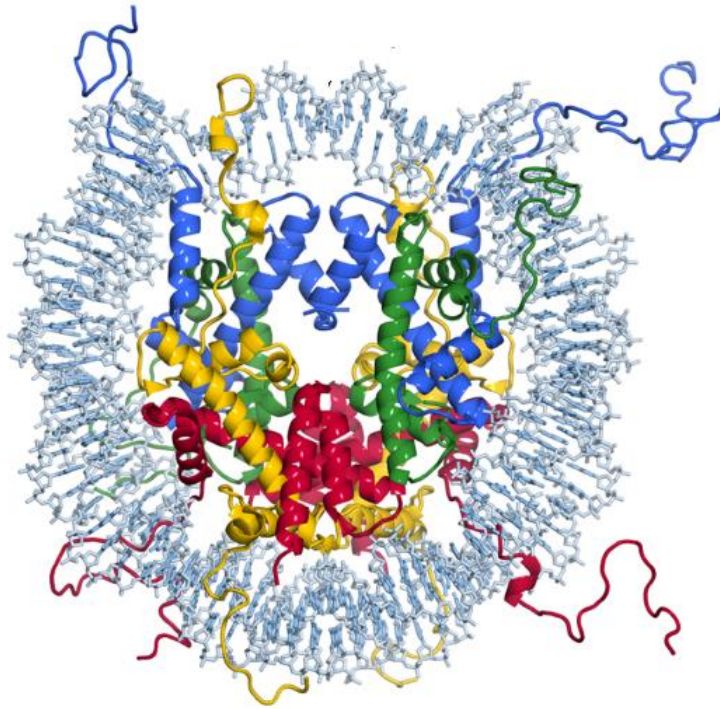


Figure 1.1 Nucleosome structure. The different histone proteins are shown: H3 in blue, H4 in green, H2A in yellow, and H2B in red; the DNA double helix is highlighted in grey.

Chromatin is a structure that may adopt two different states of compactness interchangeably which regulate the accessibility of transcriptional machinery to genes for their initial transcription into mRNA that finally gets translated into proteins. These states are heterochromatin and euchromatin. In particular, heterochromatin is a compact form that is resistant to the binding of various proteins, such as transcriptional machinery. In contrast, euchromatin is a relaxed form of chromatin that is open to modifications and transcriptional processes.

The gene accessibility to different transcriptional systems and the conformation of chromatin are dynamically modified through main modifications including DNA methylation, microRNAs (miRNAs) and histone covalent modification. The N-terminal tail of histones can carry post-translational modifications such as acetylation, phosphorylation, ubiquitination, methylation, sumoylation and ADP ribosylation. In this regard, these post-translational

modifications (PTMs) act as epigenetic marks that collaborate to influence a multitude of cellular processes including transcription, replication, DNA repair, genome integrity and cell cycle progression.³ Over the past years, different proteins have been identified and characterized as epigenetic actors (Figure 1.2). *Writers* are enzymes able to catalyse the insertion of chemical modifications into either histone tails or the DNA. Epigenetic *erasers* are enzymes able to remove the added modifications. Epigenetic *readers* are domains able to selectively recognize the inserted epigenetic marks.

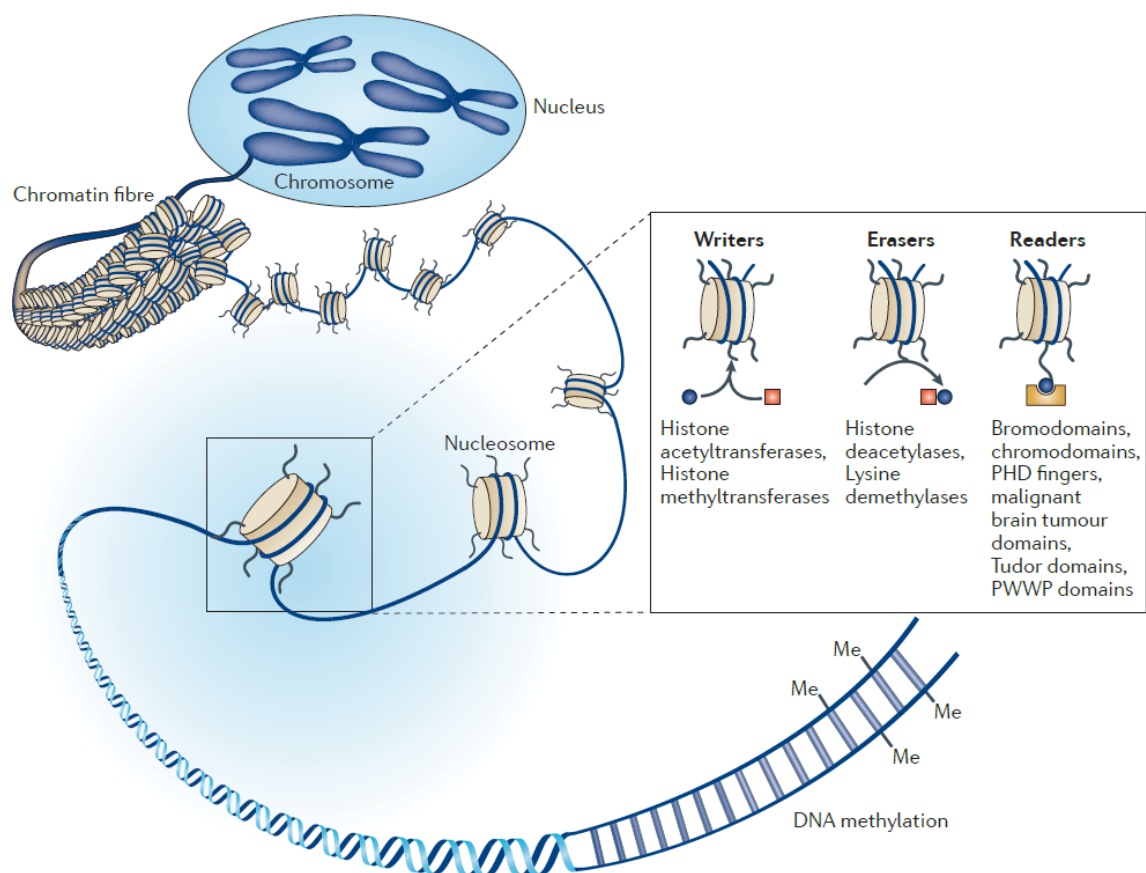


Figure 1.2 Representation of the proteins which insert (*writers*), remove (*erasers*) and read (*readers*) the epigenetic modifications.

1.2. Methylation: an important epigenetic mark

The methylation mark is one of the main epigenetic post translational modifications since it is implicated in several biological processes such as transcriptional regulation, splicing, DNA

damage and RNA maturation.^{4,5} Three classes of epigenetic target play a key role in this process. Protein methyltransferases (PMTs) act as writers by inserting methyl groups on histone and non-histones substrates. PMTs consist of more than 60 members and are distinguished according to the amino acid residue they go on to methylate. In particular, they are divided into lysine methyltransferases (PKMTs) and arginine methyltransferases (PRMTs).⁶ The catalytic mechanism, which applies to both families, involves the transfer of a methyl group from the S-5'-adenosyl-L-methionine (SAM) cofactor to a lysine or arginine residue of different substrates. However, lysine residues can be mono-, di-, and/or trimethylated by PKMTs, arginine residues can only be mono- and/or dimethylated by PRMTs. The second class of involved proteins is histones demethylases (HDMs) that induce lysine or arginine demethylation. These proteins are classified into two classes: the lysine-specific demethylase (LSD) family and the Jumonji C-containing demethylases.⁷ In particular, the lysine-specific demethylase utilizes flavin adenine dinucleotide (FAD) dependent amine oxidase family, and the Jumonji C-containing proteins are non-heme iron [Fe(II)]- and 2-oxoglutarate (2-OG)-dependent oxygenases. However, most of the aforementioned proteins target lysine-methylated residues and only few examples of arginine demethylase are reported so far. In this regard, Jumonji domain-containing 6 has been identified as arginine demethylase, catalysing the demethylation of histone H3/H4.⁸ Also, recent studies suggest that JMJD6 catalyses lysine hydroxylation.⁹ The second example is the enzyme peptidyl arginine deiminase 4 (PAD4) that converts methyl-arginine residues into citrulline.¹⁰ Nevertheless, PAD4 is not considered a classic demethylase as it cannot demethylate dimethylated arginine and can also act on unmodified arginine. Finally, the last class of epigenetic actors is made up by readers containing specialized domains that facilitate the recognition of the methyl mark. Readers of methyl-lysine residues are intensely described and includes Tudor domain, Chromo domain, plant homeodomain (PHD), WD40, ADD (ATRX-DNMT3-DNMT3L), Ankyrin and bromo-adjacent homology (BAH).¹¹ On the other

hand, readers of methyl-arginine have yet to be fully characterized and only Tudor domain-containing proteins have been reported, so far.^{12,13}

1.3. Protein Arginine Methyltransferases (PRMTs)

Arginine methylation is catalysed by a family of enzymes called protein arginine methyltransferases (PRMTs), and nine PRMTs have been identified in mammals to date.

PRMTs are divided into three types according to their catalytic activity (Figure 1.3): type I (PRMT1, 3, 4, 6 and 8) catalyses the production of ω -NG-monomethylarginines (MMA) and ω -NG,NG-asymmetric dimethylarginines (aDMA), type II (PRMT5 and PRMT9) catalyses the formation of MMA and ω -NG, N'G-symmetric dimethylarginines (sDMA); PRMT7 is the only known member of class III and catalyses the formation of ω -NG- MMA.¹⁴ The transfer of the methyl group to the guanidino nitrogen atoms of arginine prevents a potential hydrogen bond, without altering the charge of the arginine residue. In addition, arginine dimethylation by creating steric bulkiness and increasing hydrophobicity, affects protein-protein interactions in both negative and positive ways.

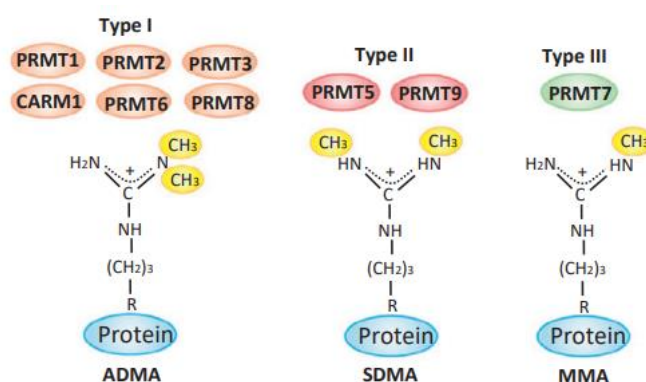


Figure 1.3 Types of arginine methylation. All PRMTs generate monomethyl-arginine (MMA or Rme1). Type I enzymes (PRMT1-4, 6, 8) catalyse the formation of asymmetrical dimethyl-arginines (aDMA or Rme2a). Type II enzymes (PRMT5 and 9) produce symmetrical dimethyl-arginines (sDMA or Rme2s). Type III enzyme (PRMT7) catalyses the production of monomethylarginines (MMA).

All PRMTs that have been structurally characterized to date share a conserved catalytic core of about 300 amino acids, and several PRMTs own additional domain (TIM barrel, zinc finger, SH3 and TPR) which are responsible for substrate specificity and regulation of protein activity.¹⁴ Among the nine mammalian PRMT members, only the structure of PRMT9 has yet to be determined. The monomeric structure of all PRMTs share two canonical domains featuring the N-terminal Rossmann fold (also referred to as the AdoMet-binding domain) and the C-terminal β -barrel domain. Protein crystallography revealed a homodimeric structure for all members except for PRMT7 which shows a pseudo-dimeric structure. In the homodimeric structure, the dimerization arm extends out of the β -barrel of one monomeric subunit and interacts with the Rossmann fold of another subunit. In particular, the homodimeric structure of type I PRMTs arranged in a head-to-tail pattern (Figure 1.4). It was postulated that the monomeric subunits are both catalytically active according to their ability to bind cofactor SAM and substrate arginine. PRMTs must maintain at least a dimer state (or pseudo dimer for PRMT7) to be functionally active.^{15,16} In type I and type III PRMTs, a dynamic α -helix (α X, α Y and α Z) is also present at the N-terminal of Rossmann fold, which is essential for cofactor SAM binding.¹⁷

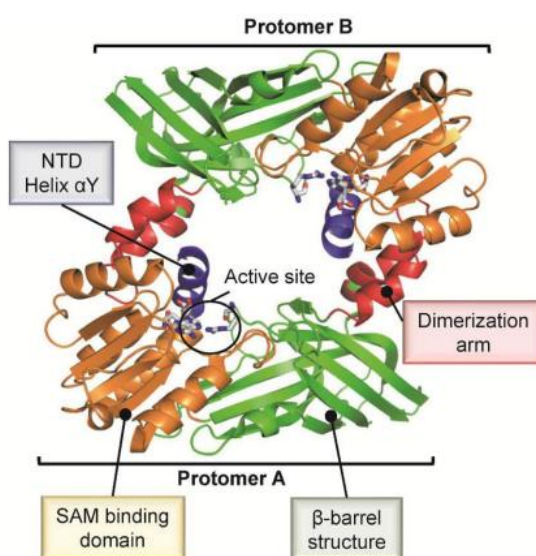


Figure 1.4 Type I PRMTs exist as a head-to-tail dimeric protein.¹⁸

In the catalytic core of all PRMTs members, it is possible to find five common, essential motifs for methyltransferases activity including (i) motif I (VLD/EVGXGXG) shapes the core of the AdoMet binding site with three highly conserved glycine; (ii) post-I motif (L/V/IXG/AXD/E) bearing glutamic or aspartic acid residue is responsible for the hydrogen bond with the ribose hydroxyl moiety of AdoMet; (iii) motif II (F/I/VDI/L/K) stabilizes motif I by the formation of a parallel β -sheet; (iv) motif III (LR/KXXG) also called “double-E loop” featuring two glutamic acid residues that is crucial for the correct positioning of arginine substrate; (v) the THW loop which is near to the active site and it is fundamental for substrate recognition.¹⁹

Name	Domain structure	Classification	Cellular localization
PRMT1		type I	cytoplasm/nucleus
PRMT2		type I	cytoplasm/nucleus
PRMT3		type I	cytoplasm
CARM1		type I	cytoplasm/nucleus
PRMT5		type II	cytoplasm/nucleus
PRMT6		type I	nucleus
PRMT7		type III	cytoplasm/nucleus
PRMT8		type I	plasma membrane
PRMT9		type II	cytoplasm

Figure 1.5 The mammalian PRMT family. Nine PRMTs were identified, and these have unique signatures (dark blue lines) with high sequence similarity (a, Motif I: VLD/EVGXGXG; b, Post-I: V/IXG/AXD/E; c, Motif II: F/I/VDI/L/K; d, Motif III: LR/KXXG; e, THW loop).²⁰

On the other side, structural evidence revealed numerous differences among the PRMTs as the presence of the N-terminal non-catalytic domains. In particular, PRMT3 harbors a zinc finger domain which is a small protein moiety and generally is able to bind DNA, RNA, proteins and lipid substrates. The zinc finger domain of PRMT3 is essential for the recognition of RNA-associated substrate.²¹ PRMT4 contains a pleckstrin homology (PH) domain which is known to bind to lipids or protein. PH domain-containing proteins play essential roles in different biological processes, including signal transduction, nuclear transport as well as DNA repair.²² Thus, deletion of this domain in PRMT4 induces a decrease in methylation activities. PRMT8 contains an N-myristoylation domain which trigger the association of the protein with the plasma membrane.²¹ Finally, the PRMT5 N-terminal domain possesses a TIM barrel domain that plays dual structural roles taking part in dimer formation and recruiting MEP50 for substrate interaction.²³ PRMT7 is the only known type III PRMT and shows distinctive features. In addition to adopting a pseudo-dimeric structure, structural studies have displayed the lack of AdoMet binding pocket in the second subunit which is considered non- catalytically active.

1.4. Biological role of PRMTs

Arginine methylation plays a key role in gene regulation, and it is involved in several biological processes, including transcription, DNA repair, protein stability, cell signaling, pre-mRNA splicing and receptor trafficking. The aberrant functions of PRMTs are involved in several human diseases such as cancer, inflammation, and neurodegenerative diseases. Over the past few years, the development of PRMTs chemical probes allowed to better characterize their biological functions and their potential as therapeutic targets.

The most studied biological roles of each arginine methyltransferase proteins and their ligands are summarized in the following sections.

1.4.1. PRMT1

The first mammalian PRMT discovered was PRMT1, which is responsible for most of arginine methylation in cells.²⁴ Due to alternative splicing, there are seven isoforms of the protein, all varying in their N-terminal domain, which are expressed in a tissue-specific manner and have distinct subcellular localization patterns.²⁵ PRMT1 has broad substrate specificity with over 40 targets. For example, PRMT1 catalyses the asymmetric dimethylation of arginine residues localized in glycine/arginine rich regions namely RGG motifs, commonly found in RNA binding proteins (RBPs).²⁶ These methylated targets are responsible for regulation of RNA- protein and protein-protein interactions. Other substrates are typically employed in signaling pathways mediated by DNA damage, growth factors, metabolites, and the immune response. Other critical substrates of PRMT1 are represented by histones. In particular, the formation of asymmetrically methylated histone H4 Arg3 (H4R3me2a) serves to activate gene expression and facilitate the recruitment of several histone acetyltransferases such as p300. In leukaemia, the oncogenic activity of PRMT1 was widely validated. In fact, PRMT1 and lysine-specific demethylase 4C cooperate with the mixed-lineage leukaemia (MLL) transcriptional complex, removing the repressing modification H3K9me3 in order to activate leukaemia genes.²⁷

Another interesting cooperation occurs between PRMT1 and enhancer of zeste homolog 2 (EZH2) that results asymmetrically dimethylated at R342 (meR342-EZH2) promoting breast cancer proliferation.²⁸ Moreover, the methylated product H4R3me2a results in a critical mark for cancer cell proliferation, migration as well as cell proliferation in multiple developing organs.^{29,30}

Although the role of PRMT1 in pre-mRNA regulation is not yet completely elucidated, the function and localization of several RBPs appear to be regulated by PRMT1. Likewise, deletion of PRMT1 has been correlated with the aberrant alternative splicing of four genes in juvenile

cardiomyocytes from which the new protein isoforms were ubiquitylated and degraded by ubiquitin-proteasome system. Another significant pattern is the methylation of RNA-binding protein 15 which regulates splicing of genes critical to megakaryocytic differentiation. On the other hand, PRMT1 overexpression is associated to blockade of differentiation and promotion of leukemogenesis.³¹ PRMT1 is also required for responses to DNA damage, methylating MRE11, 53BP1, hnRNPUL1, and BRCA1, which are essential to maintain genomic stability.^{32,33,34} The mammalian MRE11–RAD50–Nijmegen breakage syndrome 1 (NBS1) complex, known as the MRN complex, has crucial roles in homologous recombination repair of DNA double-strand breaks that are induced by ionizing radiation or that occur during DNA replication. Methylation of MRE11 within its GAR motif regulates its exonuclease activity on double-stranded DNA. Further investigation showed that cells containing hypomethylated MRE11 displayed intra-S phase DNA damage checkpoint defects. Likewise, 53BP1, which is involved in the early events of detection, signaling and repair of damaged DNA, also has a GAR motif and is methylated by PRMT1. Blocking of 53BP1 methylation by treating cells with methyltransferase inhibitors perturbs 53BP1 localization to damaged DNA and forms fewer γ H2AX foci. Furthermore, the PRMT1-catalyzed methylation plays a key role in the signaling pathways of bone morphogenetic protein (BMP), transforming growth factor- β (TGF- β) and epidermal growth factor (EGF). In particular, BMPs are a subclass of TGF- β family ligands which promotes activation of their signaling effectors, the Smads. This binding induces the interaction of PRMT1 with the inhibitory Smad6, resulting in Smad6 methylation that lead to its dissociation and the subsequent recruitment and activation of the BMP effectors Smad1 and Smad5.³⁵ In a very similar mechanism, PRMT1 is also required for TGF-induced SMAD3 activation, promoting the TGF-induced EMT and epithelial stem-cell generation.³⁶ It is thus not surprising that in mouse neural crest cells deletion of PRMT1 results in cleft palate and craniofacial malformations owing to defective activation of Smads.²⁹

PRMT1 catalyses the methylation of ER α at the DNA binding site, confining it to the cytoplasm. Methylation of ER α is required for its assembly with Src (tyrosine kinase) and activation of Akt (serine and threonine kinase). Activation of the Src-PI3K-FAK (Src-Phosphoinositide-3 Kinase - Focal adhesion kinase) and Akt cascade are essential for the coordination of cell proliferation and survival. However, it has been demonstrated that hypermethylation of ER α in breast cancer might cause hyperactivation of this signaling pathway, thus ascribing a selective survival advantage to tumour cells, even in the presence of anti-oestrogen drugs.³⁷ Also, viral proteins from several viruses are methylated by PRMT1, including SARS-CoV-2 nucleocapsid (N) protein the methylation of which at residues R95 and R177 is crucial for viral replication.³⁸

1.4.2. PRMT2

This protein represents one of the least characterized members among all arginine methyltransferases regarding structure and pathophysiological roles, probably because no adequate chemical probes have been developed so far. PRMT2 was found predominantly in the nucleus and to a lower degree in the cytoplasm of mammalian cells.³⁹ PRMT2 is a type I PRMT, catalysing the formation of MMA and aDMA residues on histones H4 and H3.^{40,41} Notwithstanding all common structural motifs are conserved, PRMT2 also exhibits a characteristic N-terminal Src homology 3 (SH3) domain that can bind to proline-rich proteins. In addition, it is able to bind non-histone substrates such as estrogen receptor alpha (ER α), retinoblastoma, and splicing factors to regulate transcription.^{42,43,44} An overexpression of PRMT2 has recently been found in glioblastoma multiforme cells (GBM) and knockdown of PRMT2 reduces GBM cell growth.⁴¹ On the other hand, the nuclear loss of PRMT2 appears to link with expression of cyclin D1 and tumor growth.⁴⁵ PRMT2 is also implicated in regulation of vascular smooth muscle cells where it inhibits angiotensin II-induced proliferation and

inflammation by reducing levels of proinflammatory cytokines, interleukin 6 and interleukin 1 β .⁴⁶

1.4.3. PRMT3

Initially, PRMT3 was identified as PRMT1-binding partner and only later classified as type-I protein. In contrast with other PRMTs, it contains a zinc finger motif at its N-terminus which is responsible for substrate specificity such as RNA-associated substrates. In fact, the 40S ribosomal protein S2 was validated as the major substrate of PRMT3.⁴⁷ Nevertheless, the binding with several substrates of type I PRMTs as high mobility group (HMG) A1 protein, histone H4 (residue 1–24) and poly(A)-binding protein nuclear 1 (PABPN1) was observed *in vitro* studies.^{48,49,50} Similarly to PRMT2, many pathophysiological functions of this protein remain unclarified. Very intriguing is the interaction between PRMT3 and tumor suppressor protein DAL1 which inhibits PRMT3 methyltransferases activity.⁵¹ So far, epigenetic down-regulation of DAL1 has been observed in several cancers (lung cancer, especially) together with an up-regulation of PRMT3.⁵² A possible role in the development of oculopharyngeal muscular dystrophy has been hypothesized due to methylation on the recombinant nuclear polyA-binding protein (PABPN1) which is caused by polyalanine expansion in PABPN1.⁴⁹ More recently, PRMT3 was validated as an essential regulator of mesenchymal stem cells (MSC)-mediated osteogenesis and bone homeostasis. In details, PRMT3 increases H4R3me2a levels in the DNA regions 343 bp upstream and 505 bp downstream of the transcription starting site (TSS) of microRNA (miR)-3648 promoting the osteogenic differentiation of MSCs. In mice, depletion of PRMT3 reduced bone mass suggesting that this protein could have an interesting therapeutic response in osteoporosis.⁵³

1.4.4. PRMT4

PRMT4, also known as co-activator associated arginine methyltransferase 1 (CARM1), is a type I protein that catalyses the formation of MMA and aDMA at arginine residues 17 and 26

of histone H3.⁵⁴ In addition, CARM1 also methylates several non-histone proteins such as p300/CBP, PABP1, HuR, HuD, SRC-3, NCOA2, CA150, SAP49, SmB e U1C.^{14,55,56} Its expression appears to be rather ubiquitous and is regulated by various microRNAs such as miR181c, miR-223 and miR-15.⁵⁷ CARM1 was initially identified as a co-activator of steroid receptors and then became the first protein among the PRMTs to be functionally linked to transcriptional regulation, acting both as a co-activator and co-repressor. This dual nature has important implications for a large number of physiological processes including mRNA splicing, cell cycle progression, and the DNA damage response.^{58,59,60} On the other hand, a dysregulation of this protein appears to be marked in several diseases. For example, it has been validated that CARM1 is able to perturb the paraspeckle integrity which is particularly important in promoting the chromatin binding with the transcription factor SOX2, which in turn induces inner cell mass specification.⁶¹ Also, CARM1 provides the increased expression of the transcription factor CDX2, which is responsible of trophectoderm specification.⁶¹ More generally, the activity of CARM1 can negatively or positively influences several cancer cell growth. In liver cancer, the glyceraldehyde-3-phosphate dehydrogenase (GAPDH) results in hypomethylation by CARM1, in doing so, the glycolysis as well as the cancer metabolism increase. Thereby, CARM1-dependent methylation of GAPDH inhibits the growth of xenograft tumors in mice.⁶² In recent year, the SWI / SNF chromatin remodeling complex (BAF) has emerged as one of the most extensively mutated gene sets in human cancer and especially in aggressive breast cancer. The complex uses the energy of ATP hydrolysis to mobilize nucleosomes and modulate chromatin structure. CARM1-mediated methylation on arginine 1064 of BAF155 promotes activation of pro-oncogenic and metastatic pathways.⁶³ In pancreatic cancer, CARM1 affects glutamine metabolism and cell proliferation by the methylation on arginine 248 of malate dehydrogenase 1 (MDH1).⁶⁴ Recently, interplay between CARM1 and CBP/p300-mutated lymphomas has been established, wherein a down-regulation of CARM1 positively impacts on B-cell

lymphoma (DLBCL) growth.⁶⁵ It also has a role in determining ER α -dependent breast cancer, cell differentiation and proliferation. The expression level of CARM1 is inversely correlated with tumor grade. In fact, CARM1 can arrest estradiol (E2)-dependent cell cycle progression by modulating ER α -mediated transcription of proteins (p21^{WAF1}, p27^{KIP1}, Cyclin G2, MAZ, KRTAP10.12, and GATA-3).⁶⁶ Thus, it catalyses the methylation of RNA polymerases II mediator complex subunit 12 (MED12) that improves cancer cell sensitization to chemotherapy drugs.⁶⁷ Depletion of CARM1 expression in colorectal cancer cells suppresses clonal survival and anchorage-independent growth, supporting the observations from clinical samples which show that 75% of colorectal cancers have CARM1 over- expression.⁶⁸ All these relevant implications suggest that small molecules that can modulate CARM1 activity might have therapeutic potential for suppressing cancer growth. Moreover, it has been postulated that CARM1 inhibition might be beneficial in cardiovascular diseases thereby an over-expression of this protein has been detected in ischaemic hearts and hypoxic cardiomyocytes.⁶⁹ Similarly, CARM1 levels are increased in inflammatory diseases such as chronic obstructive pulmonary disease and asthma.⁷⁰

1.4.5. PRMT5

PRMT5 is a type II methyltransferases and is therefore responsible for the formation of the sDMA residues in mammalian cells. It is a distributive rather than a processive enzyme, which means that PRMT5 releases MMA before the second methylation event.⁷¹ *In vitro*, PRMT5 activity requires the formation of a hetero-octameric complex with MEP50 which mediates substrate specificity and interaction with binding partners.²³ H3R8me2s, H3 R2me2s, H2AR3me2s and H4R3me2s are the key repressive histone methylation marks that are deposited by PRMT5.^{72,73} In contrast to PRMT1 products, these marks inhibit the recruitment of several histones acetyltransferases. In this regard, PRMT5 activity has been linked to oncogene-like properties due to its ability to repress the expression of tumor suppressor genes.

For example, the expression of PRMT5 is significantly higher in lung adenocarcinoma and squamous cell carcinomas wherein PRMT5, by methylating H3R2me2s and H4R3me2s, silences epithelial junctional genes to regulate cell adhesion, morphology, and invasion, which are all essential for TGF- β response and cancer metastasis.⁷⁴ The same mark is also recognized by PHD finger protein 1 (PHF1) that silences E-cadherin and FBXW7 expression for cell growth and migration.⁷⁵ Thus, keratinocyte and osteoblast differentiation genes are repressed by PRMT5-mediated methylation which also and regulates the PIWI (P-element induced wimpy testis) pathway during germ cell development.^{76,77,78} On the other hand, PRMT5 can deposit activation marks as H3R2me1/me2s that recruiting H3K4me3 as transcriptional activator, affects cancer cell proliferation and invasion, the genotoxic stress response and growth hormone production. In addition to histone modifications, PRMT5 plays a crucial role in splicing wherein by methylating Sm proteins, it promotes their assembly in snRNPs (small nuclear ribonucleoproteins) that are essential for spliceosome function.⁷⁹ Furthermore, to promote efficient splicing, PRMT5 also methylates serine/arginine-rich splicing factor 1 (SRSF1).⁸⁰ The effect of PRMT5 depletion reduces spliceosome assembly, resulting in exon skipping and retention of introns with weak 5' splice donor sites. Then, the absence or inhibition of PRMT5 directs to mis-splicing of hundreds of genes that are implicated in proliferation and signaling in neural stem cells. For example, one splicing event that is particularly sensitive to PRMT5 depletion is MDM4, a key repressor of the p53 pathway, which can express a long mRNA isoform, or a short isoform generated by a premature stop codon that is degraded by the non-sense-mediated decay pathway. In the absence of PRMT5, this pathway shift towards the expression of the short MDM4 isoform followed by blocking of p53 repression.⁸¹ This has been reported in several cancers as melanoma and leukaemia.^{82,83} Moreover, PRMT5 also methylates zinc finger 326 contained in the DBIRD complex, safeguarding the correct exclusion of AT-rich exons in the nucleus.⁸⁴ In fact, the improper inclusion of AT-rich exons leads to aberrant

destabilization of mRNAs of important breast cancer oncogenes as FOXM1 and AP4.⁸⁵ Moreover, PRMT5 has been shown to contribute to prostate cancer development by acting as a cofactor for the androgen receptor. PRMT5 activity, then, promotes carcinogenesis by regulating protein levels of the transcription factor KLF4. Indeed, PRMT5-induced methylation of the transcription factor prevents its VHL-mediated ubiquitination. Accumulation of KLF4, consequently, induces an increase in its targets, including breast cancer-associated oncogenes.⁸⁶ Nevertheless, PRMT5 anti-tumor activity has been reported in several studies. In particular, PRMT5 methylates IFN-g-inducible protein 16 (IFI16), which is component of the cyclic guanosine monophosphate (GMP)-AMP synthase (cGAS)/stimulator of IFN genes (STING) pathway, attenuating cytosolic DNA- induced IFN and chemokine expression in melanoma cells. PRMT5 also transcriptionally downregulates NLRC5 (nucleotide-binding oligomerization domain-like receptor family caspase recruitment domain containing 5), a regulator of the MHC class I antigen presentation pathway.⁸⁷ Regarding neurodegenerative diseases, a possible role of PRMT5 in Huntington's disease (HD) has been proposed. Indeed, HD is an autosomal dominant neurogenerative disease in which the huntingtin protein (HTT) contains a polyglutamine mutant sequence. This mutant protein severely impairs the activity of PRMT5 on histones while ectopic expression of PRMT5 improves the survival of neurons expressing mutant HTT, suggesting that PRMT5 and increasing sDMA levels may play a significant role in smoothing out the HTT toxicity.⁸⁸

1.4.6. PRMT6

PRMT6 is the smallest family member (316 amino acids) and is localized predominantly in the nucleus, wherein it recognizes GAR motifs, and mono- and asymmetrically demethylates arginine residues 2 and 42 on histone H3 as well as arginine 29 on histone H2A.^{89,90,91} Typically, this modification is associated with a repressive transcriptional activity, preventing the binding between readers of methylated histone lysine residues and histone H3 tails that are marked with

gene activation.⁹² However, in analogy to other members of the family, PRMT6 acts on several non-histone proteins such as Chromatin modifiers-HMGA1a, SIRT7, DNA Polymerase β , transcription regulators (CRTC2, FOXO3, GPS2 and TOP3B), cell cycle inhibitors and tumor suppressor (P16, P21 and PTEN).^{93,94,95,96,97} The latter interactions outcome particularly important validating the oncogenic activity of PRMT6 via the addition of repressive mark on tumor suppressor gene. In general, PRMT6 expression is inversely related to global DNA methylation in many tumor cells such as colon, liver, gastric and prostate cancers. These evidence push towards a correct modulation of PRMT6 in order to exploit it as a potential therapeutic target for cancer therapy. Other interesting substrates are represented by HIV-1 proteins as TAT, REV and nucleocapsid protein p7 whose methylated products slow the course of infection.⁹⁸

1.4.7. PRMT7

The sole member of the type III group is PRMT7, which is responsible for MMA formation on histones H2B and H4.^{99,100} Nevertheless, depletion of PRMT7 decreases H4R3me2s marks, which is explained by allosteric regulation of PRMT5 after methylation of H4R17me1 by PRMT7.¹⁰¹ In contrast to other PRMTs, it exhibits a pseudo-dimeric structure and contains an amino-acid sequence duplication that engages a second putative SAM binding motif. Several roles for PRMT7 in transcription, DNA damage, signaling, stress response and antiviral response have been reported. An involvement of PRMT7 has been hypothesized in the maintenance of the pluripotent state in undifferentiated embryonic and germinal stem cells, antagonizing the MLL4-mediated differentiation.¹⁰² In skeletal muscle, this protein is highly expressed, and its deletion caused loss of proliferation, delay in differentiation and consequent loss of muscle mass with premature entry into senescence phase.¹⁰³ Also, PRMT7 has implications in genetic disorder because repressive mutations in human PRMT7 gene give rise to an intellectual disability syndrome called SBIDDS (short stature, brachydactyly, intellectual

developmental disability and seizures).¹⁰⁴ In addition, the automethylated protein version-induced breast cancer metastasis has been reported.¹⁰⁵ Thereby, other studies have also associated PRMT7 and non-small-cell lung cancer metastasis.¹⁰⁶

1.4.8. PRMT8

PRMT8 is a type I methyltransferases that is mainly present in the brain. This protein exhibits greater than 80% sequence similarity to PRMT1, but it is characterized by a unique N-terminus engaging a myristoylation motif which is responsible for the association with the plasma membrane.¹⁰⁷ PRMT8 functions are not completely understood, however, a role for PRMT8 in the regulation of neuronal function of the hippocampus, synaptic maturation and differentiation has been reported.^{108,109} In fact, disruption of PRMT8 results in a defect in motor coordination and hyperactivity.^{110,111} In addition, an aberrant activity of PRMT8 is found to be associated with cancers.^{112,113}

1.4.9. PRMT9

PRMT9 joins PRMT5 as a second type II enzyme sDMA-forming enzyme in the mammalian PRMT family. Among these proteins, PRMT9 is unique because of its strict substrate specificity and its protein apparatus that contains a second methyltransferases domain. The major and first PRMT9 substrate is the spliceosome-associated protein (SAP145) which contributes to form a protein complex. In details, PRMT9 catalyses the symmetrically dimethylation at arginine residue 508 on SAP145.^{114,115} The nature of this substrate suggests an explicit role in splicing by PRMT9, although the mechanism is not fully elucidated. In this regard, the functions of PRMT9 are not completely understood, however, a role in invasion and metastasis of hepatocellular carcinoma as well as a depletion of activity in osteosarcoma has been reported.^{116,117} To date, no selective modulators of PRMT9 have been reported that could greatly help in the understanding of biological role of this protein.

1.5. Chemical probes of PRMTs

The pivotal role played by PRMT-mediated arginine methylation in the regulation of many cellular processes and the implications in the genesis of various diseases has attracted growing interest towards PRMTs as potential therapeutic targets, so the development of modulators is the front line of current PRMT research.

In the following Paragraphs, the aim is to underline the most important inhibitors to date reported for protein arginine methyltransferases. In particular, inhibitors are treated as non-selective, pan-selective and protein-selective.

1.5.1. Non-selective inhibitors

Considering the mechanism of action of this family of proteins and especially the role of SAM as a cofactor able to donate methyl groups, it should not be surprising that SAM-analogues compounds, such as **methylthioadenosine** and **sinefungin** reported in Figure 1.6, can be classified as non-selective inhibitors towards SAM-dependent methyltransferases including PRMTs. In 2012, Wang and co-workers discovered **A36** (Figure 1.6) by pharmacophore- based virtual screening methods.¹¹⁸ This is a substrate- competitive inhibitors and it shows an IC_{50} of $12 \pm 0.2 \mu M$ on PRMT1. Despite it being 7-fold selective for PRMT1 over CARM1, it reveals itself only 2-fold selective for PRMT1 over PRMT5.

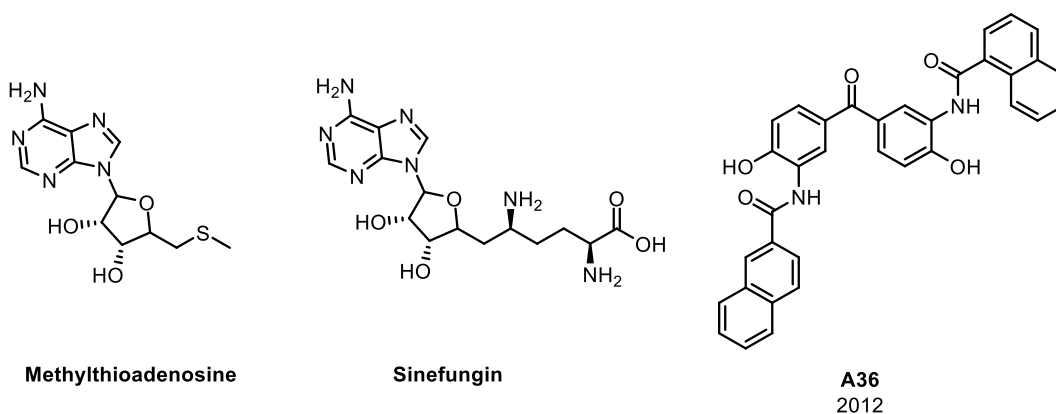


Figure 1.6 Non-selective inhibitors of PRMTs.

1.5.2. Type I pan-selective

The first inhibitors of protein arginine methyltransferases were discovered in 2004 via high-throughput screening by using the yeast arginine methyltransferase enzyme Hmt1p and the Npl3 protein as substrate. Among these inhibitors, the most active derivative, denoted as **AM1-1** (Figure 1.7), is characterized by a naphthyl sulfonic moiety that showed good activity on PRMT1 (IC_{50} of 8.8 μ M) and also a decent selectivity profile towards lysine methyltransferases.¹¹⁹ Subsequently, the EMCL Group (Epigenetic Medicinal Chemistry Laboratory) of Professor Gianluca Sbardella, synthesized several analogues structurally related to **AM1-1** and was found that the substitution of the sulfonic groups, involved in pleiotropic interactions, with the bioisosteric carboxylic group together with the formal shift of the ureidic function of the naphthalene ring, resulted in the generation of **EML108** compound (Figure 1.7) which is characterized by good activity and selectivity profiles (for details, Chapter II).¹²⁰ In 2007, Spannhoff and colleagues reported the discovery of **stilbamidine** and **allantodapsone**, that displayed a strong hypomethylating effect (Figure 1.7), using fragment-based virtual screening.¹²¹ By the same approach, they reported the identification of **RM65** (Figure 1.7) which is a cell-permeable PRMT1 inhibitor and occupies both the SAM binding pocket and the substrate arginine binding site, as supported by docking studies. **RM65** was also shown to reduce histone H4R3 methylation in HepG2 cancer cells at concentrations above 100 μ M.¹²² Further optimization resulted in the generation of even more potent inhibitors, such as the dapsone-like derivative **I**, which inhibits PRMT1 with an IC_{50} of 1.5 μ M (Figure 1.7).¹²³ In 2015, SGC in collaboration with Jin's lab reported the development of **MS023** (Figure 1.7) as a potent inhibitor of type I PRMTs, inspired by the recent discoveries of PRMT6 and CARM1 inhibitors.¹²⁴⁻¹²⁶ The design of **MS023** was based on the hypothesis that the ethylenediamino group is an excellent arginine mimetic and a critical moiety for targeting type I PRMTs. **MS023** potently inhibits PRMT1 ($IC_{50} = 30 \pm 9$ nM), PRMT3 ($IC_{50} = 119 \pm 14$ nM), PRMT4 ($IC_{50} =$

83 ± 10 nM), PRMT6 ($IC_{50} = 4 \pm 0.5$ nM), and PRMT8 ($IC_{50} = 5 \pm 0.1$ nM), while it was inactive against all type II and III PRMTs, 25 PKMTs and DNMTs, and other epigenetic enzymes including several reader proteins and histone lysine demethylases. The binding affinity of **MS023** to PRMT6 was also confirmed by ITC ($K_d = 6$ nM) and DSF ($\Delta T_m = 20$ °C). The co-crystal structure of **MS023** in complex with PRMT6 revealed that compound occupies, not surprisingly, the substrate-binding site. In MCF7 cells, **MS023** reduced levels of H4R3me2a in a dose-dependent manner ($IC_{50} = 9 \pm 0.2$ nM) and in HEK293 cells, it reduced H3R2me2a with an IC_{50} value of 56 ± 7 nM. Simultaneously, as a type I PRMTs Pan-inhibitor, it increases global levels of arginine monomethylation and arginine symmetric dimethylation. The effect on cell growth was assessed in a panel of eight cell lines, **MS023** was able to impact on cell growth at high concentrations (e.g., 10 μ M, 50 μ M). In 2016, Schapira et al. presented a new strategy to develop novel class I PRMTs inhibitors.¹²⁷ In particular, it was observed that a common characteristic of several inhibitors of type I PRMTs is the binding in the PRMT arginine binding pocket through a basic alkyl-diamino or alanine-amide tail, as previously mentioned. Starting from these considerations, a fragment library bearing these basic amino tails was screened, leading to the identification of fragment **II** (Figure 1.7) which was greatly potent for PRMT6 ($IC_{50} = 300 \pm 40$ nM), CARM1 ($IC_{50} = 1000 \pm 40$ nM), and PRMT8 ($IC_{50} = 2100 \pm 200$ nM). Importantly, it was selective for PRMT6 over PRMT1 (40-fold), PRMT3 (>60-fold), PRMT5 (inactive), and PRMT7 (inactive). The co-crystal structure of PRMT6 in complex with the fragment was obtained and showed that the ethylenediamino group is deeply buried in the substrate arginine pocket, confirming the preliminary hypothesis. In addition, the fragment inhibited asymmetric dimethylation of H3R2 in HEK293 cells (transfected with PRMT6) with an IC_{50} of 21 ± 3 μ M and no cell cytotoxicity was observed. In the same year, SGC-Jin's lab also discovered **MS049** (Figure 1.7), a dual inhibitor of PRMT4 and PRMT6, through structure-activity relationship (SAR) studies based on fragment **II**.¹²⁸ In biochemical

assays, it showed a high potency for CARM1 and PRMT6 ($IC_{50} = 34 \pm 10$ and 43 ± 7 nM, respectively) and it was inactive against other PRMTs, various epigenetic modifiers (including PKMTs, DNMTs, KDMs, and methyllysine/methylarginine reader proteins) and non-epigenetic targets (including GPCRs, ion channels, transporters, and kinases). In addition, the direct binding of **MS049** to both enzymes was confirmed by ITC and DSF. In the kinetic based mechanism of action studies **MS049** is noncompetitive with SAM and peptide but considering its similar chemical structure to fragment, the inhibitor most likely occupies the substrate (arginine) binding site of PRMT4 and PRMT6. It was proposed that the substrate binds outside the catalytic pocket of CARM1 with significant affinity, and it is not completely displaced by the inhibitor in kinetic assays. Another potential hypothesis is that protein conformational changes are induced by the binding of **MS049** and traditional enzyme kinetics may not apply. **MS049** displayed cellular activity against CARM1 and PRMT6 reducing the levels of Med12me2a and H3R2me2a ($IC_{50} = 1.4 \pm 0.1$ μ M, $IC_{50} = 0.97 \pm 0.05$ μ M, respectively) in HEK293 cells. In 2017, virtual screening and subsequent chemical modifications led to the discovery of **DCPR049_12** and **DCPR049_13** (Figure 1.7) as new type I pan-inhibitors, which displayed an IC_{50} values of 5.3 nM and 6.0 nM for PRMT1, respectively.¹²⁹ Although in the kinetic based mechanism of action studies compounds are noncompetitive with SAM and peptide, the binding in the peptide-substrate pocket was hypothesized according to the presence of a mimetic arginine group and previous studies. Not surprisingly, they showed different inhibitory activities against type I PRMTs, indicating their role as pan inhibitors. Nevertheless, they are selective against other methyltransferases including 7 PKMTs (EZH2, DOT1L, G9a, MLL1, PRDM9, SMYD2, and SUV39H1), as well as DNA methyltransferases (DNMT1 and DNMT3A/3L) and histone acetyltransferase GCN5. The effects of compounds on cell proliferation were investigated in eight leukemia cell lines (KOPN-8, KMS11, MV4-11, THP-1, RS4.11, RCH-ACV, REH, and U937) using Cell Titer-Glo assay. In the most sensitive MV4-

11 cell line, inhibitors treatment resulted in a potently and concentration-dependently inhibited cell proliferation. Compounds treatment (48 h exposure) of MV4-11 cells reduced global levels of aDMA and concurrently increase the global levels of sDMA in a concentration-dependent manner. Moreover, treatment with the two compounds led to cell cycle arrest, apoptosis induction, and leukemogenic gene regulation in MLL leukemia cells. In 2019, Fedoriw et al. reported the discovery of **GSK3368715** (Figure 1.7, also known as **EPZ019997**), a potent, reversible and S-adenosyl-L-methionine (SAM) uncompetitive type I protein arginine methyltransferases inhibitor.¹³⁰ The derivate was constituted by a pyrazolic core which was functionalized at 3- position with 1,1-bis(methoxymethyl)cyclohexane and at 4- position with ethylendiamino group well used in inhibitors of class I. In biochemical assays, **GSK3368715** was highly potent for PRMT1 ($IC_{50} = 3.1$ nM), PRMT2 ($IC_{50} = 48$ nM), PRMT4 ($IC_{50} = 1148$ nM), PRMT6 ($IC_{50} = 5.7$ nM), PRMT8 ($IC_{50} = 1.7$ nM). *In vivo*, **GSK3368715** alters exon usage and inhibits tumor growth or cause regressions of tumor models. Moreover, it causes a shift in arginine methylation state from aDMA to MMA and sDMA; the combination with a PRMT5 inhibitor tones down the gathering of MMA and sDMA. Given that **GSK3368715** and as well as **GSK3326595** (PRMT5 inhibitor) are in clinical development, this combination could be a significant and timely therapeutic strategy for cancer.

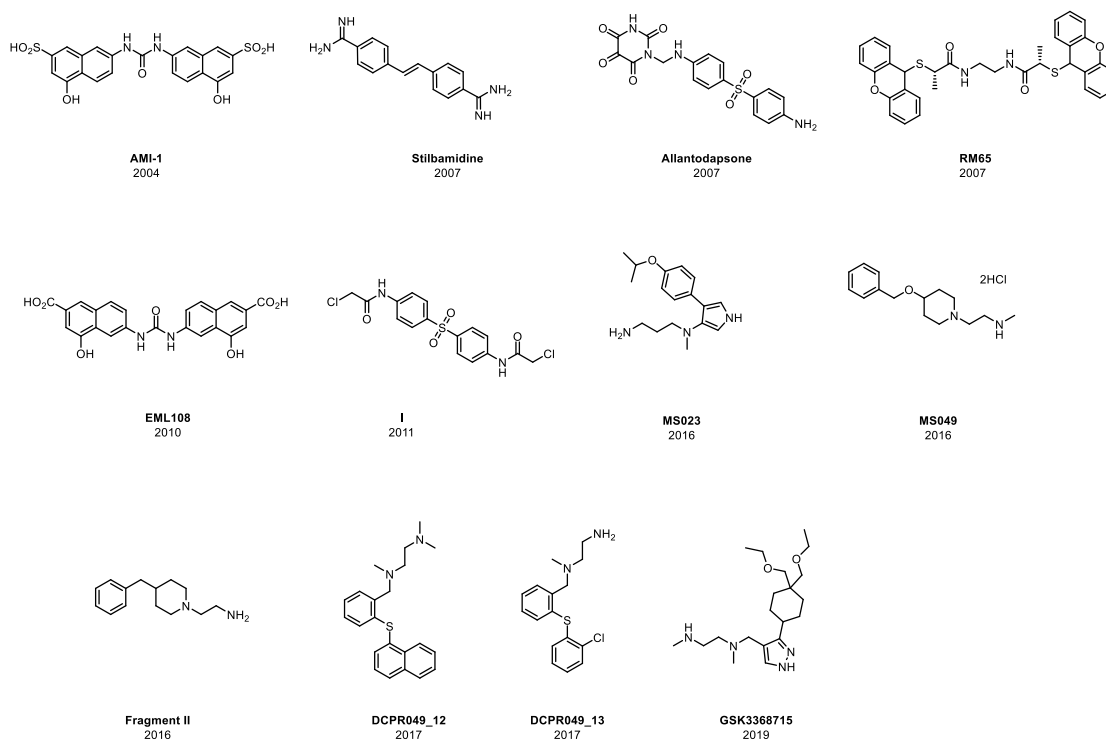


Figure 1.7 Type I-pan selective inhibitors

1.5.3. *PRMT3-selective inhibitors*

In 2012, the discovery of a first selective and sub-micromolar inhibitor of PRMT3 was reported via screening of a library of 16000 compounds. Subsequently, structure-based optimization led the identification of **SGC707** (Figure 1.8), a more potent, selective and cell-active compound which bearing an isoquinoline scaffold featuring an ureidic chain and a pyrrolidine amide moiety.¹³¹ **SGC707** inhibits PRMT3 methyltransferase activity with an IC_{50} value of 31 ± 2 nM by SPA and 66 nM by LC-MS detection assay. To confirm the binding with PRMT3, ITC and surface plasmon resonance (SPR) assays were performed (K_d values of 53 ± 2 nM and 85 ± 1 nM, respectively). As hit compound, it showed noncompetitive inhibition pattern with cofactor and peptide substrate and crystal structure confirmed an allosteric mechanism of action. The binding of **SGC707** to an allosteric site induce conformational constraints on the α -helix, a dynamic secondary element that is conserved in class I PRTMs, that prevents formation of a catalytically competent state. The cellular target engagement was

demonstrated using InCELL Hunter assay, which directly detect the intracellular binding of **SGC707** to the methyltransferase domain of PRMT3 in cell lines expressing the methyltransferase domain of PRMT3 tagged with a short fragment of β -galactosidase. Binding of compound to PRMT3(211-531)-ePL increases the fusion protein half-life. **SGC707** stabilized PRMT3 in both HEK293 and A549 cells with EC_{50} values of 1.3 μ M and 1.6 μ M, respectively. The effect of **SGC707** in cells on both endogenous and exogenously H4R3me2a, introduced GFP-tagged H4, was investigated to assess the cellular activity. The results submitted that **SGC707** was able to reduce the increment (IC_{50} of 225 nM) of endogenous H4R3me2a induced by an overexpressed PRMT3 and also inhibited asymmetric dimethylation of exogenous H4R3 with an IC_{50} of 91 nM. In addition, pharmacokinetic (PK) properties were evaluated, and the acquired data suggested that **SGC707** was suitable for animal studies. In 2018, H. Kaniskan et al. performed detailed SAR studies, starting from **SGC707** and resulting in the discovery of other potent, selective and cell-active allosteric inhibitors of PRMT3 (compound III-VI, Figure 1.8).¹³² Respect to **SGC707**, compounds **III**, and **IV** containing a substituted pyrrolidine while compound **V** and **VI** featuring a substituted isoquinoline scaffold. *In vitro*, they showed a good potency with IC_{50} values of ~10–36 nM and are selective for PRMT3 over 31 other methyltransferases and 55 other protein targets. In addition, compounds engaged PRMT3 in cells (A549 and HEK293) and inhibited its methyltransferase activity.

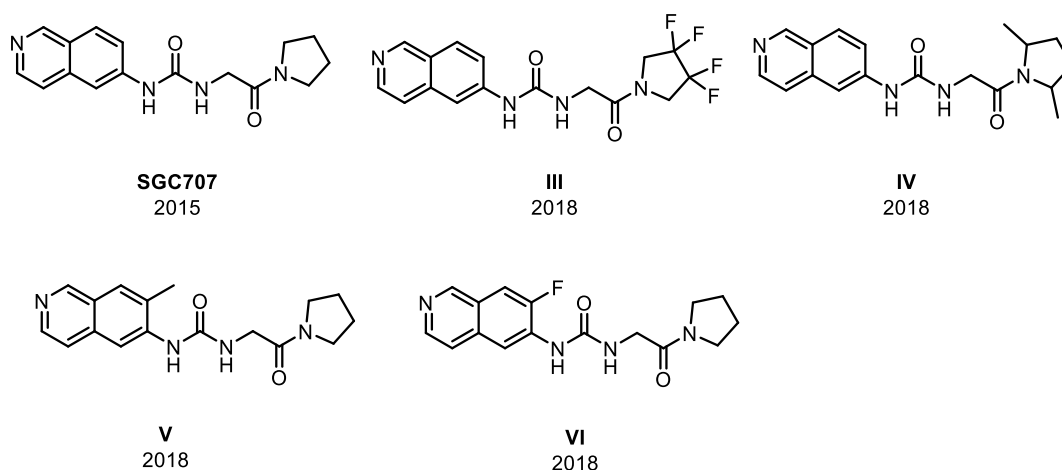


Figure 1.8 PRMT3-selective inhibitors

1.5.4. *CARM1 (PRMT4)-selective inhibitors*

Several high-throughput screening efforts and SAR studies led to the identification of pyrazole and benzo[d]imidazole derivatives as selective CARM1 inhibitors.^{133,134,135,136} Further hit-to-lead campaigns resulted in the discovery of potent CARM1 inhibitors **CMPD1** and **CMPD2** (Figure 1.9) with IC_{50} values of 27 nM and 30 nM, respectively.¹²⁵ Inspired by the structural information of these compounds, Ferreira et al. conducted a virtual screening and subsequent optimization of hits identified, led to the development of **SGC2085** (Figure 1.9) as a potent CARM1 inhibitor with an IC_{50} of 50 ± 20 nM in SPA.¹³⁷ It was selective over other PRMTs and over a panel of 21 methyltransferases with the exception of PRMT6 ($IC_{50} = 5.2$ μ M, around 100-fold selective for CARM1). It showed non-competitive inhibition pattern with cofactor and peptide substrate despite the binding at the substrate pocket, as previously shown for other protein methyltransferase inhibitors. The compound was found to be inactive in cell, probably due to its low cellular permeability. In 2017, Epizyme identified new compounds as CARM1 inhibitors through rationale design. Later, potency of these compounds was improved by SAR study, resulting in the discovery of **EPZ0025654** (Figure 1.9), which displayed an IC_{50} of 3 nM in biochemical assays and an in-cell Western IC_{50} value of 11 nM.¹³⁸ Despite its utility as a cell-based chemical probe, possessed poor pharmacokinetic (PK) properties in animals. To

improve PK properties of **EPZ0025654** and make it suitable for *in vivo* studies, Epizyme conducted further optimization and discovered **EZM2302** (Figure 1.9).¹³⁸ It potently inhibited CARM1 with an $IC_{50} = 6 \pm 3$ nM and displayed a > 100 -fold selectivity for CARM1 over diverse HMTs in the Epizyme enzyme panel. A crystal structure of **EZM2302** in complex with CARM1 and SAH revealed that the inhibitor binds in the arginine pocket, even though it showed noncompetitive inhibition with substrate and cofactor. In addition, the inhibition of CARM1 was observed in a dual inhibitor study which displays a synergistic inhibition with **EZM2302** and SAH. **EZM2302** decreased methylation levels on substrate PABP1 and SmB in a concentration-dependent manner in MM cell lines. Furthermore, treatment with **EZM2302** resulted in anti-proliferative activity in multiple myeloma cell lines and in notable inhibition of tumor growth in a multiple myeloma subcutaneous xenograft tumor model. In 2018, virtual screening conducted by Takeda Pharmaceuticals in collaboration with the SGC yielded **TP-064** (Figure 1.9), a potent and selective small molecule inhibitor of PRMT4.¹³⁹ This compound has an IC_{50} of < 10 nM for PRMT4 in SPA and it exhibited high selectivity over other PRMT family members as well as 24 PKMTs and DNMTs. However, it displayed only modest selectivity over PRMT6 (IC_{50} of 1.3 ± 0.4 μ M), and PRMT8 (IC_{50} of 8.1 ± 0.6 μ M). The crystal structure of the catalytic domain of human (h)PRMT4 with **TP-064** and the cofactor product SAH, revealed that **TP-064** occupies the substrate binding pocket. The SPR experiments confirmed compound binding to PRMT4 but only in the presence of SAM or SAH (K_d value of 7.1 ± 1.8 nM). Kinetic experiments measuring IC_{50} values with varying SAM and peptide concentrations suggested a non-competitive mechanism of inhibition which has been previously shown for other PRMTs inhibitors binding at the substrate pocket. **TP-064** in a concentration-dependent manner reduced the arginine dimethylation of PRMT4 substrates, BAF155 (IC_{50} value 340 ± 30 nM) and Med12 (IC_{50} value 43 ± 10 nM), as supported by cell-based assay. In addition, it inhibits proliferation of certain multiple myeloma cell lines as NCI-H929, RPMI8226, and

MM.1R. In 2019, SGC and Luo's Lab reported the discovery of **SKI-72** (Figure 1.9) as a potent and selective CARM1 inhibitor,¹⁴⁰ inspired by earlier SAR studies of cofactor-competitive PMT inhibitors. The X-ray crystal structure revealed a peculiar binding mode, engaging both the SAM and peptide pockets of CARM1. It is believed that this binding mode, not suitable for SAM-based inhibitor, may be contributing to the high selectivity of CARM1 against other methyltransferases. However, competitive assays displayed that **SKI-72** acts on CARM1 in a SAM-competitive and substrate-noncompetitive manner. Although this compound showed a good potency in biochemical assay (IC_{50} value 43 ± 10 nM) and strongly selectivity for CARM1 over the panel of 33 diverse methyltransferases, it lacks sufficient cell permeability thus limiting its use in cell-based studies. According to this, SGC developed **SKI-73** (Figure 1.9) as a cell-permeable pro-drug of **SKI-72** in which the primary amine moiety was hidden with a redox-triggered trimethyl-locked quinone butanoate moiety. Not surprisingly, it inhibited arginine methylation on BAF155 (R1064) and PABP1 (R455/R460) substrates in MDA-MB-231 cells. Currently, Zuhao Guo et al. described the development of a novel potent, selective, and cell-active inhibitor of PRMT4, via rational design strategy in which the 1,3-diaminopropan-2-ol motif, a well-known arginine mimetic group, was used as warhead. Firstly, a scaffold hopping exercise was employed to replace the left-hand side of compounds containing the aforementioned moiety and then, a co-crystal structure of hit identified was solved. After a careful analysis of the co-crystal structure of initial hit and elegant fine-tuning of the interactions in the substrate pocket, compound **VII** (Figure 1.9) was discovered.¹⁴¹ It inhibited PRMT4 with an IC_{50} of 0.021 ± 0.005 μ M; it showed good selectivity over other PRMTs (> 100-fold) and no inhibitory activity against lysine methyltransferases and other PKMTs. In eight leukemia cell lines (MV4-11, MOLM13, THP-1, RS4.11, MOLT4, MOMOMAC6, HEL, K562), it was able to inhibit cell proliferation in a dose-dependent manner (IC_{50} of 6.93 μ M in MOLM13 cells), probably due to its ability to induce blockage of the cell cycle and apoptosis.

Also, it reduced arginine dimethylation on PRMT4 substrates, BAF155 (IC₅₀ of 0.369 μ M) and PABP1 (IC₅₀ of 0.545 μ M). In addition, it is orally bioavailable and tested in BALB/c nude mice bearing subcutaneous MOLM13 xenografts showing tumor-growth inhibition (TGI) rate of 53.5% with a 100 mg/kg daily.

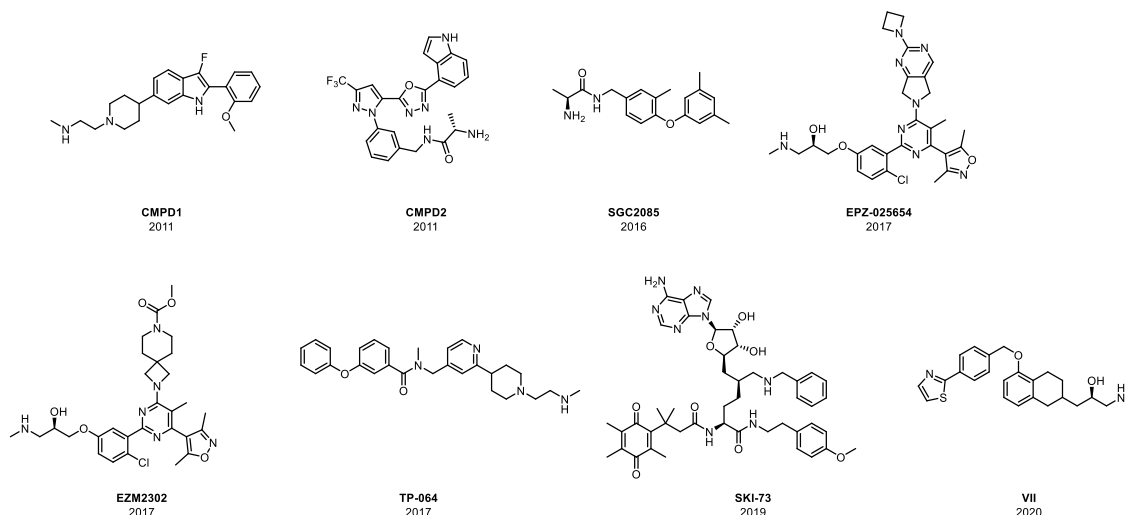


Figure 1.9 PRMT4-selective inhibitors.

1.5.5. PRMT5-selective inhibitors

In recent years, several PRMT5 inhibitors have been identified, reflecting the broad structural data about this protein, characterized by an excellent activity and selectivity profile. The discovery of the first cell-active and bioavailable inhibitor of PRMT5 was described in 2015. HTS of a 370000-compound library led to discovery of **EPZ015666** (Figure 1.10) which displayed an IC₅₀ of 22 ± 14 nM for PRMT5 in biochemical assay and it showed high selectivity over 20 other protein methyltransferases.¹⁴² However, it was not evaluated against PRMT9. **EPZ015666** appeared to be competitive with the peptide substrate ($K_i = 5 \pm 0.3$ nM) while uncompetitive with the cofactor SAM. Interestingly, the affinity for the protein target increases significantly when the cofactor SAM is present. The crystal structure of PRMT5:MEP50 in complex with **EPZ015666** and SAM confirmed these findings, revealing a single binding mode within the substrate channel of PRMT5 and a key cation- π interaction between **EPZ015666** and

the cofactor SAM. **EPZ015666** also has a cellular activity against PRMT5 manifested by reduction of cellular sDMA in a dose-dependent manner in a panel of five MCL cell lines (Z-138, Maver-1, Mino, Granta-519, and Jeko-1). The treatment of the same panel of cell lines with inhibitor compound showed antiproliferative activities with IC_{50} values of 96 nM and 450 nM in Z-138 and Maver-1 cells, respectively. Similar activities were also observed in additional MCL cell lines, with IC_{50} values ranging from 61 to 904 nM. The antitumor activity of **EPZ015666** was assessed using MCL xenograft models in immune deficiency (SCID) mice. Treatment with 200 mg/kg of **EPZ015666** administered BID for 21 days resulted in significant tumor- growth inhibition of higher than 93% in Z-138 xenograft cells and more than 70% TGI in Maver-1 xenograft cells. **EPZ01566** was further optimized through different medicinal chemistry approaches, leading to the discovery of **GSK3203591** and **GSK3326595** which are more drug-like molecules (Figure 1.10).¹⁴³ Similar to **EPZ015666**, these inhibitors are uncompetitive with SAM and competitive with peptide substrate. In biochemical assays, **GSK3326595** and **GSK3203591** were found to be potent inhibitors of PRMT5 with an IC_{50} of 6.2 ± 0.8 nM and 11 ± 8 nM, respectively and a 4000-fold selectivity for PRMT5 against a panel of 20 methyltransferases including PRMT9. In Z-138 MCL cells, both **GSK3326595** and **GSK3203591** potently reduced sDMA levels (EC_{50} values of 2.5 nM and 2.1 nM, respectively) and subsequently, cell activity of **GSK3326595** was evaluated in a panel of breast and lymphoma cell lines. Overall, **GSK3326595** inhibited sDMA in all cancer cell lines tested (EC_{50} values of 2 to 160 nM). This inhibitor has shown remarkable promise in solid and hematologic cancer cell lines, displaying antiproliferative effects and inhibition of tumor growth, especially lymphoma and breast cancer. **GSK3203591**, also known as **GSK591**, has donated to the SGC as a chemical probe while **GSK3326595** has entered phase 1 clinical trials for the treatment of solid tumors and non-Hodgkin's lymphoma. In 2017, Mao et al. performed a pharmacophore- and molecular docking based virtual screening to screen the drug-like SPECS database. The

selected compounds at the end of this virtual screening study were then tested in biochemical assays as well as Alpha LISA and radioactive methylation assay. The hits were then optimized to yield compound **VIII** (Figure 1.10) as a potent PRMT5 inhibitor with an IC_{50} value of 0.33 μ M.¹⁴⁴ This inhibitor showed a good selectivity against a panel of 10 methyltransferases (including most PRMTs), a bromodomain protein (BRD4) and a histone acetyltransferase (GCN5). This compound also achieved cellular potency diminishing sDMA in a concentration-dependent manner and preventing cell proliferation with EC_{50} value of 6.53 μ M for MV4-11 leukemia cells. M. Zhang and co-workers utilized a docking-based virtual screening approach and performed SAR studies; **DC_C01** (Figure 1.10), a PRMT5 inhibitor with an IC_{50} of 2.8 μ M in 3 H-labeled radioactive methylation assay, was identified.¹⁴⁵ Compound **DC_C01** displayed selectivity against PRMT1, DNMT3A (DNA methyltransferase 3A), and EZH2 (enhancer of zeste homolog 2), showing no inhibitory activity at up to 50 μ M. To evaluate its interaction with PRMT5, the putative binding mode of inhibitor was compared with the crystal structure of **EPZ015666**. From this comparison, similar interactions have been hypothesized and as well as the same mechanism of action. Finally, in cell-based assays, **DC_C01** demonstrated concentration-dependent antiproliferative effects with IC_{50} values of 12.7 μ M, 12.7 μ M and 10.5 μ M in Z-138, Maver-1 and Jeko-1 cancer cells, respectively. In 2018, Eli Lilly and the SGC reported the discovery of **LLY-283**, a potent and selective inhibitor of PRMT5 (Figure 1.10).¹⁴⁶ **LLY-283** potently inhibited PRMT5 with an IC_{50} of 22 nM and displayed a strongly selectivity against a panel of 32 other methyltransferases. Direct binding of **LLY-283** to PRMT5 was confirmed by SPR with high affinity (K_d = 6 nM). In addition, a co-crystal structure of **LLY-283** in complex with PRMT5:MEP50 was obtained and revealed that the inhibitor occupies the SAM cofactor binding site even through the competition assays did not show a cofactor or substrate competitive mechanism of action. The compound reduced in a dose-dependent manner symmetric dimethylation of SmBB' in MCF7 cells with an IC_{50} of 25

nM and affected MDM4 splicing with an IC₅₀ of 40 nM in A375 cells. **LLY-283** is orally bioavailable and tested in mouse xenograft models showing tumor growth inhibition, after 28 days of dosing. In 2019, a first-in-class PRMT5 covalent inhibitor was reported by Lin et al.¹⁴⁷ This hemiaminal compound **IX** (Figure 1.10) binds a cysteine residue 499, present only in PRMT5 active site, strongly reducing the sDMA levels in biochemical assay (IC₅₀ values of 11 nM). In 2021, Johnson & Johnson reported the discovery of **JNJ-64619178** (Figure 1.10), a potent and a pseudo irreversible inhibitor of PRMT5, that is being evaluated in clinical trials for the treatment of solid tumors and non-Hodgkin lymphoma.¹⁴⁸ **JNJ-64619178** can bind simultaneously the SAM- and peptide substrate- binding pockets. Importantly, oral dosing of **JNJ-64619178** resulted in dose-dependent antitumor activity in different human NSCLC and SCLC cancer mouse xenograft models. The inhibitor induced tumor growth inhibition by reducing sDMA levels of SmD1/3, proteins of the splicing machinery. In the same year, a novel 5,5-fused bicyclic nucleoside-derived class was discovered via structure-based drug design.¹⁴⁹ The authors took inspiration from cofactor SAM and the aforementioned **JNJ64619178**, with the aim to design a dual-competitive compounds able of engaging key residues in the channel connecting cofactor and substrate binding pockets. An intense and robust medicinal chemistry campaign was performed, and compound **X** (Figure 1.10) emerged as the first promising lead compound. However, monitoring the reversible inhibition and time-dependent inhibition of CYP3A4, compound **X** showed an increased risk suggesting the need to continue the optimization process. Addition efforts led to identification of compound **XI** (Figure 1.10) bearing an all-carbon 5,5-fused core and capable of reducing tumor growth and regression.

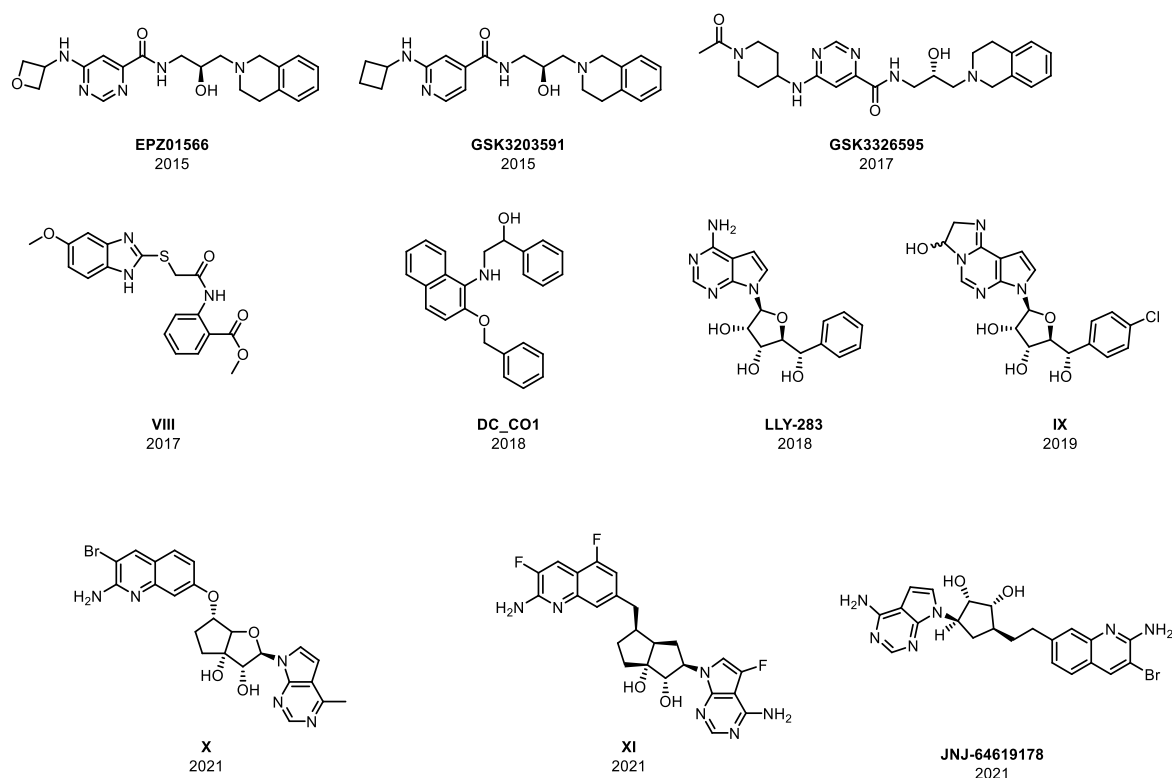


Figure 1.10 PRMT5-selective inhibitors.

1.5.6. PRMT6-selective inhibitors

The discovery of **EPZ020411** as first PRMT6 selective inhibitor was reported in 2015 (Figure 1.11).¹²⁶ The compound was developed through optimization of non-selective inhibitor of class I PRMTs which was discovered via HTS of the Epizyme internal library. **EPZ020411** was characterized by aryl pyrazole bearing a diamino side-chain that occupies the putative site of the substrate arginine side- chain, as assigned by crystal structure of tool compound with SAH and PRMT6. **EPZ020411** potently inhibited PRMT6 with an IC_{50} of 10 nM in a biochemical assay. It was 20-fold and 10-fold selective over PRMT8 (IC_{50} value of 0.223 μ M) and PRMT1 (IC_{50} value of 0.119 μ M), respectively. In addition, it was >100-fold selective for PRMT6 over other histone methyltransferases. The cellular activity of inhibitor was studied in an engineered pattern in which PRMT6 was transiently expressed in A375 cells. In this pattern, selective methylation of the PRMT6 substrate H3R2 was resolutely induced after 48 h of PRMT6 expression. PRMT6 inhibition by **EPZ020411** resulted in a concentration- dependent

decrease in H3R2 methylation ($IC_{50} = 0.637 \pm 0.241 \mu M$). SGC in collaboration with Eli Lilly, the Icahn School of Medicine at Mount Sinai, and the Ontario Institute for Cancer Research (OICR) developed **SGC6870** a potent and selective allosteric inhibitor of PRMT6 (Figure 1.11).¹⁵⁰ **SGC6870** potently inhibits PRMT6 with IC_{50} of 77 ± 6 nM and it is selective over all other PRMTs and 23 methyltransferases. It also inhibited asymmetric dimethylation of H3R2 with an IC_{50} of $0.8 \pm 0.2 \mu M$ in HEK293T cells.

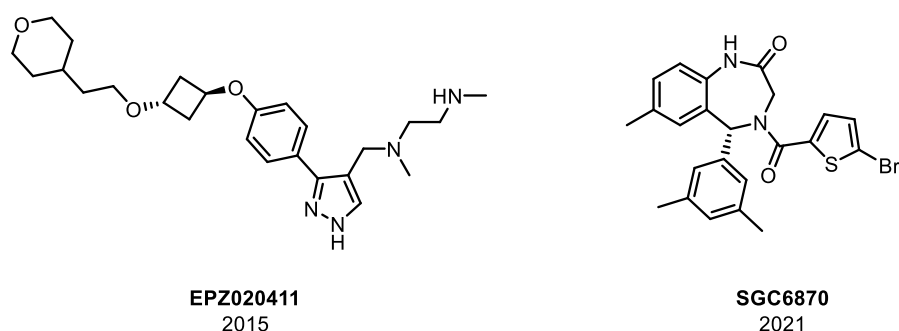


Figure 1.11 PRMT6-selective inhibitors.

1.5.7. *PRMT7-selective inhibitors*

The first PRMT7 known inhibitor is the **DS-437** compound (Figure 1.12), identified in 2015 and designed in relation to the structural characteristics of PRMT5 as it was hypothesized similarities between the two methyltransferases. **DS-437** inhibits PRMT5 and PRMT7 with a comparable IC_{50} of approximately $6 \mu M$ and is inactive toward the other methyltransferases.¹⁵¹

Currently, SGC in collaboration with Takeda and OICR described the first potent and selective small molecule inhibitor of PRMT7, **SGC3027** (Figure 1.12).¹⁵² **SGC3027** is a pro-drug which undergo oxide-reduction cellular mechanism, leading to the rapid release of active component, **SGC8158**. It was discovered via screening of a focused-library and subsequent optimization of the hit identified. **SGC81558** inhibits PRMT7 biochemical activity with an IC_{50} of 2.5 nM in SPA and it was 40-fold selective for PRMT7 over other histone methyltransferases and non-epigenetic targets. The crystal structure of mouse PRMT7 in complex with **SGC8158**

revealed this compound occupying the SAM cofactor binding pocket. The SPR experiments confirmed binding of compound to PRMT7 with a K_d value of 6.4 ± 1.2 nM. Kinetic experiments measuring IC_{50} values with varying SAM and peptide concentrations suggested that **SGC8158** exhibited a cofactor-competitive and substrate-uncompetitive MOA. **SGC8158** lacked cellular activity due to its SAM-like structure and low cell permeability often associated with SAM analogs but on the other hand, its pro-drug **SGC3027** inhibited methylation of HSP70 with IC_{50} of 2.4 ± 0.1 μ M in C2C12 cells.

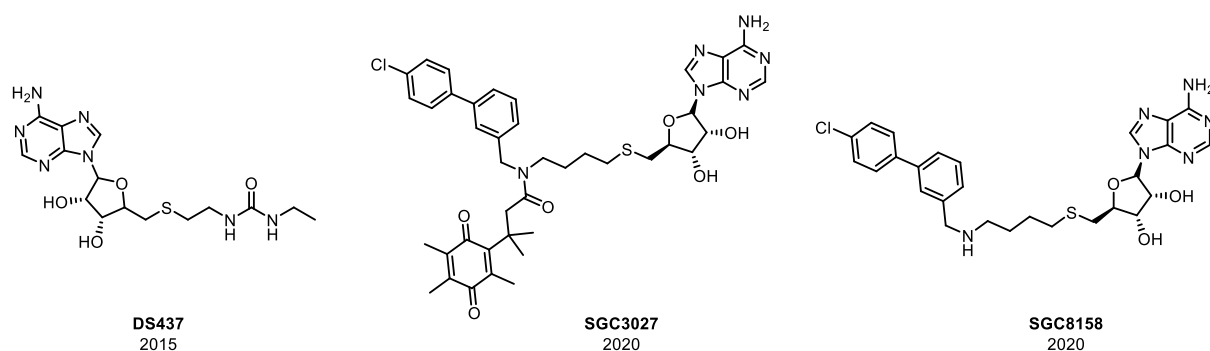


Figure 1.12 PRMT7-selective inhibitors

Unfortunately, despite many efforts into the progress of PRMT9 chemical probes, no satisfactory outcomes have been observed to date.

1.6. Aim of this Ph. D. work

As widely mentioned, over the past 15 years the medicinal chemistry community has paid a growing attention to PRMTs. Despite the excellent progress made in the PRMT field to underscore the therapeutic and pharmacological potential of targeting PRMTs, selective inhibitors are still in high demand. In fact, the greatest advancement in recent years has been the use of PRMT5 selective inhibitors to define cancer vulnerabilities to PRMT5 inhibition, and this has led to exciting clinical trials for cancer therapy. There have been several efforts to achieve similar encouraging results for type I PRMTs, but unfortunately, only a few satisfactory outcomes have been observed. Several critical points have been found in type I inhibitors,

suggesting that the development of selective and potent type I inhibitors remains a very ambitious goal to pursue.

In this regard, aim of this PhD project is the design, synthesis, biochemical and biophysical evaluation of new putative chemical probes for PRMTs. To this purpose, different medicinal chemistry approaches were applied:

1. Deconstruction-Reconstruction and Fragment Growing Approach;
2. Development of Alkene 1,3-Functionalization Reaction and Design of Ketone-based Compounds as PRMTs Inhibitors
3. Pro-drug Strategy;
4. Proteolysis-targeting chimeras: PROTACsTM;
5. Scaffold Replacement Approach.

CHAPTER II

Deconstruction-Reconstruction and Fragment Growing Approach

2.1 Background

In 2010, the EMCL (Epigenetic Medicinal Chemistry Lab) developed a series of type I PRMT inhibitors starting from 7,7'-(carbonylbis(azanediyl))bis(4-hydroxynaphthalene-2-sulfonic acid) **AMI-1** (for details, see Chapter I). Among these inhibitors, **EML108**, the isosteric bis-4-hydroxy-2-naphthoic acid, was able to prevent arginine methylation of cellular proteins in whole-cell assays, with activities comparable or even better than **AMI-1**. In addition, **EML108**, as well as its derivatives, showed a strong selectivity for PRMT family and no inhibitory activity against lysine methyltransferase SET7/9.¹²⁰ In analogy to **AMI-1**, **EML108** binds PRMT1 (chosen as representative of type I enzymes) between the S-adenosine-L-methionine (SAM) co-factor and substrate arginine binding sites without fully occupying them (Figure 2.1) as supported by molecular modelling studies (docking and binding mode analysis, confirmed by structure-based 3-D QSAR models). In particular, one of the two 4-hydroxy-2-naphthoic moieties partially occupies the substrate binding site without establishing interactions with the two conserved glutamate residues of the so-called “double-E loop” critical for chelating and orienting the Arg guanidine group. On the other hand, the binding of the second 4-hydroxy-2-naphthoic moiety seems to leave the SAM binding pocket largely unoccupied.

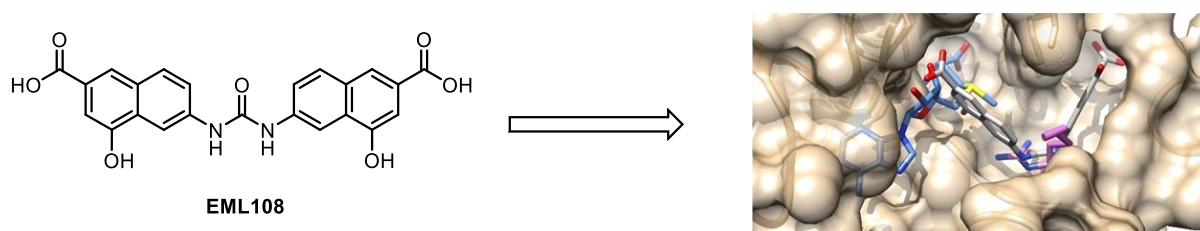


Figure 2.1 Predicted binding mode of **EML108** into PRMT1 (tan) catalytic site.^{120,153} SAM is depicted in cornflower blue, histone Arg in orchid (for clarity, only the side chain is showed).

Starting from these considerations, a “Deconstruction-Reconstruction and Fragment Growing Approach” has been adopted. The concept underlying this approach is simple: since traditional fragment-based drug discovery (FBDD) combines fragments into a final

molecule,¹⁵⁴ it is typically possible to deconstruct a known ligand to obtain a relatively smaller fragment library.^{155,156} Therefore, the structure of **EML108** has been deconstructed into a single 4-hydroxy-2-naphthoic fragment and grown into a more complex structure incorporating warheads able to better bind the abovementioned available pockets.

2.2 Previous work: First Reconstruction Step

In the first reconstruction step, a set of compounds bearing the 4-hydroxy-2-naphthoic group bridged by an amide or urea group with an arginine mimetic moiety has been designed and synthesized (Figure 2.2). The effect of the introduction of a methionine was also explored.

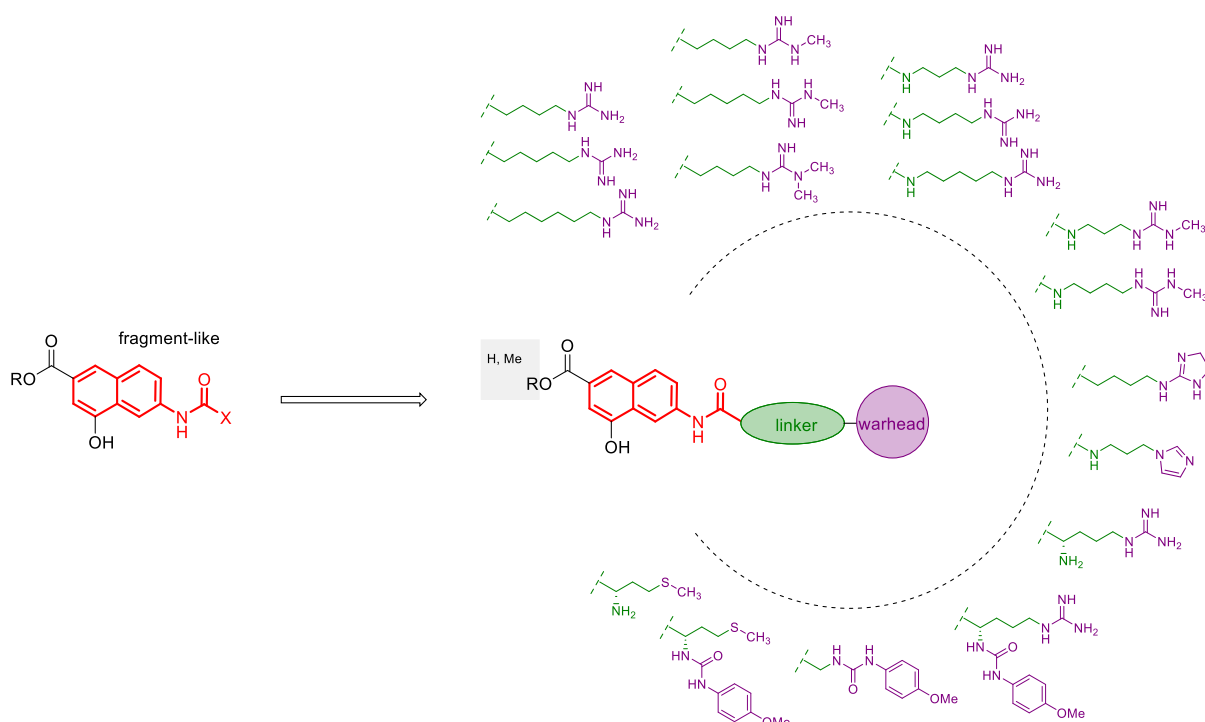
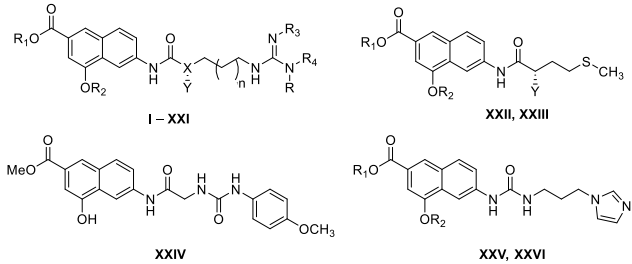


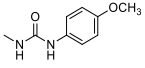
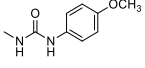
Figure 2.2 Compounds designed for the first reconstruction step.

The inhibitory activity of compounds has been evaluated against human recombinant PRMT1, chosen as representative of type I, using an in-house peptide-based AlphaLISA assay that measures the levels of H4R3me. All the compounds were tested at a fixed concentration of 100 μ M using **EML108** as the reference compound. Then, the compounds that displayed a

greater than 85% inhibition (residual enzyme activity < 15%) were selected and the corresponding IC₅₀ values were determined (Table 2.1).

Table 2.1: Inhibitory activities of **I – XXVI** compounds against *h*PRMT1

Inhibitory activities of EML compounds against <i>h</i> PRMT1										
										
Entry	R	R ₁	R ₂	R ₃	R ₄	X	Y	n	% PRMT1 residual activ. @ 100 μM ^{a,b,c}	IC ₅₀ (μM) ^{a,d}
I (EML525)	-H	-Me	-H	-H	-H	-CH-	-H-	1	35.00 ± 0.3	ND ^e
II (EML611)	-H	-Me	-H	-H	-H	-CH-	-H-	2	5.71 ± 2.1	23
III (EML737)	-H	-Me	-H	-H	-H	-CH-	-H-	3	-0.49 ± 0.1	3.8
IV (EML528)	-Me	-Me	-H	-H	-H	-CH-	-H-	1	1.22 ± 0.3	28.6
V (EML613)	-Me	-Me	-H	-H	-H	-CH-	-H-	2	1.63 ± 0.2	13.7
VI (EML530)	-Me	-Me	-H	-H	-Me	-CH-	-H	1	10.8 ± 3.7	60.4
VII (EML522)	-H	-Me	-H	-CH ₂ CH ₂ -	-H	-CH-	-H	1	121.8 ± 5.8	ND
VIII (EML526)	-H	-H	-H	-H	-H	-CH-	-H-	1	69.7 ± 2.0	ND
IX (EML612)	-H	-H	-H	-H	-H	-CH-	-H-	2	65.9 ± 1.0	ND
X (EML529)	-Me	-H	-H	-H	-H	-CH-	-H-	1	14.7 ± 1.1	28.2
XI (EML614)	-Me	-H	-H	-H	-H	-CH-	-H-	2	50.4 ± 0.2	ND
XII (EML531)	-Me	-H	-H	-H	-Me	-CH-	-H	1	36.8 ± 0.3	ND
XIII (EML523)	-H	-H	-H	-CH ₂ CH ₂ -	-H	-CH-	-H	1	25.1 ± 1.5	ND
XIV (EML732)	-H	-Me	-H	-H	-H	-N-	-H	1	0.4 ± 0.1	1.6
XV (EML538)	-H	-Me	-H	-H	-H	-N-	-H	2	2.0 ± 0.2	16.3

XVI (EML735)	-H	-Me	-H	-H	-H	-N-	-H	3	-0.91 ± 0.1	1.2
XVII (EML733)	-Me	-Me	-H	-H	-H	-N-	-H	1	0.2 ± 0.1	0.4
XVIII (EML634)	-Me	-Me	-H	-H	-H	-N-	-H	2	-0.3 ± 0.1	19.1
XIX (EML539)	-H	-H	-H	-H	-H	-N-	-H	2	31.5 ± 3.1	ND
XX (EML513)	-H	-Me	-H	-H	-H	-CH-	-NH ₂	1	34.2 ± 5.1	ND
XXI (EML516)	-H	-Me	-H	-H	-H	-CH-		1	4.9 ± 0.7	42.1
XXII (EML519)	-	-Me	-H	-	-	-	-NH ₂	-	92.1 ± 15.8	ND
XXIII (EML521)	-	-Me	-H	-	-	-		-	75.9 ± 4.8	ND
XXIV (EML533)	-	-	-	-	-	-	-	-	87.1 ± 2.9	ND
XXV (EML535)	-	-Me	-H	-	-	-	-	-	65.6 ± 2.1	ND
XXVI (EML536)	-	-H	-H	-	-	-	-	-	36.9 ± 10.5	ND
EML108	-	-	-	-	-	--	-	-	17.4 ± 0.4	9.3

^aAlphaLISA was used for both fixed dose and IC₅₀ determinations against human recombinant PRMT1 (0.9 nM, final concentration). Histone H4 (1-21) peptide, biotinylated (100 nM, final concentration) and SAM (2 μM, final concentration) were used as substrate and cofactor, respectively; ^bCompounds were tested at a 100 μM fixed concentration; ^cEnzyme residual activity percentage calculated with respect to DMSO; ^dCompounds were tested in 10-concentration IC₅₀ mode with 3-fold serial dilutions starting at 100 μM. Data were analyzed with GraphPad Prism software (version 6.0) for IC₅₀ curve fitting; eND, not determined.

Within the set of evaluated compounds, structure–activity relationship (SAR) analysis revealed that ester function is preferred to carboxylic acid group and urea compounds are more active to their amide counterparts (for example, compare inhibiting activities of compounds **EML525**, **EML611**, **EML528**, and **EML613** with those of **EML526**, **EML612**, **EML529**, **EML614**). The presence of a single methyl on one of the terminal nitrogen atoms of the guanidine groups has a positive effect only on the activity of amide compounds (compare **EML528** and **EML613** with **EML525** and **EML611**, respectively). Nevertheless, further modification on guanidine group such as the addition of a second methyl group, the replacement with an imidazole or its removal are deleterious for the activity (compare **EML530** with **EML528** and **EML535** with **EML732**). Furthermore, the effect of the methylene linker length

was investigated. In the amide compounds, the activity seems to increase with the number of carbon atoms of the linker, while an “odd/even effect” seems to occur in the urea series, wherein an even number of carbon atoms in the alkyl spacer (as in the case of **EML538** and **EML634**, $n=2$, total carbon atoms in the linker = 4) is less favourable than an odd number (as in the case of **EML732** and **EML733**— $n=1$, total carbon atoms in the linker = 3—or **EML735**— $n=3$, total carbon atoms in the linker = 5). These abovementioned effects seem to be additive. Indeed, the ester compound **EML733** bearing a methylene linker of 3 carbon atoms between urea group and the mono-methylated guanidine is the most active compound showing a submicromolar IC_{50} value (0.4 μM).

Overall, these results validate the 4-hydroxy-2-naphthoic group as a fragment, corroborating the initial hypothesis that one of the two naphthoic groups could be efficiently replaced by an arginine-mimetic group moiety.

2.3 Aim of this Ph. D. project: Design of multisubstrate CARM1 inhibitors

Intrigued by obtained results and pursuing our interest in the identification of potent and selective PRMT inhibitors, a second step of the reconstruction has been performed. Taking into account the SARs of previously described compounds, a small set of compounds (**1 – 9**) was designed. These derivatives feature an adenosine moiety (SAM mimics) anchored to the mimetic arginine portion with an alkyl linker (Figure 2.3).

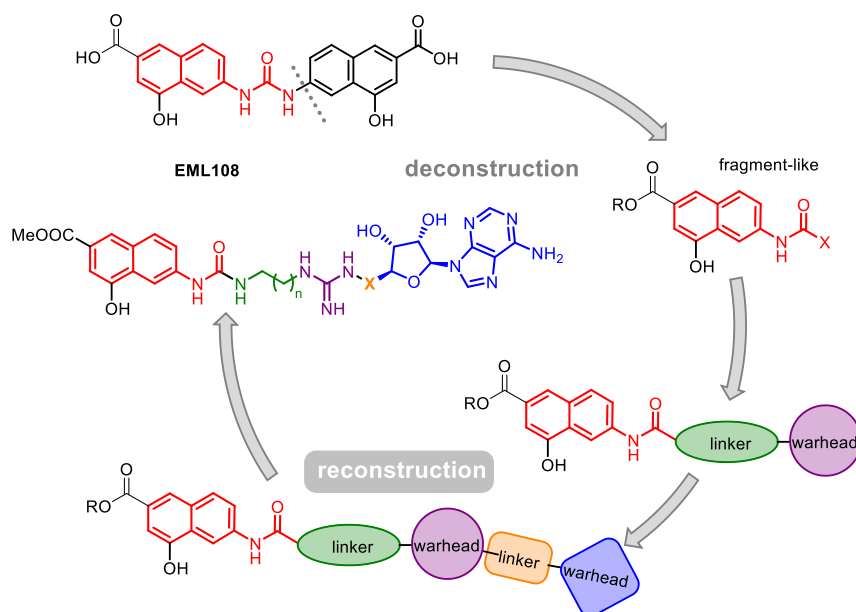
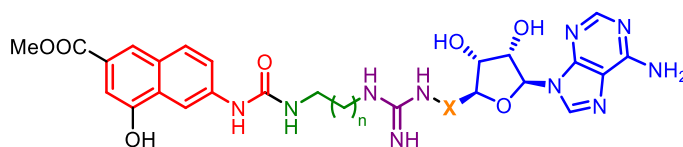


Figure 2.3 Flowchart of our design strategy.

Taken together, data in Table 2.1 indicated that the linker length had a pivotal role on activity. Moreover, several literature reports supports the correlation between the distance of the pharmacophores with PRMTs inhibition for potency and selectivity.^{157,151,158}

Based on these premises, initially we designed and synthesized three derivatives (**1 – 3**). In particular, compounds **1 – 3** were characterized by a linker between the urea and the guanidine groups of three, four or five carbon atoms, respectively and the adenosine moiety was connected to a guanidine ω -nitrogen through a methylene group (Figure 2.4).



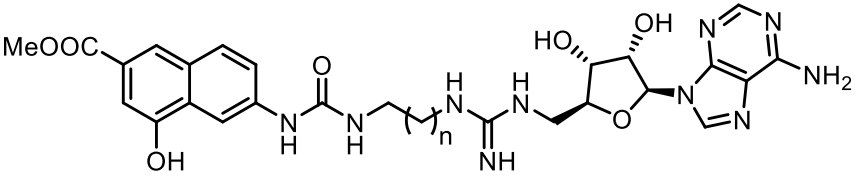
- 1** (EML734): X = CH₂; n = 2
- 2** (EML709): X = CH₂; n = 3
- 3** (EML736): X = CH₂; n = 4
- 4** (EML978): X = CH₂; n = 5
- 5** (EML979): X = CH₂; n = 6
- 6** (EML980): X = CH₂-CH₂; n = 3
- 7** (EML982): X = CH₂-CH₂-CH₂; n = 3
- 8** (EML981): X = CH₂CH=CH; n = 3
- 9** (EML1102): X = CH₂; n = 1

Figure 2.4 Compounds designed for the second fragment growing step.

2.3.1. *AlphaLISA and radioisotope-based studies of activity to PRMTs*

The effect of compounds **1 – 3** was preliminary evaluated on the catalytic activity of human recombinant PRMT1 using a purpose-developed AlphaLISA assay (Chapter VIII, Paragraph 8.3.2). The introduction of the adenosine moiety had a positive effect on the inhibitory activity against PRMT1, as all the derivatives showed IC₅₀ value in the submicromolar range (Table 2.2, values in parenthesis). Prompted by these results, to assess selectivity, the activity of the compounds was also evaluated in a radioisotope-based filter-binding assay (Chapter VIII, Paragraph 8.3.1, performed by Reaction Biology Corp.), screening them against a panel of four PRMTs (PRMT1, PRMT3, PRMT4 and PRMT5). Compared to the results obtained from the AlphaLISA assay, in the more sensitive radioisotope-based assay compounds **1 – 3** showed higher IC₅₀ values but still in the micromolar range. Notably, they were appreciably more active against PRMT4. In particular, we noticed that increasing the distance between the methyl 4-hydroxy-2-naphthoate moiety and the arginine-mimetic group had a considerable effect on PRMT4, a moderate positive effect on PRMT1 and PRMT3, but no significant effect on the activity of PRMT5. In fact, compound **3** exhibits a submicromolar activity (IC₅₀ = 0.42 μ M) only against PRMT4, with a selectivity for the latter ranging from 20-fold (over PRMT1; Table 2.2) to 122-fold (over PRMT5; Table 2.2).

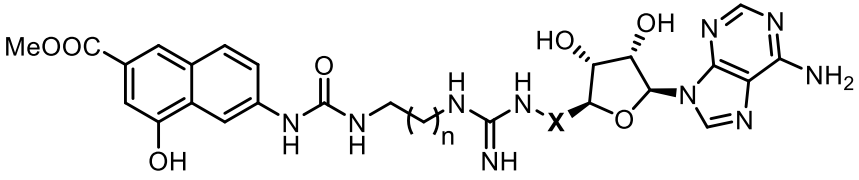
Table 2.2: Inhibitory activities of compounds **1** – **3** against various PRMTs

Inhibitory activity of compounds 1 – 3 (IC ₅₀ μM) against PRMTs					
					
Entry	n	PRMT1 ^{a,b}	PRMT3 ^{a,b}	PRMT4 ^{a,b}	PRMT5 ^{a,b}
1 (EML734)	2	32.27 (0.5) ^c	57.19	13.84	52.13
2 (EML709)	3	11.67 (0.43) ^c	43.41	2.14	76.7
3 (EML736)	4	8.46 (0.3) ^c	21.26	0.42	51.41
SAH	-	0.33	2.77	0.43	40.49

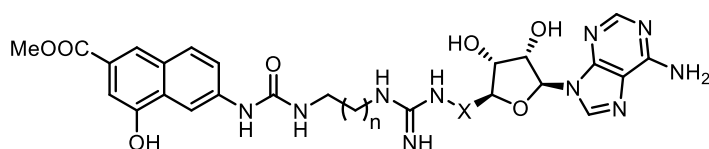
^aCompounds were tested in 10-concentration IC₅₀ mode with 3-fold serial dilutions starting at 100 μM. Data were analyzed with GraphPad Prism software (version 6.0) for IC₅₀ curve fitting; ^bUnless differently indicated, the values were obtained in a radioisotope-based filter assay, using 5 μM histone H4 (for PRMT1, PRMT3), histone H3 (for PRMT4), histone H2A (for PRMT5) as substrate and S-adenosyl-L-[methyl-3H]methionine (1 μM) as methyl donor; ^cObtained in AlphaLISA assay, using human recombinant PRMT1 (0.9 nM, final concentration). Histone H4 (1–21) peptide, biotinylated (100 nM, final concentration) and SAM (2 μM, final concentration) were used as substrate and cofactor, respectively.

Based on these outcomes, we speculated that modulation of the distance between the three pharmacophore moieties might generate potent and selective PRMT4 inhibitors. Therefore, we synthesized a second set of derivatives (compounds **4** – **8**) in which was further increased the distance between the 4-hydroxy-2-naphthoate moiety and the guanidine group (compounds **4**, **5**) or the distance between the guanidine group and the adenosine moiety (compounds **6** – **8**). The compounds were tested over a wider panel of PRMTs (including also PRMT6, PRMT7 and PRMT8) using the same radioisotope-based assay and the results were reported in Table 2.3 and summarized as heatmaps in Figure 2.5.

Table 2.3: Inhibitory activities of compounds **1** – **8** against various PRMTs

Inhibitory activities of compounds 1 – 8 (IC ₅₀ μM values) against PRMTs									
									
Entry	n	X	PRMT1	PRMT3	PRMT4	PRMT5	PRMT6	PRMT7	PRMT8
1 (EML734)	2	-CH ₂ -	32.27	57.19	13.84	52.13	72.77	0.32	8.29
2 (EML709)	3	-CH ₂ -	11.67	43.41	2.14	76.7	>100	0.55	18.68
3 (EML736)	4	-CH ₂ -	8.46	2.77	0.43	40.49	>100	0.22	5.87
4 (EML978)	5	-CH ₂ -	0.86	12.2	0.068	2.6	47	0.41	3.82
5 (EML979)	6	-CH ₂ -	2.6	12.4	0.176	3.38	35.6	0.631	5.48
6 (EML980)	3	-CH ₂ CH ₂ -	4.86	10.5	0.0097	0.115	22.7	0.226	6.00
7 (EML982)	3	CH ₂ CH ₂ CH ₂ -	1.80	13.3	0.0084	0.778	4.34	4.68	1.41
8 (EML981)	3	-CH=CHCH ₂ -	0.835	4.05	0.0032	1.46	1.75	1.68	1.95
SAH	-	-	0.15	1.2	0.12	1.61	0.33	0.22	0.17

Compounds were tested in 10-concentration IC₅₀ mode with 3-fold serial dilutions starting at 100 μM. Data were analyzed with GraphPad Prism software (version 6.0) for IC₅₀ curve fitting; The values were obtained in a radioisotope-based filter assay, using 5 μM histone H4 (for PRMT1, PRMT3), histone H3 (for PRMT4), histone H2A (for PRMT5) as substrate and S-adenosyl-L-[methyl-3H]methionine (1 μM) as methyl donor.



#	n	X	PRMT1	PRMT3	PRMT4	PRMT5	PRMT6	PRMT7	PRMT8	IC ₅₀
1 (EML734)	2	-CH ₂ -	32,270	57,190	13,870	52,130	72,770	315	8,293	1×10 ⁰ nM
2 (EML709)	3	-CH ₂ -	11,670	43,410	2,144	76,700	>100,000	554	18,680	5×10 ⁰ nM
3 (EML736)	4	-CH ₂ -	8,460	21,620	421	5,140	>100,000	222	5,871	1×10 ¹ nM
4 (EML978)	5	-CH ₂ -	860	12,160	61	2,669	47,820	413	3,818	5×10 ¹ nM
5 (EML979)	6	-CH ₂ -	2,603	12,410	176	3,383	35,600	631	5,476	1×10 ² nM
6 (EML980)	3	-CH ₂ CH ₂ -	4,858	10,470	10	115	22,730	226	5,995	5×10 ² nM
7 (EML982)	3	-CH ₂ CH ₂ CH ₂ -	1,795	13,250	8	778	4,338	4,681	1,406	1×10 ³ nM
8 (EML981)	3	-CH ₂ CH=CH-	835	4,045	3	1,462	1,749	1,675	1,948	5×10 ³ nM

#	n	X	PRMT1	PRMT3	PRMT5	PRMT6	PRMT7	PRMT8	SI
1 (EML734)	2	-CH ₂ -	2	4	4	5	0.02	315	>2000
2 (EML709)	3	-CH ₂ -	5	20	36	>47	0.26	9	2000
3 (EML736)	4	-CH ₂ -	20	51	122	>238	0.52	14	1500
4 (EML978)	5	-CH ₂ -	13	179	38	691	6	56	1000
5 (EML979)	6	-CH ₂ -	15	70	19	202	4	33	500
6 (EML980)	3	-CH ₂ CH ₂ -	501	1,082	12	2,340	23	619	100
7 (EML982)	3	-CH ₂ CH ₂ CH ₂ -	214	1,583	93	517	557	168	50
8 (EML981)	3	-CH ₂ CH=CH-	261	1,266	456	547	525	609	10

Figure 2.5 Inhibitory activities of compounds **1** – **8**: the heatmaps depict the IC₅₀ values (nM) for compounds **1** – **8** (top panel) and the selectivity index (fold) for PRMT4 over the specified PRMT (bottom).

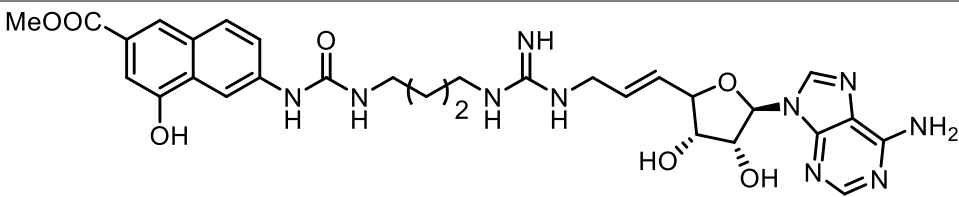
As shown in Table 2.3, increasing the linker length between the 4-hydroxy-2-naphthoate and the guanidine group up to a total of 4 or 5 carbon atoms resulted in a slight increase in the inhibitory activity against PRMT4 (6.2-fold for **4** and 2.4-fold for **5**). However, the compounds showed a similar gain also against PRMT1, PRMT5, and PRMT6 (e.g. 9.8-fold and 3.2-fold against PRMT1 and 19.8-fold and 15.2-fold against PRMT5, for **4** and **5**, respectively), with a

consequent reduction of selectivity. A lesser effect was observed against PRMT8 and a slight decrease of inhibiting activity was observed against PRMT7. The shorter compound **1**, bearing a linker length of 3 carbon atoms, displayed an interesting inhibitory activity on PRMT7 compared to PRMT4 but this behavior will be better discussed in Paragraph 2.4. On the other hand, compounds **6 – 8**, in which the distance between the guanidine group and the adenosine moiety was increased, showed an outstanding increase in potency and in selectivity over other 6 human PRMTs. In particular, compound **8** showed a 668-fold gain in potency over its shorter counterpart **2** and 261 to 1266-fold selectivity over the other PRMTs.

2.3.2. Selectivity profile of compound **8**

Subsequently, compound **8** was tested at fixed dose (1 and 10 μ M) in duplicate, evaluating its inhibitory activity against a panel of 8 lysine methyltransferases (including ASH1L, DOT1L, EZH2 complex, MLL1 complex, SET7/9, SET8, SUV39H2 and SUV420H1TV2). The obtained results showed a strong selectivity profile of compound **8**, as reported in the Table 2.4.

Table 2.4: Inhibitory activity of compound **8** against 8 Lysine Methyltransferases

Inhibitory activities of compound 8 (IC ₅₀ μ M values) against Methyltransferases		
		
Concentrations		
Methyltransferases	10 μ M	1 μ M
ASH1L	100.83	90.76
DOT1L	100.94	97.74
EZH2 Complex	84.28	84.39

MLL1 Complex	93.43	102.15
SET7/9	96.95	112.02
SET8	114.06	130.39
SUV39H2	86.70	113.51
SUV420H1TV2	91.85	104.00

Compound 8 was tested in single-dose mode, in duplicate, at 10 and 1 μ M. Data were analyzed with GraphPad Prism software (version 6.0) for IC₅₀ curve fitting; The values were obtained in a radioisotope-based filter assay, using 5 μ M Nucleosomes (for ASH1L, DOT1L, MLL1 Complex, SET8, SUV420H1TV2), histone H3 (for SUV39H2), Core Histone (for EZH2 Complex, SET7/9) as substrate and S-adenosyl-L-[methyl-3H]methionine (1 μ M) as methyl donor.

2.3.3. SPR-based studies of binding to PRMT4

The direct binding of compounds **1** – **8** on PRMT4 was evaluated using Surface Plasmon Resonance (SPR, Chapter VIII, Paragraph 8.3.3). To this aim, human PRMT4 (full length) was covalently immobilized on a sensor chip surface using an amine coupling approach and the three compounds were injected at different concentrations over the protein surface. Each compound strongly interacts with PRMT4, displaying the equilibrium dissociation constant (K_D) values in the nanomolar range for compounds **6** – **8** (Figure 2.6 and Table 2.5). In detail, compound **6** interacts with PRMT4 with higher affinity (K_D = 25.2 nM; Table 2.4) compared to **7** (K_D = 51.7 nM) and **8** (K_D = 75.9 nM). As shown by the sensorgrams depicted in Figure 2.6, compounds **6** – **8** dissociate from the protein slower than compounds **1** – **5**. Nonetheless, compound **6** showed the fastest interaction, as its residence time residence time (t_R)¹⁵⁹ values is the lowest among tested compounds (14.7 sec). Furthermore, **8** and **7** have longer residence time (62.5 and 76.9 sec, respectively) meaning that the effects of their binding to CARM1 last more. The association rate constants (K_{on}) values, being significantly higher for compounds **6** – **8** compared to compounds **1** – **5**, could be translated in the higher potency corroborating the enzymatic activity results.

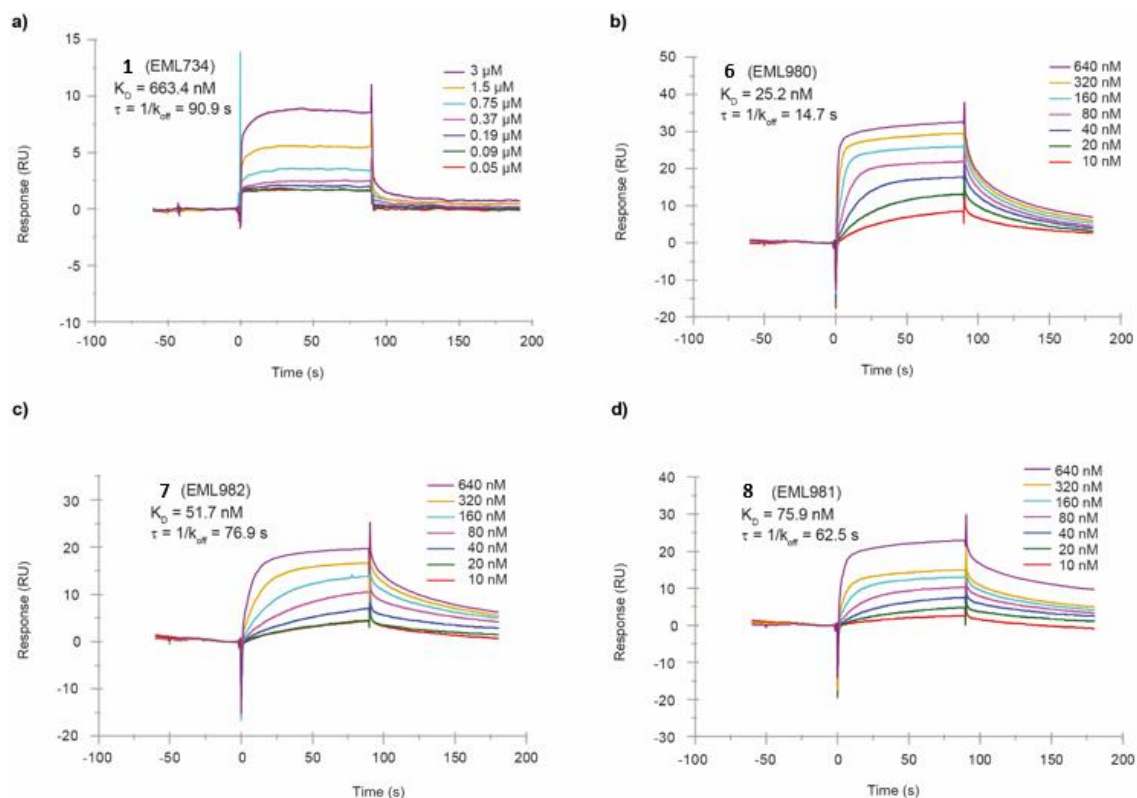


Figure 2.6 Sensorgrams obtained from the SPR interaction analysis of compounds **1** and **6 – 8** (panels a–d, respectively) binding to immobilized PRMT4. Each compound was injected at different concentrations (from 3 μM to 0.05 μM for **1** and from 640 nM to 10 nM for **6 – 8**) with an association and a dissociation time of 90 sec, with a flow rate of 30 $\mu\text{L}/\text{min}$. The equilibrium dissociation constants (K_D) were derived from the ratio between kinetic dissociation (k_{off}) and association (k_{on}) constants.

Table 2.5: Affinity and kinetic parameters derived from SPR experiments

Compound	K_D	k_{on} (1/Ms)	k_{off} (1/s)	τ_R (s)
1 (EML734)	663.4 nM	1.67×10^4	0.011	90.9
2 (EML709)	2300 nM	6.52×10^3	0.015	66.7
3 (EML726)	359.2 nM	3.49×10^4	0.013	76.9
4 (EML978)	2800 nM	2.70×10^5	0.760	1.31

5 (EML979)	603.4 nM	2.58×10^4	0.015	66.7
6 (EML980)	25.2 nM	2.70×10^6	0.068	14.7
7 (EML982)	51.7 nM	0.25×10^6	0.013	76.9
8 (EML981)	75.9 nM	0.21×10^6	0.016	62.5
SAM	9.6 nM	2.90×10^5	0.003	333.3

2.3.4. Structural studies

To study and compare the binding modes of compounds **1** – **3** (less potent and selective PRMT4 inhibitors) and **6** – **8** (more potent and selective PRMT4 inhibitors) with different PRMTs, in collaboration with Prof. Jean Cavarelli (IGBMC, University of Strasbourg), co-crystallization studies were performed using four PRMTs, namely isolated domains of *mm*PRMT4 (*Mus musculus* PRMT4, residues 130–487 or 140–497), full length *Mus musculus* PRMT2, *mm*PRMT6 (*Mus musculus* PRMT6, residues 34–378), full length *Mus musculus* PRMT7. Unfortunately, no co-crystals were obtained with PRMT2 or PRMT7. On the contrary, we were able to co-crystallize the compounds in complex with both PRMT4 and PRMT6.

Overall, the compounds co-crystallized with PRMT4 adopt a similar conformation, revealing two common anchoring platforms, the methyl 4-hydroxy-2-naphthoate and the adenosine moieties, each one occupying the same binding site on PRMT4 regardless the different linker lengths (Figure 2.7a). As expected, the adenosine moiety occupies the SAM binding pocket mainly interacting with Y150, E215, E244, M269 (Figure 2.7c,d). On the other hand, the methyl 4-hydroxy-2-naphthoate moiety partially engages the peptide substrate binding site on PRMT4, establishing major interactions with Y262, P473, F475, Y477 on one hand and F153 on the other hand (Figure 2.7c,d). Surrounded by such a “frozen” binding site, the linker of each compound assumes a unique and distinctive conformation interacting with

catalytic residues M260, E258, H415 and W416 on one side and with F153, Y154, E267 on the other side (Figure 2.7c,d). In addition, strong hydrogen bonds are established within such a "frozen" site and their number and strength markedly depend on the length and nature of the linker of each compound, according to their affinity and, consequently, the IC₅₀ values. In the case of compound **8**, the best inhibitor herein reported, the guanidine group is inserted in the binding site of the guanidine moiety of the peptide transition state, interacting with catalytic glutamate residues (E258 and E267) of the double-E loop. Moreover, the N5 atom establishes 2 hydrogen bonds with the oxygen atoms of the main chain of E258 and M260 (Figure 2.7d).

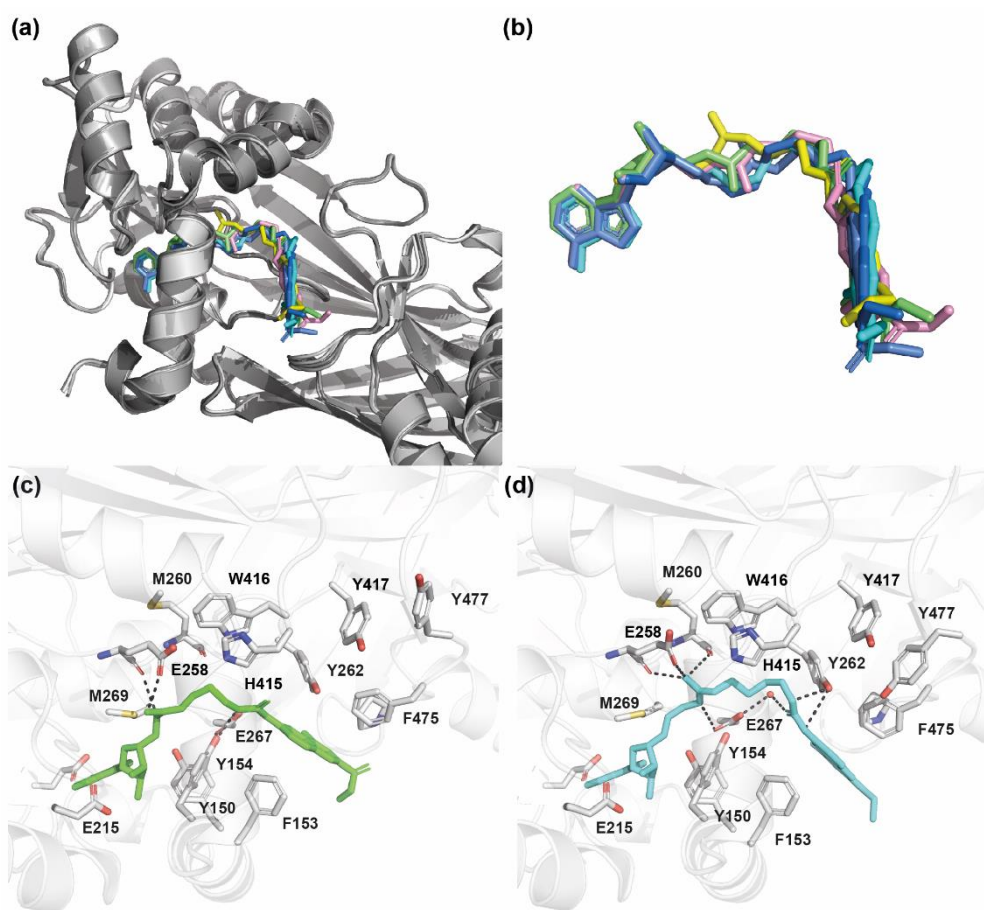


Figure 2.7 Structures of *mmPRMT4* in complex with compounds **1 – 3** and **6 – 8**. (a) Superimposition (done on protein backbones) of compounds (**1 – 3** and **6 – 8**) bound to subunit B of *mmPRMT4*. Each PRMT4 subunit is represented as cartoon (shades of grey) lime, cyan, marine, yellow, grey, pink ribbons) and compounds are represented as sticks (in lime, yellow,

pink, cornflower blue, sea blue and cyan, respectively); (b) close-up view of bound compound conformations; (c) binding interactions of compound **1** (lime sticks) with *mm*PRMT4 monomer B (ribbon); (d) binding interactions of compound **8** (cyan sticks) with *mm*PRMT4 monomer B (ribbon). Hydrogen bonds are shown as dash lines. For clarity, *N*-terminal helices (residues 135–165) of PRMT4 are not shown.

The crystal structures revealed the importance of the linker length between the adenosine moiety and the guanidine group as well as between the latter and the methyl 4-hydroxy-2-naphthoate group. In order to bring the guanidine group within the catalytic clamp formed by E258 and E267, a linker length between the guanidine group and the adenosine moiety of 2 or 3 carbon atoms is required. Compounds **1** – **3**, bearing a shorter linker, are unable to establish the two guanidine-stabilizing hydrogen bonds with the main chain of PRMT4, resulting in compounds with weaker affinity than compounds **6** – **8**. This evidence corroborates the better inhibitory ability of compounds **6** – **8** compared to compounds **1** – **3**. In addition, the double-bound in **8** imposed a trans conformation which is less constrained and, therefore, more favorable than the one adopted by the corresponding saturated compound **7**. Regarding the linker between the methyl 4-hydroxy-2-naphthoate and the guanidine group, increasing the linker length from 3 ($n=2$, **1**) to 4 ($n=3$, **2**) and 5 ($n=4$, **3**) carbon atoms result in additional Van der Waals interactions with W416 and Y262, thus supporting a higher affinity and a corresponding decrease in IC_{50} values.

In the case of PRMT6, co-crystallization studies revealed that the compounds adopt an odd distorted U-shaped conformation (Figure 2.8), wherein the guanidine moiety is unable to reach the PRMT6 double E loop clamp because the linker with the sugar is too short, even for the longer compounds **7** and **8**. On the other hand, the methyl-4-hydroxy-2-naphthoate moiety does not bind to the arginine binding site but it is sandwiched between the adenosine and the side chains of Y50 and Y51 residues of alpha helix motif I.

The adopted conformation of compounds was not able to induce strong interactions with PRMT6, supporting the higher affinity of compounds **6** – **8** on PRMT4.

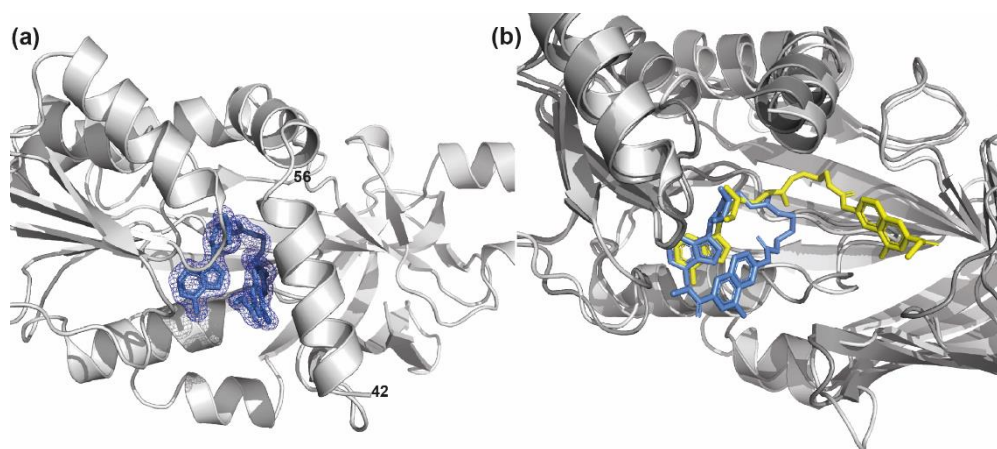


Figure 2.8 (a) Electron density ($2F_{\text{obs}}-F_{\text{calc}}$) weighted maps of compound **1** (represented as cornflower blue sticks) bound to subunit B of mmPRMT6 (represented as grey cartoon). Maps are represented as a mesh, contouring level set to 1σ . For clarity, N-terminal helices (residues 42–56) of mmPRMT6 are not shown; (b) Superimposition (done on protein backbones) of the conformations of compound **1** (yellow or cornflower blue sticks, respectively) when bound to subunit B of mmPRMT4 (represented as dark grey cartoon) and when bound to mmPRMT6 (represented as light grey cartoon). For clarity, N-terminal helices of PRMT4 and PRMT6 are not shown.

2.3.5. Assessment of cellular activity and toxicity

The aim of this work was to demonstrate the value of our approach in the development of potent and selective PRMTs inhibitors. Therefore, at this stage, the attention was not focused on *druglikeness* as well as cell permeability of compounds. The hypothesis of poor permeability of compounds **6** – **8** was confirmed by parallel artificial membrane permeability assay (PAMPA, Chapter VIII, Paragraph 8.3.4). The highly permeable drug propranolol and the poorly permeable drug furosemide were used as positive and negative controls, respectively, and the results are summarised in Table 2.6.

Table 2.6: Permeability values of compounds **6 – 8**.

Entry	PAMPA P_{app} (cm/s)
6 (EML980)	0.55×10^{-7}
7 (EML982)	0.39×10^{-7}
8 (EML981)	0.38×10^{-7}
Propranolol	60×10^{-7}
Furosemide	0.34×10^{-7}

Nevertheless, we evaluate the ability of compounds **6 – 8** to affect the activity of PRMT4 also in a cellular context. Initially, the cell toxicity of compounds **6 – 8** was evaluated using the MTT assay (Chapter VIII, Paragraph 8.3.5). HEK293T cells were treated with the compounds at three different concentrations (10, 50 and 100 μ M) and after 24 h and 72 h of incubation with the compounds, cellular viability was assessed. We find that the compounds did not reduce the number of metabolically active cells in comparison with vehicle, at all tested concentrations (up to 100 μ M, Figure 2.9a). Even after 72 h of treatment cell viability remained above 80% (Figure 2.9b).

Subsequently, in collaboration with Prof. Mark T. Bedford (MD Anderson Cancer Center) the ability of compounds **6 – 8** to reduce cellular level of arginine methylation catalyzed by PRMT4 was evaluated. To this aim, HEK293T cells were incubated for 24 h with the three compounds (at 10 and 50 μ M) or with compound TP-064 (10 μ M), used as positive control. The total cell lysates were then immunoblotted with a pan-PRMT4 substrate antibody

(PRMT4^{sub}), originally raised against the R388 site of Nuclear Factor 1 B-type (NFIB-Me) but also capable to recognize many PRMT4 substrates. As showed in Figure 2.9c, the results confirmed the proof of concept concerning the design of these derivatives. In fact, although with a lower effect compared to the cytopermeable TP-064, the compounds, in particular **8**, are able to reduce the activity of PRMT4 in a concentration-dependent way. Noteworthy, for TP-064 concentration higher than 10 μ M led to cell death.

In addition, the inhibitory activity and the antiproliferative effect of compound **8** were evaluated also on MCF7 cells, a breast cancer cell line (Figure 2.9d and 2.9f, respectively). As reported in Figure 2.9d, the inhibitory activity on PRMT4 of compound **8** is also observed in MCF7 cells after 4- and 8-days of incubation using compound TP-064 (10 μ M), as positive control. Compound **8** is able to reduce the methylation catalysed by PRMT4 in a concentration-dependent manner. More importantly, both 10 μ M TP064 and 50 μ M **8** markedly decreased proliferation of MCF7 cells, whereas no effect was observed in HEK293T cells (Figures 2.9e,f).

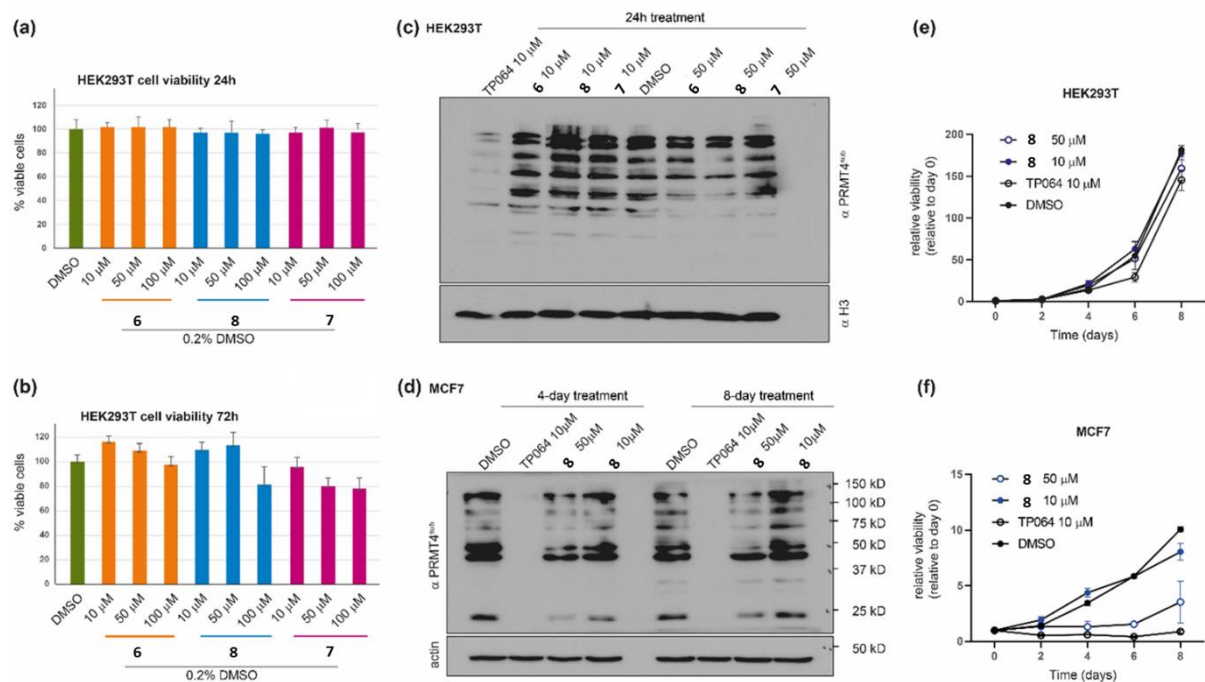


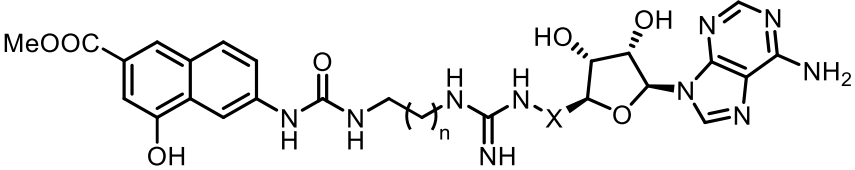
Figure 2.9 (a,b) HEK293T cells were treated with compounds **6** – **8** at three different concentrations (10, 50 and 100 μ M) for (a) 24 h and (b) 72 h. The cell viability was assessed by measuring the mitochondrial-dependent reduction of MTT to formazan, with respect to DMSO; (c,d) western blot analyses were performed (c) on lysates from HEK293T cells after treatment with compounds **6** – **8** at 10 and 50 μ M for 24 h, and (d) on lysates from MCF7 cells after treatment with compound **8** at 10 and 50 μ M for 4- and 8 days. Methylation was detected by immunoblotting with a pan-PRMT4 substrate antibody (PRMT4^{sub}). Total histone H3 (c) or actin (d) were used to check for equal loading. The cell-permeable PRMT4 inhibitor TP064 (10 μ M) was used as a reference compound; (e,f) relative proliferation of (e) HEK293T and (f) MCF7 cells with different concentration of **8** for different time points. Medium was changed at day 4. All the data points represent the relative viability normalized to day 0. The error bars represent the standard deviation of three biological replicates performed at each time point.

2.4 Identification of PRMT7 and PRMT9 inhibitors

On the basis of previous results, we assumed that modulating the distance between the pharmacophoric moieties would provide further information on the structural requirement for other PRMTs inhibition such as PRMT7 and PRMT9. In fact, despite many efforts into the progress of PRMT7 selective chemical probes, only a few satisfactory outcomes have been observed. In addition, to date, no PRMT9 inhibitor has been reported, probably due to the absence of a robust and effective biochemical assays for measuring its methyltransferase activity. Data reported in Table 2.3 and Figure 2.5 suggested that these compounds could be valuable starting points to find PRMT7 and/or PRMT9 selective inhibitors. To this aim, firstly, we looked for a suitable assay for PRMT9. We resolved to adapt the AlphaLISA technology to develop an effective assay to measure the levels of methylation catalysed by PRMT9 (Chapter VIII, Paragraph 8.3.2) because the commercially available homogenous assay kit (BPS, # 52069) did not work properly in our hands and gave an unacceptably narrow assay window. Subsequently, we extended our pool of compounds synthesizing compound **9**, featuring a linker length of 2 carbon atoms between the 4-hydroxy-2-naphthoate moiety and the guanidine group, as lower homologue of compound **1**.

The screening of selected compounds **1 – 9** was performed and the corresponding IC₅₀ values were determinate and summarized in Table 2.7. The IC₅₀ values on PRMT9 was determinate by AlphaLISA assay while the radioisotope-based assay was used to determinate the IC₅₀ value on PRMT7.

Table 2.7: Inhibitory activities of compounds **1** – **9** against PRMT7 and PRMT9

												
(IC ₅₀ μM values)					Selectivity index PRMT9 vs other PRMTs							
#	n	X	PRMT7 ^a	PRMT9 ^b	PRMT1	PRMT3	PRMT4	PRMT5	PRMT6	PRMT7	PRMT8	
1 (EML734)	2	-CH ₂ -	0.32	0.89	36	64	16	59	82	0.36	9.3	
2 (EML709)	3	-CH ₂ -	0.55	1.32	8.8	1.6	33	58	>76	0.42	14	
3 (EML736)	4	-CH ₂ -	0.22	5.8	1.5	3.7	0.07	8.9	>17	0.04	1	
4 (EML978)	5	-CH ₂ -	0.41	n.a ^c	n.a ^c	n.a ^c	n.a ^c	n.a ^c	n.a ^c	n.a ^c	n.a ^c	
5 (EML979)	6	-CH ₂ -	0.631	1.3	2.0	9.6	0.14	2.6	27	0.49	4.5	
6 (EML980)	3	-CH ₂ CH ₂ -	0.226	1.2	4.0	8.75	0.008	0.1	19	0.19	5	
7 (EML982)	3	CH ₂ CH ₂ CH ₂	4.68	>10	0.18	0.13	0.00084	0.08	0.43	0.47	0.14	
8 (EML981)	3	CH=CHCH ₂	1.68	9.3	0.089	0.43	0.0004	0.16	0.19	0.18	0.20	
9 (EML1102)	1	-CH ₂ -	0.54	2.47	>40	>100	9.2	3.8	28	0.22	17	

^aThe values were obtained in a radioisotope-based filter assay (Table 2.1 – 2.2).

^bObtained in AlphaLISA assay, using human recombinant PRMT9 (200 ng/μL, final concentration), biotinylated substrate peptide SAP-145 (aa 500–519) (Pepmic, custom synthesis) (final concentration, 100 nM), and SAM (50 μM, final concentration) were used as substrate and cofactor, respectively.

^cNot available

As expected, compounds **7** and **8**, characterized by a three-carbon linker between the adenosine part and the guanidine group, showed a strong decrease in inhibitory activity on PRMT7 and PRMT9, compared to the IC₅₀ values obtained on PRMT4. A similar selectivity profile was observed also for compound **6**, featuring a two-carbon linker between the two

aforementioned pharmacophoric moieties. On the other hand, compounds **1 – 3**, **5** and **9** in which the adenosine moiety was connected to guanidine through a methylene linker, displayed a gain in the inhibitory activity against PRMT9. Nevertheless, even if compounds **3,5** and **9** showed a good inhibitory activity on PRMT7 and PRMT9 (IC_{50} of 5.8 μ M, 1.3 μ M and 2.47 μ M, respectively), similar IC_{50} values were observed also for other PRMTs with a consequent loss of selectivity. However, decreasing the linker length between the 4-hydroxy-2-naphthoate and the guanidine group up to a total of 3 or 4 carbon atoms yielded a gain in the inhibitory activity against PRMT7 and PRMT9 over other PRMTs. In particular, compound **1** was identified as the first-in-class dual inhibitor of PRMT7 and PRMT9 (IC_{50} of 0.32 μ M and 0.89 μ M, respectively) that showed 9 to 82-fold selectivity on PRMT9 over the other human PRMTs.

Molecular modelling studies are still in course, and the preliminary data are highlighting a different binding mode of compound **1** with PRMT7 and PRMT9 compared to the previous reported binding with PRMT4. The synthesis of a new pool of compounds, bearing suitable decorated naphthoate moiety, is in course to clarify and validate the predictive model.

2.5 Conclusions

In summary, compound **EML108**, a type I inhibitor identified by EMCL in 2010, was deconstructed into a 4-hydroxy-2-naphthoic fragment and then a step-by-step growing approach was applied. First, the fragment was bridged by an amide or urea group with an arginine mimetic or methionine moiety. The inhibitory activity of the synthesized compounds (derivatives **I - XXVI**) was evaluated on the catalytic activity of human recombinant PRMT1, chosen as representative of type I PRMTs, using a purpose-developed AlphaLISA assay. On the basis of structure–activity relationships, in this Ph. D. project we designed and synthesized another series of compounds (**1 – 9**). The last bearing, in addition to the 4-hydroxy-2-naphthoic fragment of **EML108**, the adenosine scaffold as SAM mimetic moiety and a guanidine group

as arginine mimic. A radioisotope-based filter-binding assay was used as a robust and effective screening to profile the activity of the compounds against type I PRMT1, PRMT3, PRMT4, PRMT6, and PRMT8, type II PRMT5, and type III PRMT7. The overall length of the compounds and, even more, the distance of the three pharmacophoric moieties resulted to be crucial for the inhibitory activity especially against PRMT4. In fact, derivative **8** featuring a four-carbon atom linker between the 4-hydroxy-2-naphthoate and the guanidine group and a three-carbon atom linker between the latter and the adenosine resulted to be the most potent inhibitor against PRMT4 (IC_{50} of 3 nM), with a 261- to 1266-fold selectivity over the other PRMTs and no activity was observed over 8 lysine methyltransferases. The specific and strong binding interaction between PRMT4 and compound **8** ($K_D = 75.9$ nM; $\tau_R = 62.5$ sec) was confirmed also by SPR and crystallographic studies. In particular, these studies also supported the improvement in activity and selectivity observed for compound **8** compared to other compounds. Subsequently, the cell toxicity was evaluated and all tested compounds (**6** – **8**) did not reduce the number of metabolically active cells in comparison with vehicle, at all the tested concentrations (up to 100 μ M). Then, although non optimized for cell permeability, compound **8** was able to reduce the cellular activity of PRMT4 in a concentration-dependent way in two different cell lines (HEK293T and MCF7, respectively) and can be a starting point for further development of cell active PRMT4 inhibitors. In this scenario, some well-known medicinal chemistry strategies such as pro-drug, molecular simplification, bioisosteric substitutions could be applied with the aim to mask or remove the groups responsible of the low cell permeability. On the other hand, based on these results and pursuing our interest in the identification of potent and selective PRMT inhibitors, we focused our attention also on PRMT7 and PRMT9. Firstly, we expand our pool of compounds and then they were screening against PRMT9 using in-house developed AlphaLISA assay. Even in this outlook, the distance of the three pharmacophoric moieties resulted to be crucial for the inhibitory activity. Compound **1** featuring a three-carbon

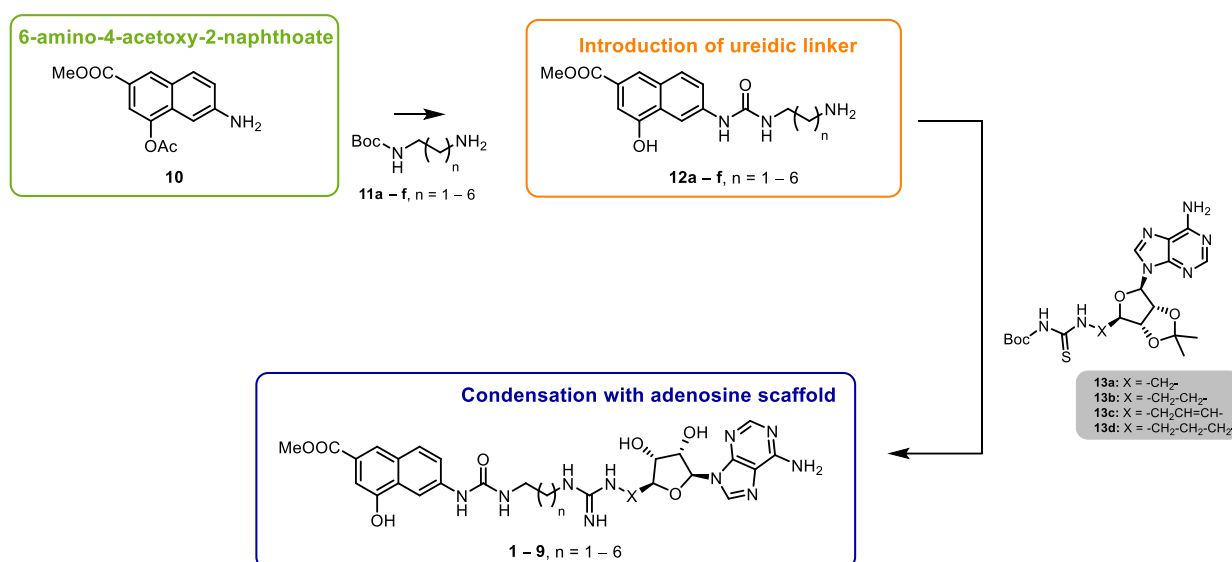
atom linker between the 4-hydroxy-2-naphthoate and the guanidine group and a methylene linker between the latter and the adenosine moiety resulted to be the most potent inhibitor against PRMT7 and PRMT9 (IC_{50} of 0.32 μ M and 0.89 μ M, respectively), with a 9- to 82-fold selectivity over the other PRMTs. In conclusion, these studies confirmed the feasibility of our deconstruction–reconstruction approach to achieve potency and selectivity against a specific PRMT isoform, leading to the identification of compound **8**, as the new nanomolar PRMT4 inhibitor, and compound **1** as the first in class dual inhibitor of PRMT7 and PRMT9.

2.6 Chemistry

In this section, the synthetic procedures adopted for the preparation of compounds **1** – **9** were described. The synthetic general route was depicted in Scheme 2.1. It was based on two key steps:

- I) Attachment of proper linkers, featuring a terminal amino group, on the 6-amino-4-hydroxy-2-naphthoic scaffold;
- II) Condensation of the terminal amino group with decorated adenosine moieties.

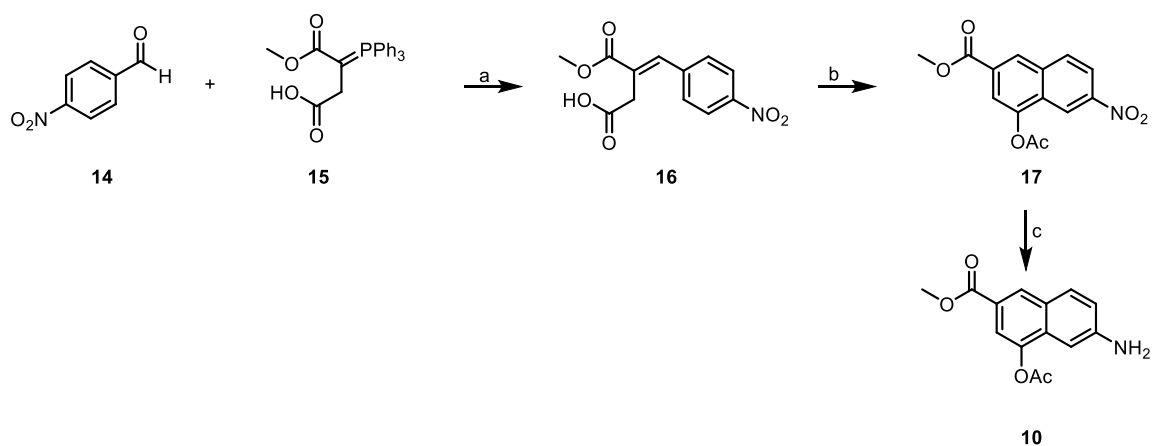
Scheme 2.1 General synthetic route.



2.6.1. Synthesis of 6-amino-4-acetoxy-2-naphthoate 10

The 6-amino-4-acetoxy-2-naphthoate **10** was prepared in excellent yields following a synthetic protocol previously developed by us (Scheme 2.2).¹²⁰ The first step involved in a Wittig reaction (compound **16**) between the commercial available 4-nitrobenzaldehyde **14** and the carboxyphosphorane **15**, followed by the microwave-assisted Friedel-Crafts-type ring closure to yield methyl 4-acetoxy-6-nitro-2-naphthoate **17**. The nitro derivative was selectively reduced with zinc dust in acetic acid (AcOH) to give the amino derivative **10**.

Scheme 2.2 General synthetic scheme for the preparation of compound **10**.



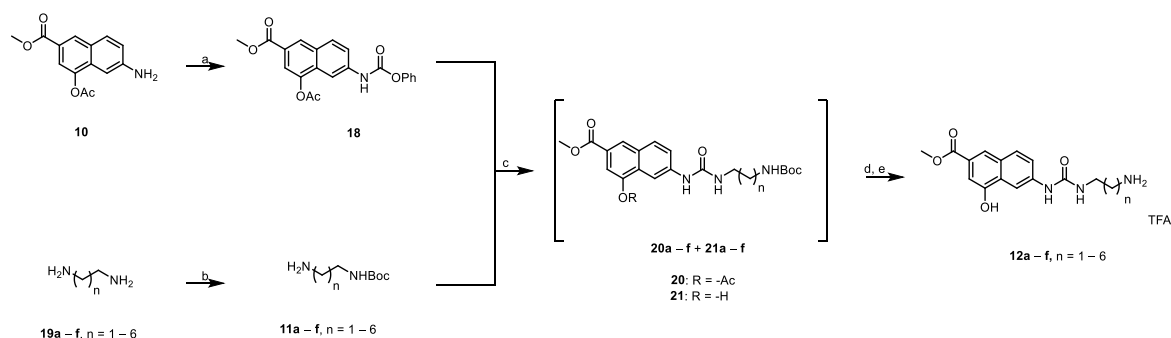
Reagents and conditions: a) toluene, r. t., 48 h (92%); b) sodium acetate, acetic anhydride, 120 °C (MW), 0.5 h, (95%); c) zinc dust, AcOH, r. t., 1 h (98%).

2.6.2. Synthesis of compounds 12a – f

The ureido derivatives **12a – f** were prepared as outlined in Scheme 2.3. The amino derivative **10** was activated with phenyl chloroformate to yield phenyl carbamate **18**. The latter was reacted with the proper mono-Boc-protected alkyldiamines **11a – f**, obtained by commercially available di-aminoalkane **19a – f**, to give a mixture of acetylated and non-acetylated derivatives **20a – f** and **21a – f**. The treatment with piperidine in

dichloromethane (DCM), followed by deprotection with trifluoroacetic acid (TFA), furnished derivatives **12a – f**.

Scheme 2.3 General synthetic scheme for the preparation of compounds **12a – f**.

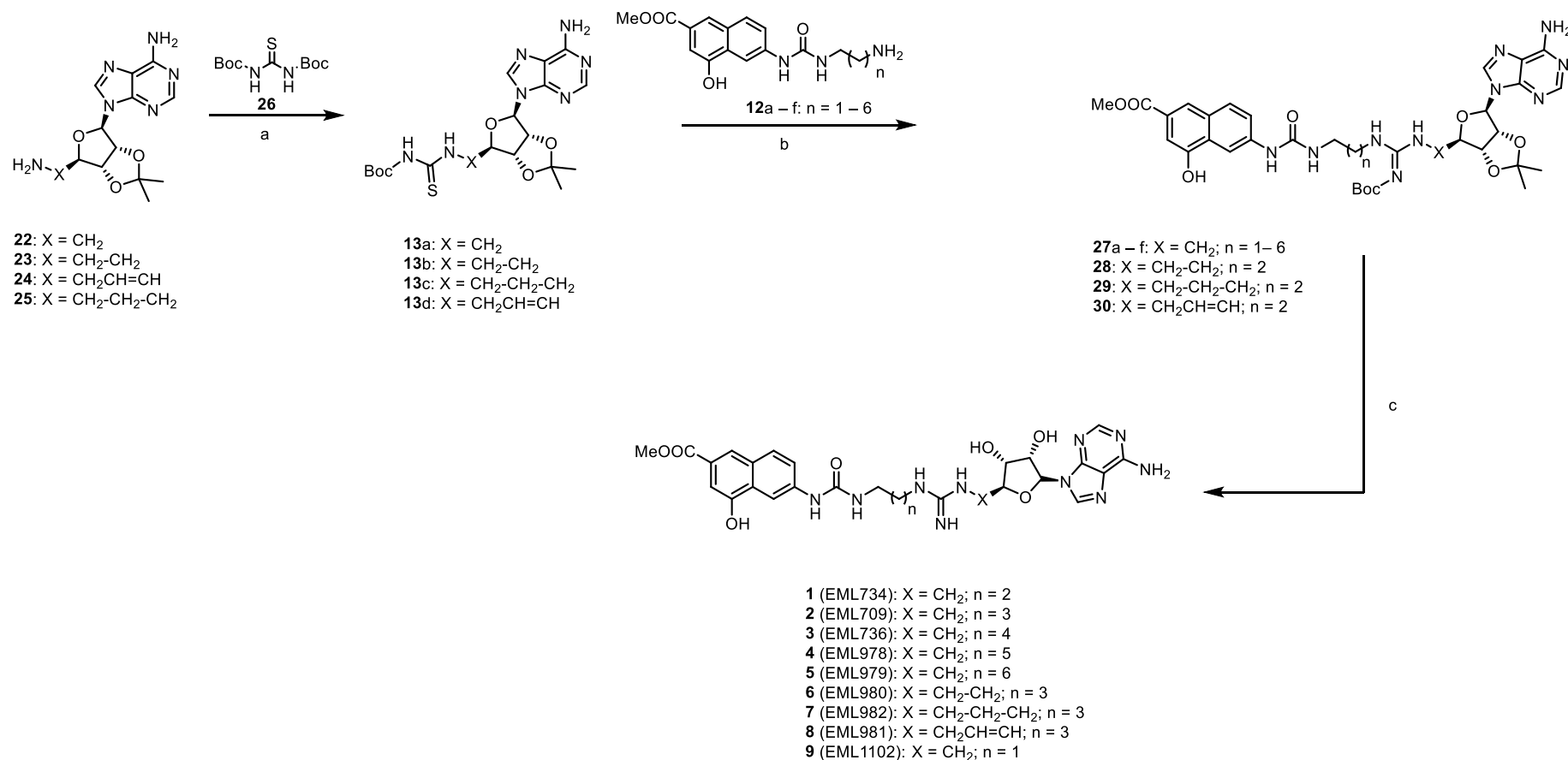


Reagents and conditions: a) phenyl chloroformate, triethylamine (TEA), ethyl acetate (AcOEt), r. t., 12 h (70%); b) Di-*tert*-butyl dicarbonate (Boc₂O), chloroform (CHCl₃), r. t., 12 h (78 – 81%); c) TEA, dry N,N-dimethylformamide (DMF), r. t., 2 h; d) piperidine, DCM, r. t., 0.5 h; e) DCM/TFA 9:1, r. t., 12 h (80 – 85% on three steps).

2.6.3. Synthesis of compounds **1 – 9**.

Compounds **1 – 9** were prepared as outlined in Scheme 2.4. Adenosine derivatives **22 – 25** were reacted with *N,N'*-di-Boc-thiourea **26** in the presence of trifluoroacetic anhydride (TFAA) and sodium hydride (NaH), to give thioureas **13a – d**. Coupling reaction with amino derivatives **12a – f** in the presence of 1-Ethyl-3-(3-dimethylaminopropyl) carbodiimide (EDC) hydrochloride as activating agent and triethylamine (TEA) as a base yielded derivatives **27a – f**, **28 – 30** which were deprotected with TFA to obtain the target compounds **1 – 9**.

Scheme 2.4 General synthetic scheme for the preparation of compounds **1–9**.

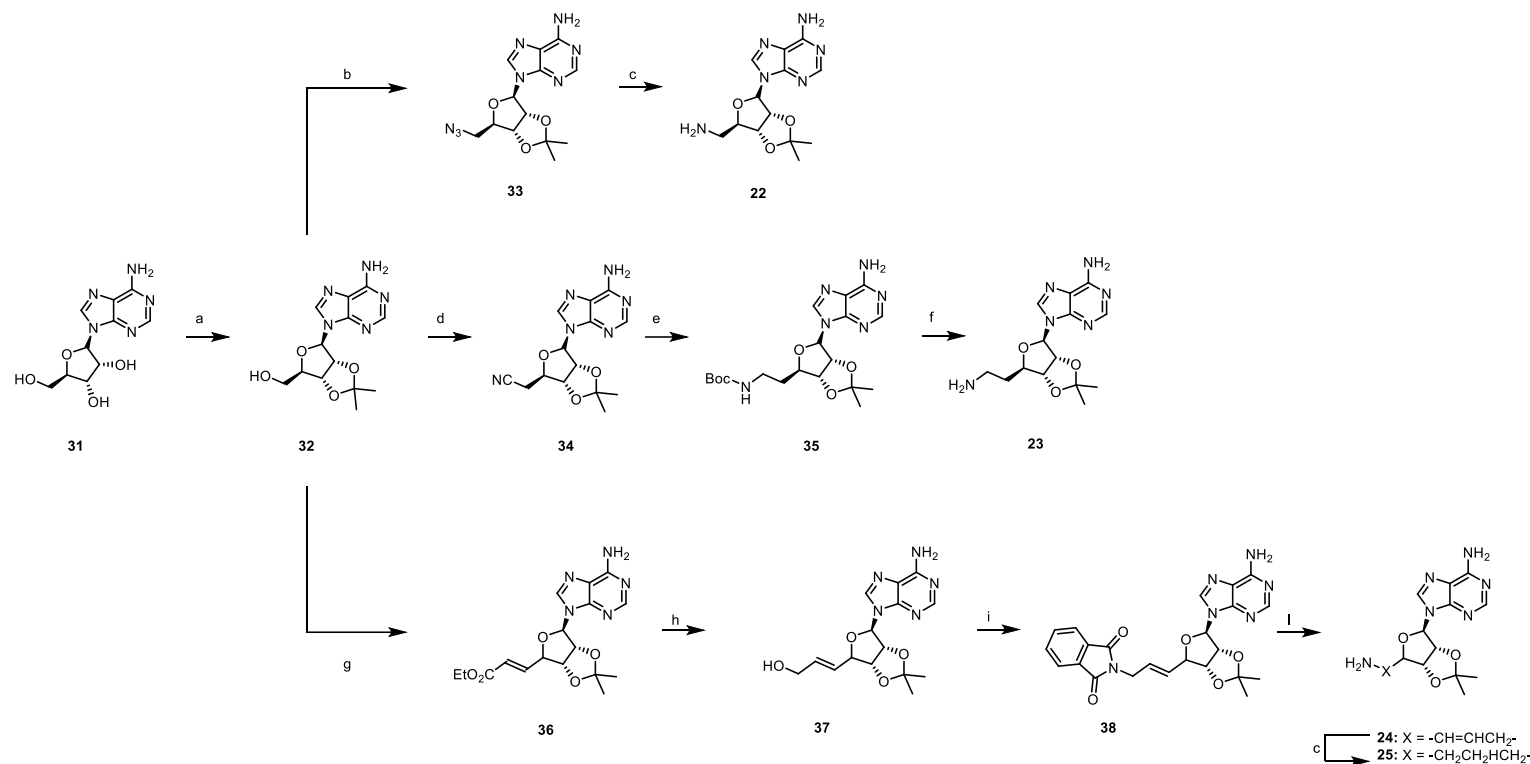


Reagents and conditions: a) NaH (60% mineral oil), TFAA, dry tetrahydrofuran (THF), r. t., 16 h (33 – 53 %); b) EDC hydrochloride, TEA, DCM, r. t. 18 h (72 – 81%); c) DCM/TFA/H₂O, 7:3:0.1, r. t., 2 h (74 – 80%).

2.6.4. Synthesis of amino-adenosine derivatives **22** – **25**

Amino-adenosine derivatives **22** – **25** were obtained according to a slight modification of previously reported procedures, as depicted in Scheme 2.5.^{160,161} Key building block is the 3',4'-acetonide adenosine **32**, synthesized from commercial available adenosine **31** and perchloric acid (HClO₄) in acetone. Nucleophilic substitution with diphosphorylazide (DPPA) and sodium azide (NaN₃), in presence of 1,8-Diazabicyclo(5.4.0)undec-7-ene (DBU), led to azide **33** which was reduced into the corresponding amino-derivative **22** by palladium-catalysed hydrogenation. The synthesis of compound **23** began with the one carbon homologation of **32** via Mitsunobu reaction employing triphenylphosphine (PPh₃), diethyl azodicarboxylate (DEAD), and acetone cyanohydrin allowed to obtain the nitrile derivative **34**. The latter was firstly reduced to the Boc-protected amine **35**, in presence of sodium borohydride (NaBH₄) and nickel(II) chloride hexahydrate (NiCl₂·6H₂O) using methanol (MeOH) as a solvent. Subsequently, the protected-amine was treated with TFA in DCM to give amino-adenosine **23**. Finally, oxidation of primary alcohol of **32** with 2-iodoxybenzoic acid (IBX) led to the *in situ* generation of the corresponding aldehyde which was directly converted into alkene **36** via a Wittig reaction with triphenylcarbethoxymethylenephosphorane. The selective reduction of the ester with diisobutylaluminum hydride (DIBAL-H) yielded the alcohol **37**. Subsequent Mitsunobu reaction allowed to straightforward insert the phthalimide group (**38**) which was then removed with hydrazine hydrate (NH₂NH₂ · H₂O) to obtain the amino-adenosine **24** which was in turn converted into its saturated analogue **25** by palladium-catalysed hydrogenation.

Scheme 2.5 General synthetic scheme for the preparation of amino-adenosine derivatives **22** – **25**.



Reagents and conditions: a) acetone, HClO₄ 70%, r. t., 5 h (81%); b) NaN₃, DPPA, DBU, 15-crown-5, dioxane, 24 h (86%); c) H₂, Pd/C 10%, MeOH, r. t., 16 h (99%); d) acetone cyanohydrin, DEAD, PPh₃, dry THF, 0 °C to 20 °C, 24 h, (89%); e) Boc₂O, NaBH₄, NiCl₂·6H₂O, dry MeOH, 0 °C, 2 h, (80%); f) DCM/TFA 95:5, r. t., 8 h, (65%); g) IBX, CH₃CH₂O₂CCH=P(C₆H₅)₃, dimethyl sulfoxide (DMSO), 20 °C, 72 h (70%); h) DIBAL-H, DCM, -78 °C, 2 h, (98%); i) phthalimide, DEAD, PPH₃, dry THF, 20° C, 16 h (70%); j) NH₂NH₂ · H₂O, MeOH, 0 °C to 25 °C, 16 h (90%).

CHAPTER III

Development of Alkene 1,3- Functionalization Reaction and Design of Ketone-based Compounds as PRMTs Inhibitors

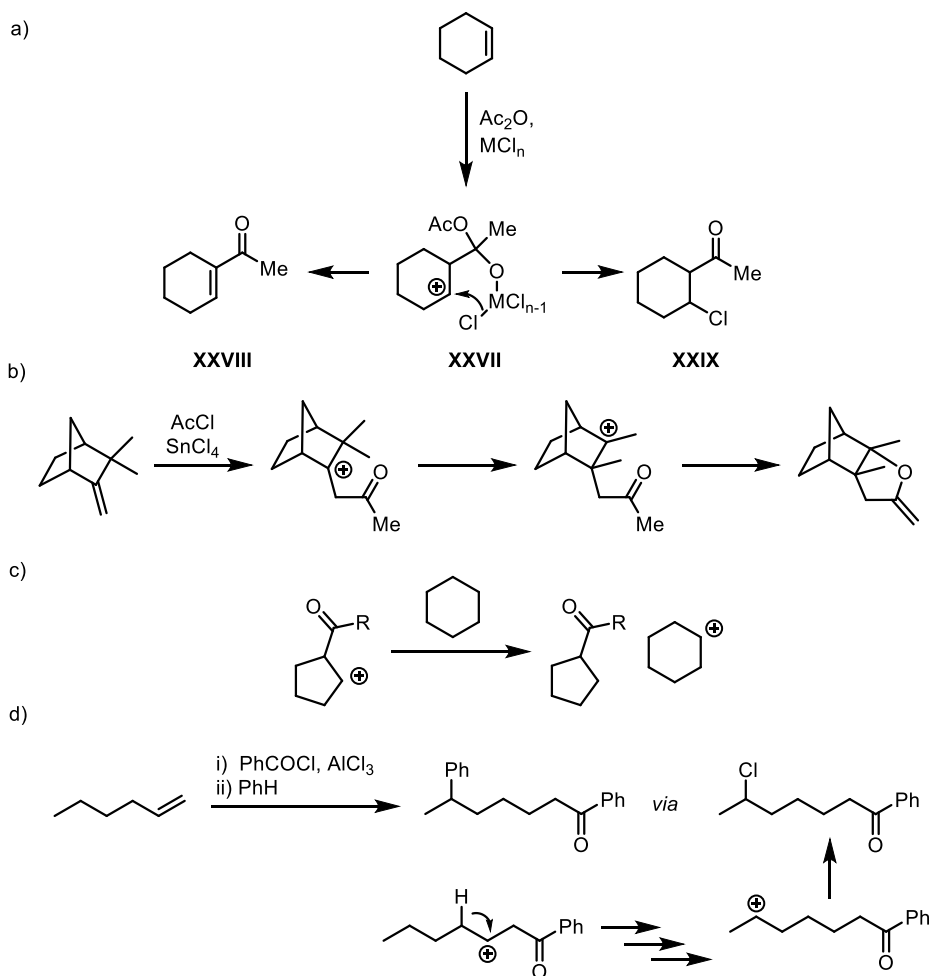
With the aim of improving my knowledge in organic chemistry, I spent seven months at the Institute of Organic Chemistry (University of Vienna) under the supervision of Prof. Nuno Maulide, wherein I was involved in the development of a new synthetic methodology defined as “Alkene 1,3-Functionalization”. This expertise was then applied to design new PRMTs inhibitors, structurally related to those described in Chapter II.

3.1. Alkene 1,3-Functionalization reaction

3.1.1. *Introduction*

The reaction of alkenes with acylium ions is a process that was intensely studied around the middle of the 20th century.¹⁶² Typically generated by the reaction of an acyl halide with a Lewis-acid metal salt (e.g. AlCl₃), acylium ions were shown to undergo a wide range of Friedel-Crafts-type processes with alkenes, leading to an array of possible products (Scheme 3.1). The attack of the double bond on the acylium ion can initially form a β -carbonyl cation **XXVII**, the most straight-forward reactions of which are α -deprotonation, generating the α , β -unsaturated carbonyl compound **XXVIII**, or direct capture by an anion (e.g. halide), affording the corresponding β -halo carbonyl compounds **XXIX** (Scheme 3.1a). However, according on reaction conditions, choice of Lewis acid and further, as of yet unknown, factors, these cations can also undergo other types of transformations, including alkyl shifts (Scheme 3.1b), intermolecular hydride transfers (Scheme 3.1c) and, probably most interestingly, sequential intramolecular 1,2-hydride shifts (Scheme 3.1d).

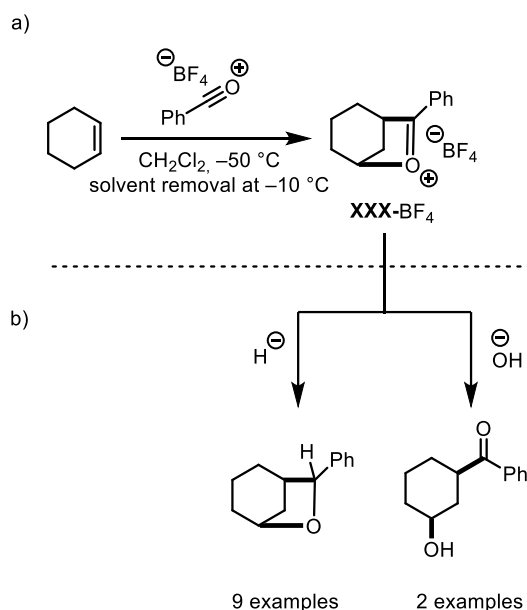
Scheme 3.1 Diverse reaction pathways of β -carbonyl cations.



The possibility to harness the tendency of hydrides to shift intramolecularly in such a fashion that the positive charge effectively migrates away from the electron-withdrawing carbonyl functionality is particularly intriguing. In this context, the research work reported in Scheme 3.2 presents interesting precedent, seeing as the formation of bridged oxocarbenium ion (**XXX**- BF_4) through the reaction of a range of alkenes with acylium tetrafluoroborates is reported (Scheme 3.2a). The initial ionic products are further transformed to the corresponding cyclic ethers and, for two isolated substrates, to the diastereomerically pure γ -hydroxylated ketones, as depicted in Scheme 3.2b.^{163,164}

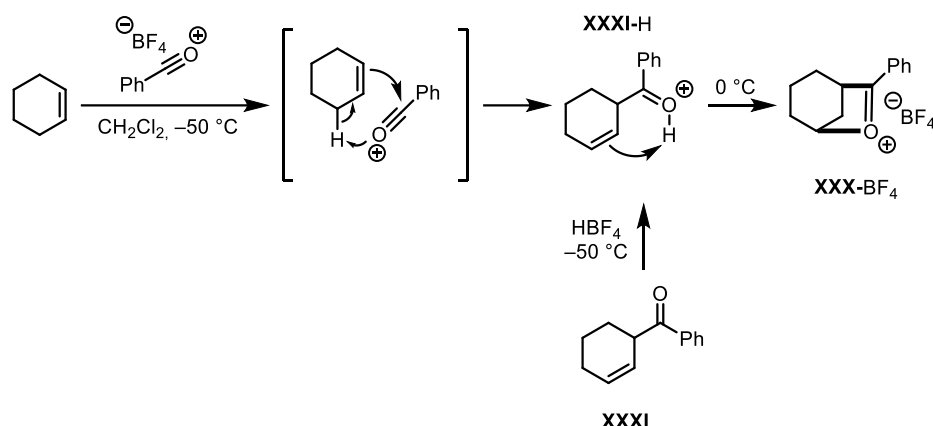
A key consideration for the formation of **XXX**-BF₄ is the nature of the counter anion employed; the use of an anion such as tetrafluoroborate, being virtually non-basic and non-nucleophilic, is imperative to suppress competing reactions, such as deprotonation (leading to elimination) and nucleophilic capture of the cationic intermediate.

Scheme 3.2 The reaction of cyclohexene with acylium tetrafluoroborates.



The proposed mechanism involves an ene-type reaction of the acylium ion with the allylic system of cyclohexene, initially forming the protonated β , γ -unsaturated ketone **XXXI** at cryogenic temperatures (as observed by NMR studies). Upon warming to 0 °C, the authors report the transformation of **XXXI**-H into **XXX**-BF₄, which is stable and isolable. This proposal is further underlined by the fact that **XXXI** can be protonated by tetrafluoroboric acid to form **XXXI**-H, which further rearranges to **XXX**-BF₄ upon warming (Scheme 3.3).

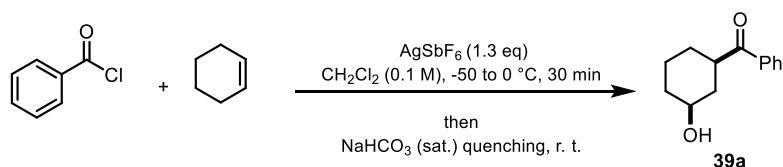
Scheme 3.3 Mechanism hypothesis for the formation of **XXX-BF₄**.



3.1.2. Aim of our study

Inspired by the aforementioned literature reports, we started to investigate the oxocarbenium ion, which is prone to rearrangement reactions. While the procedure described above (Scheme 3.3) showed generally good yields of the bridged oxocarbenium species, a major drawback is the necessity of using non-complexed (neat) boron trifluoride and acyl fluorides, which are considerably less ubiquitous than acyl chlorides, for the formation of the acylium ions which, in addition, have to be isolated prior to addition to the alkene. With the aim to develop a more versatile and useful suite of reaction, our initial attempt involved the in-situ formation of oxocarbenium- SbF_6 by treatment of benzoyl chloride with silver hexafluoroantimonate(V) (AgSbF_6) in DCM followed by the addition of cyclohexene (Scheme 3.4). Pleasingly, employing the same temperature profile as reported in the literature, the yield of compound **39a** was determined to be 75% by NMR.

Scheme 3.4 Initial tested conditions



3.1.3. Optimization of reaction conditions

In an attempt to optimize and, especially, simplify the reaction conditions, several parameters such as time, temperature, solvent and Lewis acid were evaluated, as outlined in Table 3.1. The reactions were carried out on a 0.2 mmol scale in a flame-dried Schlenk tube using cyclohexene as alkene, lauroyl chloride as aliphatic acyl chloride and/or benzoyl chloride as aromatic acyl chloride as aromatic acyl chloride.

Table 3.1 Optimization of the reaction conditions.

$\text{R} = \text{- benzene}$
 - undecane

40a, R = -benzene
40b, R = -undecane

39a, R = -benzene
39b, R = -undecane

Entry	Solvent	Lewis Acid	Acyl Chlorides	Time	Solvent	40a,b ^(b)	39a, b ^(a)
1	DCM	AgSbF ₆	Benzoyl chloride	10 min	35 °C	-	83%
2	DCM	AgOTf	Benzoyl chloride	30 min	0 °C	39%	-
3	DCM	AgSbF ₆	Lauroyl chloride	10 min	0 °C	46%	52%
4	DCM	AgSbF ₆	Lauroyl chloride	10 min	25 °C	30%	62%
5	DCM	AgSbF ₆	Lauroyl chloride	10 min	35 °C	20%	70%
6	DCE	AgSbF ₆	Lauroyl chloride	10 min	35 °C	57%	23%
7	Difluoro Benzene	AgSbF ₆	Lauroyl chloride	10 min	35 °C	58%	12%
8	Cyclohexane	AgSbF ₆	Lauroyl chloride	10 min	35 °C	32%	30%

9	THF	AgSbF ₆	Lauroyl chloride	10 min	35 °C	-	-
10	CHCl ₃	AgSbF ₆	Lauroyl chloride	10 min	35 °C	62%	22%
11	DCM	AgSbF ₆	Lauroyl chloride	30 min	35 °C	20%	63%
12	DCM	AgSbF ₆	Lauroyl chloride	60 min	35 °C	25%	55%

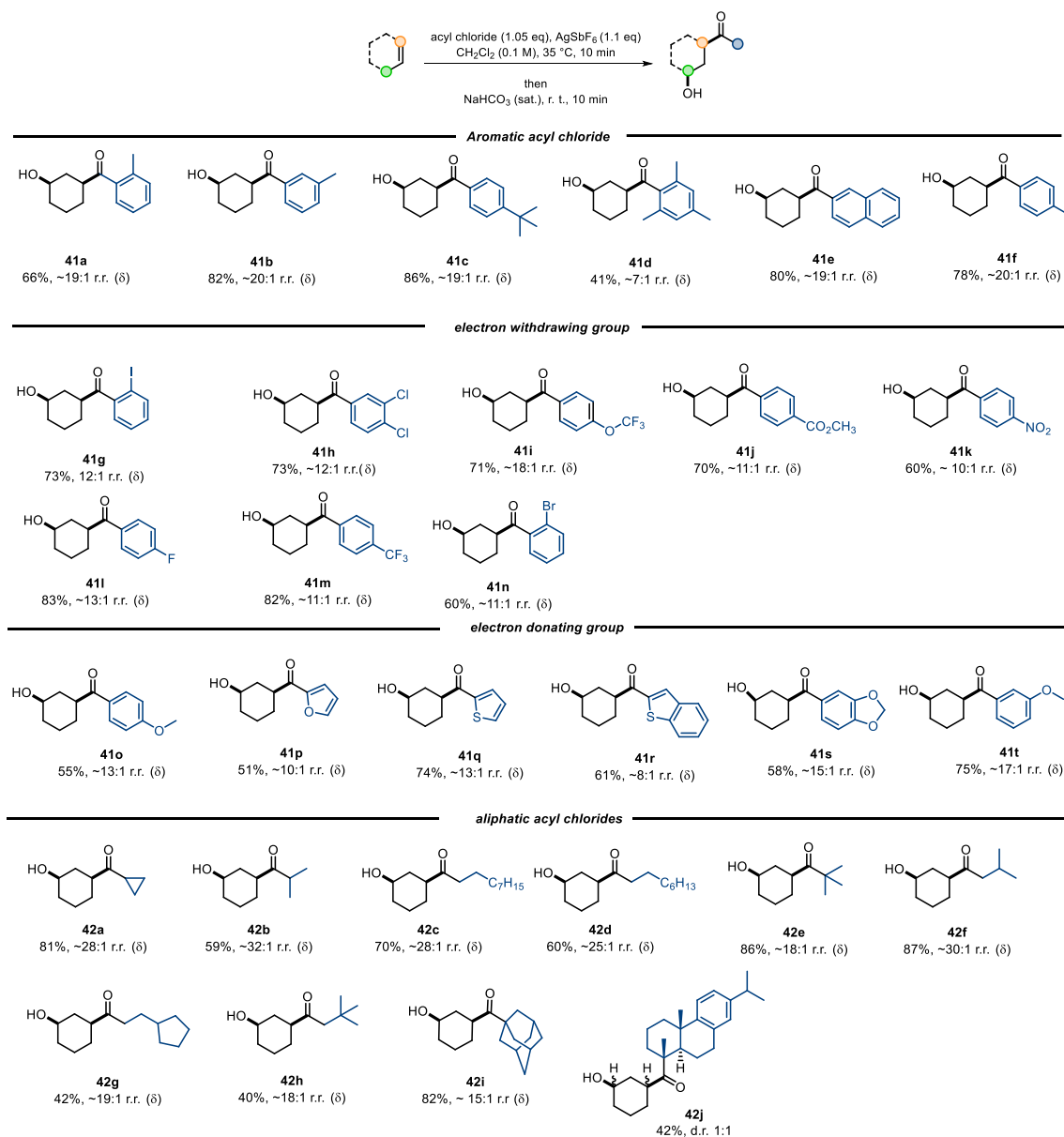
^(a)obtained by isolated product
^(b)obtained by NMR

3.1.4. Results and Discussion

Extensive optimization led to development of a “one-pot” manner reaction. The combination of acyl chloride, AgSbF₆, DCM as solvent, and the reaction temperature at 35 °C were found to be the optimal reaction conditions, affording product **39** in 83% isolated yield (Table 3.1, entry 1). When AgSbF₆ was replaced by silver triflate (AgOTf) or when aliphatic acyl chloride was used at lower temperature (Table 3.1, entry 2 – 3), α , β -unsaturated ketone **40** was detected. Moreover, any efforts to screen different solvents (Table 3.1, entry 6 – 10) resulted in the formation of the α , β -unsaturated ketone derivative. Notably, this result is hardly compatible with the reported ene-reaction mechanism (Scheme 3.3), as the presence of α , β -unsaturated ketone demands for the transient formation of a β -carbonyl cation. Finally, increasing the reaction time resulted in a slightly lower yield of desired compound **39** (Table 3.1, entry 11 – 12 compared to entry 5).

Then, with reliable reaction conditions in hand, we proceeded to investigate the scope of this reaction, initially focusing on the decorated acyl chlorides (Scheme 3.5).

Scheme 3.5 Alkene 1,3-Functionalization of substituted acyl chlorides: scope of reaction.

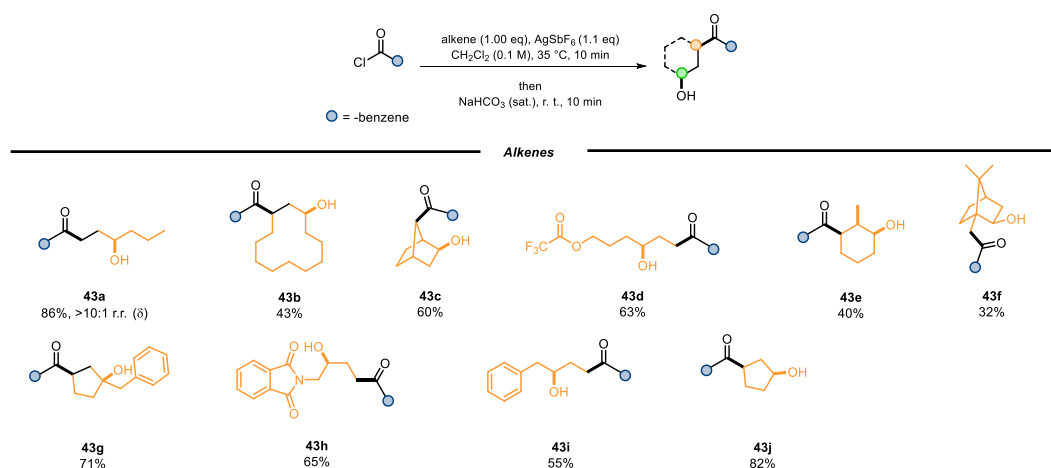


Excellent yields were obtained using aromatic acyl chlorides bearing electron-neutral or electron-withdrawing substituents. Additionally, acyl chlorides bearing electron-rich substituents, such as thiophene, benzothiophene, benzodioxole and furan were all suitable, resulting in their corresponding products with high yields. Reactions of aliphatic acyl chlorides were examined, and desired products were obtained in 40 – 87% yields. As shown in Scheme 3.5, all products were achieved as single diastereoisomers and with an extraordinary

regioisomeric ratio, as determined by ^1H NMR analysis (for details, see reported mechanism in Scheme 3.8).

Following the study of different acyl chlorides, our focus shifted to the investigation of the alkene compatibility (Scheme 3.6).

Scheme 3.6 Alkene 1,3-Functionalization of alkene: scope of reaction.



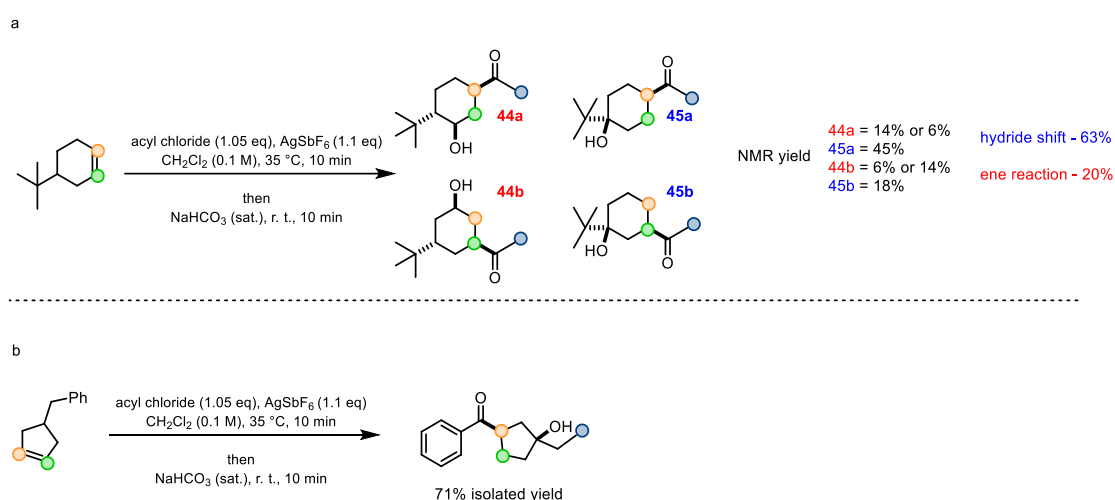
Linear alkene and/or cyclic alkene with different ring sizes showed good yields (40 – 86%) as well as the introduction of the alcohol functional group. On the basis of these auspicious results, we turned our attention to some more complex systems such as norborene, camphene, phthalimide that afforded the corresponding hydroxylation in good yield. It is noteworthy that camphene hydroxylation proceeds via non-classical carbocation pathway.

This process proved to possess an excellent functional group (FG) compatibility. However, some limits have been found in our study. Typically, halogen in proximity of the carbonyl group failed to react, and no conversion was observed. Unfortunately, nitrogen containing functional group such as nitrile, amine, amide and sulfonamide were not tolerated as substrates.

Subsequently, we conducted further studies with the aim to shed light on the mechanism of this functionalization. As depicted in Scheme 3.7 and supported by data in optimization step,

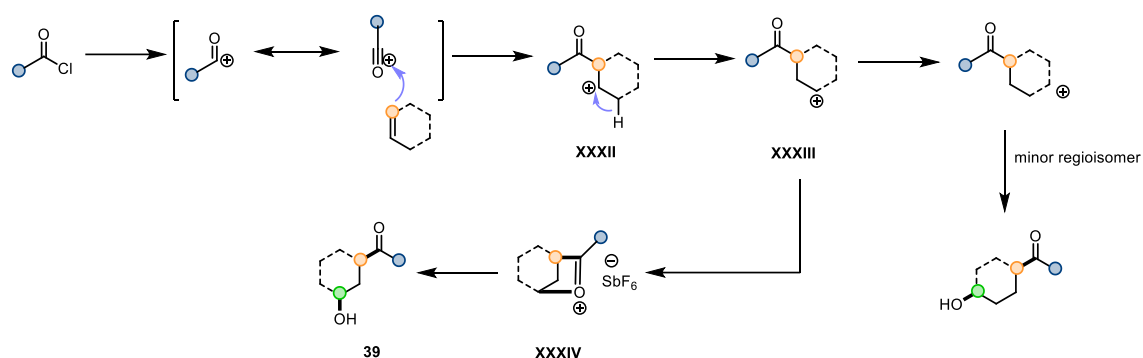
we give supporting evidence that our reaction is hardly compatibility with the mechanism involving an ene-reaction. In particular, when 4-*tert*-butylcyclohexene was subjected to the reaction conditions, four products were detected (Scheme 3.7a). The red compounds (**44a,b**) could be compatible with an ene-reaction but the blues (**45a,b**), are only accessible through additional hydride shifts. Furthermore, the reaction with 4-substituted cyclopentene showed a total selectivity toward hydroxylation in δ -position (Scheme 3.7b).

Scheme 3.7 Hydride shift evidence.



This result hints at the involvement of an additional hydride shifts pathway. In details, our proposed mechanism invokes a carbocation intermediate **XXXII**, following the formation of the acylium ion and consequent reaction with the alkene, which cyclizes by means of a [1,2]-hydride shift (intermediate **XXXIII**) forming the key oxocarbenium intermediate **XXXIV** that forms the desired alcohol **39** under slight basic conditions (Scheme 3.8).

Scheme 3.8 Our proposed mechanism.



In conclusion, we have developed a new method to functionalize alkene via hydride shift mediate by oxocarbenium formation. This methodology is general, diastereoselective, broad in substrate scope, and affords the desired products in good to excellent yields. The identification of late-stage reactions such as further manipulations of oxocarbenium are in course.

3.2. Design of ketone-based compounds

3.2.1. Aim of work

Considering the broad scope of 1,3-alkene functionalization, this approach could be used to achieve new versatile scaffolds in medicinal chemistry. Therefore, we decided to apply this methodology to our PRMT4 inhibitors (compounds **2**, **6** – **8**, discussed in Chapter II), in which the 4-hydroxy-2-naphthoic group was replaced by a sp³-rich fragment with a view to strengthen the intermolecular interactions with the protein target and to increase the *druglikeness* of compounds. In particular, we chose as sp³-rich fragment the 3-hydroxy-(cyclohexyl)phenyl-methanone, yielding from cyclohexene and 4-nitro benzoyl chloride. Taking into account our previous studies (Chapter II), we selected our most potent PRMT4 inhibitors **6** – **8** and their shorter counterpart **2** to design a small pool of ketone-based compounds (**46** – **49**, Figure 3.1).

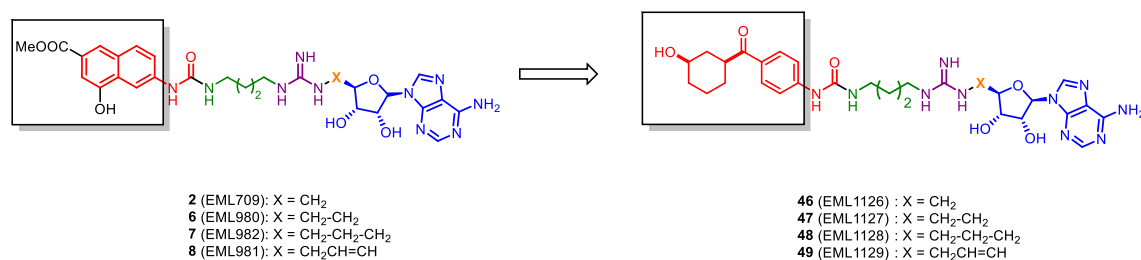


Figure 3.1 Design of ketone-based compounds.

3.2.2. Results

To explore the effects of this replacement we resolved to study the direct binding of compounds **46** – **49** on PRMT4 using an in-house optimized SPR protocol (Chapter VIII, Paragraph 8.3.3). As reported in Figure 3.2 and in Table 3.2, compounds **47** – **49**, bearing a linker length between the guanidine group and the adenosine moiety of 2 or 3 carbon atoms, showed a very strong binding interaction with PRMT4 and confirmed a K_D values in the nanomolar range. As shown by sensorgrams depicted in Figure 3.2 and residence time (τ_R) values reported in Table 3.2, compounds **47** – **49** dissociate from the protein very slowly. On the other hand, compound **46** display a K_D value in micromolar range and a residence time (τ_R) much lower than other compounds. These results are consistent with the ones obtained with their 4-hydroxy-2-naphthoic counterparts. Moreover, it is noteworthy that the K_D values of compounds **47** – **49** are 10-fold higher over its related naphthalene derivatives. This aspect is also supported by their residence time (τ_R) values (105.1, 150.3 and 171.0 s for **47** – **49** compared to 14.7, 76.9 and 62.5 s for **6** – **8**).

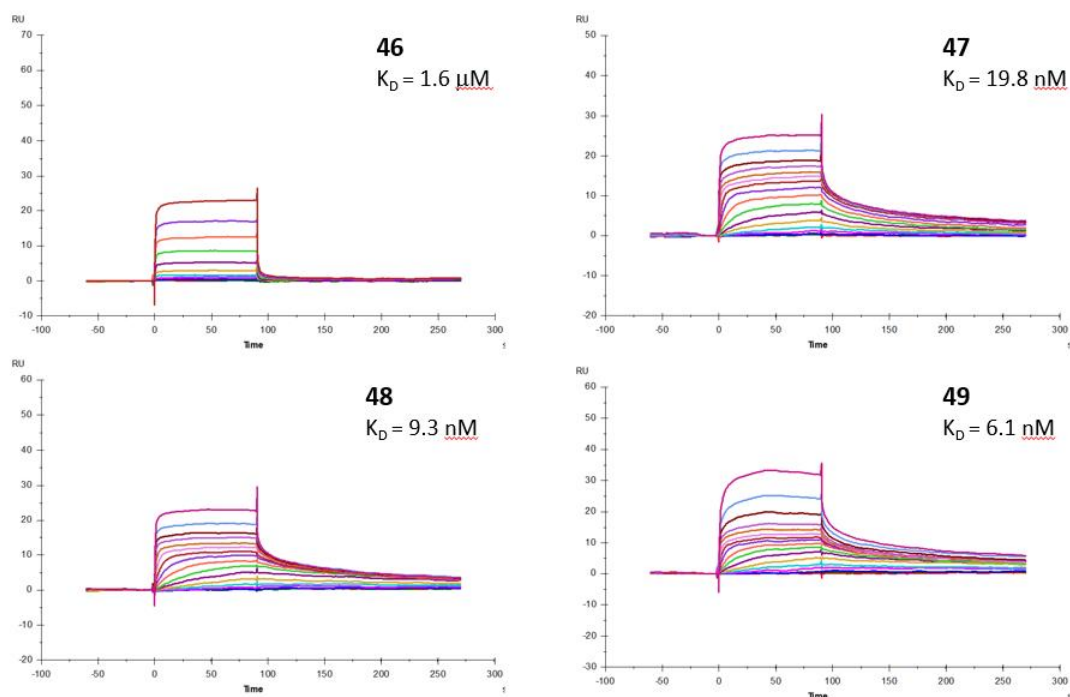


Figure 3.2 Sensorgrams obtained from the SPR interaction analysis of compounds **46 - 49** binding to immobilized PRMT4. Each compound was injected at different concentrations (from 20 μM to 0.02 μM for **46** and from 20 μM to 0.3 nM for **47 – 49**) with an association and a dissociation time of 90 sec, with a flow rate of 30 $\mu\text{L}/\text{min}$. The equilibrium dissociation constants (K_D) were derived from the ratio between kinetic dissociation (k_{off}) and association (k_{on}) constants.

Table 3.2: Affinity and kinetic parameters derived from SPR experiments.

Compound	K_D	k_{on} (1/Ms)	k_{off} (1/s)	t_R (s)
46 (EML1126)	1605 nM	4.45×10^4	0.714	1.4
47 (EML1127)	19.9 nM	4.78×10^5	0.009	105.1
48 (EML1128)	9.2 nM	7.20×10^5	0.007	150.3
49 (EML1129)	6.1 nM	9.64×10^5	0.006	171.0
SAM	9.6 nM	2.90×10^5	0.003	333.3

Prompted by these results, we are planning to separate the two diastereoisomers for the best candidates (**47** – **49**) to assess the role of stereoselectivity in affinity. With this aim, future efforts will be focused on optimization of chromatographic method to efficiently separate the two diastereoisomers or on their enantioselective synthesis starting from chirally pure 3-hydroxy-(cyclohexyl)phenyl-methanone enantiomers.

3.2.3. *Conclusions*

During my period abroad at the Institute of Organic Chemistry (University of Vienna) under the supervision of Prof. Nuno Maulide, I have been implicated in the development of a new synthetic methodology defined as 1,3-alkene functionalization. The latter was applied to develop analogues of compounds **2** and **6** – **8** (Chapter II) bearing sp³-rich fragments with a view to strengthen the intermolecular interactions with protein target (PRMT4). Ketone-based compounds **46** – **49** were prepared and their binding to PRMT4 was evaluated by SPR assay. The preliminary results suggested that the 4-hydroxy-2-naphthoic group could be efficiently replaced by a 3-hydroxy-(cyclohexyl)phenyl-methanone scaffold. In fact, compounds **47** – **49** showed a higher affinity on PRMT4 compared their naphthalene analogues and, at the same time, the similar SARs were obtained as the compounds with a longer linker showed to be the most potent.

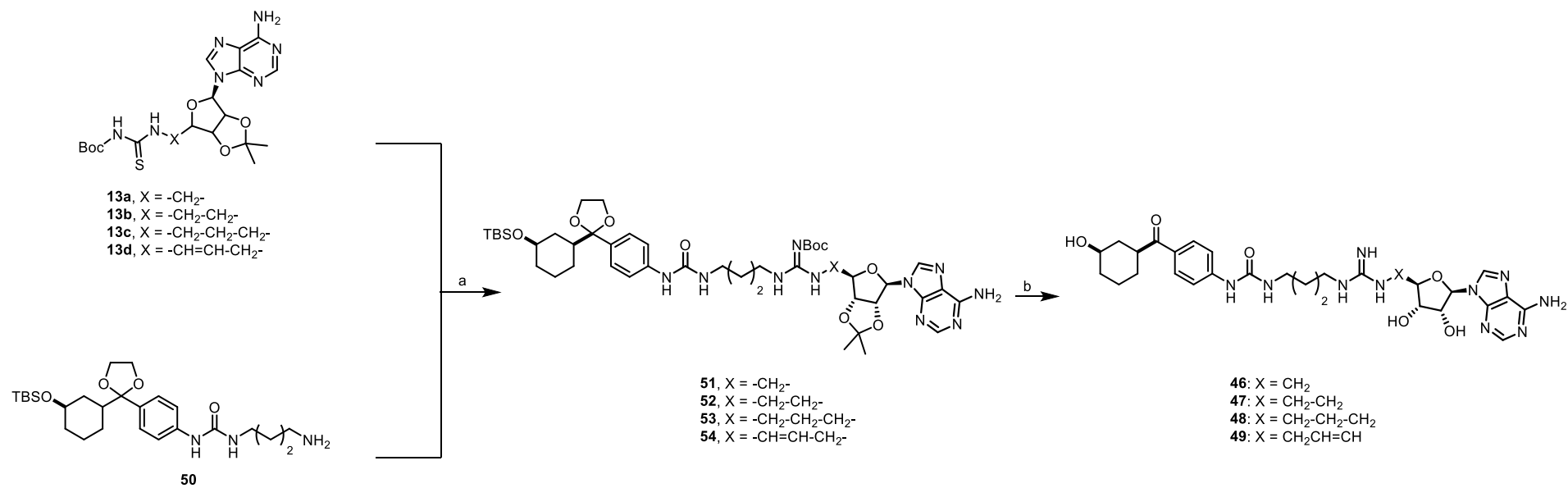
3.2.4. *Chemistry*

3.2.4.1. *Synthesis of compounds 46 – 49*

This section describes the synthetic procedures adopted for the preparation of compounds **46** – **49**. The synthetic general route was depicted in Scheme 3.9. In analogy to previously described compounds, the synthesis of ketone-based compounds is based on the condensation between decorated adenosine moieties (**13a** – **d**) and ureidic intermediate (**50**), followed by a one-pot deprotection of all protecting groups. Following the same procedure mentioned for

compounds **27a – f**, **28 – 30** (Chapter II, Paragraph 2.5.4, Scheme 2.4), the intermediates **51 – 54** were obtained in excellent yield. The one-pot deprotection reaction required 24 hours and a higher amount of TFA (50 %) and H₂O (10%) compared to the previous reported conditions.

Scheme 3.9 General synthetic scheme for the preparation of compounds **46** – **49**.

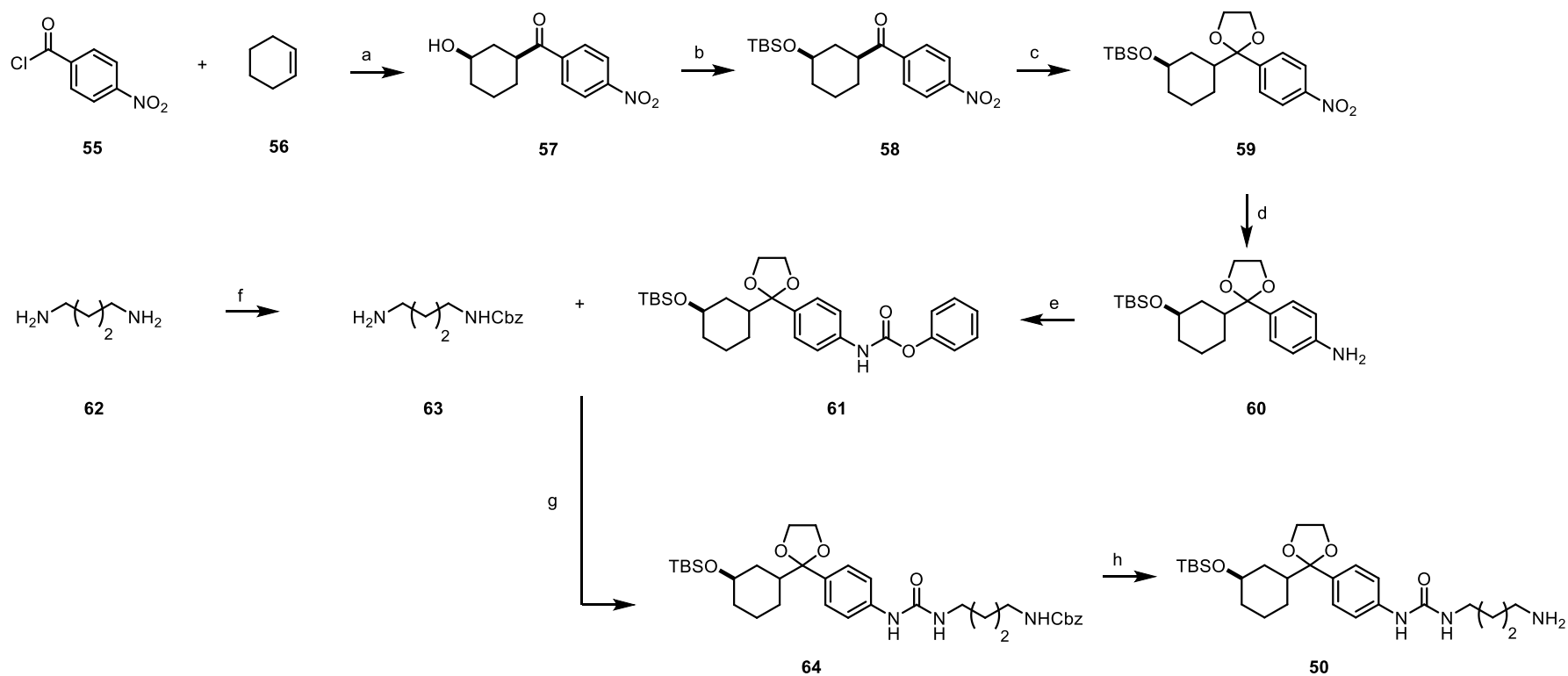


Reagents and conditions: a) EDC hydrochloride, TEA, dry DCM, r. t., 48 h (65 – 80%), b) DCM/TFA/H₂O (40:50:10), r. t., 24 h (70 – 80%).

3.2.4.2. *Synthesis of compound 50*

Compound **50** was prepared as outlined in Scheme 3.10. The first synthetic step involved in an alkene 1,3-functionalization using 4-nitrobenzoyl chloride (**55**) and cyclohexene (**56**) in presence of AgSbF_6 that acts as a Lewis acid to form the alcohol intermediate **57**. The latter was protected on the alcohol (**58**) and ketone (**59**) group to avoid the formation of by-products in the following steps, using *tert*-Butyldimethylsilyl chloride (TBDMSCl) and ethylene glycol, respectively. The nitro group on the protected intermediate **59** was selectively reduced by palladium-catalysed hydrogenation to amine **60** which was activated with phenyl chloroformate (**61**) and reacted with the intermediate **63**, obtained by reaction of the aliphatic amine commercially available (**62**) with benzyl chloroformate. Finally, the amino-protecting group of the ureidic compound **64** was removed by palladium-catalysed hydrogenation, affording compound **50** in excellent yield.

Scheme 3.10 General synthetic scheme for the preparation of intermediate **50**.



Reagents and conditions: a) AgSbF_6 , 35 °C, 10 min, then NaHCO_3 for 10 min (63%); b) TBDMSCl, imidazole, dry DCM, r. t., 1 h (97%); c) ethylene glycol, boron trifluoride diethyl etherate, dry DCM, 0 °C to r. t., 12 h (99%); d) H_2 , Pd/C 10 %, AcOEt, r. t., 36 h (63%); e) phenylchloroformate, TEA, AcOEt, r. t., 12 h (80%); f) benzyl chloroformate, dry DCM, r. t., 16 h (85%); g) TEA, dry DMF, r. t., 12 h (80%); h) $\text{NH}_4\text{CO}_2\text{H}$, Pd/C 10%, MeOH, reflux, 2 h (99%).

CHAPTER IV

Pro-drug Strategy

4.1. Background

In 2016, the EMCL developed a set of pyrrole-based inhibitors toward CARM1 and **EML660 – 699 – 701** emerged as the most active compounds.¹⁶⁵ The pyrrolic structural motif, commonly found in pharmaceutical drugs and natural products, was explored as a bioisosteric substitution of pyrazole, an interesting scaffold used in the development of CARM1 inhibitors. Indeed, the first example of pyrazole-based inhibitor against CARM1 was reported by Purandare et al. in 2008 via high-throughput screening and compound **65** (Figure 4.1) emerged as the best candidate, showing an interesting *in vitro* activity (IC_{50} value of 1.8 μM). Nevertheless, **65** and its analogues resulted completely inactive in cell due to their low cytopermeability.¹³⁴ In 2009, several optimization efforts were performed in collaboration with Nerviano Medical Sciences.^{166,133} Extensive SAR studies of pyrazole-based compounds have attributed to (S)-alanine, inserted as a substituent of the phenyl ring at the N1 position of pyrazole, an important role in the high *in vitro* potency for CARM1. In fact, this warhead interacts with arginine substrate binding pocket and any modification are not tolerated. Then, several substitutions occurred on C-5 position of pyrazole ring, wherein benzyl amines were found to be superior to others substitution such as aniline and aliphatic amines. These studies led to the identification of compound **66** (Figure 4.1), which displayed a 22-fold increase *in vitro* inhibitory potency (IC_{50} value of 0.08 μM) over hit compound **65**. However, no satisfactory outcomes were reported to improve their cytopermeability.

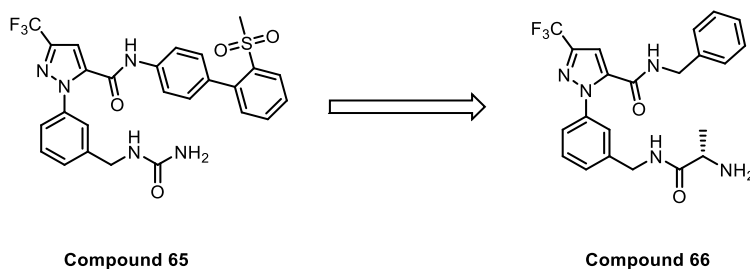


Figure 4.1 Identification of pyrazole-based CARM1 inhibitors: hit to lead stage.

With the aim to overcome this issue and to develop a more versatile chemical scaffold for CARM1 inhibitors, EMCL hypothesized that the replacement of the nitrogen at position 2 of the pyrazole ring with a methylene could increase the lipophilicity and therefore the cytopermeability of the molecules. The first pyrrole-based compound (**EML568**) was designed and synthesized retaining the same key substitution pattern of pyrazole **66**, used as lead compound. Compound **EML568** (Figure 4.2) showed an IC_{50} value of 7.3 μM , which is lower than the parent pyrazole derivative but supported the further evaluation of pyrrole as putative bioisosteric cycle of pyrazole for this class of PRMT inhibitors.

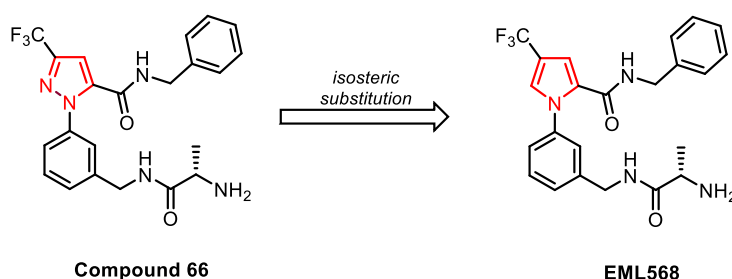


Figure 4.2 Design of first pyrrole-based compound as CARM1 inhibitor.

With the aim to increase the potency of this derivatives, substitution at C-4 position of pyrrole was explored and ethyl ester was identified as a good replacement for the trifluoromethyl group. Moreover, the (S)-alanine moiety was directly attached on the N-phenyl pyrrole substituent, leading to the identification of **EML660** as the best pyrrole-based candidate, showing an increased *in vitro* inhibitory potency (IC_{50} value of 3.68 μM) over parent compound **EML568** (Figure 4.3). Subsequently, computational studies (Prof. Giuseppe Bifulco, DIFARMA, University of Salerno) were performed to further improve potency and, at the same time, to increase lipophilicity to promote cell permeability. These efforts enabled the identification of **EML699** and **EML701** compounds (Figure 4.3), which showed an increase in inhibitory activity against CARM1 compared to **EML660** but all synthesized compounds did

not evidence a significant cellular activity, mainly also due to their low cellular permeability, in analogy to pyrazole-based compounds.

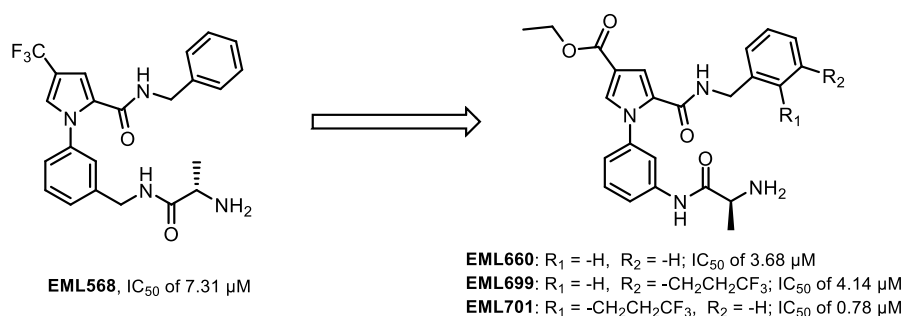


Figure 4.3 Development of most promising pyrrole-based compounds as CARM1 inhibitors.

4.2. Aim of work

As no further manipulations of the molecules could be done without negatively affect the activity, in this Ph. D project, we have considered to design the pro-drug of our pyrrole-based compounds **67** – **72**, depicted in Figure 4.4.

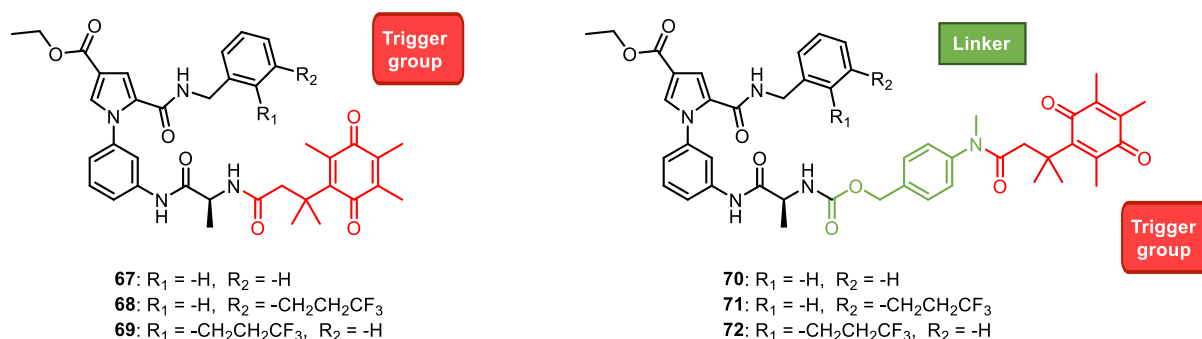


Figure 4.4 Development of pro-drug compounds.

In our pro-drug design, we resolved to mask the primary amino group of alanine to increase the lipophilicity of compounds and promote their cell permeability. As carrier moieties, we selected the colored portions depicted in Figure 4.4. In particular, pro-drug system is characterized by a trigger group named “trimethyl lock” bearing quinone propionic acid (Q₃PA). In response to oxide-reduction cellular mechanism, mediated by NAD(P)H-dependent

enzymes, Q₃PA undergo intramolecular cyclization to form lactone leading to the rapid release of chemical moiety. The attack of the chemical moiety on the trigger group can be direct or mediated by a linker (Figure 4.5). In this case, intramolecular cyclization is followed by self-immolative 1,6-elimination reaction.¹⁶⁷

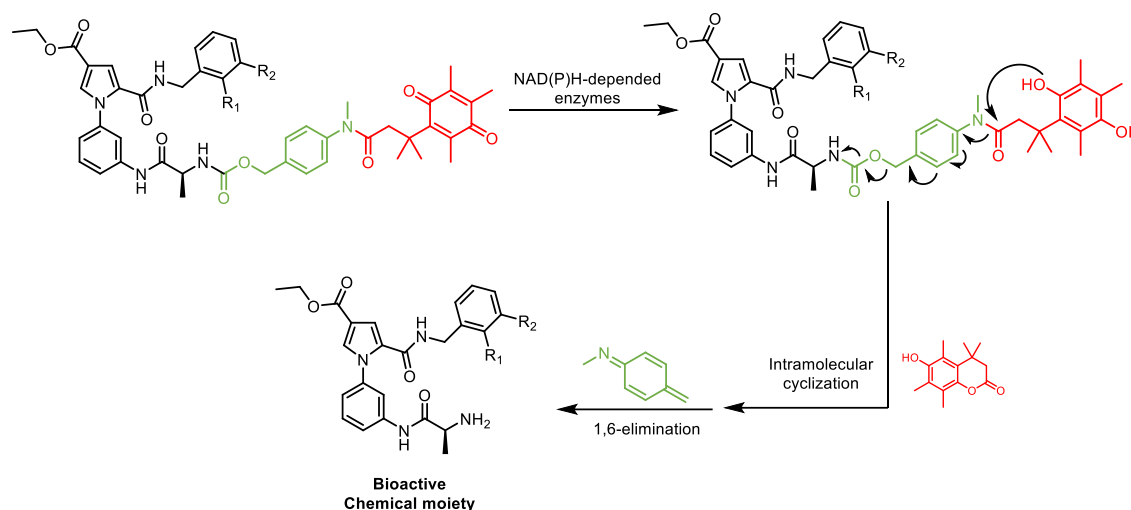


Figure 4.5 Metabolic pathway to generate bioactive molecule from the pro-drug.

4.3. Results

The inhibitory activity of designed and synthesized pro-drug **67 – 72** was directly evaluated in cellular context, in collaboration with Prof. Mark T. Bedford (Chapter VIII, Paragraph 8.3.6). In particular, the effect of pro-drug on cellular methylation of Nuclear Factor 1 B-type (NFIB-Me), one of the reported PRMT4 substrates, was investigated. Pro-drug **67 – 72** were profiled in two different cell lines HEK293T and Hela, respectively. The cells were incubated for 24, 48 and 72 h with compounds **67 – 72** (at 10, 20 and 50 μ M) or with compound TP-064 (10 μ M), used as positive control. Unfortunately, no significant inhibitory activity for all tested compounds was observed.

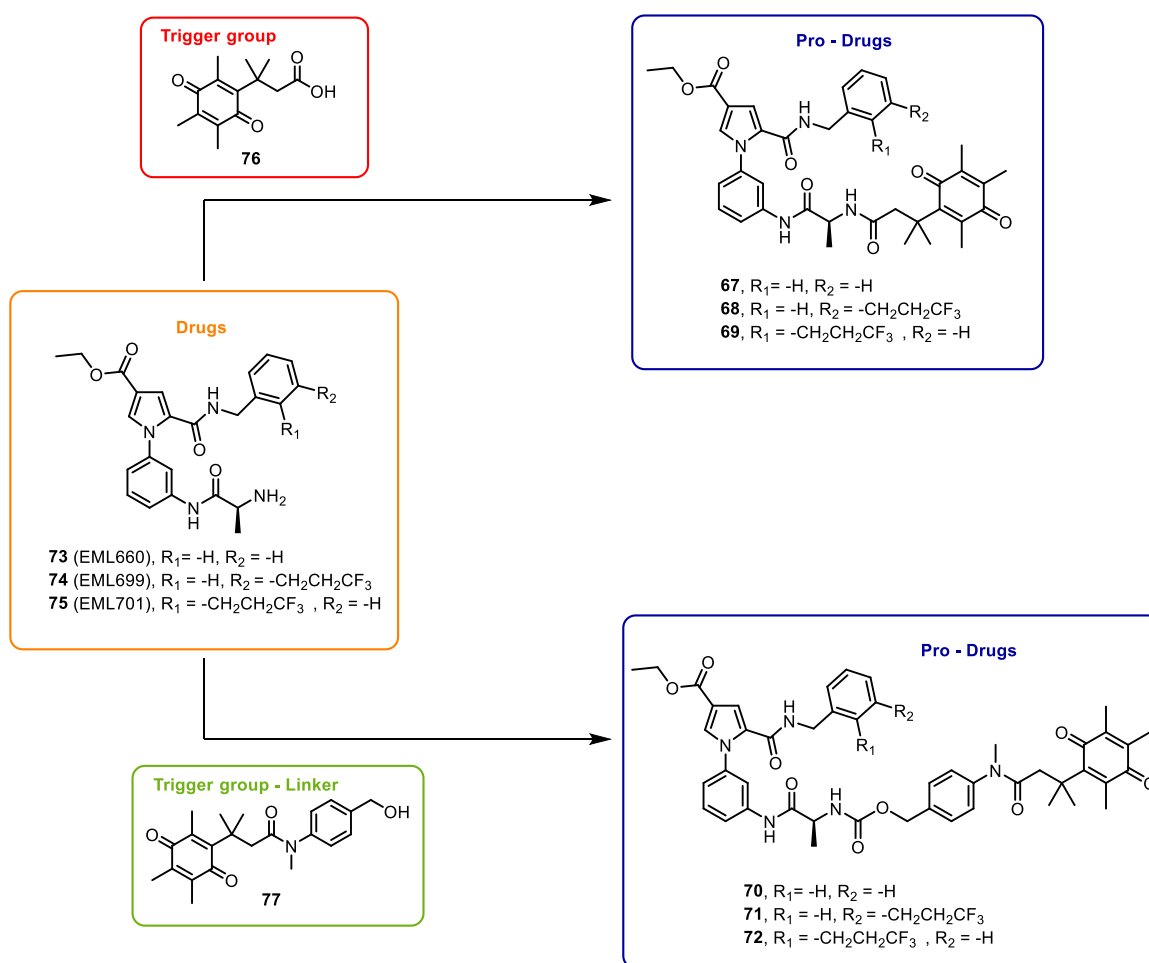
4.4. Conclusions

In this approach, we investigated the pro-drug strategy applied to promising pyrrole-based compounds previously identified as PRMT inhibitors. Indeed, despite their interesting *in vitro* activity, these compounds resulted completely inactive in cells, mainly due to their low cellular permeability. The pro-drug strategy has been used to mask the primary amino group of alanine to promote their cell permeability. A small pool of pro-drug compounds was synthesized, and their cellular activity was evaluated. Unfortunately, none of the prepared compounds showed an interesting activity in cellular context. This unsuccessful result prompted us to not further investigate on this pyrrolic scaffold. This choice was also strengthened by the decision of Nerviano Medical Science to give up with pyrazole-based compounds as CARM1 inhibitors. As a matter of fact, no new compounds bearing to this class have been released in the last 10 years.

4.5. Chemistry

This section describes the synthetic procedures adopted for the preparation of pyrrole-based pro-drug **67** – **72**. The synthetic general route is depicted in Scheme 4.1. It is based on the synthesis of chemical moieties **73** – **75**, which were condensed with a trigger group **76** or its correspondent **77** bearing a self-immolative linker leading to the formation of target compounds.

Scheme 4.1 General synthetic route.

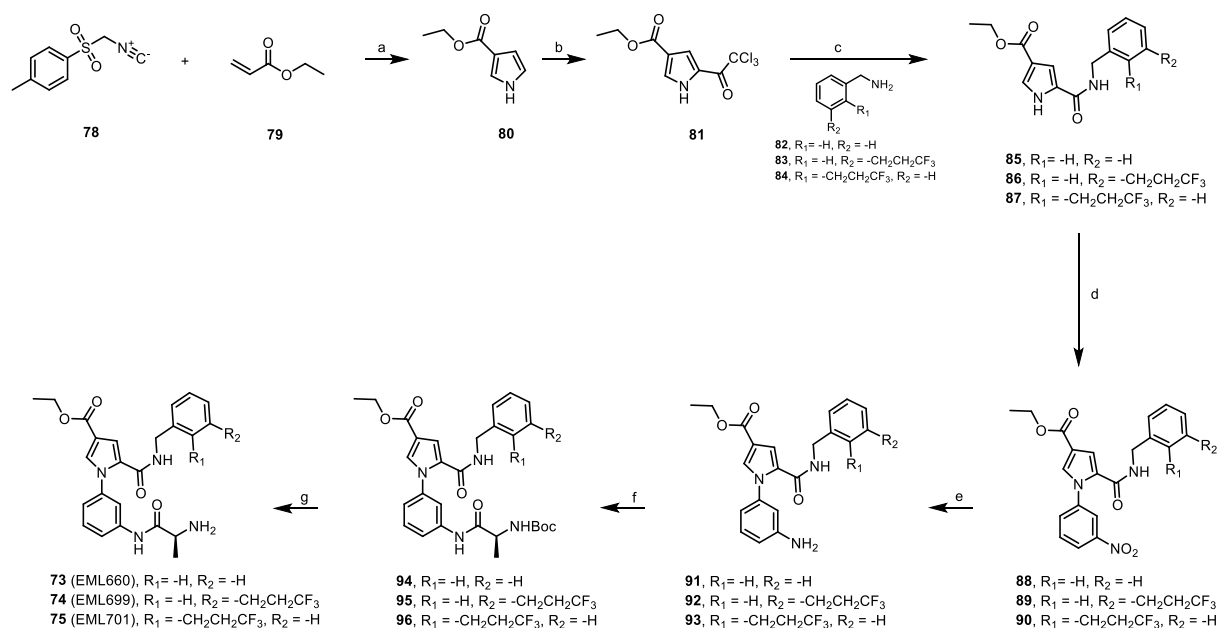


4.5.1. Synthesis of compounds **73** – **75**

Compounds **73** – **75** were prepared as outlined in Scheme 4.2. The first step involved a Van-Leusen type reaction for smoothly obtaining the pyrrole scaffold **80**, using tosylmethyl-

isocyanide (**78**, TOSMIC) and ethyl acrylate (**79**). Friedel-Crafts acylation with trichloroacetyl chloride (**81**), followed by nucleophilic substitution with benzylamines **82** – **84** provided the easily functionalization at the C-2 position of intermediate **81**, obtaining compounds **85** – **87**. N-Aryl compounds **88** – **90** were prepared under Ullman-type conditions under microwave irradiation. Subsequently, reduction of nitro group using zinc dust in AcOH (**91** – **93**), followed by coupling reaction with N-(*tert*-Butoxycarbonyl)-L-alanine (L-Boc-Ala-OH) provided Boc-protected compounds **94** – **96**. Deprotection with TFA in DCM yielded target compounds **73** – **75**.

Scheme 4.2 General synthetic scheme for the preparation of compounds **73** – **75**.

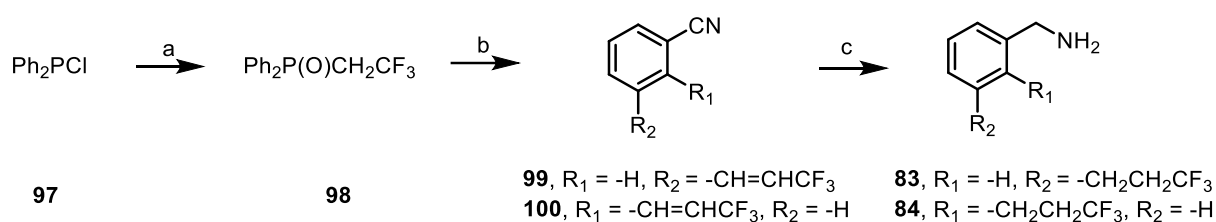


Reagents and conditions: a) NaH (60% mineral oil), dry DMF, dry THF, 5 h (88%); b) trichloroacetyl chloride, dry DCM, 80 °C, 18 h (50%); c) TEA, DCE, 80 °C, 5 h (80 – 85%); d) 1-bromo-3-nitrobenzene, copper(I) iodide (CuI), N,N'-dimethylethylenediamine, potassium phosphate (K₃PO₄), dry dioxane, 130 °C (MW), 0.5 h (79 – 83%); e) zinc dust, AcOH, r. t. 1 h (99%); f) Boc-L-Ala-OH, EDC hydrochloride, hydroxybenzotriazole (HOBt), N-methylmorpholine, dry DMF, r. t., 18 h (78 – 86%); (g) DCM/TFA (9:1), r. t., 0.5 h (99%).

4.5.1.1. Synthesis of benzylamines **83**, **84**

The benzylamines **83**, **84** were prepared using the procedure depicted in Scheme 4.3. Briefly, the phosphonate **98**, obtained by diphenylchlorophosphine **97** and TFA, underwent Wittig-Horner reaction with proper aldehydes to yield cyano derivatives **99** and **100**. Reductions of cyano group and carbon-carbon double bond afforded the desired amino intermediates **83** and **84**.

Scheme 4.3 General synthetic scheme for the preparation of benzylamines **83**, **84**.

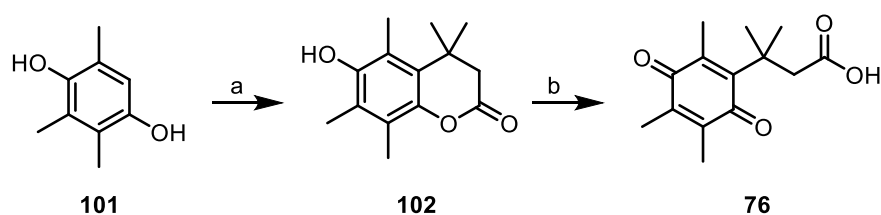


Reagents and conditions: a) TFA, H_2O , 0 to 100 °C, 3 h (55%); b) 3-formylbenzonitrile and 2-formylbenzonitrile, Tetra-*n*-butylammonium fluoride (TBAF 1M in THF solution), dry THF, r. t., 2 h (35 – 70%); c) Sulfuric acid (H_2SO_4), H_2 Pd/C 10%, EtOH, r. t., 24 h (97 – 99%).

4.5.2. Synthesis of compound **76**

The trigger group **76** was prepared as outlined in Scheme 4.4, according to reported procedure.¹⁶⁷ The reaction between 2,3,5- trimethylbenzene-1,4-diol (**101**) and 3-methylbut-2-enoic acid in the presence of methanesulfonic acid provided **102**, which was further treated with N-Bromosuccinimide (NBS) to afford **76**.

Scheme 4.4 General synthetic scheme for the preparation of compound **76**.

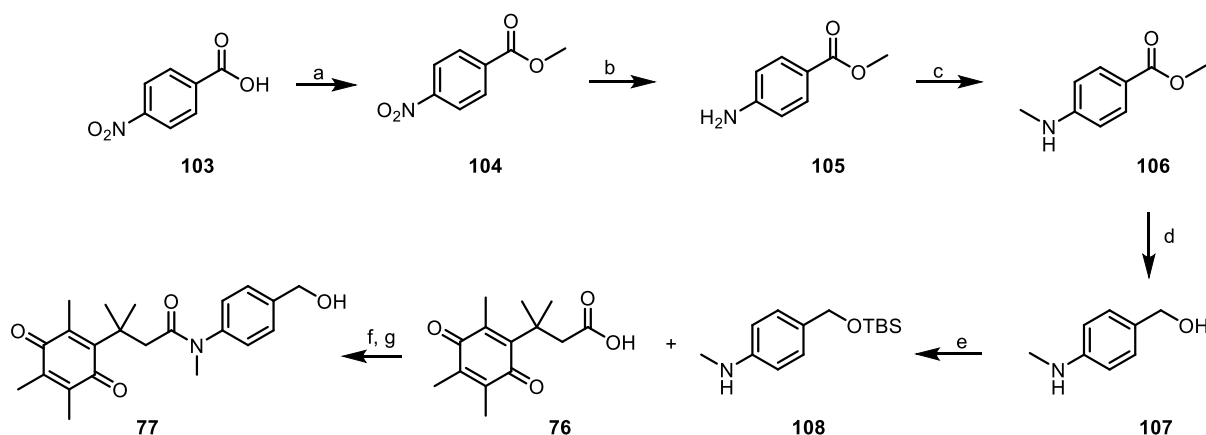


Reagents and conditions: a) 3-methylbut-2-enoic acid, methanesulfonic acid, 85 °C, 3 h (80%); (b) NBS, ACN, 1 h (99%).

4.5.3. Synthesis of compound 77

The synthesis of compound **77** is depicted in Scheme 4.5. The esterification of benzoic acid **103** led to formation of compound **104**, which was converted into the amino derivate **105** via palladium-catalysed hydrogenation. Then, the aniline was monomethylated using iodomethane and potassium carbonate (K₂CO₃) in dry ACN (**106**). The reduction of ester with lithium aluminium hydride (LiAlH₄) afforded alcohol **107**, which was protected (**108**) using TBDMSCl. Condensation of **108** and trigger group **76**, followed by deprotection using TBAF, provided compound **77**.

Scheme 4.5 General synthetic scheme for the preparation of compound **77**.

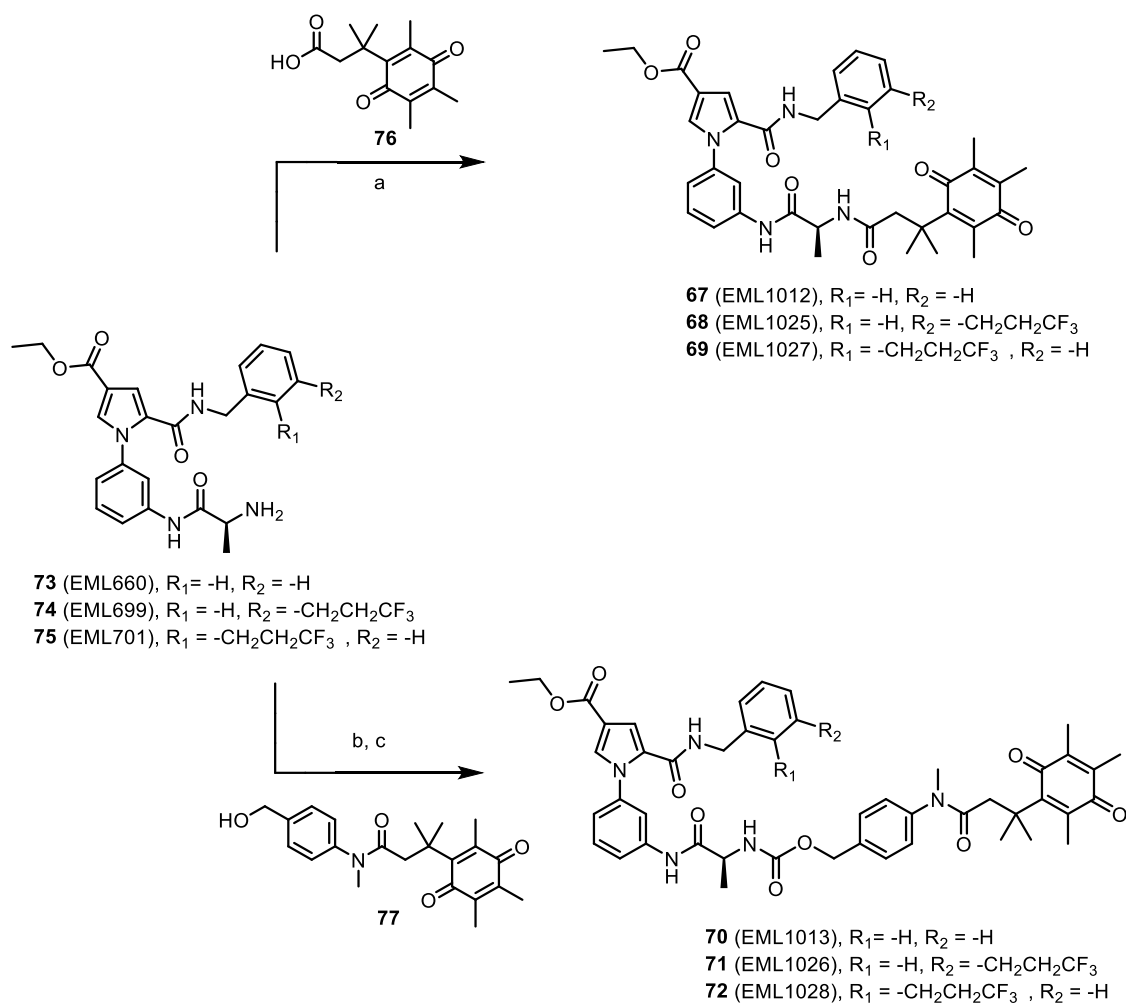


Reagents and conditions: a) H₂SO₄, MeOH, reflux, 18 h (99%); b) NH₄HCO₂, Pd/C 10%, MeOH, reflux, 1 h (99%); c) iodomethane, K₂CO₃, dry ACN, 80 °C, 3 h (49%); d) LiAlH₄, dry THF, 0 °C to 25 °C, 18 h (97%); e) TBDMSCl, imidazole, DCM, r. t., 1 h (90%); f) N-methylmorpholine, isobutyl chloroformate, dry DCM, -78 °C, 5 h; g) TBAF 1M in THF, r. t., 1 h (90%).

4.5.4. Synthesis of compounds 67 – 72

The target compounds **67 – 72** were prepared as outlined in Scheme 4.6. Compounds **67 – 69** were prepared by condensation of **73 – 75** with carboxylic acid **76** using a mixture of EDC hydrochloride and HOBt as coupling agents. Compounds **73 – 75** were linked to **77** using triphosgene and carbamate bond formation furnished target compounds **70 – 72**

Scheme 4.6 General synthetic scheme for the preparation of compounds **67** – **72**.



Reagents and conditions: a) EDC hydrochloride, HOBT, N-methylmorpholine, dry DMF, r. t., 18 h (80 – 88%); b) triphosgene, 4-dimethylaminopyridine (DMAP), dry DCM, 0 °C to 25 °C, 6 h; c) TEA, dry DMF, 0 °C to 25 °C, 18 h (68 – 74% on two steps).

CHAPTER V

Proteolysis-targeting chimera: PROTACTM

5.1. PROTAC approach

Over the past few years, an emerging strategy to inhibit proteins activity is their selective induced-degradation using Proteolysis Targeting Chimeras (PROTACsTM) compounds. PROTACsTM are heterobifunctional molecules that hijack the target protein to ubiquitin-proteasome machinery (UPS) for their selective degradation. Structurally, a PROTACTM compound includes a ligand for the protein of interest (POI) and a ligand for the E3 ubiquitin ligase connected by a linker. In this way, these heterobifunctional molecules are able to bridge the target protein and an E3 ubiquitin ligase. The latter binds to an E2 enzyme, promoting the polyubiquitination of the protein. The polyubiquitinated target is recognized as a substrate by the proteasome and is consequently degraded. As the PROTACTM remains unmodified, it can initiate a new degradation event, working in a catalytic manner (Figure 5.1).^{168,169}

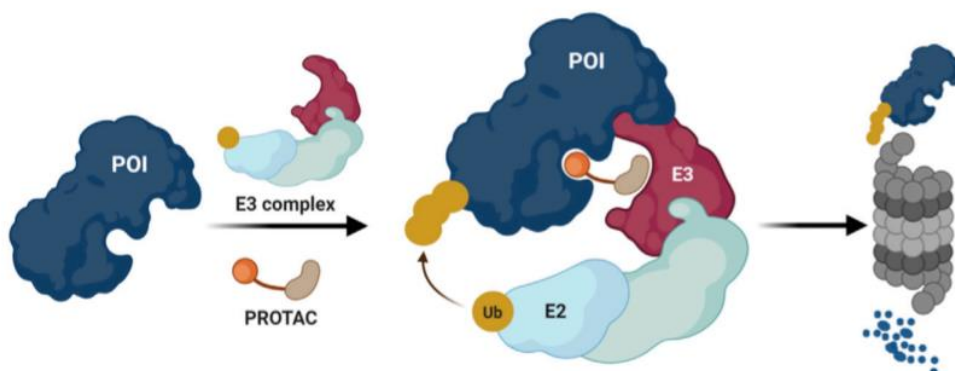


Figure 5.1 Schematic mechanism of PROTACsTM.¹⁷⁰

This approach can offer several advantages to inactivate a target protein compared to traditional approaches such as small-molecules inhibition. As mentioned, the PROTACsTM mechanism of action is catalytic and therefore, their concentrations result much lower than classical small-molecules, avoiding off-target effects due to high doses. In addition, PROTACsTM can recruit protein target via any binding site, changing the target from "undruggable" to "druggable". In addition, it is necessary to have selective modulators to achieve important therapeutic benefits. Considering the high structural similarity and sequence identity among protein isoforms, this is often a difficult aim to fulfil. PROTACTM approach has been revealed to be helpful in achieving isoform selectivity,¹⁷¹ taking advantage from the stability of each ternary complex (Protein-PROTACTM-E3 ligase) that can positively or negatively affect degradation outcomes. On the other hand, PROTACsTM have several limits due to their structure, physicochemical properties, and their mode of action. Considering the high molecular size and the structure complexity, the synthetic procedures as well as the purification steps are quite difficult. Moreover, the correct attachment point of linker on the ligand should be assessed to not alter the binding with protein target. In addition, the nature and length of linkers should be carefully examine in order to bring the protein target in close proximity to E3 ligase, avoiding steric repulsive effects. Furthermore, the linker could be representing an easier target for metabolic enzymes, reducing or inactivating the PROTACTM itself. The formation of a stable ternary complex (Protein – PROTACTM – E3 ligase) instead of a binary system (Protein – PROTACTM or PROTACTM – E3 ligase) is necessary to start a degradation event. High concentrations of PROTAC can promote the binary system occurring in the so called, "Hook effect". Finally, the rate of protein degradation should be faster than the *de novo* resynthesis.

Despite the complexity of PROTACTM technology, numerous small-molecule degraders for several protein targets have been successfully developed in the last twenty years. However, a

very few small-molecule degraders of histone methyltransferases have been reported to date.^{172,173}

Among these, the only example of VHL (Von Hippel Lindau)-based PRMT5 PROTACsTM was reported in 2020.¹⁷³ This compound (**MS4322**, Figure 5.2) which features VHL ligand as E3 recruiter, **EPZ015666** as warhead, and a PEG4 as a linker, is highly selective against PRMT5 reducing the sDMA level in MCF-7 cells in a concentration-, time-, PRMT5-, VHL-, and proteasome-dependent manner. Furthermore, **MS4322** can strongly reduce PRMT5 protein levels in cancer lines such as Hela, A549, A172, and Jurkat cells and inhibit the proliferation of these cells.

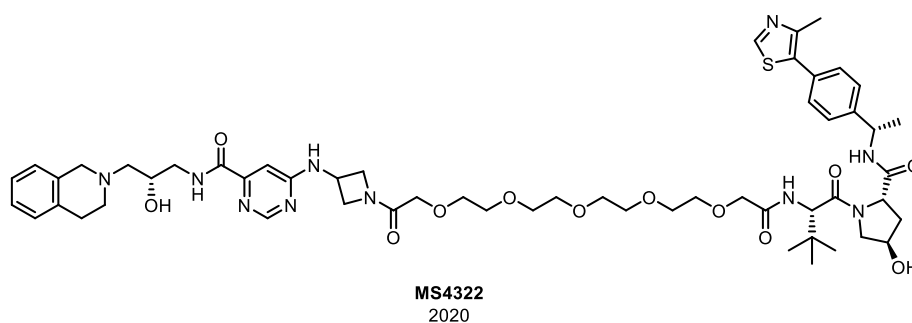


Figure 5.2 First-in-Class Protein Arginine Methyltransferase 5 (PRMT5) Degrader.

5.2. Aim of work

In this Ph. D. project, a small pool of PROTACsTM of type I PRMTs was designed and synthesized. **MS023** (for details, see Chapter I Introduction), a reported unselective ligand for PRMTs of class I, is chosen as protein binder with a view to improve its selectivity toward specific PRMT isoforms. To define the putative proper connection position, the crystal structure of **MS023** was exploited (Figure 5.3).¹²⁴

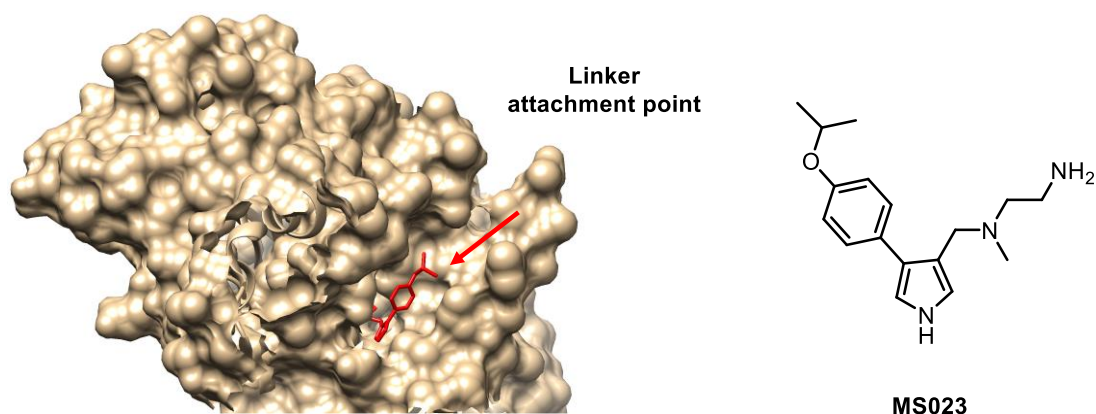


Figure 5.3 Crystal Structure of Human HMT1 hnRNP methyltransferase-like protein 6 in complex with **MS023** (PDB 5E8R).

Isopropoxy group on phenyl ring is solvent exposed and it seems to be not involved in important interactions with the protein. Therefore, this position was identified as linker-attachment point and functionalized with an alkyl group for proper linker connection. As mentioned, the nature and length of linkers result a critical aspect in PROTACsTM design. Polyethylene glycol (PEG) of different lengths were selected (L1-L3). A thalidomide derivative was used as E3 ligase Cereblon (CRBN) ligand and a proline-based compound as von Hippel–Lindau (VHL) ligand. The combination of these components yielded a collection of compounds (**109a – c** and **110a – c**) as depicted in Figure 5.4.

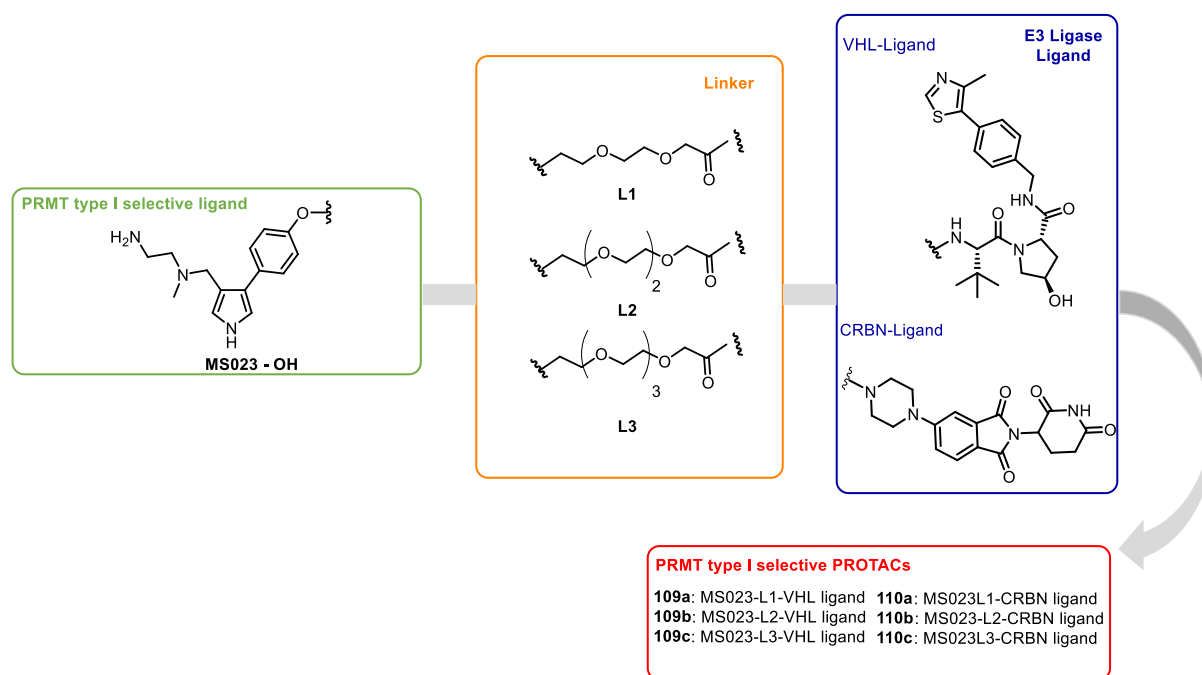


Figure 5.4 Combination of components for PROTACsTM design.

5.3. Results

The ability of PROTACsTM **109a – c** and **110a – c** to induce degradation of PRMTs was evaluated in collaboration with Prof. Mark T. Bedford (Chapter VIII, Paragraph 8.3.6). Compounds were profiled in HEK293T and Hela cells. The latter were treated for 1, 3 and 5 days with compounds at concentration of 10 μ M and then the lysates were immunoblotted with PRMT1, PRMT4 and PRMT6 specific antibodies. Unfortunately, no significant reduction in protein levels for all the compounds tested was observed.

5.4. Conclusions

In this approach, we reported the design and synthesis of a new pool of type I PRMTs PROTACTM compounds. **MS023**, a selective type I PRMTs inhibitor, was chosen as protein binder and connected to E3 ligase (VHL and CRBN) ligands by PEG linkers of different length. Their ability to induce protein degradation was evaluated in cellular context. Unfortunately, no protein degradation was observed. Although negative, these results should be analysed in the

complexity of PROTACsTM field. Indeed, the inactivity of PROTACsTM compounds is not unusual, considering that several aspects can influence their activity. Also, for our compounds the length and the nature of the linkers could be not suitable for the proper engagement of target protein and E3 ligase and can be optimized. To better investigate this aspect, a new pool of compounds bearing different linkers with aromatic or aliphatic nature could be synthesized. Moreover, other aspects will be evaluated. For example, to verify the formation of the binary complex between PROTACsTM and protein target, we have planned SPR assays. In fact, it is quite common that the presence of linkers and/or E3 ligase ligands could alter the interactions with proteins. After the evaluation of these aspects, the ability of PROTACsTM to promote the formation of a stable ternary complex will be resolved using SPR and/or MicroScale Thermophoresis (MST) assays.^{174,175} Furthermore, we can also speculate that the complex structure of compounds could negatively affect the cellular permeability, which might be improved using electroporation.

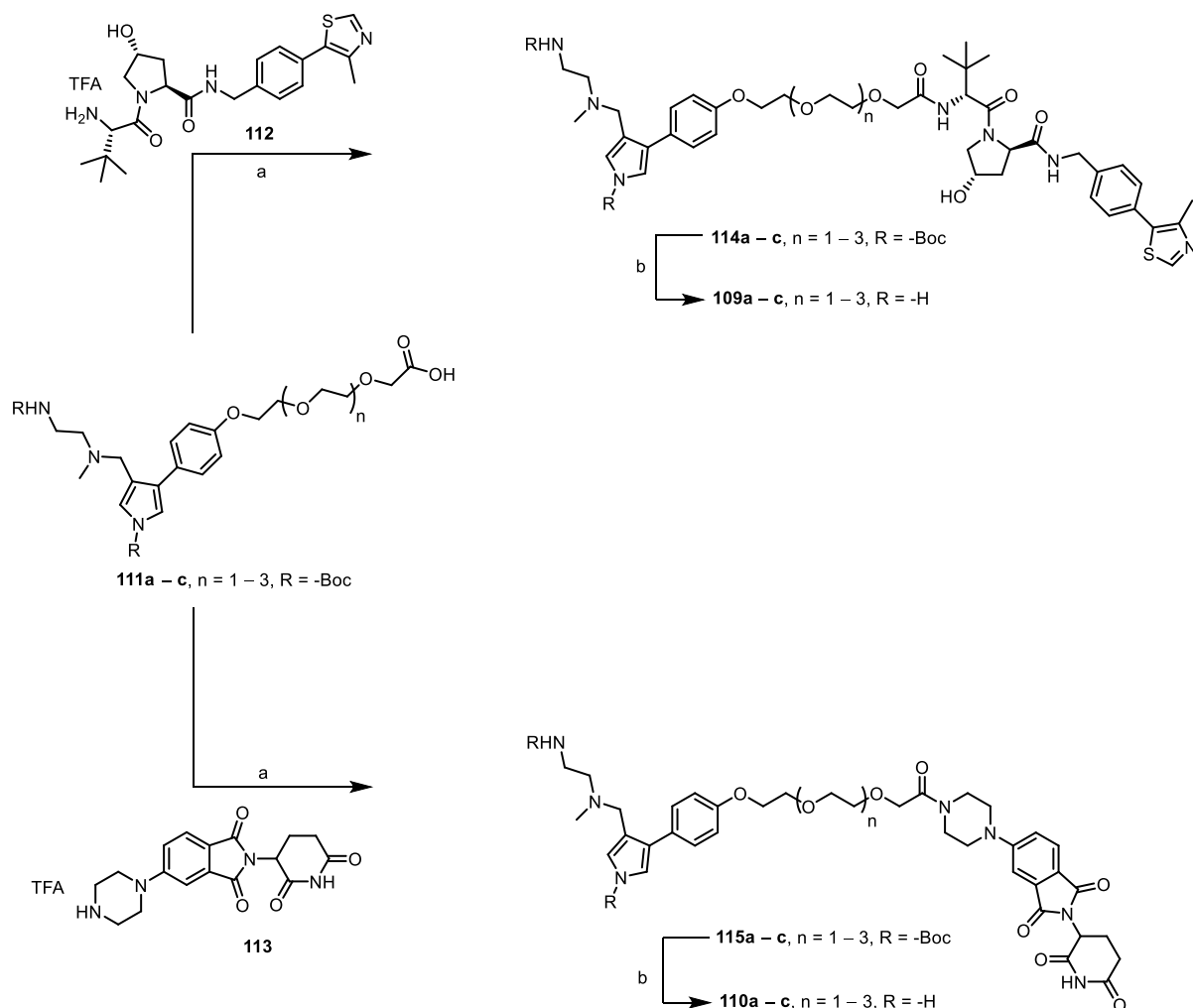
5.5. Chemistry

5.5.1. *Synthesis of compounds 109a – c and 110a – c*

This section describes the synthetic procedures adopted for the preparation of PROTACsTM **109a – c** and **110a – c**. The synthetic general route is depicted in Scheme 5.1. Final compounds were obtained via peptide coupling between the carboxylic function of proper linkers attached on protein binders (**111a – c**) and the primary amino group of VHL (**112**) or CRBN ligand (**113**), giving compounds **114a – c** and **115a – c**, respectively. The coupling reaction was performed using COMU as activating reagent, *N,N*-diisopropylethylamine (DIPEA) as a base in anhydrous DMF. Finally, deprotection in acidic conditions affords the target compounds **109a – c** and **110a – c**.

VHL ligand (**112**) and CRBN ligand (**113**) were prepared according to literature.¹⁷⁶ Linkers and the functionalized protein binder (**111a – c**) were prepared as described in the following sections.

Scheme 5.1 General synthetic scheme for the preparation of PROTAC compounds **109a – c** and **110a – c**.



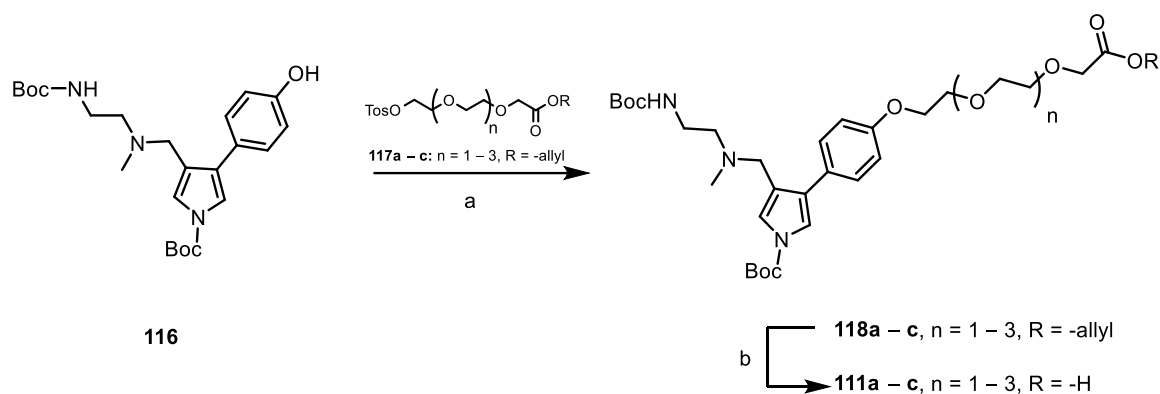
Reagents and conditions: a) COMU, DIPEA, dry DMF, r. t., 4 – 5 h (20 – 50%); b) DCM/TFA 9:1, r. t., 6 h (95 – 96%).

5.5.2. Synthesis of functionalized protein binders **111a – c**

The attachment of linkers on protein binder **116** was performed as outlined in Scheme 5.2. The phenolic portion of **116** was anchored on proper linker **117a – c** through nucleophilic

substitution to give compounds **118a – c**. Selective Tetrakis(triphenylphosphine)palladium(0)-catalysed ester hydrolysis, using pyrrolidine as an allyl trap, afforded the intermediates **111a – c**.

Scheme 5.2 General synthetic scheme for the preparation of compounds **111a – c**.

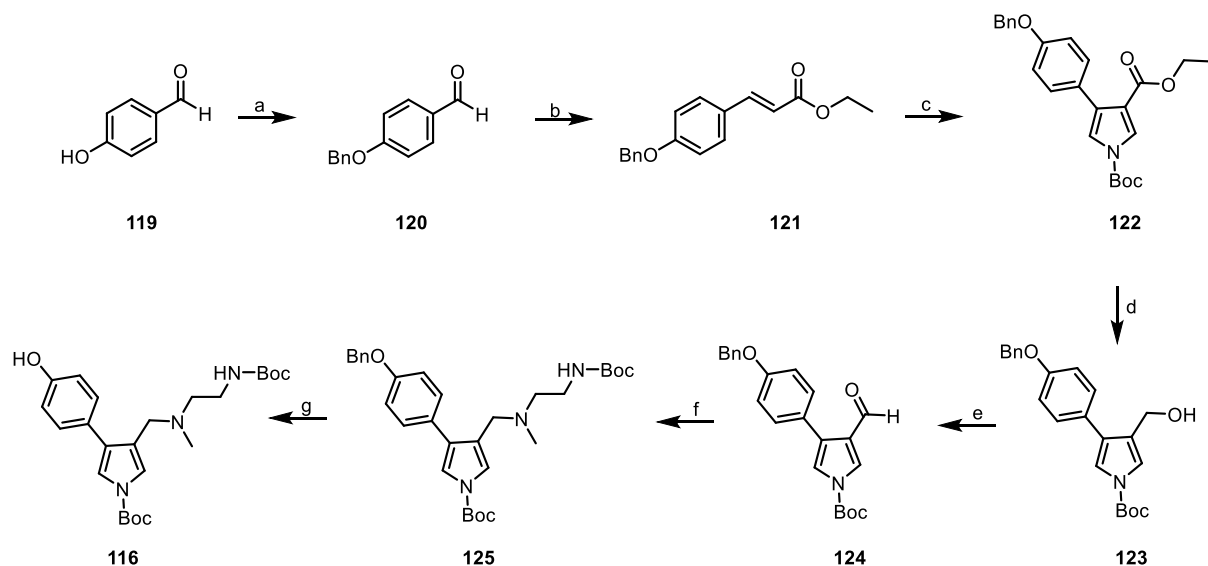


Reagents and conditions: a) K_2CO_3 , dry DMF, 80 °C, 18 h (45 – 60%); b) TETRAKIS, PPh_3 , pyrrolidine, dry DCM, r. t., 15 min (90 – 99%).

5.5.3. Synthesis of compound **116**

Compound **116** was synthesized according to a slight modification of previously reported procedure (Scheme 5.3).¹²⁴ The first step involved in a benzylation of 4-hydroxy benzaldehyde **119** using benzyl bromide in DMF to give **120** which undergoes Wittig reaction with ethyl 2-(diethoxyphosphoryl)acetate. The obtained alkene **121** was involved in a Van-Leusen type reaction to yield the pyrrole scaffold **122**. The ester group at C3 position was reduced to alcohol **123** which was subsequently oxidated to aldehyde (**124**) using Dess-Martin periodinane in anhydrous DCM. Reductive amination between aldehyde **124** and the commercially available *tert*-butyl (2-(methylamino)ethyl)carbamate afforded compound **125**, using sodium triacetoxyborohydride ($NaBH(OAc)_3$) as reducing agent. Finally, *O*-debenzylation, catalysed by palladium on carbon, furnished compound **116**.

Scheme 5.3 General synthetic scheme for the preparation of compound **116**.

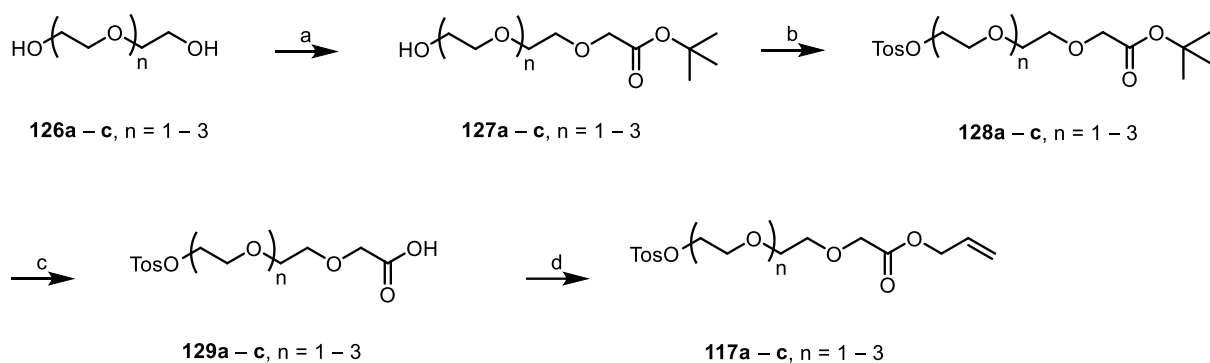


Reagents and conditions: a) Benzyl bromide, K_2CO_3 , DMF, r. t., 18 h (97%); b) ethyl 2-(diethoxyphosphoryl)acetate, KOH, THF, r. t., 4 h (82%); c) TOSMIC, NaH (60% mineral oil), DMF/THF, 0 °C to 25 °C, 4 h (75%); d) DIBAL-H, dry DCM, -78 °C, (60%); e) Dess-Martin, dry DCM, 2 h (90%); f) *tert*-butyl (2-(methylamino)ethyl)carbamate, $NaBH(OAc)_3$, dry DCM, 18 h (94%); g) H_2 , Pd/C 10%, MeOH, r. t., 2 h (99%).

5.5.4. Synthesis of linkers **117a – c**.

Linkers **117a – c** were prepared as outlined in Scheme 5.4. The commercially available glycols **126a – c** reacted with *tert*-butyl 2-bromoacetate in presence of NaH to give the intermediates **127a – c**. The latter were activated for the subsequent nucleophilic substitutions using tosyl chloride (TsCl) and TEA in anhydrous DCM affording the tosylated intermediates **128a – c**. Subsequently, the *tert*-butyl esters were hydrolysed to carboxylic acid **129a – c** and treated with allyl iodide and cesium carbonate (Cs_2CO_3) to obtain the allyl esters **117a – c**.

Scheme 5.4 General synthetic scheme for the preparation of linkers **117a – c**.



Reagents and conditions: a) *tert*-butyl 2-bromoacetate, NaH (60% mineral oil), dry DMF, r. t., 18 h (68 – 71%); b) TsCl, TEA, dry DCM, r. t., 18 h (60 – 66%); c) DCM/TFA 9:1, r. t., 2 h (99%); d) allyl iodide, Cs₂CO₃, dry DMF, r. t., 3 h (97 – 99%).

CHAPTER VI

Scaffold Replacement Approach

6.1. Aim of work

Another class of designed compounds is based on scaffold replacement approach. The latter refers to a type of replacement where the central core (scaffold) of a template-chemical structure is replaced by another chemical moiety, maintaining some of essential features. Generally, this replacement aims to improve the ADMET (absorption, distribution, metabolism, excretion, and toxicity) profile as well as potency or selectivity toward the target protein. We postulated that this approach could be helpful to achieve a gain in selectivity toward PRMTs isoform. In fact, as highlighted in our PRMT4 inhibitors (Chapter II), even minor modifications in the structure of PRMTs inhibitors might offer enhanced potency and remarkable improvement for the selectivity. Thus, we applied this well-acknowledged strategy to hit compound **EPZ007345** (Figure 6.1). Its optimization led to the identification of **EPZ015666**, a selective inhibitor of PRMT5 with a high potency (for details, see Chapter I).¹⁴³ Extensive SARs and structural studies on this class of derivatives accredited the role of the tetrahydroisoquinoline (THIQ) scaffold in the high binding affinity and selectivity for PRMT5. In fact, the THIQ core establishes a π - π stacking interaction with Phe327, an amino acid residue that has a key role in directing symmetric arginine methylation.¹⁷⁷ Moreover, the tertiary nitrogen of the THIQ ring system established a water-mediated interaction with Glu435, an important residue thought to be important for enzyme catalysis. On the other hand, the decorated phenyl ring of the hit compound **EPZ007345**, and especially the pyrimidine moiety of the lead compound **EPZ015666** are poised for π - π stacking interactions with two aromatic amino acid, likely contributing to their high inhibitory potency.

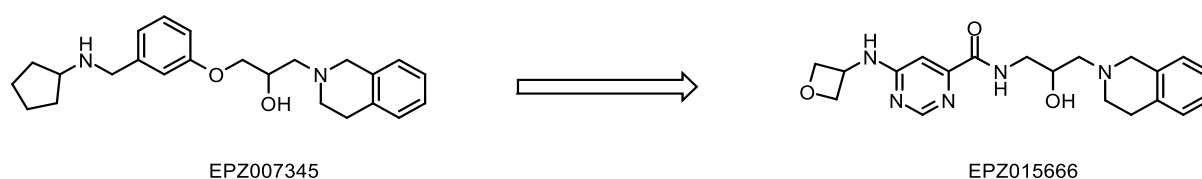


Figure 6.1 Hit-to-lead stage.

Based on these considerations, a small set of compounds (**130a,b**, **131a,b** and **132a,b**) was designed in which the THIQ core is replaced with the methyl 4-hydroxy-2-naphthoate moiety (Figure 6.2), previously identified as privileged scaffold for inhibition of PRMTs of type I (see Chapter II). This replacement could result in higher activity toward arginine methyltransferases of type I. The methyl 4-hydroxy-2-naphthoate scaffold was linked to the hydroxyaminopropanol central portion by a urea moiety and the terminal phenyl ring was decorated with three different amines bearing cyclopropyl, oxetane and cyclopentyl groups.

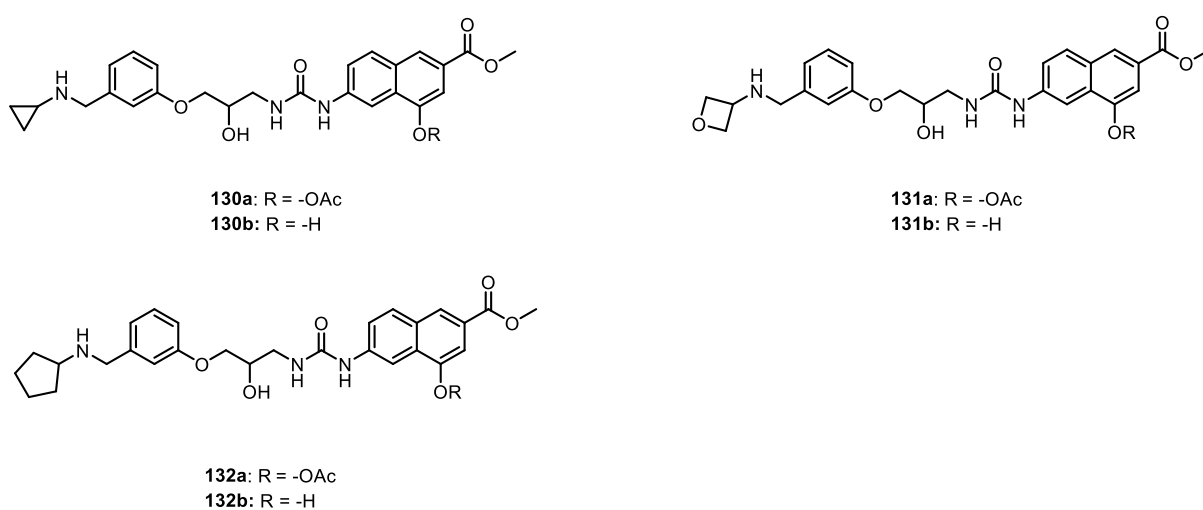


Figure 6.2 Design of compounds using a scaffold replacement approach.

6.2. Results

The binding of compounds **130a,b**, **131a,b** and **132a,b** with PRMT4, a type I methyltransferases, was determined by our optimized SPR protocol (Chapter VIII, Paragraph 8.3.3). Equilibrium dissociation constant (K_D) values were derived from the ratio between the kinetic dissociation (k_{off}) and association (k_{on}) constants, obtaining the results reported in the Figure 6.3. Compounds **130a,b** and **132a,b** bearing a cyclopropyl and cyclopentyl amine respectively, were shown to weakly interact with the immobilized CARM1, with K_D values in the micromolar range. Moreover, the deacetylated compounds displayed a slightly higher affinity compared to their acetylated analogues. On the other hand, no interaction was observed

for compounds **131a,b**. We can speculate that the presence of oxetanamine as substituent on the phenyl moiety had a deleterious effect, resulting in total lack of affinity with the protein target.

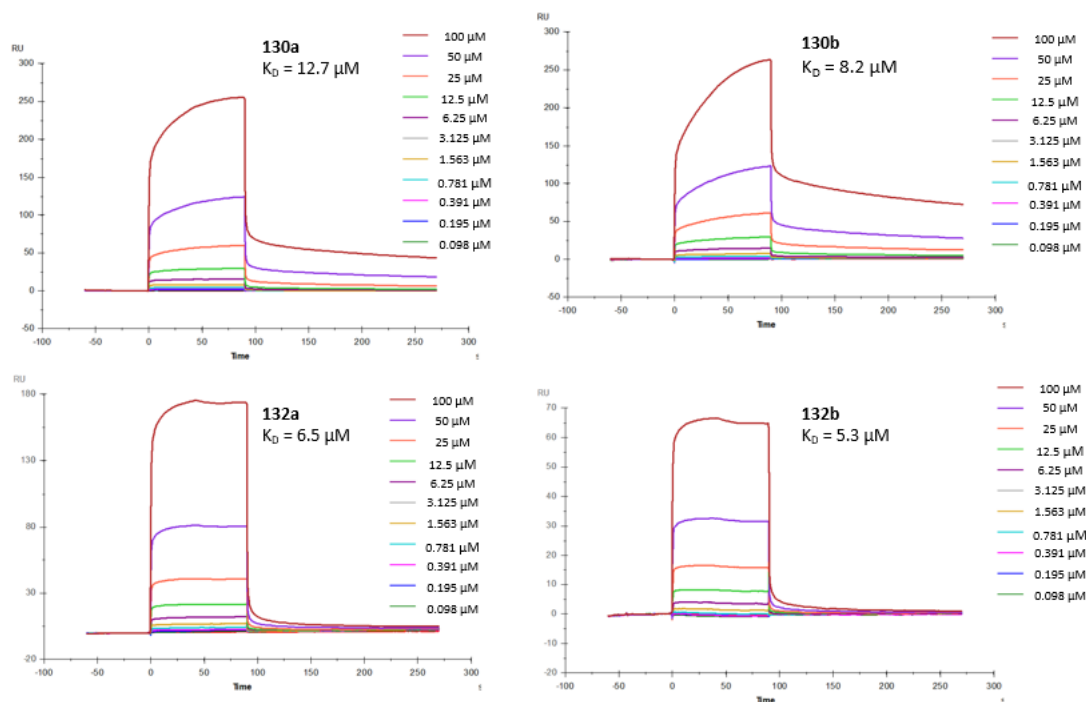


Figure 6.3 Sensorgrams obtained from the SPR interaction analysis of compounds **130a,b** and **132a,b** binding to immobilized PRMT4. Each compound was injected at different concentrations (from 100 μ M to 0.098 μ M) with an association and a dissociation time of 90 and 180 sec, with a flow rate of 30 μ L/min. The equilibrium dissociation constants (K_D) were derived from the ratio between kinetic dissociation (k_{off}) and association (k_{on}) constants.

6.3. Conclusions

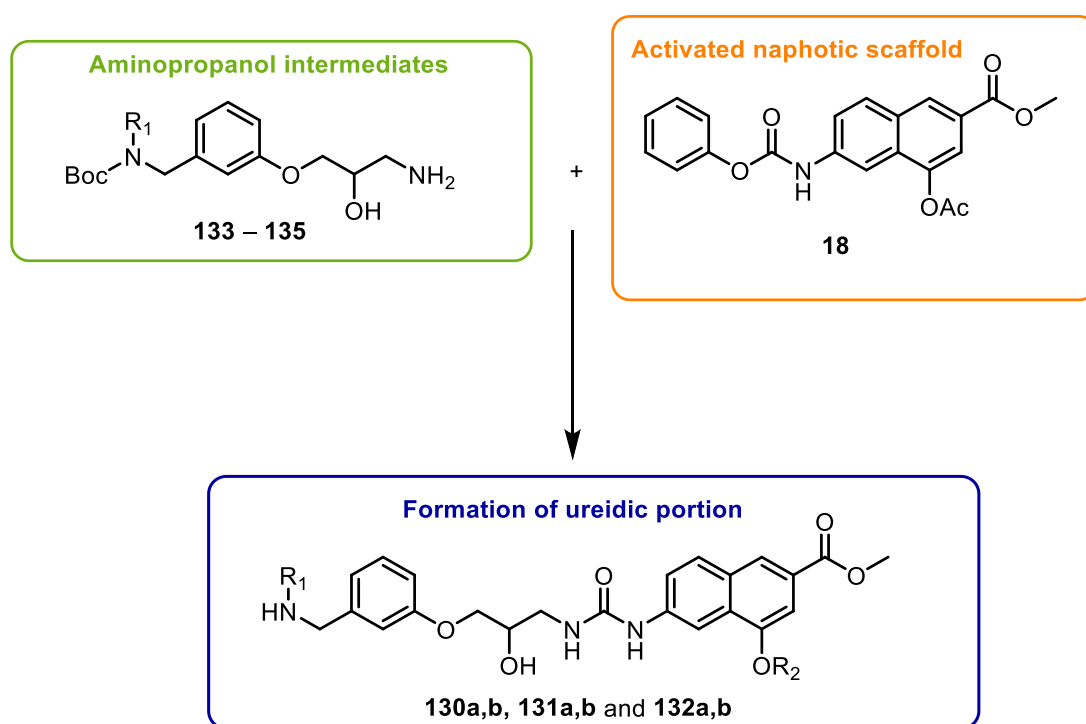
In this approach, the tetrahydroisoquinoline core of the hit compound **EPZ007345**, a reported PRMT5 inhibitor, was replaced by our validated amino hydroxynaphtoeic scaffold, in order to obtain new putative type I PRMTs inhibitors. We designed and synthesized a small pool of compounds bearing the aforementioned scaffold which was connected with 2-hydroxyaminopropanol linker to a phenyl ring, which was characterized by three different

amine groups. With the aim to validate our initial hypothesis, we resolved to study the direct binding of compounds with CARM1 using an in-house optimized SPR protocol. Compounds **130a,b** and **132a,b** displayed a modest affinity with the protein target with K_D values in the micromolar range. These outcomes showed wide margins for improvement, considering the designed compounds as a starting point for further evaluation and optimization. In fact, the introduction of our amino hydroxy naphthoic scaffold, allowed us to obtain a discrete binding with a PRMT of class I (PRMT4). The next step will be to evaluate different substitutions on the aromatic ring in order to confidently improve the interactions with protein target, similar to the study reported for the starting derivatives (**EPZ007345** and **EPZ015666**).

6.4. Chemistry

This section describes the synthetic procedures adopted for the preparation of compounds **130a,b**, **131a,b** and **132a,b**. The synthetic general route was depicted in Scheme 6.1. It was based on the preparation of aminopropanol intermediates (**133 – 135**) that were condensed with the activated naphthoic scaffold **18** (for the synthesis, see Chapter II), to give the target compounds.

Scheme 6.1 General synthetic route

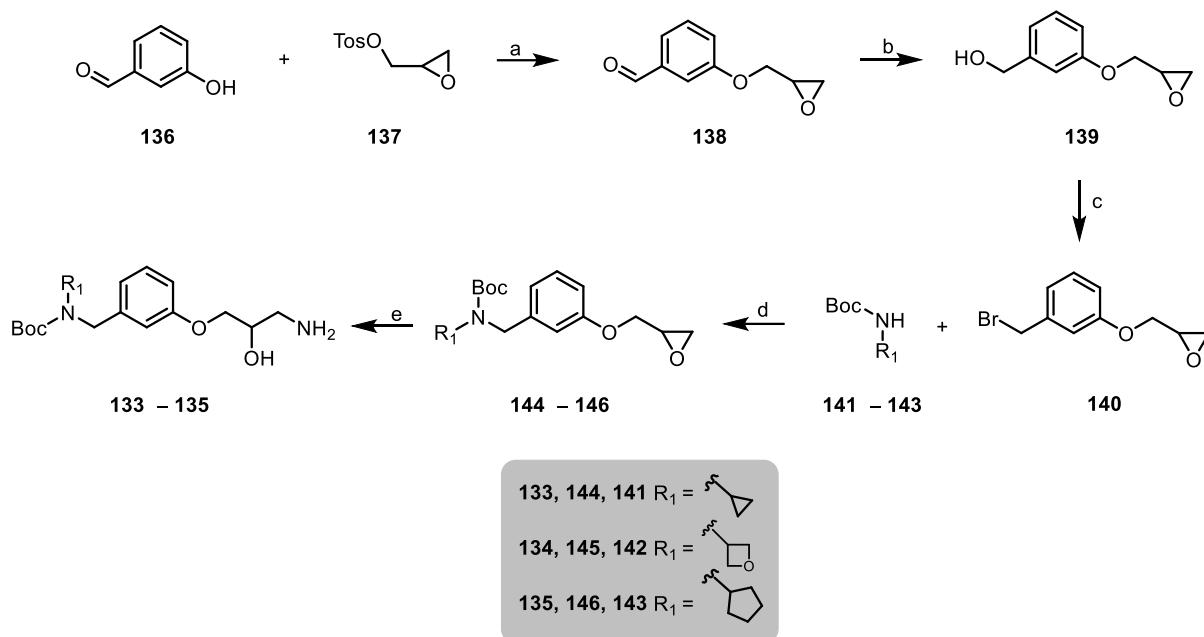


6.4.1. Synthesis of compounds 133 – 135

The aminopropanol intermediates **133 – 135** were prepared as outlined in Scheme 6.2. The first synthetic step involved in the introduction of the epoxy function on the phenolic core through the reaction of 3-hydroxybenzaldehyde **136** with glycidol tosylate **137** in the presence of K_2CO_3 . The obtained aldehyde **138** was reduced to alcohol **139** using NaBH_4 in dry MeOH. Appel-type reaction was used to convert the resulting benzyl alcohol into bromide **140** by reaction with NBS and triphenyl phosphine. Nucleophilic substitution reaction between benzyl

bromide **140** and the amines **141** – **143** furnished derivatives **144** – **146**. Finally, the aminoalcohols **133** – **135** were obtained in quantitative yields by opening the epoxy ring in the presence of ammonium hydroxide (NH₄OH).

Scheme 6.2 General synthetic scheme for the preparation of intermediates **133** – **135**.

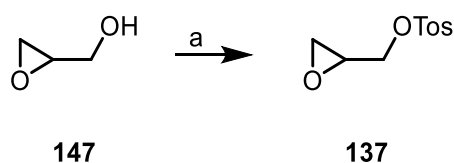


Reagents and conditions: a) K₂CO₃, dry ACN, reflux, 3 h (95%); b) NaBH₄, dry MeOH, r. t., 30 min (77%); c) NBS, PPh₃, THF, 0 °C, 0.5 h (42%); d) NaH (60% mineral oil), dry DMF, r. t., 2 h (60 – 89%); e) NH₄OH 33%, MeOH, 0 °C, r. t., 18 h (99%).

6.4.1.1. Synthesis of compound **137**

Compound **137**, not commercially available, was prepared by treatment of glycidol **147** with TsCl in the presence of TEA and DMAP (Scheme 6.3).

Scheme 6.3 General synthetic scheme for the preparation of intermediate **137**.

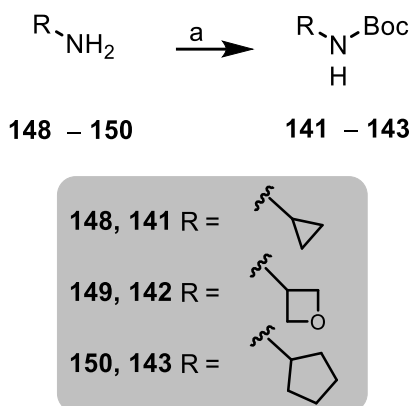


Reagents and conditions: a) TsCl, TEA, DMAP, dry DCM, 0 to 25 °C, 18 h (74%).

6.4.1.2. Synthesis of compounds **141** – **143**

The amines **141** – **143** were obtained by reaction with di-*tert*-butylcarbonate (Boc₂O) in dry DCM, starting from the corresponding aliphatic amines commercially available (**148** – **150**), as outlined in the Scheme 6.4.

Scheme 6.4 General synthetic scheme for the preparation of intermediates **141** – **143**

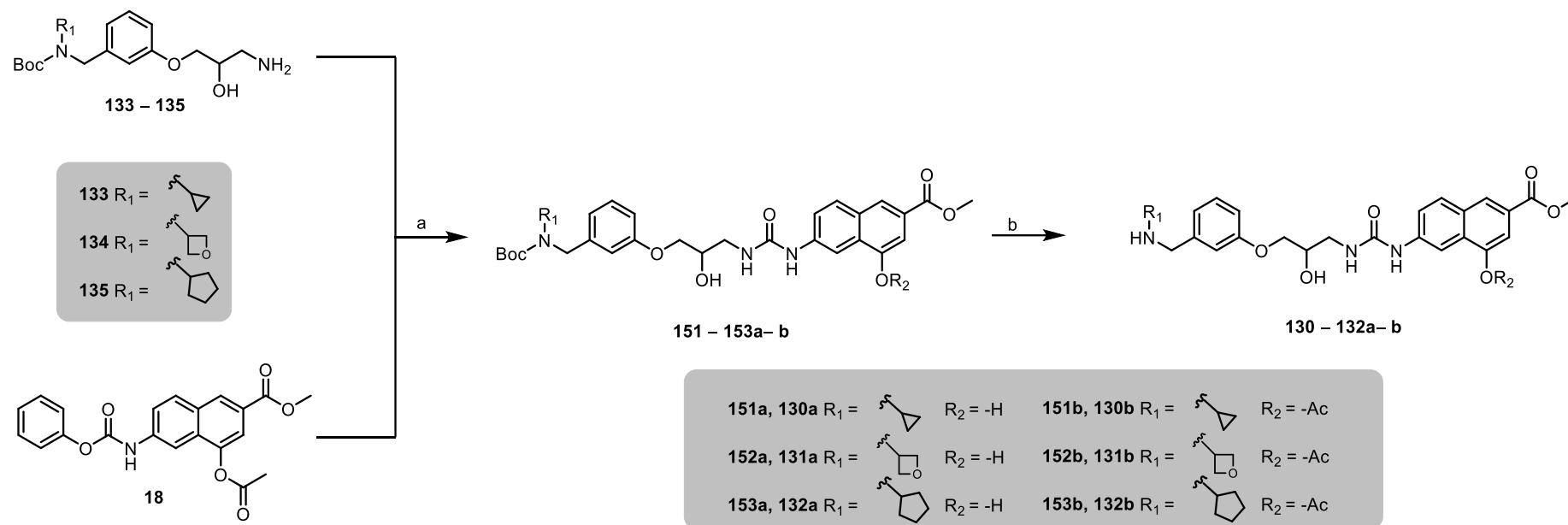


Reagents and conditions: a) Boc₂O, dry DCM, r. t., 16 h (90 – 98%).

6.4.2. Synthesis of compounds **130a,b**, **131a, b** and **132a, b**

The target compounds **130a, b**, **131a, b** and **132a, b** were prepared as outlined in Scheme 6.5. The first synthetic step involved a condensation between aminopropanol intermediates **133** – **135** and naphthoic compound **18** (see Chapter II) in the presence of TEA in dry DMF, obtaining a mixture of acetylated and non-acetylated products (compounds **151a** – **153a** and **151b** – **153b**, respectively). The acetylated and non-acetylated compounds were then easily separated by direct phase chromatography in order to deprotect them separately. Finally, the target compounds (**130a,b**, **131a,b** and **132a,b**) were obtained by removal of the Boc-protecting group in presence of TFA and DCM.

Scheme 6.5 General synthetic scheme for the preparation of compounds **130a,b**, **131a,b** and **132a,b**.



Reagents and conditions: a) TEA, dry DMF, r. t., 2 h (31 – 63%); (b) DCM/TFA 95:5, r. t., 2 h (52 – 74%).

CHAPTER VII

Conclusions

This Ph. D. project reported the design, synthesis and *in vitro* evaluation of new inhibitors of PRMTs. Despite the excellent progress made in the PRMT field to underscore the therapeutic and pharmacological potential of targeting PRMTs, selective inhibitors are still in high demand. To this aim, different medicinal chemistry approaches were applied to obtain different classes of compounds. The main strategy exploited a deconstruction–reconstruction and fragment growing approach, starting from naphthalene-based type I PRMT inhibitors, previously identified by us. These ligands were deconstructed into a 4-hydroxy-2-naphthoic fragment which was firstly bridged to an arginine mimetic group and then to an adenosine scaffold. An intensive synthetic optimization process allowed to obtain a series of compounds, with different linker length between the three aforementioned groups. A radioisotope-based filter-binding assay was used to profile the activity of these compounds against a panel of PRMTs, identifying the **EML981** as the best candidate with a nanomolar activity toward PRMT4 (IC₅₀ of 3 nM). Crystallographic and SPR studies confirmed a specific and strong binding interaction between PRMT4 and **EML981** with a K_D values in the nanomolar range (K_D = of 75.9 nM; t_R = 62.5 sec). In addition, **EML981** was able to modestly reduce the cellular activity of PRMT4 in a concentration-dependent way, offering a good starting point for further development of cell active PRMT4 inhibitors. Subsequently, based on a careful review of the results obtained, the attention was focused on PRMT7 and PRMT9 identifying the lower homologous **EML734** of **EML981** as the first in class dual inhibitor of PRMT7 and PRMT9 with an IC₅₀ of 0.32 μM and 0.89 μM, respectively. At the University of Vienna, under the supervision of Prof. Nuno Maulide, a new synthetic methodology defined as Alkene 1,3-Functionalization has been developed. This general, diastereoselective and broad in substrate scope procedure was applied to selected naphthalene compounds by developing ketone-based analogues bearing sp³-rich fragments with a view to strengthen the intermolecular interactions with protein target. In fact, ketone-based compounds showed a higher affinity on PRMT4 compared to their naphthalene

analogues, suggesting that the 4-hydroxy-2-naphthoic group could be efficiently replaced by a 3-hydroxy-(cyclohexyl)phenyl-methanone scaffold. Concurrently, three side approaches were investigated. The pro-drug strategy was applied to promising pyrrole-based lead compounds previously identified by us. Indeed, despite their interesting *in vitro* activity, these compounds did not evidence a great activity in cells, mainly due to their low cellular permeability. The pro-drug strategy has been used to mask the primary amino group of alanine to increase their lipophilicity and promote their cell permeability. Therefore, in order to verify the efficacy of our approach, the cellular activity of the new small collection of pro-drug derivatives was evaluated. Unfortunately, none of the prepared compounds showed an interesting activity in cells. The second approach involved the design and synthesis of new putative PROTACsTM (PROteolysis TArgeting Chimeras). These hetero-bifunctional molecules are able to hijack the target protein to ubiquitin-proteasome machinery for its selective degradation. Structurally, these compounds include a high affinity ligand for PRMTs (**MS023**) and two different E3 ligase (CRBN and VHL) ligands connected by different linkers. The combination of these components yielded a collection of compounds. Unfortunately, we observed no degradation on target proteins. These results need to be considered in the perspective of both the complexity of protein-induced degradation mechanism and the multifaceted aspects involved in the PROTACs design. In the third approach, the tetrahydroisoquinoline core of the hit compound **EPZ007345**, a reported PRMT5 inhibitor, was replaced by our validated amino hydroxynaphthoic scaffold, in order to obtain new putative type I PRMTs inhibitors. SPR studies were performed to evaluate the binding to the target protein (PRMT4), showing a good interaction with the immobilized PRMT4, with K_D values in the micromolar range. These outcomes showed wide margins for improvement, considering the designed compounds as a starting point for further evaluation and optimization.

CHAPTER VIII

Materials and Methods

8.1. General Information

All chemicals were purchased from Sigma-Aldrich Srl (Milan, Italy) or from Fluorochem Ltd. (Hadfield, UK) and were of the highest purity. All solvents were of reagent grade and, when necessary, were purified and dried by standard methods. All reactions requiring anhydrous conditions were conducted under a positive atmosphere of nitrogen in oven-dried glassware. Standard syringe techniques were used for anhydrous addition of liquids. Reactions were routinely monitored by thin-layer chromatography (TLC) performed on aluminum-backed silica gel plates (Merck DC, Alufolien Kieselgel 60 F254) with spots visualized by UV light ($\lambda = 254, 365$ nm) or using a KMnO₄ alkaline solution. Solvents were removed using a rotary evaporator operating at a reduced pressure of ~ 10 Torr. Organic solutions were dried over anhydrous Na₂SO₄. Chromatographic purification was done on an automated flash chromatography system (Isolera Dalton 2000, Biotage) using cartridges packed with KP-SIL, 60 Å (40–63 μ m particle size). All microwave-assisted reactions were conducted in a CEM Discover SP microwave synthesizer equipped with vertically focused IR temperature sensor. Analytical high performance liquid chromatography (HPLC) was performed on a Shimadzu SPD 20A UV/VIS detector ($\lambda = 220$ and 254 nm) using C-18 column Phenomenex Synergi Fusion - RP 80A (75 \times 4.60 mm; 4 μ m) at 25 °C using a mobile phase A (water + 0.1% TFA) and B (ACN + 0.1% TFA) at a flow rate of 1 mL/min. Preparative HPLC was performed using a Shimadzu Prominence LC-20AP with the UV detector set to 220 nm and 254 nm. Samples were injected onto a Phenomenex Synergi Fusion–RP 80A (150 \times 21 mm; 4 mm) C-18 column at room temperature. Mobile phases of A (water + 0.1% TFA) and B (ACN + 0.1% TFA) were used with a flow rate of 20 mL/min.

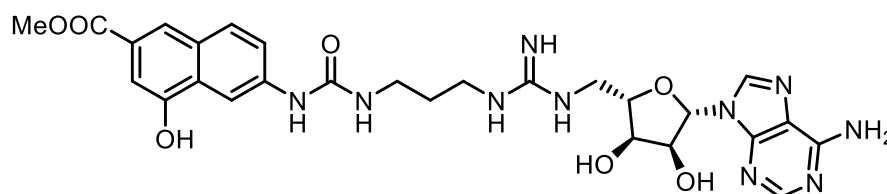
¹H spectra were recorded at 400 MHz on a Bruker Ascend 400 spectrometer while ¹³C NMR spectra were obtained by distortionless enhancement by polarization transfer quater-nary

(DEPTQ) spectroscopy on the same spectrometer. Chemical shifts are reported in δ (ppm) relative to the internal reference tetramethylsilane (TMS). Low resolution mass spectra were recorded on a Finnigan LCQ DECA ThermoQuest mass spectrometer in electrospray positive and negative ionization modes (ESI-MS). High resolution mass spectra were recorded on a ThermoFisher Scientific Orbitrap XL mass spectrometer in electrospray positive ionization modes (ESI-MS). All tested compounds possessed a purity of at least 95% established by HPLC unless otherwise noted. VHL ligand **112** and CRBN ligand **113** were prepared in according with the reported procedure and all the ^1H -NMR and ^{13}C -NMR spectra are consistent with those already reported to literature.^{176,178}

8.2. Synthetic Procedures

8.2.1. Preparation of compounds 1 – 38

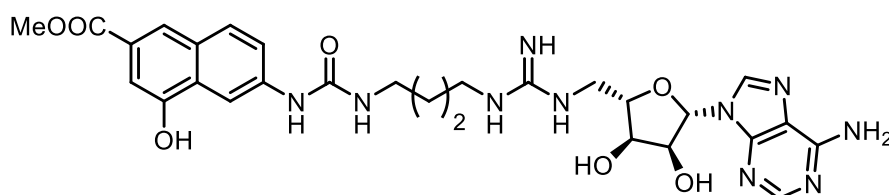
Methyl 6-(3-(3-(3-(((2R,3S,4R,5R)-5-(6-amino-9H-purin-9-yl)-3,4 dihydroxytetrahydrofuran-2-yl)methyl)guanidino)propyl)ureido)-4-hydroxy-2-naphthoate (1)



Compound **27b** (0.100 g, 0.118 mmol) was dissolved in a solution of DCM/TFA 1:1 and then a drop of water was added. The resulting mixture was stirred at room temperature for 1 h. The solvent was evaporated, and the resulting solid was washed with CHCl_3 to afford the TFA salt **1** as white solid (0.064 g, 76%). ^1H NMR (400 MHz, $\text{DMSO}-d_6$) δ 10.30 (s, 1H, exchangeable with D_2O), 8.95 (s, 1H, exchangeable with D_2O), 8.45 (s, 1H), 8.27–8.21 (m, 2H), 7.98 (s, 1H), 7.88 (d, $J = 8.9$ Hz, 1H), 7.86 (br s, 2H, exchangeable with D_2O), 7.56 (dd, $J = 9.0, 2.2$ Hz, 1H), 7.49–7.42 (m, 4H, exchangeable with D_2O), 7.30 (s, 1H), 6.39 (br t, 1H, exchangeable with D_2O), 5.95 (d, $J = 5.7$ Hz, 1H), 4.72 (t, $J = 5.4$ Hz, 1H), 4.18–4.16 (m, 1H), 4.06–4.01 (m, 1H),

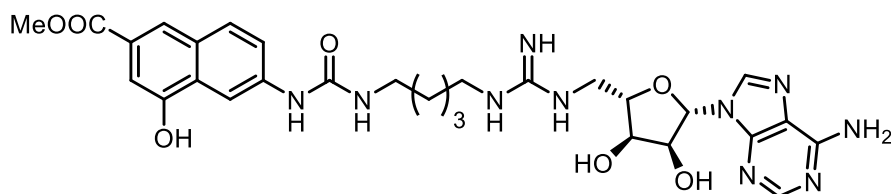
3.87 (s, 3H), 3.18–3.12 (m, 4H), 1.70–1.60 (m, 2H); ^{13}C NMR (100 MHz, DMSO- d_6) δ 166.6, 155.9, 155.3, 152.5, 149.0, 140.7, 139.7, 129.7, 128.8, 127.9, 124.7, 121.2, 120.2, 119.2, 107.2, 106.5, 87.8, 82.3, 72.7, 71.1, 51.9, 43.2, 36.5, 29.3; HRMS (ESI): m/z $[\text{M} + \text{H}]^+$ calcd. for $\text{C}_{27}\text{H}_{32}\text{N}_{10}\text{O}_7 + \text{H}^+$: 609.2528. Found: 609.2520.

Methyl 6-(3-(5-(3-(((2R,3S,4R,5R)-5-(6-amino-9H-purin-9-yl)-3,4-dihydroxy tetrahydrofuran-2-yl)methyl)guanidino)butyl)ureido)-4-hydroxy-2-naphthoate (2)



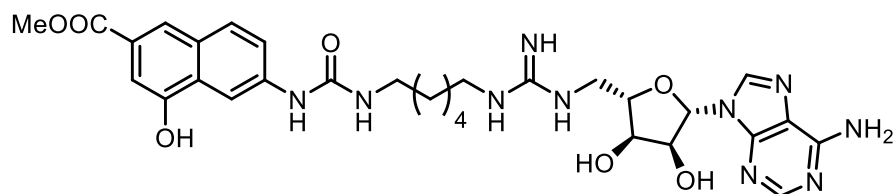
Compound **2** was obtained as a white solid (0.033 g, 75%) starting from compound **27c** (0.052 g, 0.060 mmol) following the procedure described for **1**. ^1H NMR (400 MHz, DMSO- d_6) δ 10.28 (s, 1H, exchangeable with D_2O), 8.90 (s, 1H, exchangeable with D_2O), 8.42 (s, 1H), 8.28–8.21 (m, 2H), 7.97 (s, 1H), 7.88 (d, $J = 8.9$ Hz, 1H), 7.78 (br s, 2H, exchangeable with D_2O), 7.54 (dd, $J = 8.9, 2.2$ Hz, 1H), 7.42–7.33 (m, 4H, exchangeable with D_2O), 7.30 (s, 1H), 6.34 (br t, 1H, exchangeable with D_2O), 5.93 (d, $J = 5.7$ Hz, 1H), 4.71 (t, $J = 5.7$ Hz, 1H), 4.17–4.15 (m, 1H), 4.06–3.98 (m, 1H), 3.86 (s, 3H), 3.60–3.48 (m, 2H), 3.17–3.05 (m, 4H), 1.51–1.45 (m, 4H); ^{13}C NMR (101 MHz, DMSO- d_6) δ 166.6, 155.8, 155.1, 152.5, 151.1, 149.0, 140.6, 139.8, 129.7, 128.7, 127.9, 121.2, 120.1, 119.2, 107.1, 106.4, 87.8, 82.3, 72.6, 71.0, 51.9, 43.1, 26.9, 25.9; HRMS (ESI): m/z $[\text{M} + \text{H}]^+$ calcd. for $\text{C}_{28}\text{H}_{34}\text{N}_{10}\text{O}_7 + \text{H}^+$: 623.2685. Found: 623.2689.

Methyl 6-(3-(5-(3-(((2R,3S,4R,5R)-5-(6-amino-9H-purin-9-yl)-3,4-dihydroxy tetrahydrofuran-2-yl)methyl)guanidino)pentyl)ureido)-4-hydroxy-2-naphthoate (3)



Compound **3** was obtained as a pale yellow solid (0.063 g, 78%) starting from compound **27d** (0.095 g, 0.108 mmol) following the procedure described for **1**. **¹H NMR** (400 MHz, DMSO-*d*₆) δ 10.28 (s, 1H, exchangeable with D₂O), 8.83 (s, 1H, exchangeable with D₂O), 8.38 (s, 1H), 8.25 (d, *J* = 2.2 Hz, 1H), 8.20 (s, 1H), 7.96 (s, 1H), 7.88 (d, *J* = 8.9 Hz, 1H), 7.59 (s, 2H, exchangeable with D₂O), 7.53 (dd, *J* = 8.9, 2.2 Hz, 1H), 7.37–7.32 (m, 4H, exchangeable with D₂O), 7.29 (s, 1H), 6.25 (br t, 1H, exchangeable with D₂O), 5.92 (d, *J* = 5.7 Hz, 1H), 4.71 (t, *J* = 5.4 Hz, 1H), 4.16–4.14 (m, 1H), 4.03–3.99 (m, 1H), 3.85 (s, 3H), 3.10–3.05 (m, 4H), 1.47–1.40 (m, 4H), 1.28–1.24 (m, 2H); **¹³C NMR** (100 MHz, DMSO-*d*₆) δ 167.1, 156.3, 155.6, 153.0, 149.5, 141.0, 140.3, 130.2, 129.2, 128.4, 125.1, 121.7, 120.6, 119.8, 107.5, 106.9, 88.3, 82.9, 73.1, 71.5, 52.4, 43.6, 41.5, 29.9, 28.6, 23.9; **HRMS** (ESI): *m/z* [M + H]⁺ calcd. for C₂₉H₃₆N₁₀O₇ + H⁺: 637.2841. Found: 637.2843.

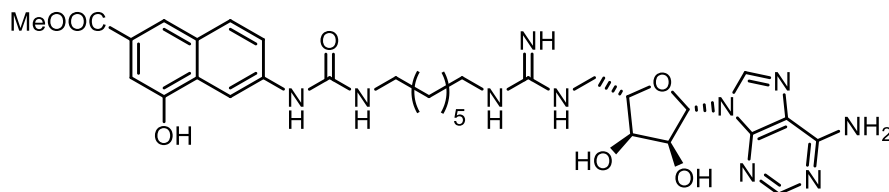
Methyl6-(3-(5-(3-(((2*R*,3*S*,4*R*,5*R*)-5-(6-amino-9*H*-purin-9-yl)-3,4-dihydroxy tetrahydrofuran-2-yl)methyl)guanidino)hexyl)ureido)-4-hydroxy-2-naphthoate (4**)**



Compound **4** was obtained as a pale yellow solid (0.065 g, 74%) starting from compound **27e** (0.092 g, 0.103 mmol) following the procedure described for **1**. **¹H NMR** (400 MHz, DMSO-*d*₆) δ 10.27 (s, 1H, exchangeable with D₂O), 8.86 (s, 1H, exchangeable with D₂O), 8.41 (s, 1H), 8.25 (d, *J* = 2.2 Hz, 1H), 8.24 (s, 1H), 7.46 (s, 1H), 7.87 (d, *J* = 8.9 Hz, 1H), 7.80 (s, 2H, exchangeable with D₂O), 7.53 (dd, *J* = 8.9, 2.2 Hz, 1H), 7.42–7.35 (m, 4H), 7.29 (s, 1H), 6.30 (br t, 1H, exchangeable with D₂O), 5.92 (d, *J* = 5.7 Hz, 1H), 4.69 (t, *J* = 5.4 Hz, 1H), 4.18–4.14 (m, 1H), 4.03–3.99 (m, 1H), 3.85 (s, 3H), 3.58–3.45 (m, 2H), 3.12–3.03 (m, 4H), 1.48–1.34 (m, 4H), 1.26–1.18 (m, 4H); **¹³C NMR** (101 MHz, DMSO-*d*₆) δ 166.6, 155.8, 155.1, 152.5, 151.0,

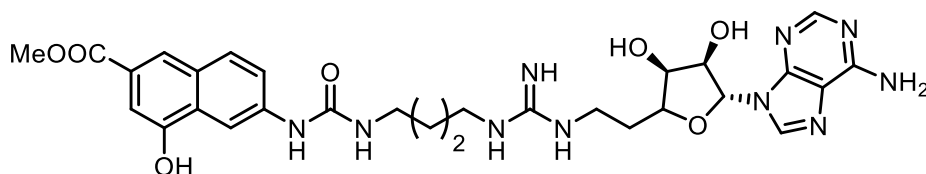
149.0, 140.6, 139.3, 129.7, 128.7, 127.9, 124.5, 121.2, 120.1, 119.2, 107.0, 106.4, 87.8, 82.4, 72.7, 71.0, 51.9, 43.1, 40.9, 29.6, 28.3, 25.9, 25.8; **HRMS** (ESI): m/z $[M + H]^+$ calcd. for $C_{30}H_{38}N_{10}O_7 + H^+$: 651.2998. Found: 651.2997.

Methyl 6-(3-(5-(3-(((2*R*,3*S*,4*R*,5*R*)-5-(6-amino-9*H*-purin-9-yl)-3,4-dihydroxy tetrahydrofuran-2-yl)methyl)guanidino)heptyl)ureido)-4-hydroxy-2-naphthoate (5)



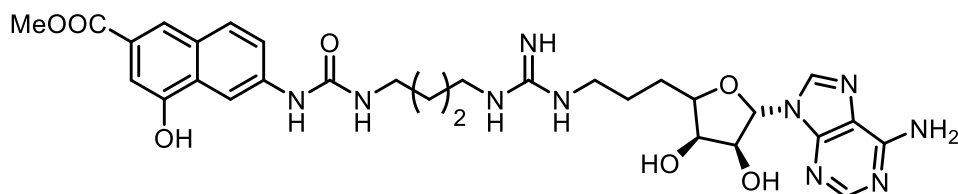
Compound **5** was obtained as a pale yellow solid (0.058 g, 75%) starting from compound **27f** (0.100 g, 0.110 mmol) following the procedure described for **1**. **¹H NMR** (400 MHz, DMSO- d_6) δ 10.28 (s, 1H, exchangeable with D₂O), 8.85 (s, 1H, exchangeable with D₂O), 8.42 (s, 1H), 8.27 (d, J = 2.1 Hz, 1H), 8.24 (s, 1H), 7.97 (s, 1H), 7.88 (d, J = 8.9 Hz, 1H), 7.80 (s, 2H, exchangeable with D₂O), 7.54 (dd, J = 8.9, 2.1 Hz, 1H), 7.42–7.26 (m, 5H, 4H exchangeable with D₂O), 6.29 (br t, 1H, exchangeable with D₂O), 5.93 (d, J = 5.7 Hz, 1H), 4.70 (t, J = 5.4 Hz, 1H), 4.17–4.14 (m, 1H), 4.03–4.01 (m, 1H), 3.86 (s, 3H), 3.56–3.50 (m, 2H), 3.13–3.03 (m, 4H), 1.44–1.40 (m, 4H), 1.29–1.24 (m, 4H); **¹³C NMR** (100 MHz, DMSO- d_6) δ 167.1, 156.3, 155.6, 153.0, 151.6, 149.5, 141.1, 140.3, 130.2, 129.2, 128.4, 125.0, 121.7, 120.6, 119.7, 107.5, 106.9, 88.3, 82.9, 73.2, 71.5, 52.4, 43.6, 41.5, 30.2, 28.8, 26.8, 26.5; **HRMS** (ESI): m/z $[M + H]^+$ calcd. for $C_{31}H_{40}N_{10}O_7 + H^+$: 665.3154. Found: 665.3148.

Methyl 6-(3-(4-(3-(2-((2*R*,3*S*,4*R*,5*R*)-5-(6-amino-9*H*-purin-9-yl)-3,4-dihydroxy tetrahydrofuran-2-yl)ethyl)guanidino)butyl)ureido)-4-hydroxy-2-naphthoate (6)



Compound **6** was obtained as a pale yellow solid (0.085 g, 80%) starting from compound **28** (0.011 g, 0.141 mmol) following the procedure described for **1**. **¹H NMR** (400 MHz, DMSO-*d*₆) δ 10.28 (s, 1H, exchangeable with D₂O), 8.90 (s, 1H, exchangeable with D₂O), 8.41 (s, 1H), 8.27 (d, *J* = 2.2 Hz, 1H), 8.22 (s, 1H), 7.97 (s, 1H), 7.88 (d, *J* = 8.9 Hz, 1H), 7.66 (br s, 2H, exchangeable with D₂O), 7.55 (dd, *J* = 8.9, 2.2 Hz, 1H), 7.34–7.24 (m, 5H, 4H, exchangeable with D₂O), 6.36 (br t, 1H, exchangeable with D₂O), 5.90 (d, *J* = 5.0 Hz, 1H), 4.69 (t, *J* = 5.4 Hz, 1H), 4.13–4.11 (m, 1H), 3.94–3.89 (m, 1H), 3.86 (s, 3H), 3.23–3.18 (m, 2H), 3.16–3.09 (m, 4H), 1.95–1.86 (m, 2H), 1.50–1.46 (m, 4H); **¹³C NMR** (100 MHz, DMSO-*d*₆) δ 167.1, 156.0, 155.6, 153.0, 149.6, 140.9, 140.3, 130.2, 129.2, 128.4, 125.1, 121.7, 120.6, 119.7, 107.6, 106.9, 88.3, 81.6, 73.8, 73.4, 52.4, 46.2, 41.1, 38.5, 32.8, 27.5, 26.5; **HRMS** (ESI): *m/z* [M + H]⁺ calcd. for C₂₉H₃₆N₁₀O₇ + H⁺: 637.2841. Found: 637.2838.

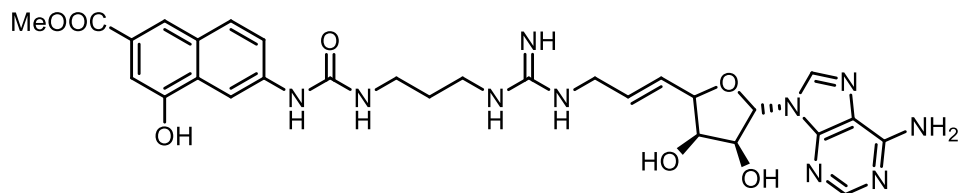
Methyl 6-(3-(4-(3-(3-((2R,3S,4R,5R)-5-(6-amino-9H-purin-9-yl)-3,4-dihydroxy tetrahydrofuran-2-yl)propyl)guanidino)butyl)ureido)-4-hydroxy-2-naphthoate (7)



Compound **7** was obtained as a white solid (0.071 g, 78%) starting from compound **29** (0.095 g, 0.120 mmol) following the procedure described for **1**. **¹H NMR** (400 MHz, DMSO-*d*₆) δ 10.29 (s, 1H, exchangeable with D₂O), 8.90 (s, 1H, exchangeable with D₂O), 8.38 (s, 1H), 8.27 (d, *J* = 2.1 Hz, 1H), 8.23 (s, 1H), 7.97 (s, 1H), 7.88 (d, *J* = 8.9 Hz, 1H), 7.70 (s, 2H, exchangeable with D₂O), 7.55 (dd, *J* = 8.9, 2.1 Hz, 1H), 7.34–7.28 (m, 5H, 4H exchangeable with D₂O), 6.36 (br t, 1H, exchangeable with D₂O), 5.87 (d, *J* = 5.0 Hz, 1H), 4.64 (t, *J* = 5.4 Hz, 1H), 4.08–4.06 (m, 1H), 3.86 (s, 3H), 3.16–3.12 (m, 6H), 1.70–1.48 (m, 8H); **¹³C NMR** (100 MHz, DMSO-*d*₆) δ 167.1, 155.9, 155.7, 153.0, 149.6, 140.9, 140.3, 130.2, 129.2, 128.4, 125.1, 121.7, 120.6,

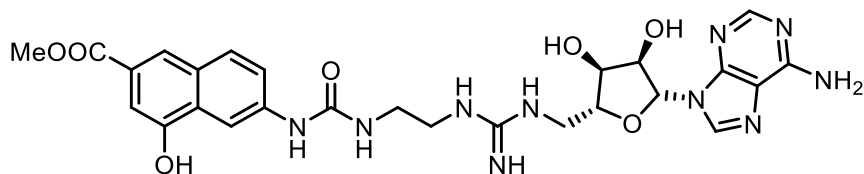
107.6, 106.9, 88.3, 83.6, 73.7, 73.5, 52.4, 41.2, 41.1, 39.1, 30.5, 27.5, 26.5, 25.5; **HRMS** (ESI): m/z $[M + H]^+$ calcd. for $C_{30}H_{38}N_{10}O_7 + H^+$: 651.2998. Found: 651.2996.

Methyl 6-(3-(4-(3-((*E*)-3-((2*R*,3*S*,4*R*,5*R*)-5-(6-amino-9*H*-purin-9-yl)-3,4-dihydroxy tetrahydrofuran-2-yl)allyl)guanidino)butyl)ureido)-4-hydroxy-2-naphthoate (8)



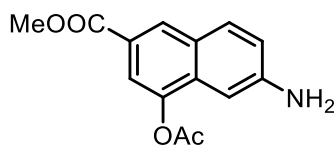
Compound **8** was obtained as a white solid (0.063 g, 78%) starting from compound **30** (0.084 g, 0.106 mmol) following the procedure described for **1**. **¹H NMR** (400 MHz, DMSO-*d*₆) δ 10.28 (s, 1H, exchangeable with D₂O), 8.92 (s, 1H, exchangeable with D₂O), 8.39 (s, 1H), 8.27 (d, J = 2.1 Hz, 1H), 8.24 (s, 1H), 7.97 (s, 1H), 7.88 (d, J = 9.0 Hz, 1H), 7.72 (s, 2H, exchangeable with D₂O), 7.57–7.49 (m, 2H, 1H exchangeable with D₂O), 7.43 (br t, 1H, exchangeable with D₂O), 7.35 (s, 2H, exchangeable with D₂O), 7.30 (s, 1H), 6.37 (br t, 1H, exchangeable with D₂O), 5.93 (d, J = 5.0 Hz, 1H), 5.89–5.86 (m, 1H), 4.69 (t, J = 5.4 Hz, 1H), 4.38–4.36 (m, 1H), 4.15–4.12 (m, 1H), 3.84 (s, 3H), 3.84–3.81 (m, 2H), 3.17–3.13 (m, 4H), 1.55–1.42 (m, 4H); **¹³C NMR** (100 MHz, DMSO-*d*₆) δ 167.1, 155.9, 155.7, 153.0, 149.6, 140.9, 140.3, 130.5, 130.2, 129.2, 128.4, 125.1, 121.7, 120.6, 88.4, 84.2, 74.4, 73.3, 54.1, 52.4, 44.7, 42.3, 41.2, 27.5, 26.5; **HRMS** (ESI): m/z $[M + H]^+$ calcd. for $C_{30}H_{36}N_{10}O_7 + H^+$: 649.2841. Found: 649.2829.

Methyl 6-(3-(3-(3-(((2*R*,3*S*,4*R*,5*R*)-5-(6-amino-9*H*-purin-9-yl)-3,4-dihydroxytetrahydrofuran-2-yl)methyl)guanidino)ethyl)ureido)-4-hydroxy-2-naphthoate (9)



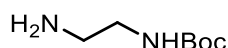
Compound **9** was obtained as a white solid (0.064 g, 76%) starting from compound **27a** (0.100 g, 0.136 mmol) following the procedure described for **1**. ¹H NMR (400 MHz, DMSO-*d*₆) δ 10.34 (s, 1H, exchangeable with D₂O), 9.17 (s, 1H, exchangeable with D₂O), 8.52 (s, 1H), 8.34 (s, 1H), 8.26 (d, *J* = 2.4 Hz, 1H), 7.97 (s, 1H), 7.89 (d, *J* = 9.0 Hz, 1H), 7.63 – 7.38 (m, 4H, exchangeable with D₂O), 7.30 (s, 1H), 6.49 (br t, *J* = 5.7 Hz, 1H, exchangeable with D₂O), 5.95 (d, *J* = 5.7 Hz, 1H), 4.69 (t, *J* = 5.5 Hz, 1H), 4.16 (t, *J* = 4.6 Hz, 1H), 4.06 (dt, *J* = 8.4, 4.2 Hz, 1H), 3.86 (s, 3H), 3.59 – 3.55 (m, 2H, overlaps with H₂O peak), 3.42 – 3.10 (m, 4H). ¹³C NMR (100 MHz, DMSO- *d*₆) δ 167.1, 156.6, 156.0, 153.1, 150.3, 149.4, 141.5, 139.9, 130.3, 129.4, 128.3, 125.3, 121.7, 120.7, 119.6, 115.1, 108.0, 106.9, 88.3, 82.8, 73.3, 71.6, 52.6, 43.7, 41.9, 38.8. HRMS (ESI): *m/z* [M + H]⁺ calcd. for C₂₆H₃₀N₁₀O₇ + H⁺: 595.2372. Found: 595.2376.

Methyl 4-acetoxy-6-amino-2-naphthoate (10)



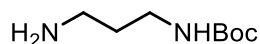
To a solution of **17** (3.00 g, 10.37 mmol) in acetic acid (50 mL), Zn dust (5.10 g, 82.40 mmol) was added. The resulting mixture was stirred for 1 h at room temperature, filtered, and concentrated in vacuo. The acid residue was dissolved in saturated aqueous solution of NaHCO₃ (50 mL) and extracted with AcOEt (3 x 50 mL). The organic layer was washed with brine (50 mL), dried (Na₂SO₄), and filtered. Vacuum evaporation of the solvent gave the title compound **10** (2.69 g, 98%) as a pale-yellow solid which was directly used in the next step without further purification. ¹H NMR (400 MHz, DMSO-*d*₆) δ 8.28 (s, 1H), 7.86 (d, *J* = 9 Hz, 1 H), 7.54 (s, 1 H), 7.06 (d, *J* = 9 Hz, 1 H), 6.79 (s, 1H), 6.04 (s, 2 H, exchangeable with D₂O), 3.87 (s, 3 H), 2.42 (s, 3H); MS (ESI) *m/z*: 260 (M+H)⁺.

Tert-butyl (2-aminoethyl)carbamate (11a)



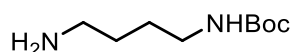
In a two necked round-bottom flask under nitrogen atmosphere, a solution of Boc_2O (1.00 g, 4.6 mmol) in dry dichloromethane (25 mL) was added dropwise to a solution of diamine **19a** (0.828 g, 13.8 mmol) in dry dichloromethane (50 mL) at 0 °C. The reaction mixture was stirred 1h at 0 °C then overnight at room temperature. Water (25mL) was added. Then, the organic layer was washed with water (2 x 25 mL) and dried over Na_2SO_4 . After filtration, solvent was removed under vacuum to afford compound **11a** (0.596 g, 81%) which was directly used in the next step without further purification step. $^1\text{H NMR}$ (400 MHz, CDCl_3) δ 4.93 (br s, 1H), 3.16 (q, $J = 5.8$ Hz, 2H), 2.79 (t, $J = 5.8$ Hz, 2H), 1.44 (s, 9H). **MS** (ESI) m/z : 161 ($\text{M}+\text{H}$) $^+$.

Tert-butyl (2-aminopropyl)carbamate (11b)



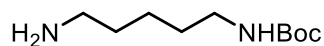
Compound **11b** was obtained as a colourless oil (0.640 g, 80%) starting from **19b** (1.03 g, 13.8 mmol) following the procedure described for **11a**. $^1\text{H NMR}$ (400 MHz, CDCl_3) δ 4.92 (s, 1H), 3.19 (t, $J = 6.2$ Hz, 2H), 2.74 (t, $J = 6.6$ Hz, 2H) 1.67 (br s, 2H), 1.59 – 1.55 (m, 4H), 1.40 (s, 9H). **MS** (ESI) m/z : 175 ($\text{M}+\text{H}$) $^+$.

Tert-butyl (2-aminobutyl)carbamate (11c)



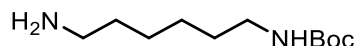
Compound **11c** was obtained as a white solid (0.743 g, 85%) starting from **19c** (1.24 g, 13.8 mmol) following the procedure described for **11a**. $^1\text{H NMR}$ (400 MHz, CDCl_3) δ 4.68 (br s, 1H), 3.13 (m, 2H), 2.70 – 2.65 (m, 2H), 1.62 – 1.33 (m, 13H). **MS** (ESI) m/z : 190 ($\text{M}+\text{H}$) $^+$.

Tert-butyl (2-aminopentyl)carbamate (11d)



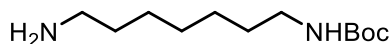
Compound **11d** was obtained as a white solid (0.754 g, 80%) starting from **19d** (1.45 g, 13.8 mmol) following the procedure described for **11a**. ¹H NMR (400 MHz, CDCl₃) δ 4.59 (br s, 1H), 3.10 – 3.07 (m, 2H), 2.68 (t, *J* = 6.6 Hz, 2H), 1.55 – 1.27 (m, 15H). MS (ESI) *m/z*: 205 (M+H)⁺.

Tert-butyl (2-aminoethyl)carbamate (11e)



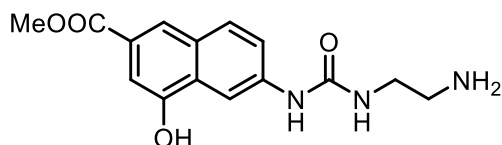
Compound **11e** was obtained as a white solid (0.789 g, 78%) starting from **19e** (1.66 g, 13.8 mmol) following the procedure described for **11a**. ¹H NMR (400 MHz, CDCl₃) δ 4.57 (br s, 1H), 3.12 – 3.05 (m, 2H), 2.64 (t, *J* = 6.6 Hz, 2H), 1.50 – 1.43 (m, 13H), 1.34 – 1.31 (m, 4H). MS (ESI) *m/z*: 220 (M+H)⁺.

Tert-butyl (2-aminoheptyl)carbamate (11f)



Compound **11f** was obtained as a white solid (0.854 g, 79%) starting from **19f** (1.87 g, 13.8 mmol) following the procedure described for **11a**. ¹H NMR (400 MHz, CDCl₃) δ 4.59 (br s, 1H), 3.10 – 3.05 (m, 2H), 2.65 (t, *J* = 6.8 Hz, 2H), 1.55 – 1.41 (m, 15H), 1.33 – 1.30 (m, 4H). MS (ESI) *m/z*: 235 (M+H)⁺.

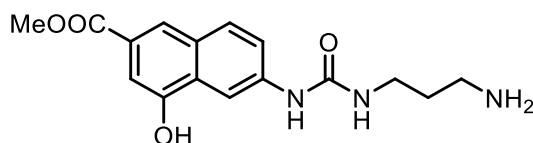
Methyl 6-(3-(3-aminoethyl)ureido)-4-hydroxy-2-naphthoate (12a)



Compound **21a** (0.700 g, 1.73 mmol) was dissolved in 10 mL of a solution of DCM/TFA (9:1) and the mixture was stirred for 48 h. The solvent was evaporated, and the resulting solid was washed with CHCl₃ to give TFA salt of compound **12a** as a brown solid (0.558 g, 80%). ¹H

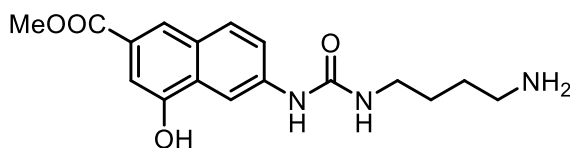
NMR (400 MHz, DMSO- d_6) δ 10.27 (s, 1H, exchangeable with D₂O), 9.01 (s, 1H, exchangeable with D₂O), 8.24 (d, J = 2.1 Hz, 1H), 7.98–7.92 (m, 1H), 7.88 (d, J = 8.9 Hz, 1H), 7.68 (br s, 3H, exchangeable with D₂O), 7.53 (dd, J = 8.9, 2.1 Hz, 1H), 7.31 (s, 1H), 6.47 (br t, 1H, exchangeable with D₂O), 3.87 (s, 3H), 3.29–3.12 (m, 2H), 2.97–2.78 (m, 2H). **MS** (ESI) m/z : 303 (M+H)⁺.

Methyl 6-(3-(3-aminopropyl)ureido)-4-hydroxy-2-naphthoate (12b)



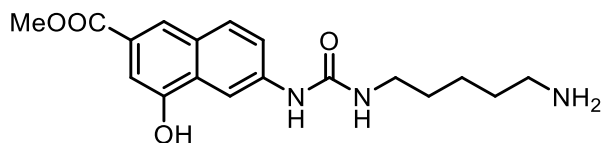
TFA salt of compound **12b** was obtained as a white solid (578 mg, 80%) starting from **21b** (700 mg, 1.67 mmol) following the procedure described for **12a**. **¹H NMR** (400 MHz, DMSO- d_6) δ 10.29 (s, 1H, exchangeable with D₂O), 9.02 (s, 1H, exchangeable with D₂O), 8.28 (d, J = 2.1 Hz, 1H), 7.99–7.94 (m, 1H), 7.89 (d, J = 8.9 Hz, 1H), 7.69 (br s, 3H, exchangeable with D₂O), 7.55 (dd, J = 8.9, 2.1 Hz, 1H), 7.30 (s, 1H), 6.49 (br t, 1H, exchangeable with D₂O), 3.86 (s, 3H), 3.29–3.10 (m, 2H), 2.99–2.79 (m, 2H), 1.85–1.58 (m, 2H).; **MS** (ESI) m/z : 318 (M+H)⁺.

Methyl 6-(3-(4-aminobutyl)ureido)-4-hydroxy-2-naphthoate (12c)



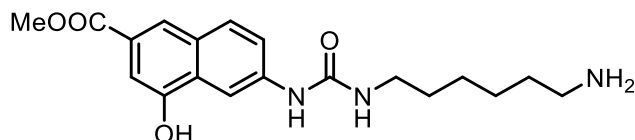
TFA salt of compound **12c** was obtained as a white solid (679 mg, 82%) starting from **21c** (800 mg, 1.86 mmol) following the procedure described for **12a**. **¹H NMR** (400 MHz, DMSO- d_6) δ 10.31 (s, 1H, exchangeable with D₂O), 8.99 (s, 1H, exchangeable with D₂O), 8.30 (d, J = 2.1 Hz, 1H), 7.98 (s, 1H), 7.86 (d, J = 8.9 Hz, 1H), 7.71 (br s, 3H, exchangeable with D₂O), 7.56 (dd, J = 8.9, 2.1 Hz, 1H), 7.31 (s, 1H), 6.45 (br t, 1H, exchangeable with D₂O), 3.85 (s, 3H), 3.16–3.08 (m, 2H), 2.83–2.74 (m, 2H), 1.66–1.43 (m, 4H); **MS** (ESI) m/z : 332 (M+H)⁺.

Methyl 6-(3-(5-aminopentyl)ureido)-4-hydroxy-2-naphthoate (12d)



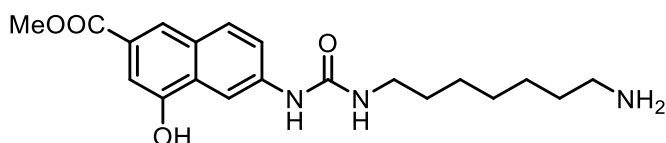
TFA salt of compound **12d** was obtained as a white solid (728 mg, 83%) starting from **21d** (850 mg, 1.91 mmol) following the procedure described for **12a**. **¹H NMR** (400 MHz, DMSO-*d*₆) δ 10.34 (s, 1H, exchangeable with D₂O), 8.95 (s, 1H, exchangeable with D₂O), 8.26 (d, *J* = 2.1 Hz, 1H), 7.97 (s, 1H), 7.89 (d, *J* = 8.9 Hz, 1H), 7.67 (br s, 3H, exchangeable with D₂O), 7.54 (dd, *J* = 8.9, 2.1 Hz, 1H), 7.29 (s, 1H), 6.85 (br t, 1H, exchangeable with D₂O), 3.86 (s, 3H), 3.11 (m, 2H), 2.85–2.73 (m, 2H), 1.63–1.42 (m, 4H), 1.39–1.27 (m, 2H).; **MS** (ESI) *m/z*: 346 (M+H)⁺.

Methyl 6-(3-(6-aminohexyl)ureido)-4-hydroxy-2-naphthoate (12e)



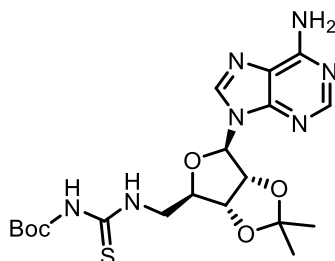
TFA salt of compound **12e** was obtained as a white solid (745 mg, 85%) starting from compound **21e** (850 mg, 1.85 mmol) following the procedure described for **12a**. **¹H NMR** (400 MHz, DMSO-*d*₆) δ 10.34 (s, 1H, exchangeable with D₂O), 8.92 (s, 1H, exchangeable with D₂O), 8.28 (d, *J* = 2.1 Hz, 1H), 7.99–7.94 (m, 1H), 7.88 (d, *J* = 8.9 Hz, 1H), 7.68 (br s, 3H, exchangeable with D₂O), 7.54 (dd, *J* = 8.9, 2.1 Hz, 1H), 7.29 (s, 1H), 6.37 (br t, 1H, exchangeable with D₂O), 3.86 (s, 3H), 3.16–3.09 (m, 2H), 2.83–2.75 (m, 2H), 1.59–1.46 (m, 6H), 1.39–1.34 (m, 2H). **MS** (ESI) *m/z*: 360 (M+H)⁺.

Methyl 6-(3-(7-aminoheptyl)ureido)-4-hydroxy-2-naphthoate (12f)



TFA salt of compound **12f** was obtained as a white solid (750 mg, 81%) starting from compound **21f** (900 mg, 1.90 mmol) following the procedure described for **12a**. ¹H NMR (400 MHz, DMSO-*d*₆) δ 10.29 (s, 1H, exchangeable with D₂O), 8.82 (s, 1H, exchangeable with D₂O), 8.27 (d, *J* = 2.2 Hz, 1H), 7.98–7.94 (m, 1H), 7.85 (d, *J* = 8.8 Hz, 1H), 7.68 (br s, 3H, exchangeable with D₂O), 7.53 (dd, *J* = 8.8, 2.2 Hz, 1H), 7.30 (s, 1H), 6.26 (br t, 1H, exchangeable with D₂O), 3.86 (s, 3H), 3.16–3.05 (m, 4H), 1.51–1.42 (m, 6H), 1.34–1.30 (m, 4H). MS (ESI) *m/z*: 374 (M+H)⁺.

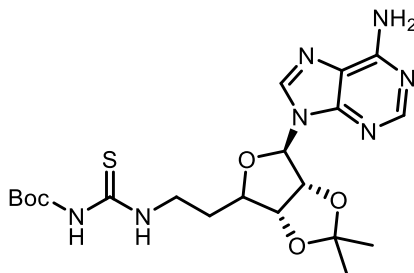
Tert-butyl (9-((3*aR*,4*R*,6*R*,6*aR*)-6-((3-*tert*-butoxythioureido)methyl)-2,2-dimethyltetrahydrofuro[3,4-*d*][1,3]dioxol-4-yl)-9*H*-purin-6-yl)carbamate (**13a**)



To a cooled solution of *N,N'*-bis-*tert*-butoxycarbonylthiourea **26** (1.00 g, 3.62 mmol) dissolved in dry THF, NaH (60% dispersion in mineral oil, 173 mg, 4.34 mmol) was added and the resulting mixture was stirred at the same temperature for 1 h. Then, TFAA (603 μL, 4.34 mmol) was added and the stirring continued for additional 1 h at 0 °C, afterward amine **22** (1.61 g, 3.96 mmol) was added and the resulting suspension was stirred for 16 h. The crude was diluted with brine (50 mL) and the aqueous phase was extracted with AcOEt (3 × 25 mL). The collected organic phases were washed with brine, dried (Na₂SO₄) and concentrated under vacuum, yielding a residue that was purified by column chromatography (gradient Hex/AcOEt 80:20 to 40:50 + 10% MeOH) to give **13a** as white solid (716 mg, 35%). ¹H NMR (400 MHz, CDCl₃) δ 9.80 (t, *J* = 4.3 Hz, 1H, exchangeable with D₂O), 8.76 (s, 1H, exchangeable with D₂O), 8.07 (s, 1H, exchangeable with D₂O), 7.92 (s, 1H), 7.84 (s, 1H), 6.14 (d, *J* = 2.5 Hz, 1H), 5.42 (dd,

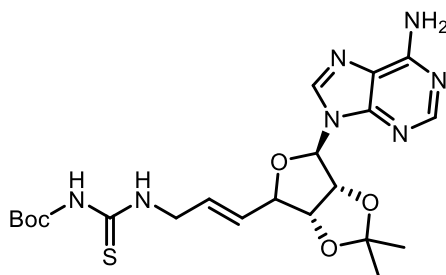
$J = 6.4, 2.5$ Hz, 1H), 5.09 (dd, $J = 6.4, 3.7$ Hz, 1H), 4.54–4.50 (m, 1H), 4.18–3.94 (m, 2H), 1.62 (s, 3H), 1.57 (s, 9H), 1.45 (s, 9H), 1.39 (s, 3H); **MS** (ESI) m/z : 566 (M+H)⁺.

Tert-butyl (9-((3*aR*,4*R*,6*R*,6*aR*)-6-((3-*tert*-butyloxythioureido)ethyl)-2,2-dimethyl tetrahydrofuro[3,4-*d*][1,3]dioxol-4-yl)-9*H*-purin-6-yl)carbamate (**13b**)



Compound **13b** was obtained as a white solid (198 mg, 53%) starting from **23** (350 mg, 1.09 mmol) following the procedure described for **13a**. **¹H NMR** (400 MHz, CDCl₃) δ 9.77 (br s, 1H, exchangeable with D₂O), 8.34 (s, 1H), 8.14 (br s, 1H, exchangeable with D₂O), 7.88 (s, 1H), 6.04 (d, $J = 2.5$ Hz, 1H), 5.89 (br s, 2H, exchangeable with D₂O), 5.47 (dd, $J = 6.6, 2.5$ Hz, 1H), 4.97 (dd, $J = 6.6, 4.0$ Hz, 1H), 4.29–4.24 (m, 1H), 3.90–3.80 (m, 1H), 3.69–3.59 (m, 1H), 2.17–2.10 (m, 2H), 1.60 (s, 3H), 1.38 (s, 12H); **MS** (ESI) m/z : 480 (M+H)⁺.

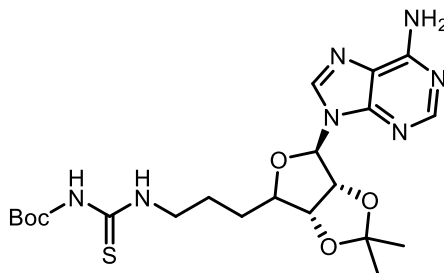
Tert-butyl (9-((3*aR*,4*R*,6*R*,6*aR*)-6-((3-*tert*-butyloxythioureido)propyl-1-en)-2,2-dimethyl tetrahydrofuro[3,4-*d*][1,3]dioxol-4-yl)-9*H*-purin-6-yl)carbamate (**13c**)



Compound **13c** was obtained as a white solid (121 mg, 33%) starting from **24** (250 mg, 0.75 mmol) following the procedure described for **13a**. **¹H NMR** (400 MHz, CHCl₃) δ 9.70 (br s, 1H exchangeable with D₂O), 8.37 (s, 1H), 8.01 (br s, 1H, exchangeable with D₂O), 7.88 (s, 1H), 6.09 (d, $J = 2.1$ Hz, 1H), 5.85–5.79 (m, 2H), 5.75 (br s, 2H, exchangeable with D₂O), 5.51 (dd,

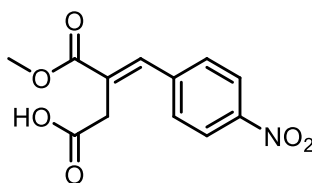
$J = 6.3, 2.0$ Hz, 1H), 5.03 (dd, $J = 6.4, 3.5$ Hz, 1H), 4.73–4.66 (m, 1H), 4.23–4.19 (m, 2H), 1.62 (s, 3H), 1.48 (s, 9H), 1.39 (s, 3H); **MS** (ESI) m/z : 492 (M+H)⁺.

Tert-butyl (9-((3*aR*,4*R*,6*R*,6*aR*)-6-((3-*tert*-butoxythioureido)propyl)-2,2-dimethyl tetrahydrofuro[3,4-*d*][1,3]dioxol-4-yl)-9*H*-purin-6-yl)carbamate (**13d**)



Compound **13d** was obtained as a white solid (191 mg, 35%) starting from **25** (250 mg, 0.75 mmol) following the procedure described for **13a**. **¹H NMR** (400 MHz, CDCl₃) δ 9.77 (br s, 1H, exchangeable with D₂O), 8.34 (s, 1H), 8.14 (br s, 1H, exchangeable with D₂O), 7.88 (s, 1H), 6.03 (d, $J = 2.5$ Hz, 1H), 5.89 (br s, 2H, exchangeable with D₂O), 5.45 (dd, $J = 6.6, 2.5$ Hz, 1H), 4.92 (dd, $J = 6.6, 4.0$ Hz, 1H), 4.29–4.24 (m, 1H), 3.70–3.58 (m, 2H), 1.82–1.74 (m, 2H), 1.70–1.64 (m, 2H), 1.61 (s, 3H), 1.47 (s, 9H), 1.38 (s, 3H); **MS** (ESI) m/z : 494 (M+H)⁺.

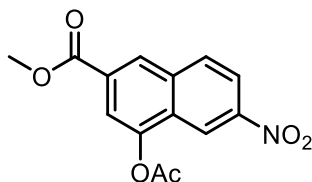
(*E*)-3-(Methoxycarbonyl)-4-(4-nitrophenyl)but-3-enoic acid (**16**)



Carboxyphosphorane **15** (13.0 g, 35.2 mmol) was suspended in toluene (150 mL) and 4-nitrobenzaldehyde **14** (5.74 g, 38.0 mmol) was then added. The resulting mixture was stirred at 25 °C for 48 h and then extracted with saturated solution of NaHCO₃ (3 x 70 mL). The aqueous phase was washed with Et₂O, acidified with concd HCl and the white solid formed was collected by filtration (8.60 g, 92%) and directly used in the following step without further purification.

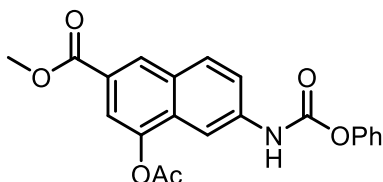
¹H NMR (400 MHz, DMSO-*d*₆) δ (d, *J* = 9 Hz, 2H), 7.86 (s, 1H), 7.69 (d, *J* = 9 Hz, 2H), 3.78 (s, 3H), 3.43 (s, 2H); **MS** (ESI) *m/z*: 266 [M+H]⁺.

Methyl 4-acetoxy-6-nitro-2-naphthoate (17)



A round-bottomed flask containing a magnetic stirring bar and fitted with a reflux condenser was charged with a mixture of **16** (5.0 g, 18.85 mmol), Ac₂O (35 mL) and NaOAc (2.30 g, 28.27 mmol). The flask was subjected to MW irradiation (power 300 W) for 15 min keeping temperature below 120°C (air flow cooling). The reaction mixture was filtered, and the filtrate was concentrated to give **17** as a yellow solid (5.17 g, 95%). **¹H NMR** (400 MHz, CDCl₃) δ 8.89 (d, *J* = 2 Hz, 1H), 8.62 (s, 1H), 8.38 (dd, *J* = 9, 2 Hz, 1H), 8.17 (d, *J* = 9 Hz, 1H), 8.05 (s, 1H), 4.05 (s, 3H), 2.59 (s, 3H); **MS** (ESI) *m/z*: 290 [M+H]⁺.

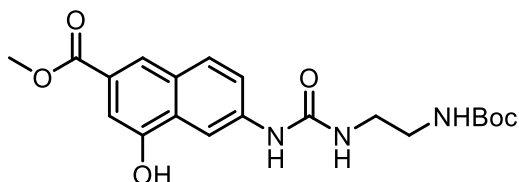
Methyl 4-acetoxy-6-((phenoxycarbonyl)amino)-2-naphthoate (18)



Compound **10** (2.68 g, 10.33 mmol) was dissolved in AcOEt and then TEA (1.58 mL, 11.37 mmol) was added. The resulting mixture was cooled at 0° C and phenyl chloroformate (1.94 mL, 15.50 mmol) was added dropwise. The yellow suspension obtained was allowed to warm to room temperature and stirred for 16 h. The reaction was then diluted with AcOEt (60 mL), washed with water (3 × 20 mL), HCl 1N (3 × 20 mL), NaHCO₃ saturated solution (3 × 20 mL), and brine (30 mL), dried over Na₂SO₄, filtered, and concentrated under reduced pressure. The resulting solid was crystallized from AcOEt to give the title compound **18** as a pale-yellow solid

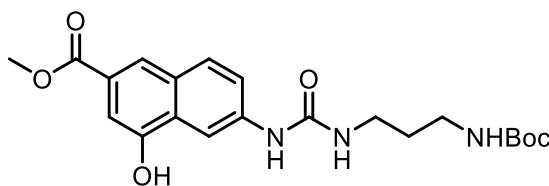
(2.74 g, 70%). **¹H NMR** (400 MHz, DMSO-*d*₆) δ 10.74 (s, 1H, exchangeable with D₂O), 8.50 (s, 1H), 8.23–8.14 (m, 2H), 7.79–7.72 (m, 2H), 7.49–7.43 (m, 2H), 7.33–7.24 (m, 3H), 3.91 (s, 3H), 2.41 (s, 3H); **MS** (ESI) *m/z*: 380 (M+H)⁺.

Methyl 6-(3-(3-((tert-butoxycarbonyl)amino)ethyl)ureido)-4-hydroxy-2-naphthoate (21a)



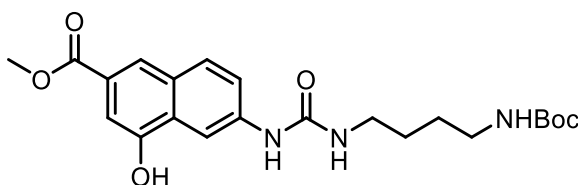
To a stirring solution of methyl 4-acetoxy-6-((phenoxycarbonyl)amino)-2-naphthoate **18** (0.40 g, 1.05 mmol) in dry DMF (5 mL), a solution of tert-butyl (2-aminoethyl)carbamate **11a** (0.336 g, 2.1 mmol) and TEA (294 μL, 2.1 mmol) in dry DMF (5 mL) was added and the reaction was stirred at room temperature for 2 h. NaHCO₃ saturated solution was added (25 mL) and the resulting mixture was extracted with AcOEt (3 × 25 mL). The combined organic layers were washed with NaHCO₃ saturated solution (2 × 10 mL) and brine (10 mL), dried over Na₂SO₄, filtered, and concentrated under reduced pressure to give a light brown solid that was purified by flash chromatography (gradient AcOEt/MeOH 100:0 to 90:10) yielding a mixture of acetylated and deacetylated compounds. Therefore, the solid was suspended in DCM (30 mL) and piperidine (580 μL) was added. After 1 h, the solvent was removed, and the crude product was diluted with AcOEt (50 mL). The organic layer was washed with HCl 1 N (3 × 20 mL) and brine (30 mL), dried over Na₂SO₄, filtered, and concentrated under reduced pressure, yielding compound **21a** as an orange solid. **¹H NMR** (400 MHz, DMSO-*d*₆) δ 10.28 (s, 1H, exchangeable with D₂O), 8.91 (s, 1H, exchangeable with D₂O), 8.27 (d, *J* = 2.1 Hz, 1H), 7.97 (s, 1H), 7.89 (d, *J* = 8.9 Hz, 1H), 7.55 (dd, *J* = 8.9, 2.1 Hz, 1H), 7.30 (s, 1H), 6.85 (t, *J* = 5.0 Hz, 1H, exchangeable with D₂O), 6.25 (t, *J* = 5.7 Hz, 1H, exchangeable with D₂O), 3.87 (s, 3H), 3.14–3.08 (m, 2H), 3.01–2.94 (m, 2H), 1.40 (s, 9H). **MS** (ESI) *m/z*: 404 (M+H)⁺.

Methyl 6-(3-(3-((tert-butoxycarbonyl)amino)propyl)ureido)-4-hydroxy-2-naphthoate (21b)



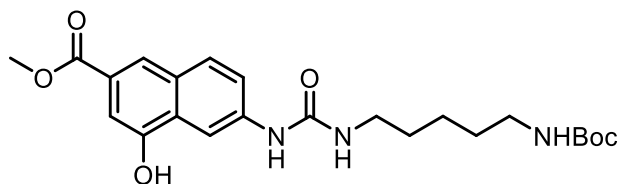
Compound **21b** was obtained as a yellow solid by reaction of **18** (856 mg, 2.26 mmol) with tert-butyl (3-aminopropyl)carbamate **11b** (786 mg, 4.51 mmol), following the procedure described for **21a**. ¹H NMR (400 MHz, DMSO-*d*₆) δ 10.28 (s, 1H, exchangeable with D₂O), 8.91 (s, 1H, exchangeable with D₂O), 8.27 (d, *J* = 2.1 Hz, 1H), 7.97 (s, 1H), 7.89 (d, *J* = 8.9 Hz, 1H), 7.55 (dd, *J* = 8.9, 2.1 Hz, 1H), 7.30 (s, 1H), 6.85 (t, *J* = 5.0 Hz, 1H, exchangeable with D₂O), 6.25 (t, *J* = 5.7 Hz, 1H, exchangeable with D₂O), 3.87 (s, 3H), 3.14–3.08 (m, 2H), 3.01–2.94 (m, 2H), 1.59–1.50 (m, 2H), 1.40 (s, 9H). MS (ESI) *m/z*: 418 (M+H)⁺.

Methyl 6-(3-(4-((tert-butoxycarbonyl)amino)butyl)ureido)-4-hydroxy-2-naphthoate (21c)



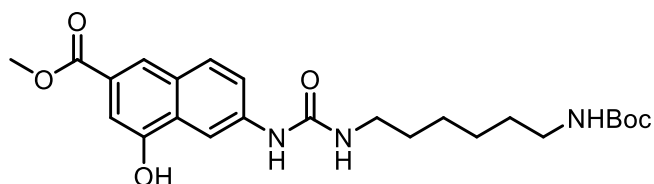
Compound **21c** was obtained as a yellow solid by reaction of **18** (856 mg, 2.26 mmol) with tert-butyl (4-aminobutyl)carbamate **11c** (849 mg, 4.51 mmol), following the procedure described for **21a**. ¹H NMR (400 MHz, DMSO-*d*₆) δ 10.30 (s, 1H, exchangeable with D₂O), 8.80 (s, 1H, exchangeable with D₂O), 8.26 (d, *J* = 2.1 Hz, 1H), 7.97 (s, 1H), 7.90 (d, *J* = 8.9 Hz, 1H), 7.54 (dd, *J* = 8.9, 2.1 Hz, 1H), 7.29 (s, 1H), 6.82 (t, *J* = 5.0 Hz, 1H, exchangeable with D₂O), 6.22 (t, *J* = 5.7 Hz, 1H, exchangeable with D₂O), 3.85 (s, 3H), 3.17–3.03 (m, 2H), 3.02–2.86 (m, 2H), 1.53–1.29 (m, 13H); MS (ESI) *m/z*: 432 (M+H)⁺.

Methyl 6-(3-(5-((tert-butoxycarbonyl)amino)pentyl)ureido)-4-hydroxy-2-naphthoate (21d)



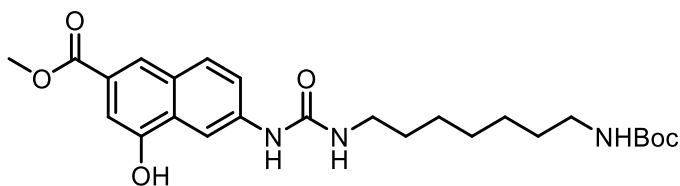
Compound **21d** was obtained as a yellow solid by reaction of **18** (856 mg, 2.26 mmol) with tert-butyl (5-aminopentyl)carbamate **11d** (911 mg, 4.51 mmol), following the procedure described for **21a**. **¹H NMR** (400 MHz, DMSO-*d*₆) δ 10.31 (s, 1H, exchangeable with D₂O), 8.83 (s, 1H, exchangeable with D₂O), 8.27 (d, *J* = 2.3 Hz 1H), 7.96 (s, 1H), 7.88 (d, *J* = 8.7 Hz, 1H), 7.52 (dd, *J* = 8.7, 2.3 Hz, 1H), 7.30 (s, 1H), 6.81 (t, *J* = 4.8 Hz, 1H, exchangeable with D₂O), 6.25 (t, *J* = 5.1 Hz, 1H, exchangeable with D₂O), 3.85 (s, 3H), 3.17–3.03 (m, 2H), 3.02–2.86 (m, 2H), 1.53–1.29 (m, 15H); **MS** (ESI) *m/z*: 446 (M+H)⁺.

Methyl 6-(3-((tert-butoxycarbonyl)amino)hexyl)ureido-4-hydroxy-2-naphthoate (21e)



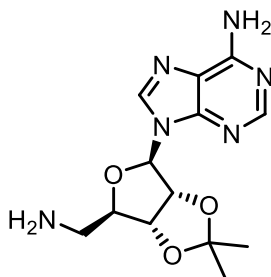
Compound **21e** was obtained as a yellow solid by reaction of **18** (856 mg, 2.26 mmol) with tert-butyl (6-aminoethyl)carbamate **11e** (974 mg, 4.51 mmol), following the procedure described for **21a**. **¹H NMR** (400 MHz, DMSO-*d*₆) δ 10.32 (s, 1H, exchangeable with D₂O), 8.84 (s, 1H, exchangeable with D₂O), 8.28 (d, *J* = 2.4 Hz 1H), 7.96 (s, 1H), 7.87 (d, *J* = 8.5 Hz, 1H), 7.52 (dd, *J* = 8.5, 2.4 Hz, 1H), 7.28 (s, 1H), 6.80 (t, *J* = 5.1 Hz, 1H, exchangeable with D₂O), 6.24 (t, *J* = 5.0 Hz, 1H, exchangeable with D₂O), 3.85 (s, 3H), 3.19–3.05 (m, 2H), 3.03–2.89 (m, 2H), 1.58–1.26 (m, 17H); **MS** (ESI) *m/z*: 460 (M+H)⁺.

Methyl 6-(3-(7-((*tert*-butoxycarbonyl)amino)heptyl)ureido)-4-hydroxy-2-naphthoate (21f)



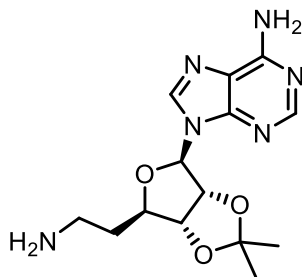
Compound **21f** was obtained as a yellow solid by reaction of **18** (856 mg, 2.26 mmol) with *tert*-butyl (7-aminoheptyl)carbamate **11f** (1.04 g, 4.51 mmol), following the procedure described for **21a**. **¹H NMR** (400 MHz, DMSO-*d*₆) δ 10.27 (s, 1H, exchangeable with D₂O), 8.82 (s, 1H, exchangeable with D₂O), 8.27 (d, *J* = 2.1 Hz, 1H), 7.97 (s, 1H), 7.88 (d, *J* = 8.9 Hz, 1H), 7.53 (dd, *J* = 8.9, 2.2 Hz, 1H), 7.30 (s, 1H), 6.81 (t, *J* = 5.0 Hz, 1H, exchangeable with D₂O), 6.26 (t, *J* = 5.2 Hz, 1H, exchangeable with D₂O), 3.86 (s, 3H), 3.16–3.05 (m, 4H), 1.51–1.42 (m, 4H), 1.53–1.30 (m, 15H). **MS** (ESI) *m/z*: 474 (M+H)⁺.

9-((4*R*,6*R*)-6-(aminomethyl)-2,2-dimethyltetrahydrofuro[3,4-*d*][1,3]dioxol-4-yl)-9*H*-purin-6-amine (22)



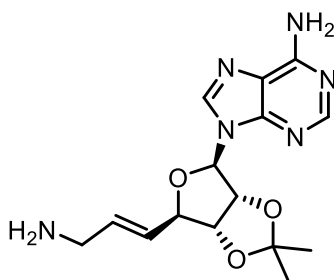
Pd/C (5 wt % on activated carbon, 0.1 equiv) was added to a solution of **33** (1.00 g, 3.01 mmol) in MeOH (100 mL) and the reaction was stirred under H₂ (1 atm, balloon) for 16 h. The reaction mixture was filtered and concentrated to give the title compound **22**, used in the next step without further purification. **¹H NMR** (400 MHz, DMSO-*d*₆) δ 8.37 (s, 1H), 8.16 (s, 1H), 7.32 (br s, 2H), 6.08 (d, *J* = 3.2 Hz, 1H), 5.45 (dd, *J* = 6.4, 3.3 Hz, 1H), 4.98 (dd, *J* = 6.4, 2.7 Hz, 1H), 4.09 (td, *J* = 5.8, 2.6 Hz, 1H), 2.70 (m, 2H), 1.54 (s, 3H), 1.33 (s, 3H); **MS** (ESI) *m/z*: 307 (M+H)⁺.

9-((4R,6R)-6-(2-aminoethyl)-2,2-dimethyltetrahydrofuro[3,4-d][1,3]dioxol-4-yl)-9H-purin-6-amine (23)



35 (0.25 g, 0.60 mmol) was dissolved in 10 mL of a solution of DCM/TFA (95:5) and the mixture was stirred at room temperature. After 24 h, the solvent was removed under vacuum, the crude was resuspended in a solution of citric acid 10%. The aqueous solution was washed with DCM (3 × 25 mL), basified with NaOH 2 N until pH 12 and then extracted with CHCl₃ (3 × 25 mL). The collected organic phases were dried (Na₂SO₄), filtered and concentrated under vacuum to give **23** as a white solid (0.30 g, 65%). ¹H NMR (400 MHz, CDCl₃) δ 8.35 (s, 1H), 7.89 (s, 1H), 6.03 (d, *J* = 2.4 Hz, 1H), 5.70 (br s, 2H), 5.48 (dd, *J* = 6.5, 2.4 Hz, 1H), 4.90 (dd, *J* = 6.5, 4.1 Hz, 1H), 4.33–4.21 (m, 1H), 2.86–2.72 (m, 2H), 1.90–1.78 (m, 2H), 1.61 (s, 3H), 1.39 (s, 3H); MS (ESI) *m/z*: 321 (M+H)⁺.

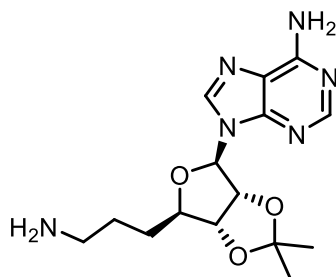
9-((4R,6R)-6-((E)-3-aminoprop-1-en-1-yl)-2,2-dimethyltetrahydrofuro[3,4-d][1,3]dioxol-4-yl)-9H-purin-6-amine (24)



To a stirred solution of compound **38** (0.40 g, 0.86 mmol) in MeOH (2 mL), a solution of hydrazine monohydrate (0.87 g, 1.73 mmol) was added, and the mixture was stirred at room temperature for 16 h. Then, the solvent was evaporated, and the crude residue was resuspended

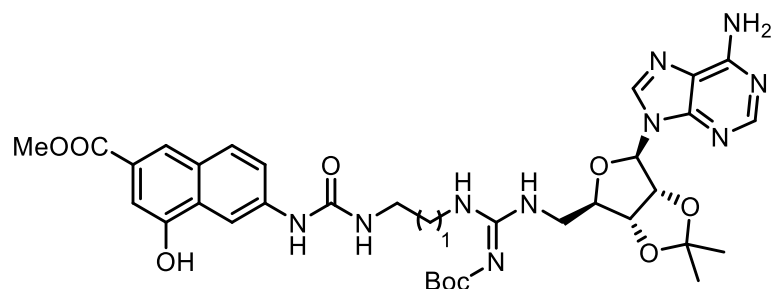
in a solution of citric acid 10%. The aqueous solution was washed with DCM (3×25 mL), basified with NaOH 2 N until pH 12 and then extracted with CHCl_3 (3×25 mL). The collected organic phases were dried (Na_2SO_4), filtered and concentrated under vacuum to give the amine **24** as a white solid (0.26 g, 90%). ^1H NMR (400 MHz, CDCl_3) δ 8.35 (s, 1H), 7.87 (s, 1H), 6.08 (d, $J = 2.0$ Hz, 1H), 5.87 (br s, 2H), 5.82–5.79 (m, 1H), 5.75–5.65 (m, 1H), 5.53 (dd, $J = 6.3, 2.0$ Hz, 1H), 4.99 (dd, $J = 6.4, 3.5$ Hz, 1H), 4.71–4.66 (m, 1H), 3.23–3.20 (m, 2H), 1.62 (s, 3H), 1.39 (s, 3H); MS (ESI) m/z : 333 ($\text{M}+\text{H}$) $^+$.

9-((4R,6R)-6-(3-aminopropyl)-2,2-dimethyltetrahydrofuro[3,4-d][1,3]dioxol-4-yl)-9H-purin-6-amine (25)



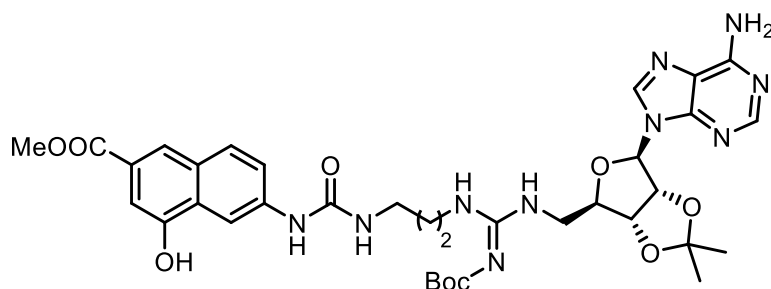
Compound **25** was obtained as a white solid (0.35 g, 99%) starting from **24** (0.35 g, 1.05 mmol) following the procedure described for **22**. ^1H NMR (400 MHz, CDCl_3) δ 8.37 (s, 1H), 7.89 (s, 1H), 6.06 (d, $J = 2.4$ Hz, 1H), 5.72 (br s, 2H), 5.48 (dd, $J = 6.5, 2.4$ Hz, 1H), 4.95 (dd, $J = 6.5, 4.1$ Hz, 1H), 4.35–4.24 (m, 1H), 2.86–2.72 (m, 2H), 1.97–1.65 (m, 4H), 1.61 (s, 3H), 1.39 (s, 3H); MS (ESI) m/z : 335 ($\text{M}+\text{H}$) $^+$.

Methyl 6-(3-(3-((E)-2-(tert-butoxycarbonyl)-3-(((3aR,4R,6R,6aR)-6-(6-((tert-butoxycarbonyl)amino)-9H-purin-9-yl)-2,2-dimethyltetrahydrofuro[3,4-d][1,3]dioxol-4-yl) methyl) guanidino)ethyl)ureido)-4-hydroxy-2-naphthoate (27a)



To a stirred suspension of **13a** (100 mg, 0.177 mmol) and **12a** (0.147 g, 0.354 mmol) in dry DCM, EDC hydrochloride (69 mg, 0.354 mmol) and TEA (74 μ L, 0.531 mmol) were added at room temperature. The resulting mixture was stirred for 18 h, then solvent was evaporated under reduced pressure and the resulting oil was taken up with water. The aqueous phase was extracted with AcOEt (3 x 25 mL), the collected organic phases were washed with brine, dried (Na_2SO_4) and concentrated under reduced pressure. The crude material was purified by flash chromatography (gradient DCM/MeOH 95:5 to 90:10) yielding **27a** as white solid (0.109 g, 74%). $^1\text{H NMR}$ (400 MHz, $\text{DMSO}-d_6$) δ 10.28 (s, 1H, exchangeable with D_2O), 10.18 (s, 1H, exchangeable with D_2O), 8.83 (s, 1H, exchangeable with D_2O), 8.66–8.62 (m, 2H), 8.24 (d, $J = 2.2$ Hz, 1H), 7.95 (s, 1H), 7.87 (d, $J = 8.9$ Hz, 1H), 7.54 (dd, $J = 8.9, 2.2$ Hz, 1H), 7.28 (s, 1H), 6.32 (br t, 1H, exchangeable with D_2O), 6.25 (s, 1H), 5.51–5.46 (m, 1H), 5.08–5.02 (m, 1H), 4.34–4.29 (m, 1H), 3.85 (s, 3H), 3.45–3.39 (m, 2H), 3.20–3.08 (m, 4H), 1.54 (s, 3H), 1.46 (s, 9H), 1.35 (s, 9H), 1.32 (s, 3H); **MS** (ESI) m/z : 835 ($\text{M}+\text{H}$) $^+$.

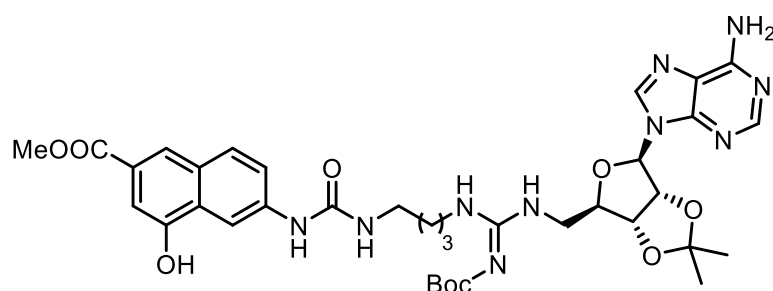
Methyl 6-(3-(3-((E)-2-(tert-butoxycarbonyl)-3-(((3aR,4R,6R,6aR)-6-(6-((tert-butoxycarbonylamino)-9H-purin-9-yl)-2,2-dimethyltetrahydrofuro[3,4-d][1,3]dioxol-4-yl)methyl)guanidino)propyl)ureido)-4-hydroxy-2-naphthoate (27b)



Compound **27b** was obtained as a white solid (114 mg, 75%) by reaction of **13a** (100 mg, 0.177 mmol) with compound **12b** (152 mg, 0.354 mmol) following the procedure described for **27a**.

¹H NMR (400 MHz, DMSO-*d*₆) δ 10.28 (s, 1H, exchangeable with D₂O), 10.18 (s, 1H, exchangeable with D₂O), 8.83 (s, 1H, exchangeable with D₂O), 8.66–8.62 (m, 2H), 8.24 (d, *J* = 2.2 Hz, 1H), 7.95 (s, 1H), 7.87 (d, *J* = 8.9 Hz, 1H), 7.54 (dd, *J* = 8.9, 2.2 Hz, 1H), 7.28 (s, 1H), 6.32 (br t, 1H, exchangeable with D₂O), 6.25 (s, 1H), 5.51–5.46 (m, 1H), 5.08–5.02 (m, 1H), 4.34–4.29 (m, 1H), 3.85 (s, 3H), 3.45–3.39 (m, 2H), 3.20–3.08 (m, 4H), 1.70–1.60 (m, 2H), 1.54 (s, 3H), 1.46 (s, 9H), 1.35 (s, 9H), 1.32 (s, 3H); **MS** (ESI) *m/z*: 849 (M+H)⁺.

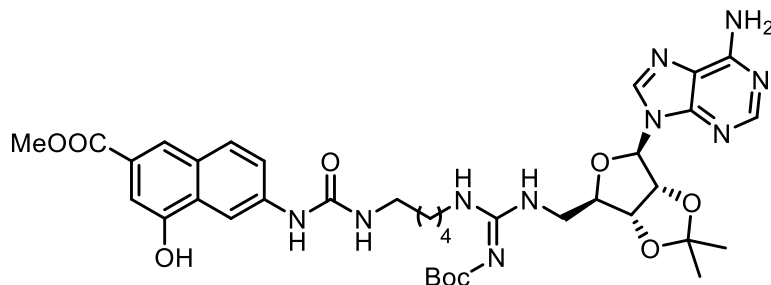
Methyl 6-(3-(4-((*E*)-2-(*tert*-butoxycarbonyl)-3-(((3*aR*,4*R*,6*R*,6*aR*)-6-(6-((*tert*-butoxycarbonyl)amino)-9*H*-purin-9-yl)-2,2-dimethyltetrahydrofuro[3,4-*d*][1,3]dioxol-4-yl)methyl)guanidino)butyl)ureido)-4-hydroxy-2-naphthoate (27c)



Compound **27c** was obtained as a white solid (37 mg, 72%) by reaction of **13a** (52 mg, 0.060 mmol) with compound **12c** (53 mg, 0.120 mmol) following the procedure described for **27a**.

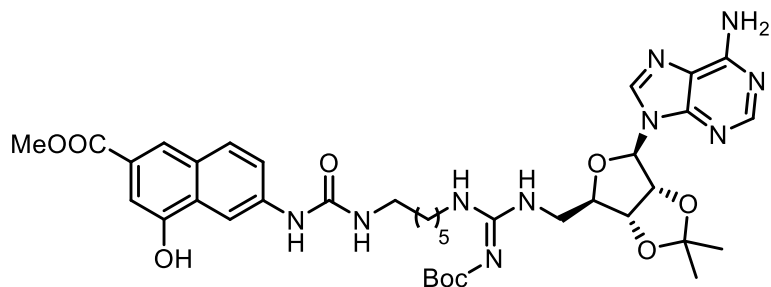
¹H NMR (400 MHz, DMSO-*d*₆) δ 10.27 (s, 1H, exchangeable with D₂O), 10.15 (s, 1H, exchangeable with D₂O), 8.86 (s, 1H, exchangeable with D₂O), 8.69–8.58 (m, 2H), 8.26 (d, *J* = 2.2 Hz, 1H), 7.96 (s, 1H), 7.87 (d, *J* = 8.9 Hz, 1H), 7.55 (dd, *J* = 8.9, 2.2 Hz, 1H), 7.29 (s, 1H), 6.31 (br t, 1H, exchangeable with D₂O), 6.24 (s, 1H), 5.53–5.45 (m, 1H), 5.12–4.94 (m, 1H), 4.39–4.28 (m, 1H), 3.85 (s, 3H), 3.44–3.38 (m, 2H), 3.17–3.07 (m, 4H), 1.58–1.51 (m, 4H), 1.49–1.46 (m, 12H), 1.37 (s, 9H), 1.30 (s, 3H); **MS** (ESI) *m/z*: 863 (M+H)⁺.

Methyl 6-(3-(5-((*E*)-2-(*tert*-butoxycarbonyl)-3-(((3*aR*,4*R*,6*R*,6*aR*)-6-(6-((*tert*-butoxycarbonyl)amino)-9*H*-purin-9-yl)-2,2-dimethyltetrahydrofuro[3,4-*d*][1,3]dioxol-4-yl)methyl)guanidino)pentyl)ureido)-4-hydroxy-2-naphthoate (27d)



Compound **27d** was obtained as a white solid (197 mg, 77%) by reaction of compound **13a** (165 mg, 0.292 mmol) with compound **12d** (268 mg, 0.584 mmol) following the procedure described for **27a**. ¹H NMR (400 MHz, DMSO-*d*₆) δ 10.29 (s, 1H, exchangeable with D₂O), 10.15 (s, 1H, exchangeable with D₂O), 8.86 (s, 1H, exchangeable with D₂O), 8.64–8.59 (m, 2H), 8.26 (d, *J* = 2.2 Hz, 1H), 7.96 (s, 1H), 7.88 (d, *J* = 8.9 Hz, 1H), 7.55 (dd, *J* = 8.9, 2.2 Hz, 1H), 7.29 (s, 1H), 6.29 (br t, 1H, exchangeable with D₂O), 6.24 (s, 1H), 5.52–5.46 (m, 1H), 5.13–5.02 (m, 1H), 4.36–4.31 (m, 1H), 3.86 (s, 3H), 3.45–3.39 (m, 2H), 3.21–3.11 (m, 4H), 1.55(s, 3H), 1.48 (s, 9H), 1.40–1.17 (m, 18H); MS (ESI) *m/z*: 878 (M+H)⁺.

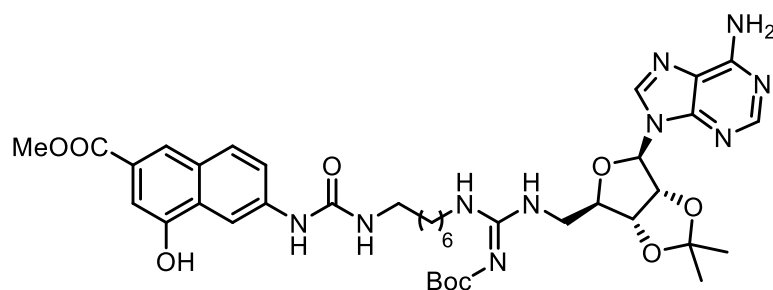
Methyl 6-(3-(6-((*E*)-2-(*tert*-butoxycarbonyl)-3-(((3*aR*,4*R*,6*R*,6*aR*)-6-(6-((*tert*-butoxycarbonyl)amino)-9*H*-purin-9-yl)-2,2-dimethyltetrahydrofuro[3,4-*d*][1,3]dioxol-4-yl)methyl)guanidino)hexyl)ureido)-4-hydroxy-2-naphthoate (27e)



Compound **27e** was obtained as a white solid (195 mg, 73%) by reaction of **13a** (170 mg, 0.300 mmol) with compound **12e** (284 mg, 0.600 mmol) following the procedure described for **27a**. ¹H NMR (400 MHz, DMSO-*d*₆) δ 10.29 (s, 1H, exchangeable with D₂O), 10.16 (s, 1H,

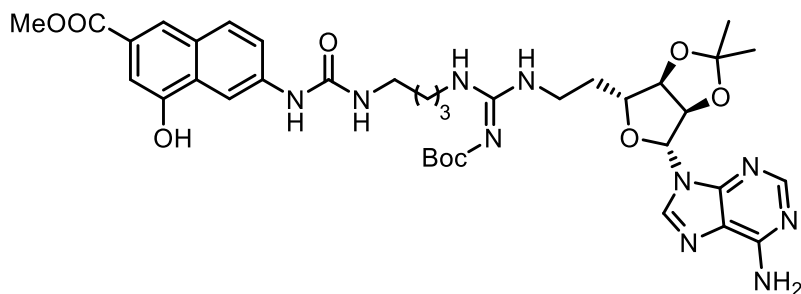
exchangeable with D₂O), 8.85 (s, 1H, exchangeable with D₂O), 8.60–8.54 (m, 2H), 8.27 (d, *J* = 2.3 Hz, 1H), 7.98 (s, 1H), 7.89 (d, *J* = 8.9 Hz, 1H), 7.61 (dd, *J* = 8.9, 2.3 Hz, 1H), 7.33 (s, 1H), 6.34 (br t, 1H, exchangeable with D₂O), 6.29 (s, 1H), 5.55–5.49 (m, 1H), 5.13–5.05 (m, 1H), 4.34–4.28 (m, 1H), 3.86 (s, 3H), 3.47–3.41 (m, 2H), 3.26–3.13 (m, 4H), 2.31–2.23 (m, 4H), 1.59 (s, 3H), 1.48–1.43 (m, 13H), 1.39–1.32 (m, 12H); **MS** (ESI) *m/z*: 892 (M+H)⁺.

Methyl 6-(3-(7-((*E*)-2-(*tert*-butoxycarbonyl)-3-(((3*aR*,4*R*,6*R*,6*aR*)-6-(6-((*tert*-butoxycarbonyl)amino)-9*H*-purin-9-yl)-2,2-dimethyltetrahydrofuro[3,4-*d*][1,3]dioxol-4-yl)methyl)guanidino)heptyl)ureido)-4-hydroxy-2-naphthoate (27f)



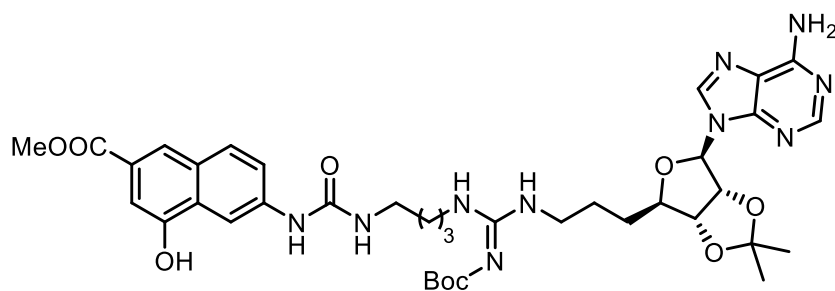
Compound **27f** was obtained as a white solid (201 mg, 72%) by reaction of compound **13a** (175 mg, 0.309 mmol) with compound **12f** (301 mg, 0.618 mmol) following the procedure described for **27a**. ¹H NMR (400 MHz, DMSO-*d*₆) δ 10.31 (s, 1H, exchangeable with D₂O), 10.25 (s, 1H, exchangeable with D₂O), 8.79 (s, 1H, exchangeable with D₂O), 8.63–8.58 (m, 2H), 8.25 (d, *J* = 1.7 Hz, 1H), 7.96 (s, 1H), 7.89 (d, *J* = 8.9 Hz, 1H), 7.51 (dd, *J* = 8.9, 1.7 Hz, 1H), 7.31 (s, 1H), 6.33 (br t, exchangeable with D₂O), 6.21 (s, 1H), 5.52–5.49 (m, 1H), 5.08–5.04 (m, 1H), 4.37–4.30 (m, 1H), 3.81 (s, 3H), 3.40–3.27 (m, 2H), 3.19–3.09 (m, 4H), 1.54 (s, 3H), 1.51–1.42 (m, 13H), 1.36 (s, 9H), 1.29–1.17 (m, 9H); **MS** (ESI) *m/z*: 906 (M+H)⁺.

Methyl 6-(3-(4-((*E*)-3-(2-(((3*aR*,4*R*,6*R*,6*aR*)-6-(6-amino-9*H*-purin-9-yl)-2,2-dimethyltetrahydrofuro[3,4-*d*][1,3]dioxol-4-yl)ethyl)-2-(*tert*-butoxycarbonyl) guanidino) butyl)ureido)-4-hydroxy-2-naphthoate (28)



Compound **28** was obtained as a white solid (129 mg, 80%) by reaction of compound **13b** (100 mg, 0.208 mmol) with compound **12c** (185 mg, 0.416 mmol) following the procedure described for **27a**. **¹H NMR** (400 MHz, DMSO-*d*₆) δ 10.26 (s, 1H, exchangeable with D₂O), 8.80 (s, 1H, exchangeable with D₂O), 8.34–8.30 (m, 2H), 8.25 (d, *J* = 2.1 Hz, 1H), 8.19–8.13 (m, 1H), 7.96 (s, 1H), 7.87 (d, *J* = 8.9 Hz, 1H), 7.54 (dd, *J* = 8.9, 2.1 Hz, 1H), 7.36–7.25 (m, 3H, 2H exchangeable with D₂O), 6.27 (br t, 1H, exchangeable with D₂O), 6.11 (s, 1H), 5.47–5.34 (m, 1H), 5.01–4.89 (m, 1H), 4.17–4.05 (m, 1H), 3.86 (s, 3H), 3.20–3.09 (m, 6H), 1.99–1.73 (m, 2H), 1.53 (s, 3H), 1.49–1.42 (m, 4H), 1.35 (s, 9H), 1.31 (s, 3H); **MS** (ESI) *m/z*: 778 (M+H)⁺.

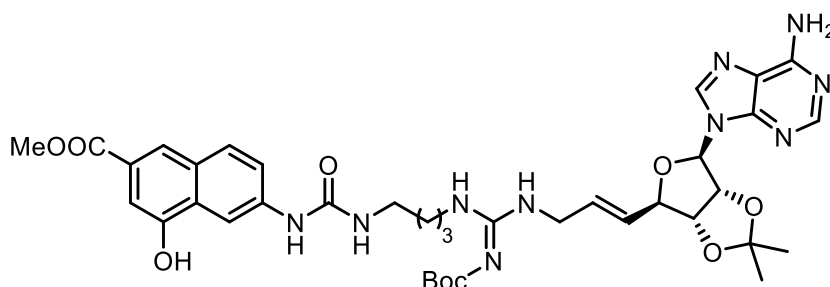
Methyl 6-(3-(4-((*E*)-3-(3-((3*aR*,4*R*,6*R*,6*aR*)-6-(6-amino-9*H*-purin-9-yl)-2,2-dimethyl tetrahydrofuro[3,4-*d*][1,3]dioxol-4-yl)propyl)-2-(tert-butoxycarbonyl) guanidino) butyl) ureido)-4-hydroxy-2-naphthoate (29)



Compound **29** was obtained as a white solid (155 mg, 79%) starting from compound **28c** (123 mg, 0.249 mmol) with compound **12c** (222 mg, 0.498 mmol) following the procedure described for **29a**. **¹H NMR** (400 MHz, DMSO-*d*₆) δ 10.29 (s, 1H, exchangeable with D₂O), 8.85 (s, 1H, exchangeable with D₂O), 8.29–8.21 (m, 2H), 8.26 (d, *J* = 2.2 Hz, 1H), 7.92 (s, 1H), 7.85 (d, *J* = 8.9 Hz, 1H), 7.56 (dd, *J* = 8.9, 2.2 Hz, 1H), 7.30–7.22 (m, 3H, 2H exchangeable with D₂O),

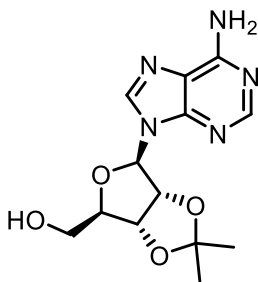
6.27 (br t, 1H, exchangeable with D₂O), 6.07 (s, 1H), 5.47–5.44 (m, 1H), 4.89–4.77 (m, 1H), 4.11–4.02 (m, 1H), 3.86 (s, 3H), 3.46–3.37 (m, 2H), 3.17–3.10 (m, 4H), 1.67–1.58 (m, 2H), 1.57–1.44 (m, 9H), 1.37 (s, 9H), 1.30 (s, 3H); **MS** (ESI) *m/z*: 791 (M+H)⁺.

Methyl 6-(3-(4-((*E*)-3-((*E*)-3-((3*aR*,4*R*,6*R*,6*aR*)-6-(6-amino-9*H*-purin-9-yl)-2,2-dimethyltetrahydrofuro[3,4-*d*][1,3]dioxol-4-yl)allyl)-2-(tert-butoxy carbonyl) guanidino)butyl)ureido)-4-hydroxy-2-naphthoate (30)



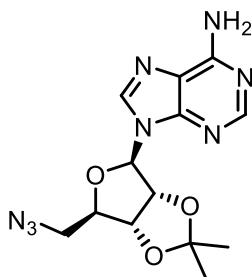
Compound **30** was obtained as a white solid (143 mg, 81%) by reaction of compound **13c** (110 mg, 0.224 mmol) with compound **12c** (199 mg, 0.448 mmol) following the procedure described for **27a**. ¹H NMR (400 MHz, DMSO-*d*₆) δ 10.27 (s, 1H, exchangeable with D₂O), 8.84 (s, 1H, exchangeable with D₂O), 8.31–8.23 (m, 2H), 8.16 (d, *J* = 1.9 Hz, 1H), 7.96 (s, 1H), 7.87 (d, *J* = 8.9 Hz, 1H), 7.54 (dd, *J* = 8.9, 1.9 Hz, 1H), 7.33–7.25 (m, 3H, 2H exchangeable with D₂O), 6.30 (br t, exchangeable with D₂O), 6.15 (s, 1H), 5.76–5.70 (m, 2H), 5.43 (m, 1H), 4.95 (m, 1H), 4.60–4.55 (m, 1H), 3.85 (s, 3H), 3.78–3.73 (m, 2H), 3.15–3.10 (m, 4H), 1.55 (s, 3H), 1.47–1.38 (m, 4H), 1.36 (s, 9H), 1.31 (s, 3H); **MS** (ESI) *m/z*: 789 (M+H)⁺.

((4*R*,6*R*)-6-(6-amino-9*H*-purin-9-yl)-2,2-dimethyltetrahydrofuro[3,4-*d*][1,3]dioxol-4-yl)methanol (32)



To a suspension of adenosine **31** (2.00 g, 7.50 mmol) in dry acetone (150 mL), 0.75 mL of HClO₄ were added dropwise. After stirring overnight, the clear solution was treated with a saturated solution of NaHCO₃ until the pH was 7. The solvent was concentrated under vacuum and the product extracted with AcOEt (3 × 25 mL). The collected organic phases were washed with brine (30 mL), dried (Na₂SO₄), filtered and concentrated under vacuum, yielding compound **32** as a white solid (1.86 g, 81%). ¹H NMR (400 MHz, DMSO-*d*₆) δ 8.16 (s, 1H), 8.00 (s, 1H), 6.48 (br s, 2H), 6.09 (s, 1H), 5.25 (s, 1H), 5.01 (s, 1H), 4.47 (s, 1H), 4.24 (m, 2H), 1.53 (s, 3H), 1.30 (s, 3H); MS (ESI) *m/z*: 308 (M+H)⁺.

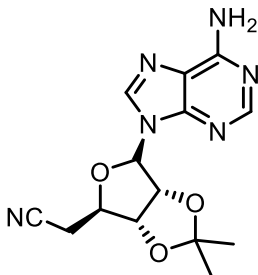
9-((4*R*,6*R*)-6-(azidomethyl)-2,2-dimethyltetrahydrofuro[3,4-*d*][1,3]dioxol-4-yl)-9*H*-purin-6-amine (33)



To a solution of **32** (1.00 g, 3.25 mmol) in dry 1,4-dioxane (10 mL), DPPA (1.48 mL, 6.50 mmol) and DBU (1.50 mL, 9.80 mmol) were added dropwise, and the reaction mixture was stirred at room temperature. After 24 h, sodium azide (1.06 g, 16.3 mmol) and 15-crown-5 (0.06 mL, 0.33 mmol) were added, and the resulting mixture was refluxed for 2 h. The mixture was warmed up to room temperature, filtered and concentrated under vacuum. The residue was taken up with CHCl₃ (50 mL), washed with water (50 mL) and brine (50 mL), dried (Na₂SO₄), filtered and concentrated under vacuum. The crude brown oil was purified by flash column chromatography (gradient DCM/AcOEt/MeOH 80:20:0 to 20:80:10) yielding the azide **33** as a yellow solid (0.93 g, 86%). ¹H NMR (400 MHz, DMSO-*d*₆) δ 8.35 (s, 1H), 8.18 (s, 1H), 7.34 (br s, 2H), 6.21 (d, *J* = 3.2 Hz, 1H), 5.52 (dd, *J* = 6.4, 3.3 Hz, 1H), 5.01 (dd, *J* = 6.4, 2.7 Hz,

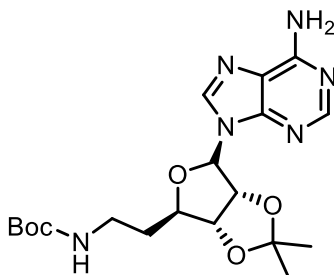
1H), 4.31 (td, $J = 5.8, 2.6$ Hz, 1H), 3.68 – 3.48 (m, 2H), 1.55 (s, 3H), 1.34 (s, 3H); **MS** (ESI) m/z : 333 (M+H)⁺.

2-((4R,6R)-6-(6-amino-9H-purin-9-yl)-2,2-dimethyltetrahydrofuro[3,4-d][1,3]dioxol-4-yl)acetonitrile (34)



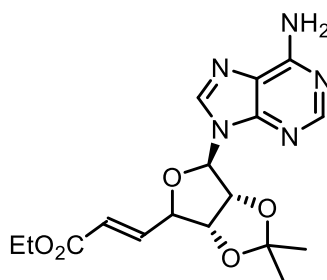
To a solution of **34** (0.76 g, 2.47 mmol) and PPh₃ (1.62 g, 6.17 mmol) in THF (25 mL), acetone cyanohydrin (0.57 mL, 6.20 mmol) was added. Within 5 min, DEAD (40% in toluene, 2.79 mL, 6.10 mmol) was added at 0 °C. The solution was stirred at the same temperature for 10 min and then warmed to room temperature. After 16 h, the solvent was evaporated, and the crude residue was purified by flash column chromatography (gradient AcOEt / MeOH 99:1 to 80:20) yielding the title compound **34** (0.70 g, 89%) as a brown oil. ¹H NMR (400 MHz, CDCl₃) δ 8.35 (s, 1H), 7.88 (s, 1H), 6.09 (s, 1H), 5.60 (br s, 2H), 5.48 (dd, $J = 6.4, 2.0$ Hz, 1H), 5.13 (dd, $J = 6.3, 3.1$ Hz, 1H), 4.56–4.50 (m, 1H), 3.03–2.86 (m, 2H), 1.62 (s, 3H), 1.40 (s, 3H); **MS** (ESI) m/z : 317 (M+H)⁺.

tert-butyl (2-((4R,6R)-6-(6-amino-9H-purin-9-yl)-2,2-dimethyltetrahydrofuro[3,4-d][1,3]dioxol-4-yl)ethyl)carbamate (35)



To a stirred solution of **34** (0.50 g, 1.58 mmol) in MeOH (20 mL), di-*tert*-butyl dicarbonate (1.03 g, 4.74 mmol) and nickel(II) chloride hexahydrate (0.04 g, 0.16 mmol) were added. The solution was cooled at 0 °C and sodium borohydride (0.42 g, 11.1 mmol) was added portion-wise, and the black suspension was stirred at room temperature for 4 h. Then, diethylenetriamine (0.17 mL, 1.58 mmol) was added and the resulting mixture was stirred for 24 h. The solvent was removed under vacuum and the crude was extracted with AcOEt (3 × 50 mL). The collected organic phases were washed with water (50 mL) and brine (50 mL), dried (Na₂SO₄), filtered and concentrated under vacuum. The crude product was purified by flash column chromatography (gradient DCM/MeOH 99:1 to 90:10) yielding the protected amine **35** as a pale-yellow solid (0.53 g, 80%). ¹H NMR (400 MHz, CDCl₃) δ 8.36 (s, 1H), 7.87 (s, 1H), 5.99 (d, *J* = 2.6 Hz, 1H), 5.60 (br s, 2H), 5.48 (dd, *J* = 6.6, 2.7 Hz, 1H), 5.03 (s, 1H), 4.91 (dd, *J* = 6.6, 4.0 Hz, 1H), 4.28–4.18 (m, 1H), 3.30–3.11 (m, 1H), 1.97–1.87 (m, 2H), 1.60 (s, 3H), 1.41 (s, 9H), 1.38 (s, 3H); MS (ESI) *m/z*: 421 (M+H)⁺.

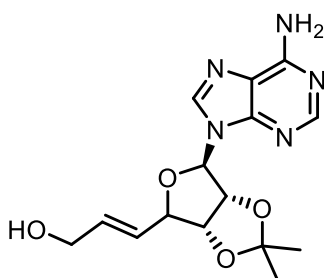
Ethyl (E)-3-(((4*R*,6*R*)-6-(6-amino-9*H*-purin-9-yl)-2,2-dimethylperhydrofuro[3,4-*d*][1,3]dioxol-4-yl)acrylate (36)



To a solution of **32** (1.50 g, 4.88 mmol) in 15 mL of DMSO, (ethoxycarbonylmethylene) triphenylphosphorane (4.25 g, 12.2 mmol) and o-iodoxybenzoic acid (IBX) (1.37 g, 12.2 mmol) were added. The mixture was stirred at room temperature for 72 h. Water (25 mL) was added and the mixture was extracted with AcOEt (3 × 50 mL). The combined organic phases were dried (Na₂SO₄), filtered and concentrated under vacuum to obtain a crude residue which was

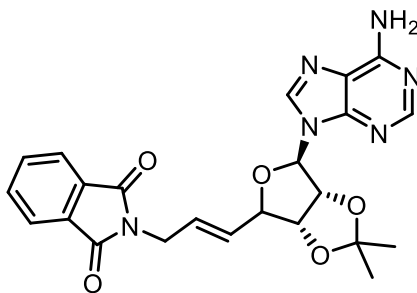
purified by column chromatography (AcOEt /MeOH 95:5) to give the title compound as an orange solid (1.28 g, 70%). **¹H NMR** (400 MHz, CDCl₃) δ 8.33 (s, 1H), 7.87 (s, 1H), 6.96 (dd, J = 15.7, 5.5 Hz, 1H), 6.13 (d, J = 1.9 Hz, 1H), 5.81 (dd, J = 15.6, 1.7 Hz, 1H), 5.61 (br s, 2H), 5.56 (dd, J = 6.2, 1.9 Hz, 1H), 5.14 (dd, J = 6.3, 3.5 Hz, 1H), 4.84–4.77 (m, 1H), 4.12 (q, J = 7.1 Hz, 2H), 1.63 (s, 3H), 1.40 (s, 3H), 1.23 (t, J = 7.1 Hz, 3H); **MS** (ESI) m/z : 376 (M+H)⁺.

(*E*)-3-((4*R*,6*R*)-6-(6-amino-9*H*-purin-9-yl)-2,2-dimethyltetrahydrofuro[3,4-*d*][1,3]dioxol-4-yl)prop-2-en-1-ol (37)



To a solution of **36** (1.00 g, 2.65 mmol) in dry DCM (10 mL), DIBAL-H (1 M in THF, 20 mL, 20.0 mmol) was added dropwise at -78 °C and the mixture was stirred for 2 hours. Then, the reaction was quenched with MeOH (8 mL) and warmed to room temperature. A saturated solution of Rochelle salt (40 mL) was added, and the resulting suspension was stirred overnight, then the aqueous phase was extracted with AcOEt (3 × 25 mL). The collected organic phases were washed with brine (30 mL), dried (Na₂SO₄) and filtered. Evaporation under vacuum of the solvent gave the title compound **37** (0.86 g, 98%) as a white yellow solid, which was directly used in the next step without further purification. **¹H NMR** (400 MHz, CDCl₃) δ 8.36 (s, 1H), 7.87 (s, 1H), 6.10 (d, J = 2.0 Hz, 1H), 5.87–5.84 (m, 1H), 5.58 – 5.53 (m, 3H), 5.02 (dd, J = 6.3, 3.4 Hz, 1H), 4.73–4.71 (m, 1H), 4.09–4.06 (m, 2H), 1.63 (s, 3H), 1.40 (s, 3H); **MS** (ESI) m/z : 334 (M+H)⁺.

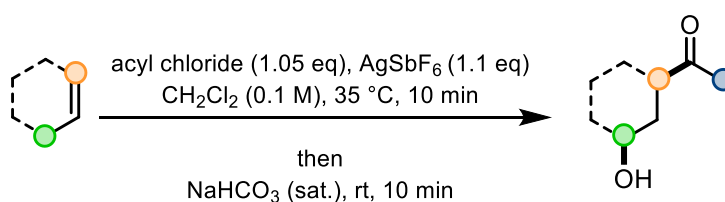
2-((*E*)-3-((4*R*,6*R*)-6-(6-amino-9*H*-purin-9-yl)-2,2-dimethyltetrahydrofuro[3,4-*d*][1,3]dioxol-4-yl)allyl)isoindoline-1,3-dione (38)



To a stirred suspension of **37** (0.48 g, 1.44 mmol), phthalimide (0.21 g, 1.44 mmol) and Ph_3P (0.38 g, 1.44 mmol) in THF (10 mL), DEAD (40% in toluene, 0.66 mL, 1.44 mmol) was added dropwise. After stirring for 1.5 h at room temperature, a colourless solid started to precipitate. Stirring was continued for 1 h, after which the mixture was cooled to 0 °C and filtered. The residue was washed with Et_2O and dried in vacuum to give **38** (0.47 g, 70%) as a white solid. ^1H NMR (400 MHz, CDCl_3) δ 8.24 (s, 1H), 7.86–7.83 (m, 3H), 7.74–7.71 (m, 2H), 6.07 (d, J = 2.0 Hz, 1H), 5.87–5.80 (m, 1H), 5.77–5.68 (m, 1H), 5.60 (br s, 2H), 5.48 (dd, J = 6.3, 2.0 Hz, 1H), 4.98 (dd, J = 6.3, 3.3 Hz, 1H), 4.71–4.65 (m, 1H), 4.21–4.18 (m, 2H), 1.59 (s, 3H), 1.37 (s, 3H); MS (ESI) m/z : 463 ($\text{M}+\text{H}$) $^+$.

8.2.2. Preparation of compounds 39 – 64

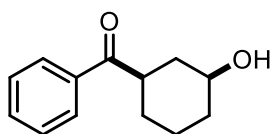
8.2.2.1. General Procedure for the 1,3-hydroxyacylation of alkenes with acylium ions



In a flame-dried Schlenk tube at ambient temperature, a solution of alkene (1.00 equiv.) and acyl chloride (1.05 equiv.) in dichloromethane (0.1 M) was treated with silver hexafluoroantimonate (1.1 equiv.) and the resulting suspension was immediately placed in a pre-heated oil bath at 35 °C. After vigorously stirring the reaction mixture at the same temperature for 10 min, the reaction vessel was removed from the oil bath and a saturated

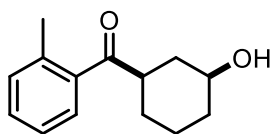
aqueous solution of sodium bicarbonate (equivalent to the amount of dichloromethane used) was added, followed by vigorous stirring for 10 min. After this time, the phases were separated, the aqueous phase was extracted with dichloromethane and the combined organic phases were dried over anhydrous Na₂SO₄, filtered and the filtrate was concentrated under reduced pressure. The resulting crude material was purified by flash column chromatography on silica gel (heptane/ethyl acetate) to give the title compound.

3-hydroxycyclohexyl)(phenyl)methanone (39)



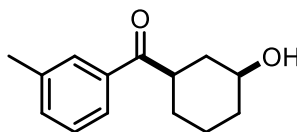
Synthesized following the general procedure, using cyclohexene (20.3 μ L, 0.20 mmol, 1.00 equiv.), benzoyl chloride (24.4 μ L, 0.21 mmol, 1.05 equiv.), silver hexafluoroantimonate (75.6 mg, 0.22 mmol, 1.10 equiv.) and dichloromethane (2 mL). Purification by flash column chromatography gave the title compound (> 50:1 r.r., 34.1 mg, 83%) as a white solid. **¹H NMR** (600 MHz, CDCl₃): δ 7.95 – 7.90 (m, 2H), 7.59 – 7.52 (m, 1H), 7.50 – 7.42 (m, 2H), 3.77 (td, J = 10.5, 4.2 Hz, 1H), 3.37 (tt, J = 11.2, 3.4 Hz, 1H), 2.18 – 2.11 (m, 1H), 2.02 (app d, J = 12.4 Hz, 1H), 1.97 – 1.81 (m, 2H), 1.58 – 1.49 (m, 1H), 1.47 – 1.39 (m, 2H), 1.33 – 1.22 (m, 1H). **¹³C NMR** (151 MHz, CDCl₃): δ 202.3, 135.9, 133.0, 128.6 (2C), 128.3 (2C), 69.9, 44.0, 37.6, 35.1, 28.5, 23.3. **HRMS (ESI⁺)**: exact mass calculated for [M+Na]⁺ (C₁₃H₁₆O₂Na) requires m/z 257.1154, found m/z 257.1153.

3-hydroxycyclohexyl)(*m*-tolyl)methanone (41a)



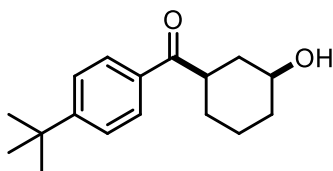
Synthesized following the general procedure, using cyclohexene (20.3 μ L, 0.20 mmol, 1.00 equiv.), *o*-toluoyl chloride (27.4 μ L, 0.21 mmol, 1.05 equiv.), silver hexafluoroantimonate (75.6 mg, 0.22 mmol, 1.10 equiv.) and dichloromethane (2 mL). Purification by flash column chromatography (heptane/ethyl acetate 90:10 to 20:80) gave the title compound (> 19:1 r.r., 28.9 mg, 66%) as a white solid. **¹H NMR** (400 MHz, CDCl₃): δ 7.56 – 7.42 (m, 1H), 7.40 – 7.29 (m, 1H), 7.29 – 7.17 (m, 2H), 3.69 (td, J = 10.5, 4.0 Hz, 1H), 3.13 (tt, J = 11.4, 4.1 Hz, 1H), 2.42 (s, 3H), 2.13 (app d, J = 12.4 Hz, 1H), 2.00 (app d, J = 11.5 Hz, 1H), 1.95 – 1.71 (m, 2H), 1.53 – 1.17 (m, 4H). **¹³C NMR** (101 MHz, CDCl₃): δ 207.1, 138.4, 137.5, 131.7, 130.7, 127.3, 125.6, 70.1, 47.3, 37.3, 35.1, 27.8, 23.3, 20.7. **HRMS** (ESI⁺): exact mass calculated for [M+Na]⁺ (C₁₄H₁₈O₂Na) requires m/z 241.1205, found m/z 241.1198.

3-hydroxycyclohexyl)(*m*-tolyl)methanone (41b)



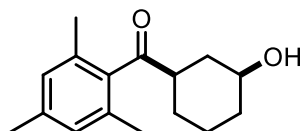
Synthesized following the general procedure, using cyclohexene (20.3 μ L, 0.20 mmol, 1.00 equiv.), *m*-toluoyl chloride (27.7 μ L, 0.21 mmol, 1.05 equiv.), silver hexafluoroantimonate (75.6 mg, 0.22 mmol, 1.10 equiv.) and dichloromethane (2 mL). Purification by flash column chromatography (heptane/ethyl acetate 90:10 to 20:80) gave the title compound (> 20:1 r.r., 35.8 mg, 82%) as a white solid. **¹H NMR** (500 MHz, CDCl₃): δ 7.77 – 7.62 (m, 2H), 7.40 – 7.30 (m, 2H), 3.87 – 3.62 (m, 1H), 3.36 (tt, J = 11.1, 3.4 Hz, 1H), 2.41 (s, 3H), 2.20 – 2.08 (m, 1H), 2.05 – 1.95 (m, 1H), 1.95 – 1.80 (m, 2H), 1.56 – 1.37 (m, 4H), 1.36 – 1.17 (m, 1H). **¹³C NMR** (126 MHz, CDCl₃): δ 201.7, 137.5, 135.0, 132.8, 127.8, 127.5, 124.5, 68.9, 42.9, 36.7, 34.2, 27.5, 22.3, 20.4. **HRMS** (ESI⁺): exact mass calculated for [M+Na]⁺ (C₁₄H₁₈O₂Na) requires m/z 241.1205, found m/z 241.1199.

(4-(tert-butyl)phenyl)((1R,3S)-3-hydroxycyclohexyl)methanone (41c)



Synthesized following the general procedure, using cyclohexene (20.3 μL , 0.20 mmol, 1.00 equiv.), 4-*tert*-butylbenzoyl chloride (41.3 μL , 0.21 mmol, 1.05 equiv.), silver hexafluoroantimonate (75.6 mg, 0.22 mmol, 1.10 equiv.) and dichloromethane (2 mL). Purification by flash column chromatography (heptane/ethyl acetate 90:10 to 20:80) gave the title compound (> 19:1 r.r., 44.6 mg, 86%) as a white solid. **^1H NMR** (600 MHz, CDCl_3): δ 7.91 – 7.85 (m, 2H), 7.54 – 7.42 (m, 2H), 3.86 – 3.66 (m, 1H), 3.43 – 3.28 (m, 1H), 2.16 – 2.06 (m, 1H), 2.08 – 1.95 (m, 1H), 1.93 – 1.78 (m, 2H), 1.60 – 1.39 (m, 4H), 1.34 (s, 9H). **^{13}C NMR** (151 MHz, CDCl_3): δ 202.1, 156.8, 133.3, 128.3 (2C), 125.5 (2C), 69.9, 43.8, 37.7, 35.2, 32.1, 31.1 (3C), 28.6, 23.3. **HRMS** (ESI⁺): exact mass calculated for $[\text{M}+\text{Na}]^+$ ($\text{C}_{17}\text{H}_{24}\text{O}_2\text{Na}$) requires m/z 283.1674, found m/z 283.1658.

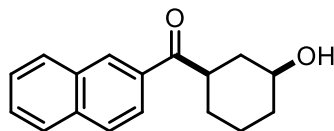
3-hydroxycyclohexyl)(mesityl)methanone (41d)



Synthesized following the general procedure, using cyclohexene (20.3 μL , 0.20 mmol, 1.00 equiv.), 2,4,6-trimethylbenzoyl chloride (35.0 μL , 0.21 mmol, 1.05 equiv.), silver hexafluoroantimonate (75.6 mg, 0.22 mmol, 1.10 equiv.) and dichloromethane (2 mL). Purification by flash column chromatography (heptane/ethyl acetate 90:10 to 40:60) gave the title compound (> 7:1 r.r., 20.5 mg, 41%) as a colorless oil. **^1H NMR** (500 MHz, CDCl_3): δ 6.84 (s, 2H), 3.68 – 3.51 (m, 1H), 2.76 (app ddd, J = 11.9, 8.8, 3.1 Hz, 1H), 2.28 (s, 3H), 2.20 – 2.16 (m, 7H), 1.98 (dd, J = 10.6, 3.3 Hz, 1H), 1.91 – 1.80 (m, 2H), 1.50 – 1.19 (m, 4H). **^{13}C NMR** (126 MHz, CDCl_3): δ 212.0, 138.7, 138.5, 133.2 (2C), 128.7 (2C), 70.3, 50.6, 36.8, 35.2,

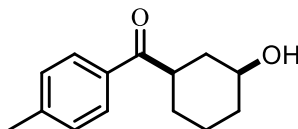
27.1, 23.5, 21.0, 19.7 (2C). **HRMS** (ESI⁺): exact mass calculated for [M+Na]⁺ (C₁₆H₂₂O₂Na) requires *m/z* 269.1518, found *m/z* 269.1513.

3-hydroxycyclohexyl)(naphthalen-2-yl)methanone (41e)



Synthesized following the general procedure, using cyclohexene (20.3 μ L, 0.20 mmol, 1.00 equiv.), 2-naphthoyl chloride (19.1 μ L, 0.21 mmol, 1.05 equiv.), silver hexafluoroantimonate (75.6 mg, 0.22 mmol, 1.10 equiv.) and dichloromethane (2 mL). Purification by flashcolumn chromatography (heptane/ethyl acetate 90:10 to 20:80) gave the title compound (> 19:1 r.r., 41.1 mg, 80%) as a white solid. **¹H NMR** (700 MHz, CDCl₃): δ 8.44 (s, 1H), 8.00 (d, *J* = 8.6 Hz, 1H), 7.96 (d, *J* = 8.1 Hz, 1H), 7.88 (dd, *J* = 17.0, 8.3 Hz, 2H), 7.60 (t, *J* = 7.4 Hz, 1H), 7.55 (t, *J* = 7.4 Hz, 1H), 3.86 – 3.80 (m, 1H), 3.54 (m, 1H), 2.21 (app d, *J* = 12.6 Hz, 1H), 2.06 (app d, *J* = 12.2 Hz, 1H), 1.92 (app d, *J* = 8.4 Hz, 2H), 1.60 (m, 1H), 1.54 – 1.44 (m, 2H), 1.33 – 1.31 (m, 1H). **¹³C NMR** (176 MHz, CDCl₃): δ 202.4, 135.5, 133.3, 132.5, 129.7, 129.5, 128.5, 128.4, 127.7, 126.8, 124.2, 70.0, 43.9, 37.8, 35.2, 28.6, 23.4. **HRMS** (ESI⁺): exact mass calculated for [M+Na]⁺ (C₁₇H₁₈O₂Na) requires *m/z* 277.1205, found *m/z* 277.1200.

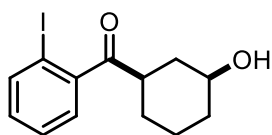
3-hydroxycyclohexyl)(p-tolyl)methanone (41f)



Synthesized following the general procedure, using cyclohexene (20.3 μ L, 0.20 mmol, 1.00 equiv.), *p*-toluoyl chloride (27.8 μ L, 0.21 mmol, 1.05 equiv.), silver hexafluoroantimonate (75.6 mg, 0.22 mmol, 1.10 equiv.) and dichloromethane (2 mL). Purification by flash column chromatography (heptane/ethyl acetate 90:10 to 20:80) gave the title compound (> 20:1 r.r., 34.2 mg, 78%) as a white solid. **¹H NMR** (400 MHz, CDCl₃): δ 7.88 – 7.78 (m, 2H), 7.31 –

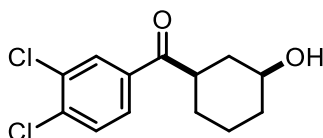
7.18 (m, 2H), 3.84 – 3.64 (tt, $J = 10.5, 3.2$ Hz, 1H), 3.41 – 3.25 (tt, $J = 10.7, 4.2$ Hz, 1H), 2.41 (s, 3H), 2.17 – 2.08 (m, 1H), 2.06 – 1.97 (m, 1H), 1.92 – 1.77 (m, 2H), 1.55 – 1.38 (m, 4H), 1.33 – 1.31 (m, 1H). ^{13}C NMR (101 MHz, CDCl_3): δ 202.1, 143.9, 133.4, 129.4 (2C), 128.5 (2C), 70.0, 43.8, 37.7, 35.2, 28.6, 23.4, 21.7. **HRMS** (ESI^+): exact mass calculated for $[\text{M}+\text{Na}]^+$ ($\text{C}_{14}\text{H}_{18}\text{O}_2\text{Na}$) requires m/z 241.1205, found m/z 241.1197.

3-hydroxycyclohexyl(2-iodophenyl)methanone (41g)



Synthesized following the general procedure, using cyclohexene (20.3 μL , 0.20 mmol, 1.00 equiv.), 2-iodobenzoyl chloride (29.0 μL , 0.21 mmol, 1.05 equiv.), silver hexafluoroantimonate (75.6 mg, 0.22 mmol, 1.10 equiv.) and dichloromethane (2 mL). Purification by flash column chromatography (heptane/ethyl acetate 90:10 to 40:60) gave the title compound ($> 12:1$ r.r., 48.0 mg, 73%) as a white solid. ^1H NMR (400 MHz, CDCl_3): δ 7.88 (d, $J = 7.9$ Hz, 1H), 7.39 (td, $J = 7.5, 0.7$ Hz, 1H), 7.28 – 7.22 (m, 2H, overlaps with CDCl_3 peak), 7.12 (td, $J = 7.7, 1.6$ Hz, 1H), 3.74 – 3.53 (m, 1H), 3.20 – 2.96 (m, 1H), 2.26 – 2.12 (m, 1H), 2.05 – 1.94 (m, 1H), 1.93 – 1.81 (m, 2H), 1.54 – 1.19 (m, 4H). ^{13}C NMR (176 MHz, CDCl_3): δ 207.0, 145.1, 140.1, 131.2, 127.9, 127.5, 91.1, 70.1, 47.9, 36.9, 35.1, 27.4, 23.4. **HRMS** (ESI^+): exact mass calculated for $[\text{M}+\text{Na}]^+$ ($\text{C}_{13}\text{H}_{15}\text{IO}_2\text{Na}$) requires m/z 353.0015, found m/z 353.0011.

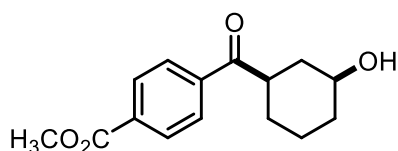
(3,4-dichlorophenyl)(3-hydroxycyclohexyl)methanone (41h)



Synthesized following the general procedure, using cyclohexene (20.3 μL , 0.20 mmol, 1.00 equiv.), 3,4-dichlorobenzoyl chloride (44.9 mg, 0.21 mmol, 1.05 equiv.), silver hexafluoroantimonate (75.6 mg, 0.22 mmol, 1.10 equiv.) and dichloromethane (2 mL).

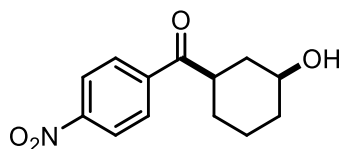
Purification by flash column chromatography (heptane/ethyl acetate 90:10 to 40:60) gave the title compound (> 15:1 r.r., 39.8 mg, 73%) as a white solid. **¹H NMR** (400 MHz, CDCl₃): δ 8.00 (s, 1H), 7.75 (d, *J* = 8.3 Hz, 1H), 7.55 (d, *J* = 8.3 Hz, 1H), 3.83 – 3.65 (m, 1H), 3.35 – 3.13 (m, 1H), 2.17 – 2.08 (m, 1H), 2.08 – 1.98 (m, 1H), 1.96 – 1.80 (m, 2H), 1.68 (brs, 1H), 1.57 – 1.20 (m, 4H). **¹³C NMR** (101 MHz, CDCl₃): δ 200.0, 137.6, 135.6, 133.4, 130.8, 130.3, 127.4, 70.0, 44.1, 37.5, 35.1, 28.3, 23.4. **HRMS** (ESI⁺): exact mass calculated for [M+Na]⁺ (C₁₃H₁₄Cl₂O₂Na) requires *m/z* 295.0269, found *m/z* 295.0249.

Methyl 4-(-3-hydroxycyclohexane-1-carbonyl)benzoate (41j)



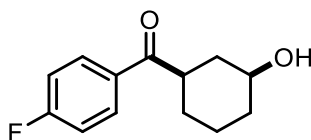
Synthesized following the general procedure, using cyclohexene (20.3 μL, 0.20 mmol, 1.00 equiv.), methyl 4-chlorocarbonylbenzoate (43.9 mg, 0.21 mmol, 1.05 equiv.), silver hexafluoroantimonate (75.6 mg, 0.22 mmol, 1.10 equiv.) and dichloromethane (2 mL). Purification by flash column chromatography (heptane/ethyl acetate 90:10 to 40:60) gave the title compound (> 11:1 r.r., 36.8 mg, 70%) as a white solid. **¹H NMR** (700 MHz, CDCl₃): δ 8.11 (d, *J* = 8.3 Hz, 2H), 7.96 (d, *J* = 8.3 Hz, 2H), 3.94 (s, 3H), 3.82 – 3.70 (m, 1H), 3.36 (tt, *J* = 11.3, 3.2 Hz, 1H), 2.21 – 2.09 (m, 1H), 2.08 – 1.98 (m, 1H), 1.95 – 1.81 (m, 2H), 1.81 – 1.65 (brs, 1H), 1.59 – 1.37 (m, 2H), 1.37 – 1.18 (m, 1H). **¹³C NMR** (176 MHz, CDCl₃): δ 201.9, 166.2, 139.3, 133.8, 129.9 (2C), 128.2 (2C), 69.9, 52.4, 44.4, 37.5, 35.1, 28.4, 23.4. **HRMS** (ESI⁺): exact mass calculated for [M+Na]⁺ (C₁₅H₁₈O₄Na) requires *m/z* 285.1103, found *m/z* 285.1102.

3-hydroxycyclohexyl(4-nitrophenyl)methanone (41k)



Synthesized following the general procedure, using cyclohexene (20.3 μ L, 0.20 mmol, 1.00 equiv.), 4-nitrobenzoyl chloride (39.0 mg, 0.21 mmol, 1.05 equiv.), silver hexafluoroantimonate (75.6 mg, 0.22 mmol, 1.10 equiv.) and dichloromethane (2 mL). Purification by flash column chromatography (heptane/ethyl acetate 90:10 to 40:60) gave the title compound (> 10:1 r.r., 30.0 mg, 60%) as a white solid. **^1H NMR** (400 MHz, CDCl_3): δ 8.31 (d, J = 7.9 Hz, 2H), 8.07 (d, J = 8.0 Hz, 2H), 3.87 – 3.64 (m, 1H), 3.43 – 3.19 (m, 1H), 2.22 – 2.10 (m, 1H), 2.09 – 2.00 (m, 1H), 1.97 – 1.79 (m, 2H), 1.78 – 1.70 (brs, 1H), 1.59 – 1.36 (m, 3H), 1.35 – 1.17 (m, 1H). **^{13}C NMR** (101 MHz, CDCl_3): δ 200.8, 150.3, 140.7, 129.3 (2C), 123.9 (2C), 69.9, 44.6, 37.4, 35.1, 28.2, 23.4. **HRMS** (ESI^+): exact mass calculated for $[\text{M}+\text{Na}]^+$ ($\text{C}_{13}\text{H}_{15}\text{NO}_4\text{Na}$) requires m/z 272.0899, found m/z 272.0893.

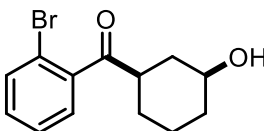
4-fluorophenyl-(3-hydroxycyclohexyl)methanone (41l)



Synthesized following the general procedure, using cyclohexene (20.3 μ L, 0.20 mmol, 1.00 equiv.), 4-fluorobenzoyl chloride (24.8 μ L, 0.21 mmol, 1.05 equiv.), silver hexafluoroantimonate (75.6 mg, 0.22 mmol, 1.10 equiv.) and dichloromethane (2 mL). Purification by flash column chromatography (heptane/ethyl acetate 90:10 to 40:60) gave the title compound (> 13:1 r.r., 37.1 mg, 83%) as a white solid. **^1H NMR** (600 MHz, CDCl_3): δ 8.01 – 7.84 (m, 2H), 7.17 – 7.02 (m, 2H), 3.84 – 3.66 (m, 1H), 3.32 (app dd, J = 15.0, 6.7 Hz, 1H), 2.17 – 2.06 (m, 1H), 2.08 – 1.97 (m, 1H), 1.93 – 1.80 (m, 2H), 1.77 (brs, 1H), 1.57 – 1.46 (m, 1H), 1.49 – 1.39 (m, 2H), 1.37 – 1.19 (m, 1H). **^{13}C NMR** (151 MHz, CDCl_3): δ 200.7, 165.6 (d, J = 253.5 Hz), 132.3 (d, J = 3.0 Hz), 130.9 (d, J = 9.0 Hz, 2C), 115.8 (d, J = 22.5 Hz,

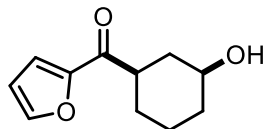
2C), 69.9, 43.9, 37.7, 35.2, 28.5, 23.3. **¹⁹F** (372 MHz, CDCl₃): δ – 107.3. **HRMS** (ESI⁺): exact mass calculated for [M+Na]⁺ (C₁₃H₁₅FO₂Na) requires *m/z* 245.0954, found *m/z* 245.0949.

3-hydroxycyclohexyl(2-bromophenyl)methanone (41n)



Synthesized following the general procedure, using cyclohexene (20.3 μL, 0.20 mmol, 1.00 equiv.), 2-bromobenzoyl chloride (27.4 μL, 0.21 mmol, 1.05 equiv.), silver hexafluoroantimonate (75.6 mg, 0.22 mmol, 1.10 equiv.) and dichloromethane (2 mL). Purification by flash column chromatography (heptane/ethyl acetate 90:10 to 40:60) gave the title compound (> 11:1 r.r., 34.2 mg, 60%) as a white solid. **¹H NMR** (400 MHz, CDCl₃): δ 7.53 (d, *J* = 7.9 Hz, 1H), 7.34 – 7.25 (m, 1H), 7.25 – 7.11 (m, 2H, overlaps with CDCl₃ peak), 3.65 – 3.47 (m, 1H), 3.07 (m, 1H), 2.23 – 2.06 (m, 1H), 1.97 – 1.87 (m, 1H), 1.99 – 1.76 (m, 2H), 1.44 – 1.07 (m, 4H). **¹³C NMR** (101 MHz, CDCl₃): δ 133.4, 131.2, 128.2, 127.3, 118.6, 70.1, 48.5, 36.9, 35.1, 27.4, 23.4. **HRMS** (ESI⁺): exact mass calculated for [M+Na]⁺ (C₁₃H₁₅BrO₂Na) requires *m/z* 305.0153, found *m/z* 305.0132 + 307.0113 (⁸¹Br).

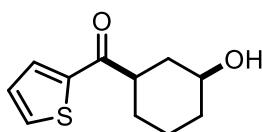
Furan-2-yl(-3-hydroxycyclohexyl)methanone (41p)



Synthesized following the general procedure, using cyclohexene (20.3 μL, 0.20 mmol, 1.00 equiv.), 2-furoyl chloride (22.7 μL, 0.21 mmol, 1.05 equiv.), silver hexafluoroantimonate (75.6 mg, 0.22 mmol, 1.10 equiv.) and dichloromethane (2 mL). Purification by flash column chromatography (heptane/ethyl acetate 90:10 to 40:60) gave the title compound (> 10:1 r.r.,

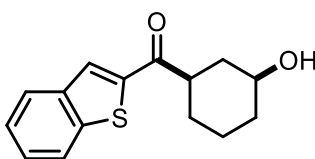
20.0 mg, 51%) as a colorless oil. **¹H NMR** (600 MHz, CDCl₃): δ 7.57 (m, 1H), 7.19 (m, 1H), 6.57 – 6.42 (m, 1H), 3.74 (tt, *J* = 10.4, 4.2 Hz, 1H), 3.18 (tt, *J* = 11.2, 3.6 Hz, 1H), 2.18 – 2.07 (m, 1H), 2.06 – 1.97 (m, 1H), 1.95 – 1.78 (m, 2H), 1.57 – 1.48 (m, 1H), 1.50 – 1.36 (m, 2H), 1.34 – 1.16 (m, 1H). **¹³C NMR** (151 MHz, CDCl₃): δ 191.4, 152.1, 146.3, 117.3, 112.3, 69.8, 44.6, 37.1, 35.0, 27.9, 23.3. **HRMS** (ESI⁺): exact mass calculated for [M+Na]⁺ (C₁₁H₁₄O₃Na) requires *m/z* 217.0841, found *m/z* 217.0837.

3-hydroxycyclohexyl)(thiophen-2-yl)methanone (41q)



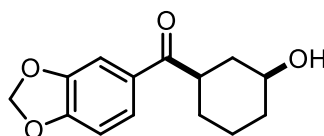
Synthesized following the general procedure, using cyclohexene (20.3 μL, 0.20 mmol, 1.00 equiv.), 2-thenoyl chloride (22.7 μL, 0.21 mmol, 1.05 equiv.), silver hexafluoroantimonate (75.6 mg, 0.22 mmol, 1.10 equiv.) and dichloromethane (2 mL). Purification by flash column chromatography (heptane/ethyl acetate 90:10 to 40:60) gave the title compound (> 13:1 r.r., 31.2 mg, 74%) as a white solid. **¹H NMR** (400 MHz, CDCl₃): δ 7.78 – 7.66 (m, 1H), 7.66 – 7.60 (m, 1H), 7.17 – 7.01 (m, 1H), 3.76 (app d, *J* = 10.2 Hz, 1H), 3.19 (m, 1H), 2.21 – 2.06 (m, 1H), 2.08 – 1.96 (m, 1H), 1.94 – 1.77 (m, 2H), 1.64 – 1.38 (m, 3H), 1.37 – 1.21 (m, 1H). **¹³C NMR** (101 MHz, CDCl₃): δ 195.3, 143.4, 133.8, 131.8, 128.2, 69.8, 45.7, 37.8, 35.1, 28.8, 23.3. **HRMS** (ESI⁺): exact mass calculated for [M+Na]⁺ (C₁₁H₁₄O₂SNa) requires *m/z* 233.0613, found *m/z* 233.0610.

Benzo[b]thiophen-2-yl(3-hydroxycyclohexyl)methanone (41r)



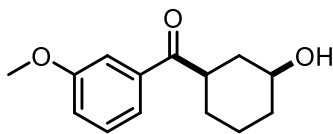
Synthesized following the general procedure, using cyclohexene (20.3 μ L, 0.20 mmol, 1.00 equiv.), benzo[*b*]thiophene-2-carbonyl chloride (42.1 mg, 0.21 mmol, 1.05 equiv.), silver hexafluoroantimonate (75.6 mg, 0.22 mmol, 1.10 equiv.) and dichloromethane (2 mL). Purification by flash column chromatography (heptane/ethyl acetate 90:10 to 40:60) gave the title compound (> 8:1 r.r., 31.9 mg, 61%) as a white solid. **¹H NMR** (600 MHz, CDCl₃): δ 7.97 (s, 1H), 7.91 – 7.83 (m, 2H), 7.49 – 7.44 (m, 1H), 7.44 – 7.39 (m, 1H), 3.84 – 3.68 (m, 1H), 3.35 (tt, *J* = 11.3, 3.2 Hz, 1H), 2.26 – 2.16 (m, 1H), 2.10 – 2.00 (m, 1H), 1.94 (m, 2H), 1.77 (app brs, 1H), 1.67 – 1.56 (m, 1H, overlaps with water peak), 1.55 – 1.44 (m, 2H), 1.37 – 1.27 (m, 1H). **¹³C NMR** (151 MHz, CDCl₃): δ 196.7, 142.8, 142.6, 139.1, 128.8, 127.5, 125.9, 125.1, 123.0, 69.9, 45.6, 37.9, 35.1, 28.8, 23.4. **HRMS** (ESI⁺): exact mass calculated for [M+Na]⁺ (C₁₅H₁₆O₂SNa) requires *m/z* 283.0769, found *m/z* 283.0765.

Benzo[d][1,3]dioxol-5-yl(-3-hydroxycyclohexyl)methanone (41s)



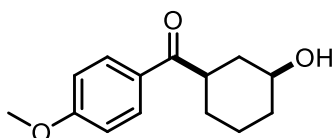
Synthesized following the general procedure, using cyclohexene (20.3 μ L, 0.20 mmol, 1.00 equiv.), piperonyl chloride (38.8 mg, 0.21 mmol, 1.05 equiv.), silver hexafluoroantimonate (75.6 mg, 0.22 mmol, 1.10 equiv.) and dichloromethane (2 mL). Purification by flash column chromatography (heptane/ethyl acetate 90:10 to 40:60) gave the title compound (> 15:1 r.r., 28.9 mg, 58%) as a white solid. **¹H NMR** (600 MHz, CDCl₃): δ 7.54 (d, *J* = 8.2 Hz, 1H), 7.41 (s, 1H), 6.85 (d, *J* = 8.1 Hz, 1H), 6.04 (s, 2H), 3.81 – 3.63 (m, 1H), 3.34 – 3.17 (m, 1H), 2.14 – 2.06 (m, 1H), 2.06 – 1.98 (m, 1H), 1.94 – 1.79 (m, 2H), 1.68 (app brs, 1H), 1.58 – 1.47 (m, 1H), 1.47 – 1.38 (m, 2H), 1.32 – 1.24 (m, 1H). **¹³C NMR** (151 MHz, CDCl₃): δ 200.4, 151.7, 148.3, 130.7, 124.4, 108.2, 107.9, 101.8, 69.9, 43.6, 37.8, 35.2, 28.7, 23.3. **HRMS** (ESI⁺): exact mass calculated for [M+Na]⁺ (C₁₄H₁₆O₄Na) requires *m/z* 271.0947, found *m/z* 271.0947.

3-hydroxycyclohexyl)(3-methoxyphenyl)methanone (41t)



Synthesized following the general procedure, using cyclohexene (20.3 μ L, 0.20 mmol, 1.00 equiv.), 3-methoxybenzoyl chloride (30.1 μ L, 0.21 mmol, 1.05 equiv.), silver hexafluoroantimonate (75.6 mg, 0.22 mmol, 1.10 equiv.) and dichloromethane (2 mL). Purification by flash column chromatography (heptane/ethyl acetate 90:10 to 40:60) gave the title compound (> 17:1 r.r., 35.5 mg, 75%) as a white solid. **^1H NMR** (700 MHz, CDCl_3): δ 7.51 (d, J = 7.6 Hz, 1H), 7.47 (s, 1H), 7.37 (t, J = 7.9 Hz, 1H), 7.11 (dd, J = 8.1, 2.4 Hz, 1H), 3.86 (s, 3H), 3.80 – 3.72 (m, 1H), 3.38 – 3.31 (m, 1H), 2.18 – 2.11 (m, 1H), 2.07 – 1.99 (m, 1H), 1.93 – 1.82 (m, 2H), 1.76 – 1.68 (app br s, 1H), 1.55 – 1.50 (m, 1H), 1.47 – 1.41 (m, 2H), 1.34 – 1.27 (m, 1H). **^{13}C NMR** (176 MHz, CDCl_3): δ 202.2, 159.9, 137.4, 129.4, 120.7, 119.3, 112.8, 70.0, 55.4, 44.1, 37.7, 35.1, 28.6, 23.4. **HRMS** (ESI^+): exact mass calculated for $[\text{M}+\text{Na}]^+$ ($\text{C}_{14}\text{H}_{18}\text{O}_3\text{Na}$) requires m/z 257.1154, found m/z 257.1150.

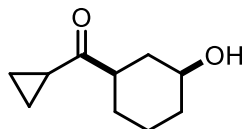
3-hydroxycyclohexyl)(4-methoxyphenyl)methanone (41u)



Synthesized following the general procedure, using cyclohexene (20.3 μ L, 0.20 mmol, 1.00 equiv.), 4-methoxybenzoyl chloride (28.4 μ L, 0.21 mmol, 1.05 equiv.), silver hexafluoroantimonate (75.6 mg, 0.22 mmol, 1.10 equiv.) and dichloromethane (2 mL). Purification by flash column chromatography (heptane/ethyl acetate 90:10 to 40:60) gave the title compound (> 13:1 r.r., 26.1 mg, 55%) as a white solid. **^1H NMR** (700 MHz, CDCl_3): δ 7.92 (d, J = 8.0, 2H), 6.93 (d, J = 8.0, 2H), 3.86 (s, 3H), 3.79 – 3.70 (m, 1H), 3.37 – 3.30 (m, 1H), 2.13 – 2.09 (m, 1H), 2.03 – 1.96 (m, 1H), 1.90 – 1.76 (m, 2H), 1.57 – 1.51 (m, 1H), 1.46

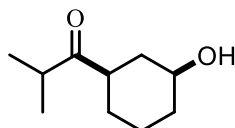
– 1.41 (m, 2H), 1.34 – 1.26 (m, 1H). **¹³C NMR** (176 MHz, CDCl₃): δ 200.9, 163.4, 130.6 (2C), 128.8, 113.8 (2C), 69.9, 55.4, 43.5, 37.7, 35.2, 28.6, 23.3. **HRMS** (ESI⁺): exact mass calculated for [M+Na]⁺ (C₁₄H₁₈O₃Na) requires *m/z* 257.1154, found *m/z* 257.1147.

Cyclopropyl((1S,3S)-3-hydroxycyclohexyl)methanone (42a)



Synthesized following the general procedure, using cyclohexene (20.3 μL, 0.20 mmol, 1.00 equiv.), cyclopropanecarbonyl chloride (19.1 μL, 0.21 mmol, 1.05 equiv.), silver hexafluoroantimonate (75.6 mg, 0.22 mmol, 1.10 equiv.) and dichloromethane (2 mL). Purification by flash column chromatography (heptane/ethyl acetate 90:10 to 40:60) gave the title compound (> 28:1 r.r., 31.0 mg, 81%) as a white solid. **¹H NMR** (600 MHz, CDCl₃): δ 3.65 (tt, *J* = 10.1, 4.2 Hz, 1H), 2.59 (tt, *J* = 11.0, 3.7 Hz, 1H), 2.15 – 2.08 (m, 1H), 1.97 – 1.89 (m, 2H), 1.87 – 1.83 (m, 1H), 1.83 – 1.78 (m, 1H), 1.39 – 1.26 (m, 3H), 1.22–1.19 (m, 1H), 0.97 – 0.92 (m, 2H), 0.84 – 0.80 (m, 2H). **¹³C NMR** (151 MHz, CDCl₃): δ 212.7, 69.7, 49.9, 36.8, 35.2, 27.5, 23.0, 19.0, 11.0, 10.9. **HRMS** (ESI⁺): exact mass calculated for [M+Na]⁺ (C₁₀H₁₆O₂Na) requires *m/z* 191.1042, found *m/z* 191.1043.

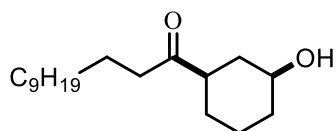
3-hydroxycyclohexyl)-2-methylpropan-1-one (42b)



Synthesized following the general procedure, using cyclohexene (20.3 μL, 0.20 mmol, 1.00 equiv.), isobutyryl chloride (22.0 μL, 0.21 mmol, 1.05 equiv.), silver hexafluoroantimonate (75.6 mg, 0.22 mmol, 1.10 equiv.) and dichloromethane (2 mL). Purification by flash column chromatography (heptane/ethyl acetate 90:10 to 20:80) gave the title compound (> 32:1 r.r., 20.0 mg, 59%) as a white solid. **¹H NMR** (600 MHz, CDCl₃): δ

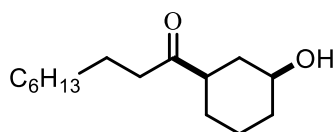
3.62 (tt, $J = 10.4, 4.2$ Hz, 1H), 2.78 – 2.70 (m, 1H), 2.58 (tt, $J = 11.3, 3.6$ Hz, 1H), 2.05 – 1.97 (m, 1H), 1.97 – 1.90 (m, 1H), 1.85 – 1.79 (m, 1H), 1.75 – 1.67 (m, 1H), 1.37 – 1.16 (m, 4H), 1.09 – 0.97 (m, 6H). ^{13}C NMR (151 MHz, CDCl_3): δ 216.4, 69.9, 47.4, 38.9, 37.1, 35.1, 27.6, 23.2, 18.5, 18.4. **HRMS** (ESI^+): exact mass calculated for $[\text{M}+\text{Na}]^+$ ($\text{C}_{10}\text{H}_{18}\text{O}_2\text{Na}$) requires m/z 193.1187, found m/z 193.1192.

3-hydroxycyclohexyl)undecan-1-one (42c)



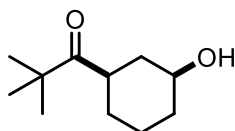
Synthesized following the general procedure, using cyclohexene (20.3 μL , 0.20 mmol, 1.00 equiv.), lauroyl chloride (50.6 μL , 0.21 mmol, 1.05 equiv.), silver hexafluoroantimonate (75.6 mg, 0.22 mmol, 1.10 equiv.) and dichloromethane (2 mL). Purification by flash column chromatography (heptane/ethyl acetate 90:10 to 20:80) gave the title compound (> 15:1 r.r., 39.7 mg, 70%) as a white solid. ^1H NMR (600 MHz, CDCl_3): δ 3.64 (tt, $J = 10.4, 4.2$ Hz, 1H), 2.46 – 2.41 (m, 3H), 2.14 – 2.03 (m, 1H), 2.00 – 1.90 (m, 1H), 1.87 – 1.76 (m, 2H), 1.59 – 1.50 (m, 1H, overlaps with water peak), 1.40 – 1.16 (m, 22H), 0.88 (t, $J = 7.0$ Hz, 3H). ^{13}C NMR (151 MHz, CDCl_3): δ 213.0, 69.9, 49.1, 40.7, 36.9, 35.1, 31.9, 29.6 (2C), 29.5, 29.4, 29.3, 29.2, 27.4, 23.7, 23.2, 22.7, 14.1. **HRMS** (ESI^+): exact mass calculated for $[\text{M}+\text{Na}]^+$ ($\text{C}_{18}\text{H}_{34}\text{O}_2\text{Na}$) requires m/z 305.2457, found m/z 305.2449.

3-hydroxycyclohexyl)nonan-1-one (42d)



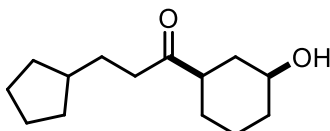
Synthesized following the general procedure, using cyclohexene (20.3 μ L, 0.20 mmol, 1.00 equiv.), nonanoyl chloride (37.9 μ L, 0.21 mmol, 1.05 equiv.), silver hexafluoroantimonate (75.6 mg, 0.22 mmol, 1.10 equiv.) and dichloromethane (2 mL). Purification by flash column chromatography (heptane/ethyl acetate 90:10 to 20:80) gave the title compound (> 28:1 r.r., 32.1 mg, 66%) as a white solid. **^1H NMR** (600 MHz, CDCl_3): δ 3.64 (tt, J = 10.4, 4.2 Hz, 1H), 2.48 – 2.38 (m, 3H), 2.11 – 2.04 (m, 1H), 1.98 – 1.90 (m, 1H), 1.87 – 1.74 (m, 2H), 1.57 – 1.52 (m, 2H), 1.36 – 1.17 (m, 15H), 0.88 – 0.86 (m, 3H). **^{13}C NMR** (151 MHz, CDCl_3): δ 213.0, 69.9, 49.2, 40.7, 36.9, 35.1, 31.8, 29.4, 29.3, 29.1, 27.5, 23.7, 23.2, 22.6, 14.1. **HRMS** (ESI^+): exact mass calculated for $[\text{M}+\text{Na}]^+$ ($\text{C}_{15}\text{H}_{28}\text{O}_2\text{Na}$) requires m/z 263.1987, found m/z 263.1974.

3-hydroxycyclohexyl)-2,2-dimethylpropan-1-one (42e)



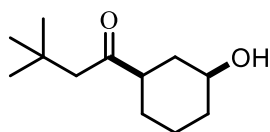
Synthesized following the general procedure, using cyclohexene (20.3 μ L, 0.20 mmol, 1.00 equiv.), pivaloyl chloride (25.9 μ L, 0.21 mmol, 1.05 equiv.), silver hexafluoroantimonate (75.6 mg, 0.22 mmol, 1.10 equiv.) and dichloromethane (2 mL). Purification by flash column chromatography (heptane/ethyl acetate 90:10 to 40:60) gave the title compound (> 17:1 r.r., 31.6 mg, 86%) as a white solid. **^1H NMR** (500 MHz, CDCl_3): δ 3.62 (app ddd, J = 14.3, 10.2, 3.9 Hz, 1H), 2.98 – 2.84 (m, 1H), 2.02 – 1.93 (m, J = 12.5 Hz, 1H), 1.92 – 1.79 (m, 2H), 1.63 – 1.53 (m, 1H, overlaps with water peak), 1.46 – 1.23 (m, 4H), 1.14 (s, 9H). **^{13}C NMR** (126 MHz, CDCl_3): δ 217.7, 70.3, 43.3, 39.9, 38.8, 35.5, 29.2, 26.3 (3C), 23.9. **HRMS** (ESI^+): exact mass calculated for $[\text{M}+\text{Na}]^+$ ($\text{C}_{11}\text{H}_{20}\text{O}_2\text{Na}$) requires m/z 207.1361, found m/z 207.1355.

3-cyclopentyl-1-(-3-hydroxycyclohexyl)propan-1-one (42g)



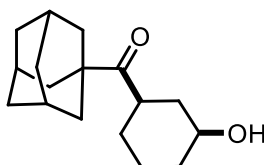
Synthesized following the general procedure, using cyclohexene (20.3 μ L, 0.20 mmol, 1.00 equiv.), cyclopentanepropionyl chloride (32.2 μ L, 0.21 mmol, 1.05 equiv.), silver hexafluoroantimonate (75.6 mg, 0.22 mmol, 1.10 equiv.) and dichloromethane (2 mL). Purification by flash column chromatography (heptane/ethyl acetate 90:10 to 40:60) gave the title compound (> 19:1 r.r., 19.1 mg, 42%) as a white solid. **^1H NMR** (400 MHz, CDCl_3): δ 3.64 (app dq, J = 10.2, 4.9, 4.1 Hz, 1H), 2.59 – 2.27 (m, 3H), 2.09 (app dd, J = 11.6, 4.6 Hz, 1H), 1.96 (app dd, J = 12.1, 4.7 Hz, 1H), 1.89 – 1.63 (m, 6H), 1.65 – 1.44 (m, 7H), 1.41 – 1.18 (m, 5H). **^{13}C NMR** (151 MHz, CDCl_3): δ 213.1, 69.9, 49.1, 40.0 (2C), 39.7, 36.9, 35.1, 32.5, 29.9, 27.5, 25.1 (2C), 23.2. **HRMS** (ESI^+): exact mass calculated for $[\text{M}+\text{Na}]^+$ ($\text{C}_{14}\text{H}_{24}\text{O}_2\text{Na}$) requires m/z 247.1674, found m/z 247.1666.

3-hydroxycyclohexyl)-3,3-dimethylbutan-1-one (42h)



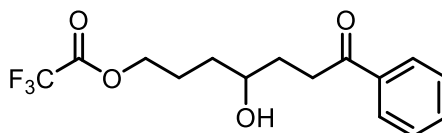
Synthesized following the general procedure, using cyclohexene (20.3 μ L, 0.20 mmol, 1.00 equiv.), 3,3-dimethylbutyryl chloride (29.4 μ L, 0.21 mmol, 1.05 equiv.), silver hexafluoroantimonate (75.6 mg, 0.22 mmol, 1.10 equiv.) and dichloromethane (2 mL). Purification by flash column chromatography (heptane/ethyl acetate 90:10 to 20:80) gave the title compound (> 18:1 r.r., 16.0 mg, 40%) as a white solid. **^1H NMR** (400 MHz, CDCl_3) δ 3.77 – 3.29 (m, 1H), 2.47 – 2.34 (m, 1H), 2.34 (s, 2H), 2.05 (ddt, J = 12.4, 4.0, 2.1 Hz, 1H), 1.99 – 1.87 (m, 1H), 1.89 – 1.71 (m, 2H), 1.27 (m, 4H), 1.00 (s, 9H). **^{13}C NMR** (101 MHz, CDCl_3): δ 212.7, 69.9, 52.9, 50.6, 36.7, 35.1, 31.0, 29.7 (3C), 27.2, 23.2. **HRMS** (ESI^+): exact mass calculated for $[\text{M}+\text{Na}]^+$ ($\text{C}_{12}\text{H}_{22}\text{O}_2\text{Na}$) requires m/z 221.1518, found m/z 221.1505.

Adamantan-1-yl(-3-hydroxycyclohexyl)methanone (42i)



Synthesized following the general procedure, using cyclohexene (20.3 μ L, 0.20 mmol, 1.00 equiv.), adamantane-1-carbonyl chloride (41.7 mg, 0.21 mmol, 1.05 equiv.), silver hexafluoroantimonate (75.6 mg, 0.22 mmol, 1.10 equiv.) and dichloromethane (2 mL). Purification by flash column chromatography (heptane/ethyl acetate 90:10 to 20:80) gave the title compound (> 15:1 r.r., 43.1 mg, 82%) as a white solid. **^1H NMR** (400 MHz, CDCl_3): δ 3.75 – 3.36 (m, 1H), 2.95 (tt, J = 11.3, 3.5 Hz, 1H), 2.05 (m, 3H), 2.00 – 1.92 (m, 1H), 1.91 – 1.62 (m, 15H), 1.54 (app dd, J = 9.9, 4.3 Hz, 1H), 1.46 – 1.18 (m, 4H). **^{13}C NMR** (101 MHz, CDCl_3): δ 216.8, 70.0, 46.9, 41.9, 38.2, 37.7 (3C), 36.5 (3C), 35.2, 28.6, 27.8 (3C), 23.6. **HRMS** (ESI^+): exact mass calculated for $[\text{M}+\text{Na}]^+$ ($\text{C}_{17}\text{H}_{26}\text{O}_2\text{Na}$) requires m/z 285.1831, found m/z 285.1822.

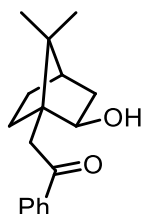
4-hydroxy-7-oxo-7-phenylheptyl 2,2,2-trifluoroacetate (43d)



Synthesized following the general procedure, using hex-5-en-1-yl 2,2,2-trifluoroacetate (39.2 mg, 0.20 mmol, 1.00 equiv.), benzoyl chloride (24.2 μ L, 0.21 mmol, 1.05 equiv.), silver hexafluoroantimonate (75.6 mg, 0.22 mmol, 1.10 equiv.) and dichloromethane (2 mL), with a reaction time of 30 minutes. Purification by flash column chromatography (heptane/ethyl acetate 90:10 to 20:80) gave the title compound (> 19:1 r.r., 40.1 mg, 63%) as a pale orange oil. **^1H NMR** (400 MHz, CDCl_3): δ 8.03 – 7.85 (m, 2H), 7.62 – 7.52 (m, 1H), 7.47 (t, J = 7.7 Hz, 2H), 4.44 – 4.30 (m, 2H), 3.72 (dt, J = 8.2, 4.1 Hz, 1H), 3.17 (t, J = 6.7 Hz, 2H), 2.17 (brs, 1H), 2.04 – 1.92 (m, 2H), 1.92 – 1.80 (m, 2H), 1.66 – 1.49 (m, 2H). **^{13}C NMR** (101 MHz, CDCl_3): δ 200.8, 157.3, 136.7, 133.3, 128.6 (2C), 128.1 (2C), 115.9, 70.8, 68.2, 34.9, 33.6, 31.4, 24.6.

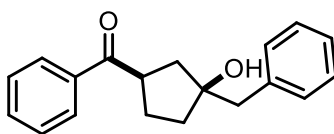
¹⁹F NMR (376 MHz, CDCl₃) δ -75.09. **HRMS** (ESI⁺): exact mass calculated for [M+H]⁺ (C₁₅H₁₇F₃O₄H) requires *m/z* 319.1079, found *m/z* 319.1143.

2-hydroxy-7,7-dimethylbicyclo[2.2.1]heptan-1-yl)-1-phenylethan-1-one (43f)



Synthesized following the general procedure, using (±)-camphene (64.2 μL, 0.40 mmol, 1.00 equiv.), benzoyl chloride (48.4 μL, 0.42 mmol, 1.05 equiv.), silver hexafluoroantimonate (151.2 mg, 0.44 mmol, 1.10 equiv.) and dichloromethane (4 mL), with a reaction time of 30 minutes. Purification by flash column chromatography (heptane/ethyl acetate 90:10 to 20:80) gave the title compound (33.0 mg, 32%) as a pale yellow solid. **¹H NMR** (400 MHz, CDCl₃): δ 8.00 (d, *J* = 7.4 Hz, 2H), 7.62 – 7.53 (m, 1H), 7.48 (t, *J* = 7.7 Hz, 2H), 3.89 – 3.74 (m, 1H), 3.43 (d, *J* = 2.6 Hz, 1H), 3.22 (d, *J* = 13.5 Hz, 1H), 2.83 (d, *J* = 13.5 Hz, 1H), 1.87 – 1.76 (m, 1H), 1.77 – 1.63 (m, 3H), 1.52 – 1.42 (m, 1H), 1.15 (s, 3H), 1.05 – 0.96 (m, 1H), 0.94 (s, 3H). **¹³C NMR** (101 MHz, CDCl₃): δ 203.6, 137.7, 133.4, 128.7 (2C), 128.5 (2C), 77.0, 52.5, 47.5, 44.6, 38.8, 34.7, 30.9, 27.2, 20.7, 20.1. **HRMS** (ESI⁺): exact mass calculated for [M+Na]⁺ (C₁₇H₂₂O₂Na) requires *m/z* 281.3498, 281.2499.

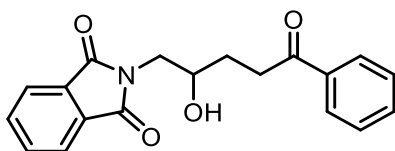
(3-benzyl-3-hydroxycyclopentyl)(phenyl)methanone (43g)



Synthesized following the general procedure, using (cyclopent-3-en-1-ylmethyl)benzene (**XX**) (31.6 mg, 0.20 mmol, 1.00 equiv.), benzoyl chloride (24.2 μL, 0.21 mmol, 1.05 equiv.), silver hexafluoroantimonate (75.6 mg, 0.22 mmol, 1.10 equiv.) and dichloromethane (2 mL), with a reaction time of 30 minutes. Purification by flash column chromatography

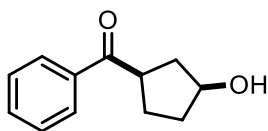
(Heptane/ethyl acetate 90:10 to 20:80) gave the title compound (42.0 mg, 71%) as a colorless oil. **¹H NMR** (400 MHz, CDCl₃): δ 7.93 – 7.76 (m, 2H), 7.49 (t, *J* = 7.4 Hz, 1H), 7.43 – 7.36 (m, 2H), 7.26 – 7.11 (m, 5H, overlaps with CDCl₃ peak), 3.95 – 3.69 (m, 1H), 3.17 (brs, 1H), 2.89 (app q, *J* = 13.4 Hz, 1H), 2.14 – 2.00 (m, 1H), 2.00 – 1.84 (m, 3H), 1.76 – 1.61 (m, 2H). **¹³C NMR** (101 MHz, CDCl₃): δ 204.6, 138.5, 136.1, 133.3, 130.3 (2C), 128.7 (2C), 128.6 (2C), 128.1 (2C), 126.2, 81.8, 45.9, 44.3, 40.9, 39.9, 29.2. **HRMS** (ESI⁺): exact mass calculated for [M+Na]⁺ (C₁₉H₂₀O₂Na) requires *m/z* 303.1361, found *m/z* 303.1353.

2-(2-hydroxy-5-oxo-5-phenylpentyl)isoindoline-1,3-dione (43h)



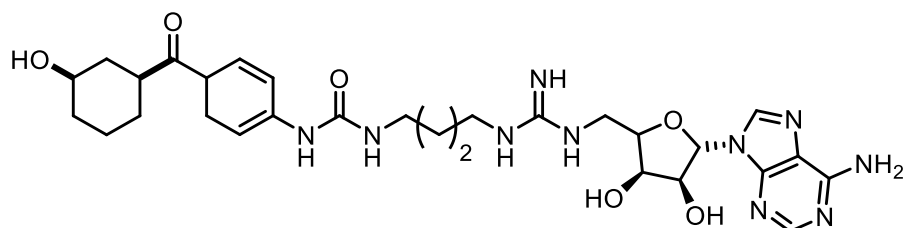
Synthesized following the general procedure, using N-(3-buten-1-yl)phthalimide (41.1 mg, 0.20 mmol, 1.00 equiv.), benzoyl chloride (24.2 μL, 0.21 mmol, 1.05 equiv.), silver hexafluoroantimonate (75.6 mg, 0.22 mmol, 1.10 equiv.) and dichloromethane (2 mL), with a reaction time of 30 minutes. Purification by flash column chromatography (toluene/ethyl acetate 100:0 to 60:40) gave the title compound (34.2 mg, 54%) as a pale yellow solid. **¹H NMR** (400 MHz, CDCl₃): δ 7.94 (d, *J* = 7.7 Hz, 2H), 7.85 (dd, *J* = 5.4, 3.1 Hz, 2H), 7.72 (dd, *J* = 5.4, 3.1 Hz, 2H), 7.61 – 7.54 (m, 1H), 7.46 (t, *J* = 7.6 Hz, 2H), 4.26 (dt, *J* = 12.4, 4.2 Hz, 1H), 3.92 (t, *J* = 6.6 Hz, 1H), 3.49 (d, *J* = 3.7 Hz, 1H), 3.32 – 2.94 (m, 2H), 1.92 (m, 2H). **¹³C NMR** (101 MHz, CDCl₃): δ 199.9, 168.7 (2C), 136.8, 134.0 (2C), 133.5, 132.1 (2C), 128.7 (2C), 128.1 (2C), 123.3 (2C), 65.3, 44.8, 35.3, 34.7. **HRMS** (ESI⁺): exact mass calculated for [M+Na]⁺ (C₁₉H₁₇NO₄Na) requires *m/z* 346.1056, found *m/z* 346.1039.

3-hydroxycyclopentyl(phenyl)methanone (43j)



Synthesized following the general procedure, using cyclopentene (17.7 μ L, 0.20 mmol, 1.00 equiv.), benzoyl chloride (24.4 μ L, 0.21 mmol, 1.05 equiv.), silver hexafluoroantimonate (75.6 mg, 0.22 mmol, 1.10 equiv.) and dichloromethane (2 mL). Purification by flash column chromatography (heptane/ethyl acetate 90:10 to 20:80) gave the title compound (26.3 mg, 78%) as a colorless oil. **¹H NMR** (500 MHz, CDCl₃): δ 7.95 – 7.90 (m, 2H), 7.59 – 7.52 (m, 1H), 7.50 – 7.42 (m, 2H), 4.37 – 4.15 (m, 1H), 3.14 – 2.98 (m, 1H), 2.01 – 1.79 (m, 4H), 1.78 – 1.71 (m, 2H), **¹³C NMR** (126 MHz, CDCl₃): δ 215.9, 133.0, 128.6 (2C), 128.3 (2C), 73.5, 48.9, 42.3, 37.5, 35.9, 31.8, 29.3, 29.2. **HRMS (ESI⁺)**: exact mass calculated for [M+Na]⁺ (C₁₂H₁₄O₂Na) requires m/z 213.0886, found m/z 213.0882.

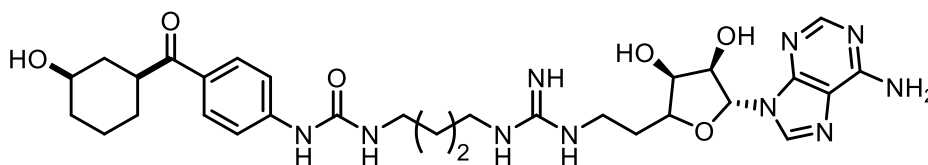
1-(3-(3-(((3*S*,4*R*,5*R*)-5-(6-amino-9*H*-purin-9-yl)-3,4-dihydroxytetrahydrofuran-2-yl)methyl)guanidino)propyl)-3-(4-((1*S*,3*R*)-3-hydroxycyclohexane-1-carbonyl)cyclohexa-1,5-dien-1-yl)urea (46)



Compound **51** (0.100 g, 0.110 mmol) was dissolved in a solution of DCM/TFA/H₂O 4:5:1. The resulting mixture was stirred at room temperature for 24 h. The solvent was evaporated, and the crude was purified by HPLC with a gradient from 5% to 90% v/v acetonitrile with 0.1% solution of TFA over 15 min to yield the TFA salt **46** as a white solid. (55 mg, 70%). **¹H NMR** (400 MHz, DMSO-*d*₆) δ 9.00 (s, 1H, exchangeable with D₂O), 8.46 (s, 1H), 8.29 (s, 1H), 7.99 (br s, 1H, exchangeable with D₂O), 7.86 (d, J = 9.0 Hz, 2H), 7.52 (d, J = 9.0 Hz, 2H), 7.45 – 7.33 (m, 4H, exchangeable with D₂O), 6.45 (br t, J = 5.9 Hz, 1H, exchangeable with D₂O), 5.95 (d, J = 5.7

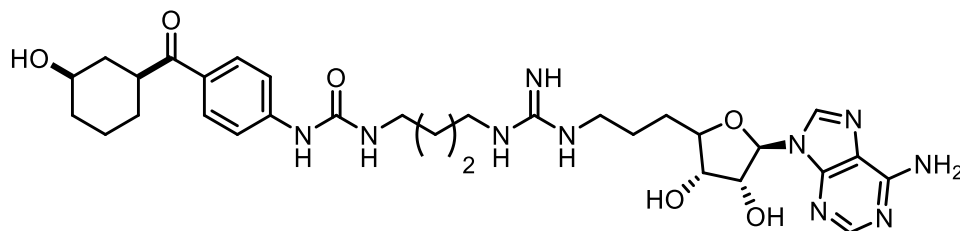
Hz, 1H), 4.71 (t, $J = 5.5$ Hz, 1H), 4.23 – 4.10 (m, 1H), 4.03 (dt, $J = 8.4, 4.2$ Hz, 1H), 3.59 – 3.48 (m, 1H, overlaps with H₂O peak), 3.43 – 3.29 (m, 1H), 3.18 – 2.97 (m, 4H), 1.96 – 1.80 (m, 2H), 1.80 – 1.71 (m, 1H), 1.71 – 1.60 (m, 1H), 1.50 – 1.34 (m, 4H), 1.26 – 0.98 (m, 4H). ¹³C NMR (100 MHz, DMSO-*d*₆) δ 200.9, 156.3, 155.3, 154.8, 150.9, 149.5, 145.6, 141.3, 130.1, 128.8, 119.7, 117.1, 88.3, 82.9, 73.2, 71.5, 68.8, 43.6, 43.3, 41.2, 35.8, 28.9, 27.4, 26.3, 23.9. HRMS (ESI): m/z [M + H]⁺ calcd. for C₂₉H₄₀N₁₀O₆ + H⁺: 625.3205. Found: 613.3209.

1-(3-(3-(2-((3*S*,4*R*,5*R*)-5-(6-amino-9*H*-purin-9-yl)-3,4-dihydroxytetrahydrofuran-2-yl)ethyl)guanidino)propyl)-3-(4-((1*S*,3*R*)-3-hydroxycyclohexane-1-carbonyl)cyclohexa-1,5-dien-1-yl)urea (47)



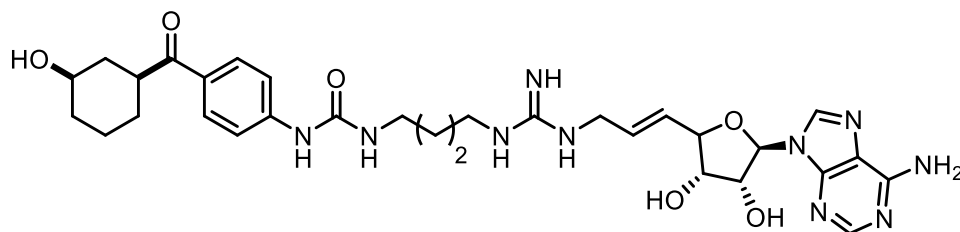
Compound **47** was obtained as a white solid (0.042 g, 75%) starting from compound **52** (0.080 g, 0.075 mmol) following the procedure described for **46**. ¹H NMR (400 MHz, DMSO-*d*₆) δ 9.01 (s, 1H, exchangeable with D₂O), 8.46 (s, 1H), 8.27 (s, 1H), 7.97 (br s, 1H, exchangeable with D₂O), 7.85 (d, $J = 9.0$ Hz, 1H), 7.52 (d, $J = 9.0$ Hz, 2H), 7.41 – 7.25 (m, 4H, exchangeable with D₂O), 6.48 (br t, $J = 5.8$ Hz, 1H, exchangeable with D₂O), 5.90 (d, $J = 5.1$ Hz, 1H), 4.67 (t, $J = 5.2$ Hz, 1H), 4.11 (t, $J = 4.9$ Hz, 1H), 3.98 – 3.91 (m, 1H), 3.41 – 3.30 (m, 1H, overlaps with H₂O peak), 3.26 – 3.16 (m, 2H), 3.20 – 2.85 (m, 5H), 1.99 – 1.80 (m, 4H), 1.79 – 1.71 (m, 1H), 1.71 – 1.61 (m, 1H), 1.52 – 1.34 (m, 4H), 1.27 – 0.98 (m, 4H). ¹³C NMR (100 MHz, DMSO-*d*₆) δ 200.9, 156.0, 155.3, 154.7, 150.8, 149.5, 145.6, 141.3, 130.1, 128.8, 119.6, 117.1, 88.4, 81.7, 73.7, 73.5, 68.8, 43.3, 41.1, 39.0, 38.5, 35.8, 32.8, 28.9, 27.4, 26.4, 23.9. HRMS (ESI): m/z [M + H]⁺ calcd. for C₃₀H₄₂N₁₀O₆ + H⁺: 639.3362 Found: 639.3360.

1-(3-(3-(3-((3*S*,4*R*,5*R*)-5-(6-amino-9*H*-purin-9-yl)-3,4-dihydroxytetrahydrofuran-2-yl)propyl)guanidino)propyl)-3-(4-((1*S*,3*R*)-3-hydroxycyclohexane-1-carbonyl)phenyl)urea (48)



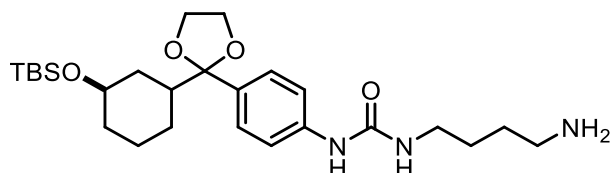
Compound **48** was obtained as a white solid (0.056 g, 80%) starting from compound **53** (0.090 g, 0.095 mmol) following the procedure described for **46**. ¹H NMR (400 MHz, DMSO-*d*₆) δ 8.99 (s, 1H, exchangeable with D₂O), 8.43 (s, 1H), 8.27 (s, 1H), 7.98 – 7.76 (m, 3H, 1H exchangeable with D₂O), 7.60 – 7.47 (m, 2H), 7.41 – 7.23 (m, 4H, exchangeable with D₂O), 6.46 (br t, *J* = 5.8 Hz, 1H, exchangeable with D₂O), 5.88 (d, *J* = 5.0 Hz, 1H), 4.64 (t, *J* = 5.1 Hz, 1H), 4.07 (t, *J* = 5.1 Hz, 1H), 3.88 – 3.79 (m, 1H, overlaps with H₂O peak), 3.59 – 3.52 (m, 1H, overlaps with H₂O peak), 3.42 – 3.31 (m, 1H), 3.20 – 3.03 (m, 6H), 1.96 – 1.81 (m, 2H), 1.79 – 1.63 (m, 4H), 1.61 – 1.52 (m, 2H), 1.51 – 1.36 (m, 4H), 1.29 – 0.93 (m, 4H). ¹³C NMR (100 MHz, DMSO-*d*₆) δ 200.9, 155.9, 155.3, 154.9, 149.5, 145.6, 141.2, 130.1, 128.8, 119.6, 117.1, 88.3, 83.7, 73.7, 73.6, 68.8, 43.5, 41.2, 41.1, 39.0, 35.8, 30.5, 28.9, 27.4, 26.4, 25.5, 23.9. HRMS (ESI): *m/z* [M + H]⁺ calcd. for C₃₁H₄₄N₁₀O₆ + H⁺: 654.7716 Found: 654.7710.

1-(4-(3-((*E*)-3-((3*S*,4*R*,5*R*)-5-(6-amino-9*H*-purin-9-yl)-3,4-dihydroxytetrahydrofuran-2-yl)allyl)guanidino)butyl)-3-(4-((1*S*,3*R*)-3-hydroxycyclohexane-1-carbonyl)phenyl)urea (49)



Compound **49** was obtained as a white solid (0.033 g, 70%) starting from compound **54** (0.060 g, 0.063 mmol) following the procedure described for **46**. **¹H NMR** (400 MHz, DMSO-*d*₆) δ 9.08 (s, 1H, exchangeable with D₂O), 8.37 (s, 1H), 8.22 (s, 1H), 7.86 (d, *J* = 9.0 Hz, 2H), 7.69 – 7.55 (m, 2H, exchangeable with D₂O), 7.58 – 7.44 (m, 3H, 1H exchangeable with D₂O), 7.38 (s, 1H, exchangeable with D₂O), 6.57 (br t, *J* = 5.8 Hz, 1H, exchangeable with D₂O), 5.96 – 5.80 (m, 2H), 5.80 – 5.61 (m, 1H), 4.69 (t, *J* = 5.0 Hz, 1H), 4.44 – 4.33 (m, 1H), 4.13 (t, *J* = 4.9 Hz, 1H), 3.92 – 3.72 (m, 2H), 3.62 – 3.33 (m, 2H, overlaps with H₂O peak), 3.22 – 3.04 (m, 4H), 1.96 – 1.82 (m, 2H), 1.80 – 1.61 (m, 2H), 1.52 – 1.37 (m, 4H), 1.29 – 1.01 (m, 4H). **¹³C NMR** (100 MHz, DMSO-*d*₆) δ 200.9, 158.7, 158.4, 155.9, 155.4, 152.0, 149.7, 145.7, 140.8, 130.5, 130.0, 128.8, 128.3, 117.1, 88.3, 84.2, 74.5, 73.3, 68.8, 43.3, 42.3, 41.2, 39.0, 35.7, 28.9, 27.4, 26.4, 23.9. **HRMS** (ESI): *m/z* [M + H]⁺ calcd. for C₃₁H₄₂N₁₀O₆ + H⁺: 651.3362 Found: 651.3359.

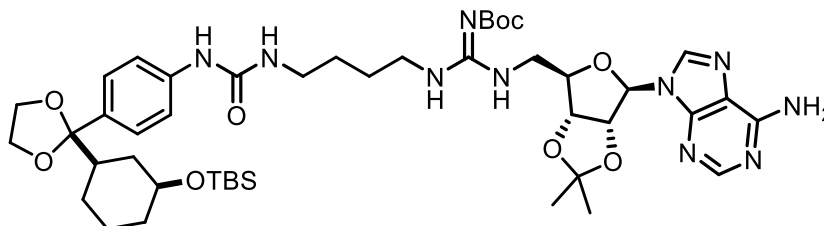
1-(4-aminobutyl)-3-(4-(2-((3R)-3-((tert-butyldimethylsilyl)oxy)cyclohexyl)-1,3-dioxolan-2-yl)phenyl)urea (50)



A mixture of **64** (0.400 g, 0.61 mmol), Pd/C 10% (0.040 g), and ammonium formate (0.800 g, 12.8 mmol) in MeOH (10 mL) was heated at reflux with stirring for 1 h. After cooling, the reaction mixture was extracted with ethyl acetate (3 x 50 mL). The extract was washed with water (50 mL) and brine (50 mL) and dried over Na₂SO₄, filtered and the solvent was concentrated under vacuum. The crude product was purified by flash column chromatography on silica gel (hexane/ethyl acetate 6:4 to 2:8) to give the title compound **50** as an uncoloured oil (0.30 g, 99%). **¹H NMR** (400 MHz, CDCl₃) δ 7.37 – 7.28 (m, 2H), 7.25 – 7.19 (m, 2H), 6.46 (br s, 1H), 5.16 (br s, 1H), 4.03 – 3.89 (m, 2H), 3.81 – 3.64 (m, 2H), 3.53 – 3.43 (m, 1H),

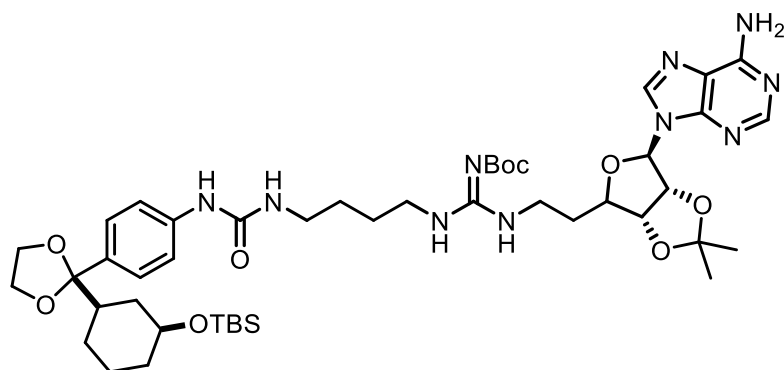
3.27 (q, $J = 7.7$ Hz, 2H), 2.73 (t, $J = 6.7$ Hz, 2H), 2.05 – 1.88 (m, 1H), 1.86 – 1.73 (m, 2H), 1.66 – 1.39 (m, 8H), 1.17 – 0.98 (m, 2H), 0.86 (s, 9H), 0.02 (s, 6H). **MS** (ESI) m/z : 492 (M+H)⁺.

1-(4-((E)-3-(((3aR,4R,6R,6aR)-6-(6-tert-butoxycarbonyl amino-9H-purin-9-yl)-2,2-dimethyltetrahydrofuro[3,4-d][1,3]dioxol-4-yl)methyl)-2-methylguanidino)butyl)-3-(4-(2-((1R,3S)-3-((tert-butyldimethylsilyl)oxy)cyclohexyl)-1,3-dioxolan-2-yl)phenyl)urea--2-methylpropan-2-ol (51)



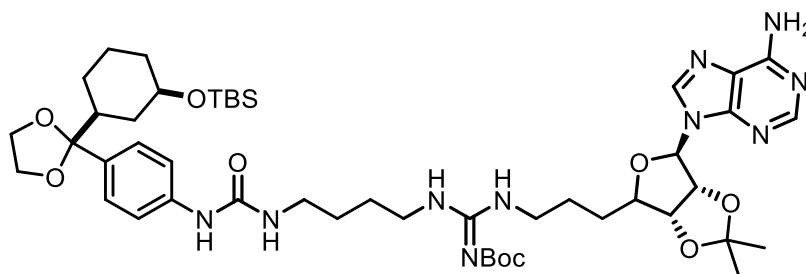
Compound **51** was obtained as a white solid (0.060 mg, 65%) starting from compound **13a** (0.047 mg, 0.10 mmol) with compound **50** (0.060 g, 0.12 mmol) following the procedure described for **27a**. **¹H NMR** (400 MHz, DMSO- d_6) δ 8.41 (br s, 1H, exchangeable with D₂O), 8.36 (s, 1H), 8.19 (s, 1H), 7.44 – 7.27 (m, 4H, 2H exchangeable with D₂O), 7.25 – 7.11 (m, 2H), 6.25 – 6.03 (m, 2H, 1H exchangeable with D₂O), 5.53 – 5.31 (m, 1H), 5.10 – 4.91 (m, 1H), 4.37 – 4.13 (m, 1H), 3.99 – 3.84 (m, 2H), 3.69 – 3.55 (m, 2H), 3.54 – 3.47 (m, 1H), 3.48 – 3.40 (m, 2H), 3.18 – 3.02 (m, 4H), 1.90 – 1.81 (m, 1H), 1.82 – 1.69 (m, 2H), 1.67 – 1.57 (m, 1H), 1.54 (s, 3H), 1.46 – 1.38 (m, 4H), 1.37 (s, 9H), 1.33 (s, 3H), 1.19 – 1.02 (m, 1H), 1.02 – 0.88 (m, 4H), 0.83 (s, 9H), 0.02 (s, 3H). **MS** (ESI) m/z : 924 (M+H)⁺.

1-(4-((E)-3-(((3aR,4R,6R,6aR)-6-(6-tert-butoxycarbonyl amino-9H-purin-9-yl)-2,2-dimethyltetrahydrofuro[3,4-d][1,3]dioxol-4-yl) ethyl)-2-methylguanidino)butyl)-3-(4-(2-((1R,3S)-3-((tert-butyldimethylsilyl)oxy)cyclohexyl)-1,3-dioxolan-2-yl)phenyl)urea--2-methylpropan-2-ol (52)



Compound **52** was obtained as a white solid (0.065 mg, 70%) starting from compound **13b** (0.048 mg, 0.10 mmol) with compound **50** (0.060 g, 0.12 mmol) following the procedure described for **27a**. ^1H NMR (400 MHz, DMSO- d_6) δ 8.40 (br s, 1H, exchangeable with D $_2$ O), 8.34 (s, 1H), 8.18 (s, 1H), 7.43 – 7.25 (m, 4H, 2H exchangeable with D $_2$ O), 7.20 – 7.13 (m, 2H), 6.25 – 6.01 (m, 2H, 1H exchangeable with D $_2$ O), 5.50 – 5.29 (m, 1H), 5.15 – 4.94 (m, 1H), 4.37 – 4.13 (m, 1H), 3.95 – 3.80 (m, 2H), 3.67 – 3.50 (m, 2H), 3.50 – 3.44 (m, 1H), 3.48 – 3.40 (m, 2H), 3.18 – 3.02 (m, 4H), 1.89 – 1.81 (m, 1H), 1.82 – 1.69 (m, 4H), 1.67 – 1.55 (m, 1H), 1.52 (s, 3H), 1.46 – 1.35 (m, 4H), 1.38 (s, 9H), 1.34 (s, 3H), 1.15 – 1.02 (m, 1H), 1.00 – 0.88 (m, 4H), 0.85 (s, 9H), 0.02 (s, 3H). MS (ESI) m/z : 938 ($M+H$) $^+$.

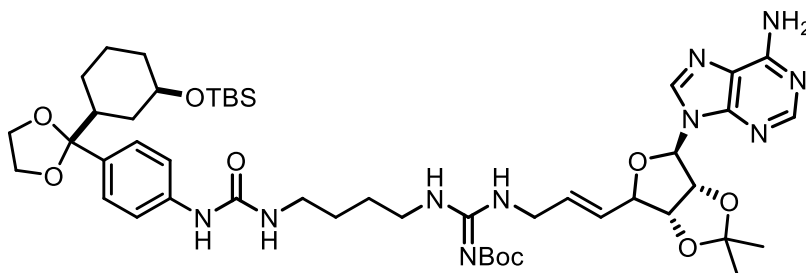
1-(4-((E)-3-(((3aR,4R,6R,6aR)-6-(6-tert-butoxycarbonyl amino-9H-purin-9-yl)-2,2-dimethyltetrahydrofuro[3,4-d][1,3]dioxol-4-yl) propyl)-2-methylguanidino)butyl)-3-(4-(2-((1R,3S)-3-((tert-butyldimethylsilyl)oxy)cyclohexyl)-1,3-dioxolan-2-yl)phenyl)urea--2-methylpropan-2-ol (53)



Compound **53** was obtained as a white solid (0.069 mg, 73%) starting from compound **13c** (0.050 mg, 0.10 mmol) with compound **50** (0.060 g, 0.12 mmol) following the procedure

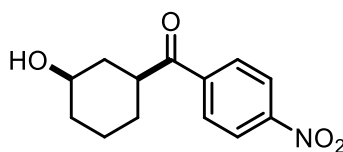
described for **27a**. $^1\text{H NMR}$ (400 MHz, DMSO- d_6) δ 8.39 (br s, 1H, exchangeable with D₂O), 8.33 (s, 1H), 8.16 (s, 1H), 7.41 – 7.23 (m, 4H, 2H exchangeable with D₂O), 7.21 – 7.17 (m, 2H), 6.24 – 6.00 (m, 2H, 1H exchangeable with D₂O), 5.51 – 5.28 (m, 1H), 5.13 – 4.93 (m, 1H), 4.37 – 4.12 (m, 1H), 3.97 – 3.80 (m, 2H), 3.65 – 3.49 (m, 2H), 3.48 – 3.42 (m, 1H), 3.40 – 3.37 (m, 2H), 3.16 – 3.02 (m, 4H), 1.89 – 1.81 (m, 1H), 1.82 – 1.69 (m, 4H), 1.67 – 1.50 (m, 3H), 1.49 (s, 3H), 1.46 – 1.37 (m, 4H), 1.36 (s, 9H), 1.33 (s, 3H), 1.12 – 1.02 (m, 1H), 1.00 – 0.89 (m, 4H), 0.82 (s, 9H), 0.02 (s, 3H). **MS** (ESI) m/z : 952 (M+H)⁺.

1-(4-((E)-3-(((3aR,4R,6R,6aR)-6-(6-tert-butoxycarbonyl amino-9H-purin-9-yl)-2,2-dimethyltetrahydrofuro[3,4-d][1,3]dioxol-4-yl)propyl)-allyl)guanidino)butyl)-3-(4-(2-((1R,3S)-3-((tert-butyldimethylsilyl)oxy)cyclohexyl)-1,3-dioxolan-2-yl)phenyl)urea--2-methylpropan-2-ol (54)



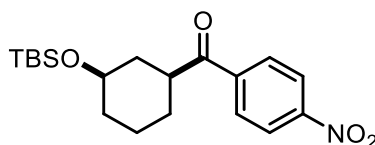
Compound **54** was obtained as a white solid (0.076 mg, 80%) starting from compound **13d** (0.049 mg, 0.10 mmol) with compound **50** (0.060 g, 0.12 mmol) following the procedure described for **27a**. $^1\text{H NMR}$ (400 MHz, DMSO- d_6) δ 8.40 (br s, 1H, exchangeable with D₂O), 8.30 (s, 1H), 8.17 (s, 1H), 7.38 – 7.27 (m, 4H, 2H exchangeable with D₂O), 7.20 – 7.10 (m, 2H), 6.21 – 5.99 (m, 2H, 1H exchangeable with D₂O), 5.80 – 5.63 (m, 2H), 5.49 – 5.31 (m, 1H), 5.02 – 4.87 (m, 1H), 4.66 – 4.50 (m, 1H), 3.94 – 3.83 (m, 2H), 3.79 – 3.71 (m, 2H), 3.65 – 3.54 (m, 2H), 3.54 – 3.45 (m, 1H), 3.16 – 3.02 (m, 4H), 1.88 – 1.82 (m, 1H), 1.81 – 1.67 (m, 2H), 1.65 – 1.55 (m, 1H), 1.55 (s, 3H), 1.35 (s, 9H), 1.24 (s, 3H), 1.18 – 1.06 (m, 1H), 1.00 – 0.87 (m, 3H), 0.82 (s, 9H), 0.02 (s, 6H). **MS** (ESI) m/z : 950 (M+H)⁺.

((1S,3R)-3-hydroxycyclohexyl)(4-nitrophenyl)methanone (57)



In a flame-dried Schlenk tube at ambient temperature, a solution of cyclohexene (103 μ L, 1 mmol) and 4-nitrobenzoylchloride (0.195 g, 1.05 mmol) in dichloromethane (10 mL) was treated with silver hexafluoroantimonate (0.378 g, 1.1 mmol) and the resulting suspension was immediately placed in a pre-heated oil bath at 35 $^{\circ}$ C. After vigorously stirring the reaction mixture at the same temperature for 10 min, the reaction vessel was removed from the oil bath and a saturated aqueous solution of sodium bicarbonate (the same amount of DCM) was added, followed by vigorous stirring for 10 min. After this time, the phases were separated, the aqueous phase was extracted with DCM (3 \times 25 mL) and the combined organic phases were dried over Na_2SO_4 , filtered and the filtrate was concentrated under reduced pressure. The resulting crude material was purified by flash column chromatography on silica gel (hexane/ethyl acetate 8:2 to 2:8) to give the title compound **57** as yellow solid (0.157 g, 63 %). ^1H NMR (400 MHz, Chloroform- d) δ 8.36 – 8.26 (m, 2H), 8.10 – 8.03 (m, 2H), 3.84 – 3.70 (m, 1H), 3.34 (ddd, J = 14.9, 7.4, 3.5 Hz, 1H), 2.21 – 2.10 (m, 1H), 2.09 – 2.00 (m, 1H), 1.99 – 1.81 (m, 2H), 1.51 – 1.39 (m, 2H), 1.38 – 1.18 (m, 2H). MS (ESI) m/z : 250 ($\text{M}+\text{H}$) $^{+}$.

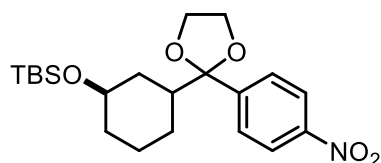
((1S,3R)-3-((*tert*-butyldimethylsilyl)oxy)cyclohexyl)(4-nitrophenyl)methanone (58)



To a solution of **57** (0.157 g, 0.63 mmol) in dichloromethane (1 mL) were added *tert*-butyldimethylsilyl chloride (0.143 g, 0.95 mmol) and imidazole (0.064 g, 0.95 mmol), and this was stirred for 1 h at room temperature. Then the reaction mixture was diluted with brine solution (25 mL) and then extracted with ethyl acetate (3 \times 25 mL). The organic phase was

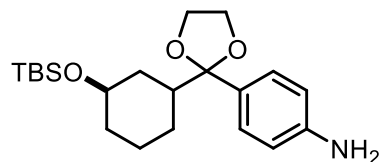
dried over anhydrous Na₂SO₄ and filtered. Solvent was removed using a rotary evaporator. The crude was directly used in the next step without further purification step. **¹H NMR** (400 MHz, Chloroform-d) δ 8.42 – 8.22 (m, 2H), 8.18 – 7.93 (m, 2H), 3.81 – 3.58 (m, 1H), 3.42 – 3.09 (m, 1H), 2.10 – 1.74 (m, 4H), 1.64 – 1.22 (m, 4H), 0.88 (s, 9H), 0.07 (s, 6H). **MS** (ESI) m/z: 364 (M+H)⁺.

tert-butyl dimethyl(((1R)-3-(2-(4-nitrophenyl)-1,3-dioxolan-2-yl)cyclohexyl)oxy)silane (59)



To a solution of **58** (0.229 g, 0.63 mmol) in dichloromethane (3 mL) were added at 0 °C 1,2-Ethanediol (0.632 mL, 11.34 mmol) and boron trifluoride diethyl etherate (0.778 mL, 6.3 mmol), and this was stirred for 12 h at room temperature. Then the reaction mixture was diluted with NaHCO₃ (25 mL) and then extracted with DCM (3 × 25 mL). The organic phase was dried over anhydrous Na₂SO₄ and filtered. Solvent was removed using a rotary evaporator. The crude was directly used in the next step without further purification step. **¹H NMR** (400 MHz, CDCl₃) δ 8.27 – 8.09 (m, 2H), 7.66 – 7.53 (m, 2H), 4.10 – 3.86 (m, 2H), 3.82 – 3.65 (m, 2H), 3.56 – 3.40 (m, 1H), 1.97 – 1.87 (m, 1H), 1.87 – 1.74 (m, 2H), 1.71 – 1.64 (m, 1H), 1.56 – 1.43 (m, 3H), 1.17 – 0.98 (m, 2H), 0.86 (s, 9H), 0.10 (s, 3H), 0.02 (s, 3H). **MS** (ESI) m/z: 408 (M+H)⁺.

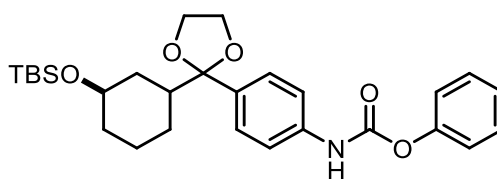
4-(2-((3R)-3-((tert-butyl dimethylsilyl)oxy)cyclohexyl)-1,3-dioxolan-2-yl)aniline (60)



A mixture of **59** (0.258 g, 0.63 mmol), Pd/C 10% (0.03 g) in EtOH (6 mL) was stirred under H₂ for 24 h. After, the reaction mixture was filtered, and the solvent was concentrated under vacuum. The resulting crude material was purified by flash column chromatography on silica

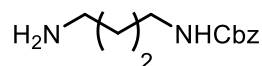
gel (hexane/ethyl acetate 8:2 to 2:8) to give the title compound **60** as pale yellow solid (0.157 g, 63%). ¹H NMR (400 MHz, CDCl₃) δ 7.21 – 7.13 (m, 2H), 6.67 – 6.57 (m, 2H), 3.97 – 3.89 (m, 2H), 3.76 – 3.70 (m, 2H), 3.65 (br s, 2H, exchangeable with D₂O), 3.55 – 3.46 (m, 1H), 2.03 – 1.92 (m, 1H), 1.82 – 1.73 (m, 2H), 1.72 – 1.64 (m, 1H), 1.17 – 1.00 (m, 4H), 0.86 (s, 9H), 0.02 (s, 6H). MS (ESI) m/z: 378 (M+H)⁺.

Phenyl (4-(2-((3R)-3-((tert-butyldimethylsilyl)oxy)cyclohexyl)-1,3-dioxolan-2-yl)phenyl)carbamate (61)



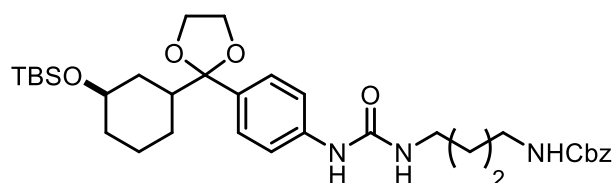
Compound **61** was obtained as a white solid (0.397 g, 80%) starting from compound **60** (0.140 g, 0.37 mmol) following the procedure described for **18**. ¹H NMR (400 MHz, CDCl₃) δ 7.47 – 7.33 (m, 5H), 7.28 – 7.23 (m, 2H), 7.22 – 7.16 (m, 2H), 6.97 (br s, 1H, exchangeable with D₂O), 3.97 – 3.87 (m, 2H), 3.76 – 3.71 (m, 2H), 3.55 – 3.45 (m, 1H), 2.00 – 1.92 (m, 1H), 1.84 – 1.72 (m, 2H), 1.71 – 1.63 (m, 1H), 1.15 – 1.00 (m, 4H), 0.84 (s, 9H), 0.02 (s, 6H). MS (ESI) m/z: 498 (M+H)⁺.

Benzyl (3-aminobutyl)carbamate (63)



Compound **63** was obtained as a white solid (1.11 g, 85%) starting from **55** (1.59 g, 17.6 mmol) with benzyl chloroformate (4.90 mL, 5.88 mmol) following the procedure described for **11a**. ¹H NMR (400 MHz, CDCl₃) δ 7.31 – 7.25 (m, 5H), 5.74 (br s, 1H), 5.06 (s, 2H), 3.14 (q, *J* = 6.0 Hz, 2H), 2.65 (t, *J* = 6.0 Hz, 2H), 1.48 – 1.33 (m, 6H). MS (ESI) m/z: 223 (M+H)⁺.

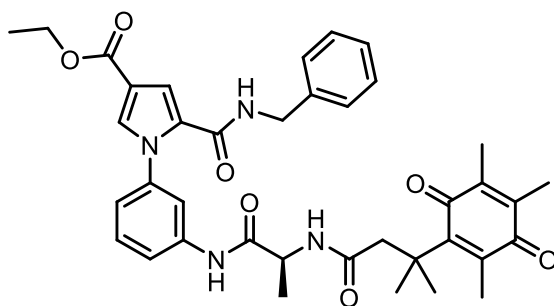
Benzyl (3-(3-(4-(2-((3*R*)-3-((*tert*-butyldimethylsilyl)oxy)cyclohexyl)-1,3-dioxolan-2-yl)phenyl)ureido)butyl)carbamate (**64**)



Compound **64** was obtained as a white solid (0.400 g, 80%) by reaction of **61** (0.397 g, 0.80 mmol) with **63** (0.355 g, 1.60 mmol), following the procedure described for **21a**. ¹H NMR (400 MHz, CDCl₃) δ 7.31 – 7.25 (m, 5H), 7.25 – 7.22 (m, 2H), 7.18 – 7.12 (m, 2H), 6.45 (br s, 1H), 5.16 (br s, 1H), 5.04 (s, 2H), 4.00 – 3.88 (m, 2H), 3.80 – 3.62 (m, 2H), 3.53 – 3.46 (m, 1H), 3.27 – 3.21 (m, 4H), 2.03 – 1.85 (m, 1H), 1.84 – 1.73 (m, 2H), 1.67 – 1.37 (m, 8H), 1.17 – 0.99 (m, 2H), 0.89 (s, 9H), 0.02 (s, 6H). MS (ESI) m/z: 626 (M+H)⁺.

8.2.3. Preparation of compounds 67 - 108

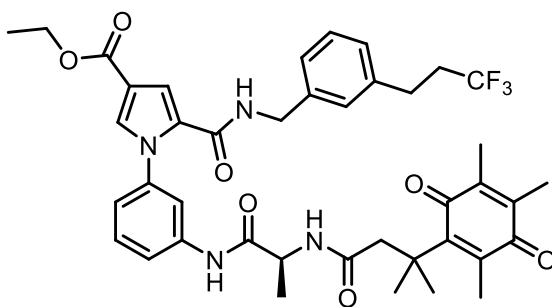
Ethyl(S)-5-(benzylcarbamoyl)-1-(3-(2-(3-methyl-3-(2,4,5-trimethyl-3,6-dioxocyclohexa-1,4-dien-1-yl) butanamido)propanamido)phenyl)-1H-pyrrole-3-carboxylate (**67**)



To a solution of **73** (0.50 g, 0.95 mmol), **76** (0.285 g, 1.14 mmol), *N*-methylmorpholine (0.52 mL, 4.75 mmol), and EDC (0.31 g, 1.61 mmol) in dry DMF (20 mL) was added HOBt (0.247 g, 1.61 mmol) under N₂ atmosphere. The reaction was left to stir at room temperature overnight, filtered, and concentrated in vacuum. The residue was dissolved in ethyl acetate (100 mL) and washed with saturated aqueous solution of NaHCO₃ (3 x 50 mL), and brine (50 mL). The

organic phase was dried on Na₂SO₄, filtered and concentrated in vacuo. The crude was purified by flash column chromatography (DCM/ethyl acetate 9:1 to 5:5) to afford the desired product **67** as yellow solid (0.54 g, 85%). **¹H NMR** (400 MHz, CDCl₃) δ 8.77 (br s, 1H, exchangeable with D₂O), 7.72 – 7.62 (m, 1H), 7.49 – 7.42 (m, 1H), 7.35 – 7.17 (m, 7H), 7.16 – 7.08 (m, 1H), 7.05 – 6.94 (m, 1H), 6.38 (t, *J* = 5.8 Hz, 1H, exchangeable with D₂O), 6.13 (d, *J* = 7.4 Hz, 1H, exchangeable with D₂O), 4.51 – 4.40 (m, 3H), 4.29 (q, *J* = 7.1 Hz, 2H), 2.86 (s, 2H), 2.08 (s, 3H), 1.92 (s, 3H), 1.88 (s, 3H), 1.45 (s, 3H), 1.41 (s, 3H), 1.36 – 1.25 (m, 6H). **¹³C NMR** (100 MHz, CDCl₃) δ 191.2, 187.4, 172.6, 170.2, 163.9, 160.3, 152.6, 143.1, 139.9, 138.8, 138.6, 138.4, 137.9, 131.5, 129.3, 128.7, 127.9, 127.7, 127.6, 121.3, 119.1, 116.9, 116.4, 114.2, 60.2, 49.3, 49.1, 43.6, 29.4, 29.4, 17.2, 14.4, 14.2, 12.7, 12.1. **HRMS** (ESI): *m/z* [M + H]⁺ calcd. for C₃₈H₄₂N₄O₇ + H⁺: 667.3126. Found: 667.3129.

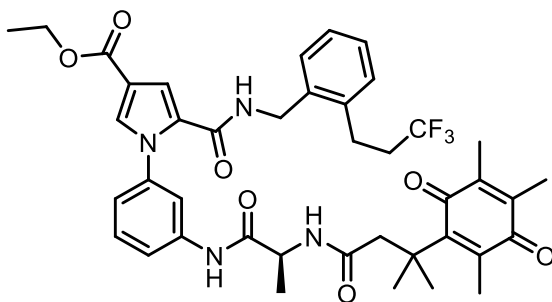
Ethyl(S)-1-(3-(2-(3-methyl-3-(2,4,5-trimethyl-3,6-dioxocyclohexa-1,4-dien-yl)butanamido)propanamido)phenyl)-5-((3-(3,3,3-trifluoropropyl)benzyl)carbamoyl)-1H-pyrrole-3-carboxylate (68)



Compound **68** was obtained as a white solid (0.92 g, 88%) by reaction of **74** (0.76 g, 1.21 mmol) following the procedure described for **67**. **¹H NMR** (400 MHz, CDCl₃) δ 8.74 (br s, 1H, exchangeable with D₂O), 7.73 – 7.69 (m, 1H), 7.47 (d, *J* = 2.0 Hz, 1H), 7.29 – 7.19 (m, 3H), 7.15 – 7.07 (m, 4H), 7.06 – 7.01 (m, 1H), 6.32 (br t, *J* = 5.8 Hz, 1H, exchangeable with D₂O), 6.04 (br s, 1H, exchangeable with D₂O), 4.52 – 4.41 (m, 3H), 4.29 (q, *J* = 7.1 Hz, 2H), 2.93 – 2.74 (m, 4H), 2.43 – 2.29 (m, 2H), 2.08 (s, 3H), 1.94 – 1.92 (m, 3H), 1.88 – 1.86 (m, 3H), 1.46

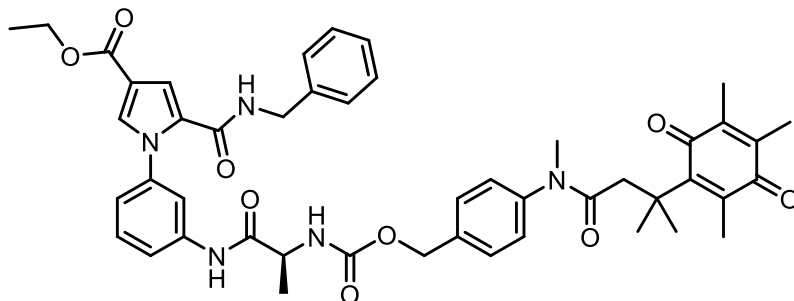
(s, 3H), 1.41 (s, 3H), 1.36 – 1.25 (m, 6H). **¹³C NMR** (100 MHz, CDCl₃) δ 191.2, 187.3, 172.9, 170.1, 163.9, 160.2, 152.1, 143.1, 140.0, 139.6, 138.9, 138.5, 138.5, 131.5, 129.2, 129.1, 127.7, 127.4, 126.0, 121.4, 119.1, 116.9, 116.4, 114.1, 60.2, 49.4, 49.1, 43.4, 35.5 (q, *J* = 28.4), 29.5, 29.4, 28.1, 16.8, 14.4, 14.1, 12.6, 12.1. **¹⁹F NMR** (377 MHz, CDCl₃) δ -66.58. **HRMS** (ESI): *m/z* [M + H]⁺ calcd. for C₄₁H₄₄F₃N₄O₇ + H⁺: 762.3240. Found: 762.3241.

Ethyl(S)-1-(3-(2-(3-methyl-3-(2,4,5-trimethyl-3,6-dioxocyclohexa-1,4-dien-1-yl)butanamido) propanamido) phenyl)-5-((2-(3,3,3-trifluoropropyl)benzyl)carbamoyl)-1H-pyrrole-3-carboxylate (69)



Compound **69** was obtained as a white solid (0.77 g, 80%) by reaction of **75** (0.64 g, 1.01 mmol) following the procedure described for **67**. **¹H NMR** (400 MHz, CDCl₃) δ 8.65 (br s, 1H, exchangeable with D₂O), 7.69 – 7.59 (m, 1H), 7.41 (d, *J* = 1.7 Hz, 1H), 7.23 – 7.12 (m, 5H), 7.12 – 7.07 (m, 1H), 7.07 – 7.04 (m, 1H), 6.99 – 6.93 (m, 1H), 6.13 (br t, *J* = 5.5 Hz, 1H, exchangeable with D₂O), 5.98 (br s, 1H, exchangeable with D₂O), 4.47 – 4.35 (m, 3H), 4.22 (q, *J* = 7.1 Hz, 2H), 2.84 – 2.61 (m, 4H), 2.35 – 2.16 (m, 3H), 2.01 (s, 3H), 1.85 (s, 3H), 1.81 (s, 3H), 1.39 (s, 3H), 1.34 (s, 3H), 1.30 – 1.22 (m, 6H). **¹³C NMR** (100 MHz, CDCl₃) δ 191.2, 187.4, 172.8, 170.1, 163.8, 160.1, 152.2, 143.1, 139.9, 138.9, 138.5, 137.1, 135.4, 131.5, 129.3, 128.9, 128.2, 127.8, 127.3, 121.4, 119.1, 116.9, 116.4, 114.2, 60.2, 49.4, 49.1, 40.7, 38.9, 35.4 (q, *J* = 28.3), 29.5, 29.4, 24.7, 16.9, 14.4, 14.2, 12.7, 12.1. **¹⁹F NMR** (377 MHz, CDCl₃) δ -66.47. **HRMS** (ESI): *m/z* [M + H]⁺ calcd. for C₄₁H₄₄F₃N₄O₇ + H⁺: 762.3240. Found: 762.3243.

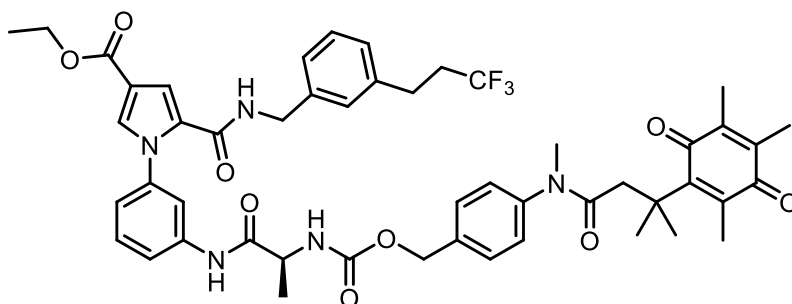
Ethyl (S)-5-(benzylcarbamoyl)-1-(3-(2-((((4-(N,3-dimethyl-3-(2,4,5-trimethyl-3,6-dioxocyclohexa-1,4-dien-1-yl)butanamido) benzyl)oxy)carbonyl) amino)propanamido) phenyl) -1H-pyrrole-3-carboxylate (70)



Under nitrogen protection, Compound **77** (0.40 g, 1 mmol) and DMAP (1.22 mg, 0.01 mmol) was dissolved in DCM (7 mL) and then cooled to 0 °C. Then triphosgene (0.30 g, 1 mmol) dissolved in DCM (3 mL) was added dropwise, then was stirred and turn to room temperature gradually for 12 h. Upon completion of the reaction, the solvent was removed, and the residue was dissolved in ethyl acetate (50 mL) and washed with brine (2 × 15 mL), dried over anhydrous Na₂SO₄, and filtered. Solvent was removed using a rotary evaporator, and the crude product was used without further purification. This acyl chloride product was dissolved DMF (2 mL). Compound **73** (0.53 g, 1 mmol) and TEA (0.14 mL, 1.1 mmol) was dissolved DMF (4 mL) and then cooled to 0 °C. Then acyl chloride solution was added to the mixture dropwise, then was stirred and turn to room temperature gradually for 24 h. Upon completion of the reaction, the solvent DMF was diluted with water (150 mL), and then extracted by ethyl acetate (3 × 50 mL) and washed with brine, dried over anhydrous Na₂SO₄, and filtered. Solvent was removed using a rotary evaporator, and the crude was purified by flash column chromatography (hexane/ethyl acetate 8:2 to 4:6) to provide compound **70** as a yellow solid (0.58 g, 74%). ¹H NMR (400 MHz, CDCl₃) δ 8.49 (br s, 1H, exchangeable with D₂O), 7.76 (s, 1H), 7.53 – 7.50 (m, 1H), 7.50 – 7.43 (m, 2H), 7.43 – 7.28 (m, 8H), 7.23 (d, *J* = 7.8 Hz, 1H), 7.17 – 7.14 (m, 2H), 7.10 (d, *J* = 7.8 Hz, 1H), 6.31 (br s, 1H, exchangeable with D₂O), 5.41 (br

s, 1H, exchangeable with D₂O), 5.24 – 5.18 (m, 1H), 5.18 – 5.14 (m, 1H), 4.54 (d, *J* = 5.8 Hz, 2H), 4.46 – 4.25 (m, 3H), 3.18 (s, 3H), 2.78 (s, 2H), 2.13 (s, 3H), 2.04 (s, 3H), 2.00 (s, 3H), 1.51 – 1.44 (m, 3H), 1.41 – 1.29 (m, 9H). ¹³C NMR (100 MHz, CDCl₃) δ 191.3, 187.9, 172.0, 170.4, 163.8, 160.3, 154.6, 143.9, 140.0, 138.5, 137.8, 136.4, 131.6, 129.4, 129.3, 128.8, 127.8, 127.7, 127.6, 121.5, 119.5, 117.2, 116.4, 114.0, 66.5, 60.2, 51.2, 47.7, 43.5, 37.1, 28.5, 18.1, 14.4, 14.1, 12.7, 12.1. **HRMS** (ESI): *m/z* [M + H]⁺ calcd. for C₄₇H₅₁N₅O₉ + H⁺: 830.3754. Found: 830.3755.

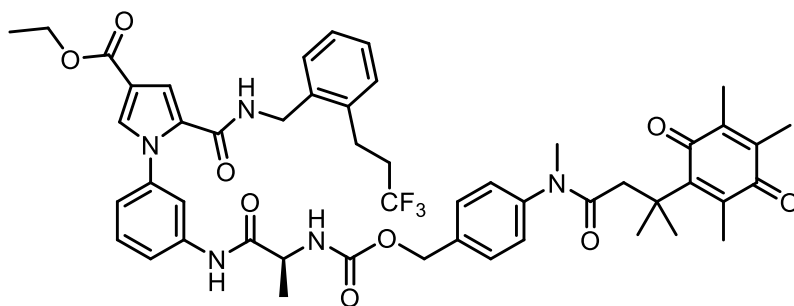
Ethyl(S)-1-(3-(2-((((4-(N,3-dimethyl-3-(2,4,5-trimethyl-3,6-dioxocyclohexa-1,4-dien-1-yl)butanami-do)benzyl)oxy)carbonyl)amino)propanamido)phenyl)-5-((3-(3,3,3-trifluoropropyl)benzyl)carbamoyl)-1H-pyrrole-3-carboxylate (71)



Compound **71** was obtained as a yellow solid (0.675 g, 73%) by reaction of **74** (0.63 g, 1.00 mmol) following the procedure described for **70**. ¹H NMR (400 MHz, CDCl₃) δ 8.61 (br s, 1H, exchangeable with D₂O), 7.80 – 7.70 (m, 1H), 7.52 – 7.46 (m, 1H), 7.47 – 7.41 (m, 2H), 7.41 – 7.34 (m, 1H), 7.34 – 7.25 (m, 3H), 7.23 – 7.17 (m, 2H), 7.18 – 7.09 (m, 4H), 7.10 – 7.03 (m, 1H), 6.36 (br t, *J* = 5.9 Hz, 1H, exchangeable with D₂O), 5.45 (br s, 1H, exchangeable with D₂O), 5.24 – 5.19 (m, 1H), 5.19 – 5.12 (m, 1H), 4.50 (d, *J* = 5.8 Hz, 2H), 4.42 – 4.25 (m, 3H), 3.16 (s, 3H), 2.92 – 2.83 (m, 2H), 2.76 (s, 2H), 2.47 – 2.30 (m, 2H), 2.12 (s, 3H), 2.02 (s, 3H), 1.98 (s, 3H), 1.45 (d, *J* = 7.0 Hz, 3H), 1.41 – 1.24 (m, 9H). ¹³C NMR (100 MHz, CDCl₃) δ 191.3, 187.3, 172.0, 170.4, 163.8, 160.3, 156.2, 154.6, 143.9, 140.1, 139.6, 138.4, 137.8, 136.4, 135.5, 131.7, 129.4, 129.2, 126.0, 121.5, 119.5, 117.2, 116.4, 114.0, 66.5, 60.3, 51.2, 47.7, 43.5,

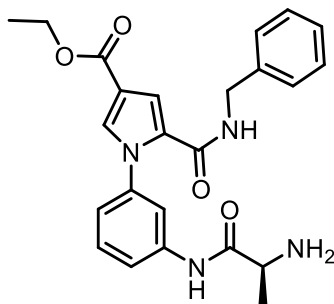
38.1, 37.1, 35.94, 35.4 (q, $J = 28.3$), 30.9, 28.8, 28.1, 18.0, 14.4, 14.0, 12.7, 12.1. **^{19}F NMR** (377 MHz, CDCl_3) δ -66.55. **HRMS** (ESI): m/z $[\text{M} + \text{H}]^+$ calcd. for $\text{C}_{50}\text{H}_{54}\text{F}_3\text{N}_5\text{O}_9 + \text{H}^+$: 926.3947. Found: 926.3944.

Ethyl (S)-1-(3-(2-((((4-(N,3-dimethyl-3-(2,4,5-trimethyl-3,6-dioxocyclohexa-1,4-dien-1-yl)butanamido)benzyl)oxy)carbonyl)amino)propanamido)phenyl)-5-((2-(3,3,3-trifluoropropyl)benzyl)carbamoyl)-1H-pyrrole-3-carboxylate (**72**)



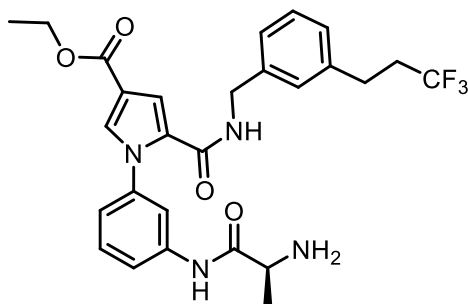
Compound **72** was obtained as a yellow solid (0.629 g, 68%) by reaction of **75** (0.63 g, 1.00 mmol) following the procedure described for **70**. **^1H NMR** (400 MHz, CDCl_3) δ 8.55 (br s, 1H, exchangeable with D_2O), 7.76 (s, 1H), 7.52 – 7.48 (m, 1H), 7.47 – 7.41 (m, 2H), 7.39 – 7.25 (m, 5H), 7.23 – 7.18 (m, 3H), 7.16 – 7.11 (m, 1H), 7.06 (d, $J = 7.6$ Hz, 1H), 6.21 (br s, 1H, exchangeable with D_2O), 5.42 (br s, 1H, exchangeable with D_2O), 5.28 – 5.19 (m, 1H), 5.17 – 5.08 (m, 1H), 4.55 (d, $J = 5.5$ Hz, 2H), 4.44 – 4.13 (m, 3H), 3.16 (s, 3H), 2.97 – 2.85 (m, 2H), 2.76 (s, 2H), 2.47 – 2.28 (m, 2H), 2.12 (s, 3H), 2.02 (s, 3H), 1.98 (s, 3H), 1.45 (d, $J = 7.2$ Hz, 3H), 1.40 – 1.20 (m, 9H). **^{13}C NMR** (100 MHz, CDCl_3) δ 191.3, 187.7, 172.0, 170.3, 163.8, 160.1, 154.6, 143.9, 140.0, 138.4, 137.9, 137.1, 136.3, 135.3, 131.7, 129.5, 129.3, 128.9, 128.3, 127.7, 127.4, 121.6, 119.5, 117.3, 116.5, 114.0, 66.6, 60.2, 51.3, 47.7, 40.8, 37.0, 35.0 (q, $J = 28.6$), 30.9, 29.7, 28.5, 24.7, 17.8, 14.4, 14.1, 12.7, 12.1. **^{19}F NMR** (377 MHz, CDCl_3) δ -66.45. **HRMS** (ESI): m/z $[\text{M} + \text{H}]^+$ calcd. for $\text{C}_{50}\text{H}_{54}\text{F}_3\text{N}_5\text{O}_9 + \text{H}^+$: 926.3947. Found: 926.3942.

(S)-ethyl 1-(3-(2-aminopropanamido)phenyl)-5-(benzylcarbamoyl)-1Hpyrrole-3-carboxylate 2,2,2-trifluoroacetate (**73**)



A mixture of TFA and DCM (1:9, 10 mL) was added to compound **94** (1.3 g, 2.45 mmol). The reaction was stirred at room temperature for 1h and then concentrated in vacuo to give the title compound **73** as a white solid (1.3 g, 99%). **¹H NMR** (400 MHz, DMSO-*d*₆) δ 10.13 (s, 1H, exchangeable with D₂O), 8.51 (t, *J* = 6.1 Hz, 1H, exchangeable with D₂O), 7.73 (s, 3H, exchangeable with D₂O), 7.20 – 7.17 (m, 2H), 7.17 – 7.12 (m, 1H), 7.01 – 6.94 (m, 1H), 6.90 – 6.84 (m, 3H), 6.82 – 6.75 (m, 3H), 6.67 – 6.58 (m, 1H), 3.87 (d, *J* = 6.0 Hz, 2H), 3.78 (q, *J* = 7.1 Hz, 2H), 3.60 – 3.53 (m, 1H), 1.01 (d, *J* = 7.0 Hz, 3H), 0.83 (t, *J* = 7.1 Hz, 3H). **MS** (ESI) *m/z*: 435 (M+H)⁺.

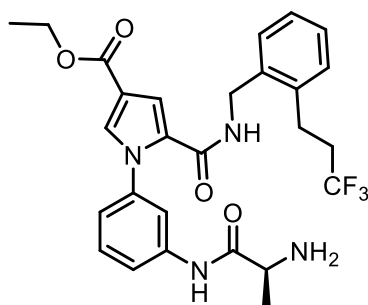
Ethyl (S)-1-(3-(2-aminopropanamido)phenyl)-5-((3-(3,3,3-trifluoropropyl)benzyl)carbamoyl)-1H-pyrrole-3-carboxylate (74)



Compound **74** was obtained as a white solid (1.52 g, 99%) by reaction of **95** (1.53 g, 2.42 mmol) following the procedure described for **73**. **¹H NMR** (400 MHz, DMSO-*d*₆) δ 10.57 (br s, 1H, exchangeable with D₂O), 8.93 (br t, *J* = 6.0 Hz, 1H, exchangeable with D₂O), 8.16 (br s, 3H,

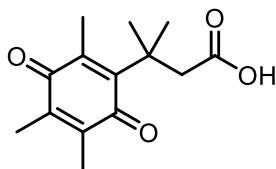
exchangeable with D₂O), 7.66 – 7.55 (m, 3H), 7.41 (t, $J = 8.0$ Hz, 1H), 7.36 – 7.31 (m, 1H), 7.30 – 7.22 (m, 1H), 7.20 – 7.15 (m, 2H), 7.15 – 7.03 (m, 2H), 4.30 (d, $J = 6.0$ Hz, 2H), 4.24 (q, $J = 7.1$ Hz, 1H), 4.01 (q, $J = 7.0$ Hz, 1H), 2.88 – 2.70 (m, 2H), 2.63 – 2.53 (m, 2H), 1.47 (d, $J = 6.9$ Hz, 3H), 1.28 (t, $J = 7.1$ Hz, 3H). **MS** (ESI) m/z : 531 (M+H)⁺.

Ethyl (S)-1-(3-(2-aminopropanamido)phenyl)-5-((2-(3,3,3-trifluoropropyl) benzyl) carbamoyl)-1H-pyrrole-3-carboxylate (75)



Compound **75** was obtained as a white solid (1.28 g, 99%) by reaction of **96** (1.28 g, 2.03 mmol) following the procedure described for **73**. **¹H NMR** (400 MHz, DMSO-d₆) δ 10.54 (br s, 1H, exchangeable with D₂O), 8.90 (br t, $J = 5.8$ Hz, 1H, exchangeable with D₂O), 7.86 (br s, 3H, exchangeable with D₂O), 7.68 – 7.53 (m, 3H), 7.41 (t, $J = 8.1$ Hz, 1H), 7.37 – 7.30 (m, 1H), 7.30 – 7.18 (m, 4H), 7.07 – 7.00 (m, 1H), 4.35 (d, $J = 5.7$ Hz, 1H), 4.24 (q, $J = 7.1$ Hz, 1H), 4.07 – 3.88 (m, 1H), 2.93 – 2.77 (m, 2H), 2.72 – 2.50 (m, 2H), 1.45 (d, $J = 7.0$ Hz, 3H), 1.28 (t, $J = 7.1$ Hz, 3H). **MS** (ESI) m/z : 531 (M+H)⁺.

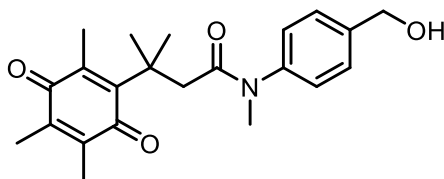
3-methyl-3-(2,4,5-trimethyl-3,6-dioxocyclohexa-1,4-dien-1-yl)butanoic acid (76)



To a solution of **102** (1.1 g, 4.8 mmol) in a mixture of acetonitrile (10 mL) and water (2.5 mL) was added NBS (0.89 g, 5.0 mmol) in portions with stirring at room temperature. After 1 h, the organic solvents were evaporated under reduced pressure, and the remaining solution was

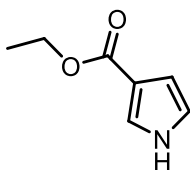
extracted with DCM (3 × 30 mL). The combined organic layer was dried over Na₂SO₄, and the solvent was removed to give a yellow solid product **76** (1.2 g, 99%). ¹H NMR (400 MHz, DMSO-d₆) δ 12.10 (s, 1H), 2.82 (s, 2H), 2.06 (s, 3H), 1.88 (s, 6H), 1.35 (s, 6H). MS (ESI) *m/z*: 251 (M+H)⁺.

N-(4-(hydroxymethyl)phenyl)-*N*,3-dimethyl-3-(2,4,5-trimethyl-3,6-dioxocyclohexa-1,4-dien-1-yl)butanamide (**77**)



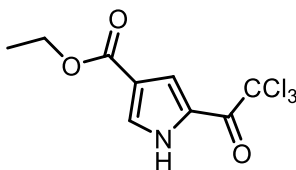
Compound **77** (1.1 g, 4.5 mmol) was dissolved in DCM (100 mL), to which was added *N*-methylmorpholine (3.04 g, 30.1 mmol). The mixture was cooled to −55 °C. Isobutyl chloroformate (0.74 g, 5.4 mmol) was then added, followed by addition of 4-(((tert-butyl)dimethylsilyl)oxy)methyl)-*N*-methylaniline (1.3 g, 5.4 mmol) after 30 min. The reaction mixture was stirred for another 5 h. The residue obtained by evaporation of the solvent under reduced pressure was dissolved in ethyl acetate (50 mL), and then washed with water (50 mL), diluted hydrochloric acid (50 mL), saturated NaHCO₃ solution (50 mL). The combined organic extracts were dried over anhydrous Na₂SO₄ and filtered. Solvent was removed using a rotary evaporator, and the crude product was dissolved THF (15 mL). Then TBAF (5.4 mL, 1 M in THF, 5.4 mmol) was added, and the solution was stirred at room temperature for 2 h. Upon completion of the reaction, the solvent was removed, and the residue was dissolved in DCM, washed with brine, dried over anhydrous Na₂SO₄, and filtered. Solvent was removed using a rotary evaporator, and the crude was purified by flash column chromatography (hexane/ethyl acetate) to provide compound **77** as a yellow solid (1.8 g, 90%). ¹H NMR (400 MHz, DMSO-d₆) δ 7.53 (d, *J* = 7.8 Hz, 2H), 7.28 (d, *J* = 7.7 Hz, 2H), 4.80 (s, 2H), 3.07 (s, 3H), 2.66 (s, 2H), 2.01 (s, 3H), 1.89 (s, 6H), 1.24 (s, 6H), 1.05 (t, *J* = 7.0 Hz, 1H). MS (ESI) *m/z*: 370 (M+H)⁺.

Ethyl 1H-pyrrole-3-carboxylate (80)



A suspension of p-Toluenesulfonylmethyl isocyanide (10.5 g, 53.1 mol) and ethyl acrylates (6.1 mL, 56.0 mol) in dry ethyl ether/DMSO (100 mL/50 mL) was added dropwise under nitrogen to a suspension of NaH (3.75 g, 93.8 mol) in diethyl ether (50 mL) at room temperature. Then the mixture was stirred for 4–5 h. Ice water (200 mL) was added into the mixture. The aqueous phase was extracted with ethyl ether (3 × 100 mL). The organic phase was dried with anhydrous Na₂SO₄, concentrated under vacuum to get light brown liquid compounds which was purified by flash chromatography (hexane/ethyl acetate 8:2 to 2:8) to give compound **80** as a yellow oil (6.5 g, 88%); ¹H NMR (400 MHz, CDCl₃) δ 9.86 (br s, 1H, exchangeable with D₂O), 7.45–7.46 (m, 1H), 6.76–6.79 (m, 1H), 6.65–6.67 (m, 1H), 4.31 (q, *J* = 7.1 Hz, 2H), 1.36 (t, *J* = 7.1 Hz, 3H). MS (ESI) *m/z*: 140 (M+H)⁺.

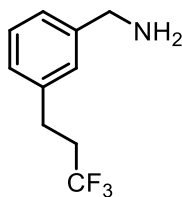
Ethyl 5-(2,2,2-trichloroacetyl)-1H-pyrrole-3-carboxylate (81)



To a solution of **80** (3.5 g, 25.1 mmol) in dry DCM (25 mL) in sealed vessel was added dropwise ClCOCCl₃ (28.2 mL, 251 mmol). The reaction was left to stir heating at 80°C for 36 h. The mixture of reaction was diluted with DCM (100 mL) and washed with saturated aqueous solution of NaHCO₃ (3 x 50 mL), brine (50 mL) and dried over Na₂SO₄. The organic layer was filtered and evaporated under reduced pressure. The crude was purified by flash column

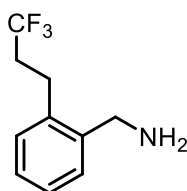
chromatography (hexane/ethyl acetate 7:3 to 2:8) to provide compound **81** as a yellow solid (3.3 g, 50%). $^1\text{H NMR}$ (400 MHz, CDCl_3) δ 9.68 (br s, 1H, exchangeable with D_2O), 7.76 – 7.72 (m, $J = 2.5$ Hz, 1H), 7.72 – 7.69 (m, $J = 3.3$ Hz, 1H), 4.34 (q, $J = 7.1$ Hz, 2H), 1.37 (t, $J = 7.1$ Hz, 3H). **MS** (ESI) m/z : 283 ($\text{M}+\text{H}$) $^+$.

(3-(3,3,3-trifluoropropyl)phenyl)methanamine (83)



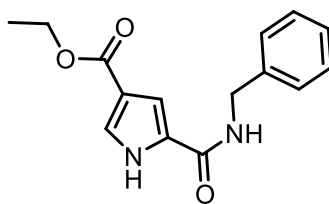
To a stirred solution of **99** (0.249 g, 1.22 mmol) in 25 mL of EtOH, H_2SO_4 (0.130 mL) and Pd/C 10% (0.03 g), were added. The reaction is stirred at room temperature, overnight under an H_2 atmosphere. The mixture was filtered; the solvent was removed under vacuum to give a yellow oil **83** that is used for the next step without further purification. $^1\text{H NMR}$ (400 MHz, $\text{DMSO}-d_6$) δ 7.25 – 7.18 (m, 5H), 4.41 – 4.31 (m, 2H), 2.80– 2.74 (m, 2H), 2.64 – 2.47 (m, 2H). **MS** (ESI) m/z : 204 ($\text{M}+\text{H}$) $^+$.

(2-(3,3,3-trifluoropropyl)phenyl)methanamine (84)



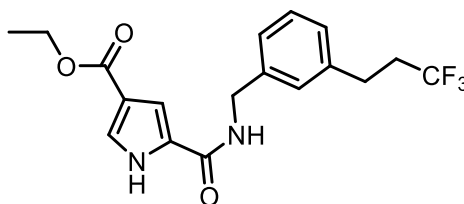
Compound **84** was obtained as a yellow solid by reaction of **100** (0.240 g, 1.22 mmol), following the procedure described for **83**. $^1\text{H NMR}$ (400 MHz, $\text{DMSO}-d_6$) δ 7.31 – 7.14 (m, 5H), 4.45 – 4.34 (m, 2H), 2.92– 2.86 (m, 2H), 2.71 – 2.58 (m, 2H). **MS** (ESI) m/z : 204 ($\text{M}+\text{H}$) $^+$.

Ethyl 5-(benzylcarbamoyl)-1H-pyrrole-3-carboxylate (85)



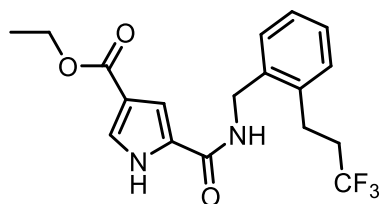
To a solution of **81** (1.1 g, 4.2 mmol) in DCM dry (20 mL) was added benzylamine (0.46 mL, 4.2 mmol). The reaction was left to stir at room temperature for 12h and evaporated under reduced pressure. The crude was purified by flash column chromatography (hexane/ethyl acetate 9:1 to 7:3) to afford the desired product as white solid (0.97 g, 85%). **¹H NMR** (400 MHz, CDCl₃) δ 10.00 (br s, 1H, exchangeable with D₂O), 7.53 – 7.46 (m, 1H), 7.41 – 7.29 (m, 5H), 7.07 – 6.92 (m, 1H), 6.29 (t, *J* = 5.8 Hz, 1H, exchangeable with D₂O), 4.61 (d, *J* = 5.8 Hz, 2H), 4.27 (q, *J* = 7.1 Hz, 2H), 1.33 (t, *J* = 7.1 Hz, 3H). **MS** (ESI) *m/z*: 273 (M+H)⁺.

Ethyl 5-((3-(3,3,3-trifluoropropyl)benzyl)carbamoyl)-1H-pyrrole-3-carboxylate (86)



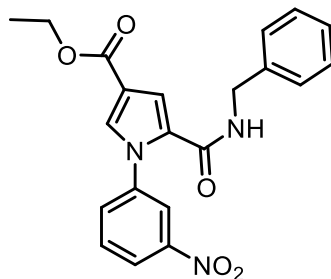
Compound **86** was obtained as a white solid (1.25 g, 81%) by reaction of amine **83** (0.85 g, 4.2 mmol) and **81** (1.1 g, 4.2 mmol) following the procedure described for **85**. **¹H NMR** (400 MHz, DMSO-*d*₆) δ 12.11 (brs, 1H, exchangeable with D₂O), 8.76 (brt, *J* = 6.1 Hz, 1H, exchangeable with D₂O), 7.41 – 7.35 (m, 1H), 7.32 – 7.13 (m, 5H), 4.41 (d, *J* = 6.0 Hz, 2H), 4.19 (q, *J* = 7.1 Hz, 2H), 2.81 – 2.76 (m, 2H), 2.65 – 2.49 (m, 2H), 1.26 (t, *J* = 7.1 Hz, 2H). **¹⁹F NMR** (377 MHz, DMSO-*d*₆) δ -64.88. **MS** (ESI) *m/z*: 369 (M+H)⁺.

Ethyl 5-((2-(3,3,3-trifluoropropyl)benzyl)carbamoyl)-1H-pyrrole-3-carboxylate (87)



Compound **87** was obtained as a white solid (1.23 g, 80%) by reaction of amine **84** (0.85 g, 4.2 mmol) and **81** (1.1 g, 4.2 mmol) following the procedure described for **85**. **¹H NMR** (400 MHz, DMSO-*d*₆) δ 12.13 (br s, 1H, exchangeable with D₂O), 8.73 (br t, *J* = 5.8 Hz, 1H, exchangeable with D₂O), 7.43 – 7.39 (m, 1H), 7.36 – 7.30 (m, 1H), 7.30 – 7.19 (m, 4H), 4.45 (d, *J* = 5.8 Hz, 2H), 4.19 (q, *J* = 7.1 Hz, 2H), 2.98 – 2.82 (m, 2H), 2.73 – 2.50 (m, 2H), 1.26 (t, *J* = 7.1 Hz, 3H). **¹⁹F NMR** (377 MHz, DMSO-*d*₆) δ -64.88. **MS** (ESI) *m/z*: 369 (M+H)⁺.

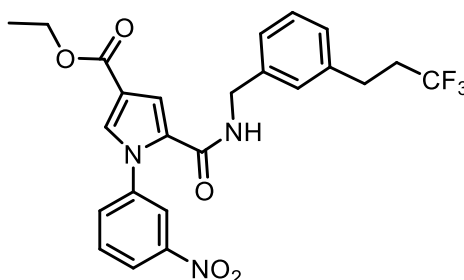
Ethyl 5-(benzylcarbamoyl)-1-(3-nitrophenyl)-1H-pyrrole-3-carboxylate (88)



3-bromobenzonitrile (0.75 g, 3.9 mmol) and CuI (0.74 g, 3.9 mmol) were suspended in Dioxane dry (5.7 mL) at room temperature in a 10 mL CEM pressure vessel equipped with a stirrer bar. The vial was degassed and N₁,N₂-dimethylethane-1,2-diamine (0.69 g, 7.92 mmol) was added to a mixture. The reaction was stirred at room temperature for 5 minutes and then compound **85** (0.97 g, 3.6 mmol) and K₃PO₄ (1.5 g, 7.2 mmol) were added. The reaction was degassed and heated in a CEM Discover microwave synthesizer (max power 300W, max pressure 250 psi) to 130 °C for 30 min, then water (25 ml) was added, and the mixture was extracted with ethyl acetate (3 x 25 mL). The combined organic layers were washed with brine (25 mL), dried on Na₂SO₄, filtered, and concentrated in vacuum. The crude was purified by flash column chromatography (hexane/ethyl acetate 9:1 to 7:3) to afford the desired product as yellow solid

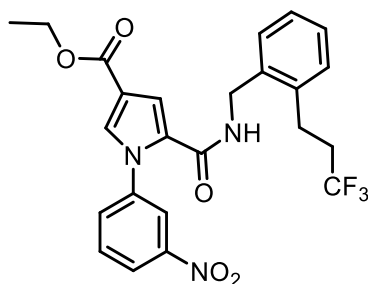
(1.1 g, 80%). **¹H NMR** (400 MHz, CDCl₃) δ 8.32 – 8.26 (m, 1H), 8.23 – 8.19 (m, 1H), 7.74 – 7.59 (m, 2H), 7.54 – 7.51 (m, 1H), 7.40 – 7.25 (m, 5H), 7.17 – 7.13 (m, 1H), 6.23 (t, *J* = 5.8 Hz, 1H, exchangeable with D₂O), 4.49 (d, *J* = 5.8 Hz, 2H), 4.31 (q, *J* = 7.1 Hz, 2H), 1.35 (t, *J* = 7.1 Hz, 3H). **MS** (ESI) *m/z*: 394 (M+H)⁺.

Ethyl 1-(3-nitrophenyl)-5-((3-(3,3,3-trifluoropropyl)benzyl)carbamoyl)-1H-pyrrole-3-carboxylate (89)



Compound **89** was obtained as a yellow solid (1.38 g, 83%) by reaction of **86** (1.25 g, 3.4 mmol) following the procedure described for **88**. **¹H NMR** (400 MHz, CDCl₃) δ 8.39 – 8.25 (m, 1H), 8.25 – 8.13 (m, 1H), 7.75 – 7.67 (m, 1H), 7.67 – 7.57 (m, 1H), 7.36 – 7.26 (m, 1H), 7.22 – 7.01 (m, 4H), 6.27 (br t, *J* = 5.8 Hz, 1H, exchangeable with D₂O), 4.48 (d, *J* = 5.8 Hz, 2H), 4.31 (q, *J* = 7.0 Hz, 2H), 2.96 – 2.70 (m, 2H), 2.55 – 2.27 (m, 2H), 1.35 (t, *J* = 7.0 Hz, 3H). **MS** (ESI) *m/z*: 490 (M+H)⁺.

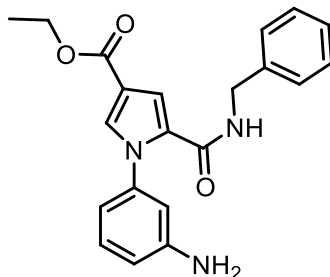
Ethyl 1-(3-nitrophenyl)-5-((2-(3,3,3-trifluoropropyl)benzyl)carbamoyl)-1H-pyrrole-3-carboxylate (90)



Compound **90** was obtained as a yellow solid (1.27 g, 79%) by reaction of **87** (1.23 g, 3.3 mmol) following the procedure described for **88**. **¹H NMR** (400 MHz, CHCl₃) δ 8.30 – 8.27 (m, 1H),

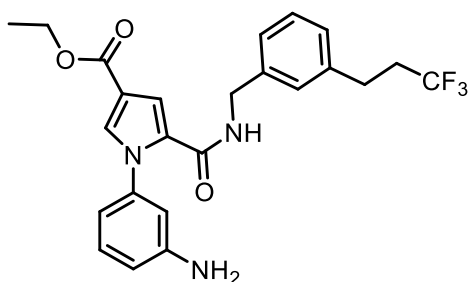
8.25 – 8.21 (m, 1H), 7.74 – 7.59 (m, 2H), 7.53 – 7.49 (m, 1H), 7.33 – 7.27 (m, 3H), 7.24 – 7.19 (m, 1H), 7.14 (d, $J = 1.7$ Hz, 1H), 6.13 (br t, $J = 5.8$ Hz, 1H, exchangeable with D₂O), 4.52 (d, $J = 5.8$ Hz, 2H), 4.31 (q, $J = 7.1$ Hz, 2H), 3.02 – 2.78 (m, 2H), 2.46 – 2.20 (m, 2H), 1.35 (t, $J = 7.1$ Hz, 3H). **MS** (ESI) m/z : 490 (M+H)⁺.

Ethyl 1-(3-aminophenyl)-5-(benzylcarbamoyl)-1H-pyrrole-3-carboxylate (91)



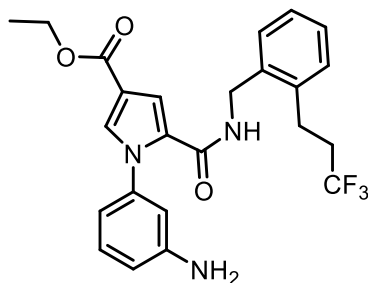
To a solution of **88** (1.1 g, 2.88 mmol) in acetic acid (60 mL) was added a powder of Zn (1.9 g, 28.8 mmol). The reaction was stirred for 1 h at room temperature, filtered, and concentrated in vacuo. The residue was dissolved in saturated aqueous solution of NaHCO₃ (250 mL) and extracted with ethyl acetate (3 × 100 mL). The combined organic layers were washed with (25 mL), dried on Na₂SO₄ and filtered. Vacuum evaporation of the solvents gave the title compound **91** (1.0 g, 99%) as a yellow solid which was directly used in the next step without further step of purification. **¹H NMR** (400 MHz, DMSO-*d*₆) δ 9.83 (t, $J = 5.5$ Hz, 1H, exchangeable with D₂O), 8.33 – 8.29 (m, 1H), 7.98 – 7.88 (m, 1H), 7.86 – 7.77 (m, 1H), 7.43 – 7.30 (m, 3H), 7.30 – 7.22 (m, 1H), 7.20 – 7.08 (m, 1H), 6.88 – 6.72 (m, 2H), 6.62 – 6.51 (m, 1H), 5.42 (s, 2H, exchangeable with D₂O), 4.52 (d, $J = 5.5$ Hz, 2H), 4.27 (q, $J = 7.0$ Hz, 2H), 1.28 (t, $J = 7.0$ Hz, 3H). **MS** (ESI) m/z : 364 (M+H)⁺.

Ethyl 1-(3-aminophenyl)-5-((3-(3,3,3-trifluoropropyl)benzyl)carbamoyl)-1H-pyrrole-3-carboxylate (92)



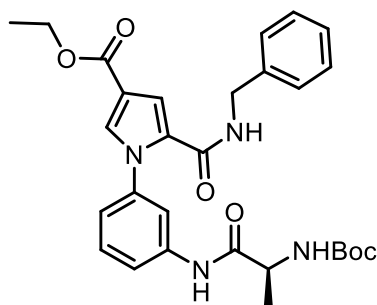
Compound **92** was obtained as a pale yellow oil (1.29 g, 99%) by reaction of **89** (1.39 g, 2.82 mmol) following the procedure described for **91**. **¹H NMR** (400 MHz, CDCl₃) δ 7.51 – 7.44 (m, 1H), 7.33 – 7.29 (m, 1H), 7.28 – 7.25 (m, 1H), 7.23 – 7.09 (m, 4H), 7.08 – 7.04 (m, 1H), 6.76 – 6.68 (m, 2H), 6.66 (br t, *J* = 5.8 Hz, 1H, exchangeable with D₂O), 4.48 (d, *J* = 5.8 Hz, 2H), 4.32 (q, *J* = 7.1 Hz, 2H), 2.95 – 2.75 (m, 2H), 2.56 – 2.31 (m, 2H), 1.36 (t, *J* = 7.1 Hz, 3H). **MS** (ESI) *m/z*: 460 (M+H)⁺.

Ethyl 1-(3-aminophenyl)-5-((2-(3,3,3-trifluoropropyl)benzyl)carbamoyl)-1H-pyrrole-3-carboxylate (93)



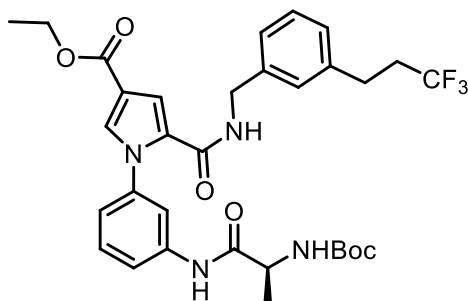
Compound **93** was obtained as a pale yellow oil (1.19 g, 99%) by reaction of **90** (1.27 g, 2.60 mmol) following the procedure described for **91**. **¹H NMR** (400 MHz, CDCl₃) δ 7.48 – 7.42 (m, 1H), 7.33 – 7.25 (m, 1H), 7.27 – 7.23 (m, 1H), 7.20 – 7.08 (m, 4H), 7.07 – 7.02 (m, 1H), 6.80 – 6.68 (m, 2H), 6.53 (br t, *J* = 5.8 Hz, 1H, exchangeable with D₂O), 4.51 (d, *J* = 5.8 Hz, 2H), 4.31 (q, *J* = 7.1 Hz, 2H), 3.00 – 2.76 (m, 2H), 2.44 – 2.23 (m, 2H), 1.34 (t, *J* = 7.1 Hz, 3H). **MS** (ESI) *m/z*: 460 (M+H)⁺.

(S)-5-(benzylcarbamoyl)-1-(3-(2-((tert-butoxycarbonyl)amino) propanamido) phenyl)-1H-pyrrole-3-carboxylate (94)



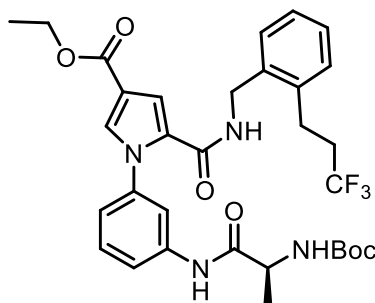
To a solution of **91** (1.1 g, 2.88 mmol), DIPEA (1.5 mL, 8.64 mmol), and Boc-L-AlaOH (0.60 g, 3.17 mmol) in dry DCM (20 mL) was added HBTU (1.4 g, 3.74 mmol) under N₂ atmosphere. The reaction was left to stir at room temperature overnight, filtered, and concentrated in vacuum. The residue was dissolved in DCM (100 mL) and washed with saturated aqueous solution of NaHCO₃ (3 x 50 mL), and brine (50 mL). The organic phase was dried on Na₂SO₄, filtered, and concentrated in vacuo. The crude was purified by flash column chromatography (hexane/ethyl acetate 9:1 to 7:3) to afford the desired product **94** as yellow solid (1.3 g, 85%). ¹H NMR (400 MHz, CDCl₃) δ 8.79 – 8.67 (m, 1H, exchangeable with D₂O), 7.79 – 7.76 (m, 1H), 7.50 – 7.48 (m, 1H), 7.38 – 7.25 (m, 8H), 7.15 – 7.12 (m, 1H), 7.09 – 7.04 (m, *J* = 7.1 Hz, 1H, exchangeable with D₂O), 6.25 (t, *J* = 5.6 Hz, 1H, exchangeable with D₂O), 5.08 – 4.99 (m, 1H), 4.50 (d, *J* = 5.7 Hz, 2H), 4.30 (q, *J* = 7.1 Hz, 2H), 1.48 (s, 9H), 1.42 (d, *J* = 7.0 Hz, 3H), 1.35 (t, *J* = 7.1 Hz, 3H). MS (ESI) *m/z*: 535 (M+H)⁺.

Ethyl (S)-1-(3-(2-((tert-butoxycarbonyl)amino)propanamido)phenyl)-5-((3-(3,3,3-trifluoropropyl) benzyl) carbamoyl)-1H-pyrrole-3-carboxylate (95)



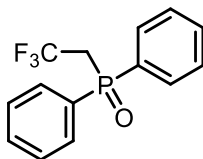
Compound **95** was obtained as a yellow solid (1.53 g, 86%) by reaction of **92** (1.29 g, 2.82 mmol) following the procedure described for **94**. **¹H NMR** (400 MHz, CDCl₃) δ 8.71 (br s, 1H, exchangeable with D₂O), 7.93 – 7.76 (m, 1H), 7.52 – 7.45 (m, 1H), 7.40 – 7.27 (m, 4H), 7.23 – 6.99 (m, 4H), 6.21 (br t, *J* = 5.6 Hz, 1H, exchangeable with D₂O), 4.99 (br s, 1H, exchangeable with D₂O), 4.49 (d, *J* = 5.6 Hz, 2H), 4.39 – 4.22 (m, 3H), 2.93 – 2.78 (m, 2H), 2.56 – 2.25 (m, 2H), 1.49 (s, 9H), 1.43 (d, *J* = 7.0 Hz, 3H), 1.36 (t, *J* = 7.1 Hz, 3H). **MS** (ESI) *m/z*: 631 (M+H)⁺.

Ethyl (S)-1-(3-(2-((tert-butoxycarbonyl)amino)propanamido)phenyl)-5-((2-(3,3,3 trifluoro propyl) benzyl) carbamoyl)-1H-pyrrole-3-carboxylate (96)



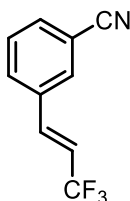
Compound **96** was obtained as a yellow solid (1.28 g, 78%) by reaction of **93** (1.19 g, 2.60 mmol) following the procedure described for **94**. **¹H NMR** (400 MHz, CDCl₃) δ 8.72 (s, 1H, exchangeable with D₂O), 7.89 – 7.71 (m, 1H), 7.53 – 7.46 (m, 1H), 7.44 – 7.32 (m, 3H), 7.26 – 7.15 (m, 4H), 7.16 – 7.09 (m, 1H), 7.10 – 7.01 (m, 1H), 6.05 (br t, *J* = 5.6 Hz, 1H, exchangeable with D₂O), 4.97 (br s, 1H, exchangeable with D₂O), 4.53 (d, *J* = 5.5 Hz, 2H), 4.35 – 4.23 (m, 2H), 2.96 – 2.76 (m, 2H), 2.43 – 2.22 (m, 2H), 1.49 (s, 9H), 1.44 (d, *J* = 7.1 Hz, 3H), 1.36 (t, *J* = 7.1 Hz, 3H). **MS** (ESI) *m/z*: 631 (M+H)⁺.

Diphenyl(2,2,2-trifluoroethyl)phosphine oxide (98)



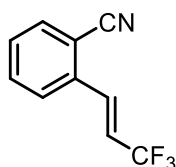
To a stirred mixture of trifluoroacetic acid (1 mL) and water (0.765 mL) was added dropwise diphenylchlorophosphine (10 mL, 56.61 mmol) at 0 °C for 30 min (syringe pump), and the mixture solidified gradually. When the mixture was allowed to warm to room temperature, it turned to a pale yellow solution. After 30 min, the mixture was heated within the range between 90 and 100 °C for 2 h. After cooling, the mixture is diluted with CHCl₃ and concentrated under reduced pressure. To the residue were added CHCl₃ and an aqueous saturated solution of NaHCO₃, and the mixture is stirred vigorously for 1 h. The organic phase was separated, and the aqueous phase was extracted with CHCl₃. The combined organic phase was washed successively with an aqueous saturated solution of NaHCO₃ followed by brine and dried over Na₂SO₄. After filtration, the filtrate was concentrated under reduced pressure, and the residue was recrystallized from AcOEt to afford **98** (2.2 g, 55%).

3-(3,3,3-trifluoropropyl)benzonitrile (99)



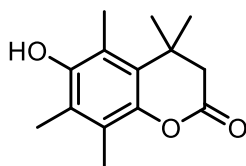
MS 4A (powder, 6 g) was added to a 1M solution of TBAF in THF (8.8 mL, 8.8 mmol) and the mixture was stirred at room-temperature overnight under an N₂ atmosphere. To the mixture were added a solution of aldehyde (0.115 g, 0.88 mmol) and phosphine oxide (0.50 g, 1.76 mmol) in THF (15 mL). After the mixture was stirred for 1 h, MS 4A was removed by filtration. Water was added to the filtrate, and the whole was extracted with AcOEt. The extract was washed with brine, dried over Na₂SO₄, and concentrated. The residue was purified using flash column chromatography on silica gel (Hex/AcOEt 9:1 → 6:4) to give **99** (0.120 g, 70%). ¹H NMR (400 MHz, DMSO-d₆) δ 7.78 – 7.59 (m, 5H), 7.21 – 7.09 (m, 1H), 6.99 – 6.85 (m, 1H).

2-(3,3,3-trifluoropropyl)benzonitrile (100)



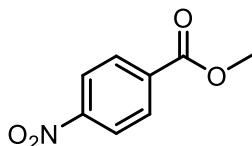
Compound **100** was obtained as a yellow solid (0.060 g, 35%) by reaction of proper aldehyde (1.15 g, 0.88 mmol) following the procedure described for **99**. $^1\text{H NMR}$ (400 MHz, DMSO- d_6) δ 7.81 – 7.63 (m, 5H), 7.25 – 7.11 (m, 1H), 6.87 – 6.78 (m, 1H).

6-hydroxy-4,4,5,7,8-pentamethylchroman-2-one (102)



2,3,5-Trimethylbenzene-1,4-diol (1.0 g, 6.6 mmol) was mixed with 3-methylbut-2-enoic acid (0.76 g, 7.5 mmol) and methanesulfonic acid (10 mL). The mixture was stirred at 85 °C under nitrogen for 3 h and then cooled to room temperature. To the mixture was added 100 g of ice with stirring. The precipitate was extracted with ethyl acetate (3×100 mL). The combined organic layer was washed with saturated NaHCO_3 (3×50 mL) and water (3×50 mL) and dried over Na_2SO_4 . After filtration and evaporation, an obtained residue was recrystallized from hexane and ethyl acetate (2:1, v/v) to give the desired product **102** as a white solid (1.1 g, 80%). $^1\text{H NMR}$ (400 MHz, CDCl_3) δ 4.70 (s, 1H), 2.56 (s, 2H), 2.37 (s, 3H), 2.23 (s, 3H), 2.19 (s, 3H), 1.46 (s, 6H). **MS** (ESI) m/z : 235 ($\text{M}+\text{H}$) $^+$.

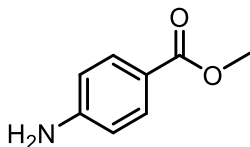
Methyl 4-nitrobenzoate (104)



A mixture of 4-nitro benzoic acid **103** (4.0 g, 23.8 mmol), conc. H_2SO_4 (96%) (15 mL) in MeOH (50 mL) was heated under magnetic stirring at 70 °C for 4 h. Then, the residue was

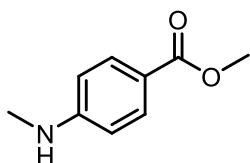
dissolved in ethyl acetate (50 mL), washed with water (50 mL), brine (50 mL), dried with Na₂SO₄, filtered and the solvent was concentrated. The product **104** was recovered as a pale yellow solid (4.2 g, 99%). ¹H NMR (400 MHz, CDCl₃) δ 8.29 (d, *J* = 6.2 Hz, 2H), 8.22 (d, *J* = 6.3 Hz, 2H), 3.99 (s, 3H). MS (ESI) *m/z*: 182 (M+H)⁺.

Methyl 4-aminobenzoate (105)



A mixture of **104** (3.0 g, 16.5 mmol), Pd/C 10% (0.3 g), and ammonium formate (20.7 g, 330 mmol) in MeOH (15 mL) was heated at reflux with stirring for 1 h. After cooling, the reaction mixture was extracted with ethyl acetate (3 x 50 mL). The extract was washed with water (50 mL) and brine (50 mL) and dried over Na₂SO₄, filtered and the solvent was concentrated under vacuum. The crude product **105** was used in the next step without further purification step. ¹H NMR (400 MHz, CDCl₃) δ 7.83 (d, 2H, *J* = 8.5 Hz), 6.62 (d, *J* = 8.5 Hz, 2H), 4.09 (br s, 2H), 3.84 (s, 3H). MS (ESI) *m/z*: 152 (M+H)⁺.

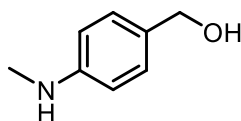
Methyl 4-(methylamino)benzoate (106)



A pressure vessel was charged with a magnetic stirring bar, aniline **105** (2.0 g, 13.2 mmol), methyl iodide (2.2 g, 15.8 mmol), potassium carbonate (1.8 g, 13.2 mmol), and acetonitrile (30 mL). The vessel was then sealed and heated to 80 °C for 3 h. After reaction cooling, water was added into the mixture. The organic phase was separated, and the aqueous layer was extracted with ethyl acetate (3 x 50 mL). The combined organic phase was washed with saturated brine

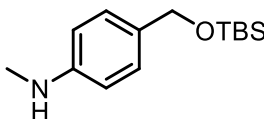
(50 mL) and dried over Na₂SO₄. The solvent was removed by rotary evaporation and the residue was transferred to a short column on silica gel hexane/ethyl acetate as the eluent to remove N,N-dimethyl substituted anilines, yielding the N-methyl aniline **106** as white solid (1.1 g, 49 %). ¹H NMR (400 MHz, CDCl₃) δ 7.90-7.86 (m, 2H), 6.58-6.53 (m, 2H), 4.18 (s, 1H), 3.85 (s, 3H), 2.89 (d, *J* = 5.1 Hz, 3H). MS (ESI) *m/z*: 166 (M+H)⁺.

(4-(methylamino)phenyl)methanol (107)



106 (1.0 g, 6.2 mmol) was dissolved in THF (20 mL) and cooled under nitrogen to 0 °C, and slowly LiAlH₄ (0.47 g, 12.4 mmol) was added. After stirring for 15 h, the reaction mixture was quenched by the sequential slow addition of 3 mL of methanol and 30 mL of Rochelle salt. The reaction was stirred for 0.5 h. The organic phase was separated, and the aqueous layer was extracted with ethyl acetate (3 x 50 mL). The combined organic phase was washed with saturated brine (50 mL) and dried over Na₂SO₄. The resulting crude material was purified by flash column chromatography on silica gel (heptane/ethyl acetate) to give the title compound **107** as an uncoloured oil (0.81 g, 97%). ¹H NMR (400 MHz, CDCl₃) δ 7.25-7.15 (m, 2H), 6.60-6.55 (m, 2H), 4.56 (d, *J* = 3.2 Hz, 2H), 4.18 (s, 1H), 2.89 (d, *J* = 5.1 Hz, 3H). MS (ESI) *m/z*: 138 (M+H)⁺.

4-(((tert-butyldimethylsilyl)oxy)methyl)-N-methylaniline (108)

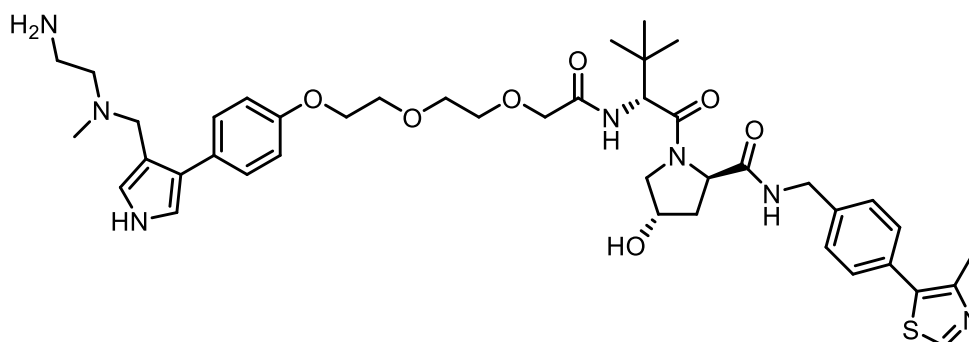


To a solution of **107** (0.81 g, 6.0 mmol) in dichloromethane (5 mL) were added tertbutyldimethylsilyl chloride (0.92 g, 6.0 mmol) and imidazole (0.42 g, 6.0 mmol), and this was stirred for 1 h at room temperature. Then the reaction mixture was diluted with brine

solution (25 mL) and then extracted with ethyl acetate (3 × 25 mL). The organic phase was dried over anhydrous Na₂SO₄ and filtered. Solvent was removed using a rotary evaporator. The crude brown-colored oil was purified by flash column chromatography on silica gel (hexane/ethyl acetate) to give the compound as a yellow solid (1.3 g, 90%). ¹H NMR (400 MHz, CDCl₃) δ 7.18 (d, *J* = 8.4 Hz, 2H), 6.72 - 6.49 (m, 2H), 4.66 (s, 2H), 2.85 (s, 3H), 0.96 (s, 9H), 0.11 (s, 6H). MS (ESI) *m/z*: 252 (M+H)⁺.

8.2.4. Preparation of compounds 109 - 129

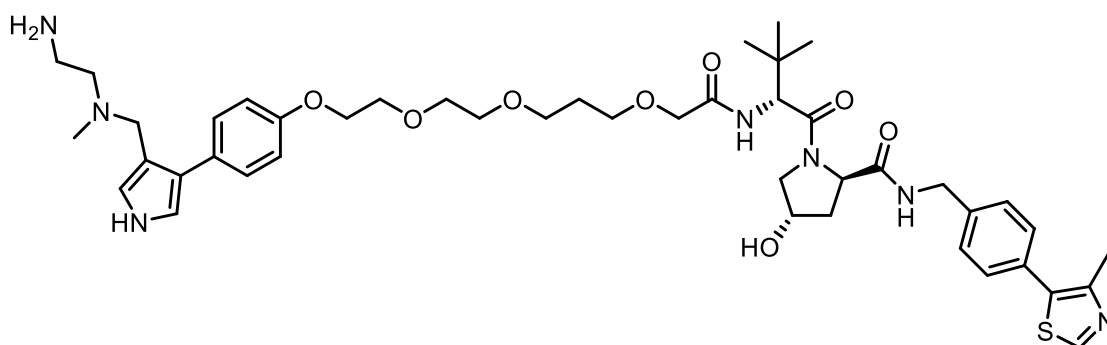
(2R,4S)-1-((R)-2-(2-(2-(2-(4-(4-(((2-aminoethyl)(methyl)amino)methyl)-1H-pyrrol-3-yl)phenoxy)ethoxy)ethoxy)acetamido)-3,3-dimethylbutanoyl)-4-hydroxy-N-(4-(4-methylthiazol-5-yl)benzyl)pyrrolidine-2-carboxamide (109a)



Compound **114a** (0.040 g, 0.040 mmol) was dissolved in a solution of DCM/TFA 9:1. The resulting mixture was stirred at room temperature for 6 h. The solvent was evaporated, and the crude product was purified by RP-HPLC (Reverse Phase High Performance Liquid Chromatography) using a mixture of H₂O/ACN + 0.1% TFA to afford the TFA salt **109a** as white solid (0.034 g, 95%). ¹H NMR (400 MHz, MeOD) δ 11.00 (s, 1H), 8.87 (s, 1H), 7.46 (d, *J* = 8.2 Hz, 2H), 7.41 (d, *J* = 8.3 Hz, 2H), 7.25 (d, *J* = 8.6 Hz, 2H), 7.13 – 7.10 (m, 1H), 7.00 – 6.94 (m, 2H), 6.88 – 6.82 (m, 1H), 4.71 – 4.68 (m, 1H), 4.60 – 4.54 (m, 1H), 4.51 (s, 2H), 4.43 (s, 2H), 4.39 – 4.31 (m, 1H), 4.18 – 4.14 (m, 2H), 4.07 (d, *J* = 3.0 Hz, 2H), 3.92 – 3.86 (m, 4H), 3.79 – 3.74 (m, 5H), 3.18 – 3.14 (m, 4H), 2.64 (s, 3H), 2.45 (s, 3H), 2.27 – 2.20 (m, 1H), 2.13 – 2.04 (m, 1H). ¹³C NMR (101 MHz, MeOD) δ 172.9, 170.8, 170.4, 157.8, 138.8, 130.1, 129.6, – 2.04 (m, 1H).

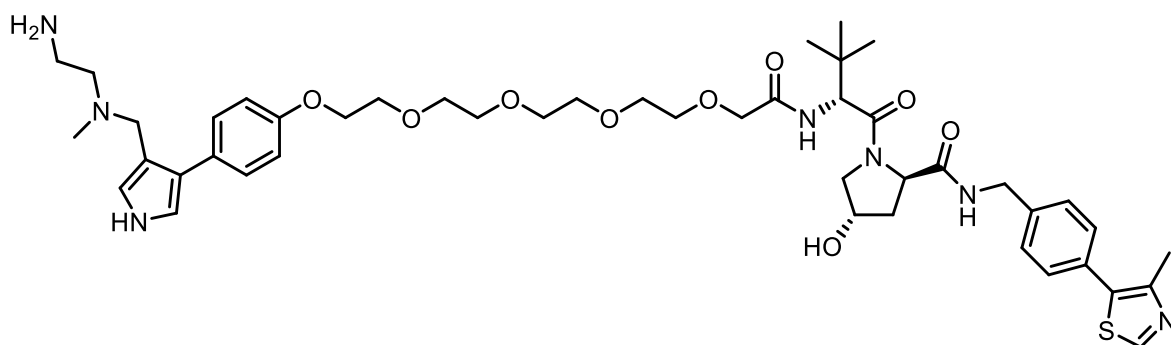
129.1, 129.0, 127.8, 127.5, 114.8, 70.9, 70.3, 69.7, 69.7, 69.6, 67.3, 59.5, 56.8, 56.7, 51.9, 50.5, 42.3, 38.8, 37.6, 35.6, 34.0, 29.3, 25.6, 14.4. **HRMS** (ESI): m/z $[M + H]^+$ calcd. for $C_{42}H_{57}N_7O_7S + H^+$: 804.4113 Found: 804.4115.

(2R,4S)-1-((R)-15-(4-(4-(((2-aminoethyl)(methyl)amino)methyl)-1H-pyrrol-3-yl)phenoxy)-2-(tert-butyl)-4-oxo-6,10,13-trioxa-3-azapentadecanoyl)-4-hydroxy-N-(4-(4-methylthiazol-5-yl)benzyl)pyrrolidine-2-carboxamide (109b)



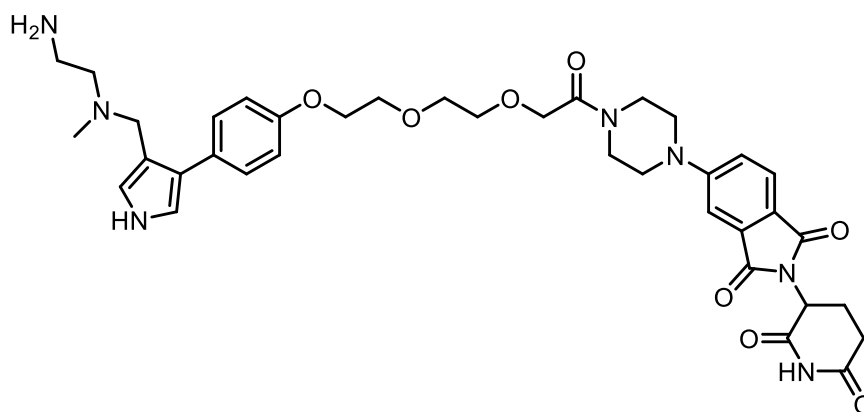
Compound **109b** was obtained as a white solid (0.036 g, 95%) starting from compound **114b** (0.042 g, 0.040 mmol) following the procedure described for **109a**. **¹H NMR** (400 MHz, MeOD) δ 10.99 (s, 1H), 8.87 (s, 1H), 7.46 (d, J = 8.4 Hz, 2H), 7.44 – 7.41 (m, 2H), 7.30 – 7.25 (m, 2H), 7.12 – 7.10 (m, 1H), 6.99 (d, J = 8.7 Hz, 2H), 6.88 – 6.85 (m, 1H), 4.69 – 4.66 (m, 1H), 4.60 – 4.55 (m, 1H), 4.52 – 4.48 (m, 2H), 4.43 (s, 2H), 4.38 – 4.31 (m, 1H), 4.14 – 4.10 (m, 2H), 4.04 (d, J = 4.3 Hz, 2H), 3.90 – 3.80 (m, 4H), 3.74 – 3.68 (m, 8H), 3.17 – 3.11 (m, 4H), 2.65 (s, 3H), 2.47 (s, 3H), 2.28 – 2.19 (m, 1H), 2.13 – 2.05 (m, 1H), 1.04 (s, 9H). **¹³C NMR** (101 MHz, MeOD) δ 184.9, 172.9, 170.7, 157.9, 151.5, 151.5, 138.9, 130.1, 129.0, 127.6, 121.6, 117.5, 114.8, 70.9, 70.4, 70.3, 70.1, 69.6, 67.3, 58.1, 51.9, 50.4, 42.3, 37.6, 35.8, 33.9, 25.6. **HRMS** (ESI): m/z $[M + H]^+$ calcd. for $C_{44}H_{63}N_7O_8S + H^+$: 862.4532 Found: 862.4535.

(2R,4S)-1-((R)-17-(4-(4-(((2-aminoethyl)(methyl)amino)methyl)-1H-pyrrol-3-yl)phenoxy)-2-(tert-butyl)-4-oxo-6,9,12,15-tetraoxa-3-azaheptadecanoyl)-4-hydroxy-N-(4-(4-methylthiazol-5-yl)benzyl)pyrrolidine-2-carboxamide (109c)



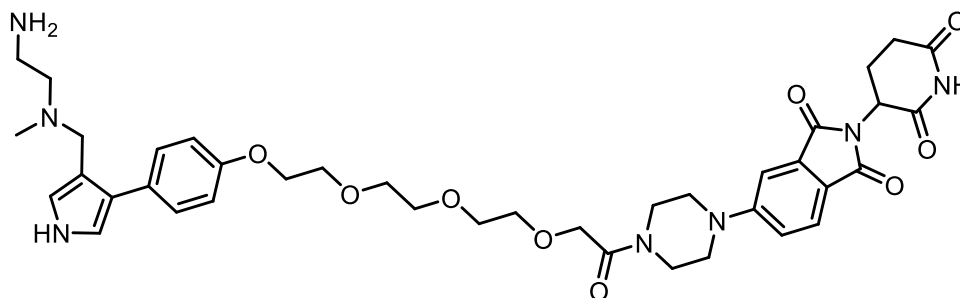
Compound **109c** was obtained as a white solid (0.036 g, 96%) starting from compound **114c** (0.030 g, 0.032 mmol) following the procedure described for **109a**. **¹H NMR** (400 MHz, MeOD) δ 11.00 (s, 1H), 8.90 (s, 1H), 7.46 (d, J = 8.5 Hz, 2H), 7.44 – 7.40 (m, 2H), 7.29 – 7.26 (m, 2H), 7.13 – 7.10 (m, 1H), 7.01 – 6.98 (m, 2H), 6.88 – 6.85 (m, 1H), 4.69 – 4.65 (m, 1H), 4.59 – 4.54 (m, 1H), 4.53 – 4.49 (m, 2H), 4.44 (s, 2H), 4.38 – 4.33 (m, 1H), 4.15 – 4.11 (m, 2H), 4.04 (d, J = 2.3 Hz, 2H), 3.89 – 3.80 (m, 4H), 3.70 – 3.64 (m, 12H), 3.17 – 3.12 (m, 4H), 2.65 (s, 3H), 2.47 (s, 3H), 2.23 (ddt, J = 13.3, 7.6, 1.8 Hz, 1H), 2.09 (ddd, J = 13.3, 9.2, 4.4 Hz, 1H), 1.04 (s, 9H). **¹³C NMR** (101 MHz, MeOD) δ 172.9, 170.8, 170.3, 157.9, 151.5, 147.6, 138.9, 130.1, 129.6, 129.3, 129.1, 129.0, 128.1, 127.6, 121.5, 114.8, 70.9, 70.8, 70.3, 70.2, 70.2, 70.2, 70.1, 69.7, 69.5, 67.7, 67.3, 59.5, 56.9, 56.8, 56.7, 51.9, 50.5, 45.5, 42.3, 38.8, 37.5, 35.64, 35.2, 33.9, 32.5, 29.3, 25.6. **HRMS** (ESI): m/z $[M + H]^+$ calcd. for $C_{46}H_{65}N_7O_9S + H^+$: 892.4637 Found: 892.4640.

5-(4-(2-(2-(2-(4-(4-(((2-aminoethyl)(methyl)amino)methyl)-1H-pyrrol-3-yl)phenoxy)ethoxy)ethoxy)acetyl)piperazin-1-yl)-2-(2,6-dioxopiperidin-3-yl)isoindoline-1,3-dione (110a)



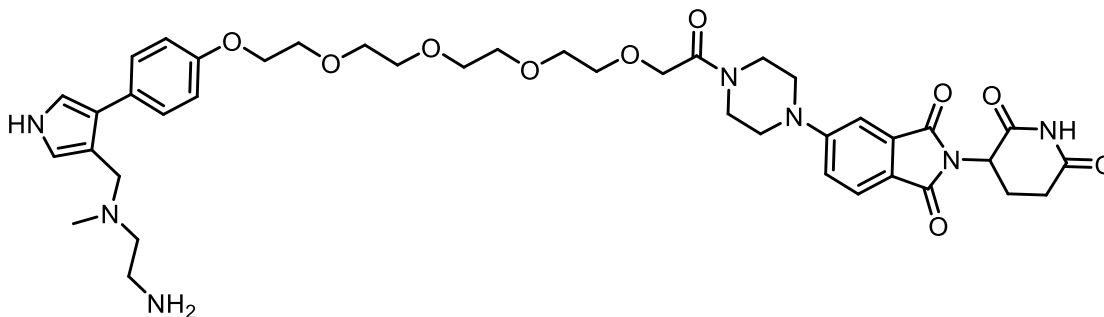
Compound **110a** was obtained as a white solid (0.017 g, 95%) starting from compound **115a** (0.020 g, 0.022 mmol) following the procedure described for **109a**. **¹H NMR** (400 MHz, MeOD) δ 7.67 (dd, J = 8.5, 1.3 Hz, 1H), 7.31 (d, J = 2.1 Hz, 1H), 7.25 – 7.21 (m, 2H), 7.19 – 7.17 (m, 1H), 7.09 (d, J = 2.1 Hz, 1H), 6.99 – 6.94 (m, 2H), 6.85 – 6.82 (m, 1H), 5.09 – 5.02 (m, 1H), 4.41 (s, 2H), 4.30 (s, 2H), 4.15 – 4.10 (m, 2H), 3.85 – 3.81 (m, 2H), 3.72 – 3.63 (m, 8H), 3.50 – 3.46 (m, 4H), 3.20 – 3.07 (m, 4H), 2.90 – 2.80 (m, 1H), 2.75 – 2.73 (m, 2H), 2.66 (s, 3H), 2.10 – 2.05 (m, 1H). **¹³C NMR** (101 MHz, MeOD) δ 172.6, 172.2, 169.5, 168.1, 167.8, 157.8, 155.5, 133.2, 129.7, 129.3, 124.7, 119.8, 118.2, 114.4, 114.1, 109.1, 71.3, 70.5, 70.2, 70.1, 69.5, 69.1, 67.5, 53.4, 52.8, 50.6, 46.7, 43.8, 41.0, 38.9, 34.1, 32.5, 30.8, 29.3, 22.8, 22.4. **HRMS** (ESI): m/z $[M + H]^+$ calcd. for $C_{37}H_{45}N_7O_8 + H^+$: 716.3403 Found: 716.3400.

5-(4-(2-(2-(2-(2-(4-(4-(((2-aminoethyl)(methyl)amino)methyl)-1H-pyrrol-3-yl)phenoxy)ethoxy)ethoxy)ethoxy)acetyl)piperazin-1-yl)-2-(2,6-dioxopiperidin-3-yl)isoindoline-1,3-dione (110b)



Compound **110b** was obtained as a white solid (0.013 g, 95%) starting from compound **115b** (0.015 g, 0.016 mmol) following the procedure described for **109a**. ¹H NMR (400 MHz, MeOD) δ 7.67 (dd, *J* = 8.5, 1.3 Hz, 1H), 7.33 (d, *J* = 2.1 Hz, 1H), 7.26 – 7.22 (m, 2H), 7.22 – 7.19 (m, 1H), 7.10 (d, *J* = 2.1 Hz, 1H), 6.99 – 6.95 (m, 2H), 6.86 – 6.84 (m, 1H), 5.10 – 5.02 (m, 1H), 4.42 (s, 2H), 4.31 (s, 2H), 4.17 – 4.10 (m, 2H), 3.86 – 3.82 (m, 2H), 3.73 – 3.66 (m, 12H), 3.54 – 3.46 (m, 4H), 3.21 – 3.07 (m, 4H), 2.91 – 2.80 (m, 1H), 2.78 – 2.71 (m, 2H), 2.66 (s, 3H), 2.12 – 2.05 (m, 1H). ¹³C NMR (101 MHz, MeOD) δ 173.6, 173.2, 169.1, 167.9, 167.5, 157.7, 155.3, 134.2, 129.6, 129.3, 124.7, 119.7, 118.0, 114.9, 114.5, 108.1, 70.3, 70.2, 70.1, 70.1, 69.6, 69.4, 67.3, 53.4, 51.8, 50.6, 46.6, 43.9, 41.1, 38.9, 34.1, 32.5, 30.8, 29.3, 22.8, 22.4. HRMS (ESI): *m/z* [M + H]⁺ calcd. for C₃₉H₄₉N₇O₉ + H⁺: 760.3665 Found: 760.3669.

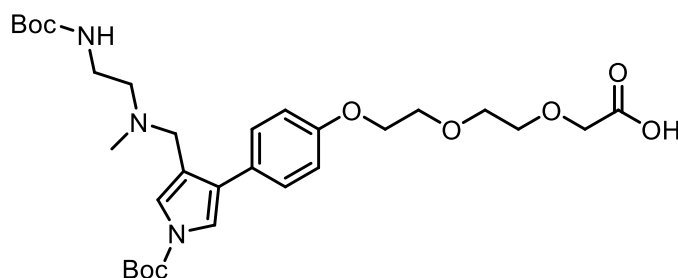
5-(4-(14-(4-(4-(((2-aminoethyl)(methyl)amino)methyl)-1H-pyrrol-3-yl)phenoxy)-3,6,9,12-tetraoxatetradecanoyl)piperazin-1-yl)-2-(2,6-dioxopiperidin-3-yl)isoindoline-1,3-dione (110c)



Compound **110c** was obtained as a white solid (0.025 g, 95%) starting from compound **115c** (0.030 g, 0.030 mmol) following the procedure described for **109a**. ¹H NMR (400 MHz, MeOD) δ 10.98 (s, 1H), 7.69 (d, *J* = 8.5 Hz, 1H), 7.37 (d, *J* = 2.3 Hz, 1H), 7.26 (d, *J* = 8.5 Hz, 2H), 7.26 – 7.20 (m, 1H), 7.12 (d, *J* = 1.9 Hz, 1H), 6.99 (d, *J* = 8.7 Hz, 2H), 6.87 (d, *J* = 1.9 Hz, 1H), 5.12 – 5.04 (m, 1H), 4.43 (s, 2H), 4.31 (s, 2H), 4.17 – 4.11 (m, 2H), 3.85 – 3.78 (m, 2H), 3.70 – 3.63 (m, 16H), 3.57 – 3.51 (m, 2H), 3.51 – 3.44 (m, 2H), 2.90 – 2.81 (m, 1H), 2.77 – 2.71 (m, 2H), 2.67 (s, 3H), 2.12 – 2.06 (m, 1H). ¹³C NMR (101 MHz, MeOD) δ 200.3, 179.7,

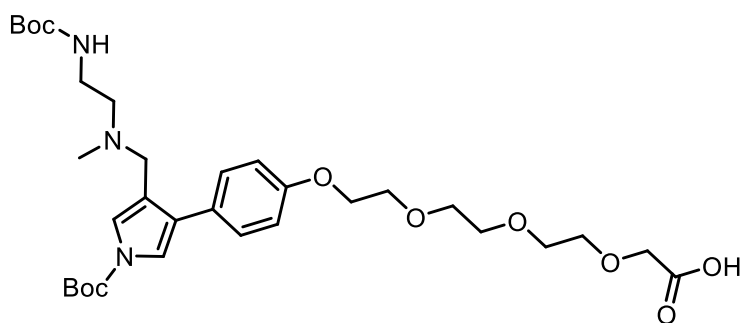
173.2, 170.3, 169.2, 167.9, 167.5, 157.8, 155.3, 155.3, 134.2, 129.6, 127.9, 124.7, 119.7, 118.1, 114.9, 108.1, 70.3, 70.2, 70.1, 70.0, 70.0, 69.5, 69.4, 67.3, 54.5, 51.8, 50.6, 43.3, 43.2, 41.1, 38.9, 34.1, 30.8, 29.3, 22.4, 17.3, 15.9. **HRMS** (ESI): m/z $[M + H]^+$ calcd. for $C_{41}H_{53}N_7O_{10} + H^+$: 804.3927 Found: 804.3924.

2-(2-(2-(4-(1-(*tert*-butoxycarbonyl)-4-(((2-((*tert*-butoxycarbonyl)amino)ethyl)(methyl)amino)methyl)-1*H*-pyrrol-3-yl)phenoxy)ethoxy)ethoxy)acetic acid (111a)



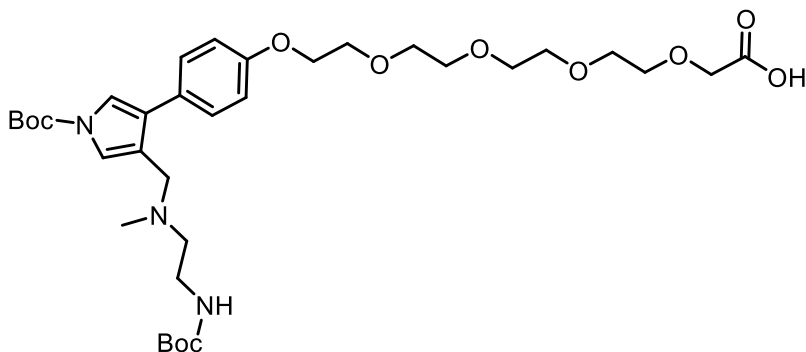
To a solution of Tetrakis(triphenylphosphine)palladium (1.28 mg, 0.001 mmol) and triphenylphosphine (1.46 mg, 0.006 mmol) in dry DCM (1 mL), **118a** (0.070 g, 0.11 mmol) was added. Then, a solution of pyrrolidine (9.8 μ L, 0.12 mmol) in dry DCM (300 μ L) was added and the resulting mixture was stirred until TLC showed disappearance of starting material. Then the reaction mixture was diluted with DCM (25 mL) and then washed with HCl 0.5 N (3×25 mL). The organic phase was dried over anhydrous Na_2SO_4 and filtered. The solvent was removed under vacuum and the product was used in the next step without further purification steps. **1H NMR** (400 MHz, $CDCl_3$) δ 11.69 (br s, 1H), 7.68 – 7.65 (m, 1H), 7.25 (d, $J = 8.5$ Hz, 1H), 7.16 (s, 1H), 6.97 (d, $J = 8.5$ Hz, 2H), 6.11 (br s, 1H), 4.13 (s, 2H), 3.95 – 3.87 (m, 2H), 3.77 – 3.65 (m, 6H), 3.38 (s, 2H), 3.06 – 2.93 (m, 2H), 2.76 – 2.63 (m, 2H), 2.17 (s, 3H), 1.63 (s, 9H), 1.41 (s, 9H). **MS** (ESI) m/z : 592 ($M+H$) $^+$.

2-(2-(2-(2-(4-(1-(*tert*-butoxycarbonyl)-4-(((2-((*tert*-butoxycarbonyl)amino) ethyl) (methyl)amino)methyl)-1*H*-pyrrol-3-yl)phenoxy)ethoxy)ethoxy)ethoxy)acetic acid (111b)



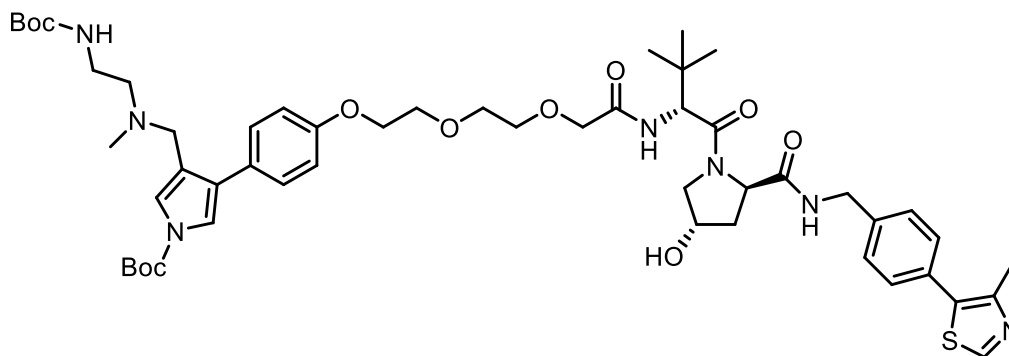
Compound **111b** was obtained as a pale yellow oil (0.058 g, 91%) starting from compound **118b** (0.067 g, 0.010 mmol) following the procedure described for **111a**. **¹H NMR** (400 MHz, CDCl₃) δ 11.64 (br s, 1H), 7.67 – 7.63 (m, 1H), 7.25 (d, *J* = 8.5 Hz, 1H), 7.15 (s, 1H), 6.94 (d, *J* = 8.5 Hz, 2H), 6.10 (br s, 1H), 4.10 (s, 2H), 3.94 – 3.88 (m, 2H), 3.75 – 3.62 (m, 10H), 3.37 (s, 2H), 3.06 – 2.93 (m, 2H), 2.76 – 2.61 (m, 2H), 2.16 (s, 3H), 1.62 (s, 9H), 1.44 (s, 9H). **MS** (ESI) *m/z*: 636 (M+H)⁺.

14-(4-(1-(tert-butoxycarbonyl)-4-(((2-((tert-butoxycarbonyl) amino) ethyl)(methyl) amino) methyl)-1H-pyrrol-3-yl)phenoxy)-3,6,9,12-tetraoxatetradecanoic acid (111c)



Compound **111c** was obtained as a pale yellow oil (0.052 g, 90%) starting from compound **118c** (0.061 g, 0.085 mmol) following the procedure described for **111a**. **¹H NMR** (400 MHz, CDCl₃) δ 11.67 (br s, 1H), 7.65 – 7.61 (m, 1H), 7.24 (d, *J* = 8.5 Hz, 1H), 7.13 (s, 1H), 6.95 (d, *J* = 8.5 Hz, 2H), 6.11 (br s, 1H), 4.12 (s, 2H), 3.94 – 3.88 (m, 2H), 3.74 – 3.61 (m, 14H), 3.38 (s, 2H), 3.07 – 2.93 (m, 2H), 2.75 – 2.61 (m, 2H), 2.17 (s, 3H), 1.64 (s, 9H), 1.43 (s, 9H). **MS** (ESI) *m/z*: 680 (M+H)⁺.

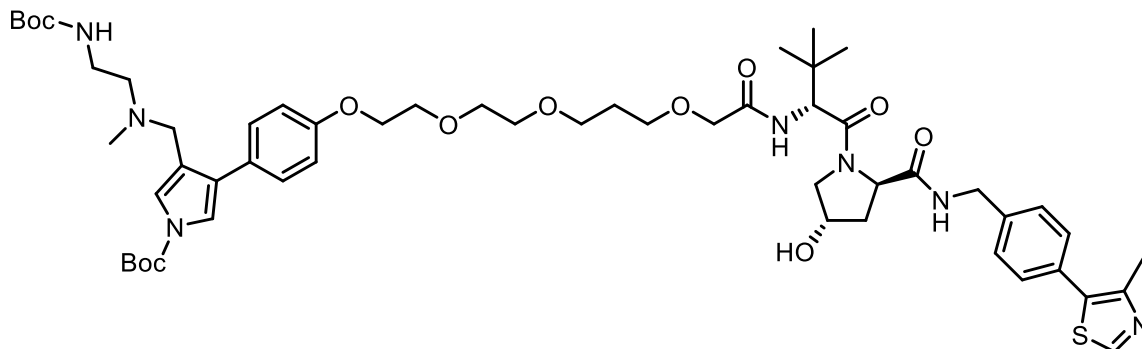
Tert-butyl 3-(((2-((tert-butoxycarbonyl)amino)ethyl)(methyl)amino)methyl)-4-(4-(2-(2-(2-(((R)-1-((2R,4S)-4-hydroxy-2-((4-(4-methylthiazol-5-yl)benzyl)carbamoyl)pyrrolidin-1-yl)-3,3-dimethyl-1-oxobutan-2-yl)amino)-2-oxoethoxy)ethoxy)ethoxy)phenyl)-1H-pyrrole-1-carboxylate (114a)



To a solution of carboxylic compound **111a** (0.058 g, 0.10 mmol) in dry DMF (2 mL), COMU (0.042 g, 0.1 mmol), compound **112** (0.052 g, 0.1 mmol) and DIPEA (0.051 mL, 0.30 mmol) were added. The reaction mixture was left to stir for 4 h at room temperature. Then, the reaction mixture was diluted with brine solution (25 mL) and then extracted with ethyl acetate (3 × 25 mL). The organic phase was dried over anhydrous Na₂SO₄ and filtered. Solvent was removed using a rotary evaporator. The crude brown-colored oil was purified by flash column chromatography on silica gel (DCM/MeOH 95:5 to 80:20) to give the compound **114a** as a yellow solid (0.040 g, 50%). ¹H NMR (400 MHz, MeOD) δ 8.88 (s, 1H), 7.45(d, *J* = 8.2 Hz, 2H), 7.40 (d, *J* = 8.3 Hz, 2H), 7.22 (d, *J* = 8.6 Hz, 2H), 7.13 – 7.10 (m, 1H), 7.01 – 6.92 (m, 2H), 6.89 – 6.82 (m, 1H), 4.71 – 4.67 (m, 1H), 4.61 – 4.54 (m, 1H), 4.51 (s, 2H), 4.42 (s, 2H), 4.39 – 4.31 (m, 1H), 4.18 – 4.13 (m, 2H), 4.05 (d, *J* = 3.0 Hz, 2H), 3.91 – 3.85 (m, 4H), 3.79 – 3.73 (m, 5H), 3.18 – 3.14 (m, 4H), 2.62 (s, 3H), 2.45 (s, 3H), 2.27 – 2.20 (m, 1H), 2.13 – 2.04 (m, 1H), 1.62 (s, 9H), 1.44 (s, 9H), 1.03 (s, 9H). MS (ESI) *m/z*: 1004 (M+H)⁺.

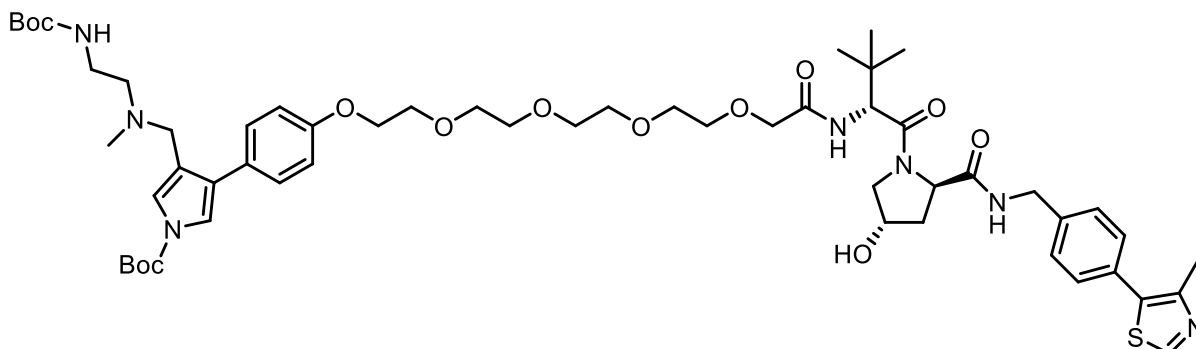
Tert-butyl 3-(((2-((tert-butoxycarbonyl)amino)ethyl)(methyl)amino)methyl)-4-(4-(((R)-14-((2R,4S)-4-hydroxy-2-((4-(4-methylthiazol-5-yl)benzyl)carbamoyl)pyrrolidine-1-carbonyl)-

15,15-dimethyl-12-oxo-3,6,10-trioxa-13-azahexadecyl)oxy)phenyl)-1H-pyrrole-1-carboxylate (114b)



Compound **114b** was obtained as a pale yellow oil (0.049 g, 47%) starting from compound **111b** (0.058 g, 0.10 mmol) following the procedure described for **114a**. ¹H NMR (400 MHz, MeOD) δ 8.89 (s, 1H), 7.45 (d, *J* = 8.2 Hz, 2H), 7.42 (d, *J* = 8.3 Hz, 2H), 7.21 (d, *J* = 8.6 Hz, 2H), 7.12 – 7.09 (m, 1H), 7.00 – 6.93 (m, 2H), 6.88 – 6.82 (m, 1H), 4.70 – 4.66 (m, 1H), 4.62 – 4.54 (m, 1H), 4.50 (s, 2H), 4.41 (s, 2H), 4.39 – 4.30 (m, 1H), 4.18 – 4.13 (m, 2H), 4.05 (d, *J* = 3.0 Hz, 2H), 3.90 – 3.85 (m, 4H), 3.74 – 3.67 (m, 8H), 3.17 – 3.14 (m, 4H), 2.62 (s, 3H), 2.45 (s, 3H), 2.31 – 2.20 (m, 1H), 2.10 – 2.04 (m, 1H), 1.61 (s, 9H), 1.42 (s, 9H), 1.04 (s, 9H). MS (ESI) *m/z*: 1062 (M+H)⁺.

Tert-butyl 3-(((2-((tert-butoxycarbonyl)amino)ethyl)(methyl)amino)methyl)-4-(4-(((R)-16-((2R,4S)-4-hydroxy-2-((4-(4-methylthiazol-5-yl)benzyl)carbamoyl)pyrrolidine-1-carbonyl)-17,17-dimethyl-14-oxo-3,6,9,12-tetraoxa-15-azaooctadecyl)oxy)phenyl)-1H-pyrrole-1-carboxylate (114c)

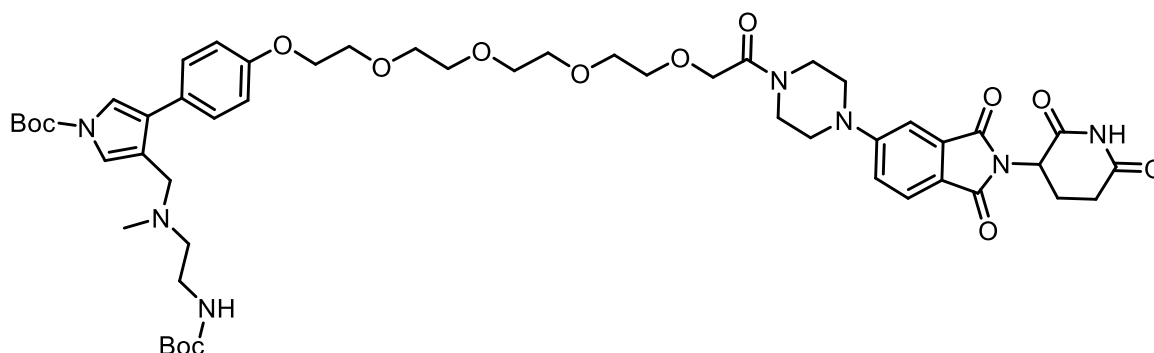


Tert-butyl 3-(((2-((tert-butoxycarbonyl)amino)ethyl)(methyl)amino)methyl)-4-(4-(2-(2-(2-(2-(4-(2-(2,6-dioxopiperidin-3-yl)-1,3-dioxoisindolin-5-yl)piperazin-1-yl)-2-oxoethoxy)ethoxy)ethoxy)ethoxy)phenyl)-1H-pyrrole-1-carboxylate (115b)



Compound **115b** was obtained as a yellow oil (0.015 g, 20%) starting from compound **111b** (0.051 g, 0.080 mmol) and compound **113** (0.030 g, 0.080 mmol) following the procedure described for **114a**. ¹H NMR (400 MHz, MeOD) δ 7.92 (s, 1H), 7.67 (d, *J* = 8.5 Hz, 2H), 7.46 (d, *J* = 8.9 Hz, 2H), 7.35 – 7.29 (m, 1H), 7.26 – 7.16 (m, 1H), 6.93 (d, *J* = 8.9 Hz, 2H), 5.08 – 5.06 (m, 1H), 4.32 (s, 2H), 4.17 – 4.10 (m, 2H), 3.91 – 3.83 (m, 2H), 3.77 – 3.65 (m, 12H), 3.53 – 3.51 (m, 4H), 3.18 – 3.09 (m, 2H), 2.66 (s, 3H), 2.45 (t, *J* = 6.5 Hz, 2H), 2.19 (s, 4H), 2.12 – 2.06 (m, 2H), 1.64 (s, 9H), 1.43 (s, 9H). MS (ESI) *m/z*: 960 (M+H)⁺.

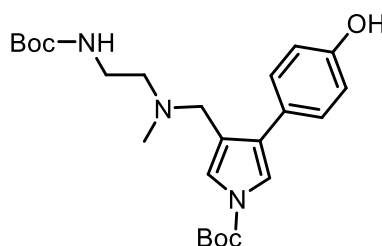
Tert-butyl 3-(((2-((tert-butoxycarbonyl)amino)ethyl)(methyl)amino)methyl)-4-(4-((14-(4-(2-(2,6-dioxopiperidin-3-yl)-1,3-dioxoisindolin-5-yl)piperazin-1-yl)-14-oxo-3,6,9,12-tetraoxatetradecyl)oxy)phenyl)-1H-pyrrole-1-carboxylate (115c)



Compound **115c** was obtained as a yellow oil (0.030 g, 36%) starting from compound **111c** (0.057 g, 0.084 mmol) and compound **113** (0.032 g, 0.084 mmol) following the procedure

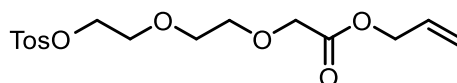
described for **114a**. **¹H NMR** (400 MHz, MeOD) δ 7.93 (s, 1H), 7.65 (d, J = 8.5 Hz, 2H), 7.45 (d, J = 8.9 Hz, 2H), 7.34 – 7.28 (m, 1H), 7.27 – 7.14 (m, 1H), 6.91 (d, J = 8.9 Hz, 2H), 5.09 – 5.06 (m, 1H), 4.30 (s, 2H), 4.15 – 4.11 (m, 2H), 3.90 – 3.82 (m, 2H), 3.75 – 3.62 (m, 12H), 3.52 – 3.52 (m, 4H), 3.15 – 3.04 (m, 2H), 2.65 (s, 3H), 2.44 (t, J = 6.5 Hz, 2H), 2.17 (s, 4H), 2.11 – 2.05 (m, 2H), 1.63 (s, 9H), 1.42 (s, 9H). **MS** (ESI) m/z : 1004 (M+H)⁺.

Tert-butyl 3-(((2-((tert-butoxycarbonyl)amino)ethyl)(methyl)amino)methyl)-4-(4-hydroxyphenyl)-1H-pyrrole-1-carboxylate (116)



A mixture of **125** (0.600 g, 0.12 mmol), Pd/C 10% (0.06 g) in EtOH (12 mL) was stirred under H₂ for 5 h. After, the reaction mixture was filtered, and the solvent was concentrated under vacuum. The product was directly used in the next step without further purification step. **¹H NMR** (400 MHz, CDCl₃) δ 7.37 (d, J = 8.6 Hz, 2H), 7.22 (s, 1H), 7.19 (s, 1H), 6.86 (d, J = 8.6 Hz, 2H), 3.41 (s, 2H), 3.22 – 3.12 (m, 2H), 2.52 – 2.39 (m, 2H), 2.17 (s, 3H), 1.61 (s, 9H), 1.44 (s, 9H). **MS** (ESI) m/z : 446 (M+H)⁺.

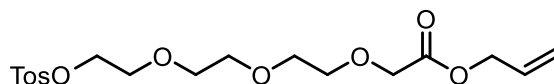
Allyl 2-(2-(2-(tosyloxy)ethoxy)ethoxy)acetate (117a)



To a solution of carboxylic acid **129a** (0.922 g, 2.9 mmol) in dry DMF (19 mL), allyl iodide (0.290 mL, 3.19 mmol) and Ce₂CO₃ (1.04 g, 3.19 mmol) were added. Then, the reaction mixture was diluted with H₂O (25 mL) and then extracted with ethyl acetate (3 × 25 mL). The organic phase was washed with NaHCO₃ (3 × 25 mL), Na₂SO₃ 5% solution (3 × 25 mL), brine solution

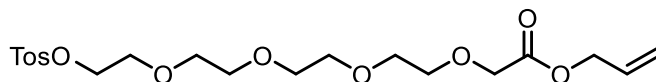
(3 × 25 mL), dried over anhydrous Na₂SO₄ and filtered. Solvent was removed using a rotary evaporator to give a pale yellow oil (1.01 g, 97%) that was used for the next step without further purification. **¹H NMR** (400 MHz, CDCl₃) δ 7.85 – 7.62 (m, 2H), 7.39 – 7.31 (m, 2H), 6.08 – 5.74 (m, 1H), 5.47 – 5.07 (m, 2H), 4.73 – 4.50 (m, 2H), 4.19 (s, 2H), 3.84 – 3.62 (m, 8H), 2.45 (s, 3H). **MS** (ESI) *m/z*: 359 (M+H)⁺.

Allyl 2-(2-(2-(2-(tosyloxy)ethoxy)ethoxy)ethoxy)ethoxy)acetate (117b)



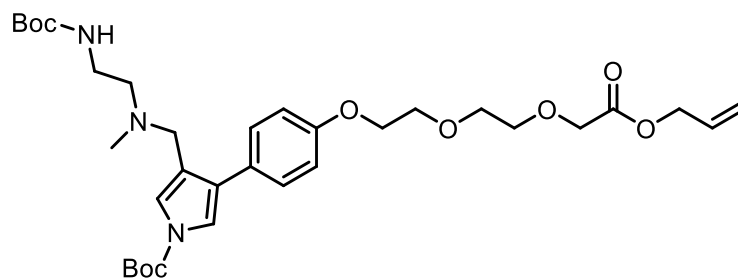
Compound **117b** was obtained as a yellow oil (0.69 g, 99%) starting from compound **129b** (0.623 g, 1.72 mmol) following the procedure described for **117a**. **¹H NMR** (400 MHz, CDCl₃) δ 7.86 – 7.63 (m, 2H), 7.40 – 7.31 (m, 2H), 6.06 – 5.73 (m, 1H), 5.45 – 5.03 (m, 2H), 4.70 – 4.50 (m, 2H), 4.21 (s, 2H), 3.83 – 3.61 (m, 12H), 2.44 (s, 3H). **MS** (ESI) *m/z*: 403 (M+H)⁺.

Allyl 15-(tosyloxy)-3,6,10,13-tetraoxapentadecanoate (117c)



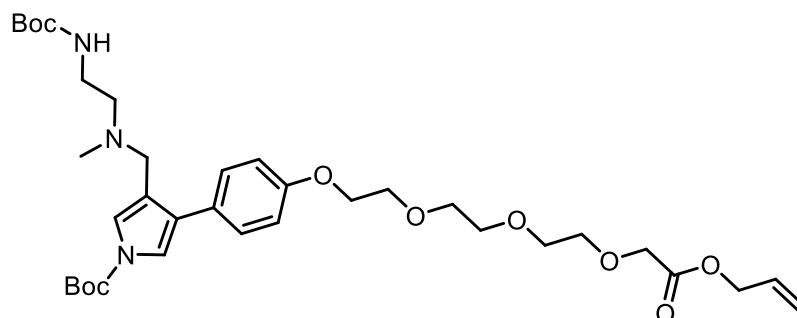
Compound **117c** was obtained as a yellow oil (0.67 g, 99%) starting from compound **129c** (0.61 g, 1.50 mmol) following the procedure described for **117a**. **¹H NMR** (400 MHz, CDCl₃) δ 7.88 – 7.63 (m, 2H), 7.39 – 7.31 (m, 2H), 6.07 – 5.73 (m, 1H), 5.44 – 5.03 (m, 2H), 4.70 – 4.48 (m, 2H), 4.20 (s, 2H), 3.91 – 3.58 (m, 16H), 2.44 (s, 3H). **MS** (ESI) *m/z*: 447 (M+H)⁺.

Tert-butyl 3-(4-(2-(2-(2-(allyloxy)-2-oxoethoxy)ethoxy)ethoxy)phenyl)-4-(((2-((tert-butoxycarbonyl)amino)ethyl)(methyl)amino)methyl)-1H-pyrrole-1-carboxylate (118a)



To a solution of **116** (0.20 g, 0.44 mmol) and **117a** (0.194 g, 0.54 mmol) in dry DMF (2.2 mL) K_2CO_3 (0.067 g, 0.48 mmol) was added. The reaction was stirred at 80° C for 24 h under an H_2 atmosphere. Then, the solution was cooled to room temperature, H_2O (25 mL) was added and then extracted with ethyl acetate (3×25 mL). The organic phase was washed with NaHCO_3 (3×25 mL), brine solution (3×25 mL), dried over anhydrous Na_2SO_4 and filtered. The crude was purified by flash column chromatography (DCM/MeOH 10:0 \rightarrow 9:1) to give the title compound **118a** as orange oil (0.170 g, 60%). ^1H NMR (400 MHz, CDCl_3) δ 7.47 (d, $J = 8.8$ Hz, 2H), 7.35 (s, 1H), 7.18 (s, 1H), 6.95 (d, $J = 8.8$ Hz, 2H), 6.04 – 5.79 (m, 1H), 5.45 – 5.14 (m, 2H), 4.77 – 4.60 (m, 2H), 4.23 (s, 2H), 4.21 – 4.07 (m, 2H), 3.91 – 3.83 (m, 2H), 3.79 – 3.69 (m, 4H), 3.40 (s, 2H), 3.22 – 3.11 (m, 2H), 2.47 (t, $J = 6.0$ Hz, 2H), 2.19 (s, 3H), 1.63 (s, 9H), 1.45 (s, 9H). MS (ESI) m/z : 632 ($\text{M}+\text{H}$) $^+$.

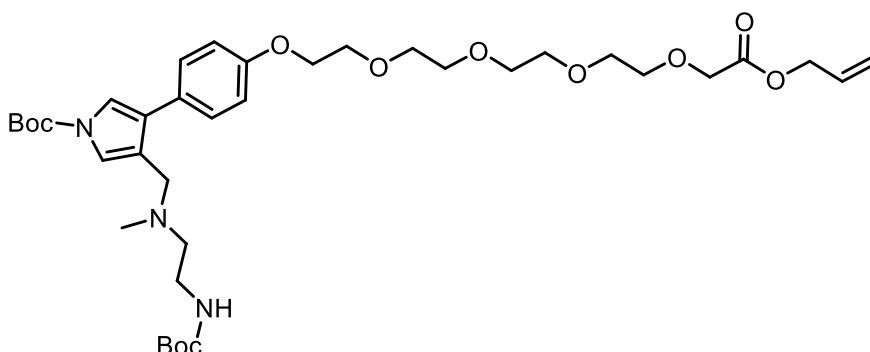
Tert-butyl 3-(((2-((tert-butoxycarbonyl)amino)ethyl)(methyl)amino)methyl)-4-(4-((11-oxo-3,6,9,12-tetraoxapentadec-14-en-1-yl)oxy)phenyl)-1H-pyrrole-1-carboxylate (118b)



Compound **118b** was obtained as a yellow oil (0.134 g, 45%) starting from compound **117b** (0.216 g, 0.54 mmol) following the procedure described for **118a**. ^1H NMR (400 MHz, CDCl_3)

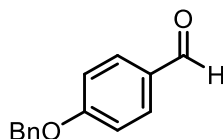
δ 7.46 (d, J = 8.7 Hz, 2H), 7.34 (s, 1H), 7.17 (s, 1H), 6.94 (d, J = 8.7 Hz, 2H), 6.04 – 5.77 (m, 1H), 5.45 – 5.13 (m, 2H), 4.75 – 4.60 (m, 2H), 4.21 (s, 2H), 4.20 – 4.05 (m, 2H), 3.93 – 3.85 (m, 2H), 3.78 – 3.65 (m, 8H), 3.43 (s, 2H), 3.21 – 3.11 (m, 2H), 2.46 (t, J = 6.0 Hz, 2H), 2.21 (s, 3H), 1.62 (s, 9H), 1.46 (s, 9H). **MS** (ESI) m/z : 676 (M+H)⁺.

Tert-butyl 3-(((2-((tert-butoxycarbonyl)amino)ethyl)(methyl)amino)methyl)-4-(4-(((14-oxo-3,6,9,12,15-pentaoxaoctadec-17-en-1-yl)oxy)phenyl)-1H-pyrrole-1-carboxylate (118c)



Compound **118c** was obtained as a yellow oil (0.122 g, 45%) starting from compound **117c** (0.240 g, 0.52 mmol) following the procedure described for **118a**. ¹H NMR (400 MHz, CDCl₃) δ 7.45 (d, J = 8.7 Hz, 2H), 7.32 (s, 1H), 7.17 (s, 1H), 6.93 (d, J = 8.7 Hz, 2H), 6.04 – 5.75 (m, 1H), 5.44 – 5.13 (m, 2H), 4.75 – 4.60 (m, 2H), 4.21 (s, 2H), 4.19 – 4.05 (m, 2H), 3.94 – 3.85 (m, 2H), 3.78 – 3.65 (m, 12H), 3.42 (s, 2H), 3.20 – 3.11 (m, 2H), 2.44 (t, J = 6.0 Hz, 2H), 2.20 (s, 3H), 1.64 (s, 9H), 1.46 (s, 9H). **MS** (ESI) m/z : 720 (M+H)⁺.

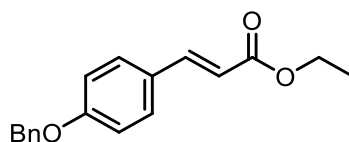
4-(benzyloxy)benzaldehyde (120)



To a stirred solution of **119** (5.0 g, 32.8 mmol) in anhydrous DMF was added K₂CO₃ (6.85 g, 44.5 mmol) and benzyl chloride (4.52 mL, 39.5 mmol) under N₂ followed. The resulting solution was stirred overnight at room temperature. After consumption of the starting material

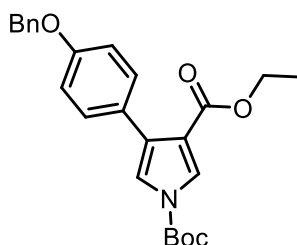
as confirmed by TLC, the reaction was quenched by addition of saturated NH_4Cl (100 mL). The resulting suspension was extracted with DCM (3×100 mL). The combined organic extracts were dried over Na_2SO_4 and filtered. The crude was purified by flash column chromatography (Hex/AcOEt 95:5 \rightarrow 80:20) to give the title compound **120** as orange oil white solid (6.74 g, 97%). $^1\text{H NMR}$ (400 MHz, CDCl_3): δ 9.77 (s, 1H), 7.72 (d, $J = 8.7$ Hz, 2H), 7.35 – 7.22 (m, 5H), 6.97 (d, $J = 8.7$ Hz, 2H), 5.03 (s, 2H). **MS** (ESI) m/z : 213 ($\text{M}+\text{H}$) $^+$.

Ethyl (E)-3-(4-(benzyloxy)phenyl)acrylate (121)



A solution of **120** (6.74 g, 31.8 mmol), ethyl 2-(diethoxyphosphoryl)acetate (7.12 g, 31.8 mmol) and KOH (3.56 g, 63.6 mmol) in anhydrous THF (50 mL) was stirred at room temperature for 4 h. The solvent was removed under reduced pressure, and the residue was purified by flash column chromatography (Hex/AcOEt 95:5 to 90:10) providing the product **121** as a white solid (7.35 g, 82%). $^1\text{H NMR}$ (400 MHz, CDCl_3) δ 7.64 (d, $J = 16.0$ Hz, 1H), 7.47 (d, $J = 8.6$ Hz, 2H), 7.45-7.28 (m, 5H), 6.97 (d, $J = 8.6$ Hz, 2H), 6.31 (d, $J = 15.8$ Hz, 1H), 5.09 (s, 2H), 4.25 (q, $J = 7.0$ Hz, 2H), 1.33 (t, $J = 7.1$ Hz, 3H). **MS** (ESI) m/z : 283 ($\text{M}+\text{H}$) $^+$.

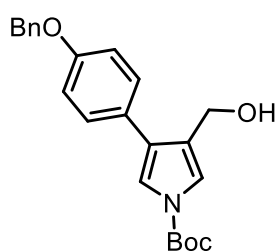
1-(tert-butyl) 3-ethyl 4-(4-(benzyloxy)phenyl)-1H-pyrrole-1,3-dicarboxylate (122)



To a stirred suspension of NaH (60% in mineral oil, 2.2 g, 55.0 mmol) in 100 mL DMF/THF (v/v, 1:1) was added a solution of TOSMIC (4.4 g, 22.9 mmol) and **121** (5.27 g, 18.7 mmol) in

100 mL DMF/THF (v/v, 1:1) slowly over 30 min at 0 °C. After completion of the addition, the reaction was warmed to room temperature and stirred for 1.5 h. The reaction was then quenched with water (50 mL) and diluted with ethyl acetate. The organic phase was washed with brine (3 × 50 mL), dried over Na₂SO₄ and concentrated to give crude compound as red brown oil. The crude product was used for the next step without purification. To a solution of the above intermediate, TEA (2.83 g, 28.05 mmol) and DMAP (228 mg, 1.87 mmol) in DCM (100 mL) was added a solution of di-tert-butyl dicarbonate (4.9 g, 22.5 mmol) in DCM (20 mL). After being stirred overnight, the reaction was quenched with water and extracted with DCM. The combined organic phase was dried over Na₂SO₄, concentrated under reduced pressure, and purified by silica gel column to give the title compound **122** (5.90 g, 75%) as pale yellow oil. ¹H NMR (400 MHz, CDCl₃): δ 7.88 (s, 1H), 7.47 (d, *J* = 8.6 Hz, 2H), 7.45 – 7.28 (m, 5H), 7.28 (d, *J* = 8.6 Hz, 2H), 7.18 (s, 1H), 5.09 (s, 2H), 4.25 (q, *J* = 7.0 Hz, 2H), 1.62 (s, 9H), 1.47 (t, *J* = 7.0 Hz, 3H). MS (ESI) *m/z*: 422 (M+H)⁺.

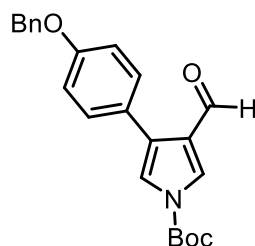
Tert-butyl 3-(4-(benzyloxy)phenyl)-4-(hydroxymethyl)-1H-pyrrole-1-carboxylate (123)



To a solution of **122** (4.22 g, 10.0 mmol) in DCM (100 mL) was added a solution of DIBAL-H (1 M in hexane, 25.0 mmol) dropwise over 30 min at -78 °C. After being stirred for 6 h, the reaction mixture was diluted with methanol (5 mL) and was slowly warmed to room temperature. Aqueous saturated potassium sodium tartrate (500 mL) was then added, and the resulting mixture was stirred vigorously until two phases separated clearly. The organic phase was dried over Na₂SO₄, filtered, concentrated and purified by flash column chromatography

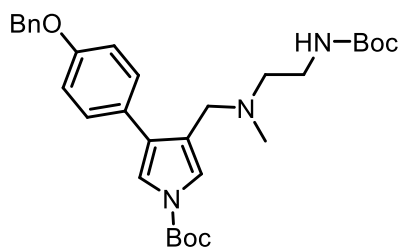
(Hex/AcOEt 90:10 to 50:50) to provide the desired alcohol **123** (2.28 g, 60%) as pale yellow oil. $^1\text{H NMR}$ (400 MHz, CDCl_3): δ 7.87 (s, 1H), 7.45 (d, $J = 8.6$ Hz, 2H), 7.44 – 7.28 (m, 5H), 7.27 (d, $J = 8.6$ Hz, 2H), 7.16 (s, 1H), 5.09 (s, 2H), 4.63 (s, 2H), 1.60 (s, 9H). **MS** (ESI) m/z : 380 ($\text{M}+\text{H}$) $^+$.

Tert-butyl 3-(4-(benzyloxy)phenyl)-4-formyl-1H-pyrrole-1-carboxylate (124)



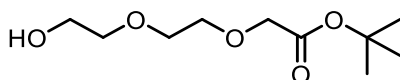
To a solution of **123** (2.10 g, 5.4 mmol) in DCM (100 mL) was added DMP (2.81 g, 6.64 mmol) slowly. The resulting suspension was warmed to room temperature and stirred for 2 h, at which time the reaction was quenched with water and extracted with DCM (3 x 25 mL). The combined organic phase was dried over Na_2SO_4 , concentrated and purified by flash column chromatography (Hex/AcOEt 95:5 to 70:30) to give aldehyde **124** (1.83 g, 90%) as yellow oil. $^1\text{H NMR}$ (400 MHz, CDCl_3): δ 9.92 (s, 1H), 7.88 (s, 1H), 7.45 (d, $J = 8.6$ Hz, 2H), 7.44 – 7.29 (m, 5H), 7.29 (d, $J = 8.6$ Hz, 2H), 7.16 (s, 1H), 5.09 (s, 2H), 1.59 (s, 9H). **MS** (ESI) m/z : 378 ($\text{M}+\text{H}$) $^+$.

Tert-butyl 3-(4-(benzyloxy)phenyl)-4-(((2-((tert-butoxycarbonyl)amino)ethyl) (methyl) amino) methyl)-1H-pyrrole-1-carboxylate (125)



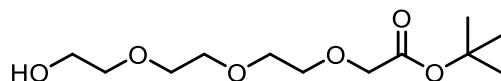
To a solution of **124** (1.4 g, 3.7 mmol) and *tert*-butyl (2- (methylamino)ethyl)carbamate (0.97 g, 5.56 mmol) in DCM (100 mL) was slowly added NaBH(OAc)₃ (1.41 g, 6.66 mmol). The resulting mixture was stirred overnight, before being quenched with water (100 mL). The aqueous phase was extracted with DCM (3 x 20 mL). The combined organic phase was dried over Na₂SO₄, concentrated and purified by flash column chromatography (DCM/MeOH 97:3 to 90:10) to give the title compound **125** (1.86 g, 94%) as pale yellow oil. ¹H NMR (400 MHz, CD₃OD): δ 7.45 (d, *J* = 8.5 Hz, 2H), 7.44 – 7.31 (m, 5H), 7.22 (s, 2H), 6.92 (d, *J* = 8.6 Hz, 2H), 3.42 (s, 2H), 3.12 (t, *J* = 6.4 Hz, 2H), 2.44 (t, *J* = 6.5 Hz, 2H), 2.19 (s, 3H), 1.62 (s, 9H), 1.41 (s, 9H). MS (ESI) *m/z*: 536 (M+H)⁺.

Tert-butyl 2-(2-(2-hydroxyethoxy)ethoxy)acetate (127a)



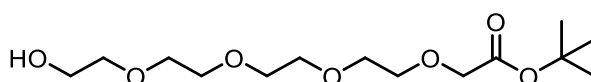
NaH 60% in mixture (0.203 g, 5.08 mmol) was added under nitrogen atmosphere to a solution of **126a** (1.35 g, 12.7 mmol) in 12 mL of dry DMF at 0 °C. The resulting mixture was stirred at 0 °C for 30 min. Then, *tert*-butyl 2-bromoacetate (0.624 mL, 4.23 mmol) was added and the final suspension was continuously stirred for 14 h at room temperature. The crude was concentrated, and the residual was taken up with saturated solution of NH₄Cl (30 mL). The aqueous phase was extracted with AcOEt (3 x 20 mL). The collected organic phases were washed with brine, dried over anhydrous Na₂SO₄ and filtered. Solvent was removed using a rotary evaporator. The crude product was purified using flash column chromatography (Hex/EtOAc 70:30 to 0:100) to yield a colorless oil **127a** (0.610 g, 70%). ¹H NMR (400 MHz, CDCl₃) δ 4.02 (s, 2H), 3.76 – 3.65 (m, 6H), 3.61 (dd, *J* = 5.3, 3.9 Hz, 2H), 1.47 (s, 9H). MS (ESI) *m/z*: 221 (M+H)⁺.

Tert-butyl 2-(2-(2-(2-hydroxyethoxy)ethoxy)ethoxy)acetate (127b)



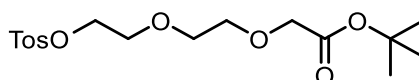
Compound **127b** was obtained as a yellow oil (0.78 g, 71%) starting from compound **126a** (1.92 g, 12.7 mmol) following the procedure described for **127a**. **¹H NMR** (400 MHz, CDCl₃) δ 4.03 (s, 2H), 3.81 – 3.62 (m, 10H), 3.60 (dd, *J* = 5.3, 3.9 Hz, 2H), 1.46 (s, 9H). **MS** (ESI) *m/z*: 265 (M+H)⁺.

Tert-butyl 14-hydroxy-3,6,9,12-tetraoxatetradecanoate (127c)



Compound **127c** was obtained as a yellow oil (0.91 g, 68%) starting from compound **126c** (2.46 g, 12.7 mmol) following the procedure described for **127a**. **¹H NMR** (400 MHz, CDCl₃) δ 4.02 (s, 2H), 3.81 – 3.59 (m, 14H), 3.57 (dd, *J* = 5.3, 3.9 Hz, 2H), 1.44 (s, 9H). **MS** (ESI) *m/z*: 309 (M+H)⁺.

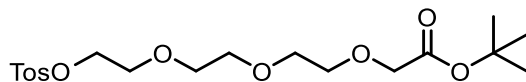
Tert-butyl 2-(2-(2-(tosyloxy)ethoxy)ethoxy)acetate (128a)



To a solution of **127a** (0.517 g, 2.34 mmol) in 26 mL of dry DCM, TEA (0.391 mL, 2.81 mmol) and TsCl (0.536 g, 2.81 mmol) were added. The resulting mixture was stirred for 18 h at room temperature under nitrogen atmosphere. Then, DCM was added (40 mL) and the organic phase was washed with HCl 1N (3 x 20 mL), saturated solution of NaHCO₃ (3 x 20 mL), brine and dried over anhydrous Na₂SO₄. After filtration and evaporation, the crude was purified by flash column chromatography (Hex/EtOAc 80:20 to 50:50) to give compound **128a** as a yellow oil (0.579 g, 66%). **¹H NMR** (400 MHz, CDCl₃) δ 7.82 (d, *J* = 8.2, 2H), 7.33 (d, *J* = 8.2 Hz, 2H),

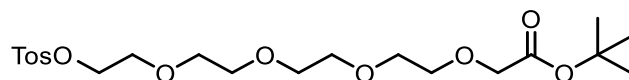
4.16 (t, $J = 4.9$ Hz, 2H), 4.03 (s, 2H), 3.73 – 3.64 (m, 6H), 2.44 (s, 3H), 1.45 (s, 9H). **MS** (ESI) m/z : 375 (M+H)⁺.

Tert-butyl 2-(2-(2-(2-(tosyloxy)ethoxy)ethoxy)ethoxy)acetate (128b)



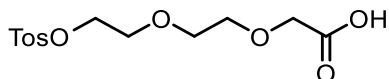
Compound **128b** was obtained as colourless oil (0.626 g, 64%) starting from compound **127b** (0.617 g, 2.34 mmol) following the procedure described for **128a**. **¹H NMR** (400 MHz, CDCl₃) δ 7.80 (d, $J = 8.2$, 2H), 7.34 (d, $J = 8.2$ Hz, 2H), 4.16 (t, $J = 4.9$ Hz, 2H), 4.00 (s, 2H), 3.73 – 3.64 (m, 10H), 2.45 (s, 3H), 1.47 (s, 9H). **MS** (ESI) m/z : 419 (M+H)⁺.

Tert-butyl 14-(tosyloxy)-3,6,9,12-tetraoxatetradecanoate (128c)



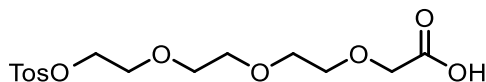
Compound **128c** was obtained as colourless oil (0.649 g, 60%) starting from compound **127c** (0.725 g, 2.34 mmol) following the procedure described for **128a**. **¹H NMR** (400 MHz, CDCl₃) δ 7.83 (d, $J = 8.2$, 2H), 7.34 (d, $J = 8.2$ Hz, 2H), 4.17 (t, $J = 4.9$ Hz, 2H), 4.04 (s, 2H), 3.81 – 3.62 (m, 14H), 2.44 (s, 3H), 1.45 (s, 9H). **MS** (ESI) m/z : 463 (M+H)⁺.

2-(2-(2-(2-(tosyloxy)ethoxy)ethoxy)ethoxy)acetic acid (129a)



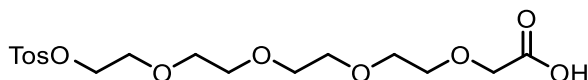
Compound **129a** was obtained as colourless oil (0.477 g, 99%) starting from compound **128a** (0.580 g, 1.5 mmol) following the procedure described for **12a**. **¹H NMR** (400 MHz, CDCl₃) δ 7.78 (d, $J = 8.2$, 2H), 7.34 (d, $J = 8.2$ Hz, 2H), 4.16 (t, $J = 4.9$ Hz, 2H), 4.10 (s, 2H), 3.74 – 3.62 (m, 6H), 2.43 (s, 3H). **MS** (ESI) m/z : 319 (M+H)⁺.

2-(2-(2-(2-(tosyloxy)ethoxy)ethoxy)ethoxy)ethoxy)acetic acid (129b)



Compound **129b** was obtained as colourless oil (0.543 g, 99%) starting from compound **128b** (0.626 g, 1.5 mmol) following the procedure described for **12a**. $^1\text{H NMR}$ (400 MHz, CDCl_3) δ 7.77 (d, $J = 8.2$, 2H), 7.32 (d, $J = 8.2$ Hz, 2H), 4.15 (t, $J = 4.9$ Hz, 2H), 4.11 (s, 2H), 3.75 – 3.66 (m, 10H), 2.44 (s, 3H). **MS** (ESI) m/z : 363 ($\text{M}+\text{H}$) $^+$.

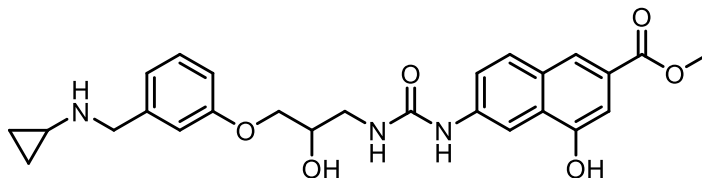
14-(tosyloxy)-3,6,9,12-tetraoxatetradecanoic acid (129c)



Compound **129c** was obtained as colourless oil (0.610 g, 99%) starting from compound **128c** (0.650 g, 1.5 mmol) following the procedure described for **12a**. $^1\text{H NMR}$ (400 MHz, CDCl_3) δ 7.79 (d, $J = 8.2$, 2H), 7.32 (d, $J = 8.2$ Hz, 2H), 4.17 (t, $J = 4.9$ Hz, 2H), 4.10 (s, 2H), 3.75 – 3.62 (m, 14H), 2.44 (s, 3H). **MS** (ESI) m/z : 407 ($\text{M}+\text{H}$) $^+$.

8.2.5. Preparation of compounds 130 - 153

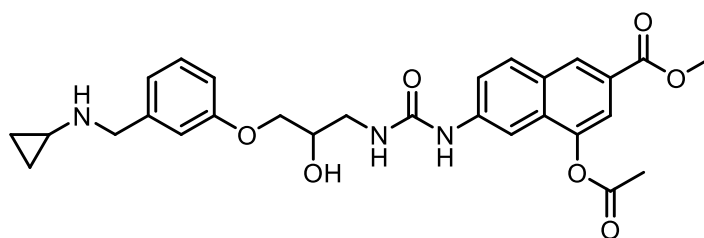
Methyl 6-(3-(3-(3-((cyclopropylamino)methyl)phenoxy)-2-hydroxypropyl)ureido)-4-hydroxy-2-naphthoate (130a)



A mixture of TFA and DCM (1:9, 2 mL) was added to compound **151a** (0.050 g, 0.09 mmol). The reaction was stirred at room temperature for 3h. Then, the solvent was concentrated under vacuum and the crude was purified by flash column chromatography (DCM/MeOH 9:1 to 8:2) to afford the title compound **130a** as a white solid (0.023 g, 53%). $^1\text{H NMR}$ (400 MHz, DMSO-

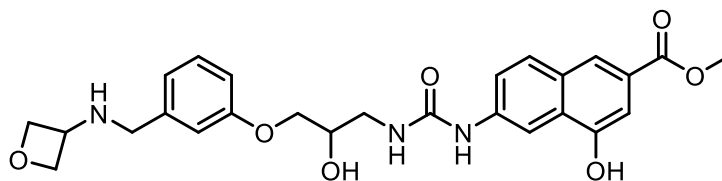
d₆) δ 10.28 (br s, 1H, exchangeable with D₂O), 8.99 (br s, 1H, exchangeable with D₂O), 8.27 (d, J = 2.4 Hz, 1H), 7.97 (s, 1H), 7.89 (d, J = 9.1 Hz, 1H), 7.53 (dd, J = 9.1, 2.4 Hz, 1H), 7.33 – 7.28 (m, 1H), 7.21 (t, J = 7.9 Hz, 1H), 6.98 – 6.85 (m, 2H), 6.83 – 6.78 (m, 1H), 6.36 (br t, J = 5.8 Hz, 1H, exchangeable with D₂O), 5.39 (br d, J = 5.0 Hz, 1H, exchangeable with D₂O), 3.96 – 3.82 (m, 6H), 3.69 (s, 2H), 3.60 – 3.50 (m, 1H), 3.24 – 3.08 (m, 1H), 2.03 (dt, J = 6.6, 3.0 Hz, 1H), 0.38 – 0.30 (m, 2H), 0.30 – 0.20 (m, 2H). **¹³C NMR** (100 MHz, DMSO-d₆) δ 167.1, 159.0, 155.7, 153.0, 143.3, 140.2, 130.2, 129.5, 129.2, 128.4, 125.1, 121.7, 120.8, 120.5, 114.5, 112.9, 107.5, 106.9, 70.5, 68.6, 53.2, 52.4, 42.9, 30.3, 6.6. **HRMS** (ESI): m/z [M + H]⁺ calcd. for C₂₆H₂₉N₃O₆ + H⁺: 480.2129. Found: 480.2126.

Methyl 4-acetoxy-6-(3-(3-(3-((cyclopropylamino)methyl)phenoxy)-2-hydroxypropyl)ureido)-2-naphthoate (130b)



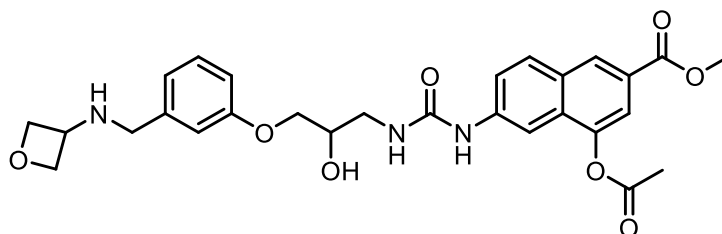
Compound **130b** was obtained as a white solid (0.027 g, 74%) by reaction of **151b** (0.045 g, 0.07 mmol) following the procedure described for **130a**. **¹H NMR** (400 MHz, DMSO-d₆) δ 9.17 (br s, 1H, exchangeable with D₂O), 8.44 (s, 1H), 8.13 – 8.04 (m, 2H), 7.71 – 7.65 (m, 1H), 7.57 (dd, J = 9.0, 2.0 Hz, 1H), 7.20 (t, J = 7.9 Hz, 1H), 6.97 – 6.85 (m, 2H), 6.80 (dd, J = 9.1, 2.0 Hz, 1H), 6.44 (br t, J = 5.7 Hz, 1H, exchangeable with D₂O), 5.32 (br d, J = 5.0 Hz, 1H, exchangeable with D₂O), 4.06 – 3.81 (m, 6H), 3.69 (s, 2H), 3.52 – 3.32 (m, 1H), 3.25 – 3.11 (m, 1H), 2.44 (s, 3H), 2.13 – 1.89 (m, 1H), 0.37 – 0.29 (m, 2H), 0.28 – 0.20 (m, 2H). **¹³C NMR** (100 MHz, DMSO-d₆) δ 167.1, 159.0, 155.7, 153.0, 143.3, 140.2, 130.2, 129.5, 129.2, 128.4, 125.1, 121.7, 120.8, 120.5, 114.5, 112.9, 107.5, 106.9, 70.5, 68.6, 53.2, 52.4, 42.9, 30.3, 22.6, 6.6. **HRMS** (ESI): m/z [M + H]⁺ calcd. for C₂₈H₃₁N₃O₇ + H⁺: 522.2235. Found: 522.2238.

Methyl 4-hydroxy-6-(3-(2-hydroxy-3-(3-((oxetan-3-ylamino)methyl)phenoxy)propyl)ureido)-2-naphthoate (131a)



Compound **131a** was obtained as a white solid (0.018 g, 52%) by reaction of **152a** (0.040 g, 0.07 mmol) following the procedure described for **130a**. **¹H NMR** (400 MHz, DMSO-*d*₆) δ 10.28 (br s, 1H, exchangeable with D₂O), 8.99 (br s, 1H, exchangeable with D₂O), 8.26 (d, *J* = 2 Hz, 1H), 7.99–7.92 (m, 1H), 7.88 (d, *J* = 9 Hz, 1H), 7.55 (dd, *J* = 9 Hz, 2 Hz, 1H), 7.31–7.24 (m, 2H), 6.91–6.84 (m, 3H), 6.37 (br t, *J* = 5.4 Hz, 1H, exchangeable with D₂O), 5.33 (br d, *J* = 5.0 Hz, 1H, *J* = 5 Hz), 5.01 (t, *J* = 5.7 Hz, 1H, exchangeable with D₂O), 4.56 – 54.50 (m, 1H), 4.31 (t, *J* = 8.8 Hz, 1H), 4.19 – 4.05 (m, 2H), 3.98 – 3.88 (m, 3H), 3.86 (s, 3H), 3.68 – 3.60 (m, 2H), 3.59 – 3.49 (m, 2H), 3.23 – 3.10 (m, 1H). **¹³C NMR** (100 MHz, DMSO-*d*₆) δ 167.2, 159.3, 155.7, 153.0, 140.1, 138.8, 129.3, 128.4, 125.1, 121.7, 120.6, 120.4, 114.4, 113.8, 107.6, 106.9, 70.5, 68.6, 64.8, 59.7, 55.8, 52.4, 45.5, 42.9. **HRMS** (ESI): *m/z* [M + H]⁺ calcd. for C₂₆H₂₉N₃O₇ + H⁺: 496.2079. Found: 496.2076.

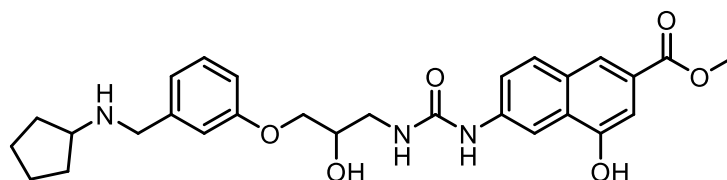
Methyl 4-acetoxy-6-(3-(2-hydroxy-3-(3-((oxetan-3-ylamino)methyl)phenoxy)propyl)ureido)-2-naphthoate (131b)



Compound **131b** was obtained as a white solid (0.030 g, 62%) by reaction of **152b** (0.055 g, 0.09 mmol) following the procedure described for **131a**. **¹H NMR** (400 MHz, DMSO-*d*₆) δ 9.17 (br s, 1H, exchangeable with D₂O), 8.52 – 8.40 (m, 1H), 8.15 – 8.01 (m, 2H), 7.68 (d, *J* =

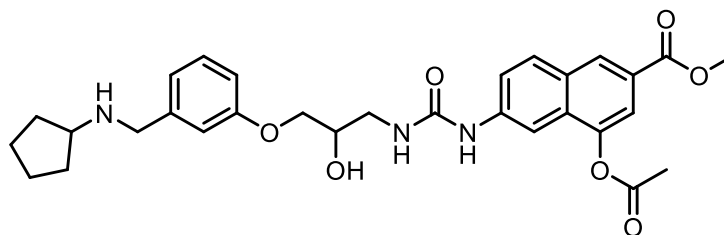
1.6 Hz, 1H), 7.58 (dd, $J = 8.9, 2.2$ Hz, 1H), 7.36 – 7.22 (m, 1H), 6.97 – 6.84 (m, 3H), 6.45 (br t, $J = 5.6$ Hz, 1H, exchangeable with D₂O), 5.39 (br d, $J = 5.0$ Hz, 1H, exchangeable with D₂O), 5.02 (br t, $J = 5.4$ Hz, 1H, exchangeable with D₂O), 4.56 (d, $J = 15.5$ Hz, 1H), 4.37 – 4.27 (m, 1H), 4.19 – 4.03 (m, 2H), 3.97 – 3.85 (m, 6H), 3.69 – 3.60 (m, 1H), 3.60 – 3.52 (m, 1H), 3.48 – 3.36 (m, 2H), 3.25 – 3.14 (m, 1H), 2.44 (s, 3H). **¹³C NMR** (100 MHz, DMSO-d₆) δ 169.7, 166.3, 159.3, 155.6, 146.1, 141.9, 138.9, 131.0, 130.4, 130.2, 129.1, 128.7, 124.4, 121.0, 120.4, 118.1, 114.5, 113.8, 105.6, 70.6, 68.5, 64.8, 59.8, 55.8, 52.7, 45.5, 42.9, 21.2. **HRMS** (ESI): m/z [M + H]⁺ calcd. for C₂₈H₃₁N₃O₈ + H⁺: 538.2184. Found: 538.2186.

Methyl 6-(3-(3-(3-((cyclopentylamino)methyl)phenoxy)-2-hydroxypropyl)ureido)-4-hydroxy-2-naphthoate (132a)



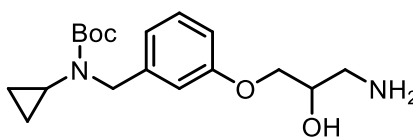
Compound **132a** was obtained as a white solid (0.040 g, 69%) by reaction of **153a** (0.070 g, 0.115 mmol) following the procedure described for **130a**. **¹H NMR** (400 MHz, DMSO-d₆) δ 10.31 (br s, 1H, exchangeable with D₂O), 9.09 (br s, 1H, exchangeable with D₂O), 8.28 (d, $J = 2.5$ Hz, 1H), 7.97 (s, 1H), 7.89 (d, $J = 9.0$ Hz, 1H), 7.53 (dd, $J = 8.9, 2.5$ Hz, 1H), 7.38 – 7.26 (m, 2H), 7.19 – 7.11 (m, 1H), 7.05 (d, $J = 7.9$ Hz, 1H), 7.00 (dd, $J = 8.9, 2.5$ Hz, 1H), 6.47 (br t, $J = 5.7$ Hz, 1H, exchangeable with D₂O), 5.37 (br d, $J = 5.0$ Hz, 1H, exchangeable with D₂O), 4.06 (s, 2H), 4.01 – 3.90 (m, 3H), 3.86 (s, 3H), 3.55 – 3.32 (m, 2H, overlaps with water peak), 3.24 – 3.12 (m, 1H), 2.02 – 1.88 (m, 2H), 1.75 – 1.44 (m, 6H). **¹³C NMR** (100 MHz, DMSO-d₆) δ 167.1, 159.2, 155.7, 153.0, 140.2, 130.3, 129.2, 125.1, 122.3, 121.7, 120.5, 116.2, 115.2, 107.53, 106.9, 70.6, 68.4, 58.7, 52.4, 49.9, 42.9, 30.0, 24.1. **HRMS** (ESI): m/z [M + H]⁺ calcd. for C₂₈H₃₃N₃O₆ + H⁺: 508.2442. Found: 508.2444.

Methyl 4-acetoxy-6-(3-(3-(3-((cyclopentylamino)methyl)phenoxy)-2-hydroxypropyl)ureido)-2-naphthoate (132b)



Compound **132b** was obtained as a white solid (0.024 g, 52%) by reaction of **153b** (0.055 g, 0.008 mmol) following the procedure described for **130a**. **¹H NMR** (400 MHz, DMSO-*d*₆) δ 9.23 (br s, 1H, exchangeable with D₂O), 8.55 – 8.41 (m, 1H), 8.32 (s, 1H), 8.15 – 8.00 (m, 2H), 7.68 (d, *J* = 1.6 Hz, 1H), 7.58 (dd, *J* = 9.0, 2.1 Hz, 1H), 7.33 (t, *J* = 7.9 Hz, 1H), 7.11 (s, 1H), 7.07 – 6.92 (m, 2H), 6.50 (br t, *J* = 5.7 Hz, 1H, exchangeable with D₂O), 5.37 (br d, *J* = 5.0 Hz, 1H, exchangeable with D₂O), 4.03 – 3.93 (m, 5H), 3.90 (s, 3H), 3.45 – 3.30 (m, 2H, overlaps with water peak), 3.22 – 3.11 (m, 1H), 2.44 (s, 3H), 2.02 – 1.84 (m, 2H), 1.73 – 1.61 (m, 4H), 1.61 – 1.44 (m, 4H). **¹³C NMR** (100 MHz, DMSO-*d*₆) δ 169.6, 166.3, 159.1, 155.6, 152.9, 146.1, 141.9, 130.9, 129.1, 128.6, 124.4, 122.2, 120.9, 118.0, 116.2, 115.1, 105.6, 70.6, 58.6, 52.7, 49.9, 42.9, 30.1, 24.1, 21.1. **HRMS** (ESI): *m/z* [M + H]⁺ calcd. for C₃₀H₃₅N₃O₇ + H⁺: 550.2548. Found: 550.2545.

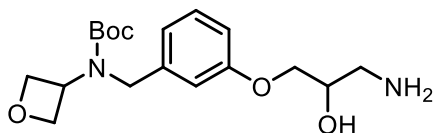
Tert-butyl (3-(3-amino-2-hydroxypropoxy)benzyl)(cyclopropyl)carbamate (133)



Compound **144** (0.230 g, 0.72 mmol) was solubilized in MeOH (0.300 mL) and 33% NH₄OH (1.10 mL, 9.30 mmol) was added. After 16 h, addition 10 eq of 33% NH₄OH were added. The end of the reaction was monitored by HPLC. The solvent was removed under reduced pressure. The residue was washed with toluene (3 x 5 mL) and with EtOH (3 x 5 mL). The yield was quantitative. **¹H NMR** (400 MHz, CDCl₃) δ 7.22 (dd, *J* = 8 Hz, 3 Hz, 1H), 6.87 – 6.77 (m, 3H),

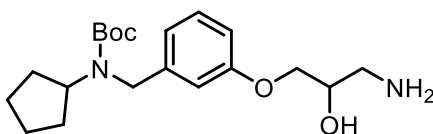
4.40 (d, $J = 3$ Hz, 2H), 4.01 – 3.92 (m, 3H), 3.01 – 2.82 (m, 2H), 2.47 (s, 1H), 1.46 (d, $J = 3$ Hz, 9H), 0.75 – 0.61 (m, 4H); **MS** (ESI) m/z : 337 ($M+H$)⁺.

Tert-butyl (3-(3-amino-2-hydroxypropoxy)benzyl)(oxetan-3-yl)carbamate (134)



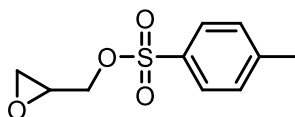
Compound **134** was obtained as a white solid by reaction of **145** (0.313 g, 0.93 mmol) following the procedure described for **133**. **¹H NMR** (400 MHz, CDCl₃) δ 7.26 – 7.20 (m, 1H), 6.82 – 6.70 (m, 3H), 4.73 – 4.58 (m, 4H), 4.54 (s, 2H), 4.01 – 3.94 (m, 3H), 3.00 – 2.78 (m, 2H), 1.43 (s, 9H); **MS** (ESI) m/z : 353 ($M+H$)⁺.

Tert-butyl (3-(3-amino-2-hydroxypropoxy)benzyl)(cyclopentyl)carbamate (135)



Compound **135** was obtained as a white solid (0.201 g, 99%) by reaction of **146** (0.190 g, 0.55 mmol) following the procedure described for **133**. **¹H NMR** (400 MHz, CDCl₃) δ 7.23 – 7.18 (m, 1H), 6.81 – 6.77 (m, 3H), 4.33 (s, 2H), 3.96 (d, $J = 9$ Hz, 3H), 3.72 (q, $J = 7$ Hz, 1H), 1.77 (d, $J = 14$ Hz, 2H), 1.62 (s, 2H), 1.53 – 1.45 (m, 4H), 1.39 (s, 9H); **MS** (ESI) m/z : 365 ($M+H$)⁺.

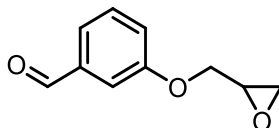
Oxiran-2-ylmethyl 4-methylbenzenesulfonate (137)



The commercially available glycidol (2.00g, 27.0 mmol) was dissolved in dry DCM (30 mL), TEA (7.52 mL, 54 mmol) and DMAP (0.165g, 1.35 mmol) were added under nitrogen. The reaction mixture was cooling to 0 ° C. A solution containing tosyl chloride (4.88g, 25.7 mmol), previously solubilized in dry DCM (20 mL) was slowly added in 2h. Then, a solution of KHSO₄

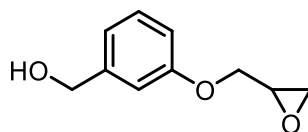
(0.5M, 50 mL) was added and the aqueous phase was extracted with DCM (3 x 50 mL). The organic phase was washed with brine (50 mL), dried over Na₂SO₄ and filtrate. The solvent was removed at reduced pressure. The residue was purified by flash chromatography (Hex/AcOEt 9: 1 to 1: 1) to recover the product **137** as a colorless oil (4.57 g, 74%). ¹H NMR (400 MHz, CDCl₃) δ 7.83 – 7.79 (m, 2H), 7.36 (d, *J* = 8 Hz, 2H), 4.27 – 4.22 (m, 1H), 3.99 – 3.92 (m, 1H), 3.21 – 3.16 (m, 1H), 2.81 (t, *J* = 4Hz, 1H), 2.62 – 2.57 (m, 1H), 2.45 (s, 3H); MS (ESI) m/z: 229 (M+H)⁺.

3-(oxiran-2-ylmethoxy)benzaldehyde (138)



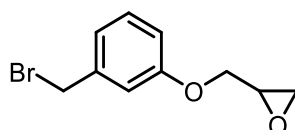
Compound **137** (4.52g, 19.8 mmol) and 3-hydroxy benzaldehyde **136** (2.20g, 18 mmol) were solubilized in dry ACN (90 mL) and K₂CO₃ (2.74g, 19.8 mmol) was added, under nitrogen. The mixture reaction was heated to reflux. After 2h, the reaction mixture was cooling, and water was added. The mixture obtained was concentrated in the rotavapor. The aqueous phase was extracted with AcOEt (3 x 50 mL). The organic phase was washed with brine (50 mL), dried over Na₂SO₄ and filtrate. The solvent was removed under reduced pressure. The residue was purified via flash chromatography (DCM/AcOEt 10:0 to 8:2) to give the desired compound as a colorless oil (3.06g, 95%). ¹H NMR (400 MHz, CDCl₃) δ 9.98 (s, 1H), 7.51–7.34 (m, 3H), 7.24 – 7.19 (m, 1H), 4.35 – 4.32 (m, 1H), 4.01 – 3.97 (m, 1H), 3.42 – 3.34 (m, 1H), 2.93 (t, *J* = 5 Hz, 1H), 2.81 – 2.77 (m, 1H); MS (ESI) m/z: 179 (M+H)⁺.

(3-(oxiran-2-ylmethoxy)phenyl)methanol (139)



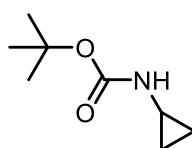
Aldehyde **138** (0.500g, 2.81 mmol) was solubilized in dry MeOH (14 mL). The mixture reaction was cooling to 0 ° C and NaBH₄ (0.064g, 1.69 mmol) was added, under nitrogen. After 1h, water was added, and the reaction mixture was concentrated to the rotavapor. The aqueous phase was extracted with AcOEt (3 x 50 mL). The organic phase was washed with brine (50 mL), dried over Na₂SO₄ and filtrate. The solvent was removed under reduced pressure. The crude was used in the next step without further purification steps (0.390g, 77%). **¹H NMR** (400 MHz, CDCl₃) δ 7.28 (d, *J* = 8 Hz, 1H), 6.96 (d, *J* = 6 Hz, 2H), 6.85 (dd, *J* = 8 Hz, 3 Hz, 1H), 4.68 (s, 2H), 4.27 – 4.22 (m, 1H), 3.99 – 3.96 (m, 1H), 3.39 – 3.32 (m, 1H), 2.91 (t, *J* = 4.5 Hz, 1H), 2.79 – 2.74 (m, 1H); **MS** (ESI) *m/z*: 181 (M+H)⁺.

2-((3-(bromomethyl)phenoxy)methyl)oxirane (140)



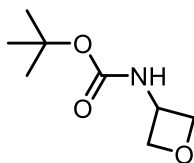
139 (0.380 g, 2.11 mmol) was dissolved in THF (4 mL). The reaction was cooling to 0 ° C and PPH₃ (0.565 g, 2.15 mmol) and N-bromosuccinimide (0.368 g, 2.07 mmol) were added. The reaction was monitored by TLC, then the solvent was removed under reduced pressure. The residue was directly purified by flash chromatography (Hex/AcOEt 95: 5 to 7: 3) to afford the desired compound as a white solid (0.214g, 42%). **¹H NMR** (400 MHz, CDCl₃) δ 7.31 – 7.27 (m, 1H), 7.05 – 6.95 (m, 2H), 6.89 (dd, *J* = 8, 2.5 Hz, 1H), 4.48 (s, 2H), 4.28 – 4.24 (m, 1H), 4.03 – 3.94 (m, 1H), 3.40 – 3.33 (m, 1H), 2.94 (t, *J* = 5 Hz, 1H), 2.81 – 2.77 (m, 1H); **MS** (ESI) *m/z*: 243 (M+H)⁺.

Tert-butyl cyclopropylcarbamate (141)



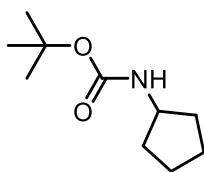
Compound **141** was obtained as a colourless oil (1.10 g, 96%) starting from **148** (0.412 g, 7.22 mmol) following the procedure described for **11a**. **¹H NMR** (400 MHz, CDCl₃) δ 4.78 (br, 1H), 2.53 (s, 1H), 1.45 (s, 9H), 0.68 (d, *J* = 6.0 Hz, 2H), 0.49 (s, 2H); **MS** (ESI) *m/z*: 158 (M+H)⁺.

Tert-butyl oxetan-3-ylcarbamate (142)



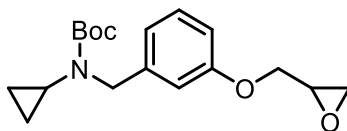
Compound **142** was obtained as a colourless oil (1.05 g, 90%) starting from **149** (0.500 g, 6.85 mmol) following the procedure described for **11a**. **¹H NMR** (400 MHz, DMSO) δ 7.2 (br s, 1H), 5.10 – 5.06 (m, 2H), 4.78 – 4.65 (m, 3H), 1.44 (s, 9H); **MS** (ESI) *m/z*: 174 (M+H)⁺.

Tert-butyl cyclopentylcarbamate (143)



Compound **143** was obtained as a colourless oil (1.85 g, 98%) starting from **150** (0.700 mL, 10.1 mmol) following the procedure described for **11a**. **¹H NMR** (400 MHz, CDCl₃) δ 4.45 (br s, 1H), 3.91 (m, 1H), 1.92 (m, 2H), 1.50-1.70 (m, 4H), 1.43 (s, 9H), 1.35 (m, 2H); **MS** (ESI) *m/z*: 186 (M+H)⁺.

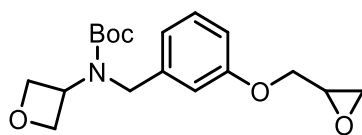
Tert-butyl cyclopropyl(3-(oxiran-2-ylmethoxy)benzyl)carbamate (144)



The amine **141** (0.146 g, 0.93 mmol) was solubilized in dry DMF (2 mL). The reaction was cooling to 0 ° C and NaH (0.010g, 0.41 mmol) was added. After stirring for 30 min at room

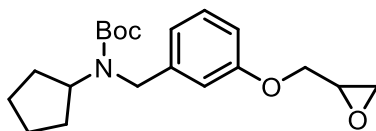
temperature, compound **140** (0.100 g, 0.41 mmol) was added dropwise, under nitrogen, to the first solution in dry DMF (1.7 mL). The reaction mixture was heated to room temperature and stirred for 24h. Then, water was added. The aqueous phase was extracted with AcOEt (3 x 10 mL). The organic phase was washed with NaHCO₃ (3 x 10 mL), with brine (25 mL), dried over Na₂SO₄ and filtrate. The solvent was removed a reduced pressure. The crude residue was purified by flash column chromatography (Hex/ AcOEt 95:5 to 5:5) to afford the desired product **144** (0.245 g, 82%). ¹H NMR (400 MHz, CDCl₃) δ 7.25 – 7.19 (m, 1H), 6.87 – 6.77 (m, 3H), 4.39 (s, 2H), 4.23 – 4.17 (m, 1H), 3.98 – 3.92 (m, 1H), 3.37 – 3.32 (m, 1H), 2.93 – 2.87 (m, 1H), 2.78 – 2.73 (m, 1H), 1.46 (s, 9H), 0.74 – 0.59 (m, 4H); MS (ESI) m/z: 320 (M+H)⁺.

Tert-butyl oxetan-3-yl(3-(oxiran-2-ylmethoxy)benzyl)carbamate (145)



Compound **145** was obtained as a colourless oil (0.110 g, 89%) by reaction of **142** (0.065 g, 0.37 mmol) following the procedure described for **144**. ¹H NMR (400 MHz, CDCl₃) δ 7.28 (s, 1H), 6.86 – 6.76 (m, 3H), 4.74 – 4.70 (m, 4H), 4.57 (s, 2H), 4.26 – 4.22 (m, 1H), 3.98-3.94 (m, 1H), 3.40 – 3.34 (m, 1H), 2.94 (t, *J* = 5 Hz, 1H), 2.80 – 2.76 (m, 1H), 1.47 (s, 9H); MS (ESI) m/z: 336 (M+H)⁺.

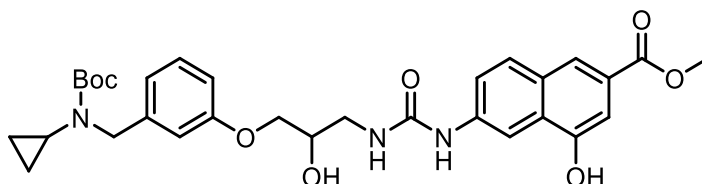
Tert-butyl cyclopentyl(3-(oxiran-2-ylmethoxy)benzyl)carbamate (146)



Compound **146** was obtained as a colourless oil (0.190 g, 60%) by reaction of **143** (0.172 g, 0.93 mmol) following the procedure described for **144**. ¹H NMR (400 MHz, CDCl₃) δ 7.22 –

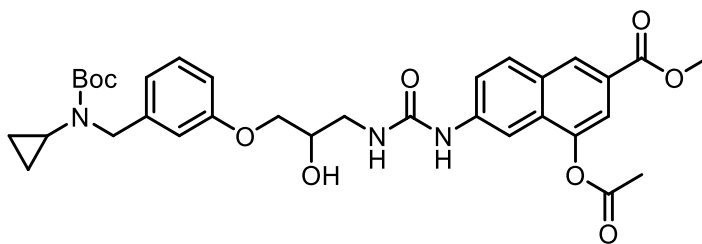
7.17 (m, 1H), 6.83 – 6.71 (m, 3H), 4.36 – 4.29 (m, 2H), 4.23 – 4.17 (m, 1H), 4.02 – 3.90 (m, 1H), 3.38 – 3.31 (m, 1H), 2.90 (t, $J = 5$ Hz, 1H), 2.79 – 2.73 (m, 1H), 1.77 (d, $J = 13$ Hz, 2H), 1.63 (s, 2H), 1.48 (d, $J = 9$ Hz, 4H), 1.39 (s, 9H); **MS** (ESI) m/z : 348 (M+H)⁺.

Methyl 6-(3-(3-(3-(((tert-butoxycarbonyl)(cyclopropyl)amino)methyl)phenoxy)-2-hydroxypropyl)ureido)-4-hydroxy-2-naphthoate (151a)



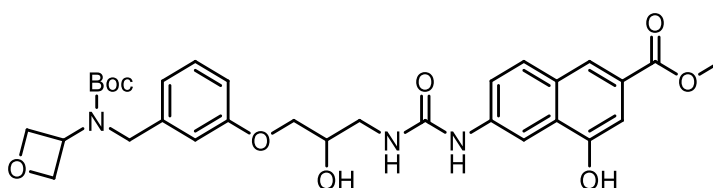
Compound **133** (0.242 g, 0.72 mmol) and **18** (0.138 g, 0.36 mmol) were solubilized in dry DMF (2.1 mL). Under nitrogen, TEA (0.060 mL, 0.43 mmol) was added. The disappearance of the starting material was monitored by TLC, then water was added. The aqueous phase was extracted with AcOEt (3 x 10 mL). The phase organic was washed with NaHCO₃ (3 x 10 mL), brine (10 mL) dried over Na₂SO₄ and filtrate. The solvent was removed under reduced pressure. The crude residue was purified by flash column chromatography (Hex/AcOEt/DCM/MeOH 1: 1: 0: 0 to 0: 0: 97: 3 to 0: 0: 85: 15) to afford the title compound **151a** as white solid (0.153 g, 63%). **¹H NMR** (400 MHz, DMSO-*d*₆) δ 10.27 (s, 1H), 8.98 (s, 1H), 8.26 (d, $J = 2$ Hz, 1H), 7.96 (s, 1H), 7.88 (d, $J = 9$ Hz, 1H), 7.52 (dd, $J = 9$ Hz, 2 Hz, 1H), 7.29 (d, $J = 2$ Hz, 1H), 7.23 – 7.17 (m, 1H), 6.94 – 6.86 (m, 2H), 6.80 (dd, $J = 8$ Hz, 2.5 Hz, 1H), 6.38 – 6.30 (m, 1H), 5.30 (d, $J = 4$ Hz, 1H), 3.04 – 3.88 (m, 6H), 3.68 (s, 2H), 3.44 – 3.35 (m, 2H), 1.40 (s, 9H), 0.67 – 0.55 (m, 4H); **MS** (ESI) m/z : 580 (M+H)⁺.

Methyl 4-acetoxy-6-(3-(3-(3-(((tert-butoxycarbonyl)(cyclopropyl)amino)methyl)phenoxy)-2-hydroxypropyl)ureido)-2-naphthoate (151b)



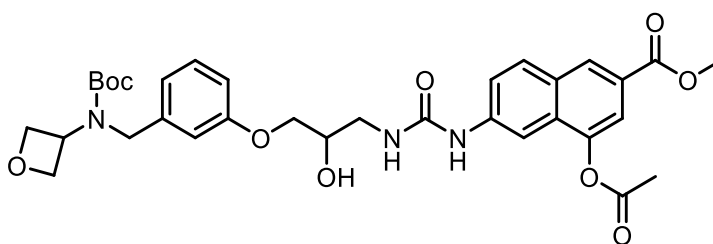
Compound **151b** was obtained as a colourless solid (0.107 g, 48%) following the procedure described for **151a**. **¹H NMR** (400 MHz, DMSO-*d*₆) δ 8.43 (s, 1H), 8.07 (d, *J* = 9 Hz, 2H), 7.67 (d, *J* = 2 Hz, 1H), 7.57 (dd, *J* = 9 Hz, 2 Hz, 1H), 7.30–7.22 (m, 1H), 6.87–6.75 (m, 3H), 4.32 (s, 2H), 3.95–3.83 (m, 6H), 3.56–3.40 (m, 3H), 2.43 (s, 3H), 1.39 (s, 9H), 0.66–0.54 (m, 4H); **MS** (ESI) *m/z*: 622 (M+H)⁺.

Methyl 6-(3-(3-(3-(((tert-butoxycarbonyl)(oxetan-3-yl)amino)methyl)phenoxy)-2-hydroxypropyl)ureido)-4-hydroxy-2-naphthoate (152a)



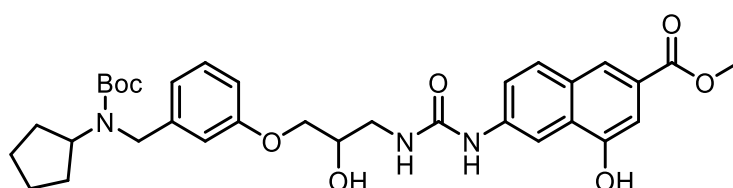
Compound **152a** was obtained as a white solid (0.052g, 41%) by reaction of **134** (0.150 g, 0.43 mmol) following the procedure described for **151a**. **¹H NMR** (400 MHz, DMSO-*d*₆) δ 8.32–8.23 (m, 1H), 7.96 (s, 1H), 7.91–7.85 (m, 1H), 7.55–7.50 (m, 1H), 7.31–7.22 (m, 2H), 6.85 (d, *J* = 8 Hz, 1H), 6.74 (d, *J* = 8 Hz, 2H), 4.60–4.41 (m, 7H), 3.90 (d, *J* = 3 Hz, 4H), 3.86 (s, 3H), 1.36 (s, 9H); **MS** (ESI) *m/z*: 596 (M+H)⁺.

Methyl 4-acetoxy-6-(3-(3-(3-(((tert-butoxycarbonyl)(oxetan-3-yl)amino)methyl)phenoxy)-2-hydroxypropyl)ureido)-2-naphthoate (152b)



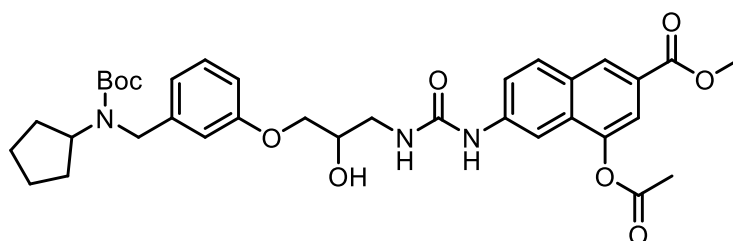
Compound **152b** was obtained as a colourless solid (0.073 g, 54%) following the procedure described for **151a**. ¹H NMR (400 MHz, DMSO-d₆) δ 8.45 – 8.41 (m, 1H), 8.07 (d, *J* = 9 Hz, 2H), 7.67 (d, *J* = 2 Hz, 1H), 7.57 (dd, *J* = 9 Hz, 2 Hz, 1H), 7.29 – 7.21 (m, 1H), 6.87 – 6.83 (m, 1H), 6.74 (d, *J* = 8 Hz, 2H), 4.57 (t, *J* = 7 Hz, 4H), 4.44 (d, *J* = 5 Hz, 3H), 3.95 – 3.85 (m, 7H), 2.43 (s, 3H), 1.36 (s, 9H); MS (ESI) *m/z*: 638 (M+H)⁺.

Methyl 6-(3-(3-(3-(((tert-butoxycarbonyl)(cyclopentyl)amino)methyl)phenoxy)-2-hydroxypropyl)ureido)-4-hydroxy-2-naphthoate (153a)



Compound **153a** was obtained as a white solid (0.105 g, 63%) by reaction of **135** (0.200 g, 0.55 mmol) following the procedure described for **151a**. ¹H NMR (400 MHz, DMSO-d₆) δ 8.32 – 8.25 (m, 1H), 7.97 – 7.85 (m, 2H), 7.52 (dd, *J* = 9 Hz, 2 Hz, 1H), 7.30 – 7.19 (m, 2H), 6.82 – 6.72 (m, 3H), 4.30 (s, 2H), 3.94 – 3.78 (m, 6H), 1.66 – 1.62 (m, 2H), 1.58 – 1.50 (m, 2H), 1.44 – 1.32 (m, 4H), 1.34 (s, 9H); MS (ESI) *m/z*: 608 (M+H)⁺.

Methyl 4-acetoxy-6-(3-(3-(3-(((tert-butoxycarbonyl)(cyclopentyl)amino)methyl)phenoxy)-2-hydroxypropyl)ureido)-2-naphthoate (153b)



Compound **153b** was obtained as a colourless solid (0.055 g, 31%) following the procedure described for **151a**. ¹H NMR (400 MHz, DMSO-d₆) δ 8.38 (s, 1H), 8.04 (s, 1H), 7.82 – 7.76 (m, 2H), 7.35 (dd, *J* = 9 Hz, 2 Hz, 1H), 7.20 – 7.14 (m, 1H), 6.73 – 6.53 (m, 3H), 4.32 (s, 2H),

4.04 – 3.93 (m, 3H), 3.94 – 3.85 (m, 6H), 2.44 (s, 3H), 1.82 – 1.77 (m, 2H), 1.63 – 1.50 (m, 2H), 1.49 – 1.43 (m, 4H), 1.41 (s, 9H); **MS** (ESI) m/z: 650 (M+H)⁺.

8.3. Biological Protocols

8.3.1. *Radioisotope-based filter-binding assay*

The effects of compounds on the catalytic activity of PRMT1, PRMT3, PRMT4, PRMT5, PRMT6, PRMT7, and PRMT8 were determined with a radioisotope-based filter-binding assay (HotSpot) PRMT activity assay by Reaction Biology Corporation (Malvern, PA, USA) according to the company's standard operating procedure. The radioisotope-based filter-binding assay is a well-established technology useful for detecting total methylation of any substrate on both lysine and arginine residues. This assay is based on the use of tritium-labeled SAM (^3H -SAM) as the methyl donor by the selected methyltransferase which catalyses the introduction of the radioactive methyl group from the tritium-labeled SAM to the histone substrate. After the reaction mixture incubation, filtration and washing steps, the bound radiolabelled substrate is detected. This assay represents a highly sensitive and reliable technology to detect enzyme activity without substrate modifications, coupling enzymes, or the need for specific antibodies for detection.¹⁷⁹

Briefly, a mixture of the proper substrate (histone H4 for PRMT1, PRMT3, and PRMT8; histone H3.3 for PRMT4; histone H2A for PRMT5/MEP50; GST-GAR for PRMT6 and PRMT7; final concentration 5 μM) in freshly prepared reaction buffer (50 mM Tris-HCl (pH 8.5), 5 mM MgCl_2 , 50 mM NaCl, 1 mM DTT, 1 mM PMSF, 1% DMSO) was treated and gently mixed with the full-length human recombinant proteins PRMT1 (residues 2–371, C-terminus; with an N-terminal GST-tag; MW = 68.3 kDa; Genbank Accession # NM_001536) or PRMT3 (residues 2–531, C-terminus; with an N-terminal His-tag; MW = 62.0 kDa; Genbank Accession # NM_005788), or PRMT4 (residues 2–608, C-terminus; with an N-terminal GST-tag; MW = 91.7 kDa; Genbank Accession # NM_199141), or PRMT5/MEP50 complex (residues PRMT5 2–637, C-terminus, and MEP50 2–342, C-terminus; with an N-terminal FLAG-tag, PRMT5, or

His-tag, MEP50; MW = 73.7/39.9 kDa; Genbank Accession # NM_006109, NM_006109), or PRMT6 (residues 2–375, C-terminus; with an N-terminal GST-tag; MW = 67.8 kDa; Genbank Accession # NM_018137), or PRMT7 (residues 2–692, C-terminus; with an N-terminal His-tag; MW = 81.7 kDa; Genbank Accession # NM_019023), or Δ N(1–60)-PRMT8 (residues 61–394, C-terminus; with C- and N-terminal His-tags; MW = 43.2 kDa; Genbank Accession # NM_019854). The DMSO solution of compounds **1** – **9** was transferred into the PRMT reaction mixture by using Acoustic Technology (Echo 550, LabCyte Inc. Sunnyvale, CA), and incubated for 20 min. Then, ^3H -SAM (final concentration 1 μM) was added. After incubation for 60 min at 30 °C, the reaction mixture was transferred to filter-paper for detection (as assessed by scintillation). Data were analyzed using Excel and GraphPad Prism 6.0 software (GraphPad Software Inc., San Diego, CA) for IC₅₀ curve fits using sigmoidal dose vs. response - variable slope (four parameters) equations.

8.3.2. *AlphaLISA*

PRMT1 and PRMT9 activity assays were performed Dott.ssa Alessandra Feoli (EMCL, University of Salerno) using AlphaLISA homogeneous proximity assay. AlphaLISA bead-based technology is a highly sensitive homogeneous luminescent amplification assay that relies on the use of donor and acceptor beads to capture the target analyte. Specifically, the streptavidin-coated donor binds to a biotinylated antibody and, similarly, a second antibody binds to the AlphaLISA acceptor beads. Following addition into the sample, the analyte binds with the two antibodies, bringing the donor and acceptor beads into close proximity. After excitation of the donor beads at 680 nm, a photosensitizer within them converts ambient oxygen into an excited singlet state, initiating several chemical events in the neighbouring acceptor beads, resulting in chemiluminescent emission at 615 nm. The amount of light is comparable to the amount of analyte present in the sample.¹⁸⁰

8.3.2.1. *PRMT1 activity assay*

The assays were performed in white opaque OptiPlate-384 (PerkinElmer, # 6007299) at 22°C in a final volume of 25 μ L, using a proper assay buffer (30 mM Tris–HCl pH 8.0, 1 mM DTT, 0.01% BSA, 0.01% Tween-20). In each well, 3 μ L of human recombinant PRMT1 (BPS BioScience, # 51041) (final concentration, 0.9 nM) was incubated for 30 min with 2.5 μ L of each compound (dissolved in DMSO and diluted in assay buffer to obtain 1% DMSO). Then, 4.5 μ L of a mixture of histone H4 (1–21), peptide biotinylated (AnaSpec, # 62555) (final concentration, 100 nM) and SAM (Sigma, # A7007) (final concentration, 2 μ M) was added and the reaction was incubated for 60 min. Then, it was stopped by the addition of 5 μ L of anti-methyl-histone H4 arginine 3 (H4R3me) AlphaLISA acceptor beads (PerkinElmer, # AL150) (final concentration, 20 μ g/mL) diluted in Epigenetic Buffer 1X (PerkinElmer, # AL008). After an incubation of 60 min, 10 μ L of streptavidin donor beads (PerkinElmer, # 6760002) diluted in Epigenetic Buffer 1X was added in each well (final concentration, 20 μ g/mL) and incubated for 30 min. Signals were read in Alpha mode with a PerkinElmer EnSight mul-timode microplate reader (excitation at 680 nm and emission at 615 nm). For each incubation step, the OptiPlate was sealed with protective foil to prevent evaporation and contamination. Donor and Acceptor beads were added in subdued light. The 100% activity (positive control) was reached using vehicle (DMSO) while the 0% activity (negative control) was obtained without the protein. Data were analyzed using Excel software. Values obtained for each compound are mean \pm SD determined for three separate experiments.

8.3.2.2. *PRMT9 activity assay*

PRMT9 activity assay was performed by AlphaLISA on the basis of the “PRMT9 Homogeneous assay Kit” (BPS BioScience, #52069), which was opportunely modified.

The assays were performed in white opaque OptiPlate-384 (PerkinElmer, # 6007299) at 22°C in a final volume of 30 μ L, using the HMT assay buffer 2A (BPS-BioScience #52170-A). In each well, 2 μ L of human recombinant PRMT9 (BPS BioScience, # 79124) (50 ng/ μ L) was first incubated for 30 min with 3 μ L of each compound (dissolved in DMSO and diluted in assay buffer to obtain 1% DMSO). Then, in each well 0.5 μ L of the biotinylated substrate peptide SAP-145 (aa 500–519) (Pepmic, custom synthesis) (final concentration, 100 nM), 1 μ L of SAM 250 μ M, 1.5 μ L of water and 2 μ L of 4x HMT assay buffer 2A were added to reach the final volume of 10 μ L. The reaction was incubated for 60 min. Subsequently, in each well 5 μ L of a 1:100 dilution of Primary antibody 28 (BPS BioScience, #52140Z3) in Detection buffer (BPS BioScience) and 5 μ L of anti-Rabbit acceptor beads (PerkinElmer, #AL104C) were added to obtain a final concentration of 20 μ g/mL. After an incubation of 60 min, 10 μ L of streptavidin donor beads (PerkinElmer, # 6760002) diluted in detection buffer was added in each well (final concentration, 20 μ g/mL). After an incubation of 30 min, signals were read in Alpha mode with a PerkinElmer EnSight multimode microplate reader (excitation at 680 nm and emission at 615 nm).

For each incubation step, the OptiPlate was sealed with protective foil to prevent evaporation and contamination. Donor and Acceptor beads were added in subdued light. The 100% activity (positive control) was reached using vehicle (DMSO) while the 0% activity (negative control) was obtained without the protein. Data were analyzed using Excel and Prism softwares. Values obtained for each compound are mean \pm SD determined for three separate experiments.

8.3.3. *SPR*

The direct binding of compounds with PRMT4 was evaluated by Dott.ssa Alessandra Feoli (EMCL, University of Salerno) using Surface Plasmon Resonance (SPR). SPR is an

optical technique for the qualitative and quantitative characterization of the specific binding of a mobile analyte to a binding partner, immobilized on the sensor surface. Briefly, an analyte is covalently bound to the sensor surface, a prism coated with a thin film of metal (usually silver or gold). In the buffer flow, a second mobile reagent is injected in fixed doses over the sensor surface. As a result of the binding of the two analytes, the refractive index of the metal film changes, causing a shift in the resonance angle that, to a good approximation, has been shown to be proportional to the surface concentration of the macromolecules. The cycle of binding, dissociation and regeneration of the sensor surface is repeated using different concentrations of the mobile reagent. The obtained sequence of binding curves allows the determination of the chemical rate and thermodynamic equilibrium constants.¹⁸¹

SPR experiments were performed on a Biacore T200 biosensor (Cytiva). PBS buffer (phosphate buffered saline, pH 7.4) supplemented with 0.05% Tween-20 was used as the running buffer. Full length recombinant PRMT4 (Active motif, # 81107) was diluted at the concentration of 50 µg/mL in 10 mM of sodium acetate pH 4.5 and then immobilized on a Series S Sensor Chip CM5 at a flow rate of 10 µL/min by using standard amine-coupling protocols to obtain densities of 4.6 kRU. One flow cell was left empty for background subtractions. Compounds were diluted in PBS supplemented with 0.05% Tween-20, keeping a final 2% DMSO concentration. Each compound was tested in 12 serial dilutions, prepared starting from 640 nM to 10 nM. Binding experiments were performed at 25 °C by using a flow rate of 30 µL/min, with 90 s monitoring of association and 90 s monitoring of dissociation. Regeneration of the surfaces was performed, when necessary, by a 10 s injection of 5 mM NaOH. The sensorgrams obtained at the 12 concentrations of each compound were first corrected taking advantage of the solvent correction performed by the instrument (correction range from 1.5% to 2.8% DMSO), then they were double referenced. The corrected sensorgrams for each compound were fitted simultaneously using a 1:1 Langmuir model to

obtain equilibrium dissociation constants (K_D) and kinetic dissociation (k_{off}) and association (k_{on}) constants.

8.3.4. PAMPA

The apparent cellular permeability of compounds was evaluated by Dott.ssa Alessandra Feoli (EMCL, University of Salerno) using the Parallel Artificial Membrane Permeability Assay (PAMPA). PAMPA is a screening technique for evaluating the passive permeability of compounds across various biological membrane systems in a microplate format. This assay is based on the use of a "sandwich-type" multiwell microplate, consisting of an acceptor plate and a donor plate that are separated by a lipid-infused microporous filter. The compound is added into the donor plate and allowed to pass through the lipid layer during an incubation period. After that, samples from the acceptor plate are transferred to a UV-Vis-compatible microplate and measured optically or sampled by mass-spectrometric analysis. Compounds with high and low permeability are added as positive and negative controls, respectively. In this way, the ability of the compound to passively cross the membrane can be assessed.¹⁸²

Donor solution (0.2 mM) was prepared by diluting 20 mM dimethylsulfoxide (DMSO) compound stock solution using phosphate buffer (pH 7.4, 0.01 M). Filters were coated with 5 μ L of a 1% (w/v) dodecane solution of L- α -phosphatidylcholine. Donor solution (150 μ L) was added to each well of the filter plate. To each well of the acceptor plate, 300 μ L of solution (5% DMSO in phosphate buffer) was added. Selected compounds were tested in triplicate, propranolol and furosemide were used as positive and negative controls, respectively. The sandwich was incubated for 24 h at room temperature under gentle shaking. After the incubation time, the sandwich plates were separated and 250 μ L of the acceptor plate was transferred to a UV quartz microtiter plate and measured by UV spectroscopy, using a Multiskan GO microplate spectrophotometer (Thermo Fisher Scientific) at 250–500 nm at a step of 5 nm.

Reference solutions (250 µL) were prepared diluting the sample stock solutions to the same concentration as that with no membrane barrier. The apparent permeability value P_{app} is determined from the ratio r of the absorbance of compound found in the acceptor chamber divided by the theoretical equilibrium absorbance (determined independently), the Faller modification of Sugano equation:

$$P_{app} = -\frac{V_D V_R}{(V_D + V_R)At} \times \ln(1 - r)$$

In this equation, V_R is the volume of the acceptor compartment (0.3 cm³), V_D is the donor volume (0.15 cm³), A is the accessible filter area (0.24 cm²), and t is the incubation time in seconds.

8.3.5. *MTT assay*

The cell toxicity of compounds was evaluated by Dott.ssa Alessandra Feoli (EMCL, University of Salerno) using the MTT assay. This method is a widely used procedure to assess the *in vitro* cytotoxic effects of compounds, using metabolic activity as an indicator of cell viability. This colorimetric assay is based on the conversion of MTT (3-[4,5-dimethylthiazol-2-yl]-2,5-diphenyl tetrazolium bromide) into purple formazan crystals by live cells, which are characterized by mitochondrial activity. Indeed, total mitochondrial activity is strongly associated with the number of viable cells, the only ones that contain NAD(P)H-dependent oxidoreductase enzymes that catalyse the reduction. Insoluble formazan crystals are dissolved, and the resulting-coloured solution is quantified by measuring absorbance at 500-600 nm with a multi-well spectrophotometer. The obtained solution colour is directly proportional to the number of viable, metabolically active cells.

The HEK293T cell line was cultured in DMEM (Euroclone) supplemented with 10% (v/v) fetal bovine serum (Euroclone), 100 U/mL penicillin, 100 µg/mL streptomycin

(Euroclone) and 2 mM L-glutamine (Euroclone) at 37 °C in a 5% CO₂ atmosphere. A total of 200 µL of cells seeded in 96-well microtiter plates (5×10^4 cells/mL) were exposed for 24h to different concentrations of compounds (10, 50 and 100 mM) in media containing 0.2% DMSO. The resulting formazan was solubilized in DMSO, and absorbance was measured at 550 nm and corrected for 620 nm background. Experiments were performed in quadruplicate and all values are expressed as the percentage of the control containing 0.2% DMSO.

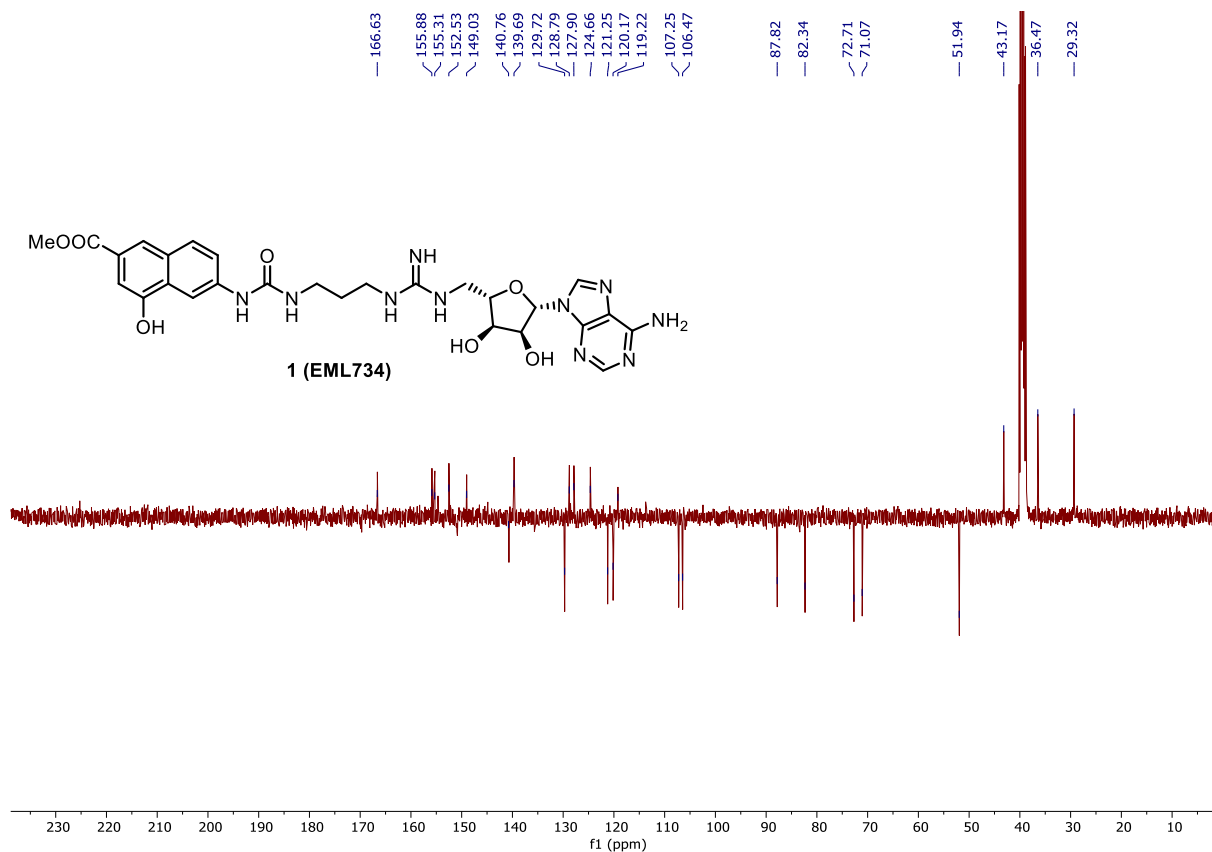
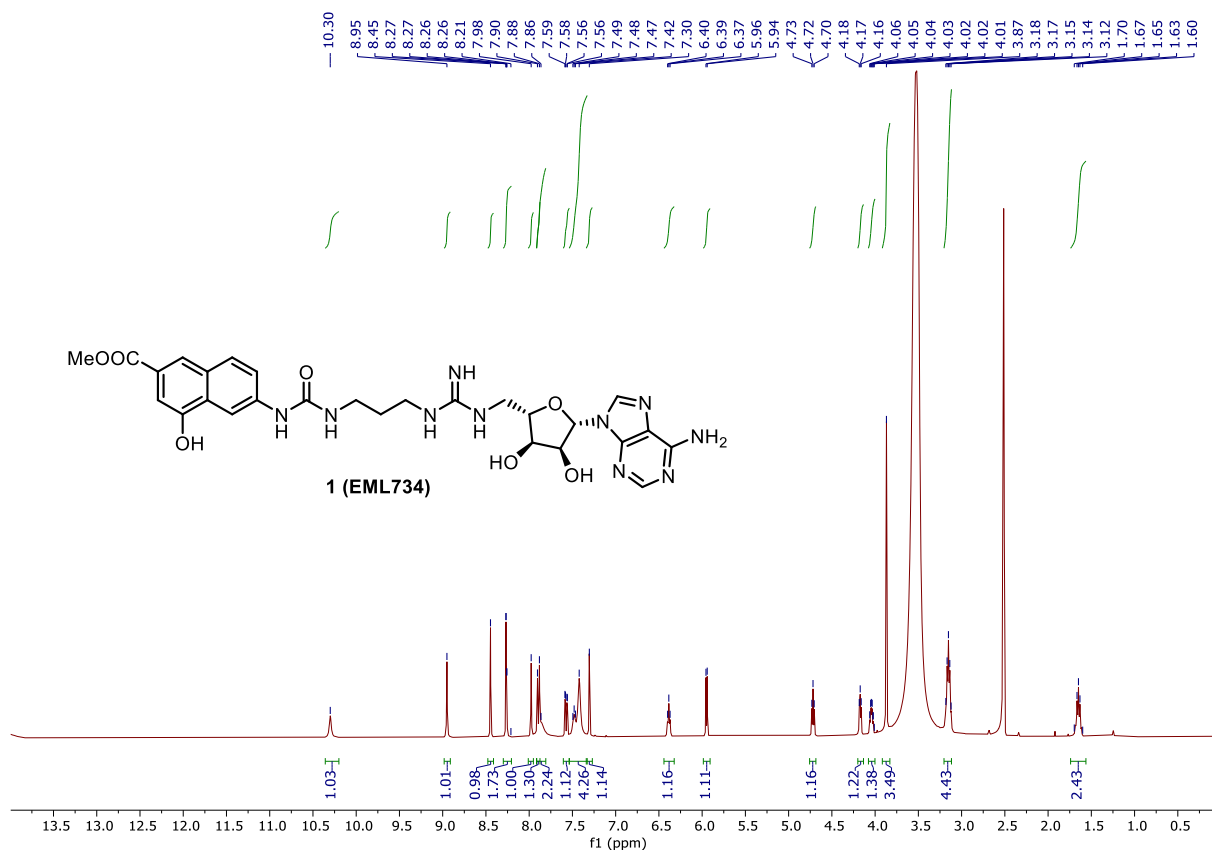
8.3.6. Western blot

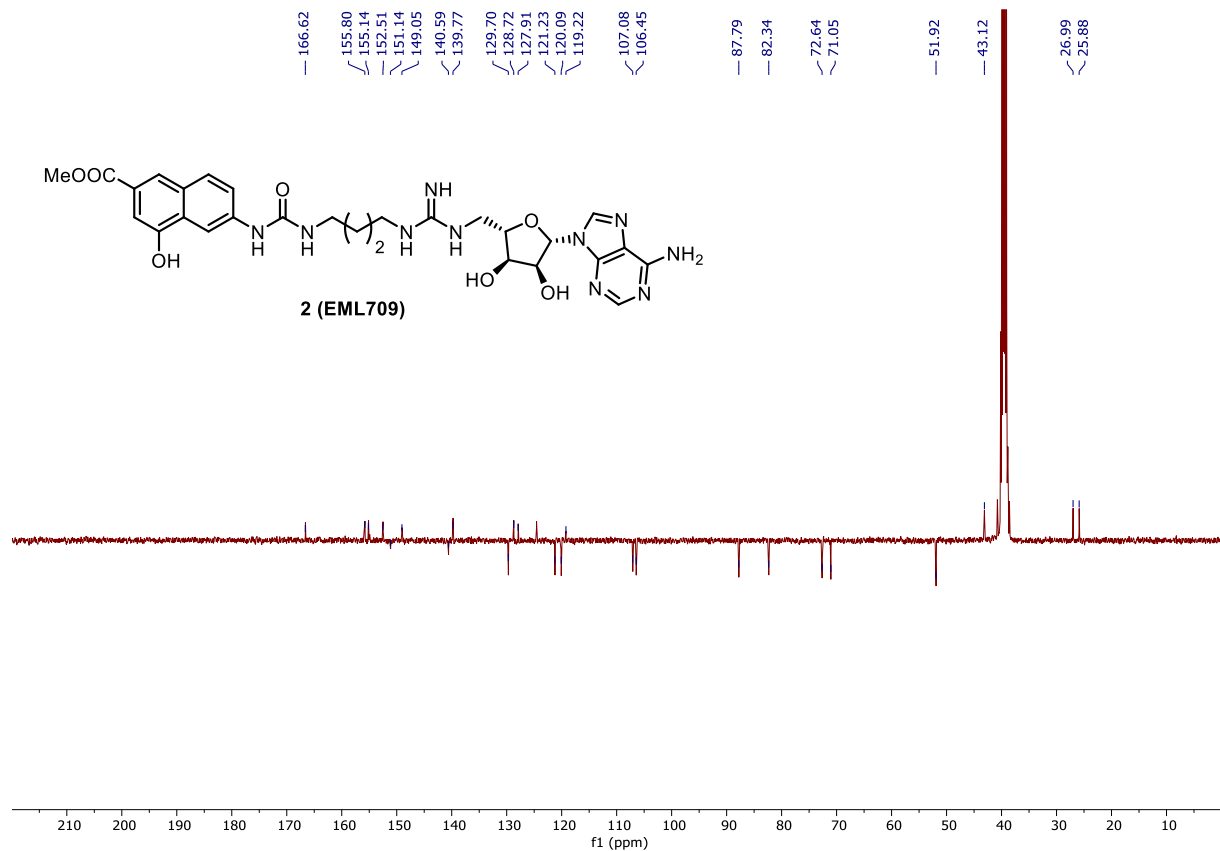
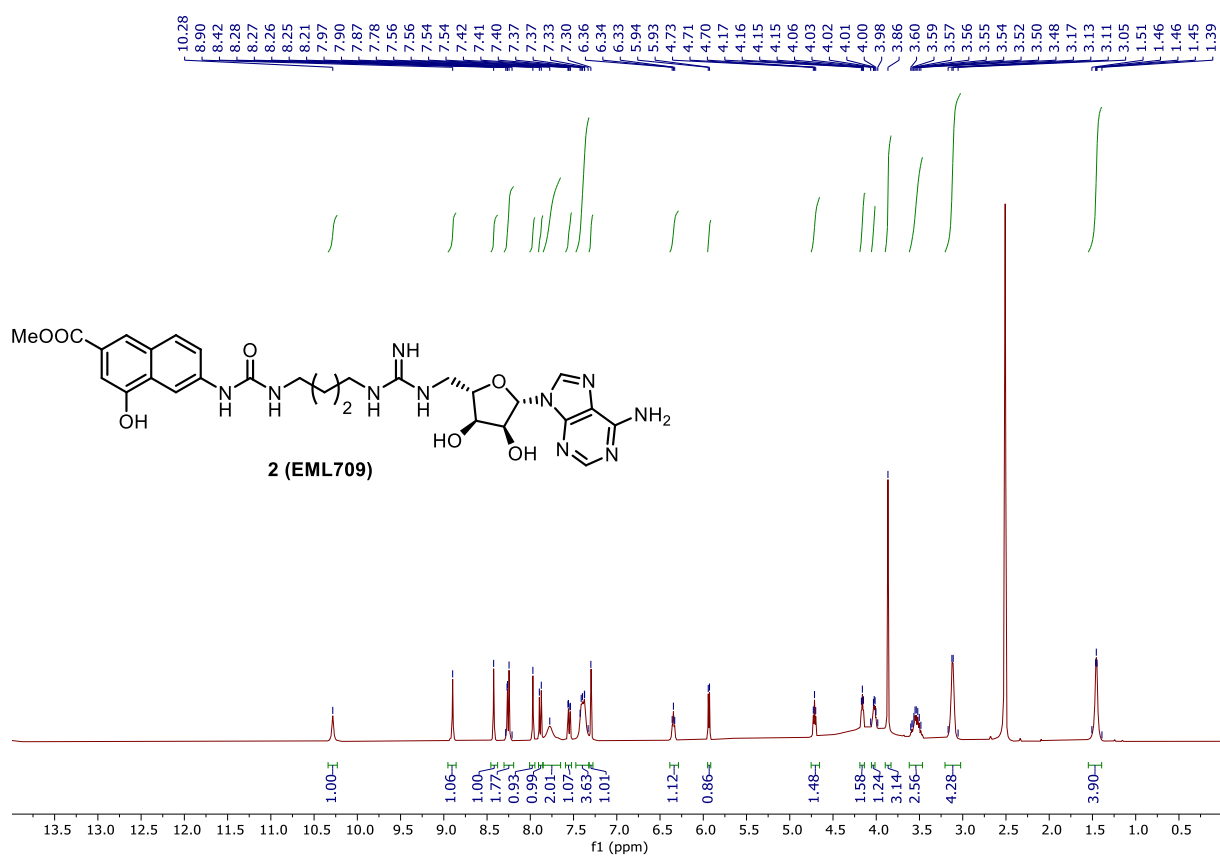
Cellular activity of compounds was evaluated by western blotting in collaboration with Prof. Mark Bedford. Western blotting is an important method for separating specific proteins from a mixture of proteins extracted from cells. Basically, a mixture of proteins is separated by molecular weight through an electrophoresis gel. The latter is transferred to a solid membrane support to obtain a band for each protein. After incubation with an appropriate primary and secondary antibody, the target protein is visualized as a single band, considering that the antibodies bind only to the protein of interest. The thickness of the band corresponds to the amount of protein present and therefore the use of a standard can reveal the amount of protein present.

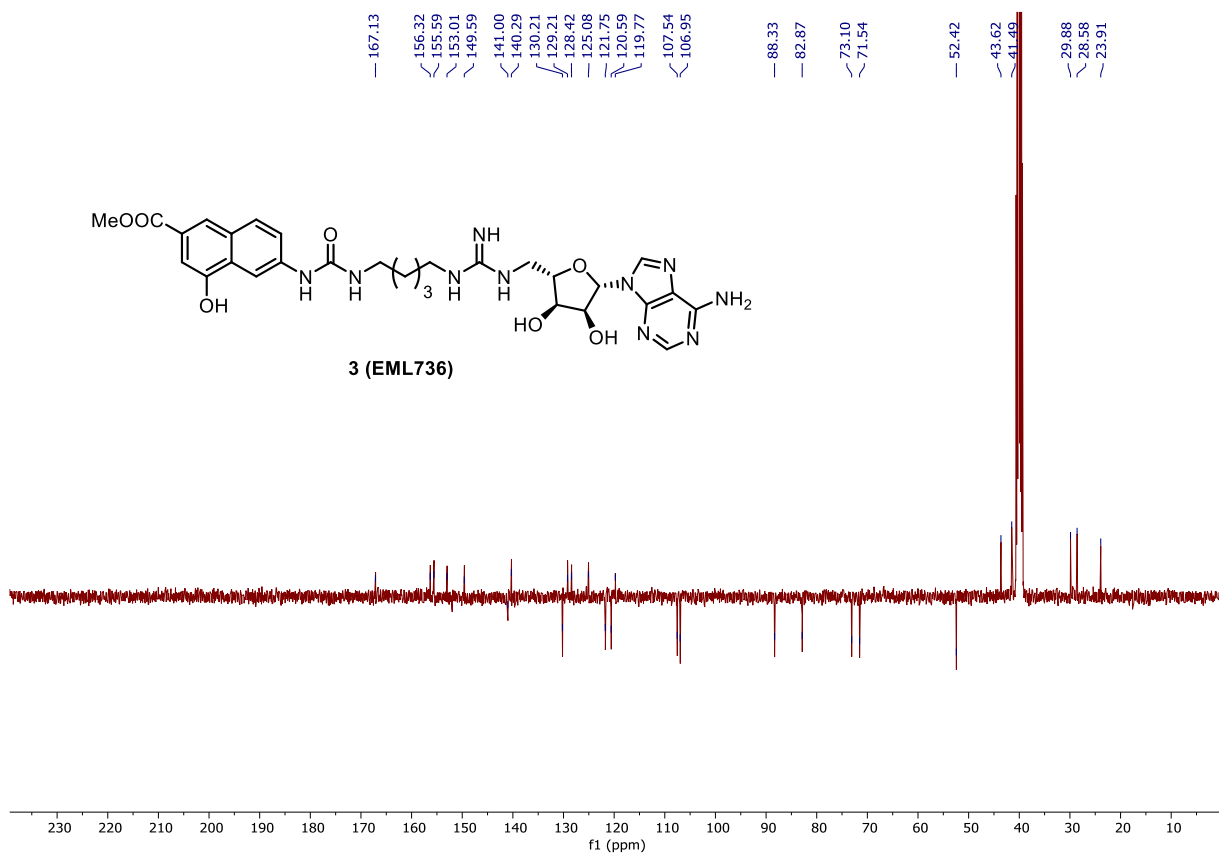
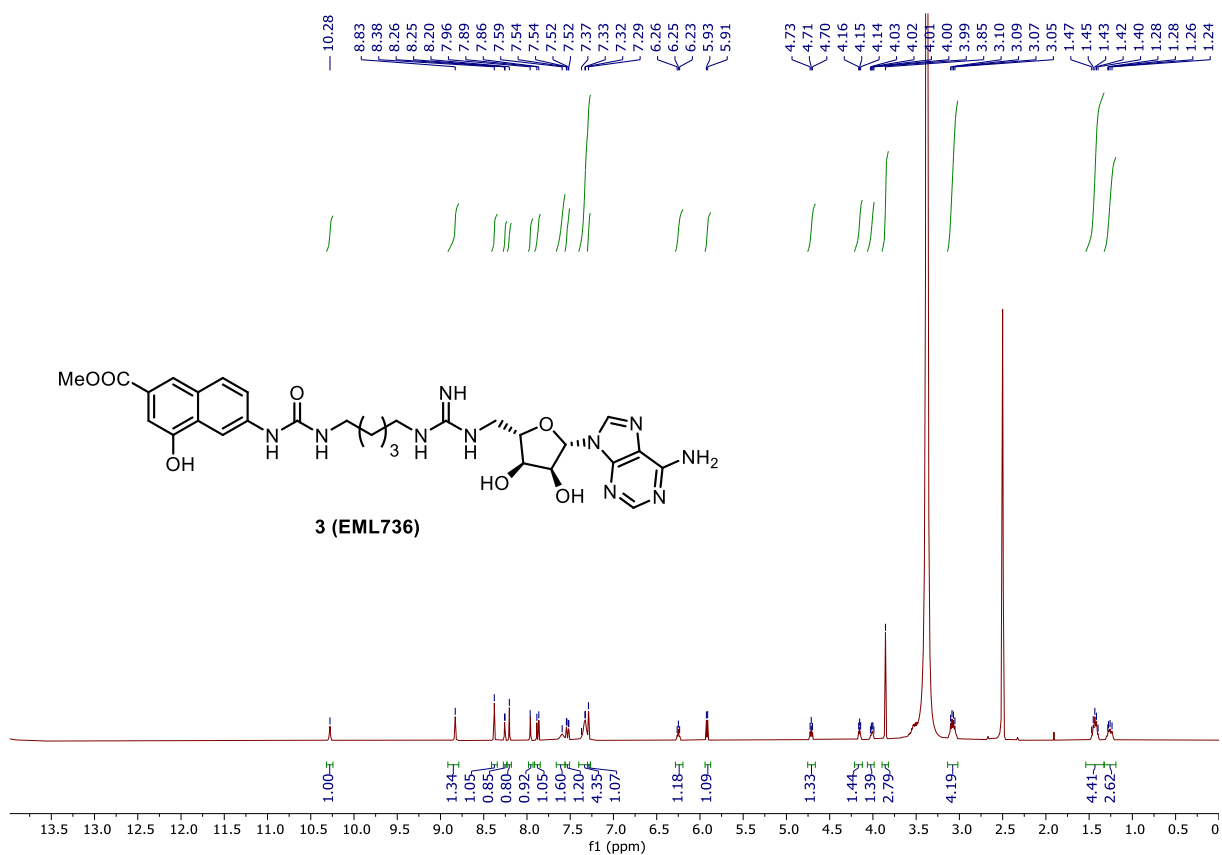
Cells were collected and lysed, and the cell lysates were applied to Western blot analysis. In brief, cells were harvested and washed three times with cold PBS, and then cell lysis buffer (50 mM Tris-HCl, pH 7.5, 150 mM NaCl, 1% Nonidet P-40, 0.1% SDS, 1% sodium deoxycholate, 5 mM EDTA, supplemented with proteinase inhibitor mixture) was added to obtain the cell lysates. Cell debris was pelleted and discarded, whereas the supernatant was kept. Protein samples were added with SDS loading buffer and boiled for 10 minutes, followed by SDS-PAGE. Then the proteins were transferred to a PVDF membrane. The membrane was blocked with 5% fat-free milk for 1 h at room temperature and then incubated with the proper

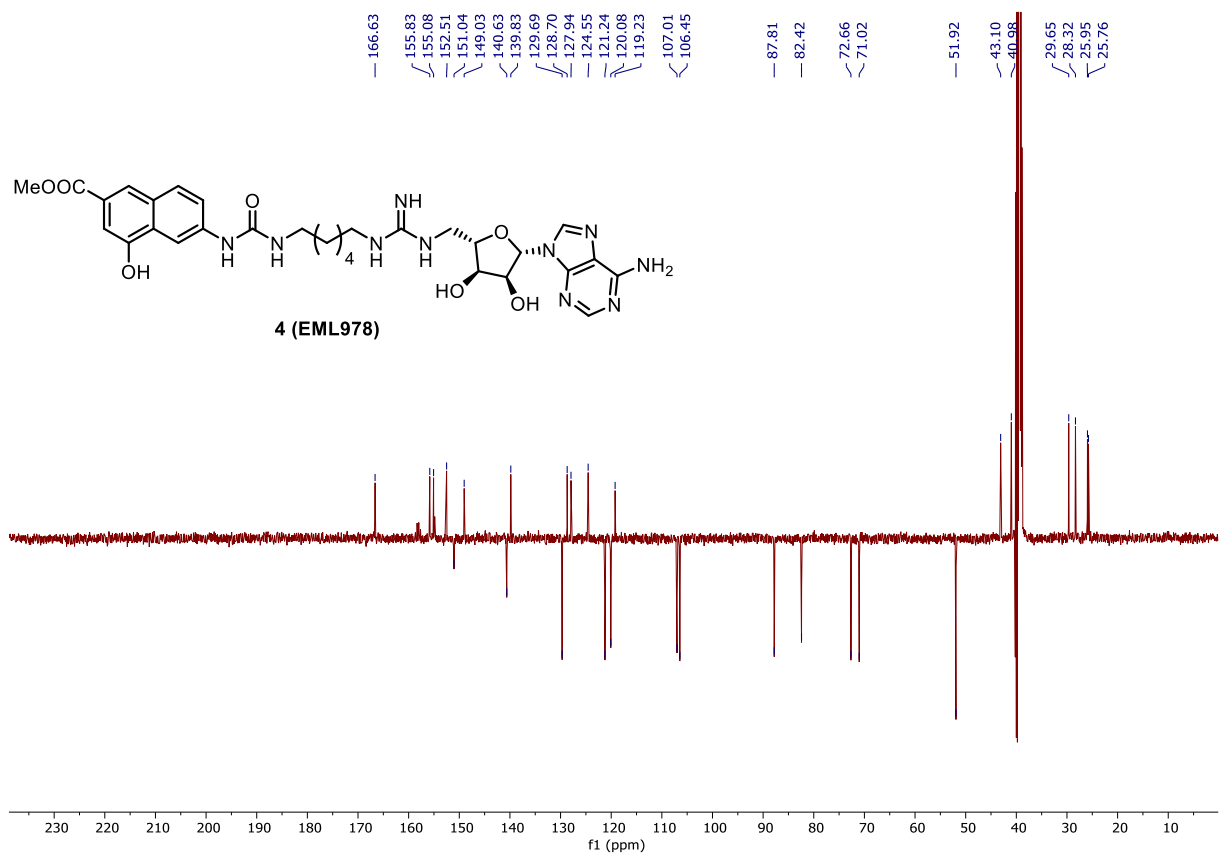
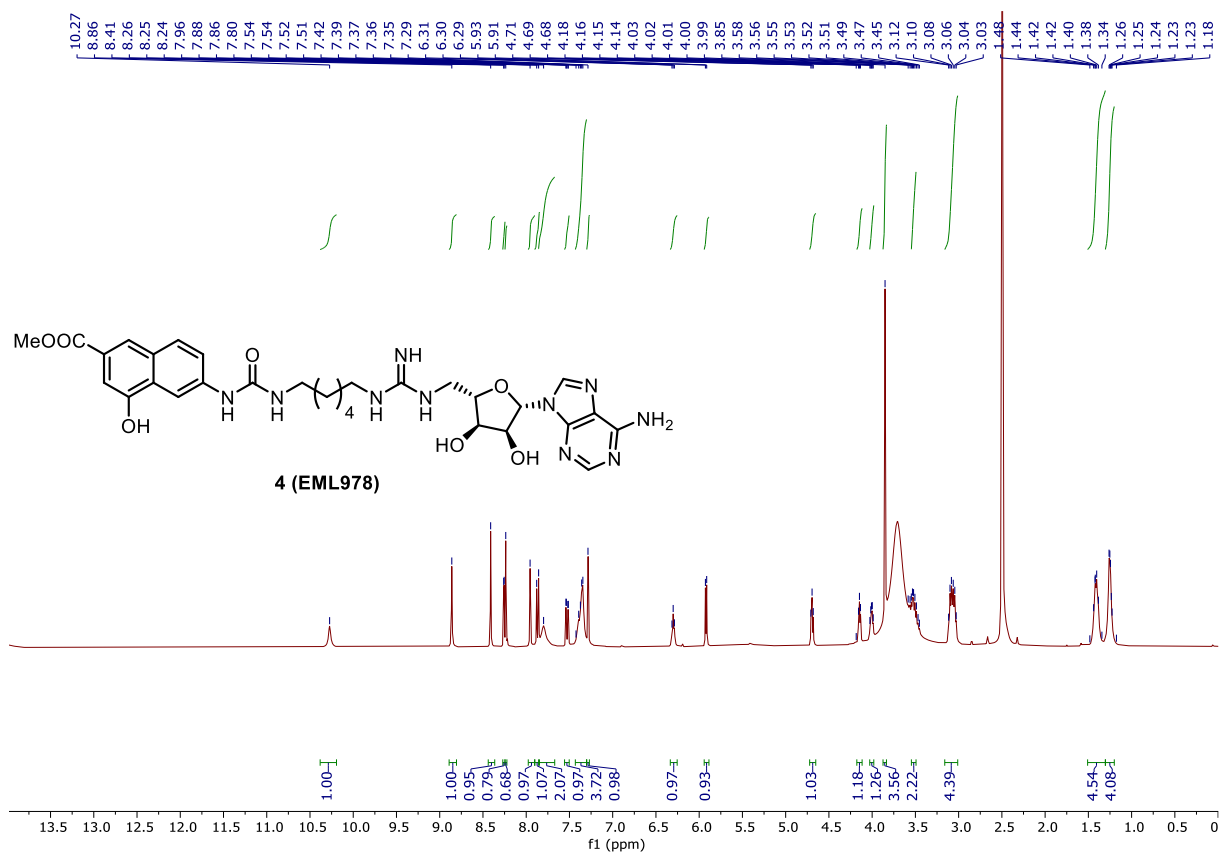
primary antibodies (anti-histone H3, Abcam, #ab18521; pan-PRMT4 substrate antibody, made in-house; anti-PRMT1, anti-PRMT4, anti-PRMT6) at 4 °C overnight. The blot was then washed three times with PBST and incubated with secondary antibodies for 1 h at room temperature. After washing three times with PBST, the membrane was incubated with ECL reagent, and the signals were detected on X-ray film.

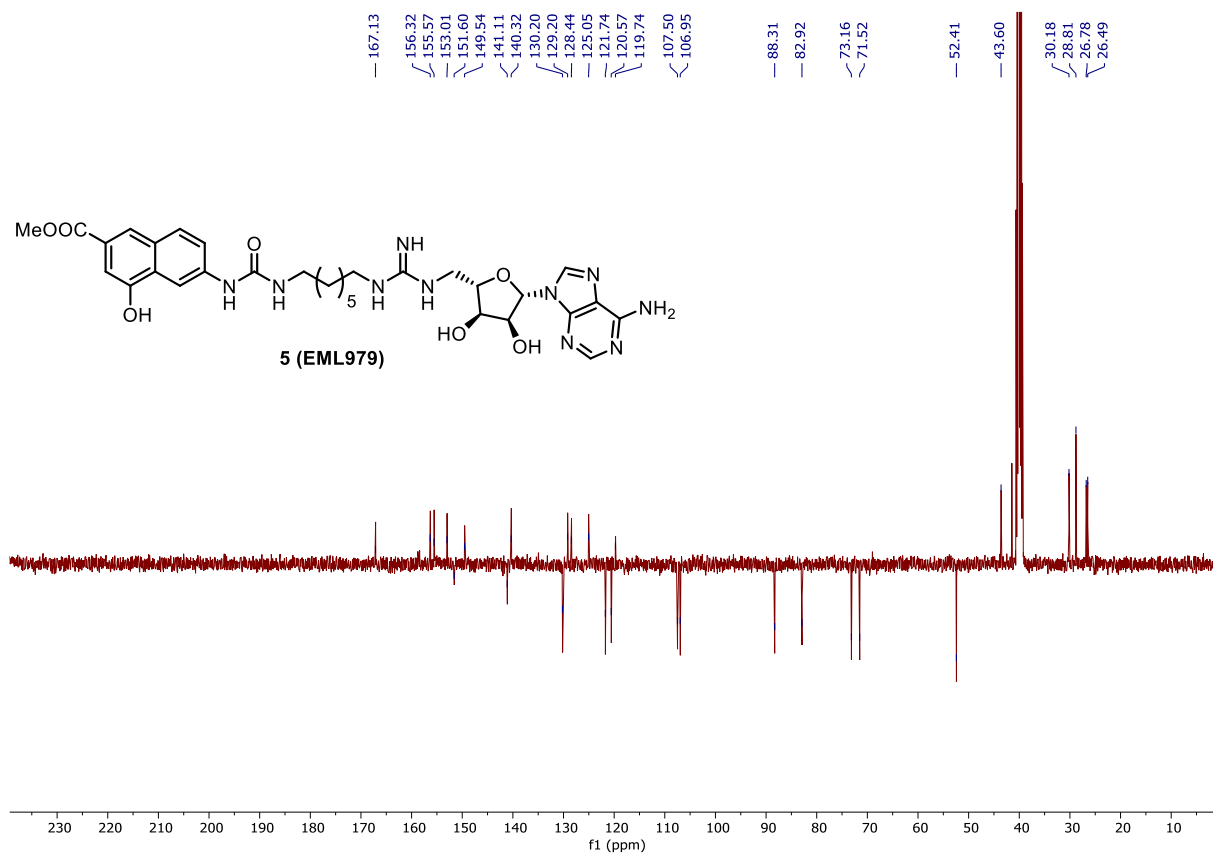
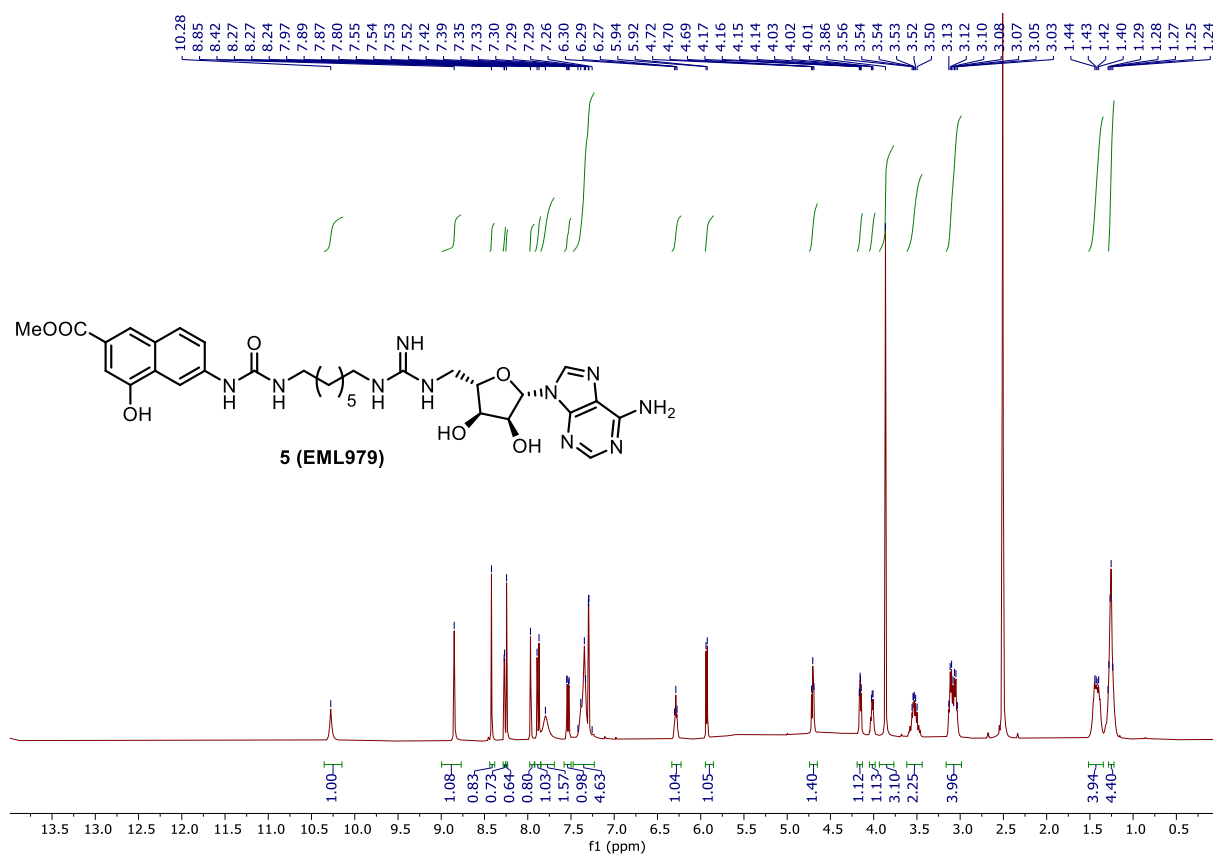
8.4. NMR DATA

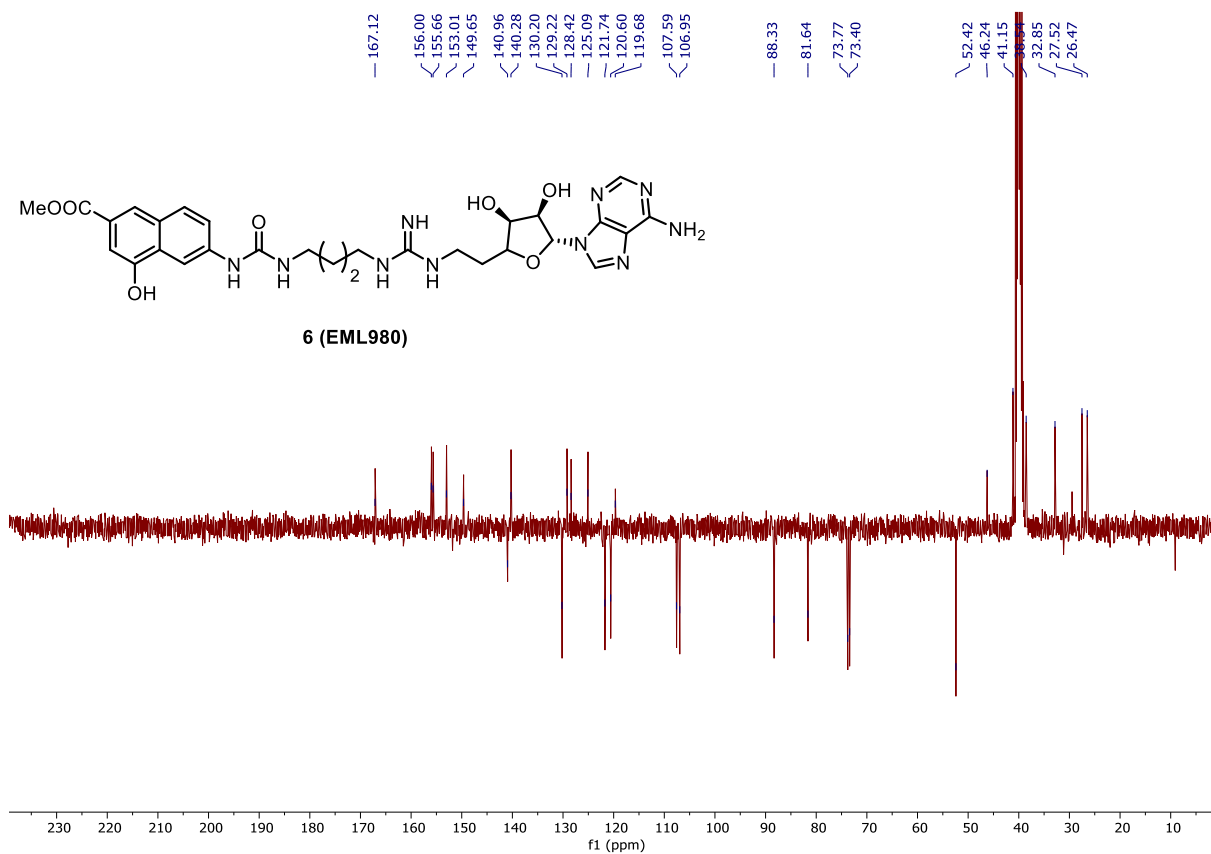
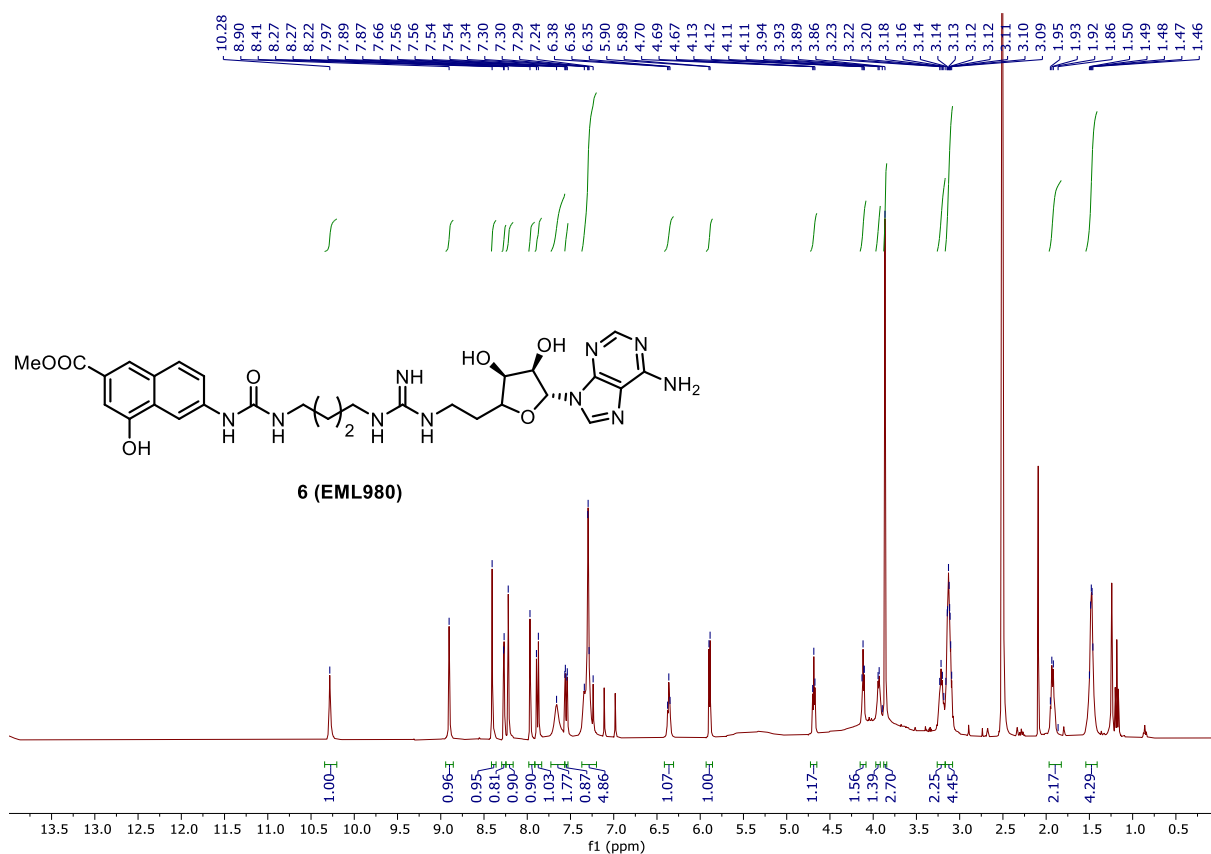


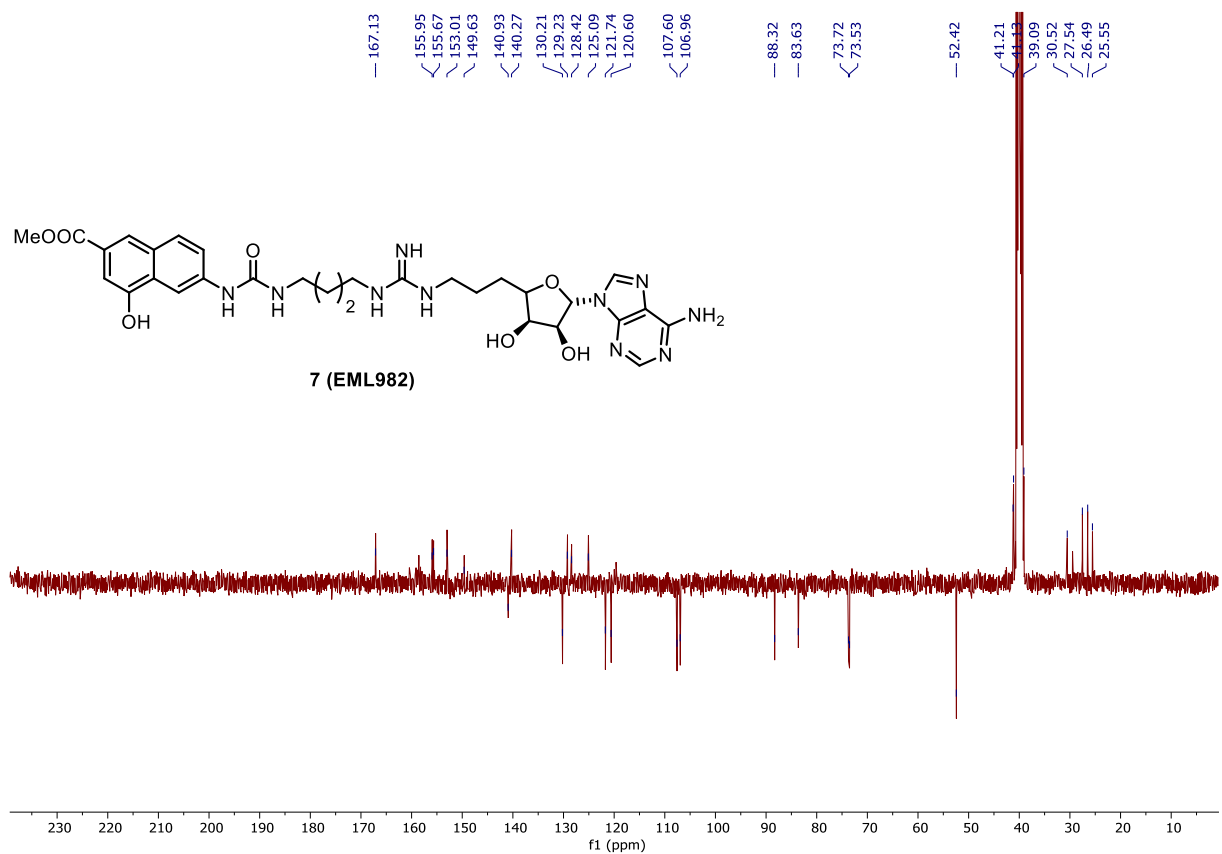
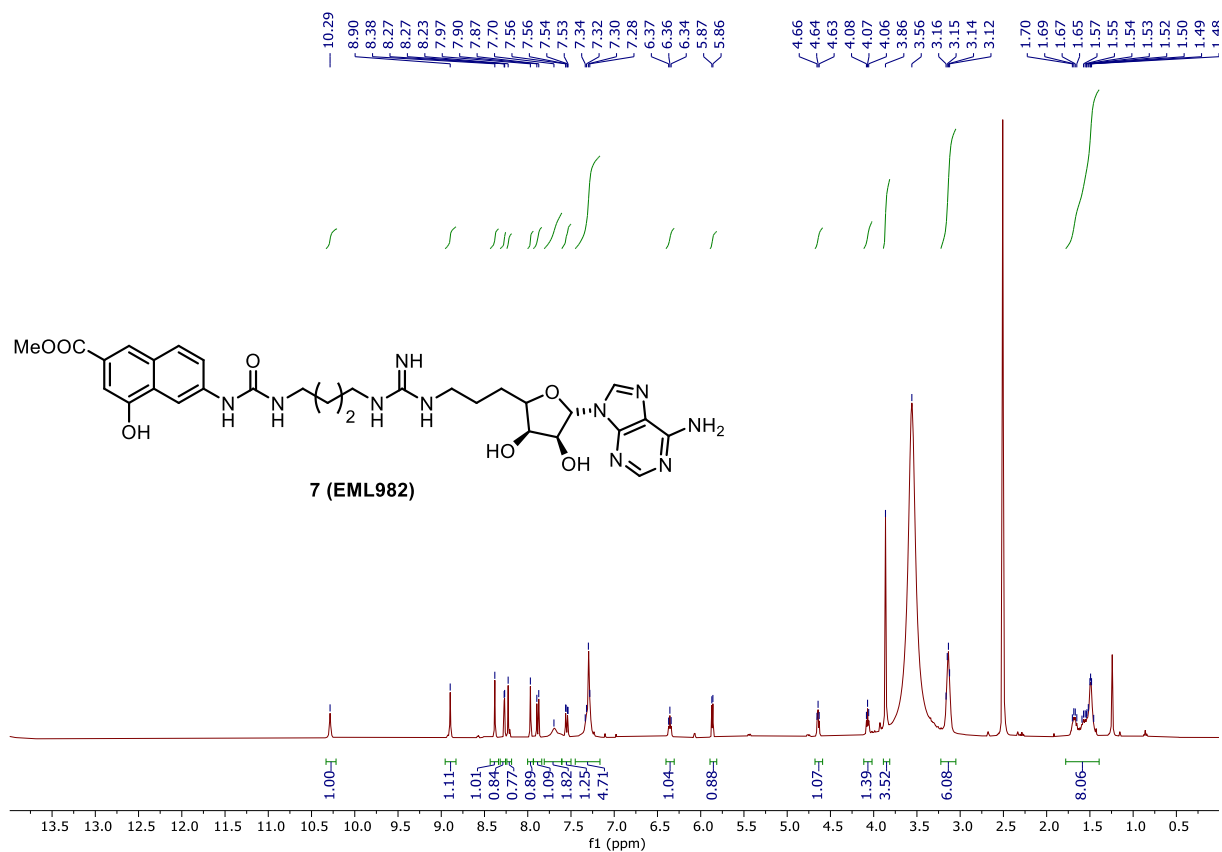


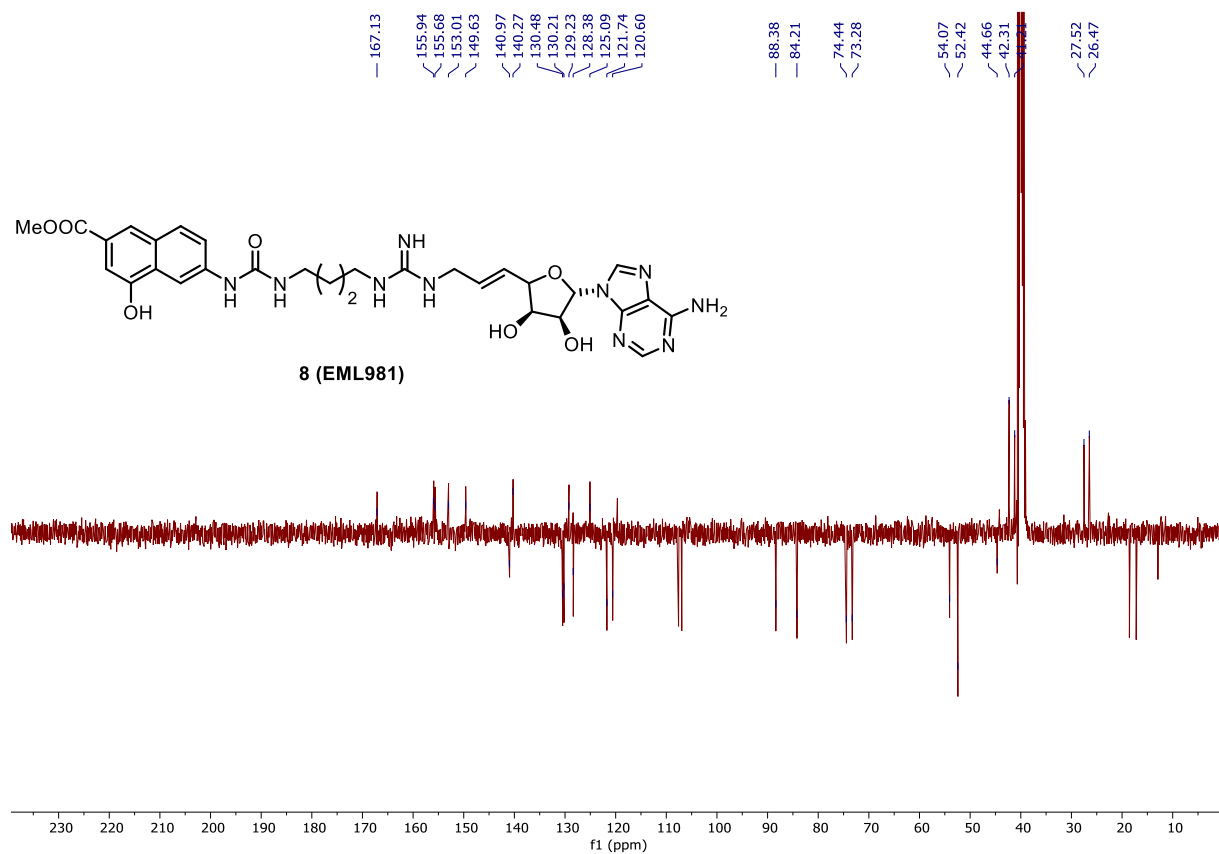
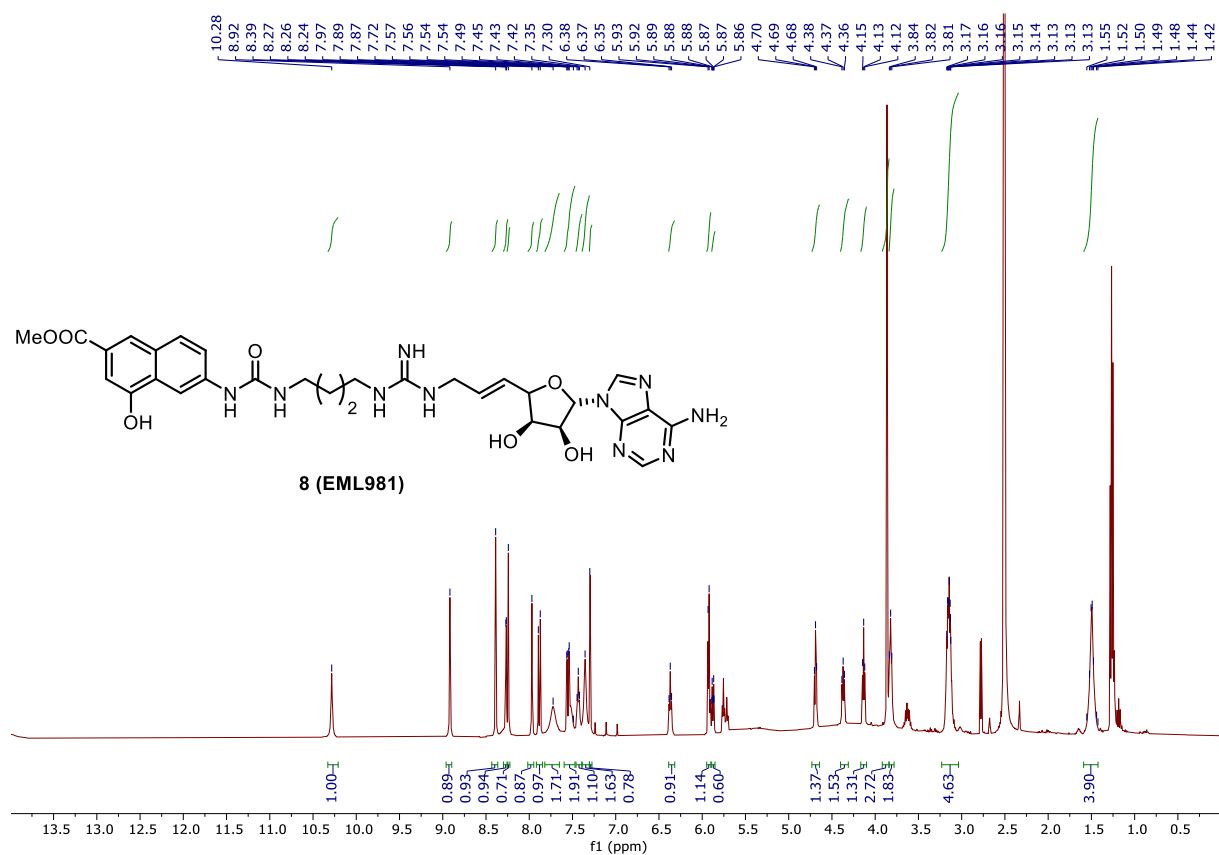


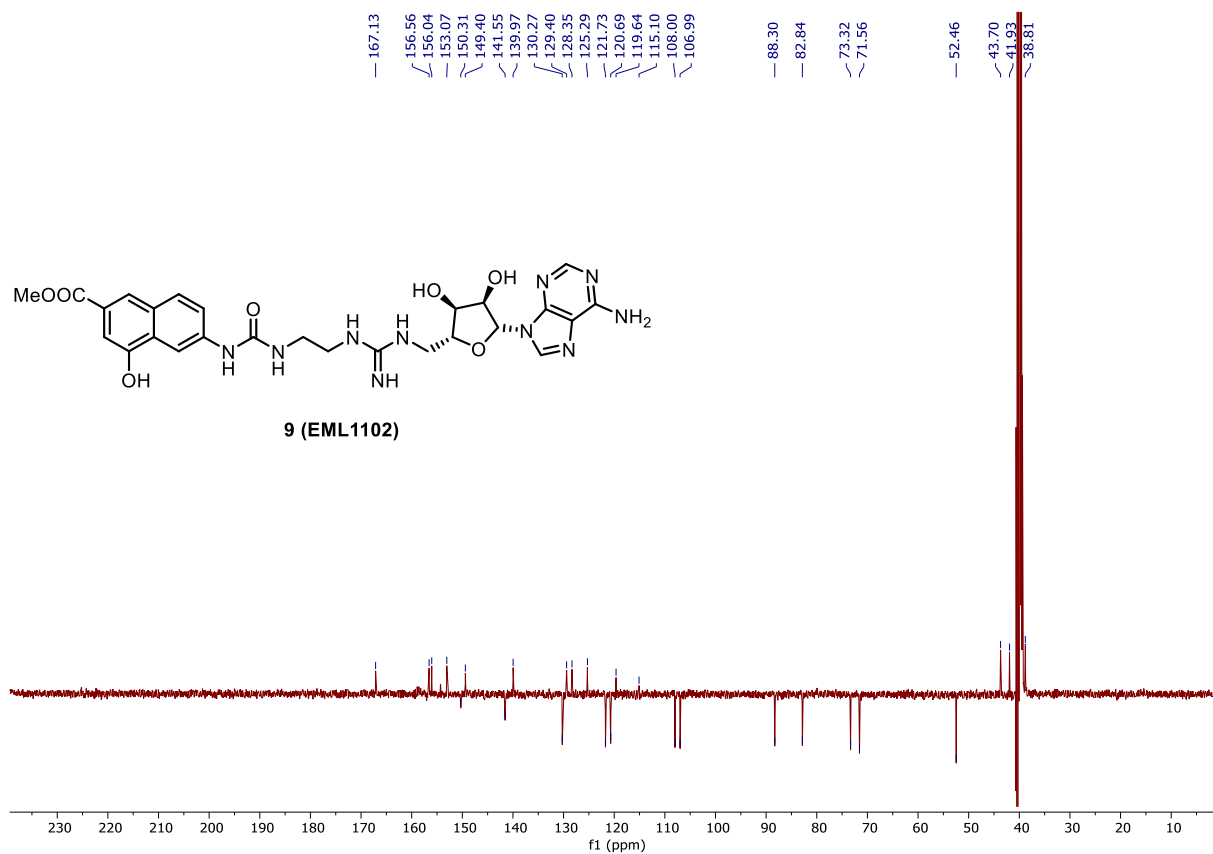
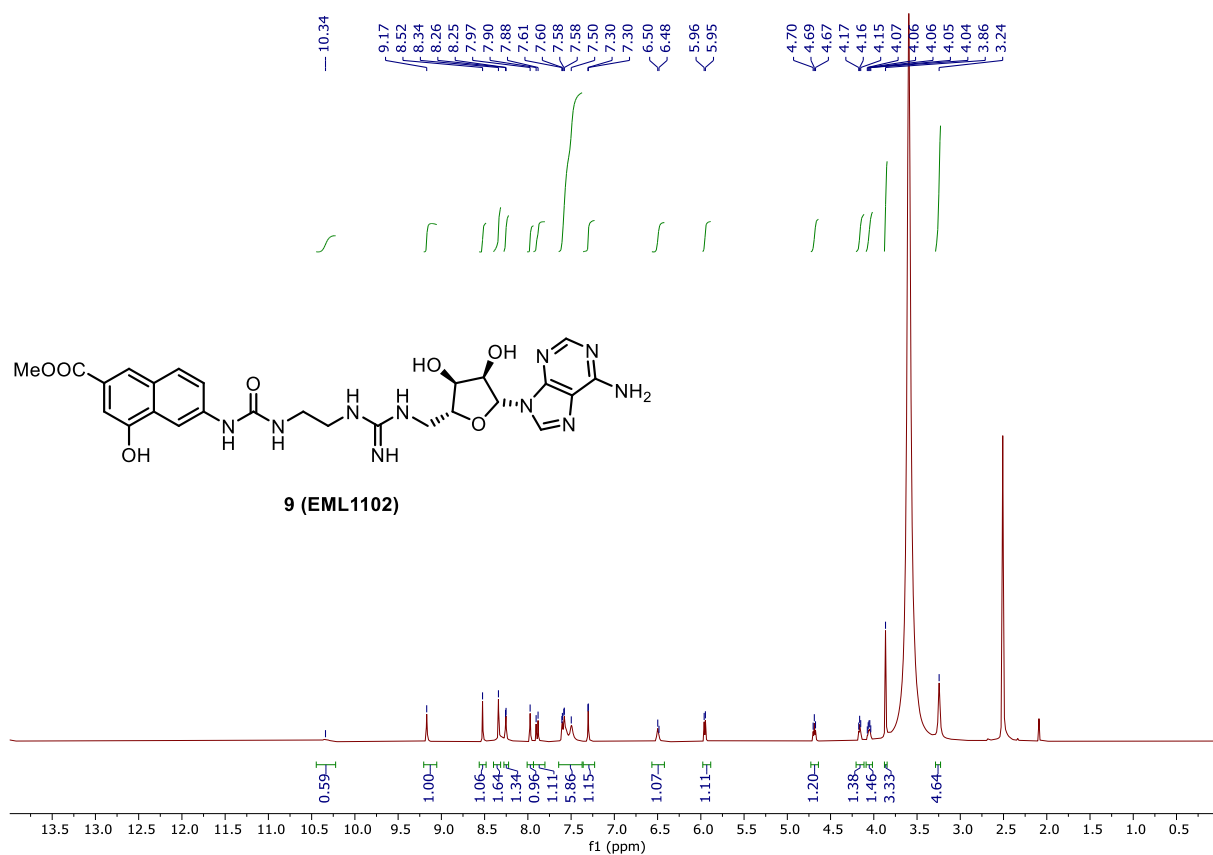


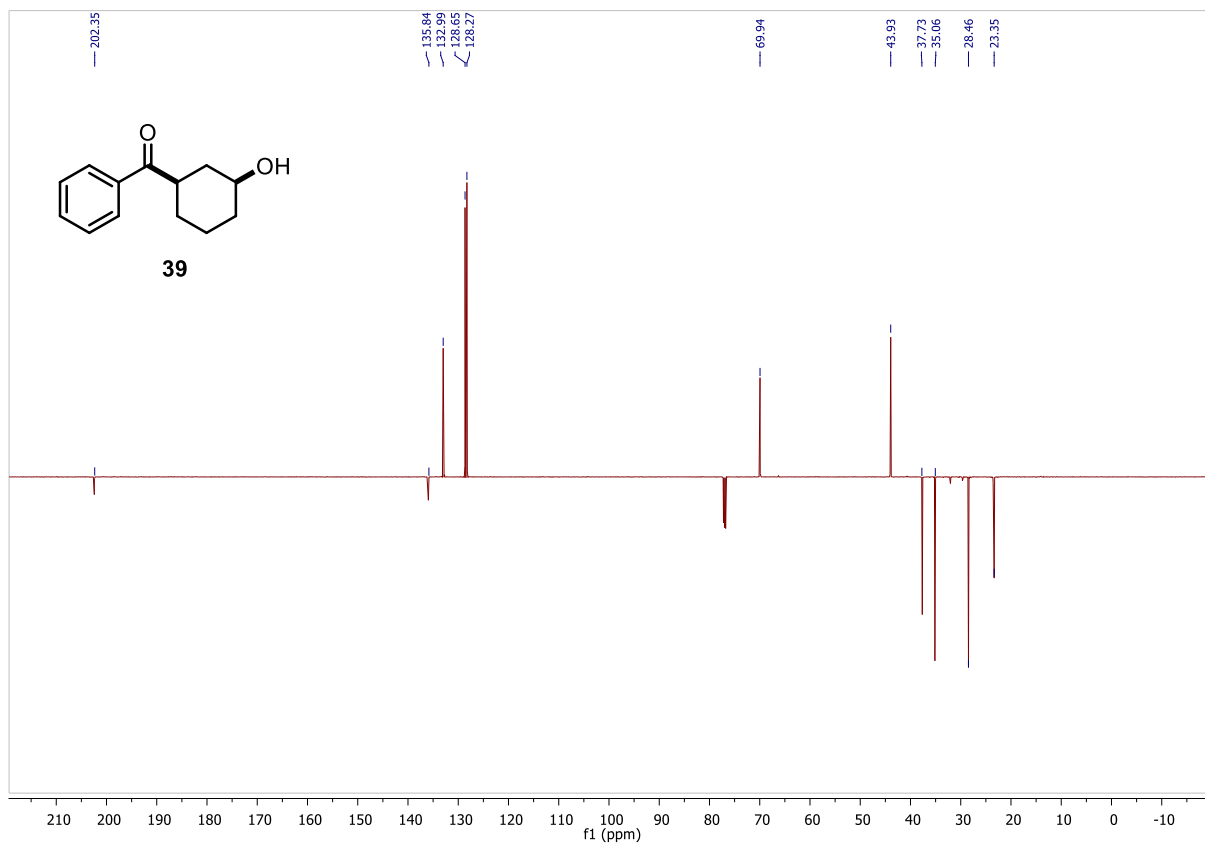
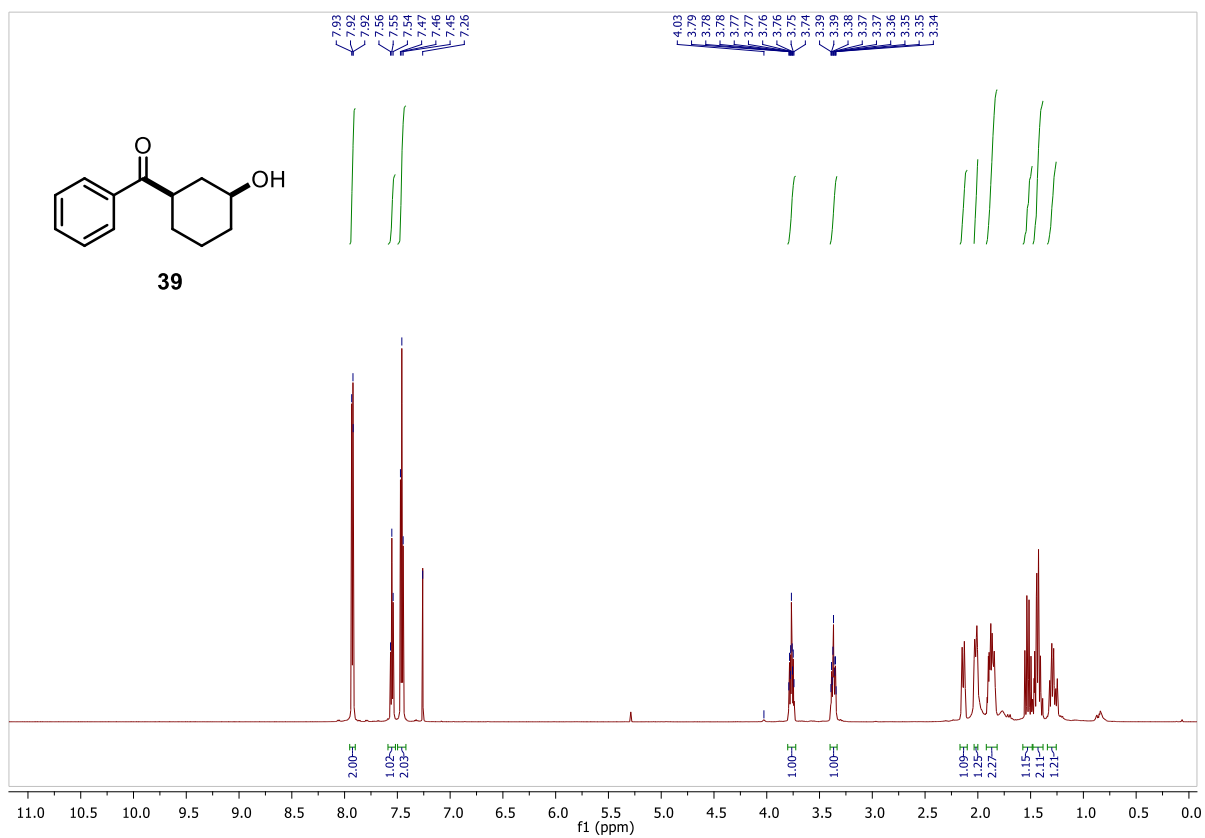


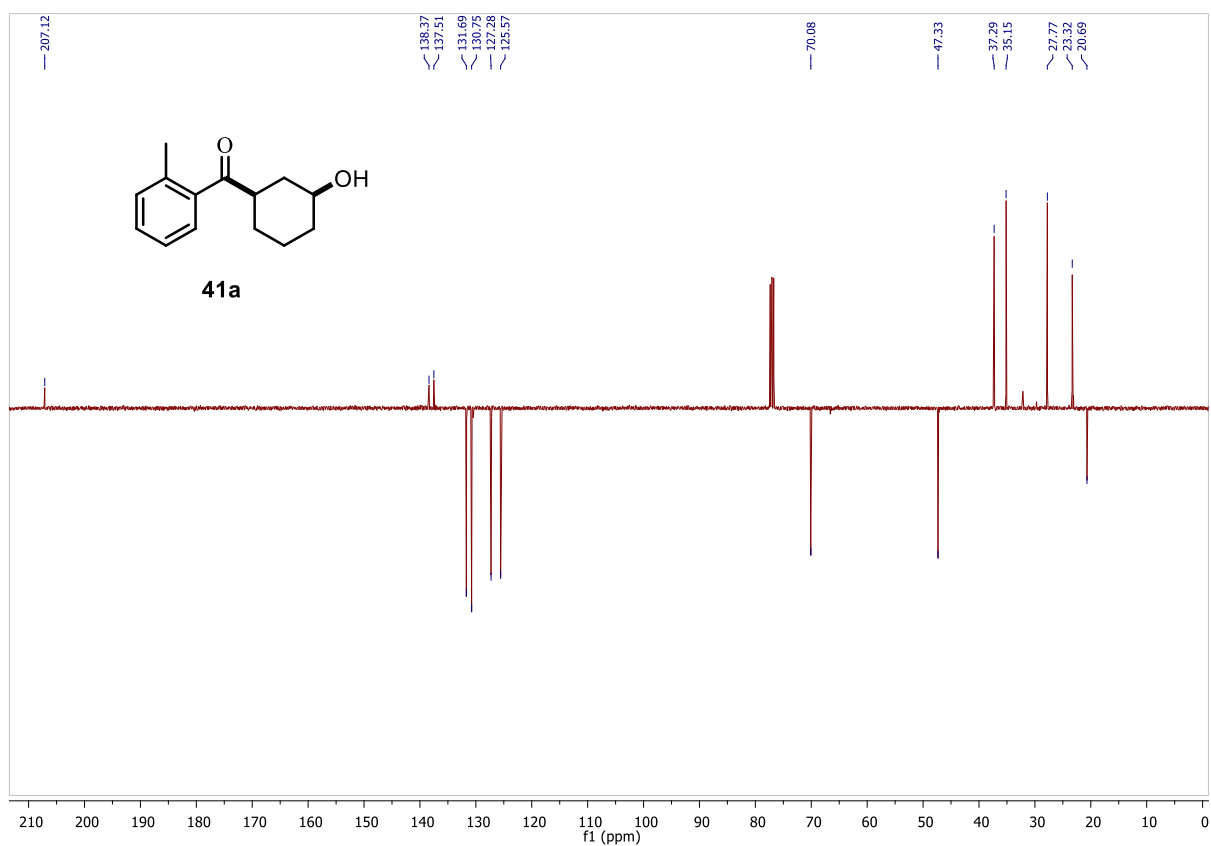
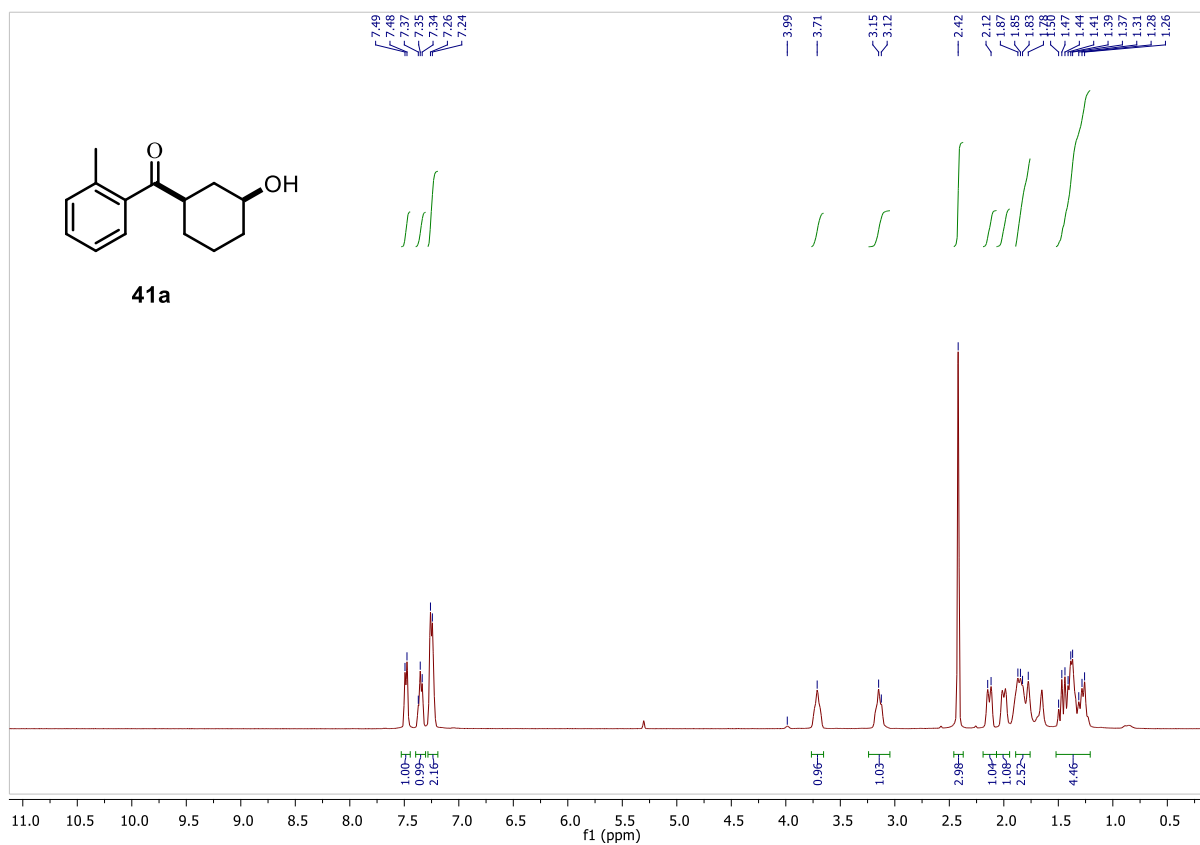


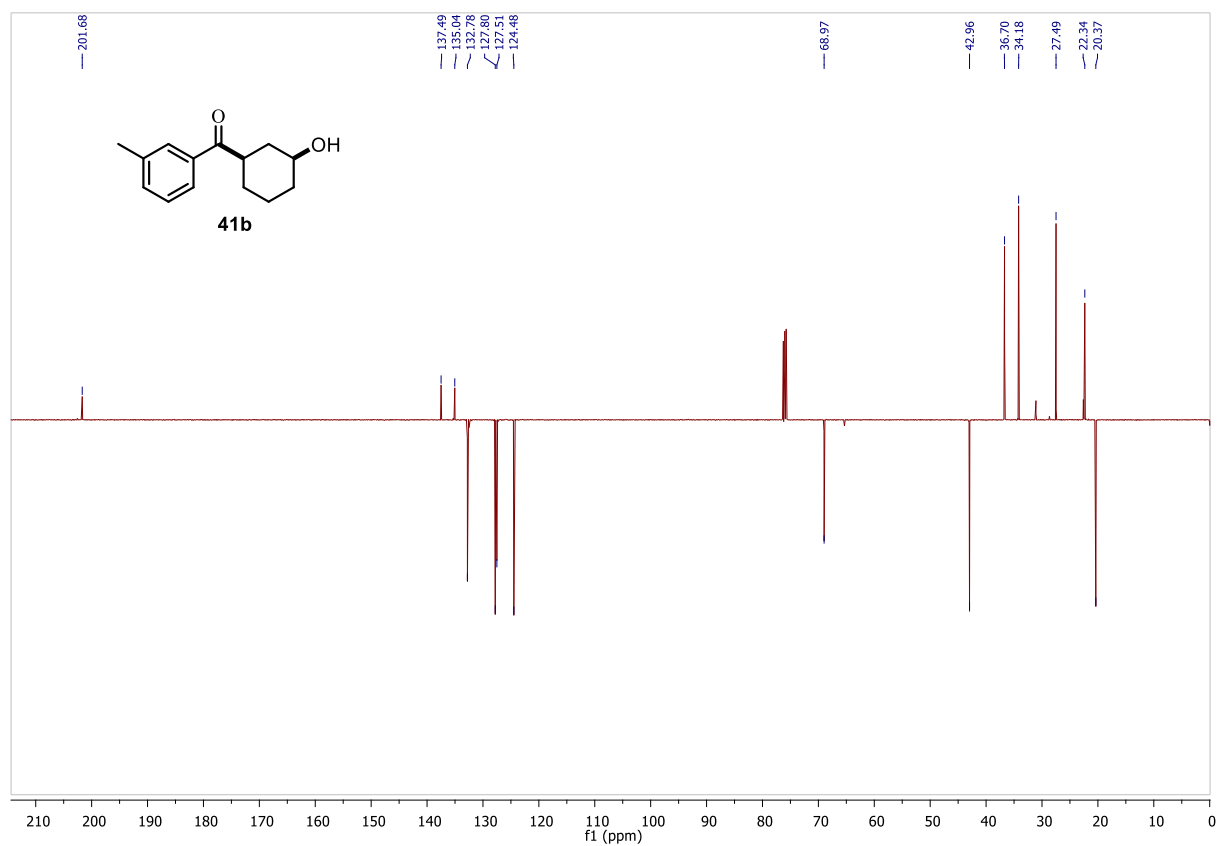
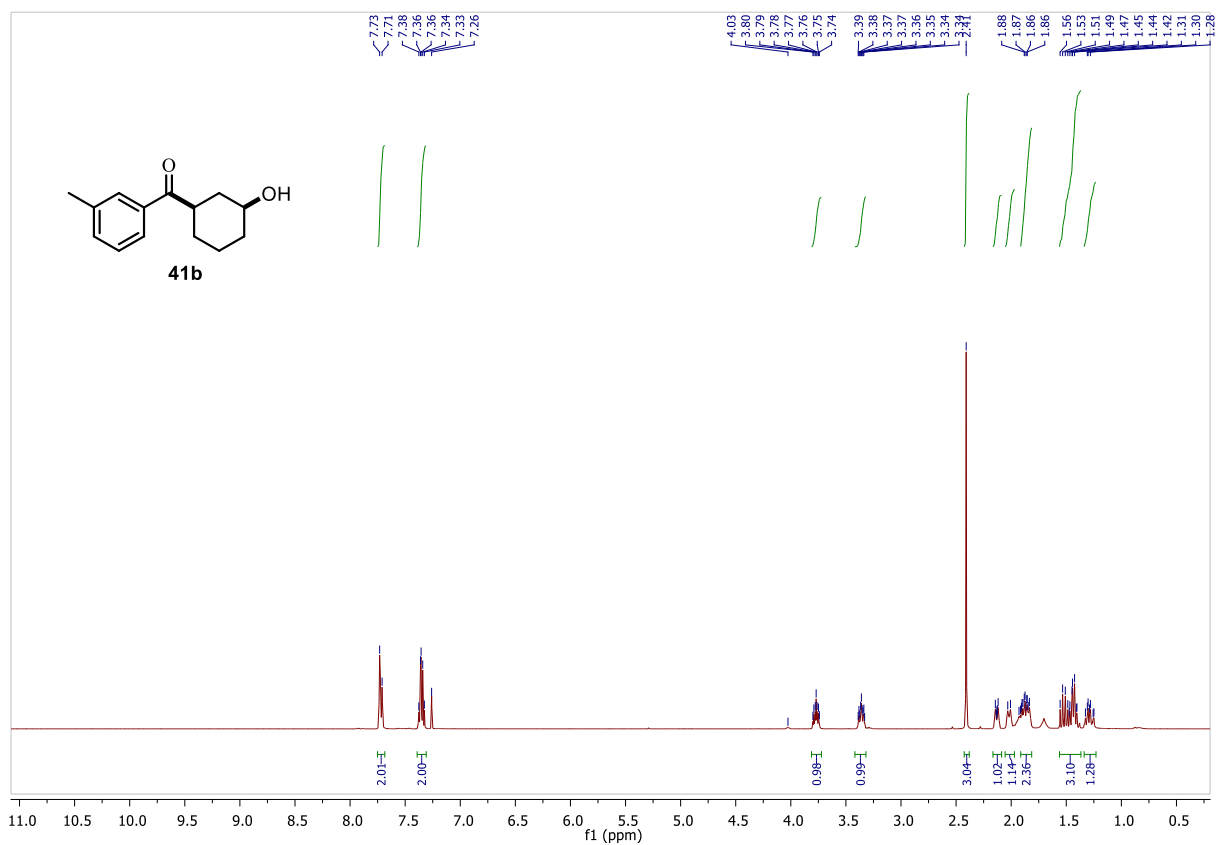


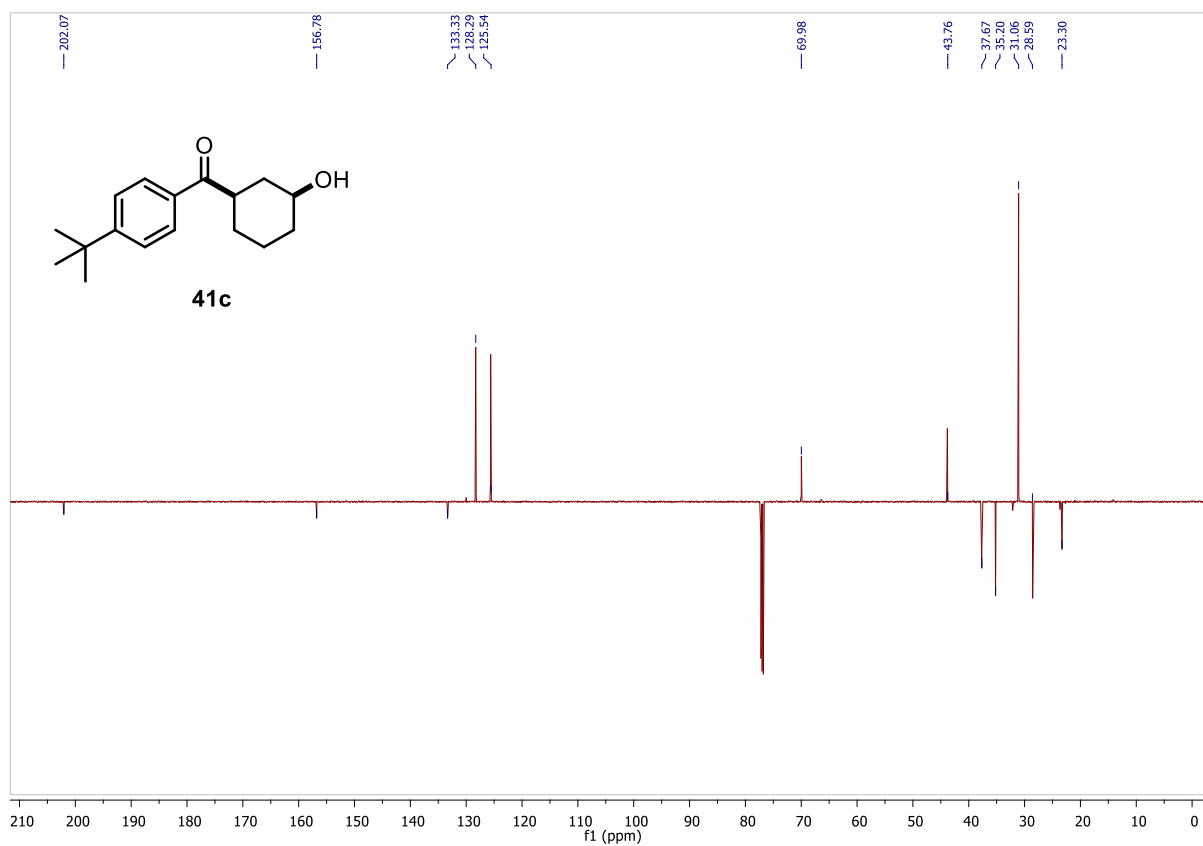
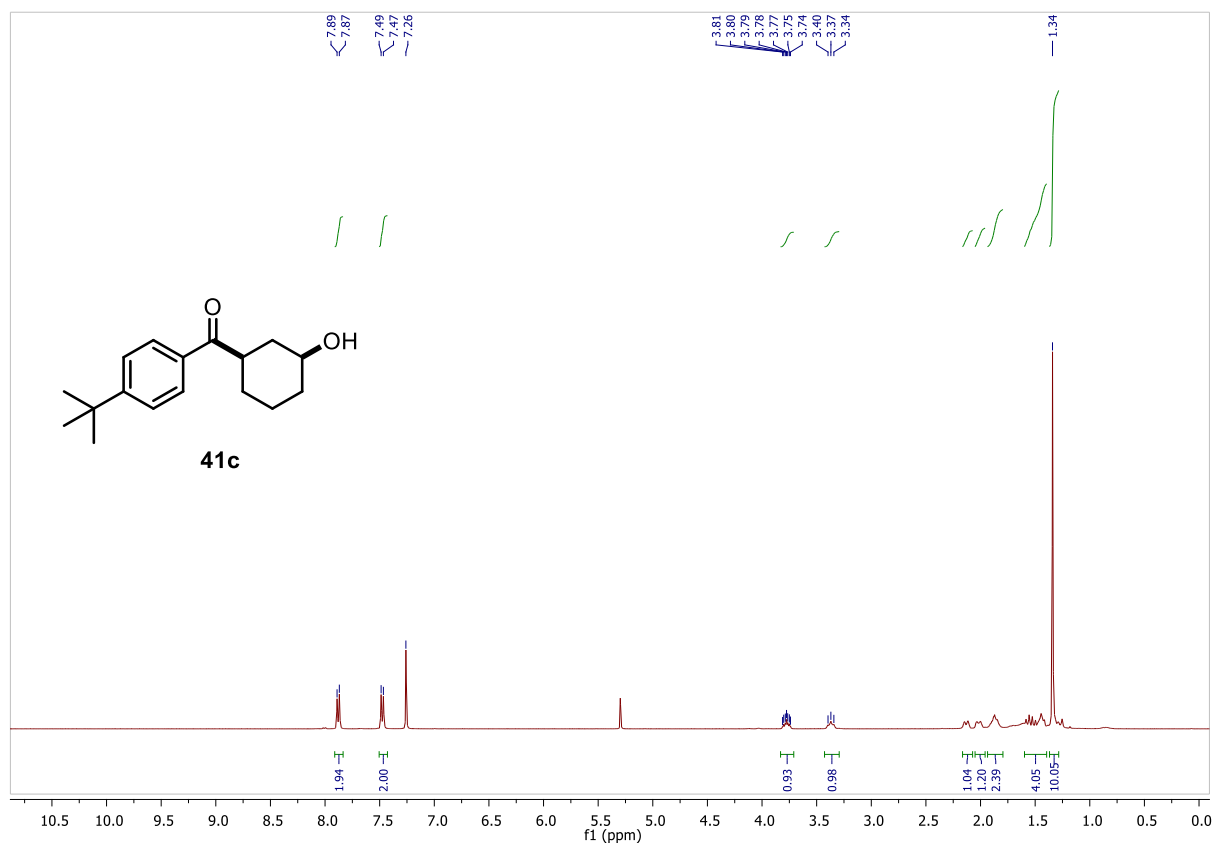


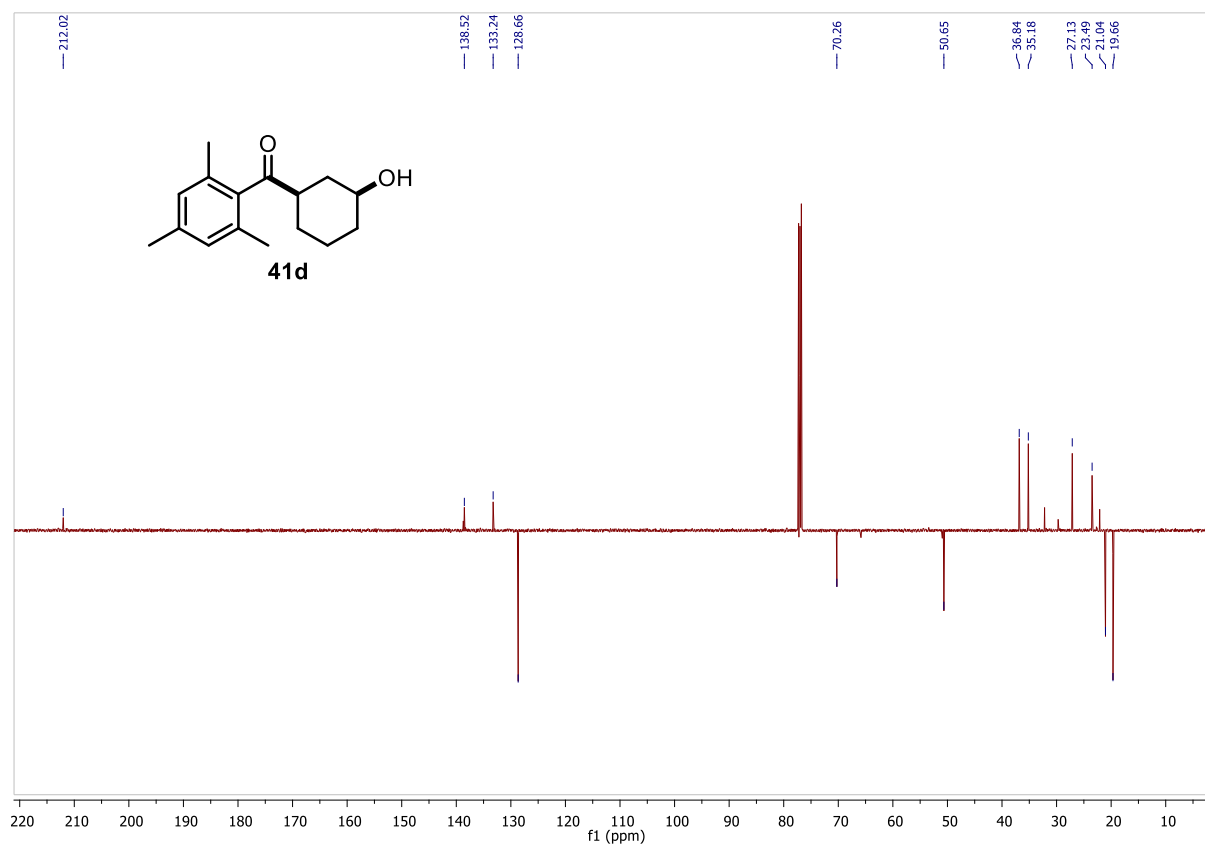
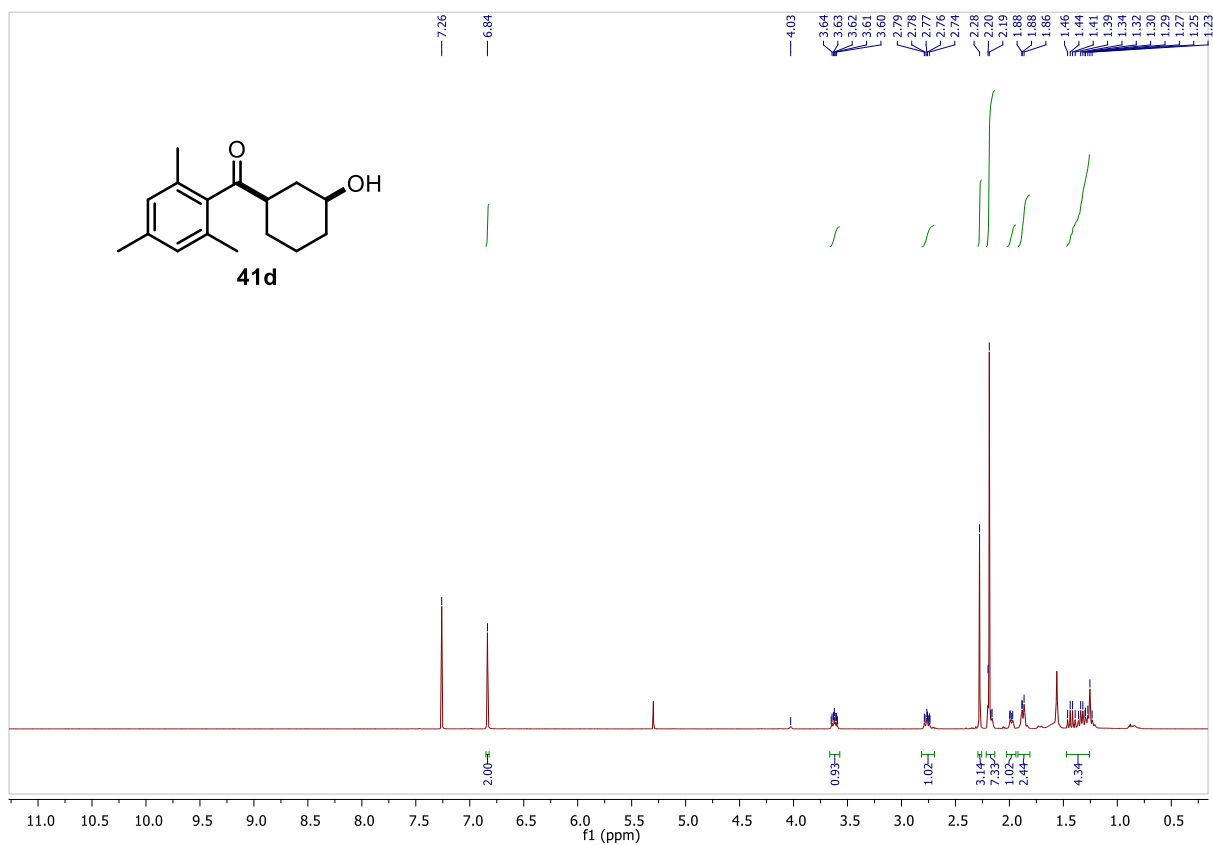


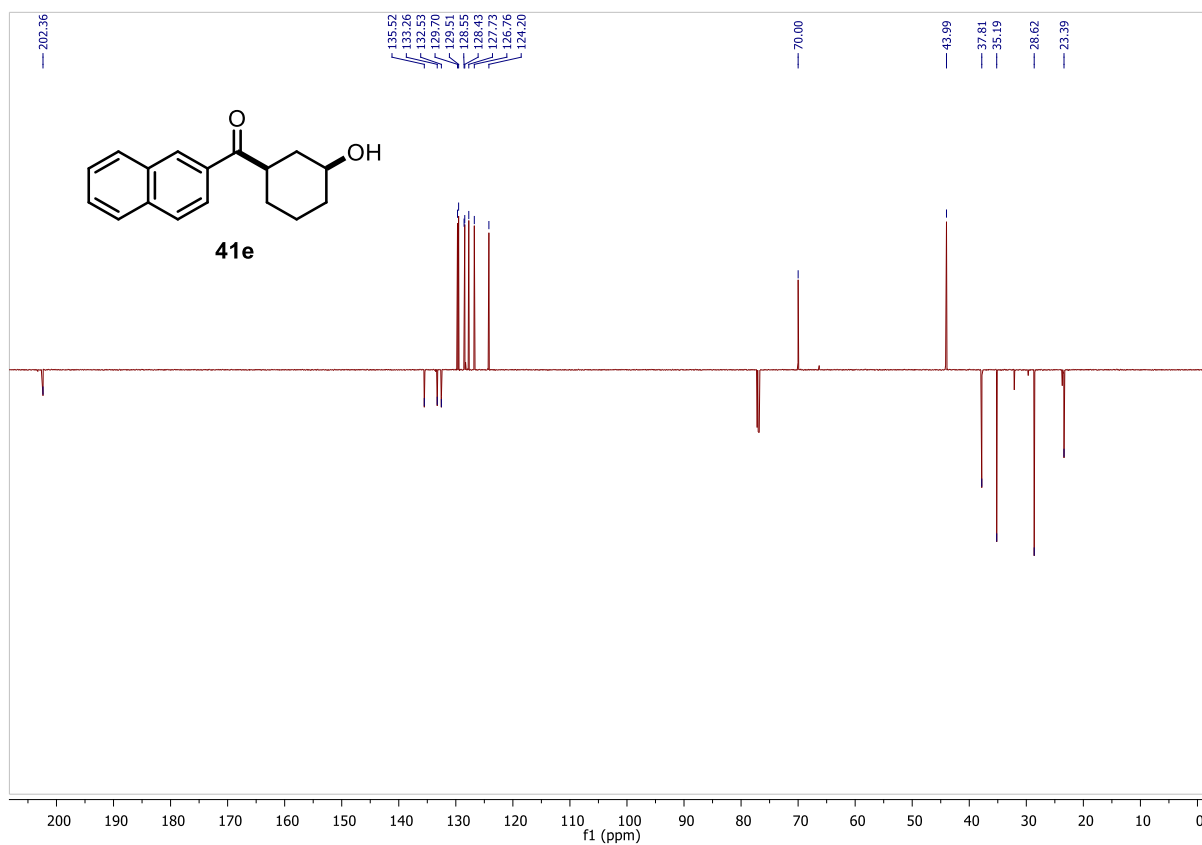
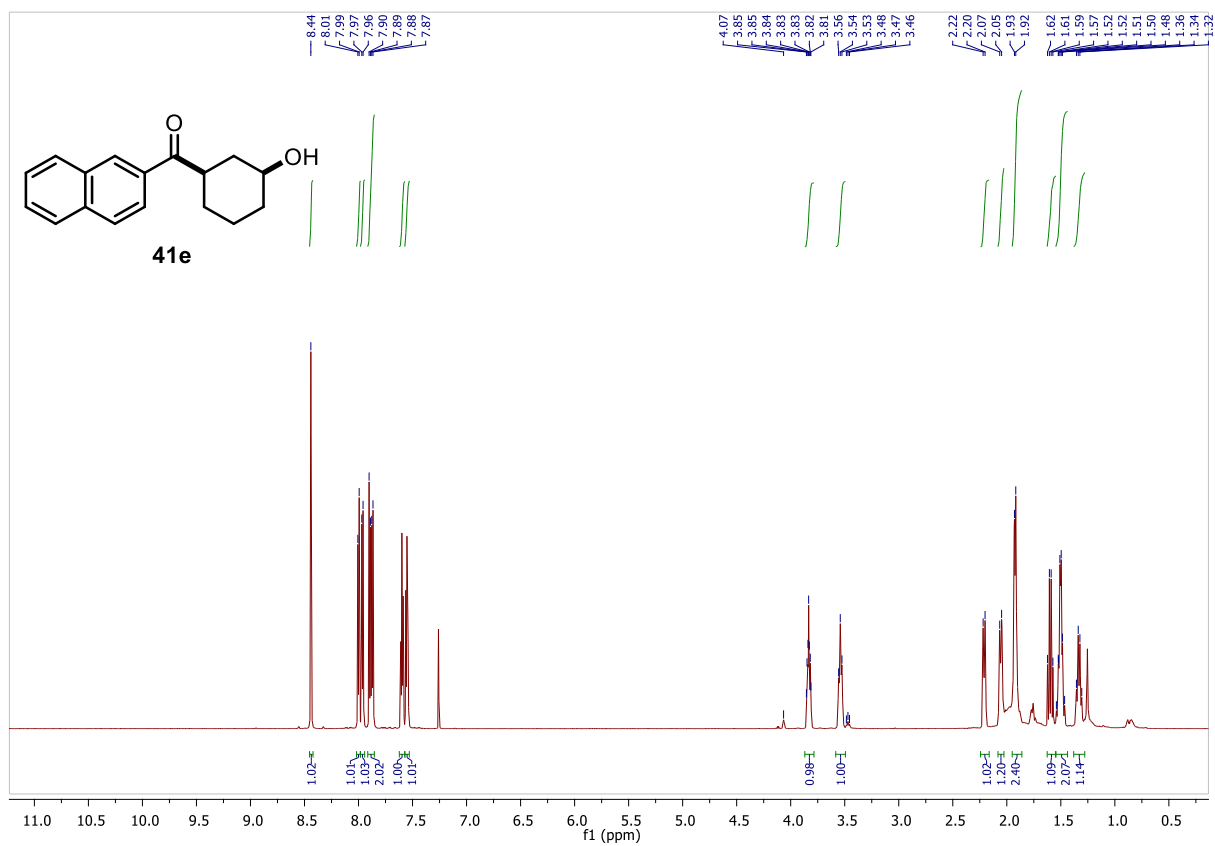


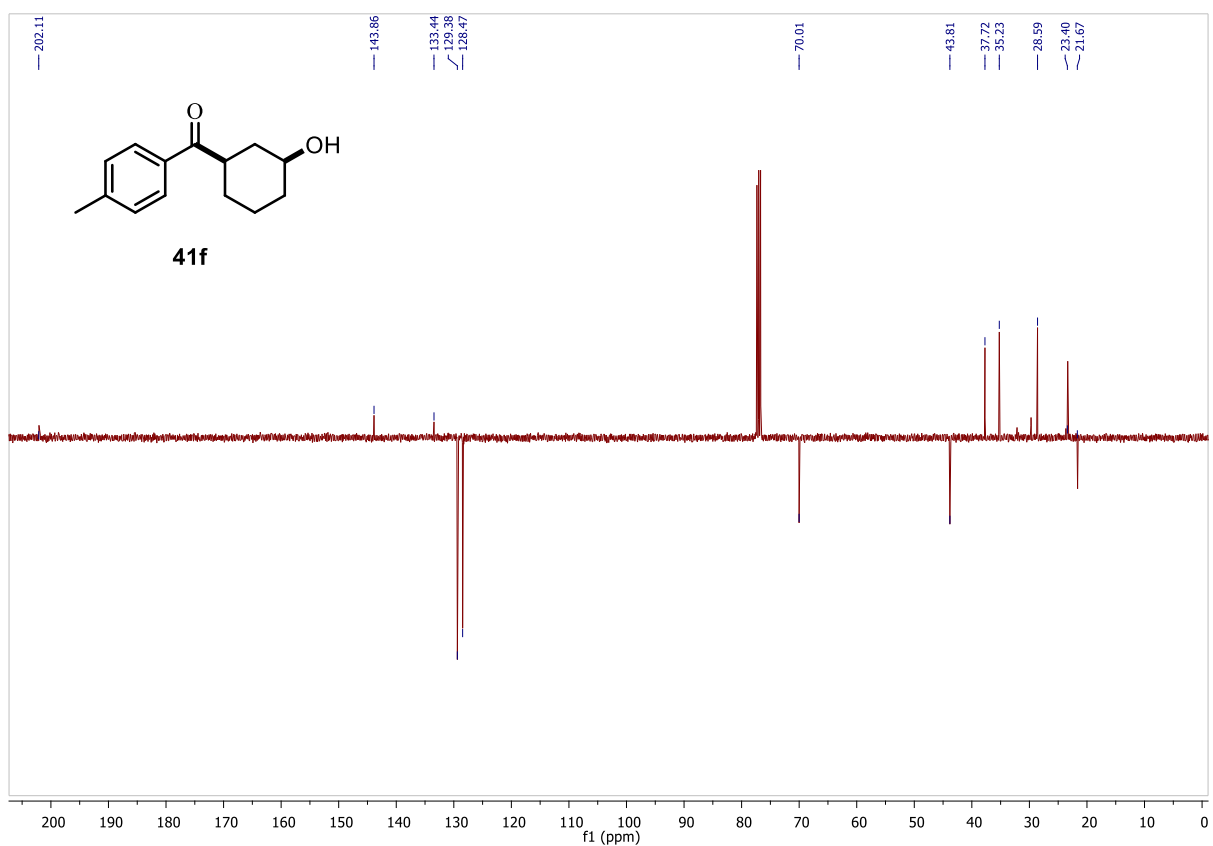
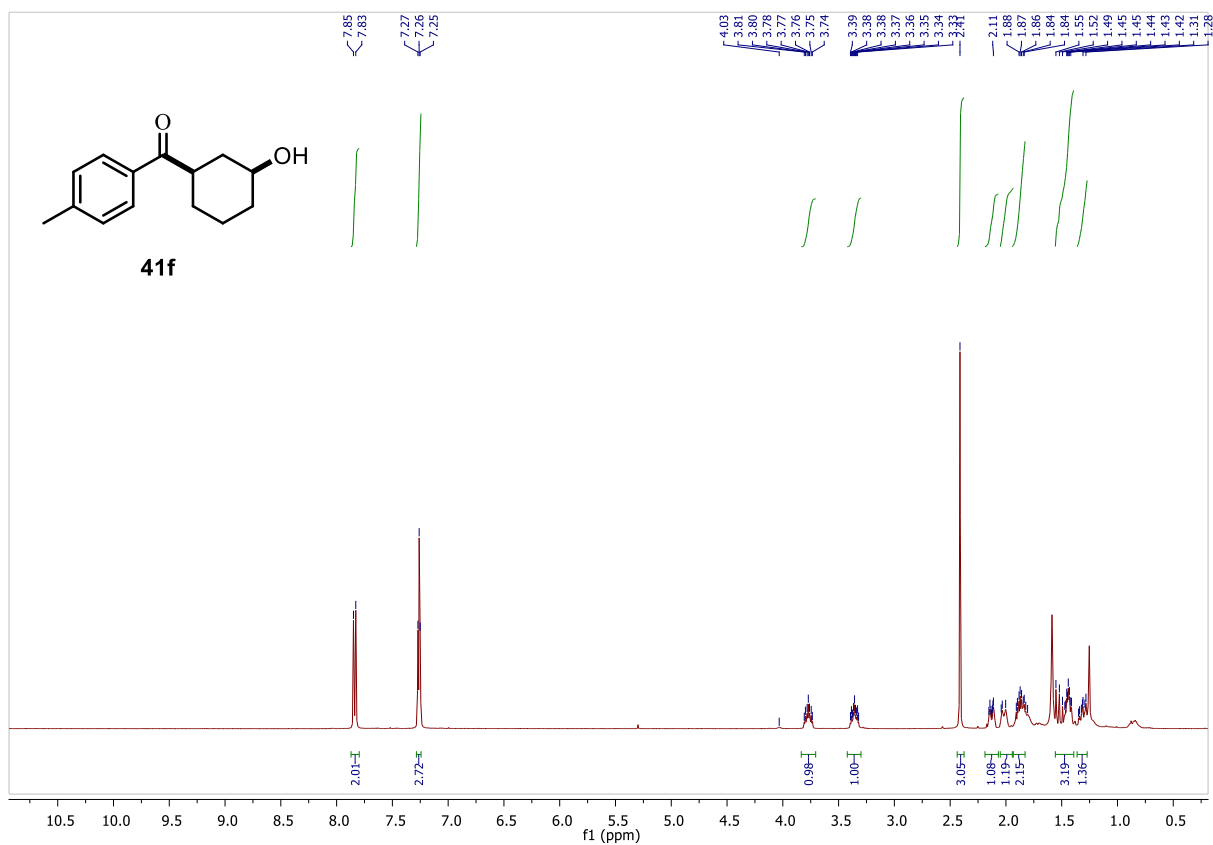


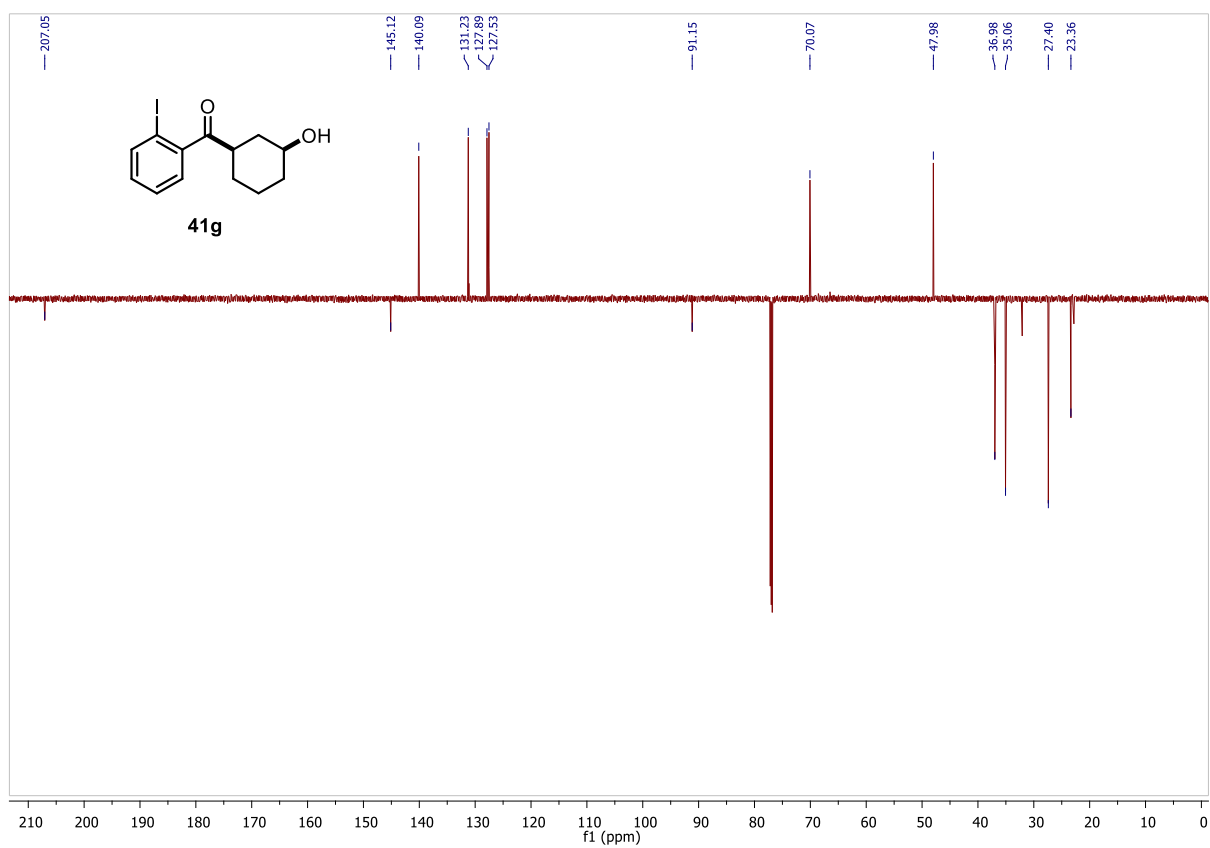
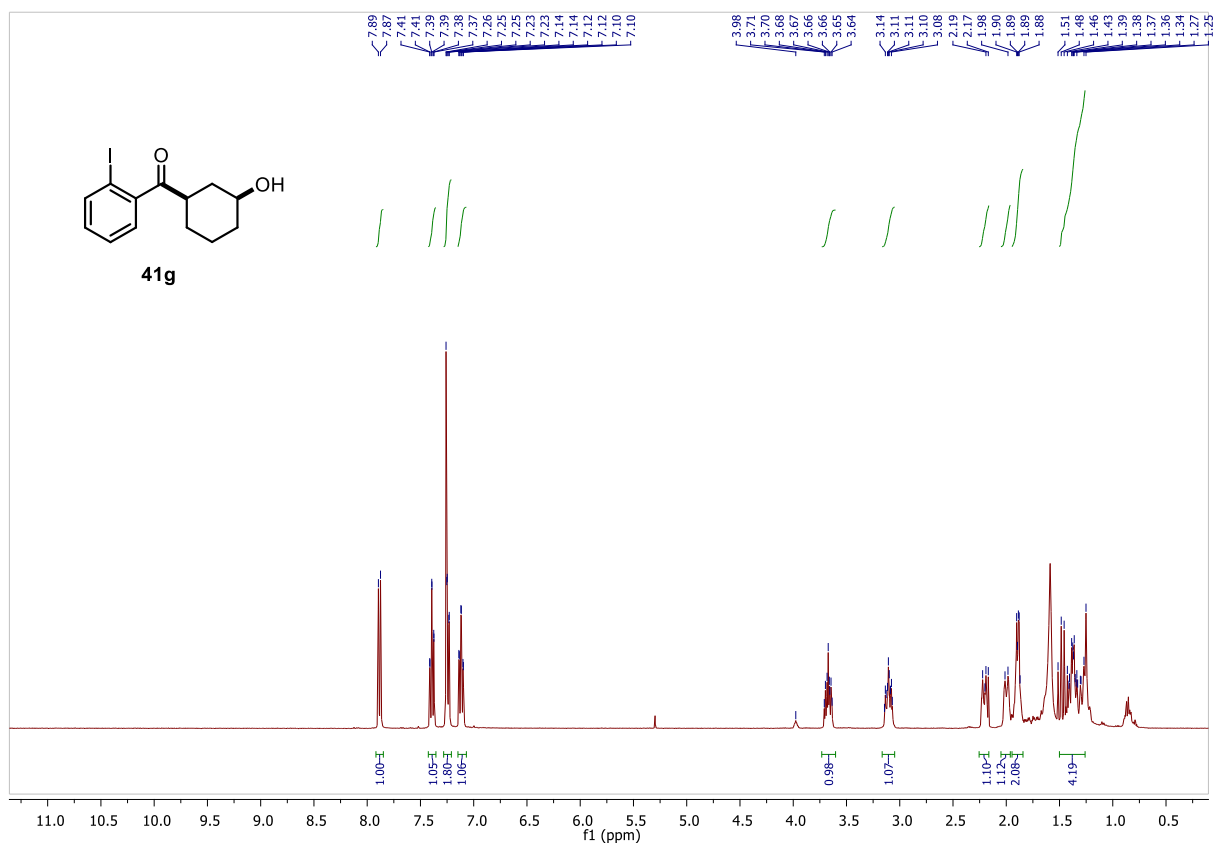


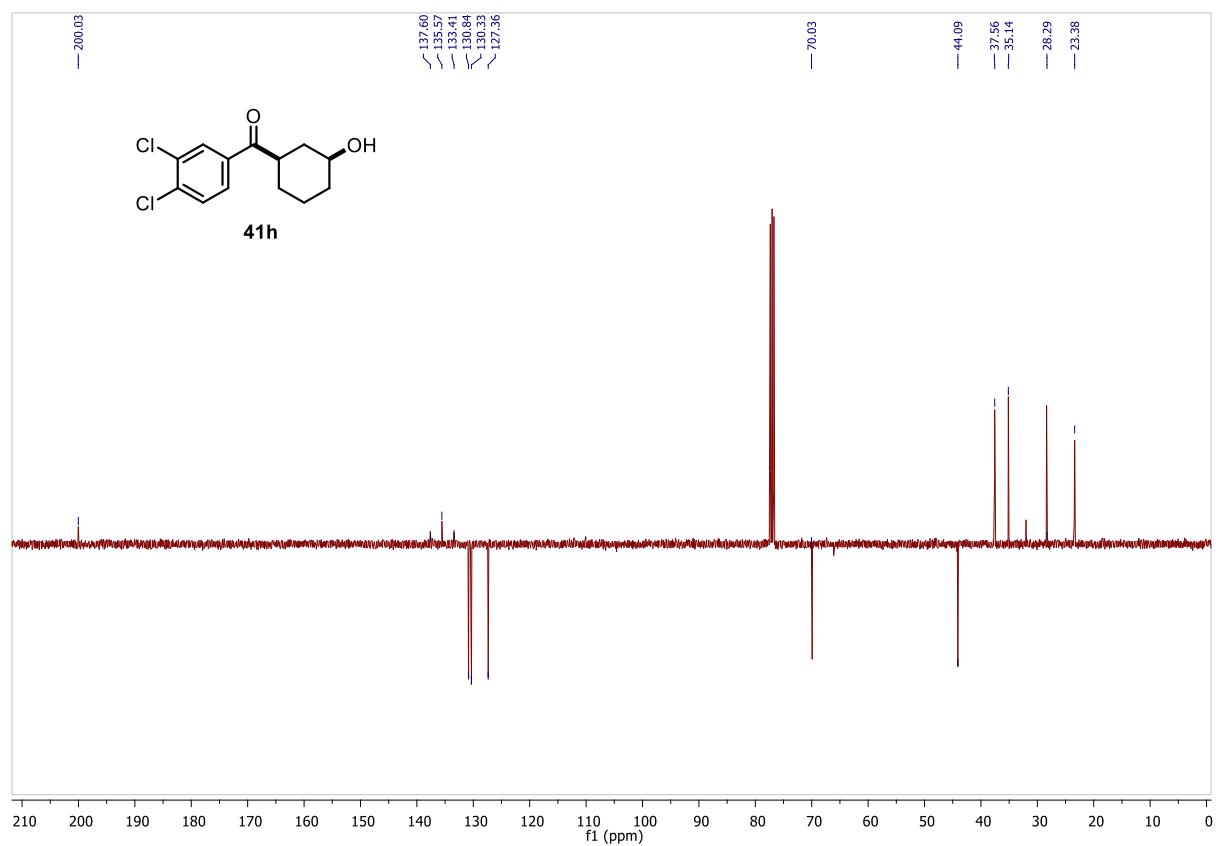
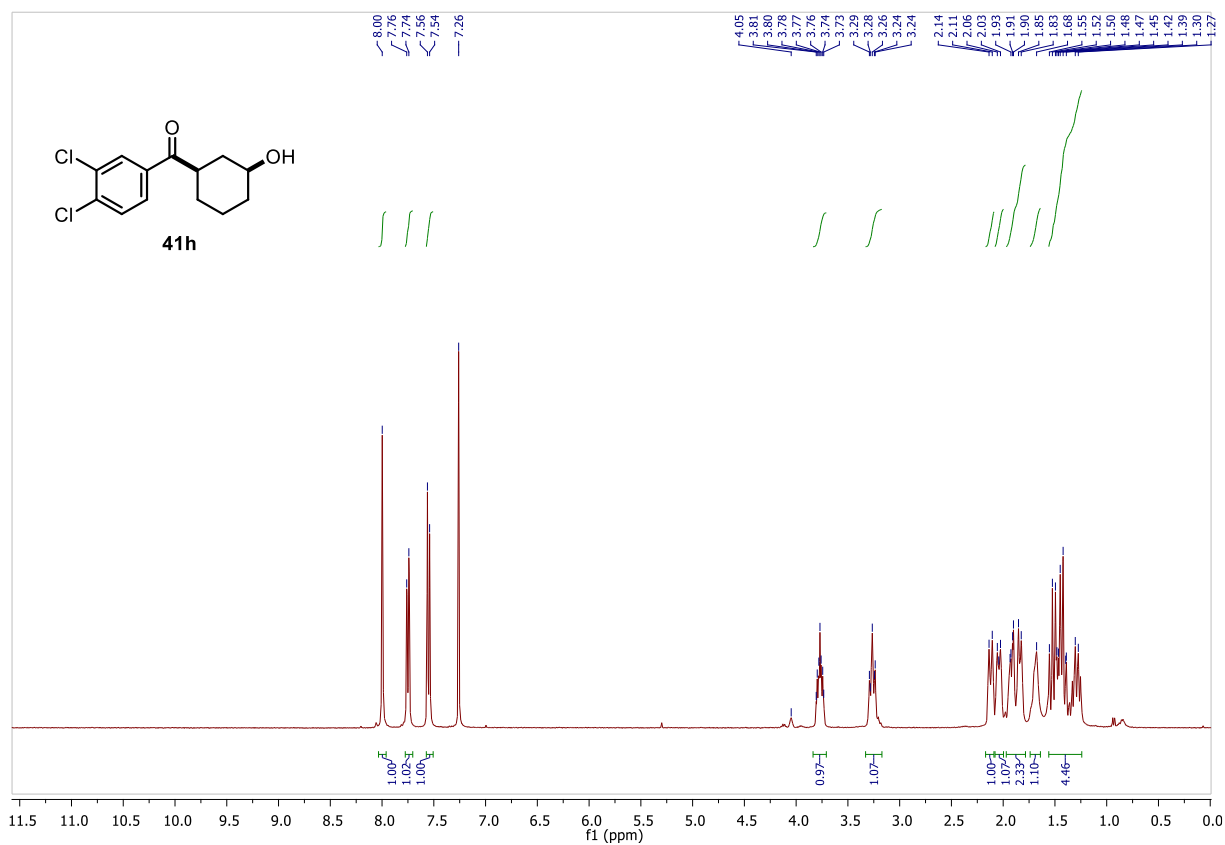


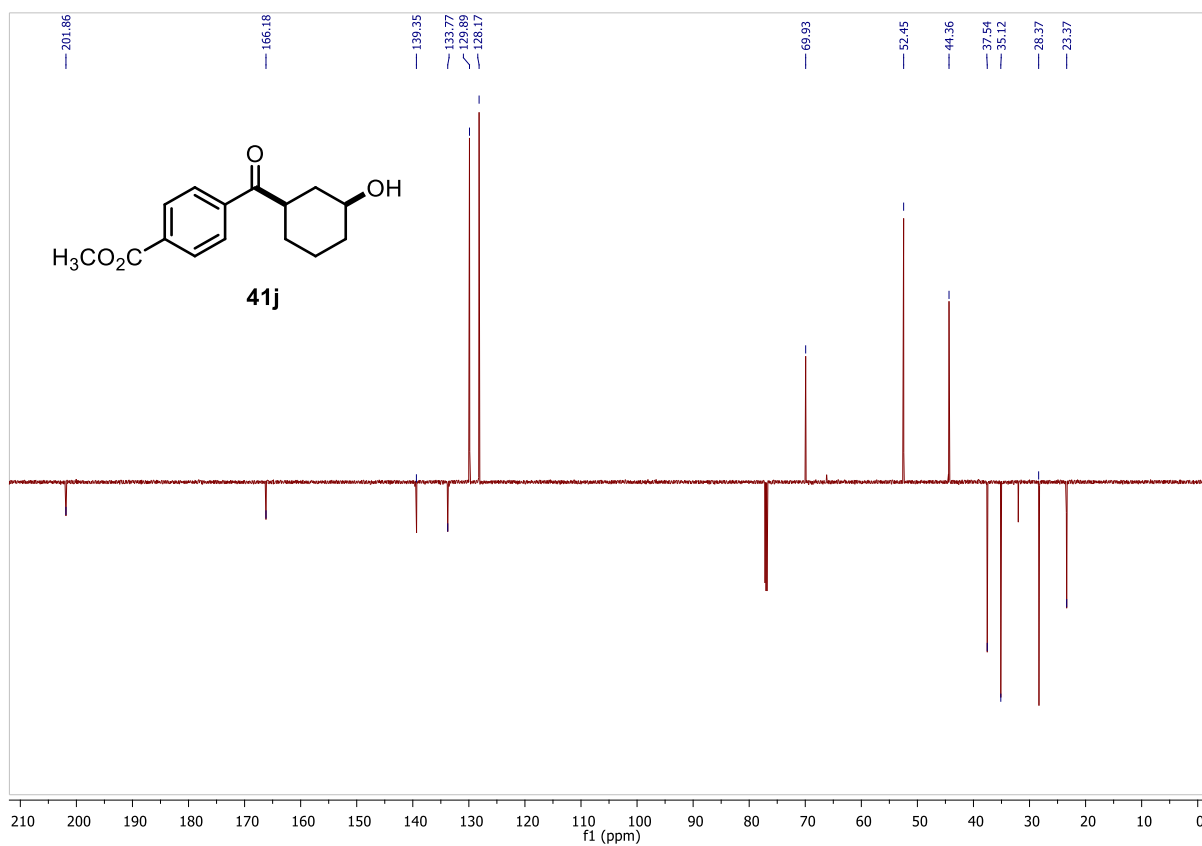
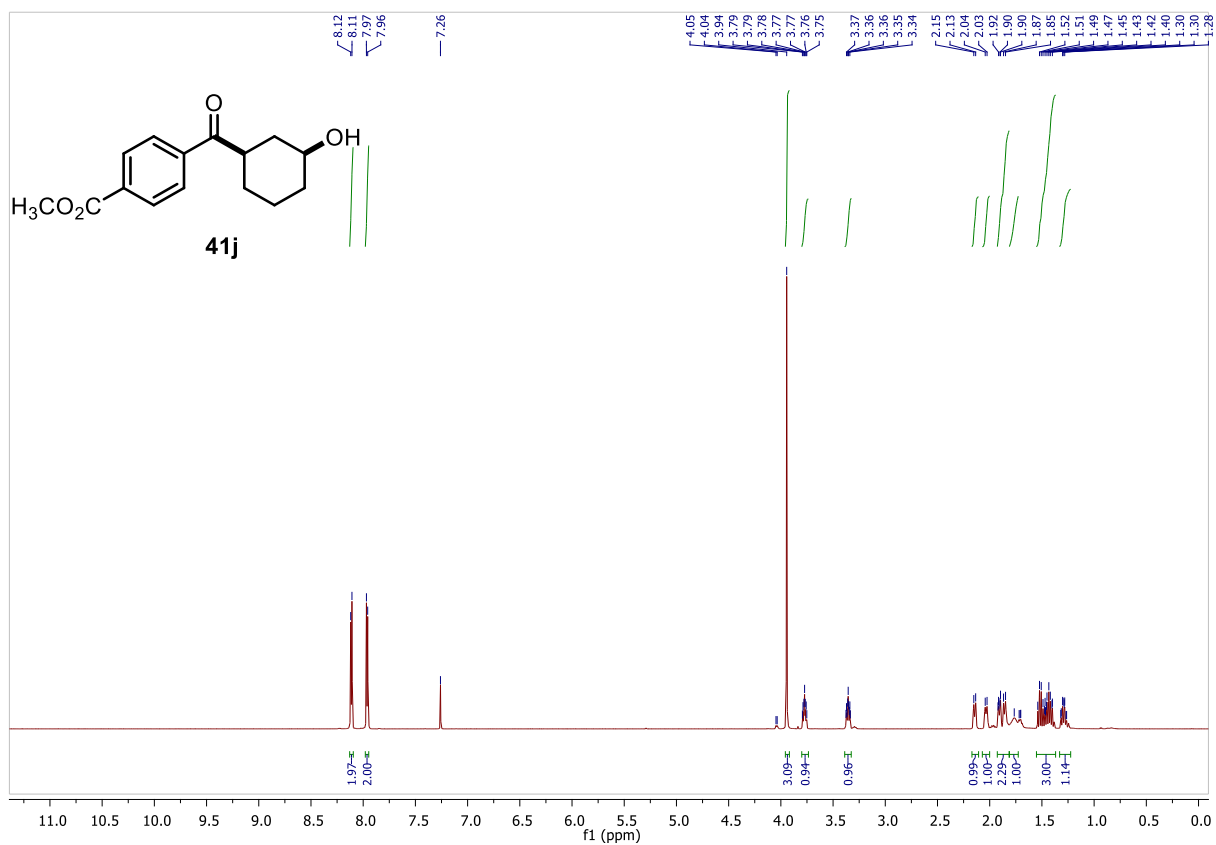


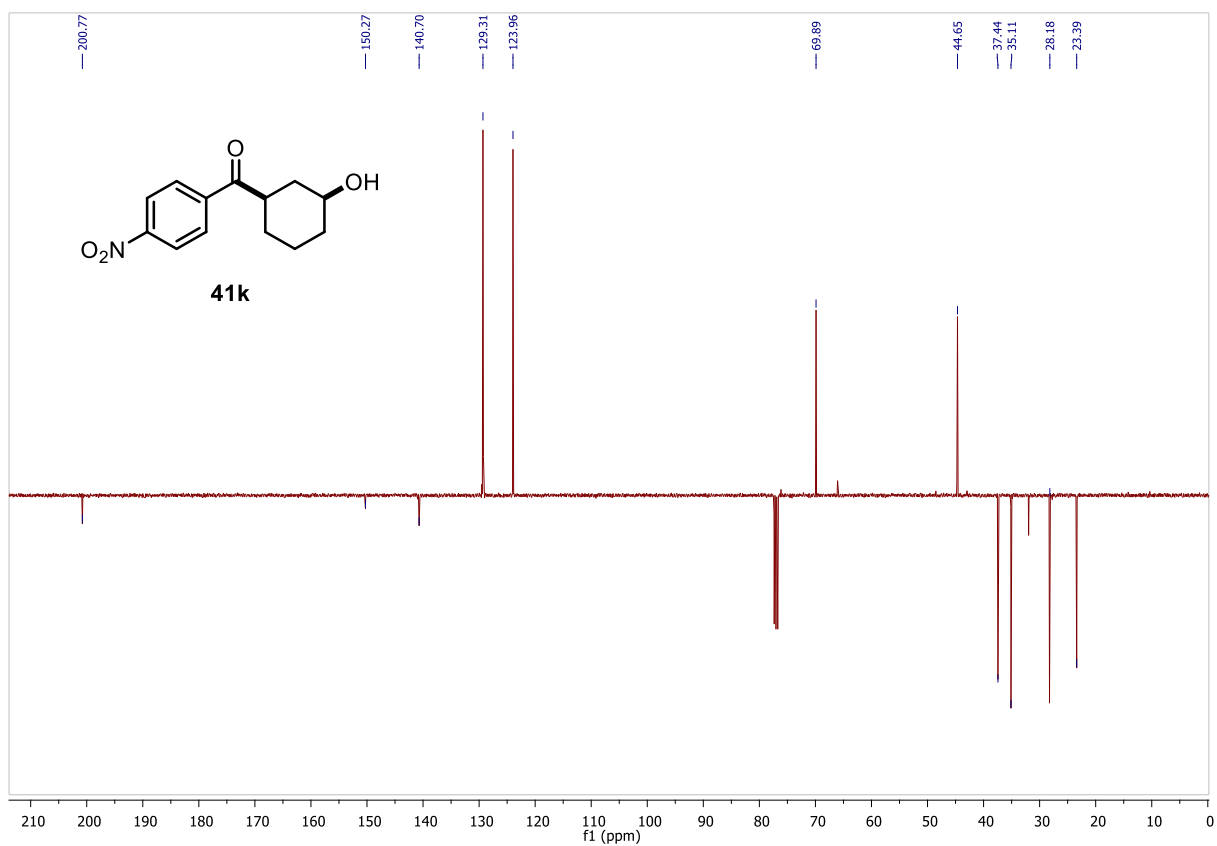
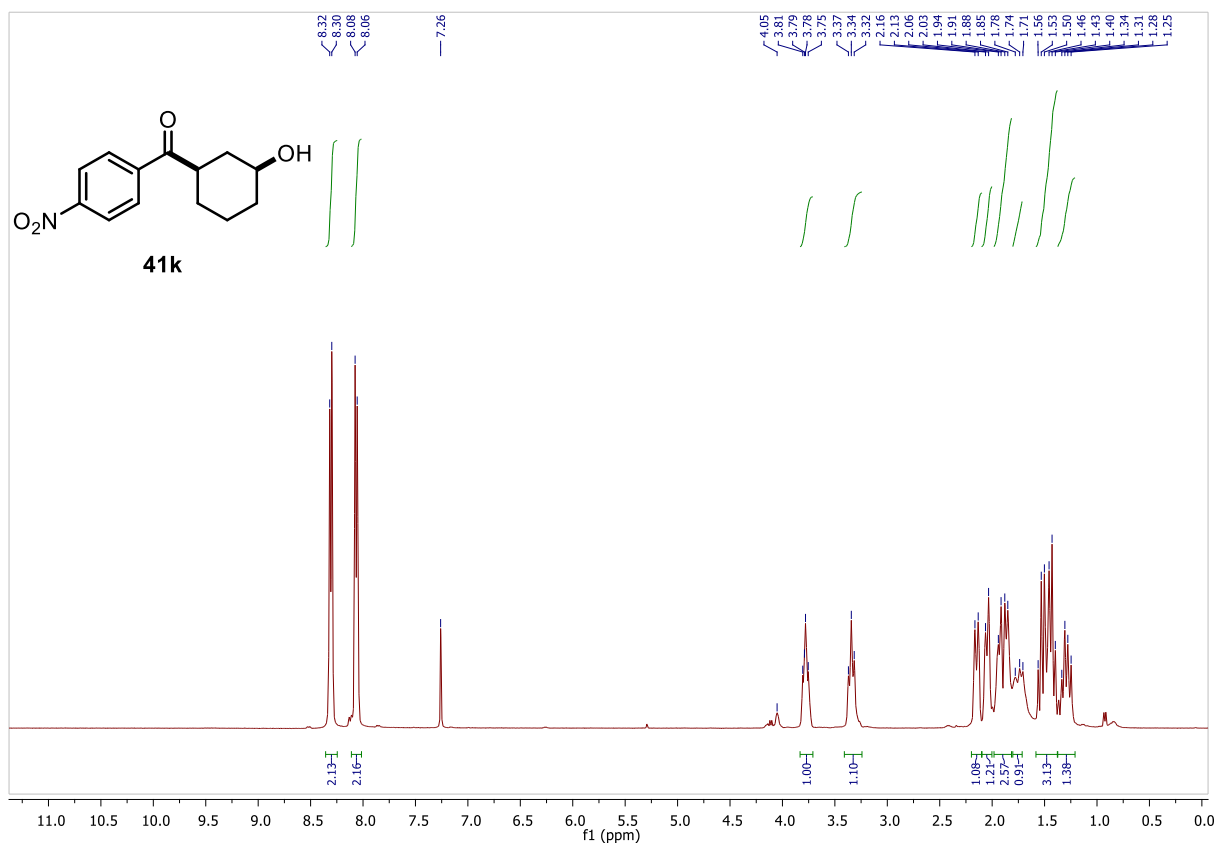


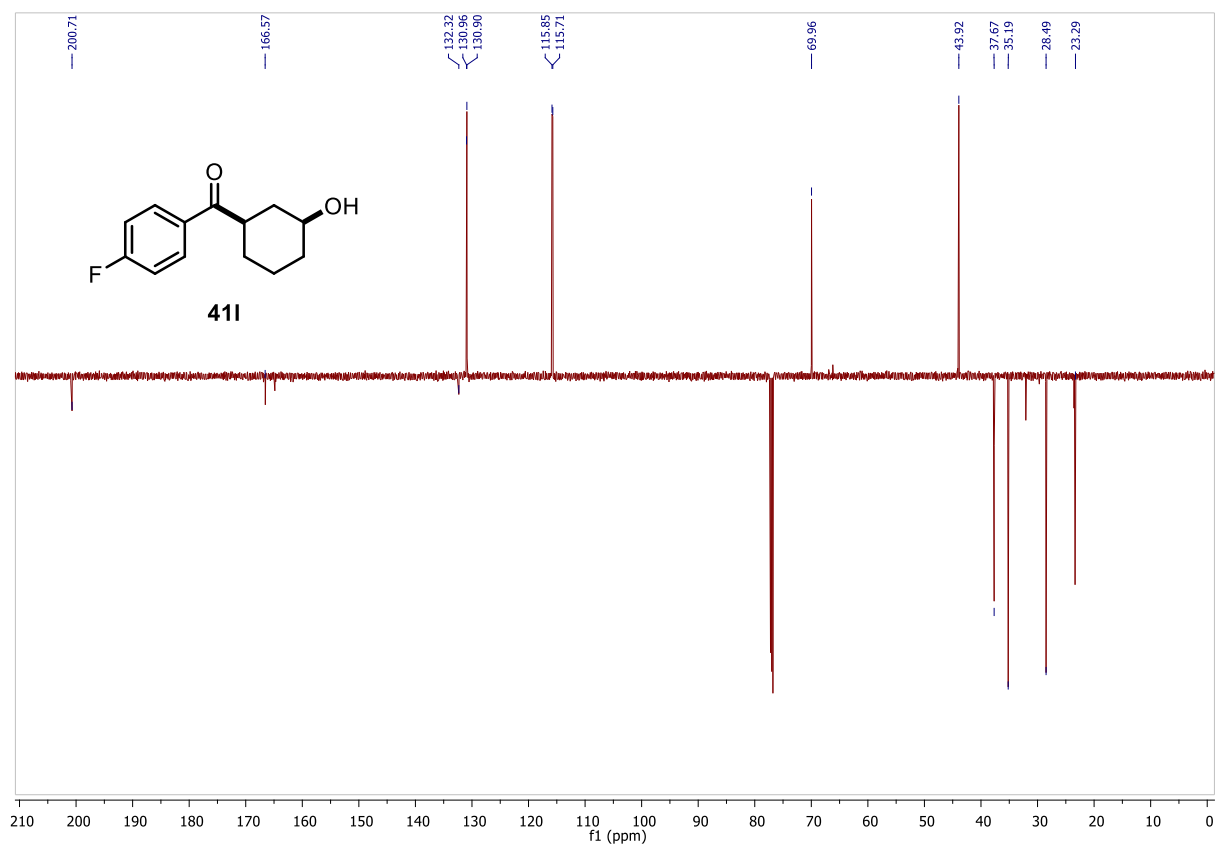
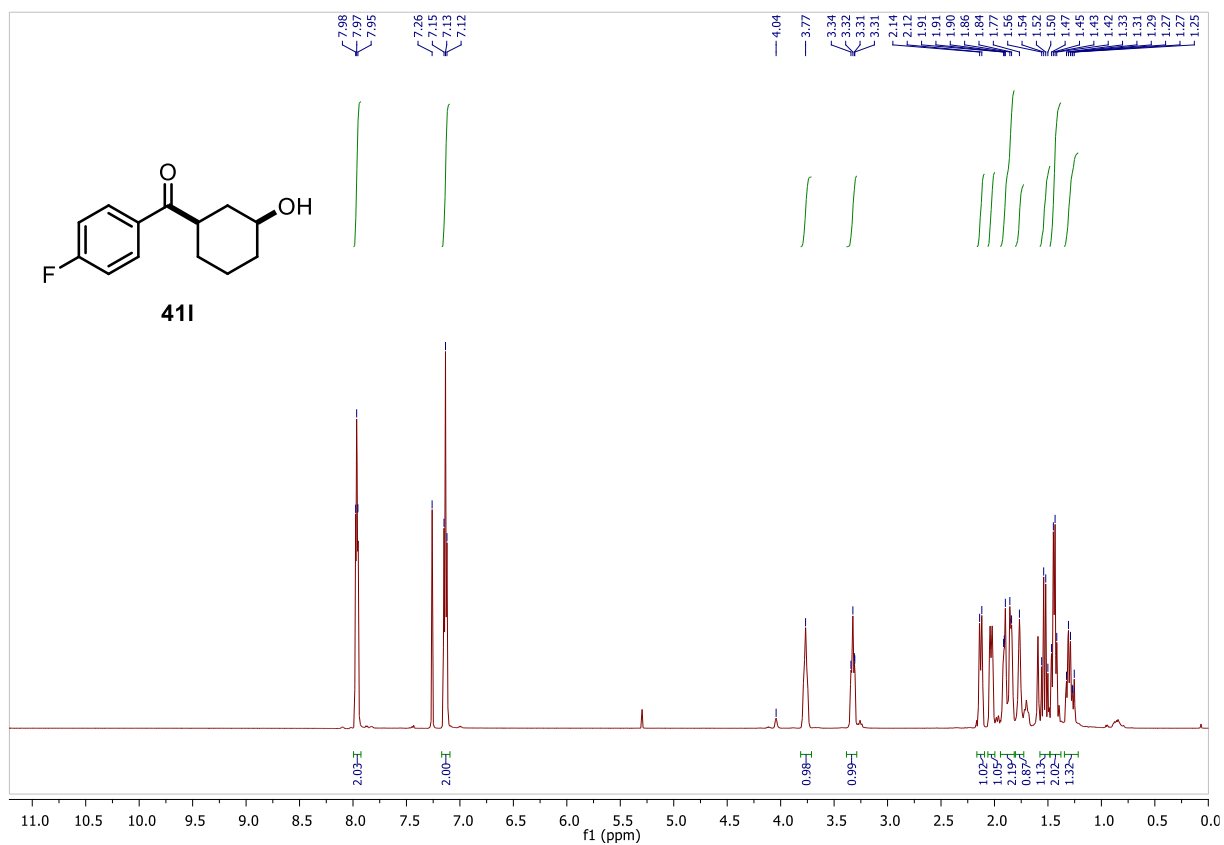


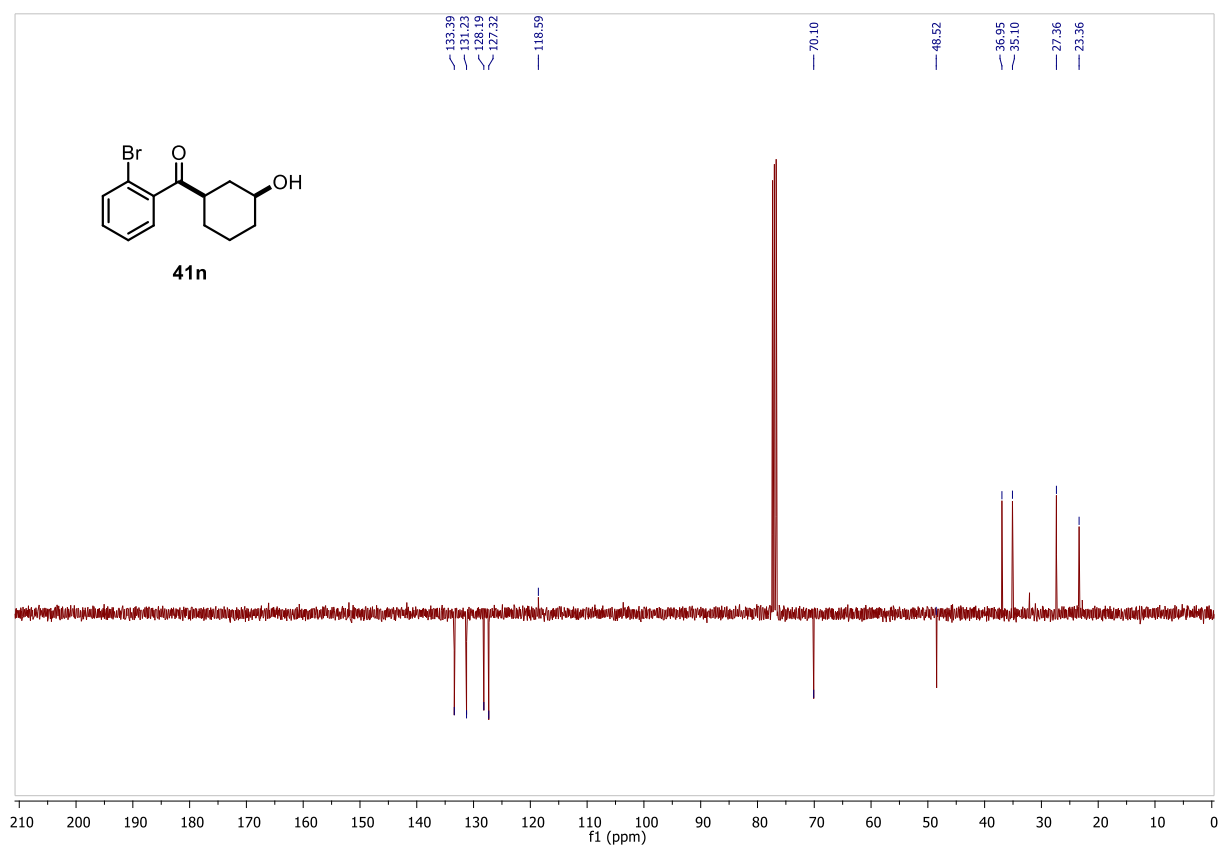
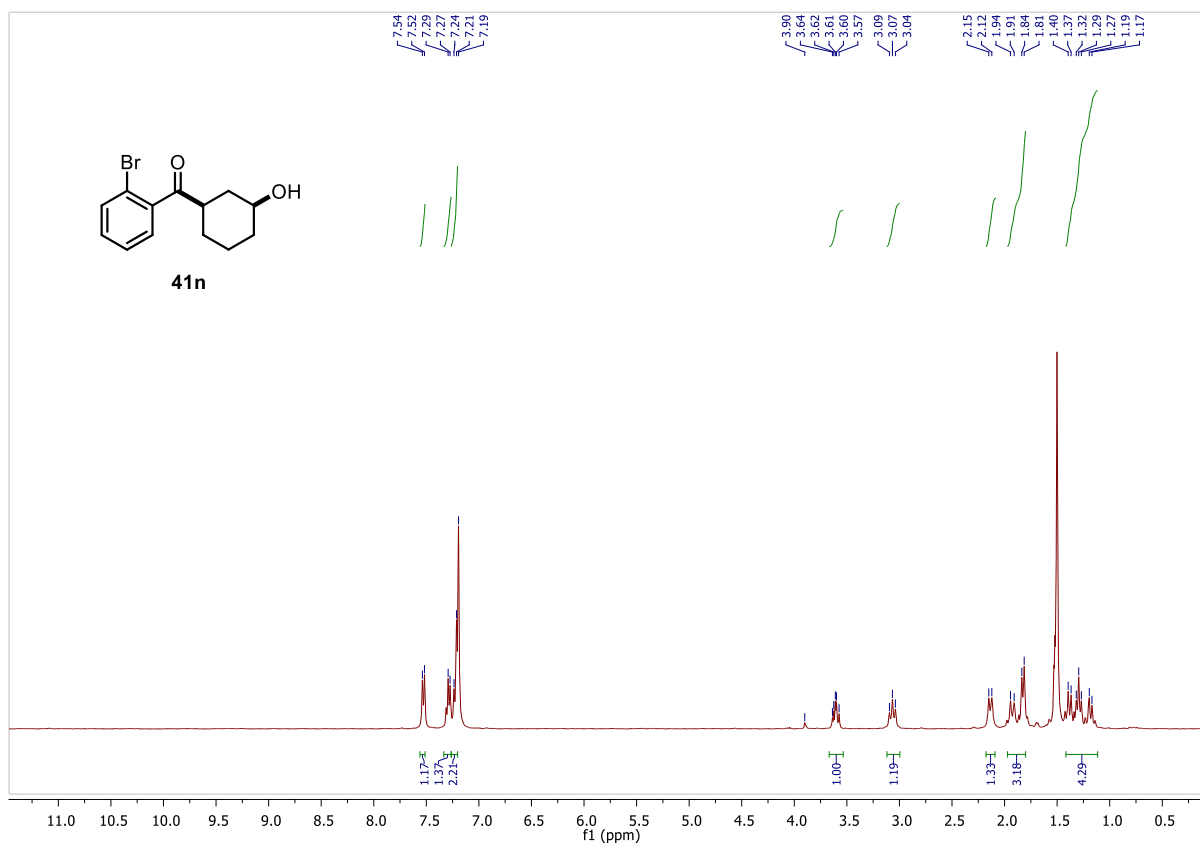


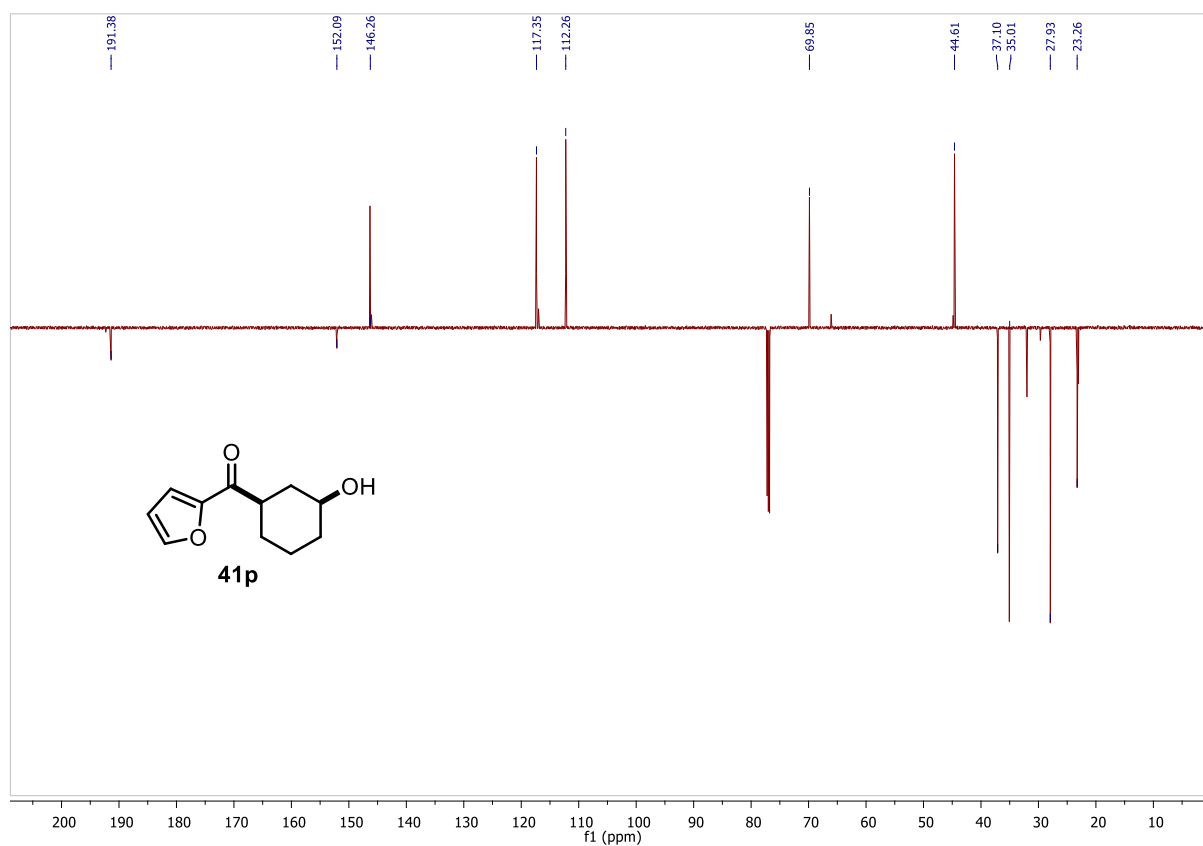
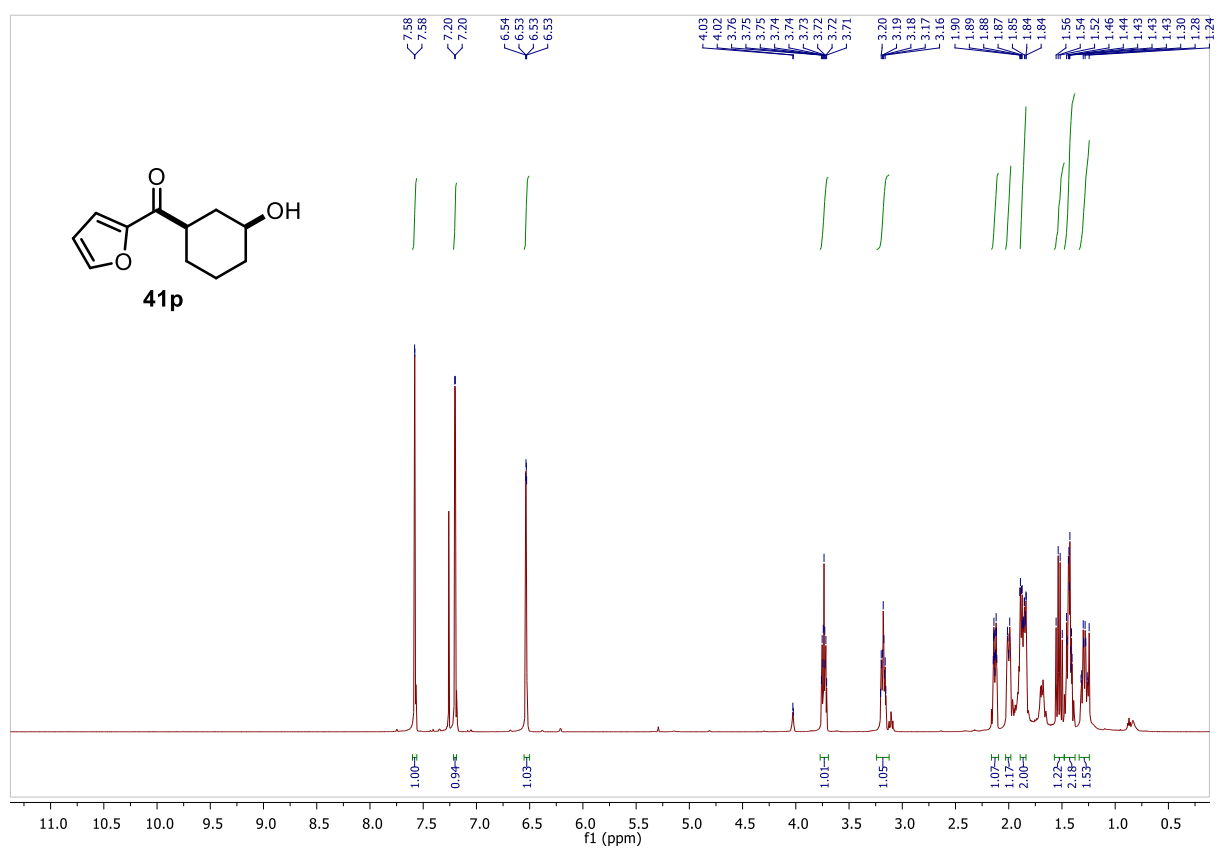


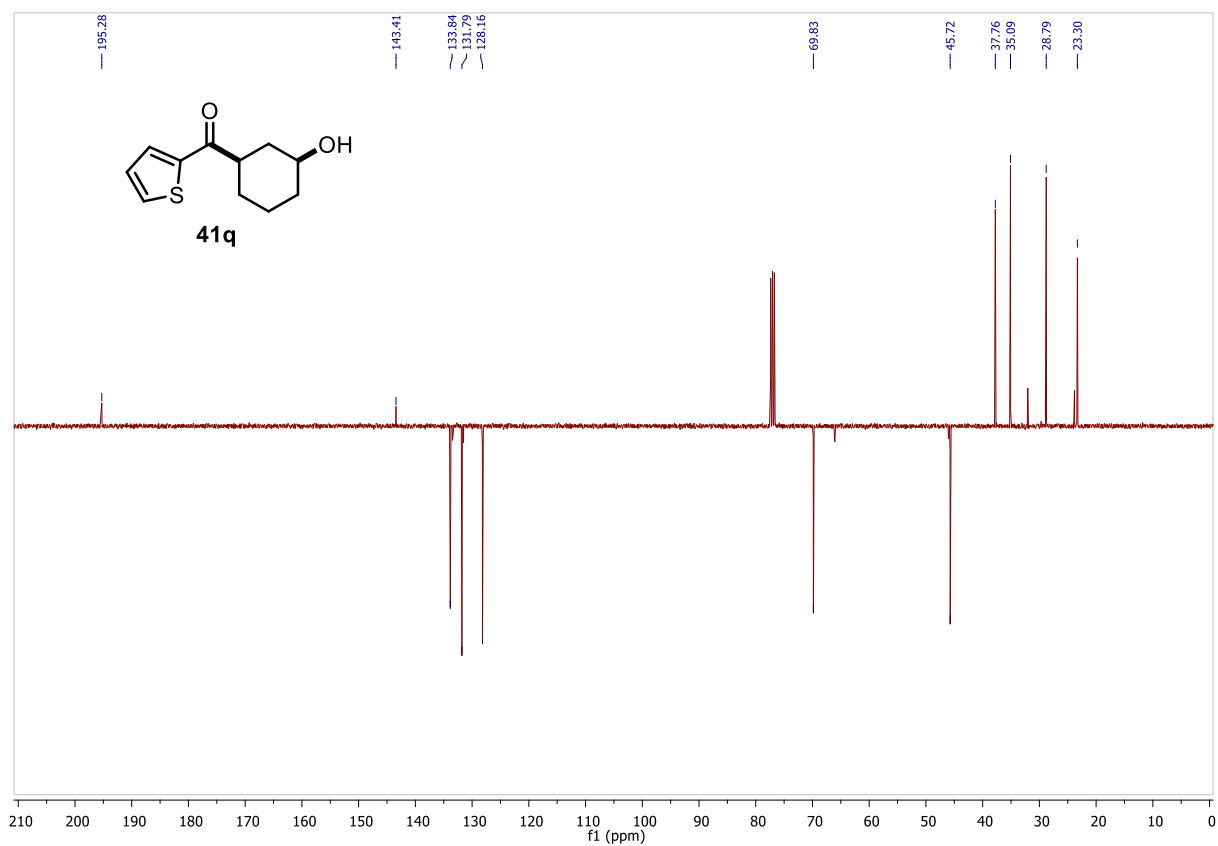
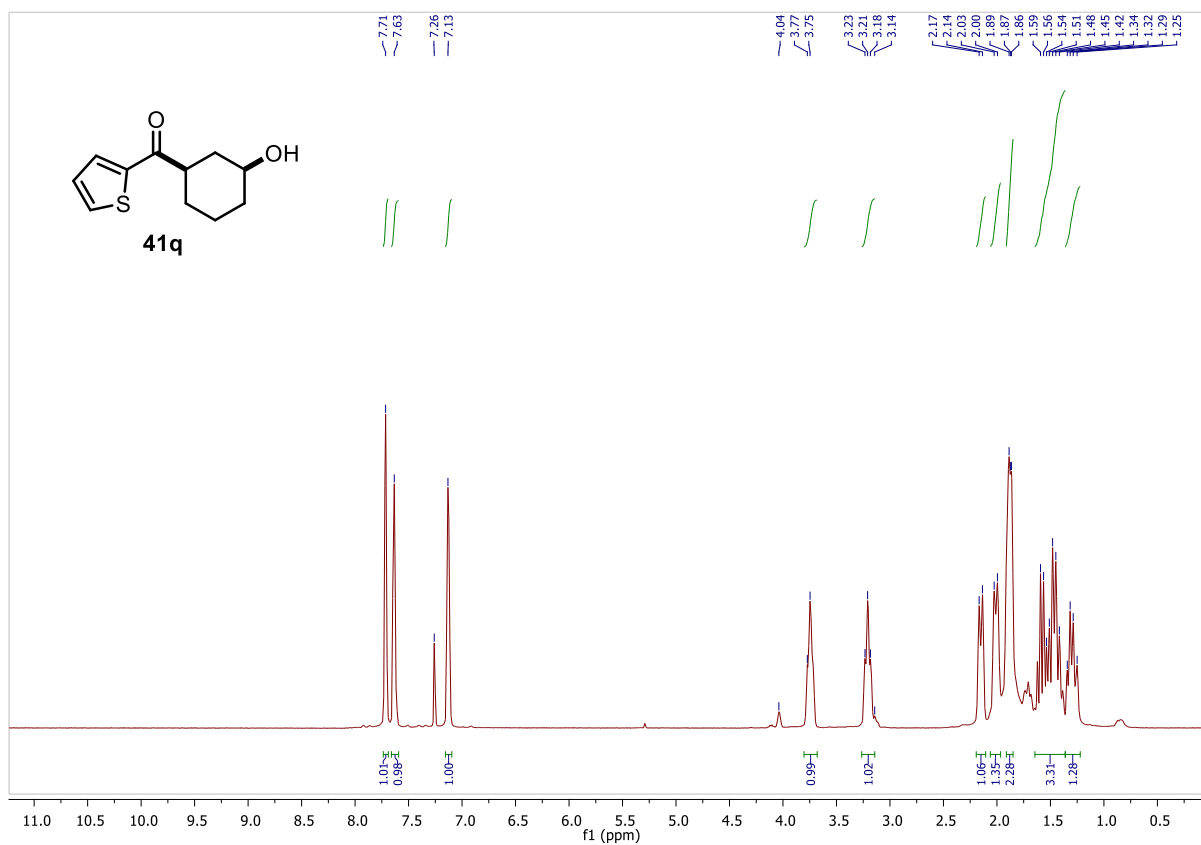


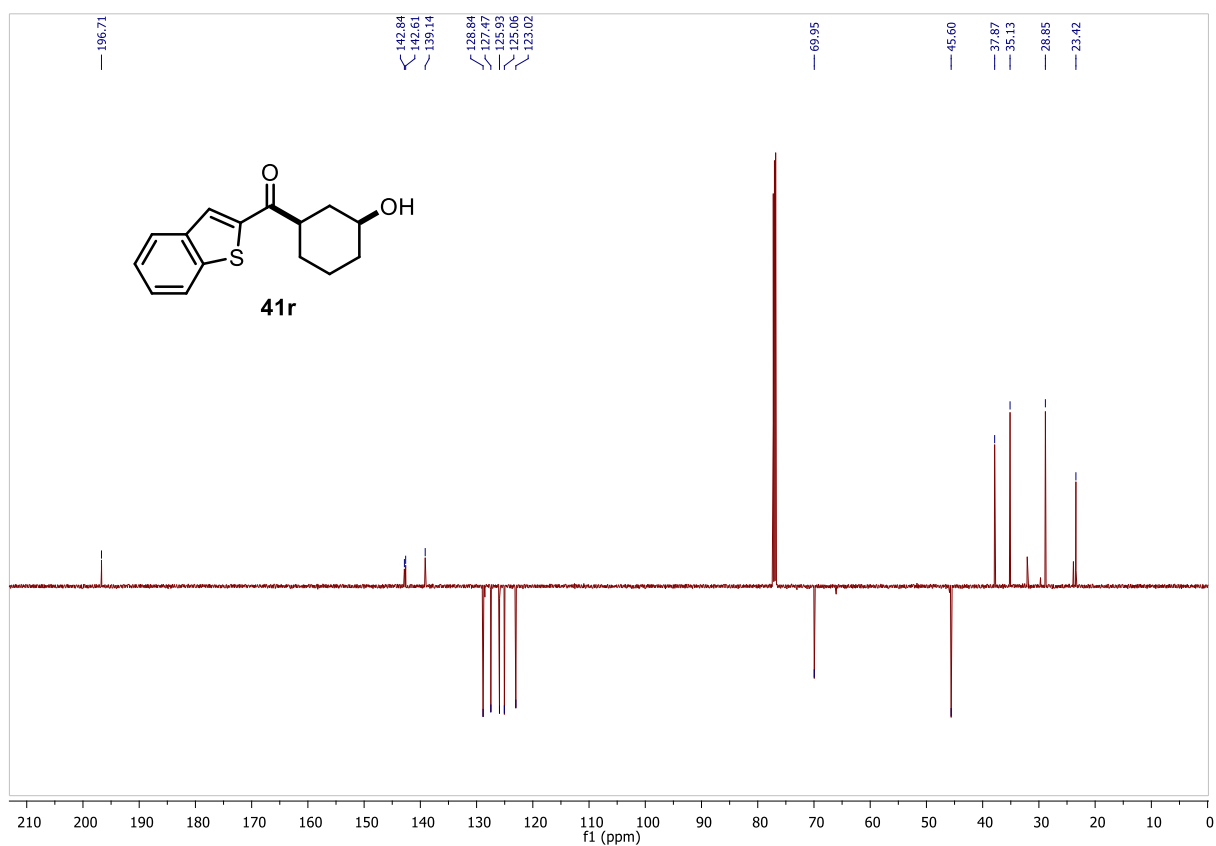
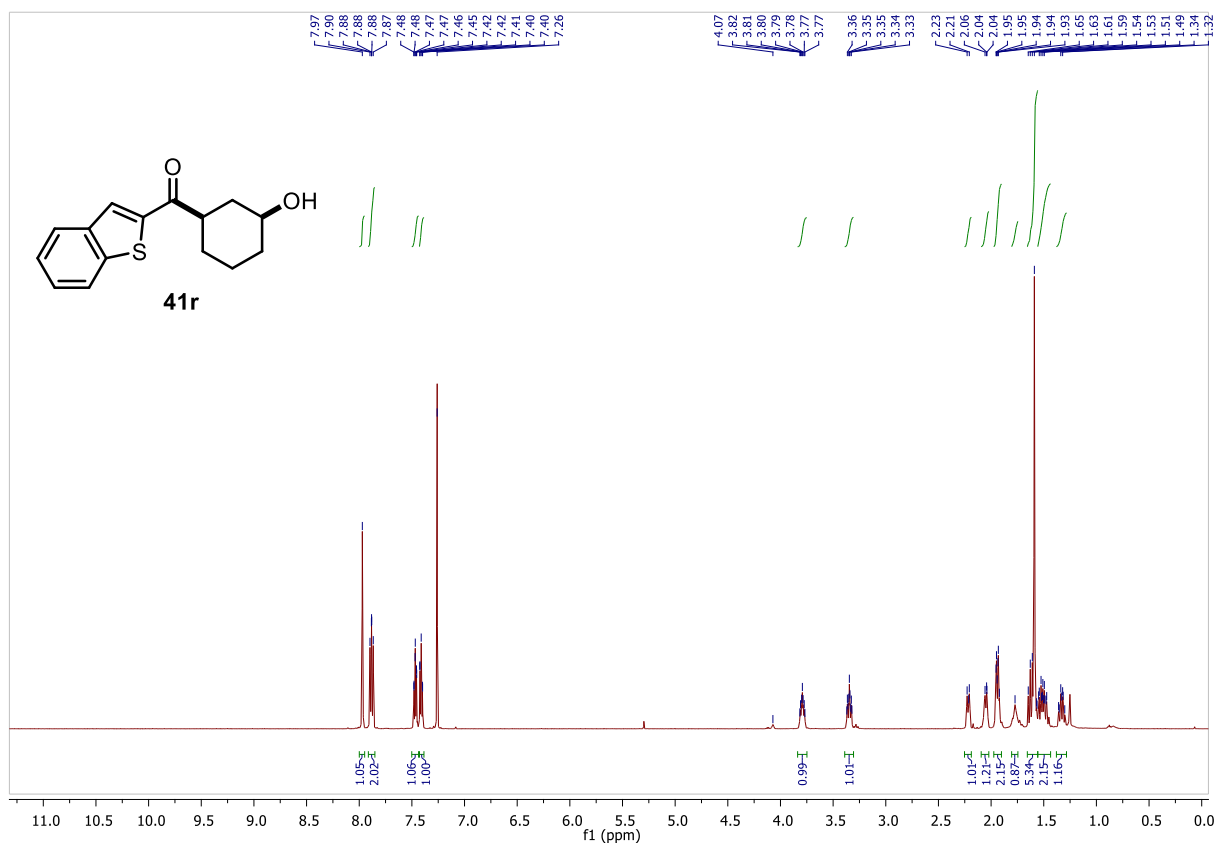


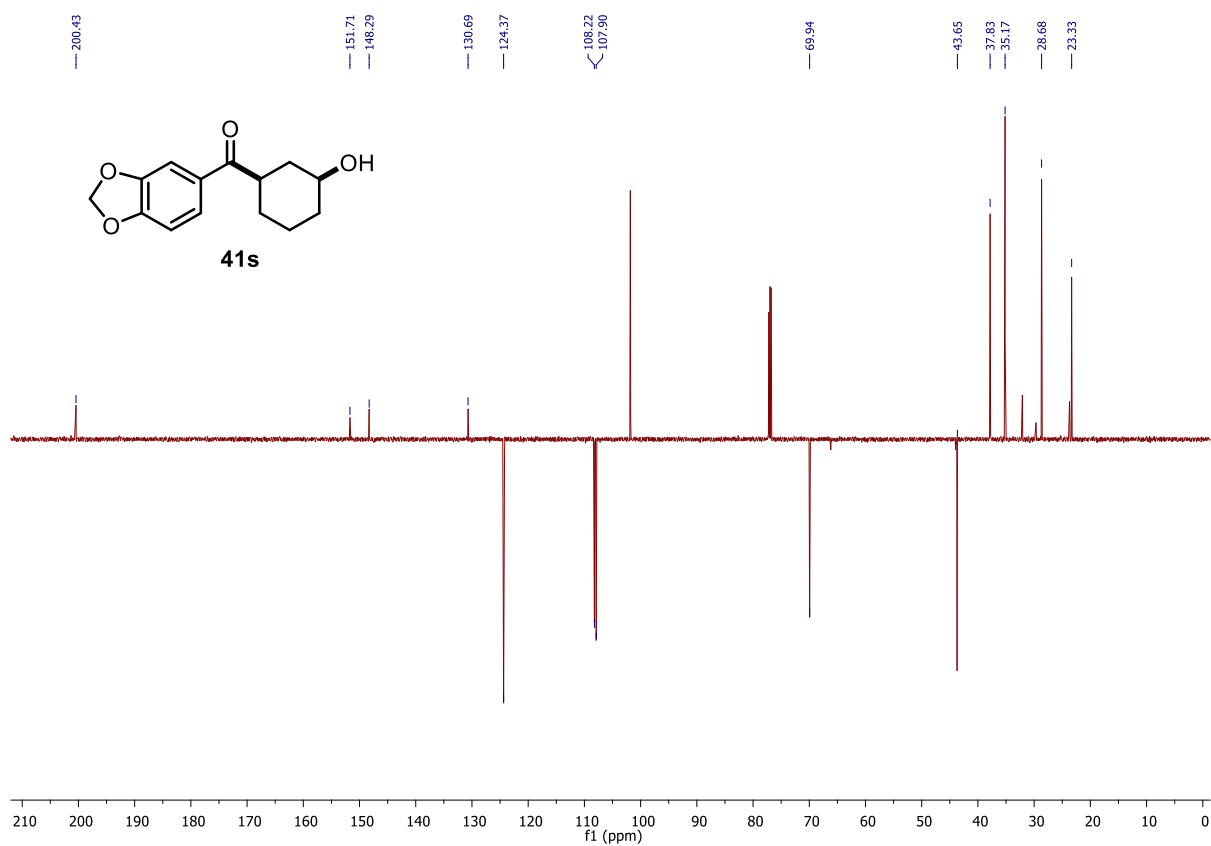
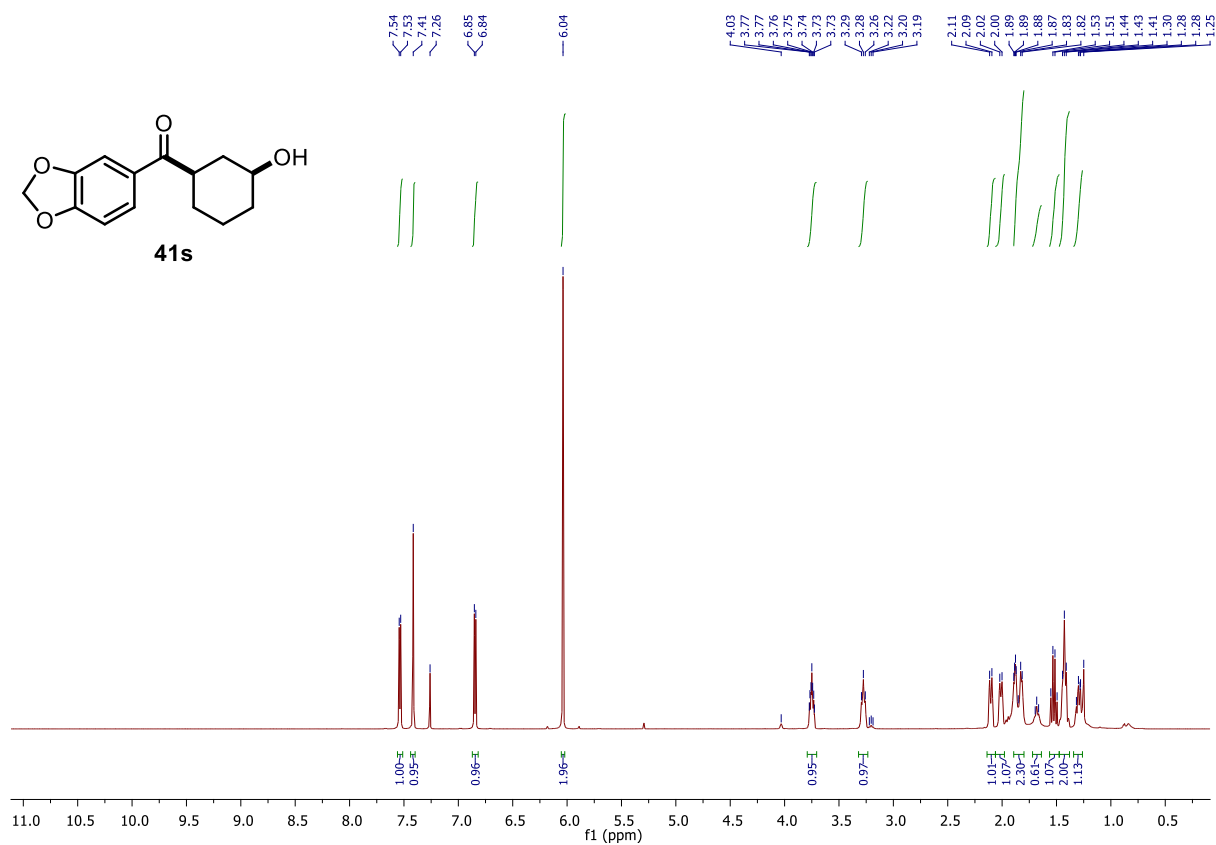


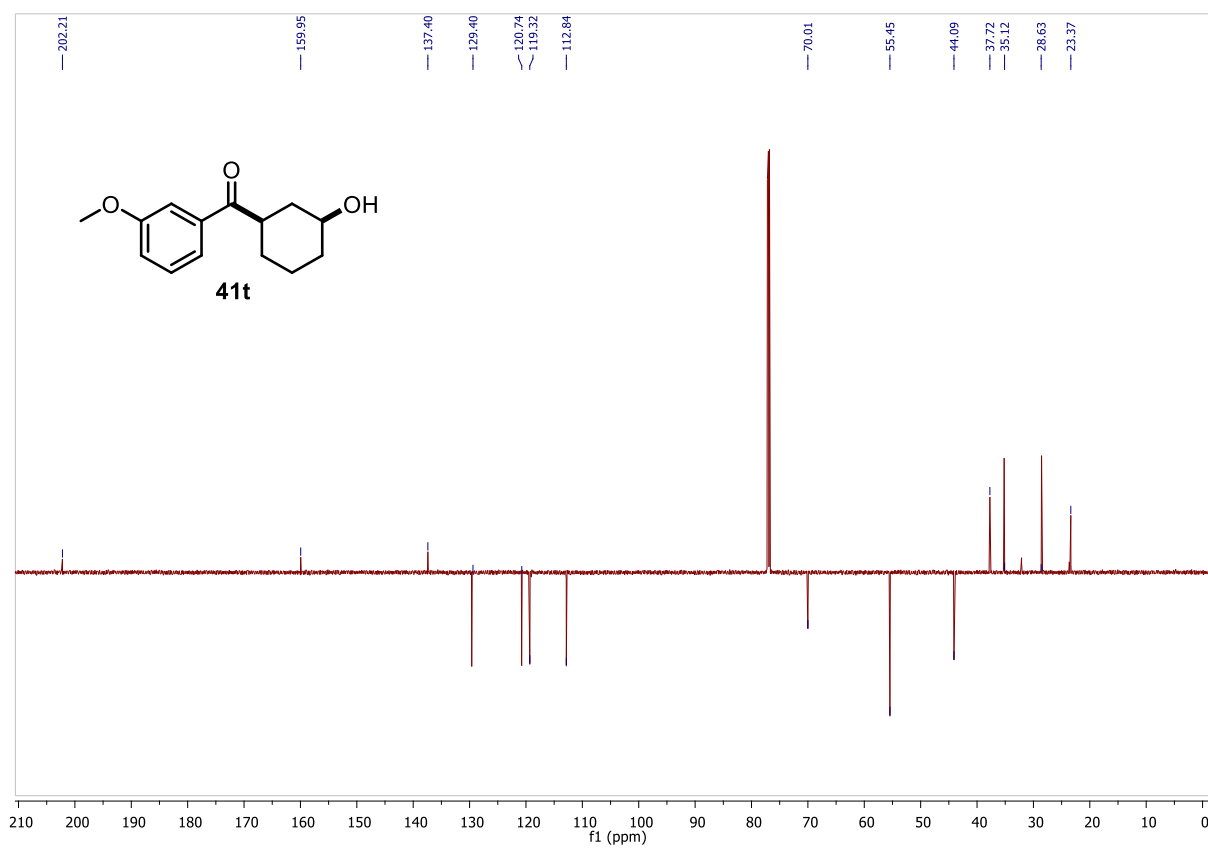
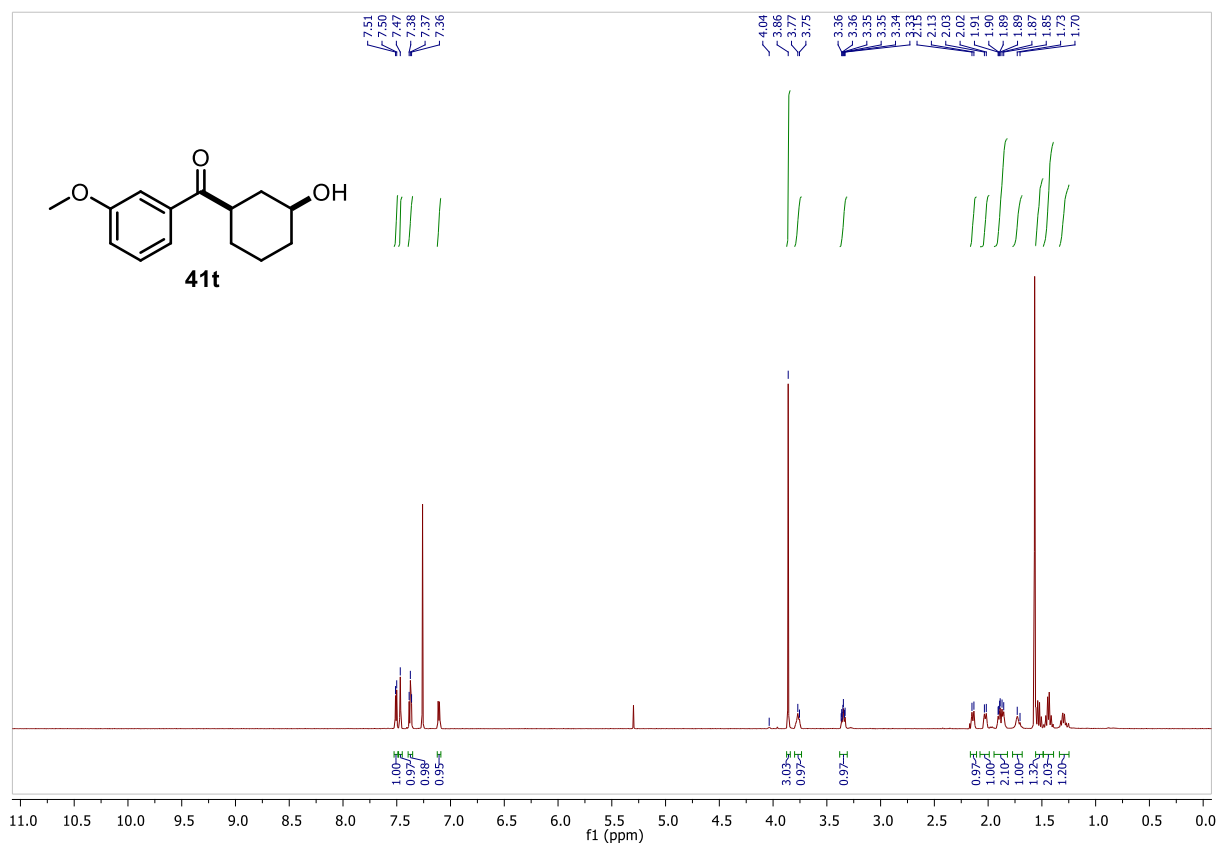


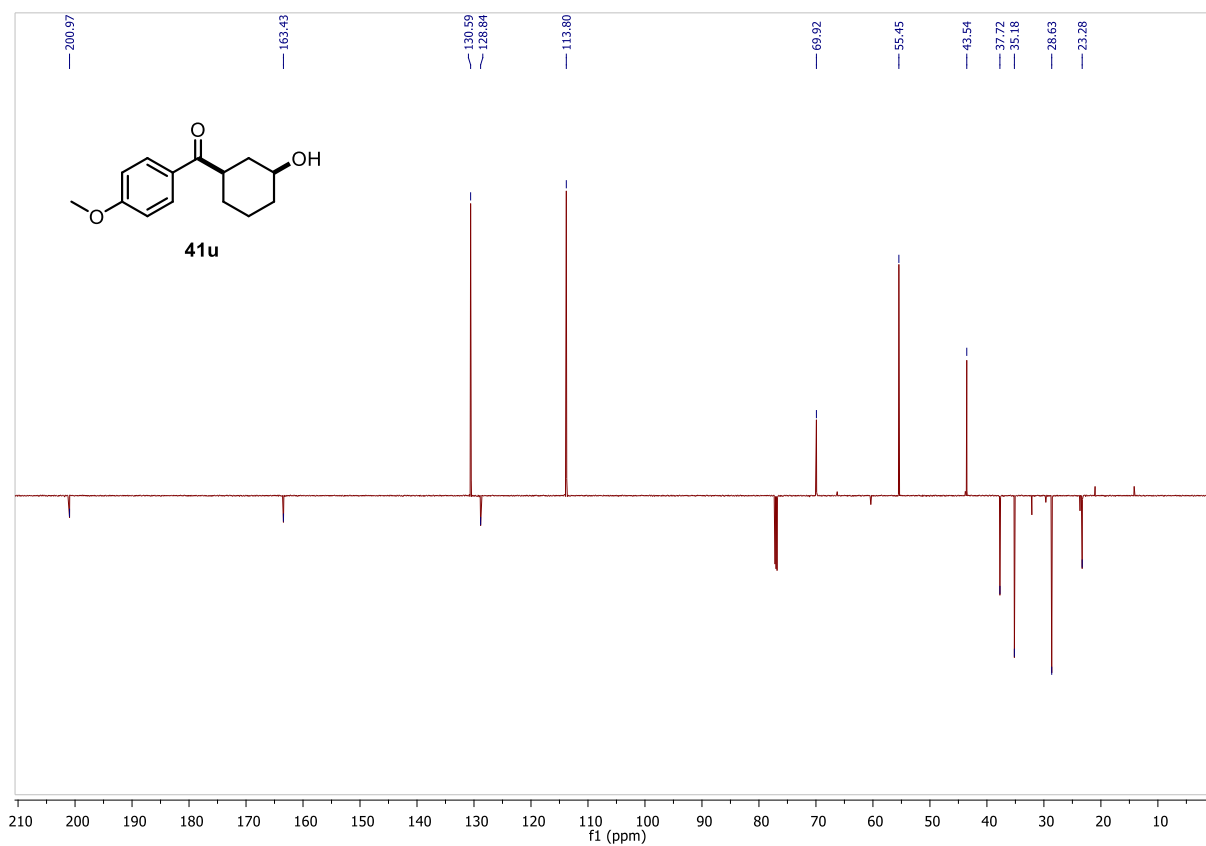
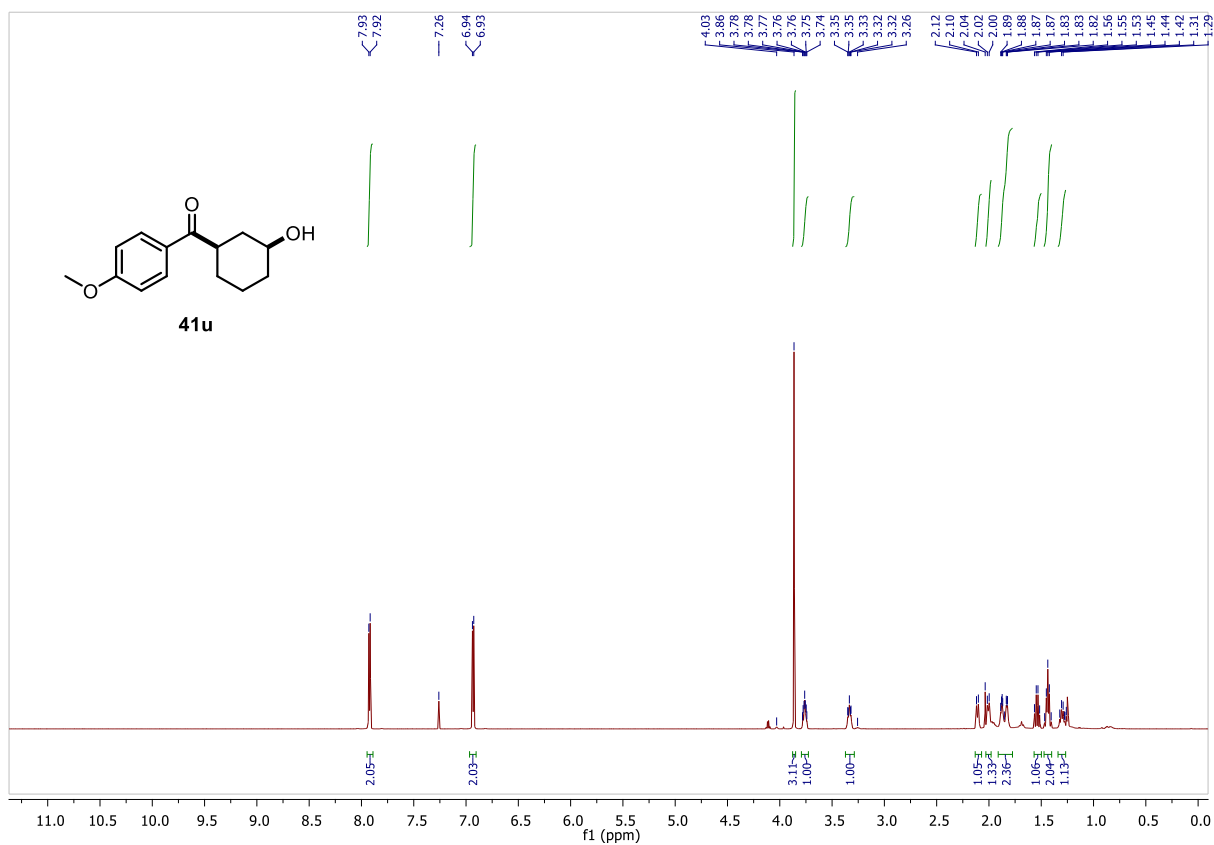


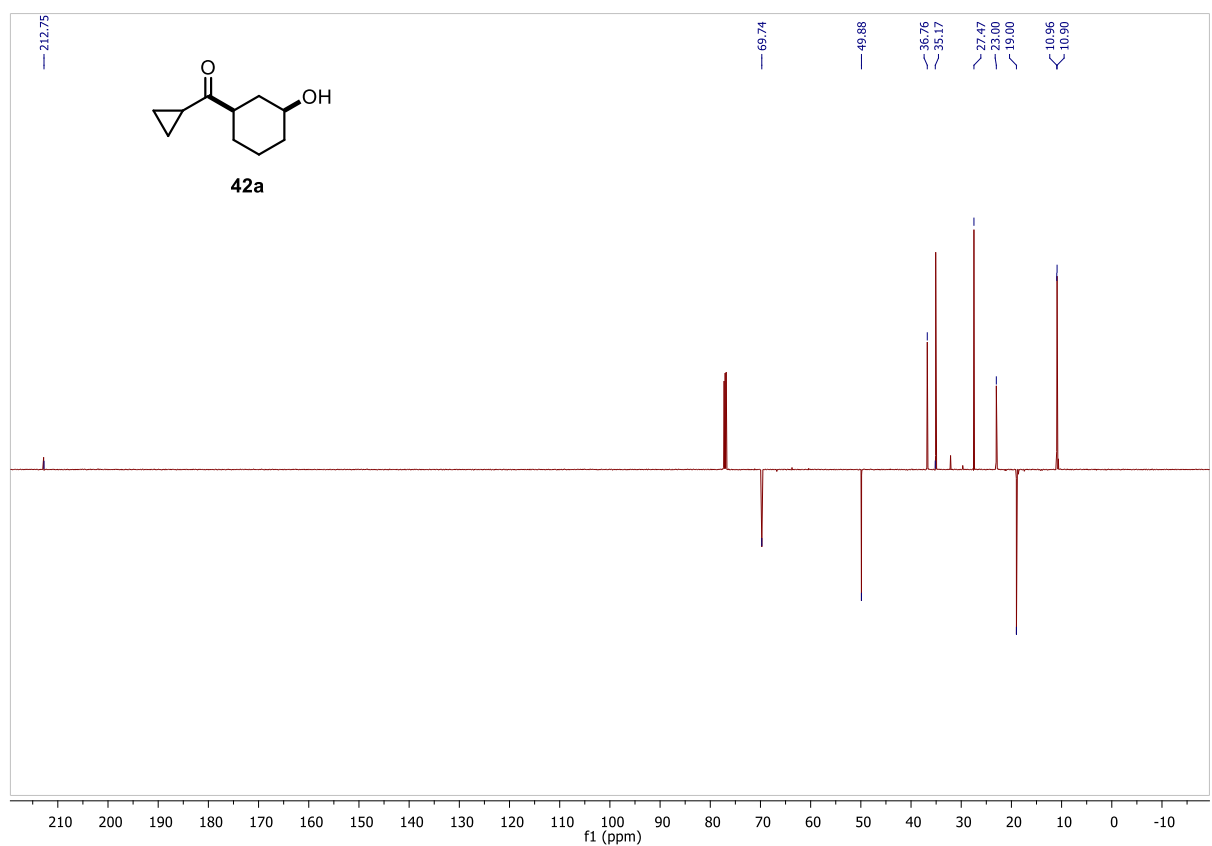
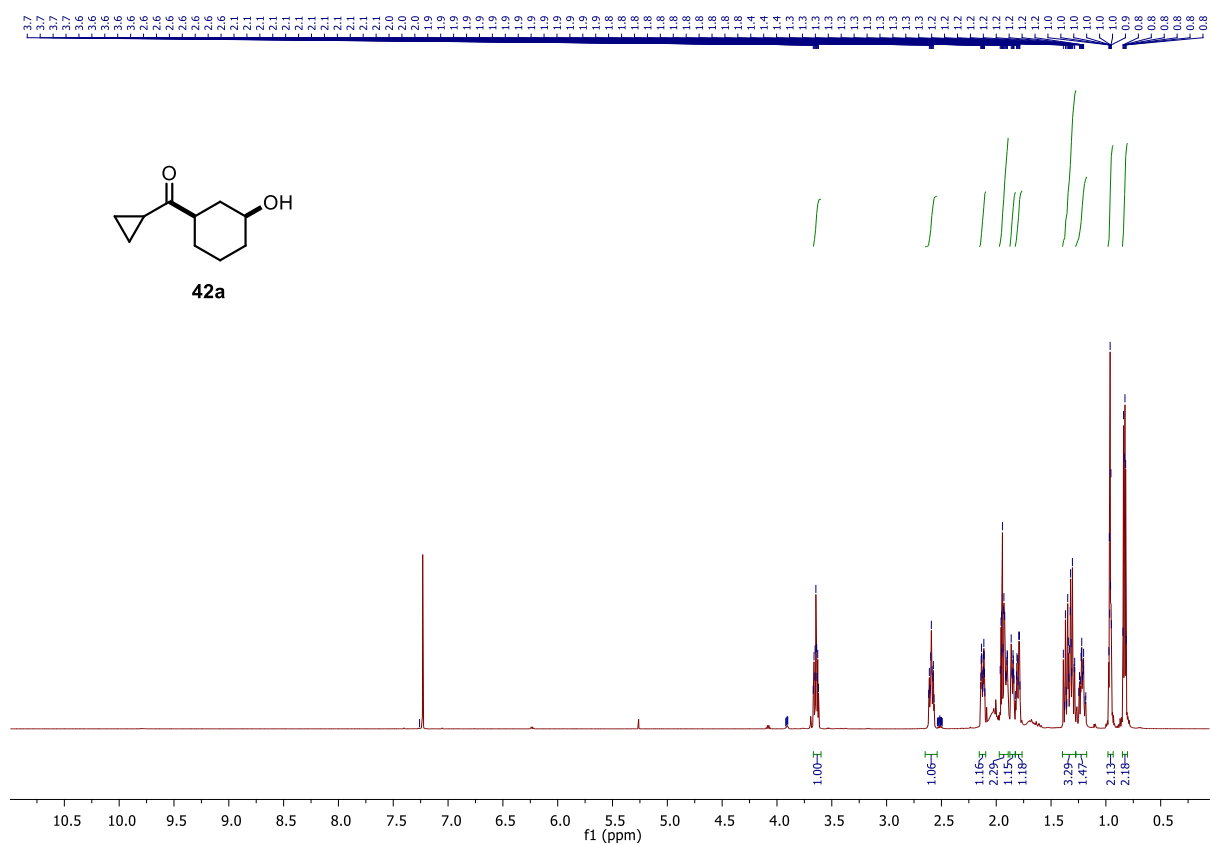


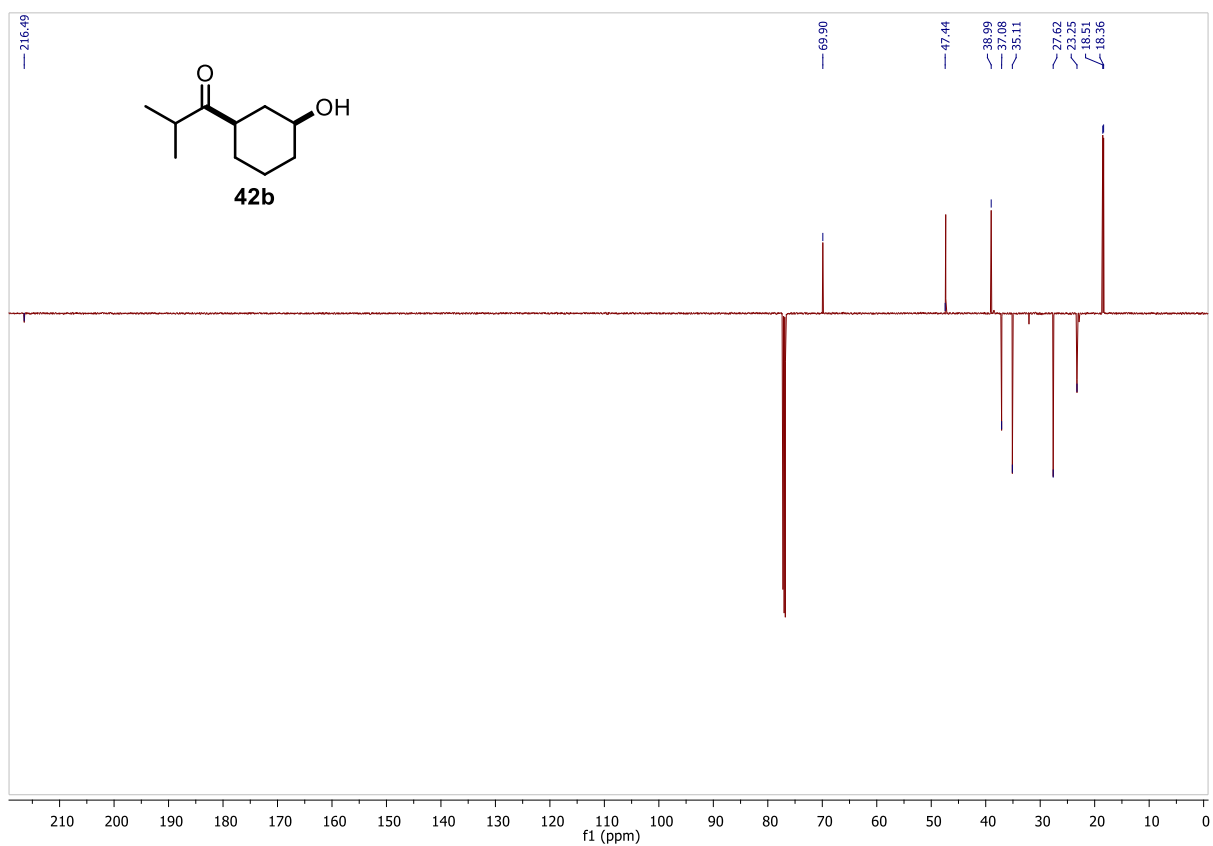
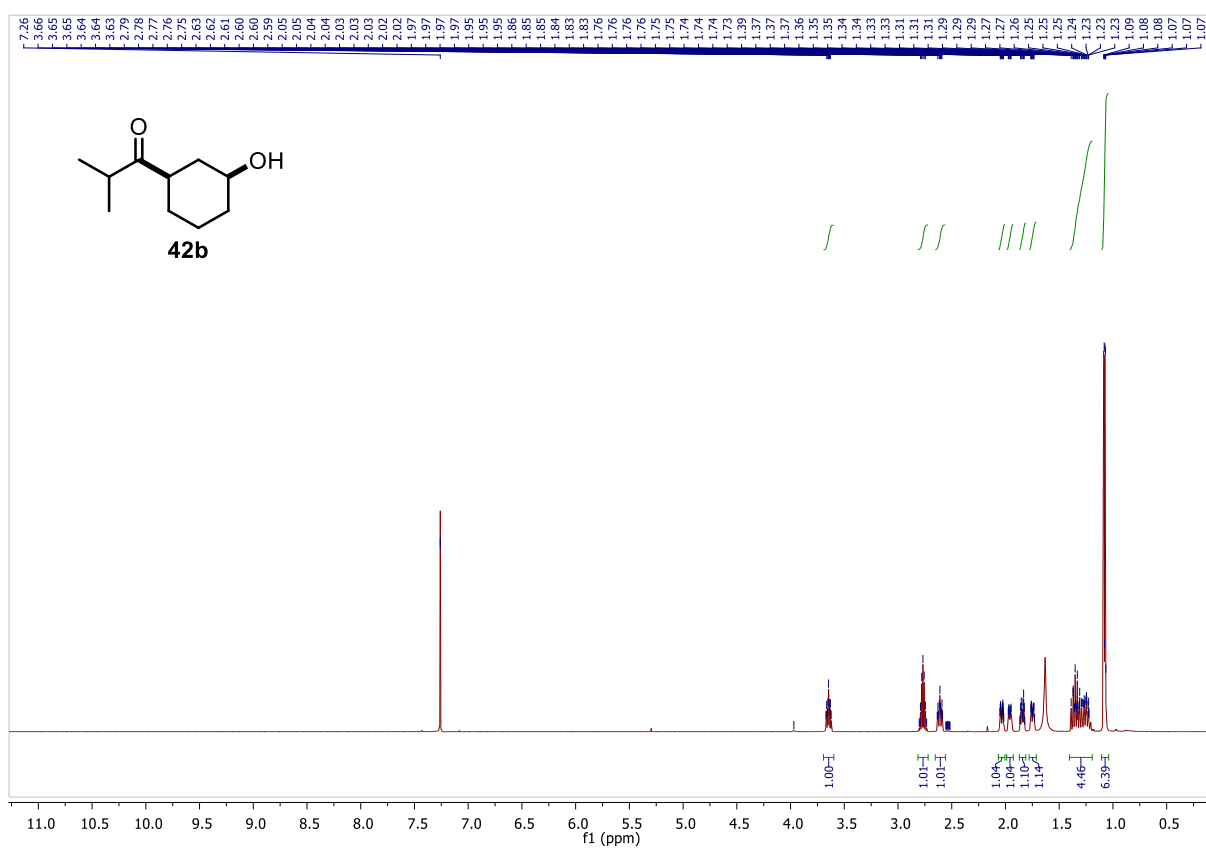


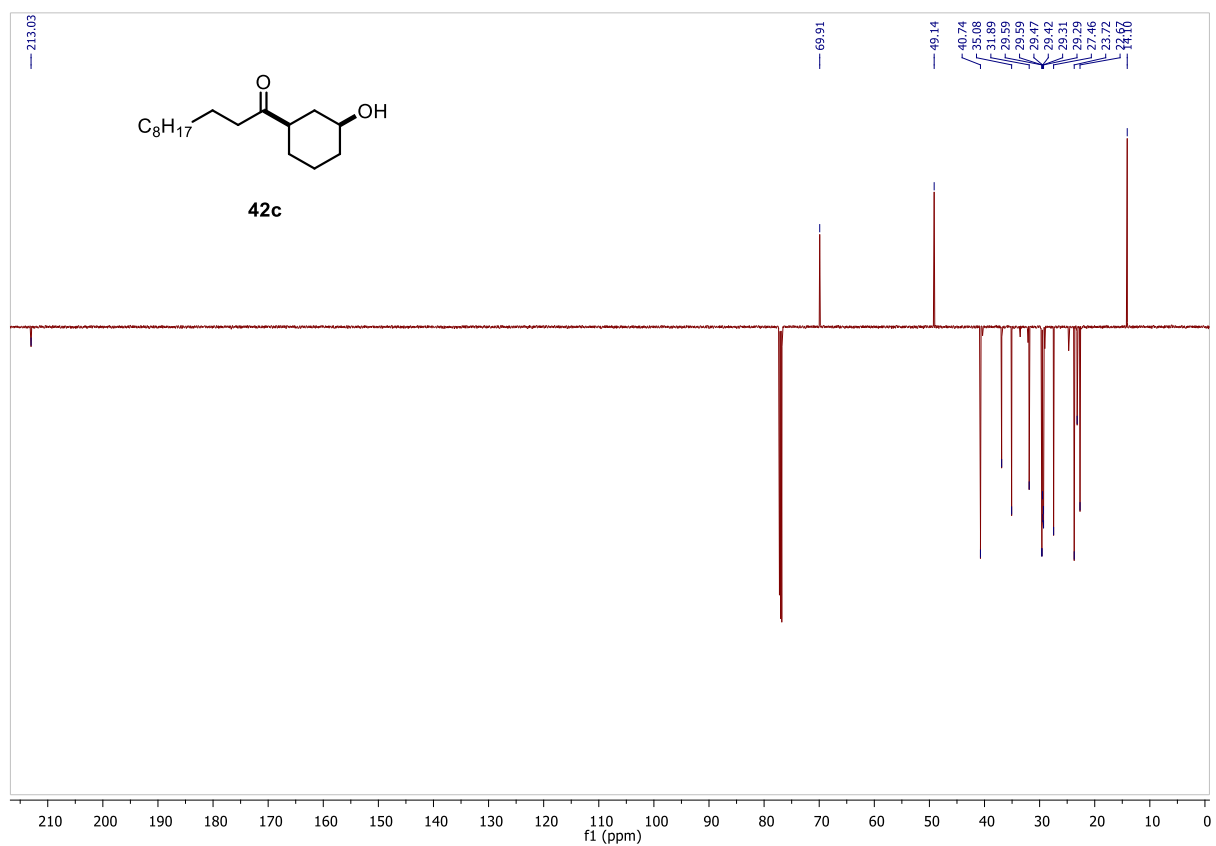
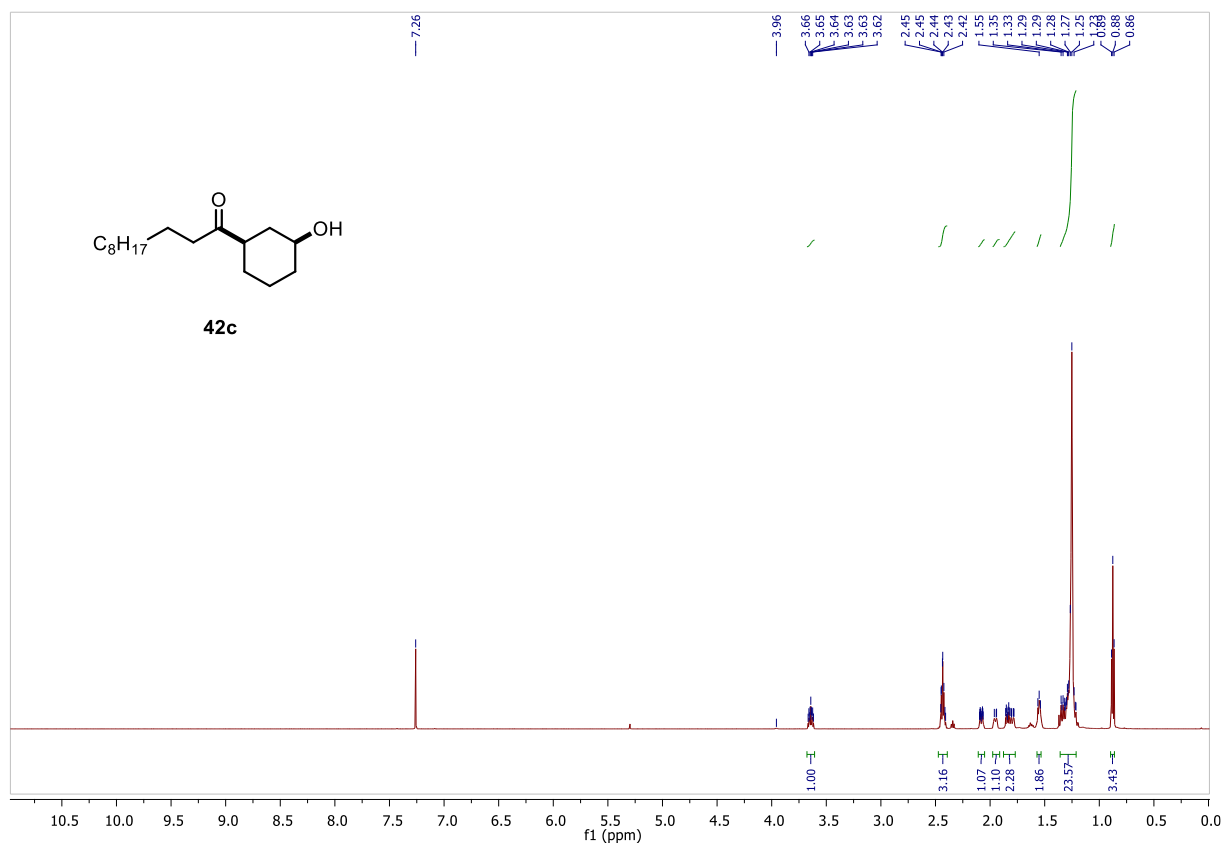


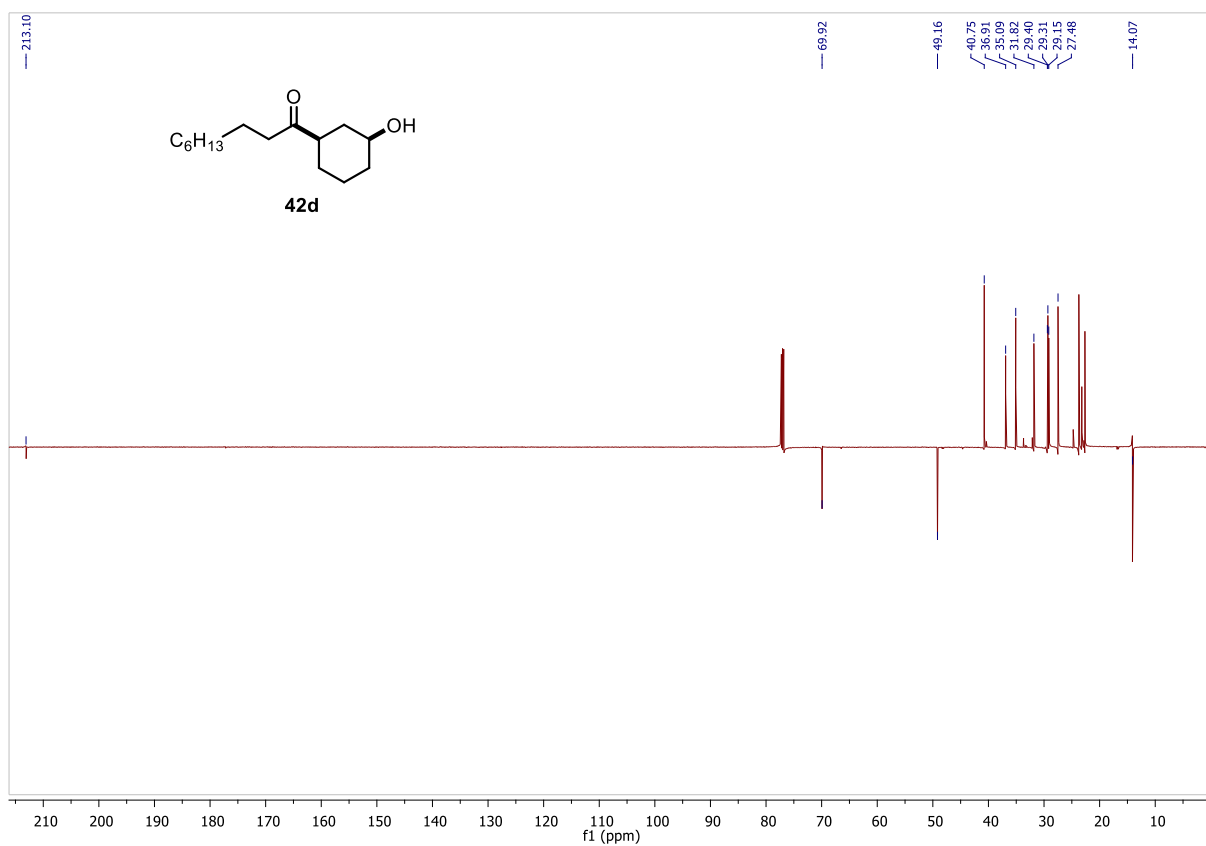
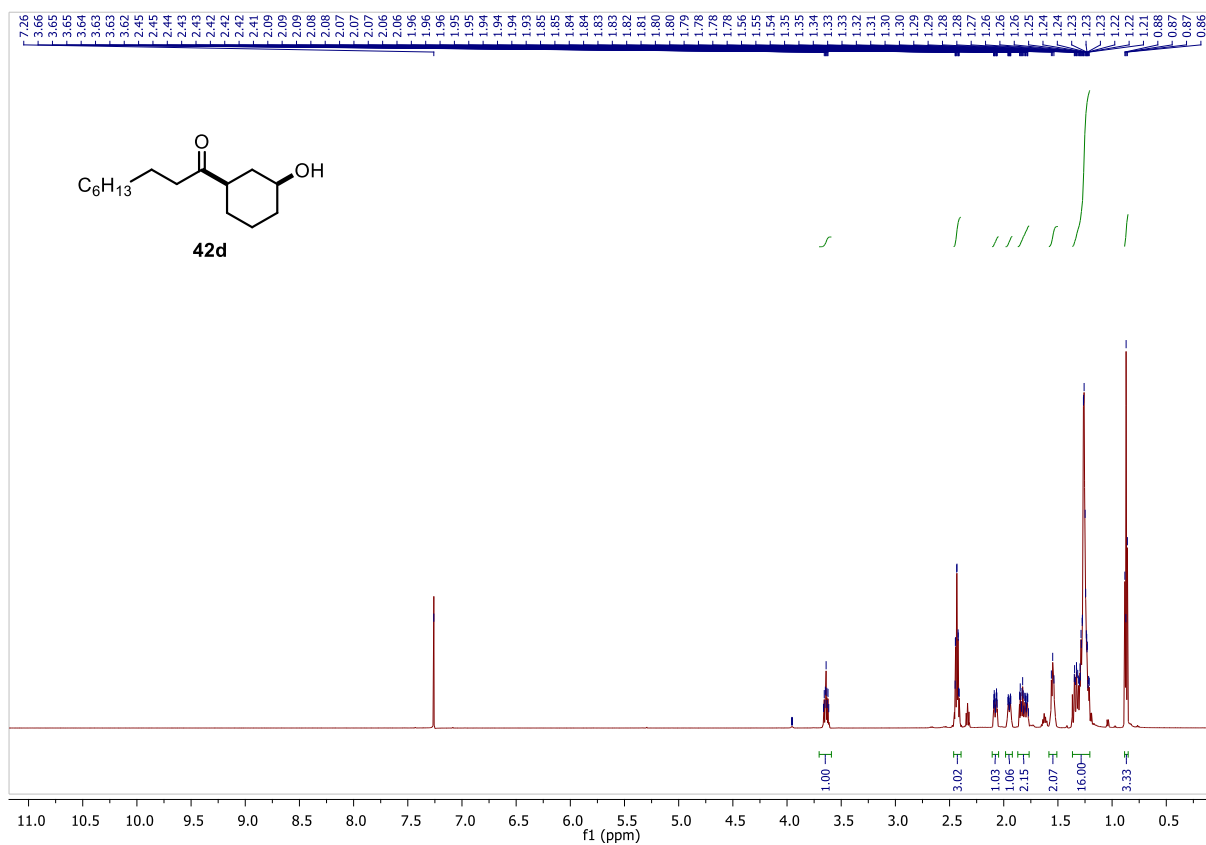


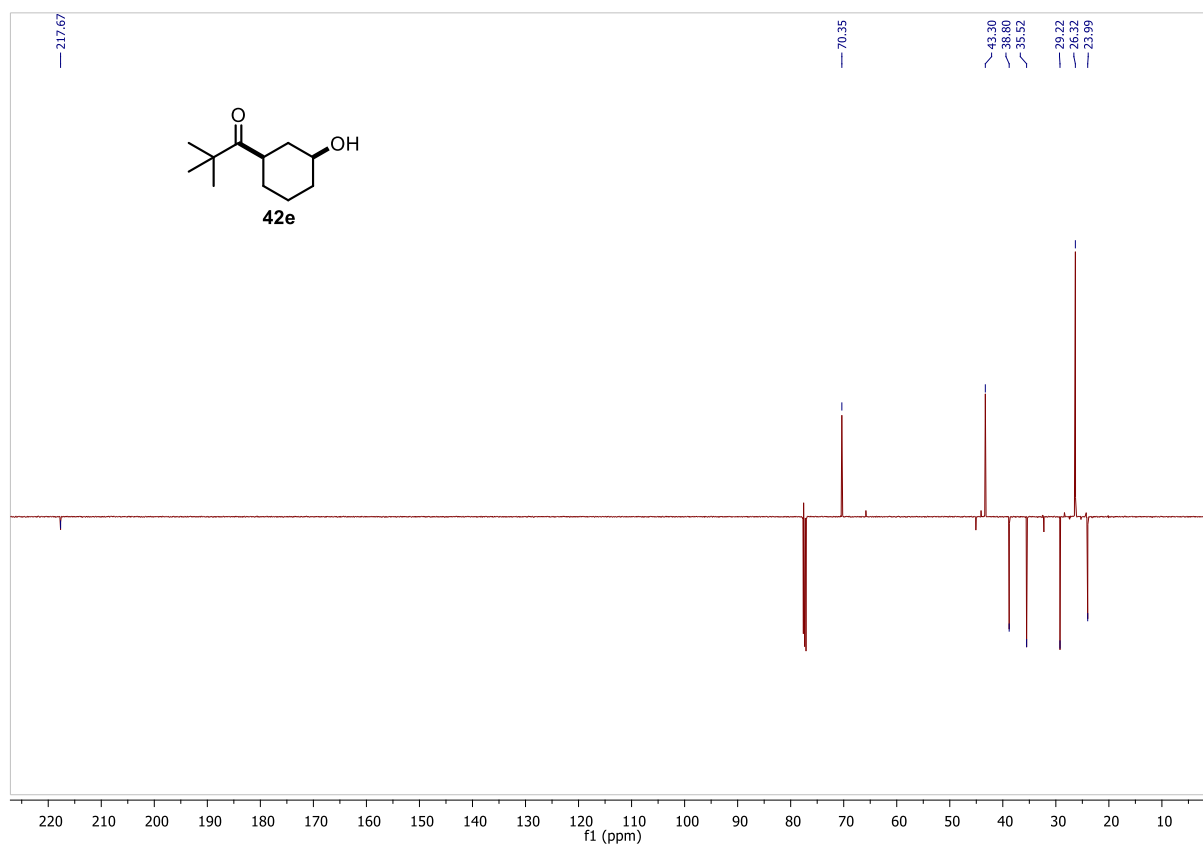
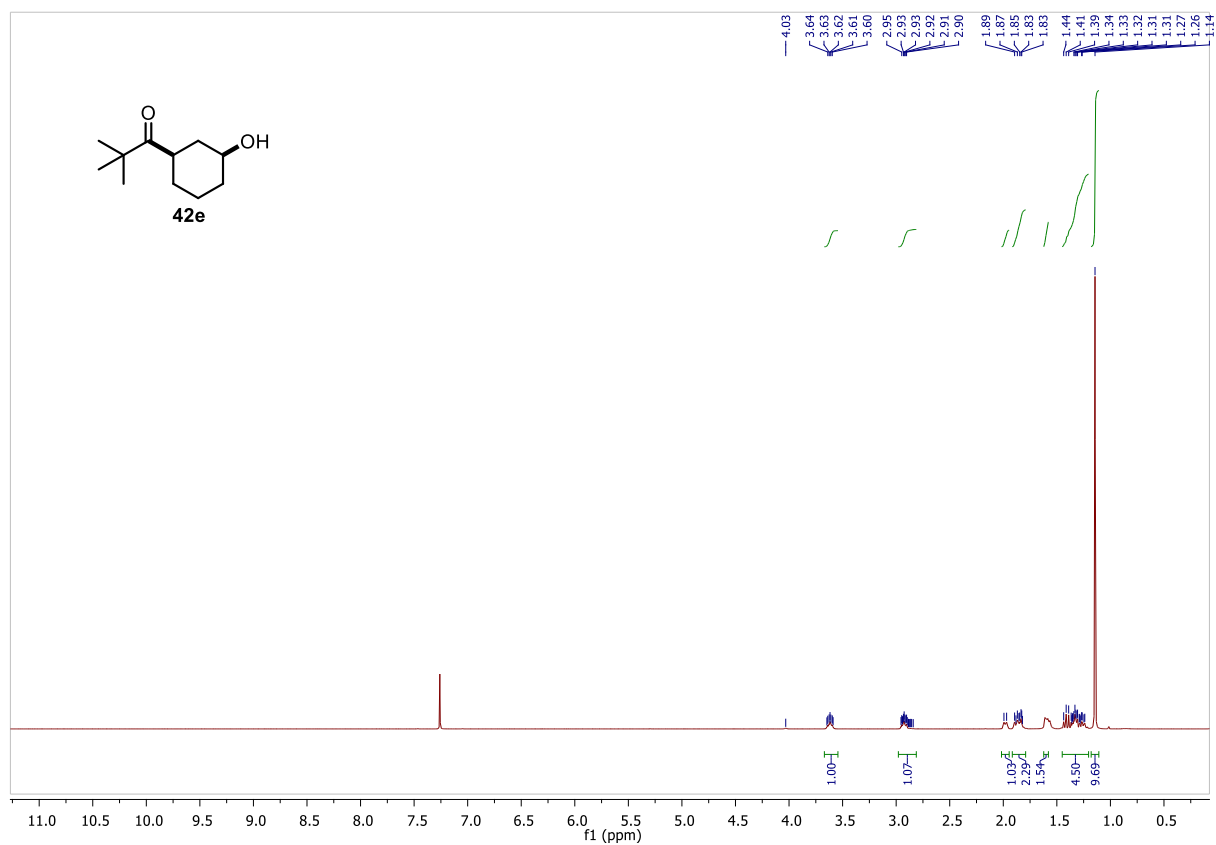


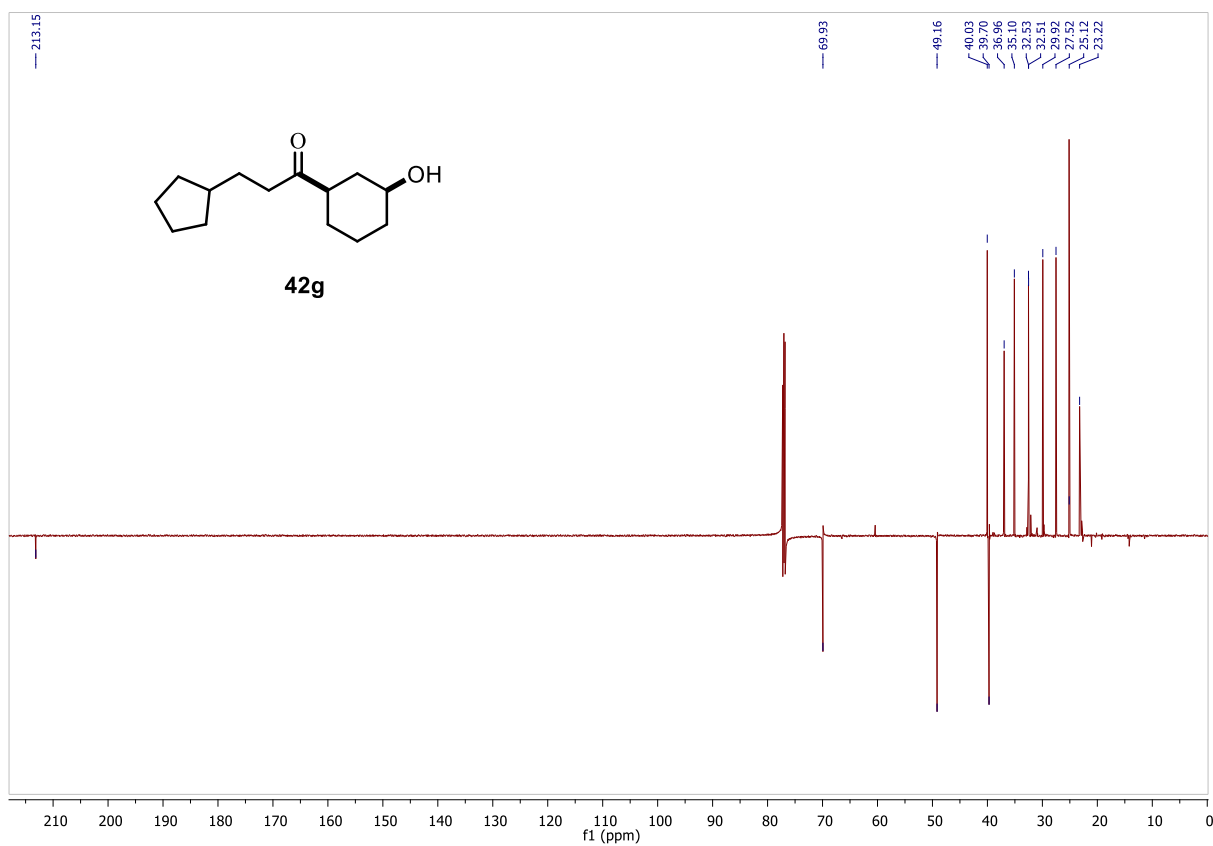
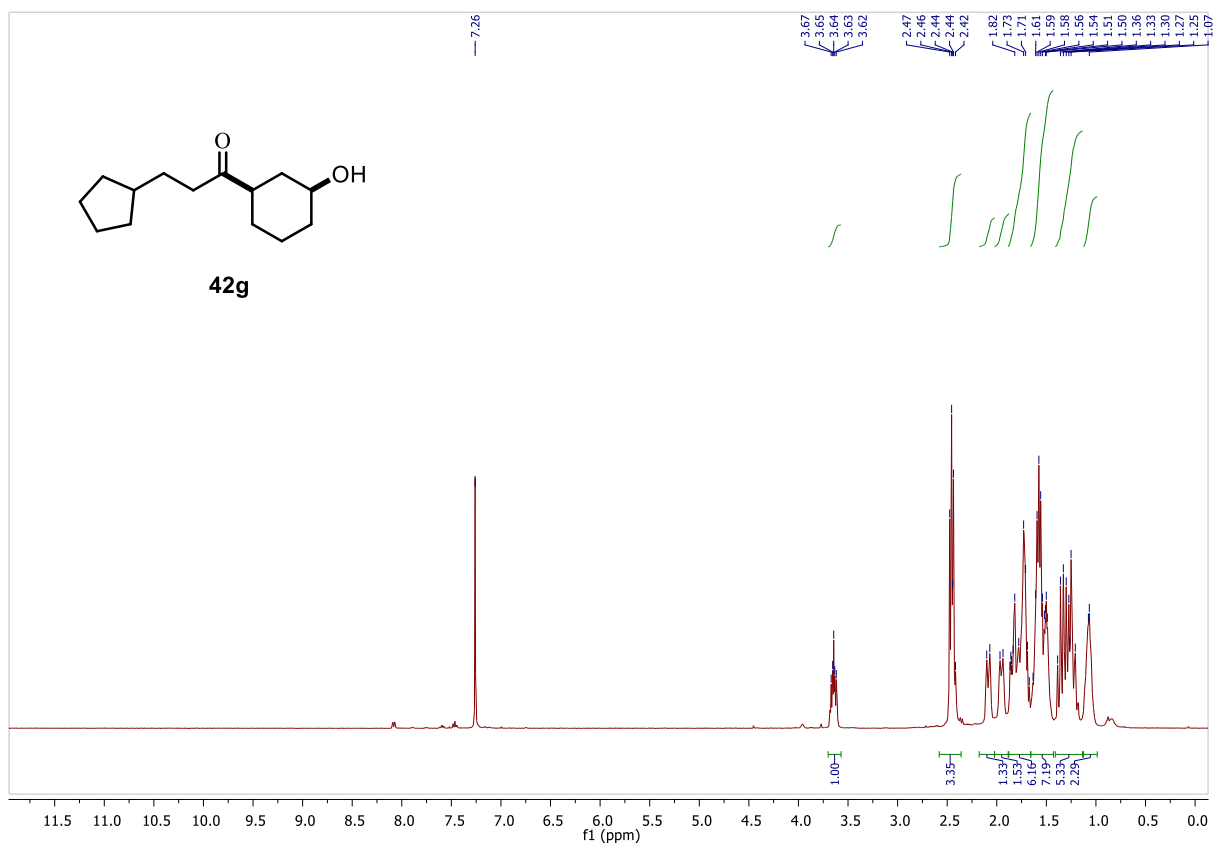


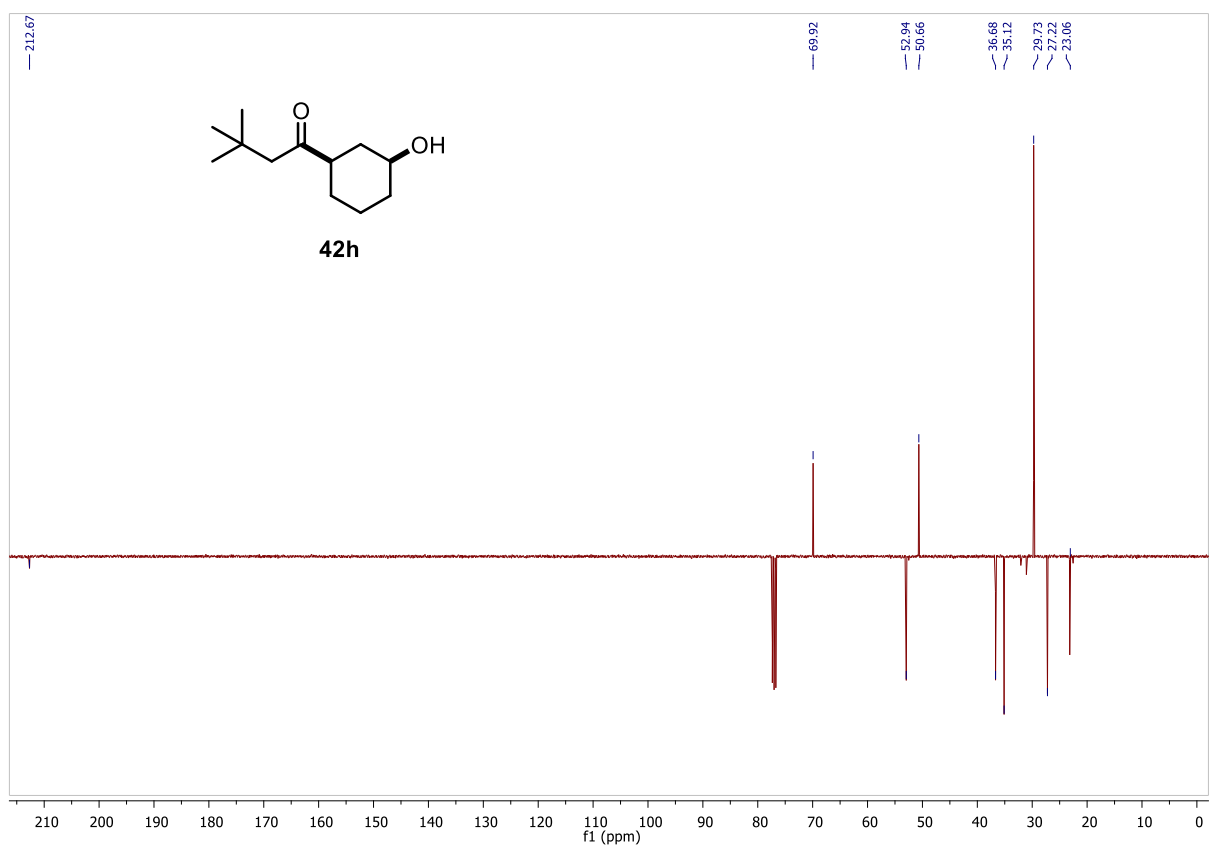
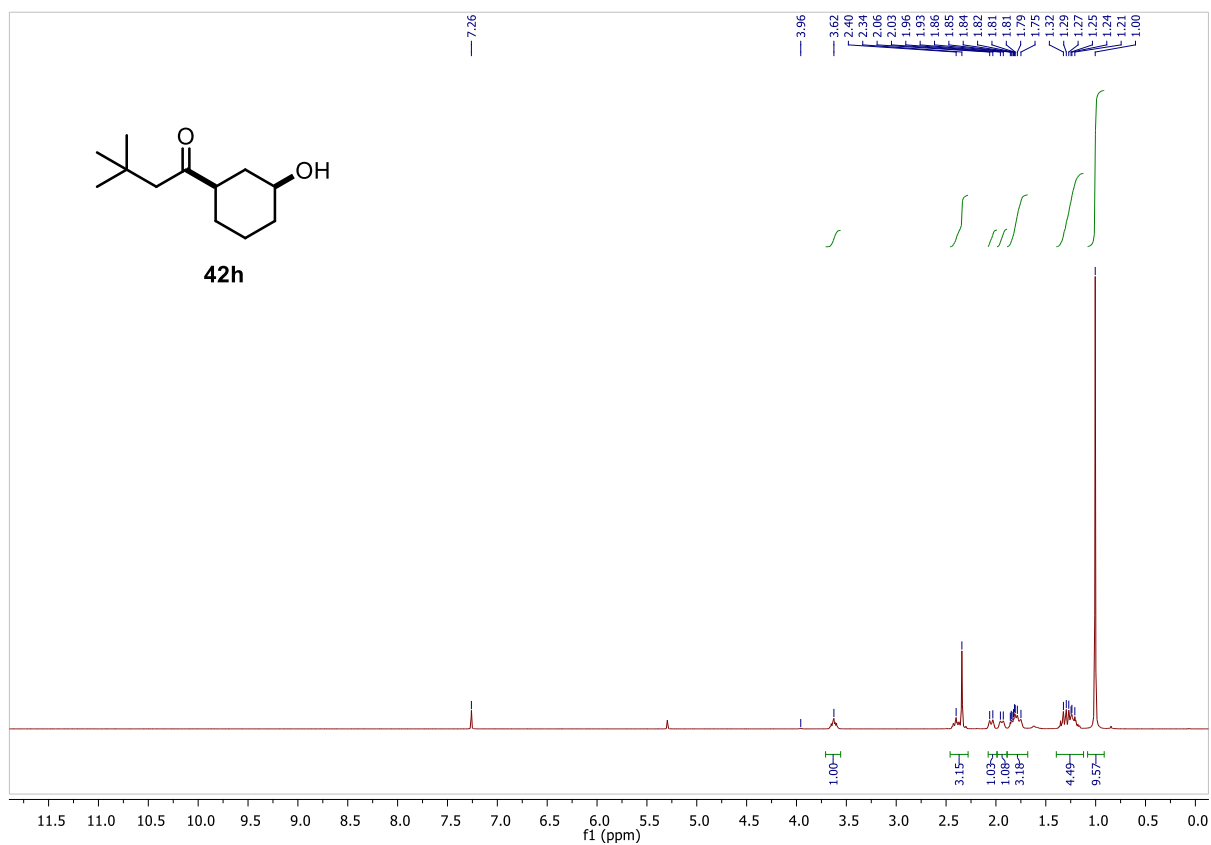


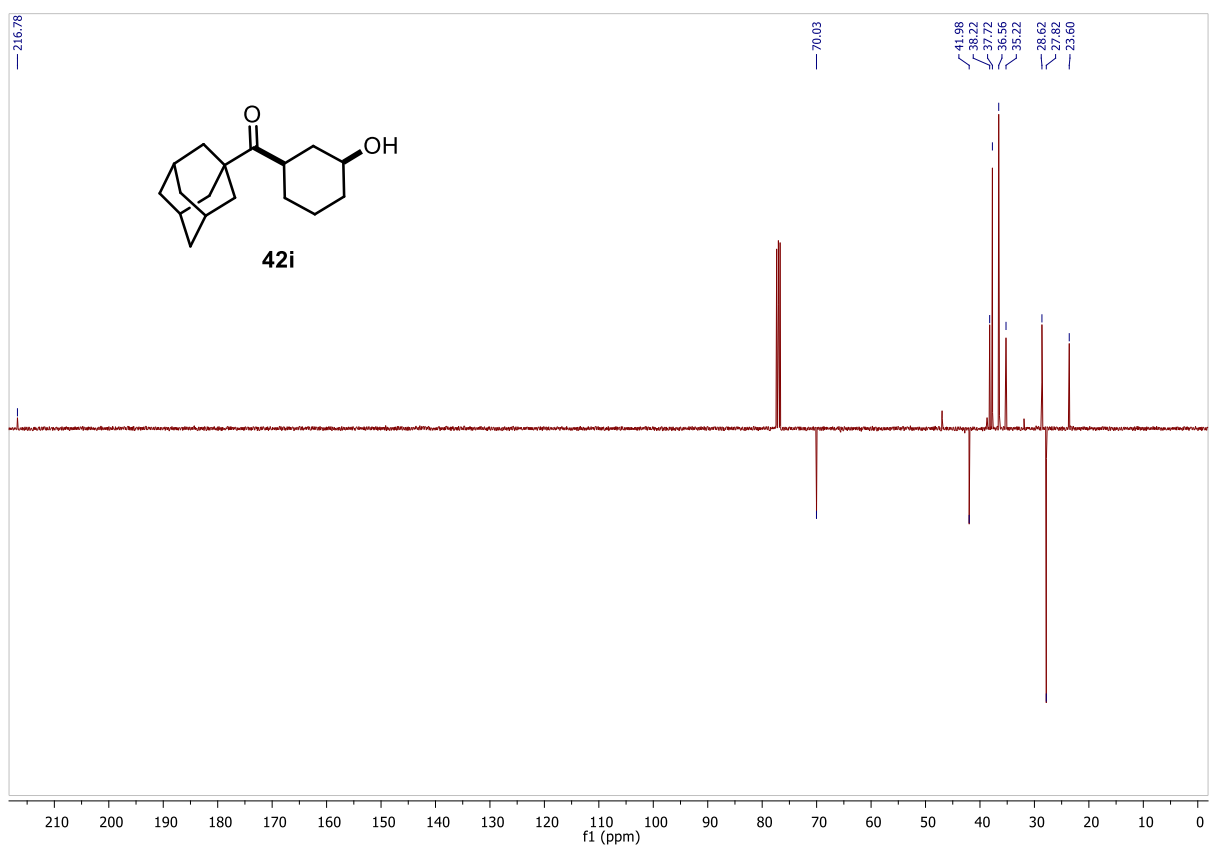
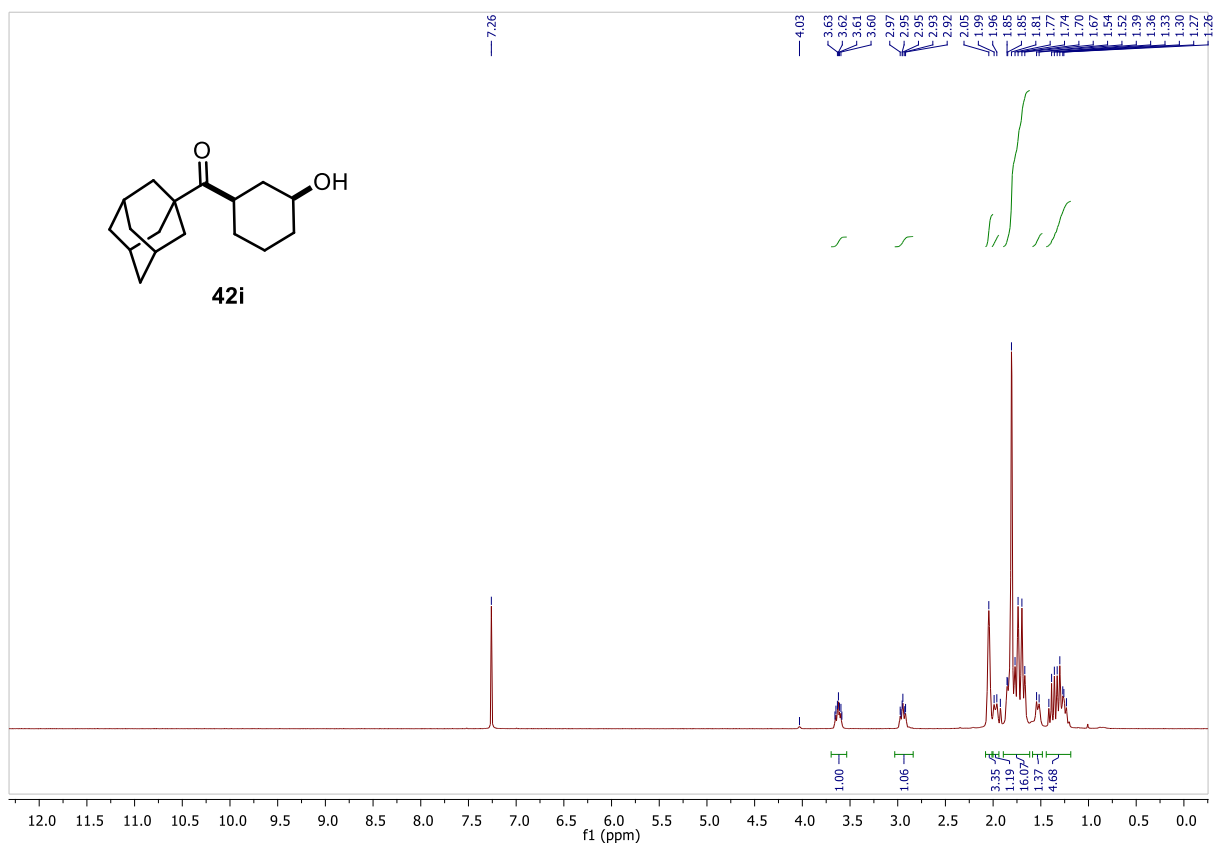


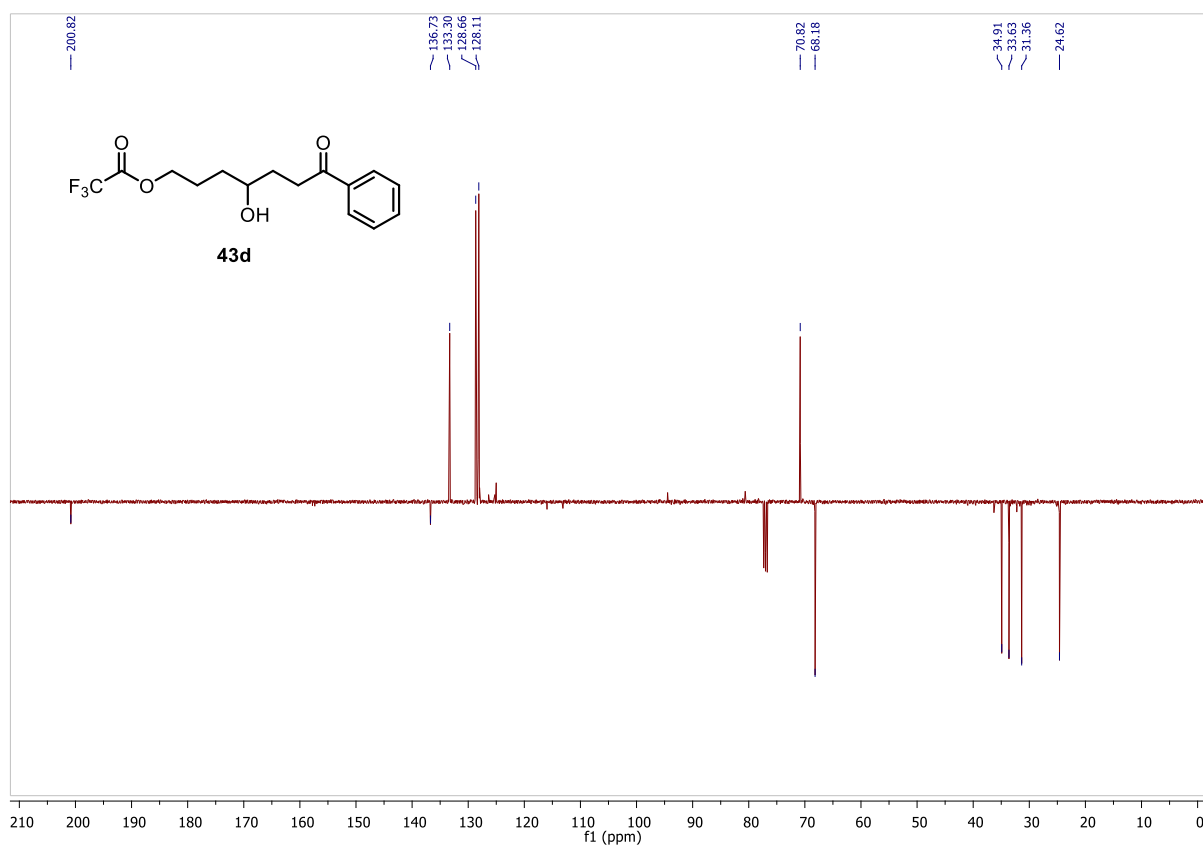
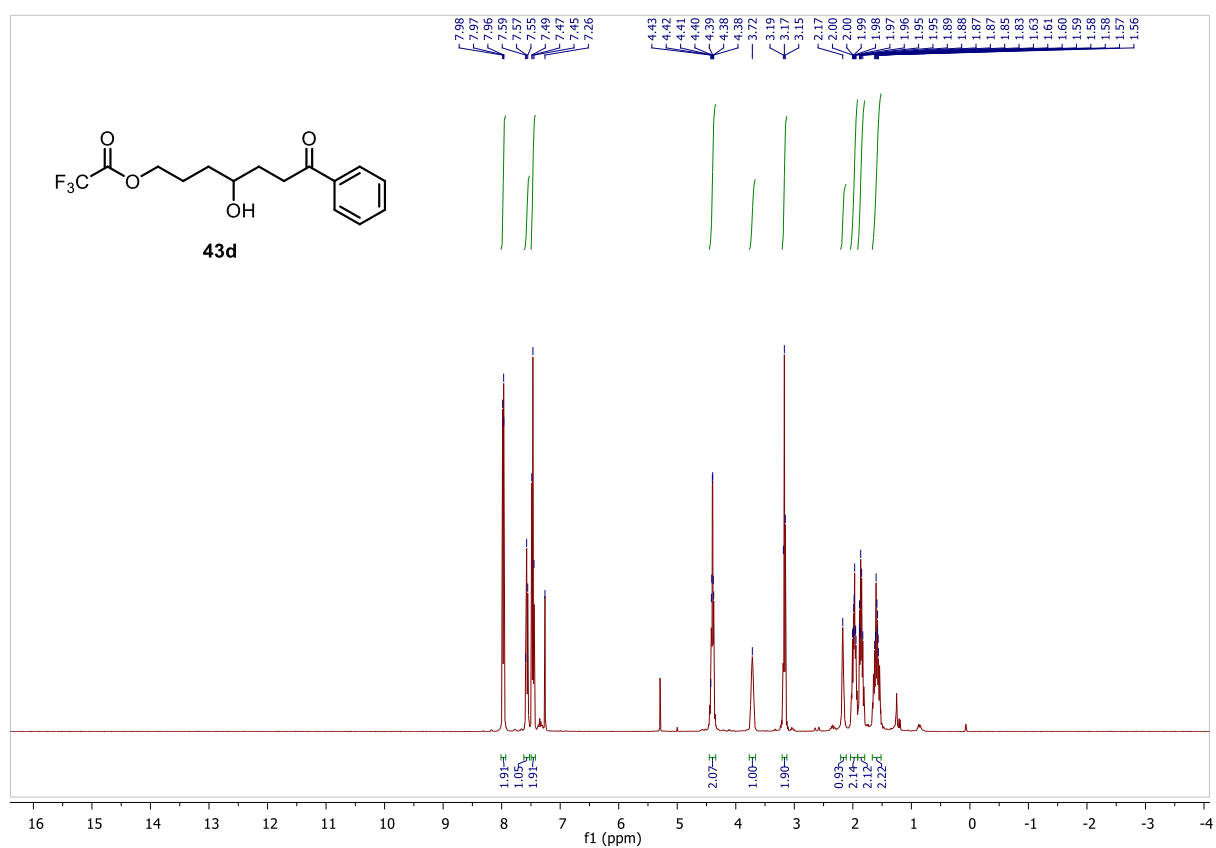


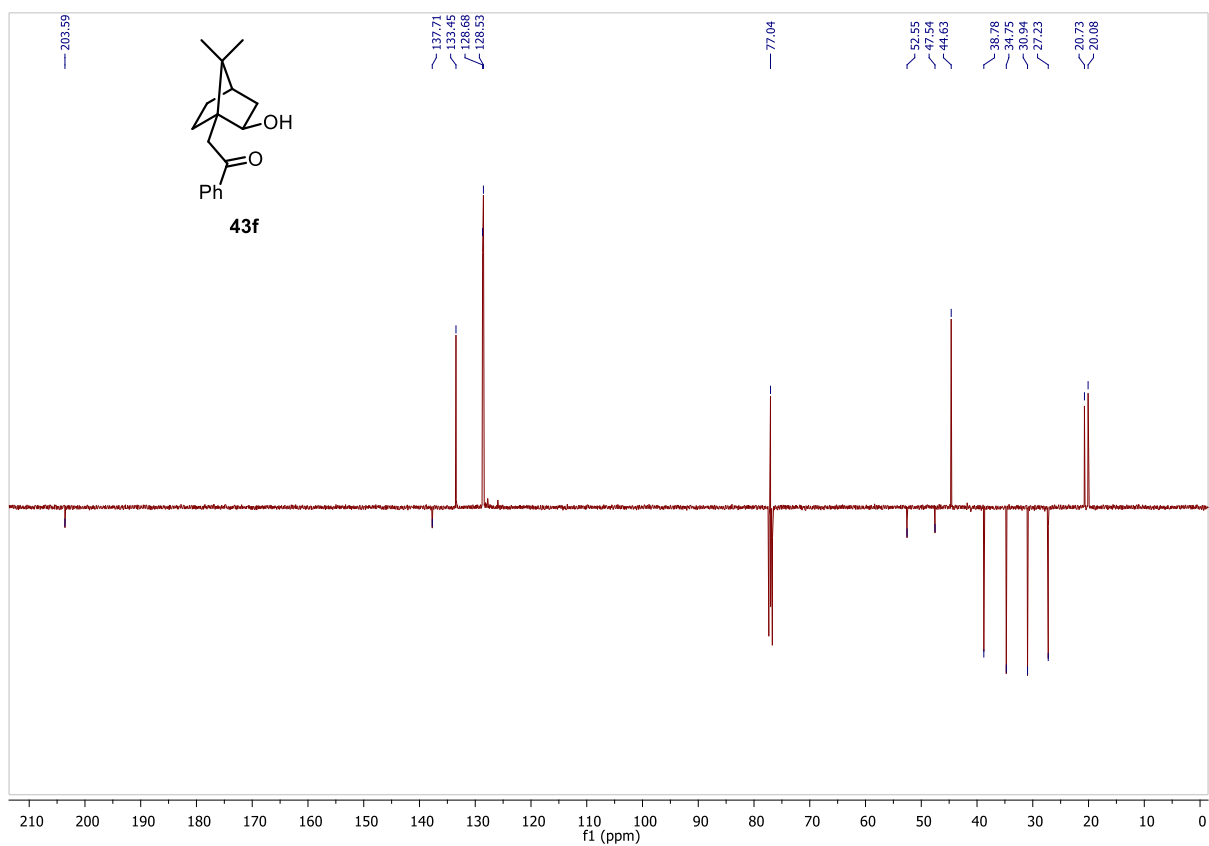
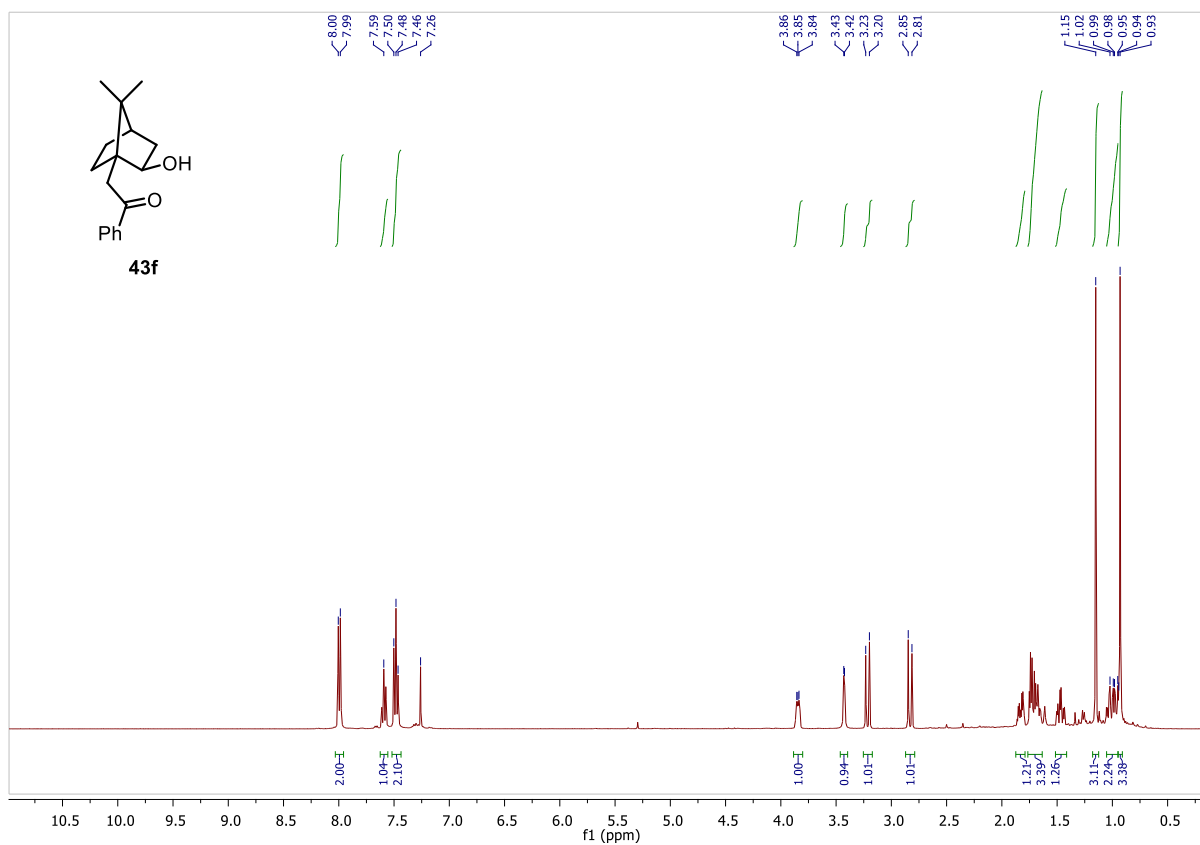


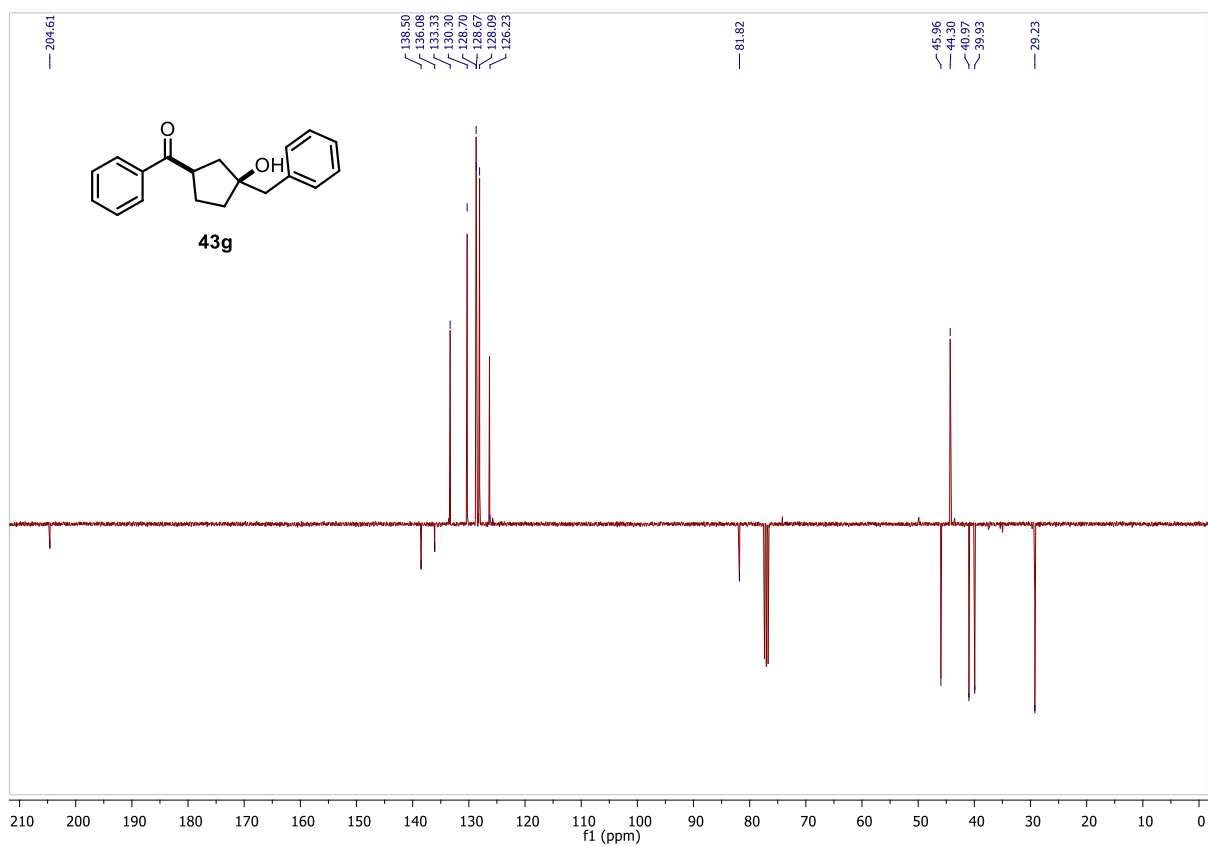
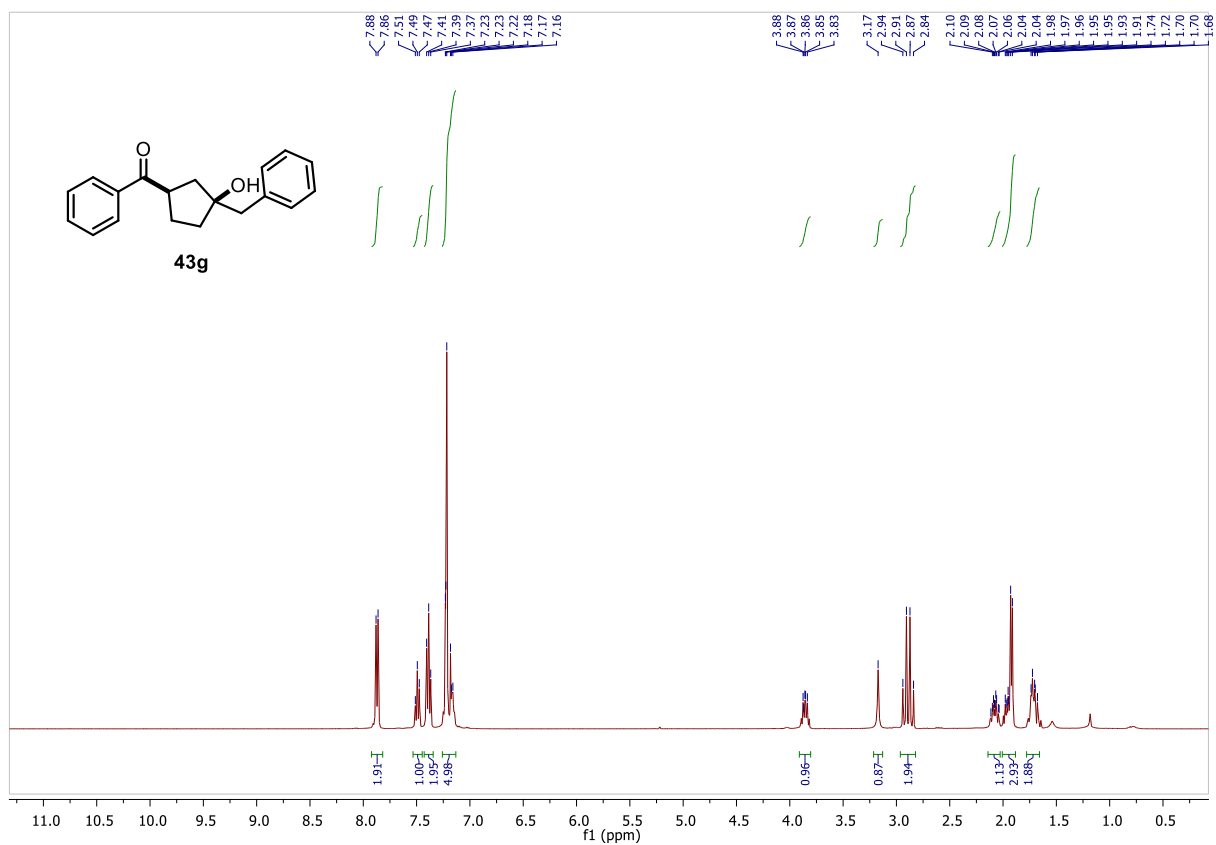


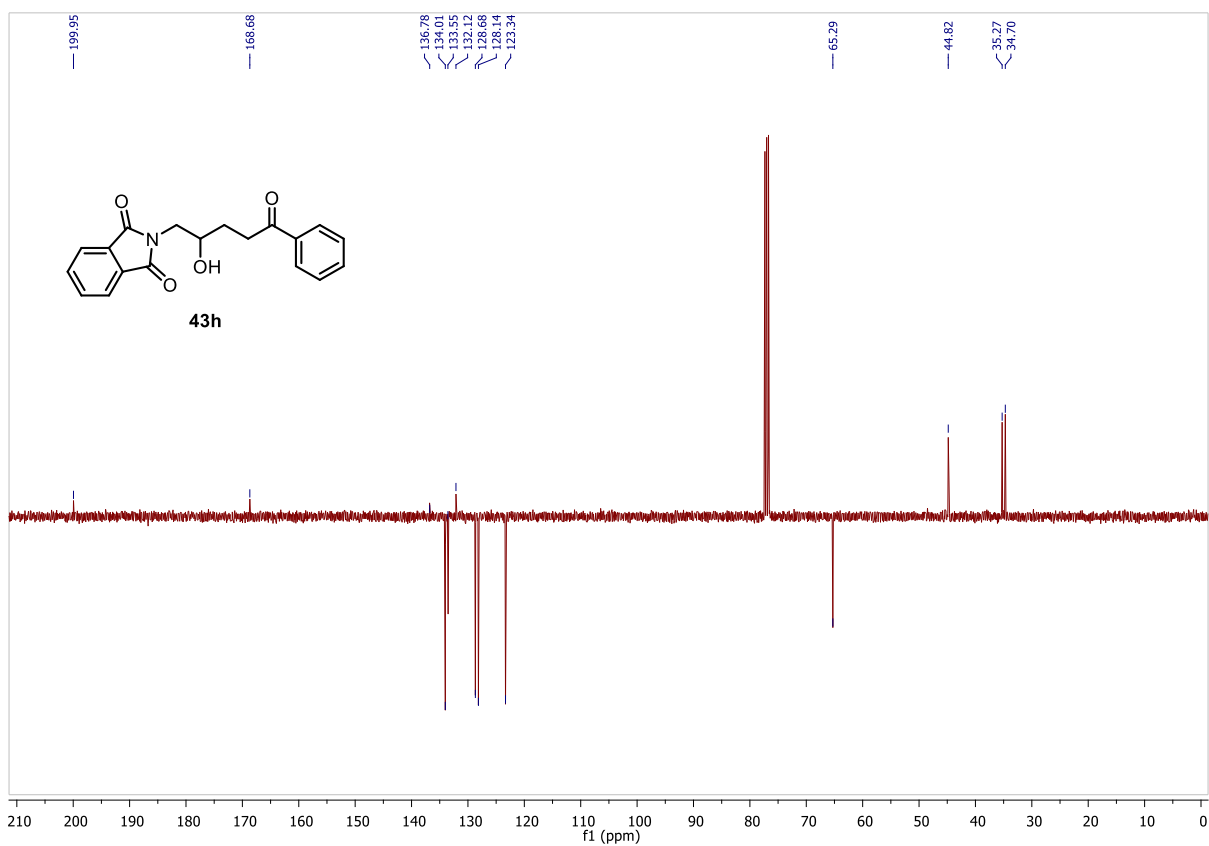
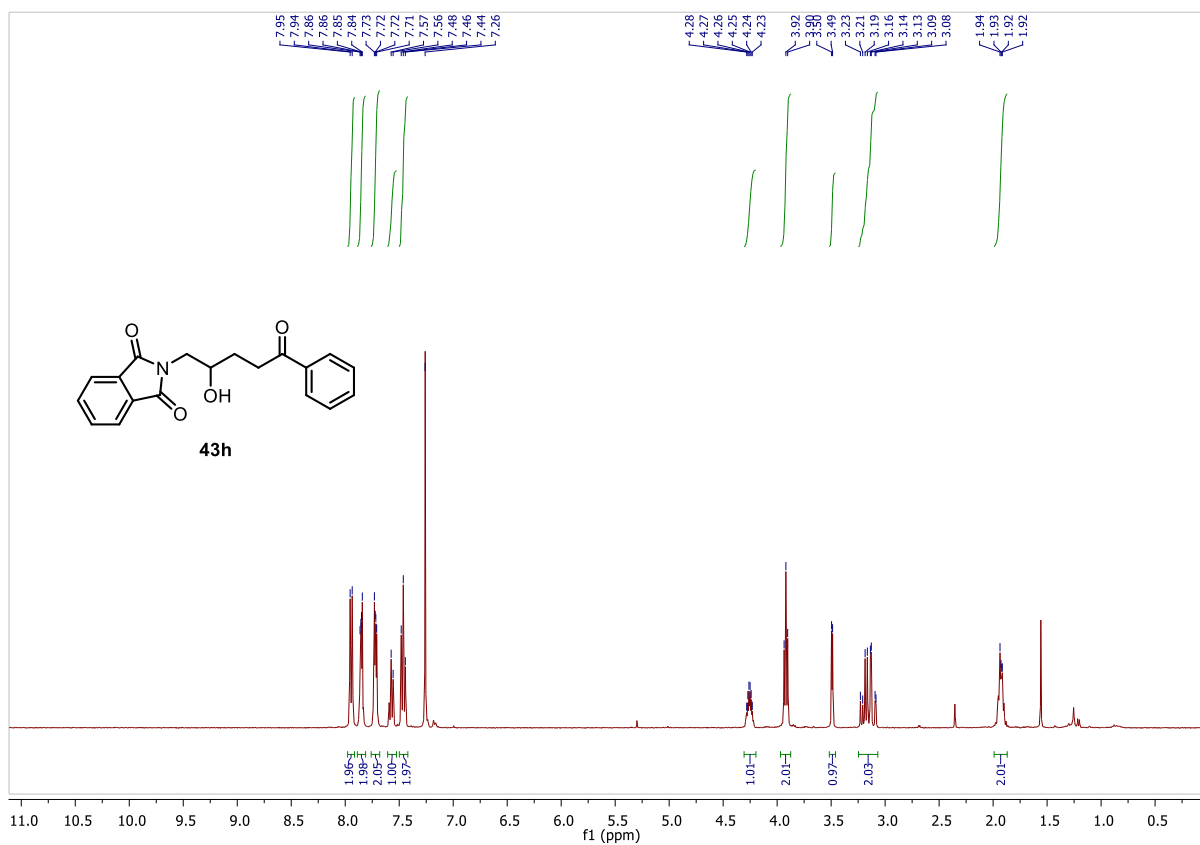


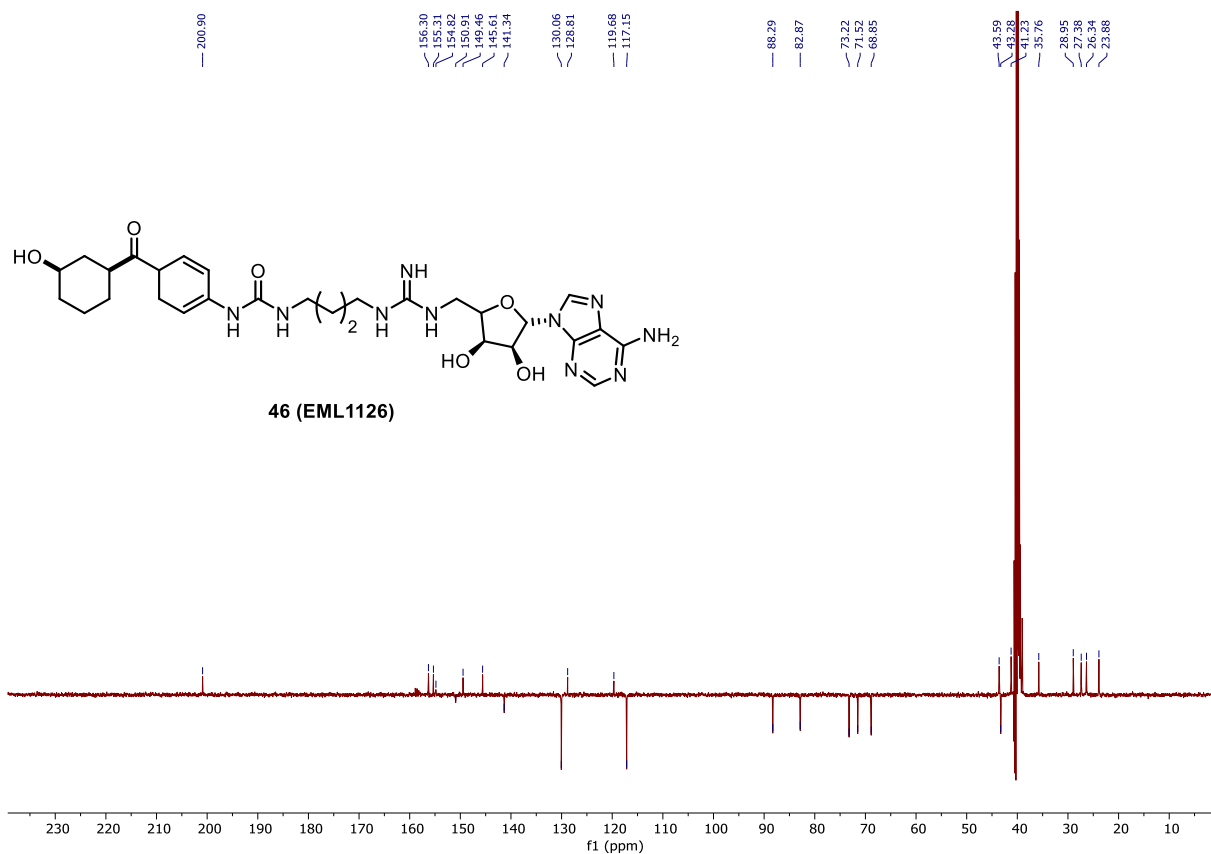
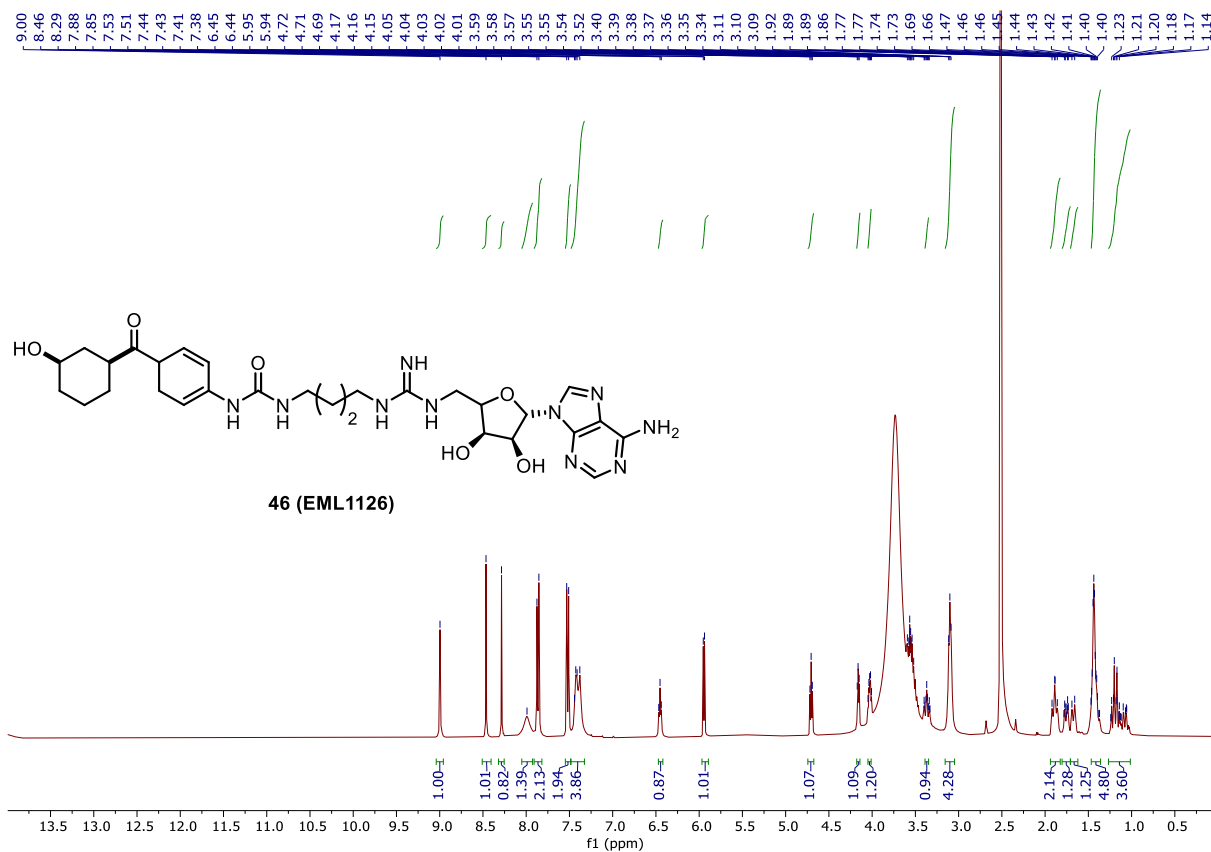


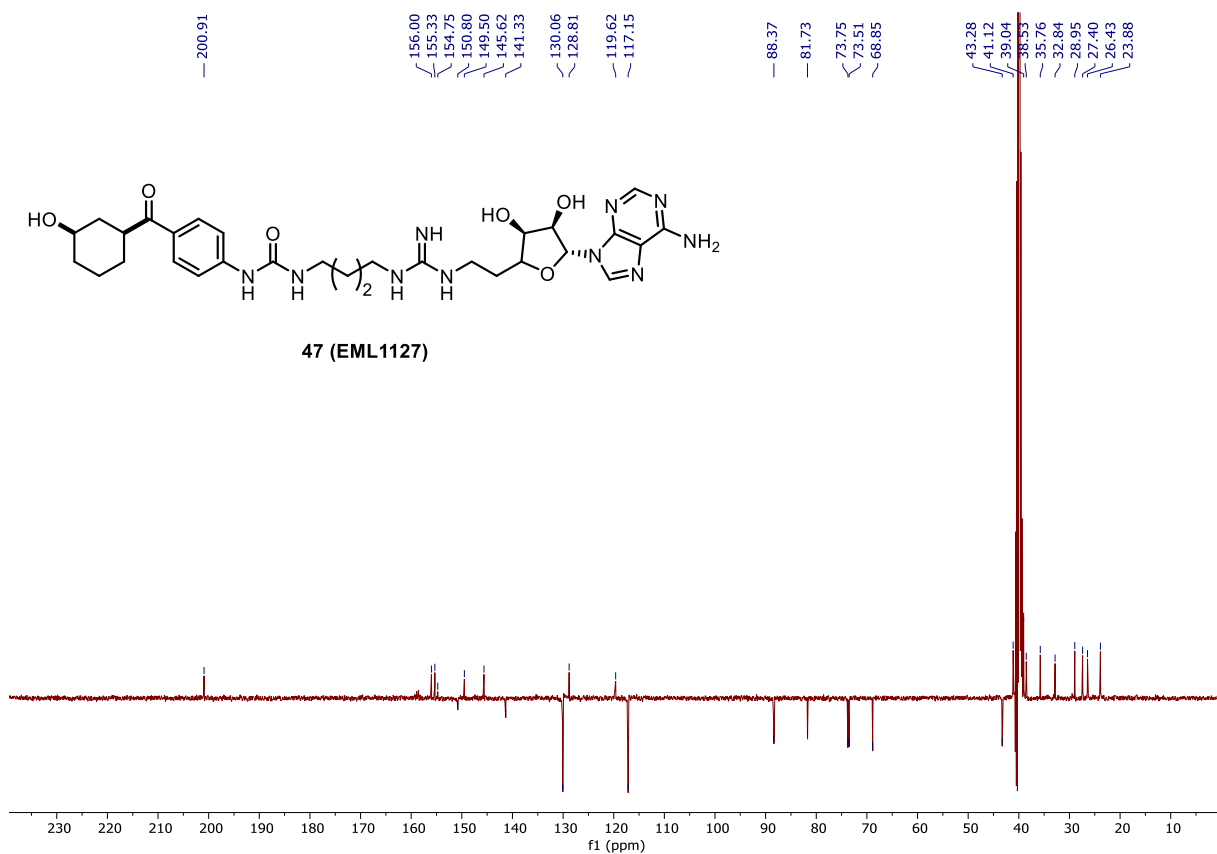
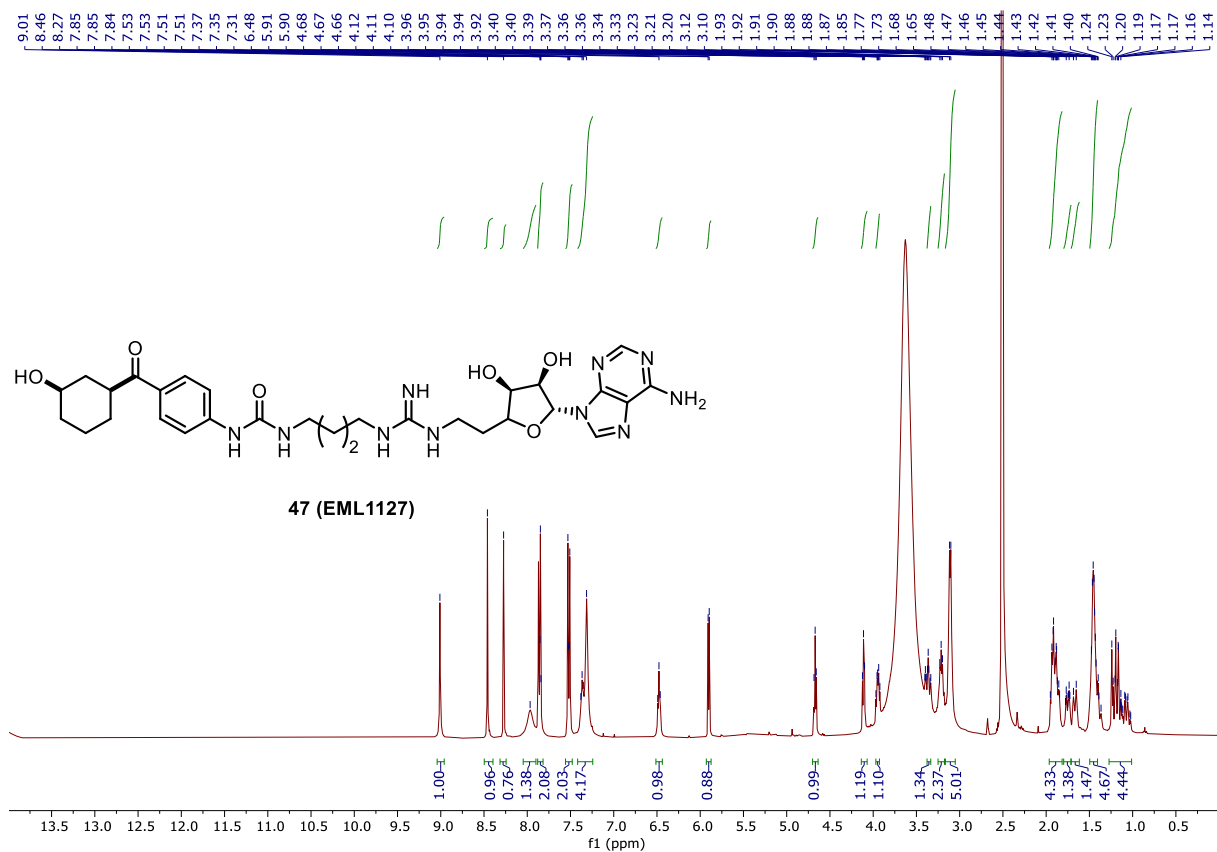


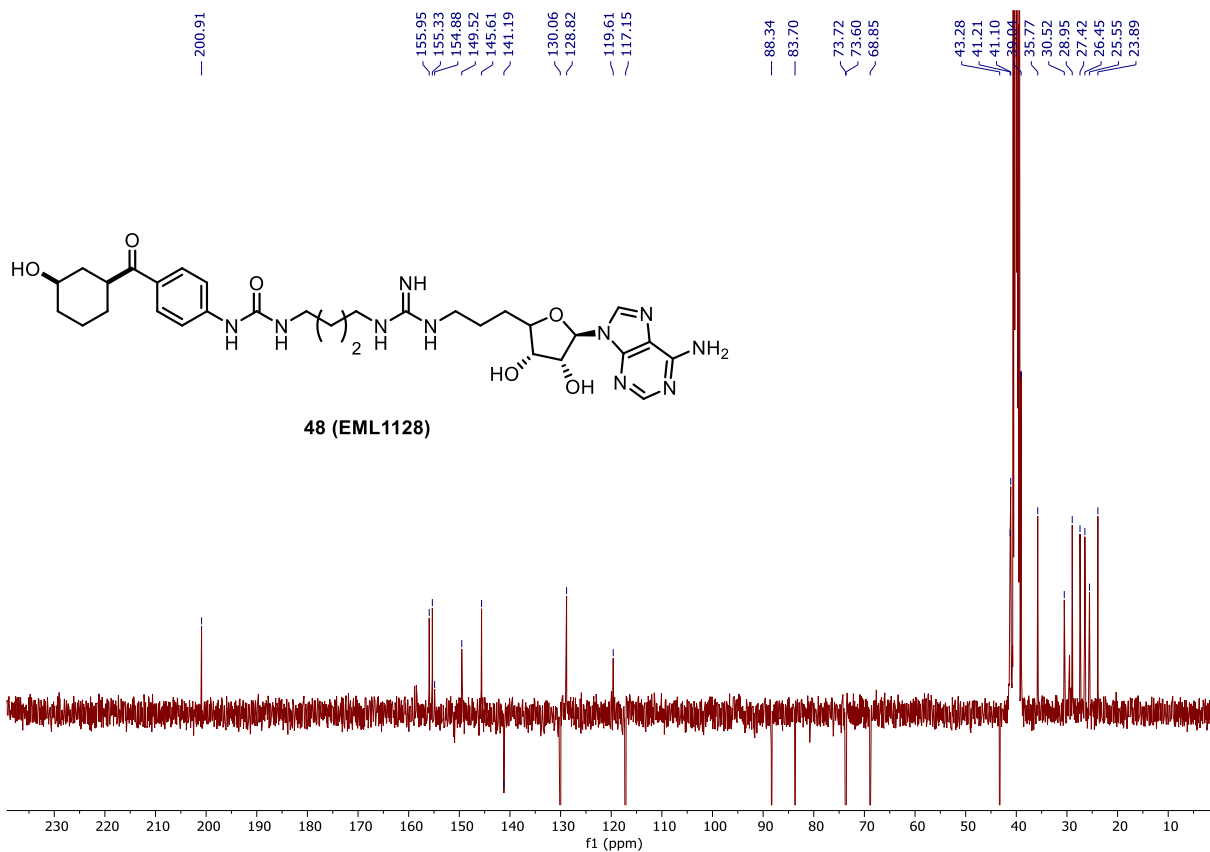
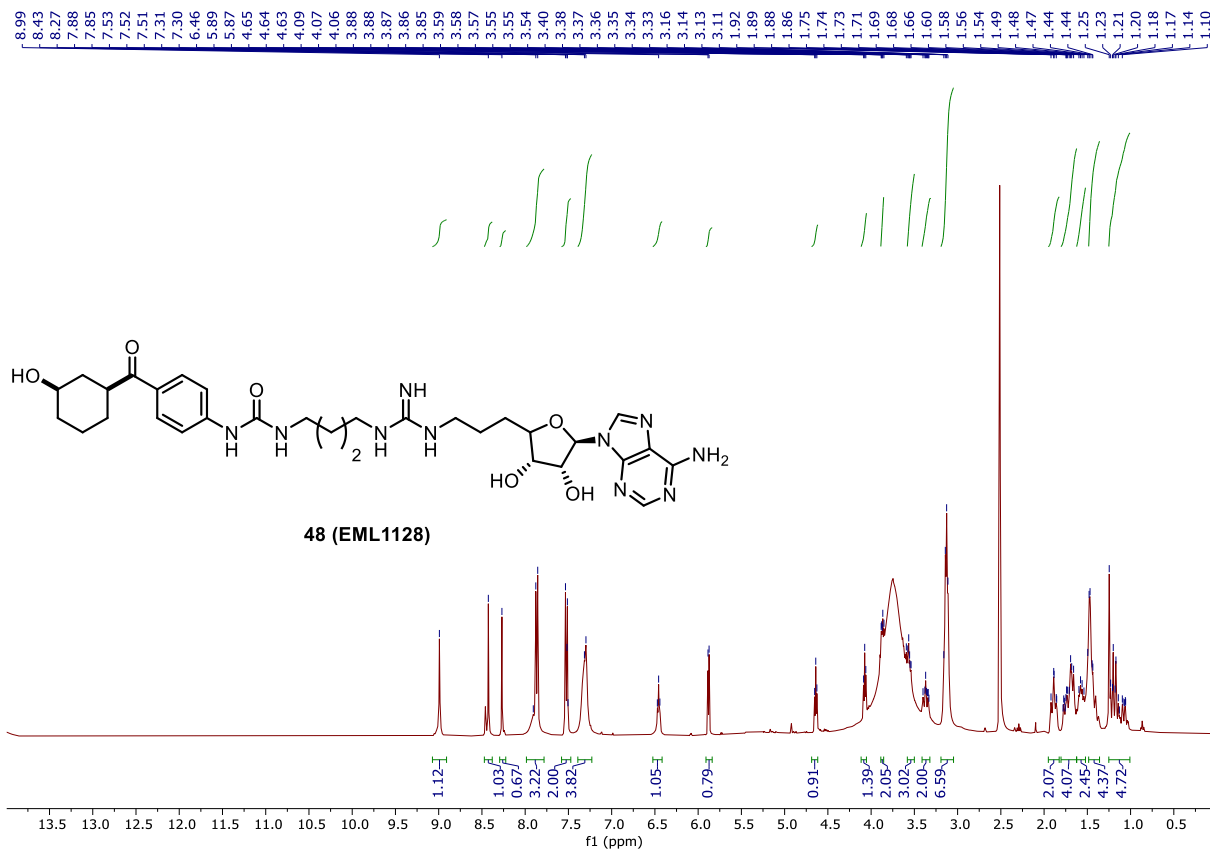


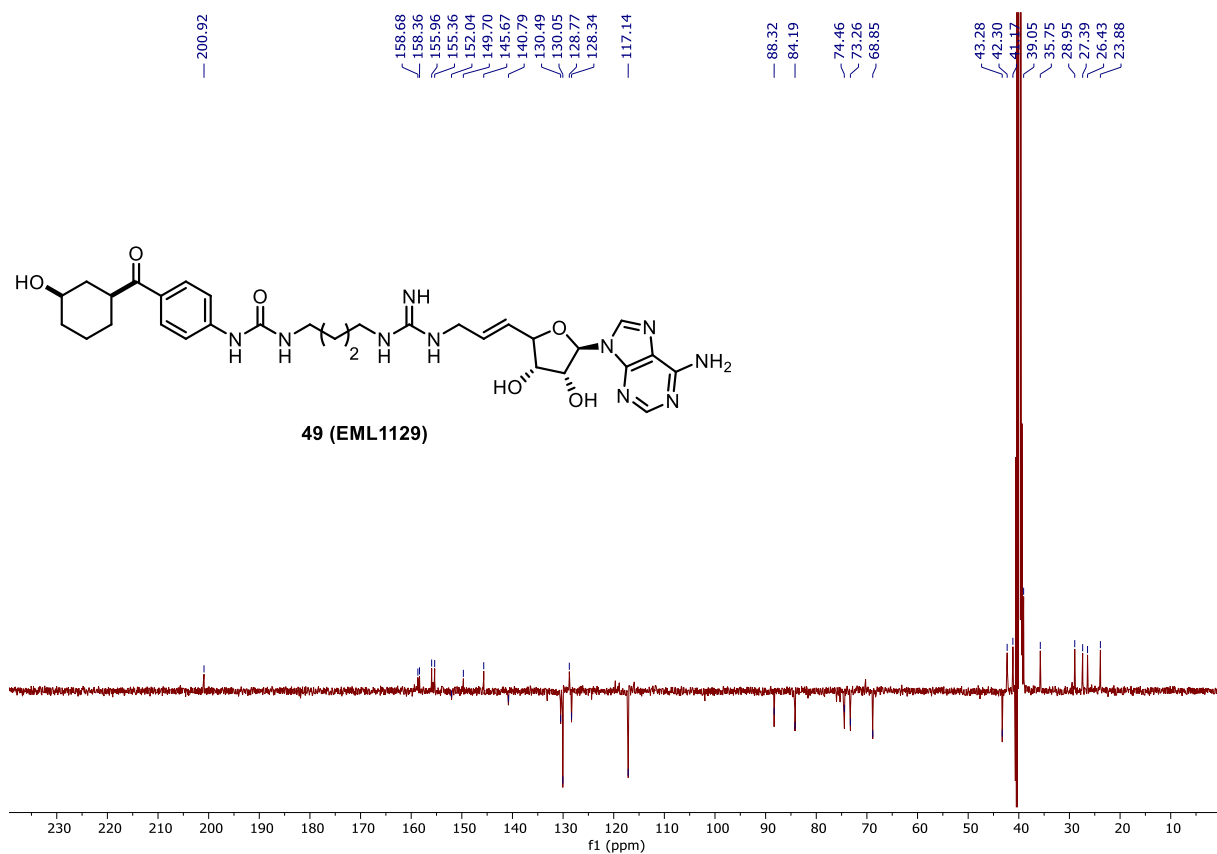
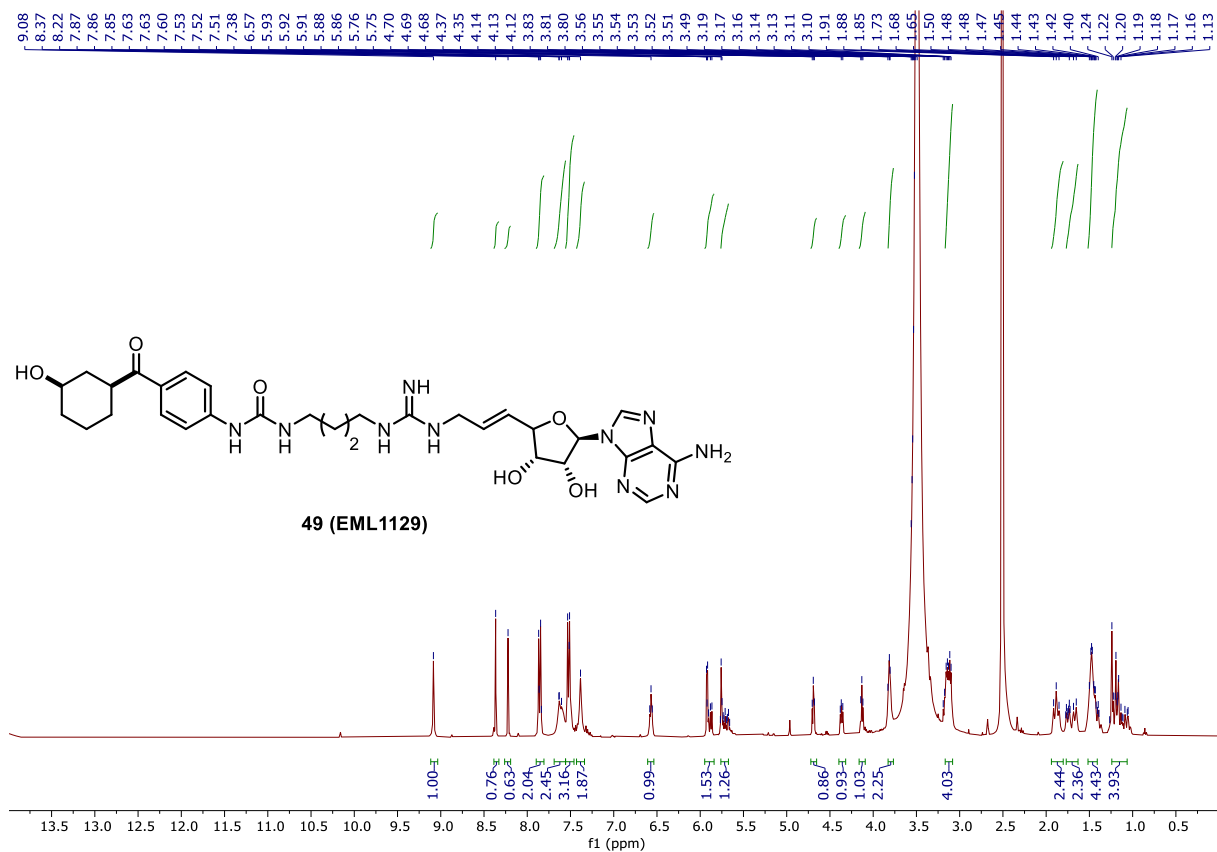


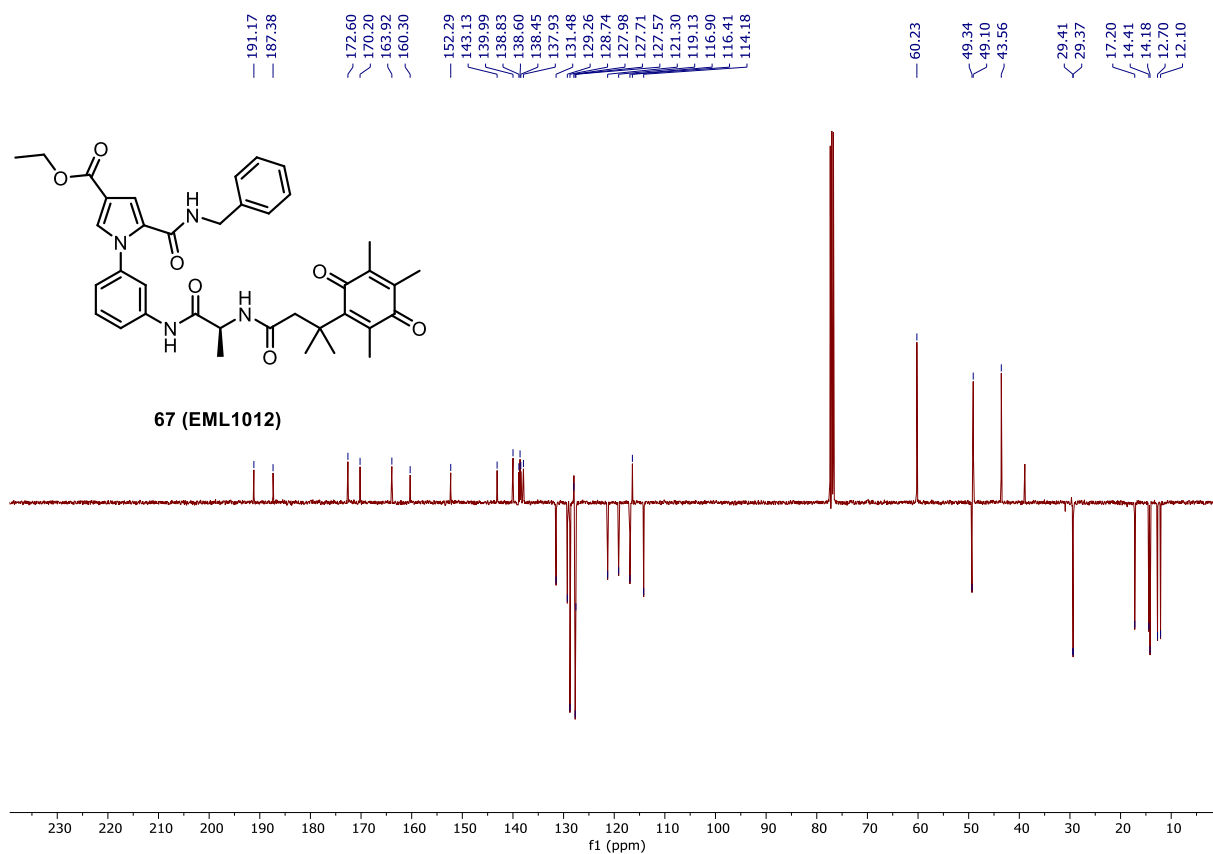
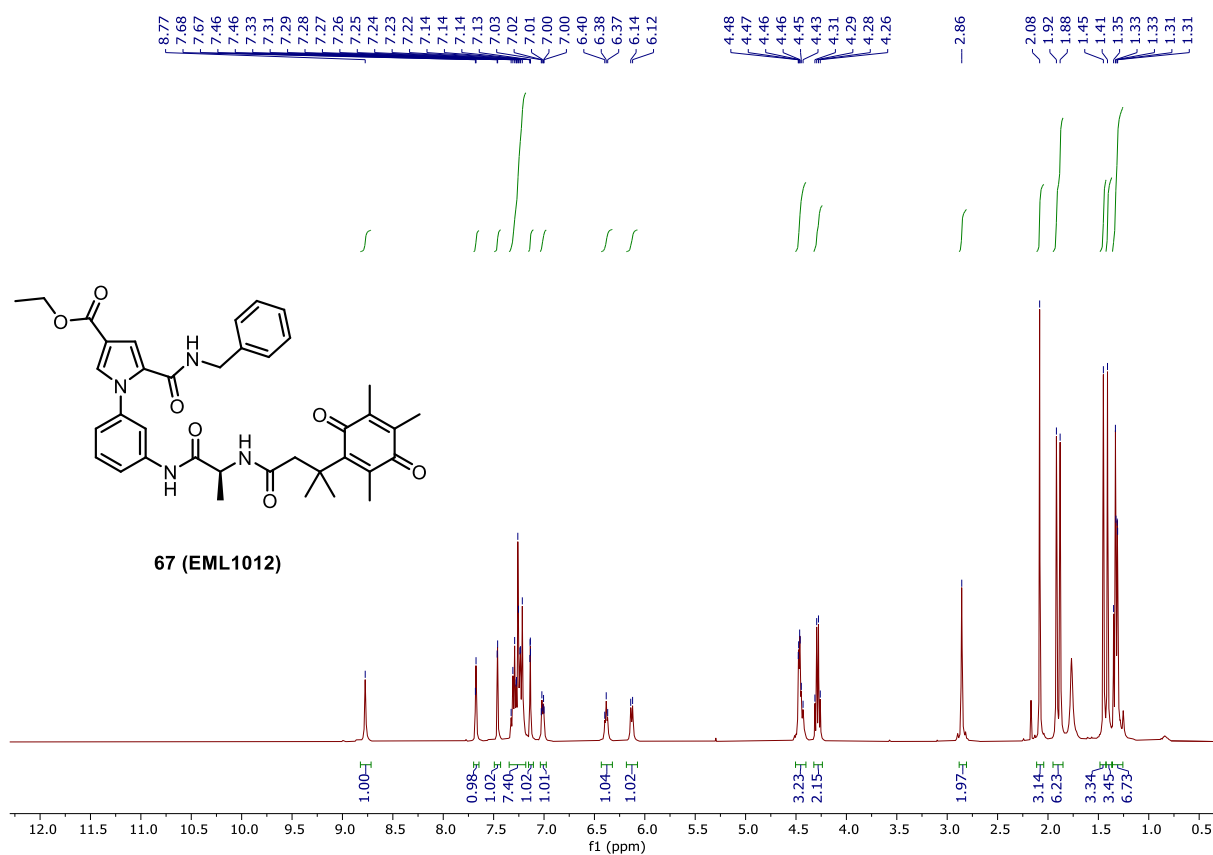


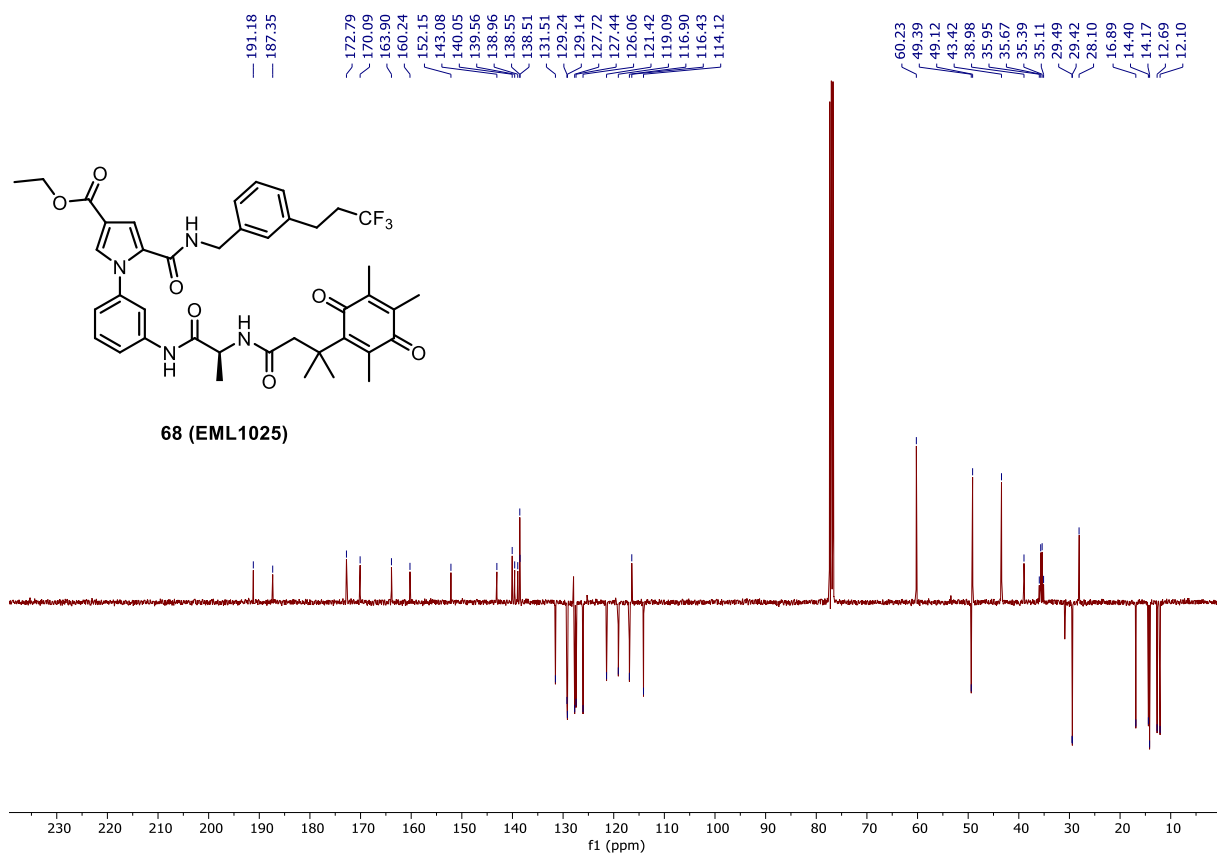
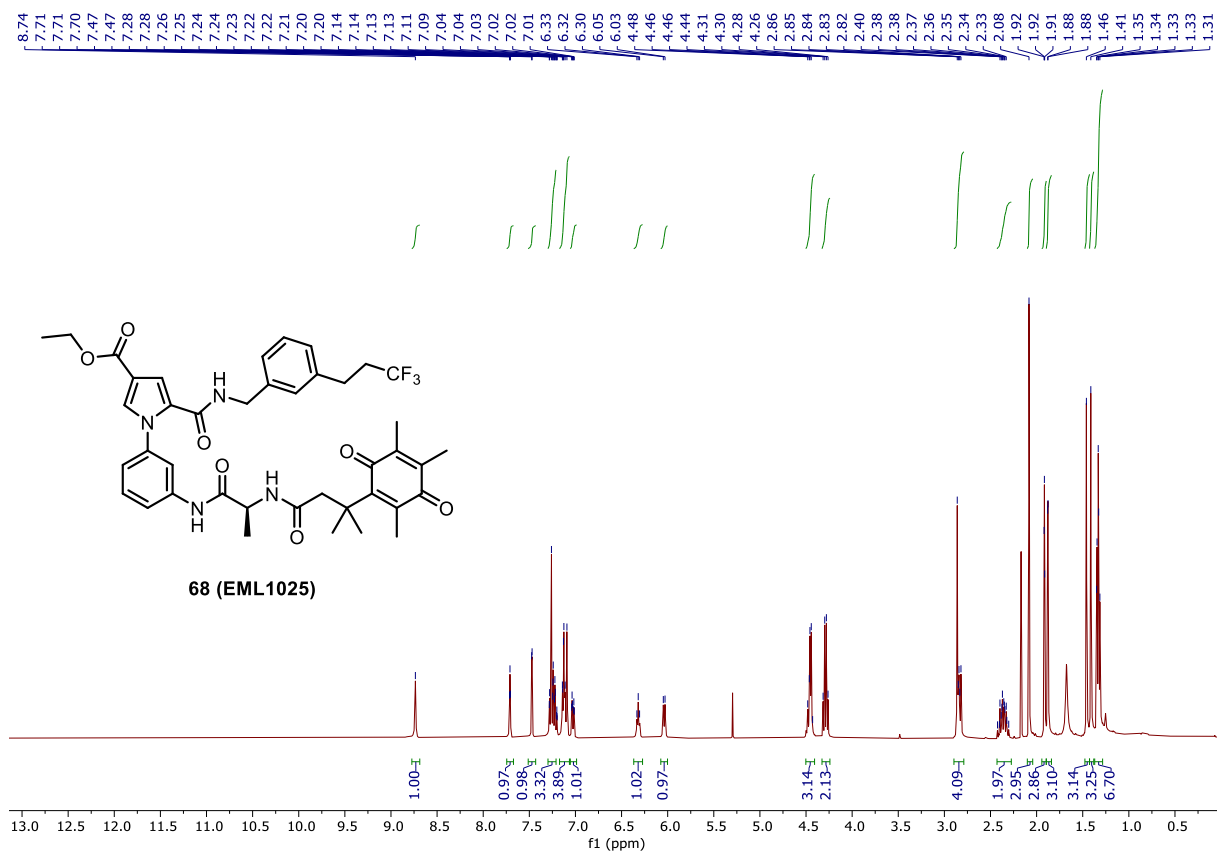


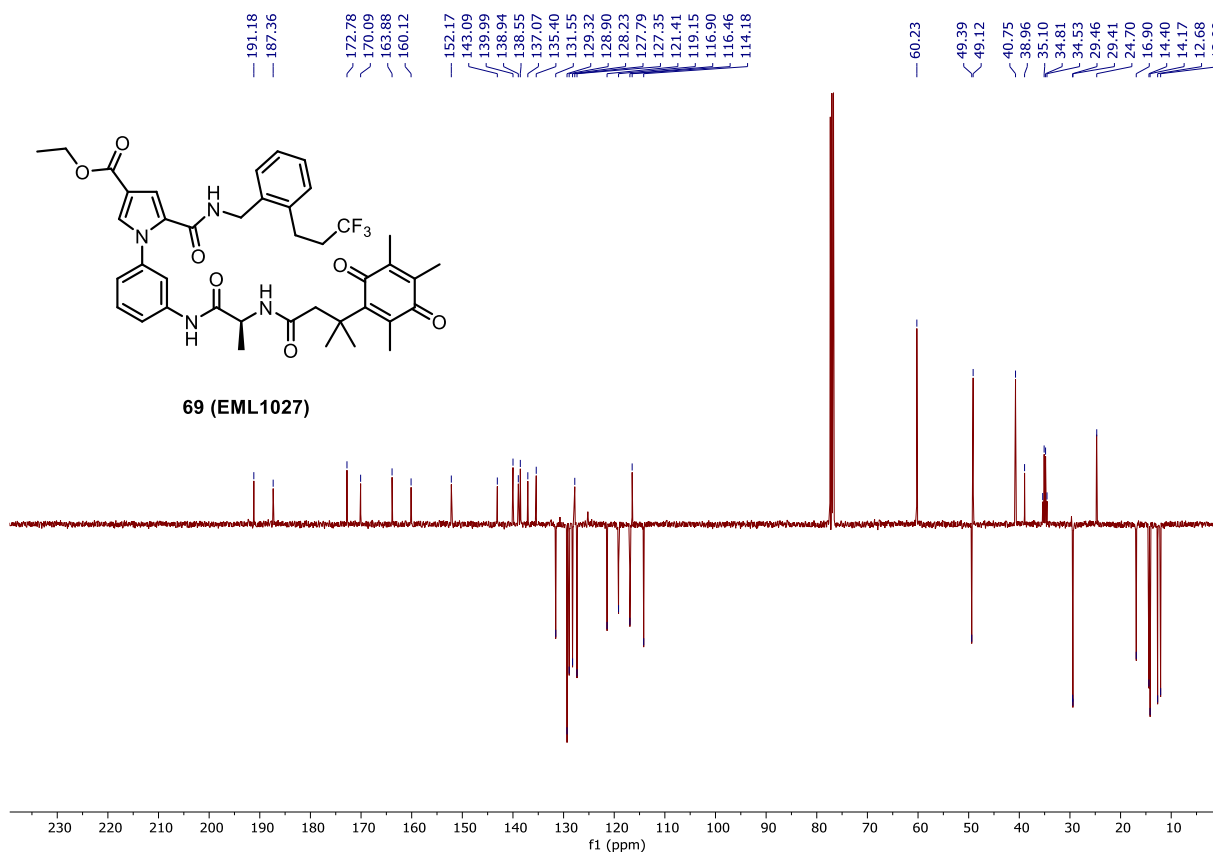
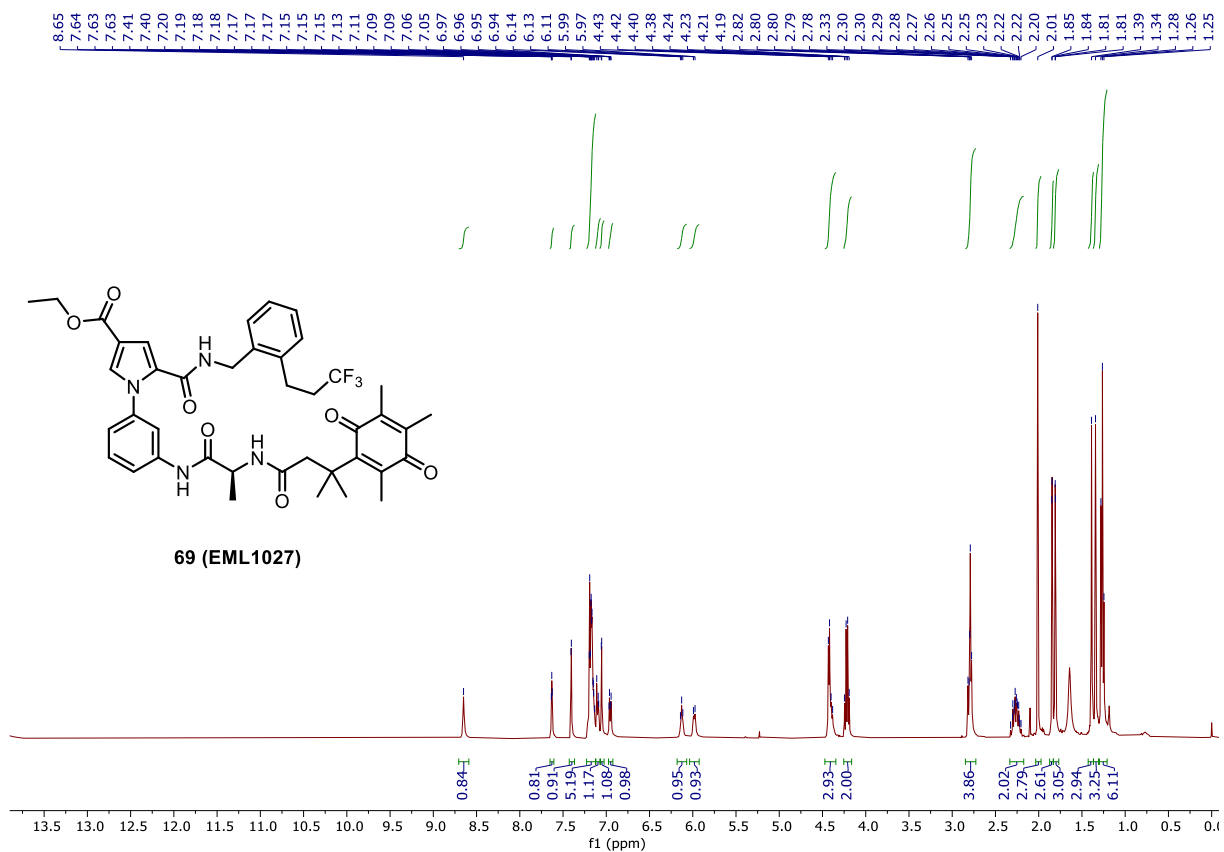


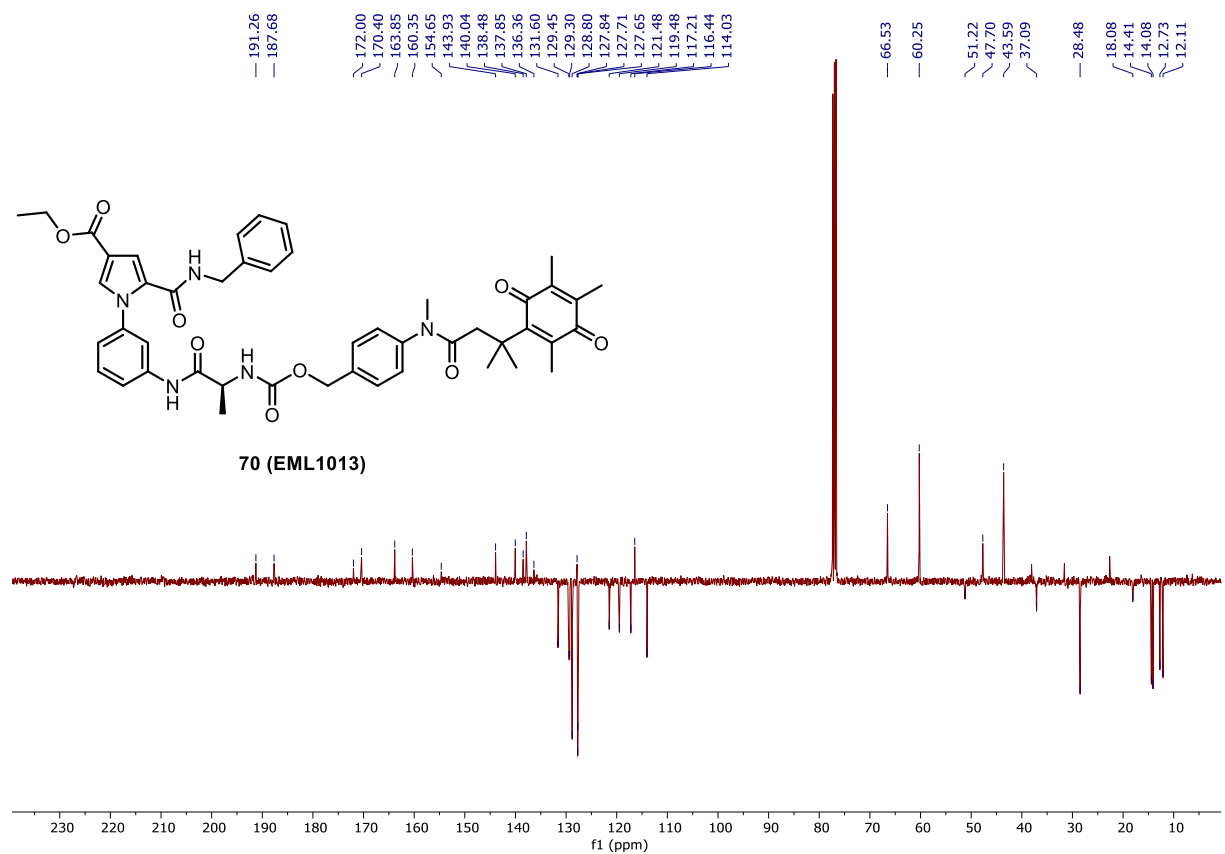
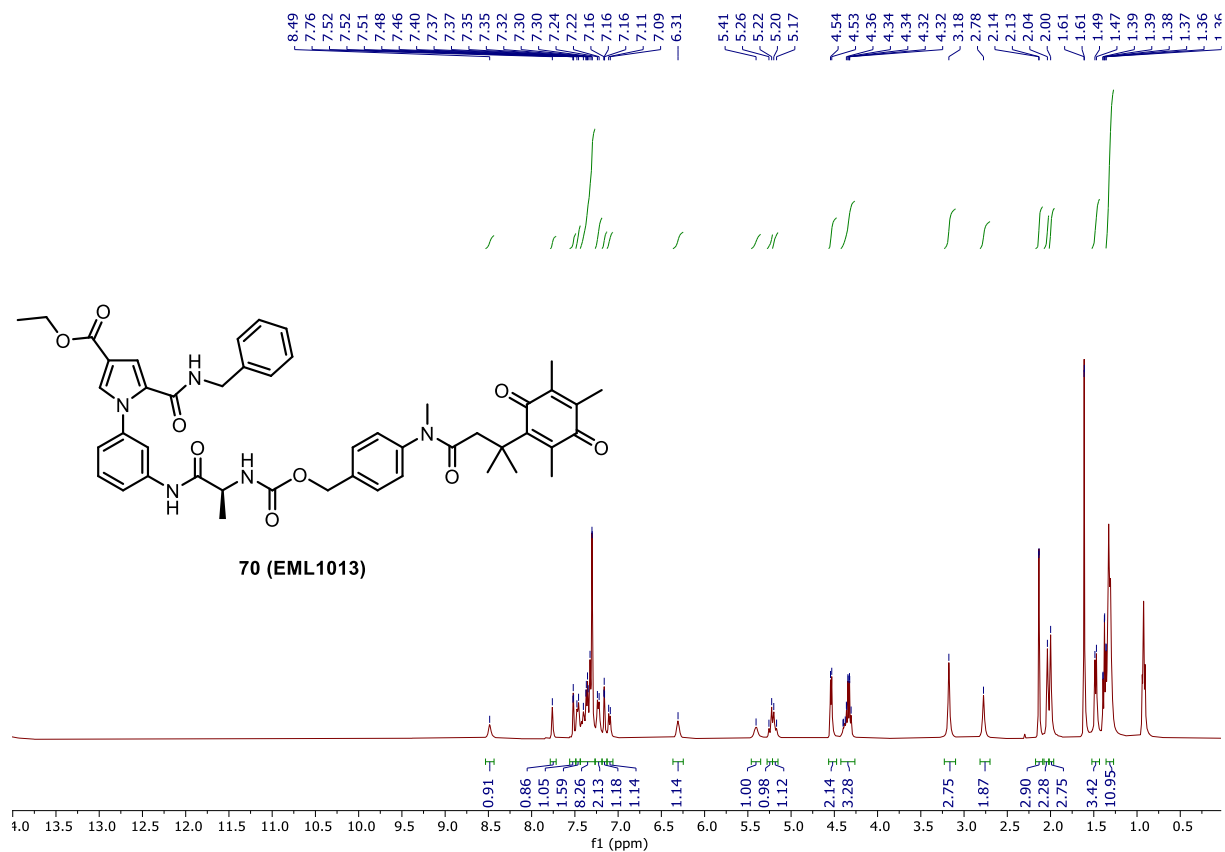


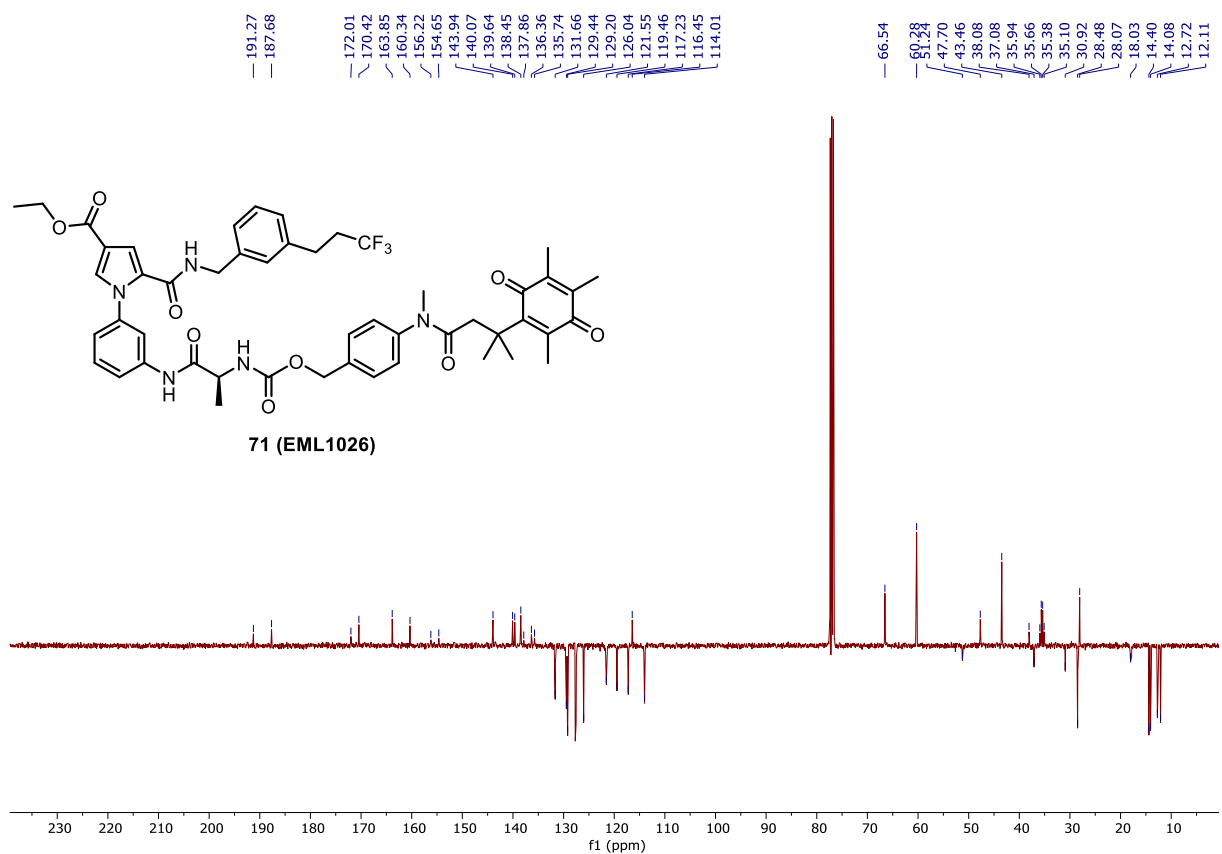
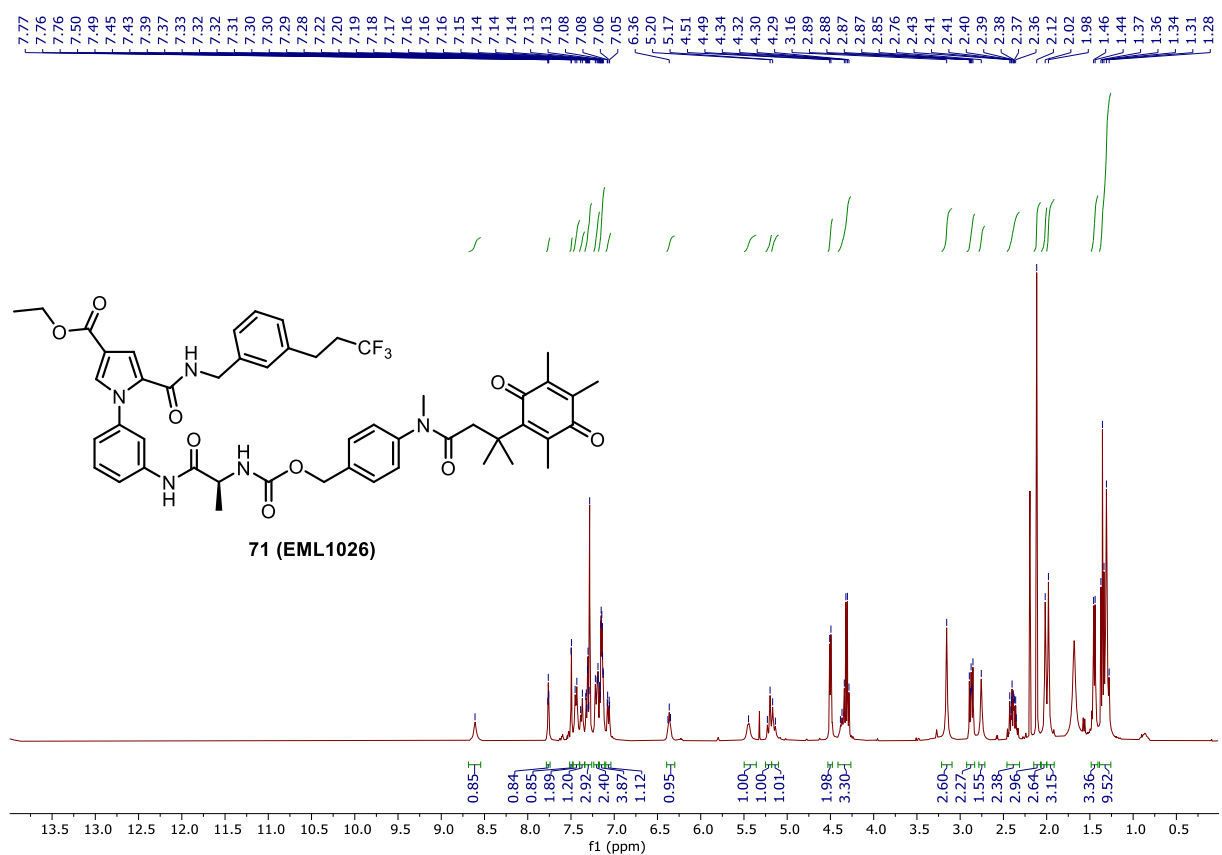


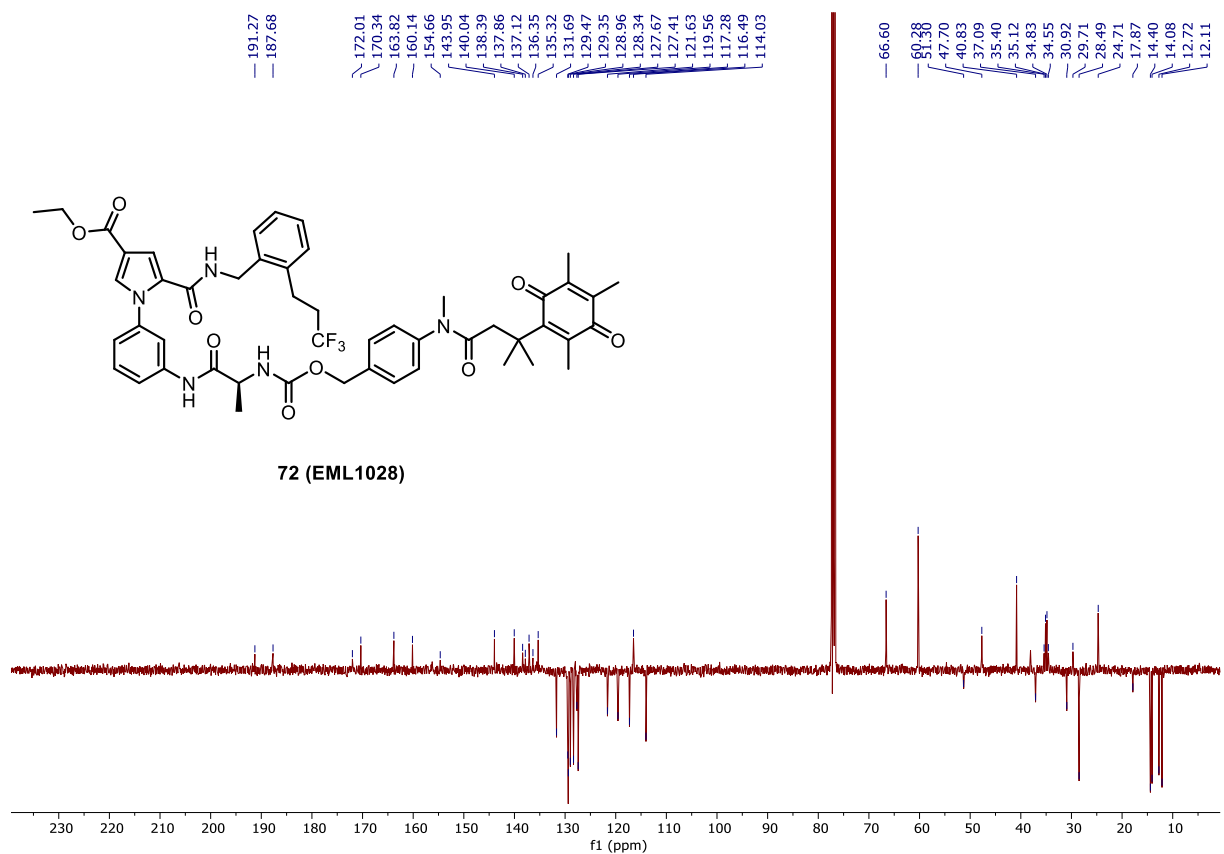
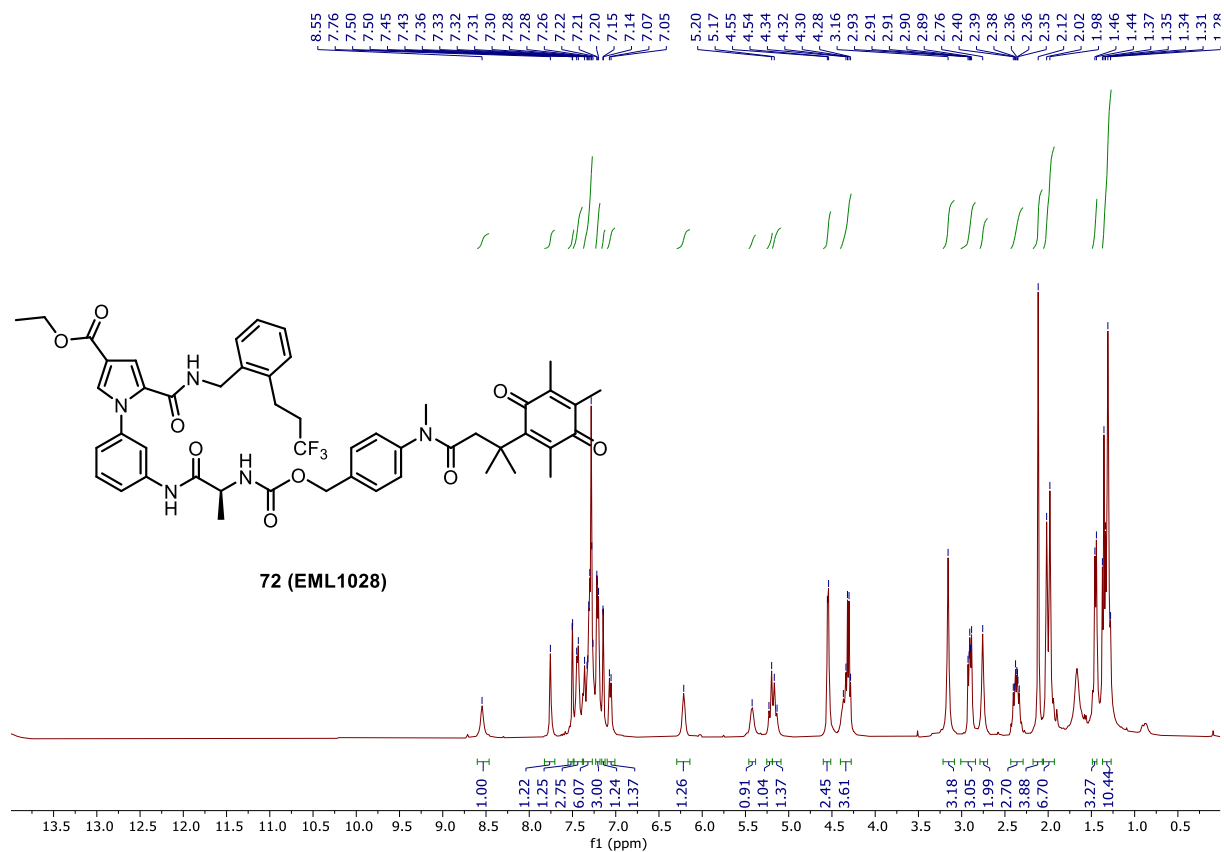


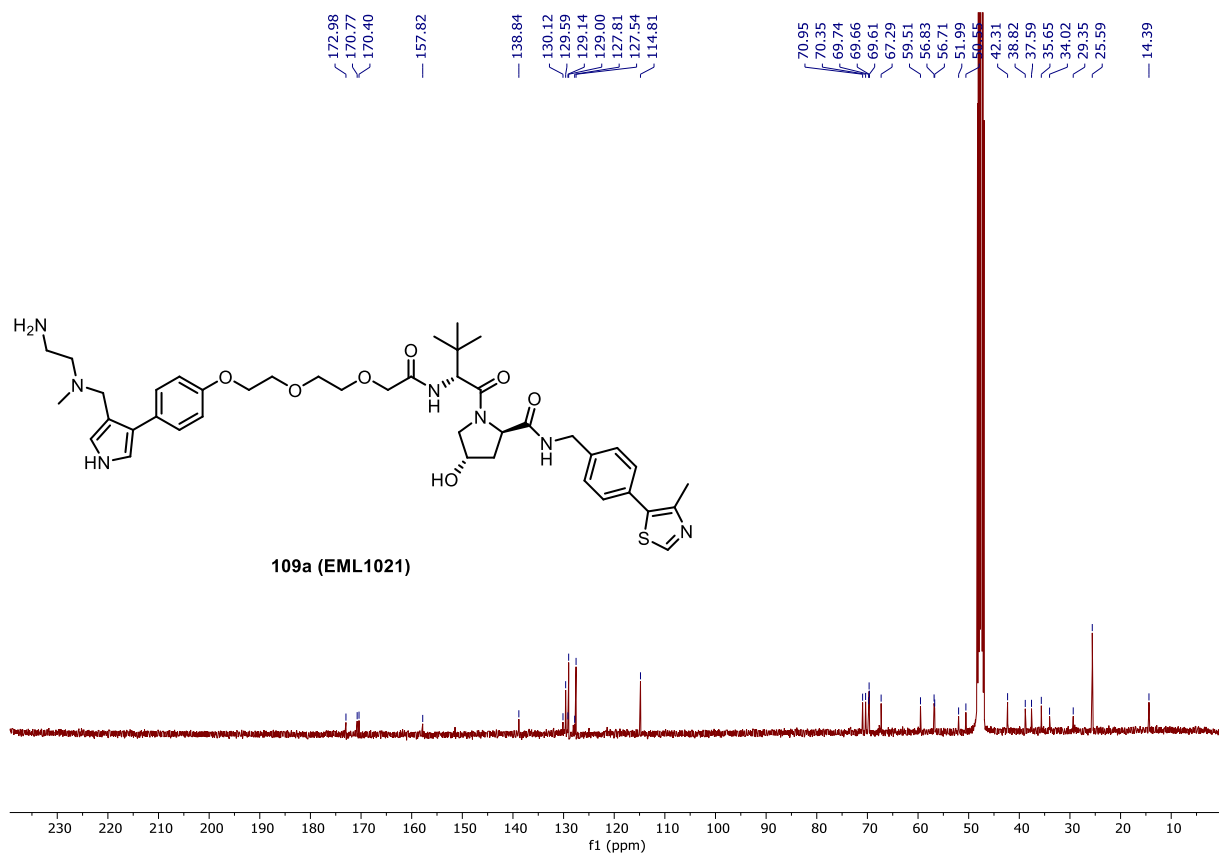
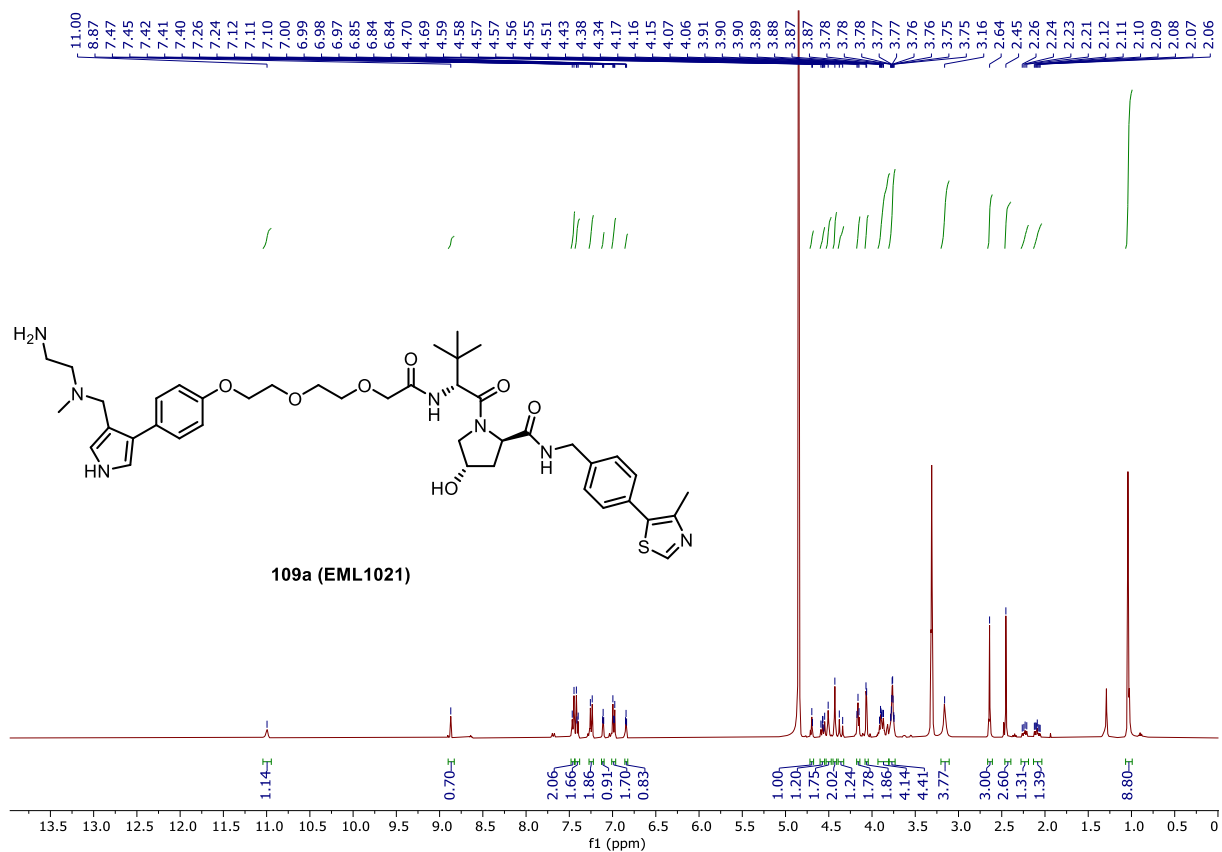


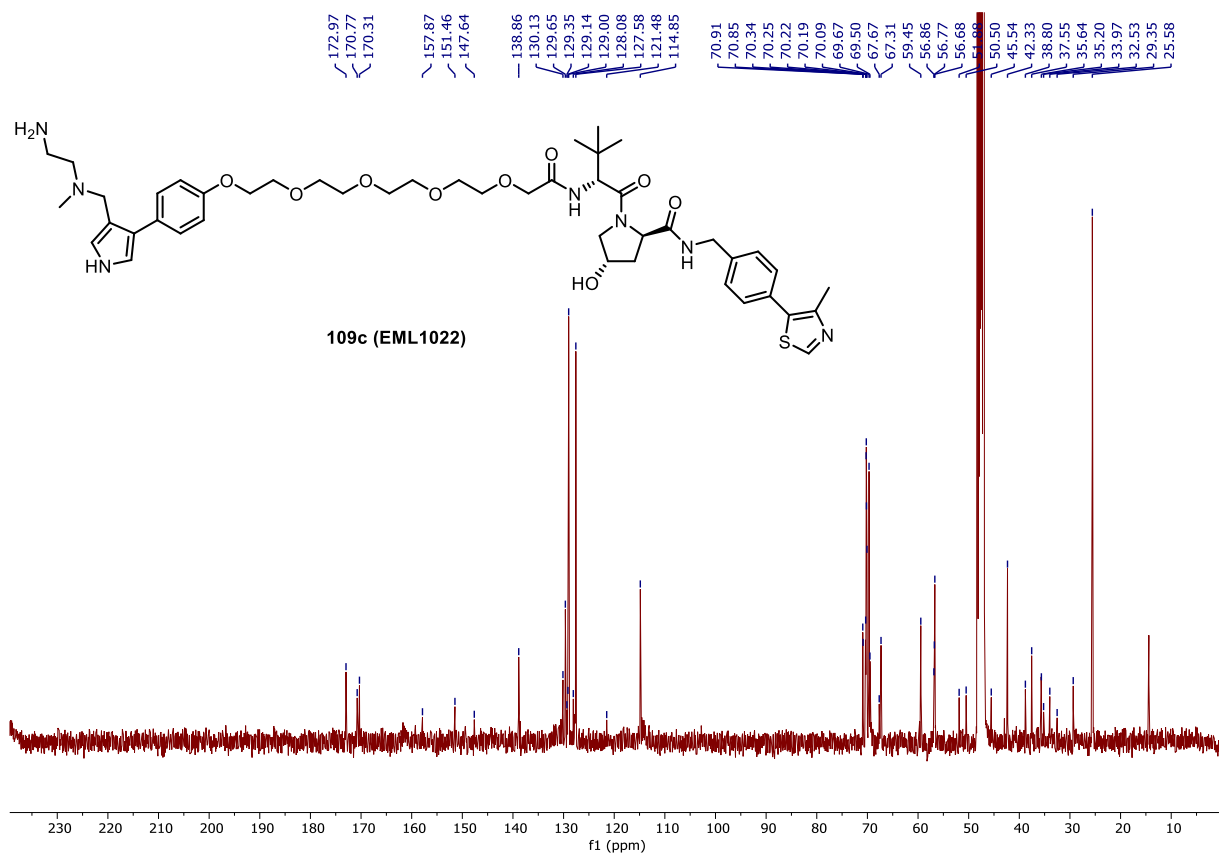
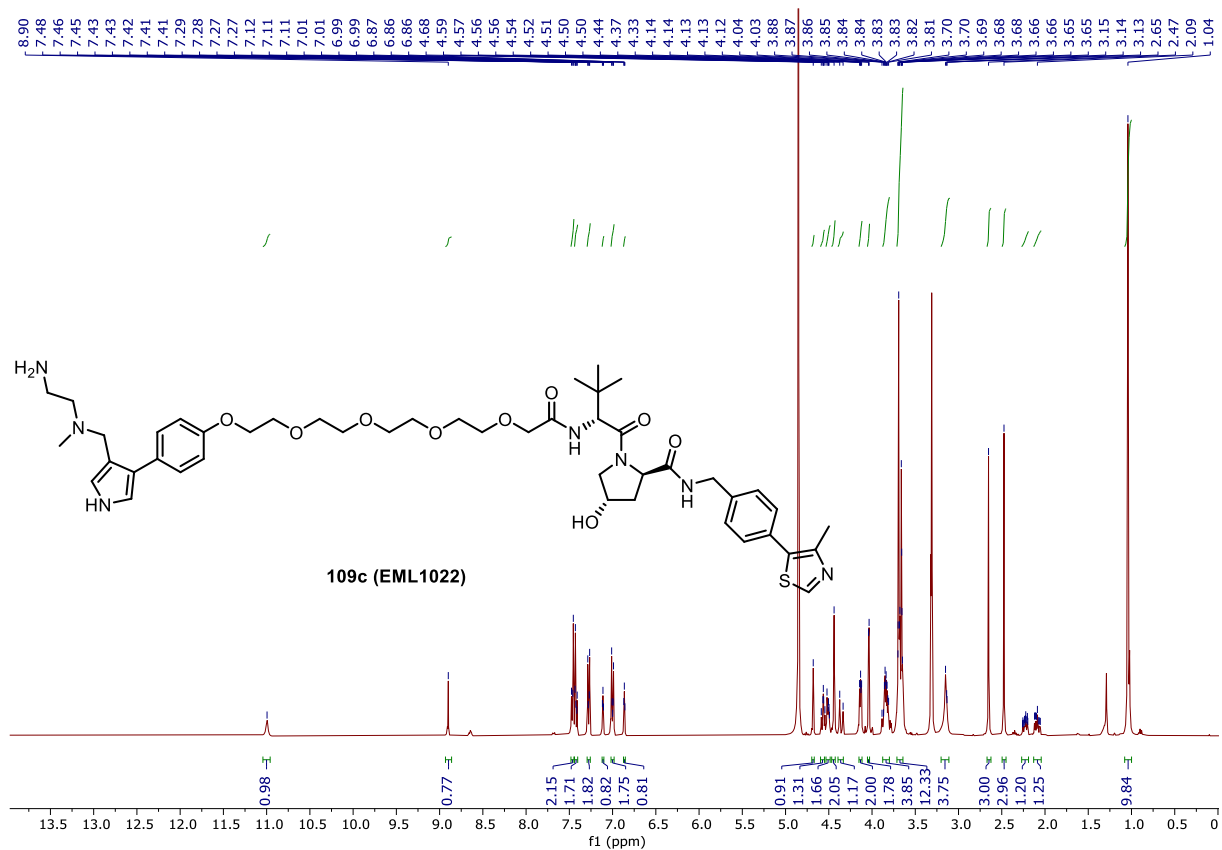


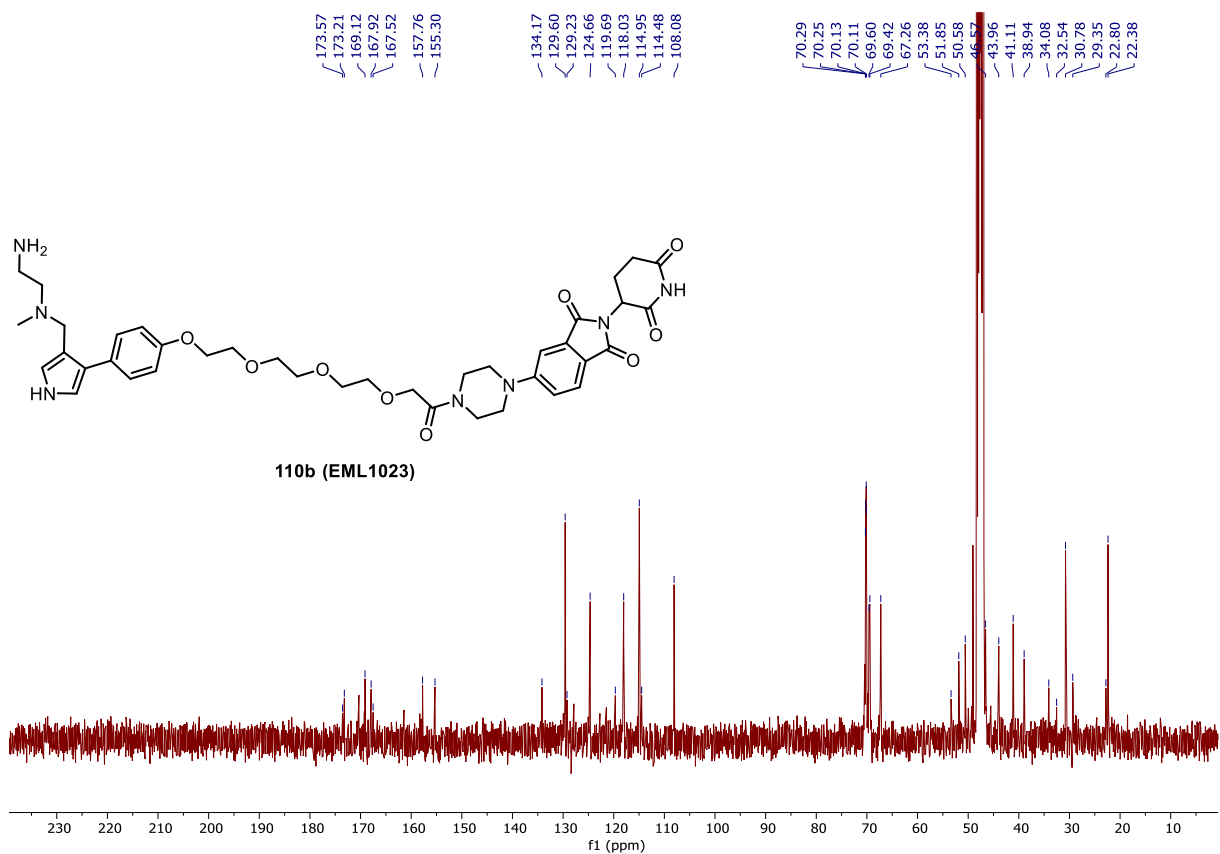
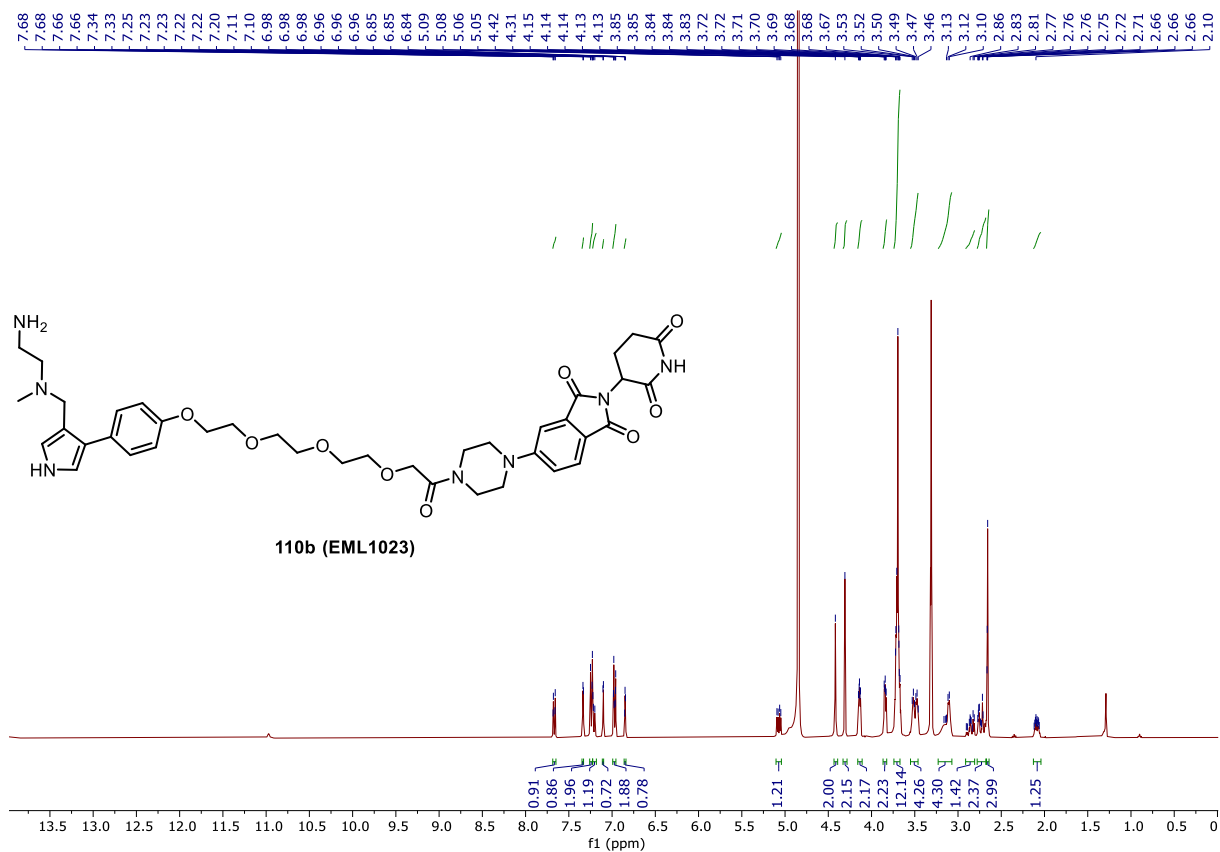


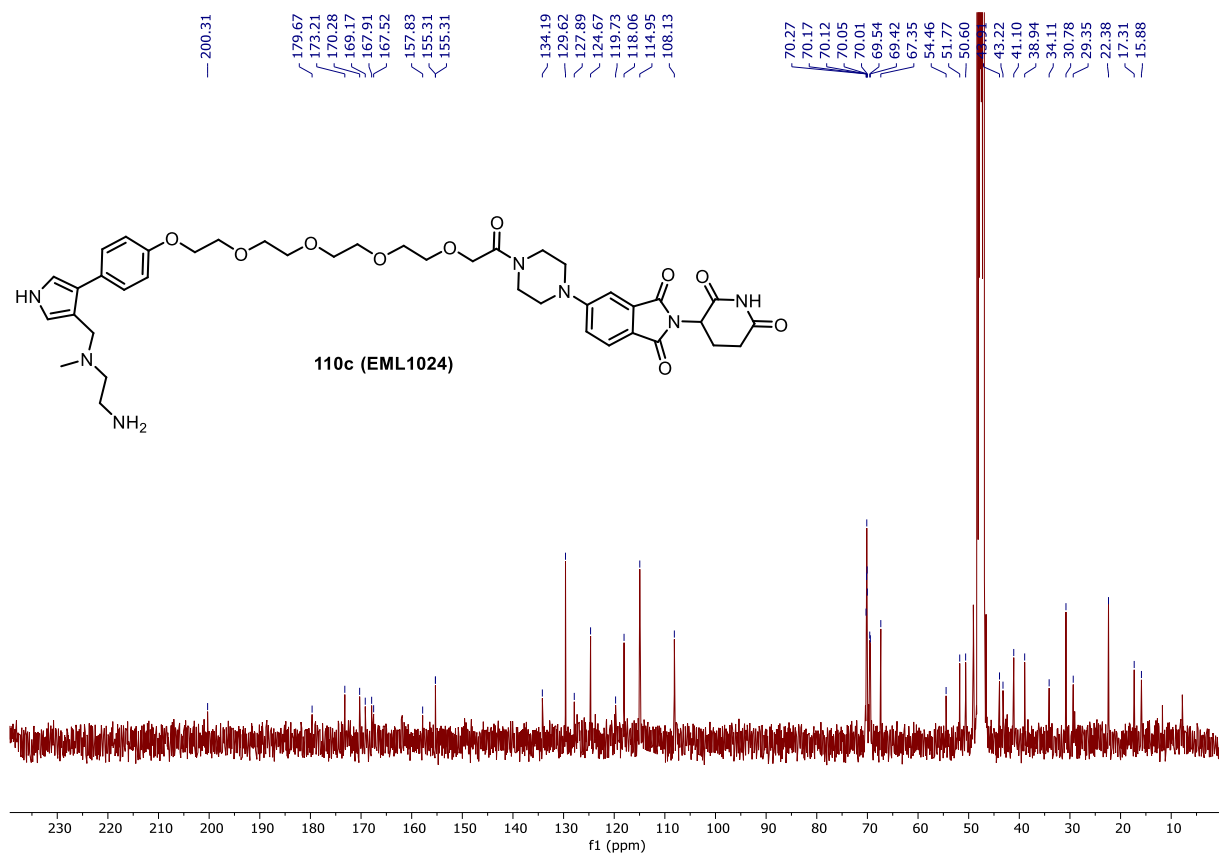
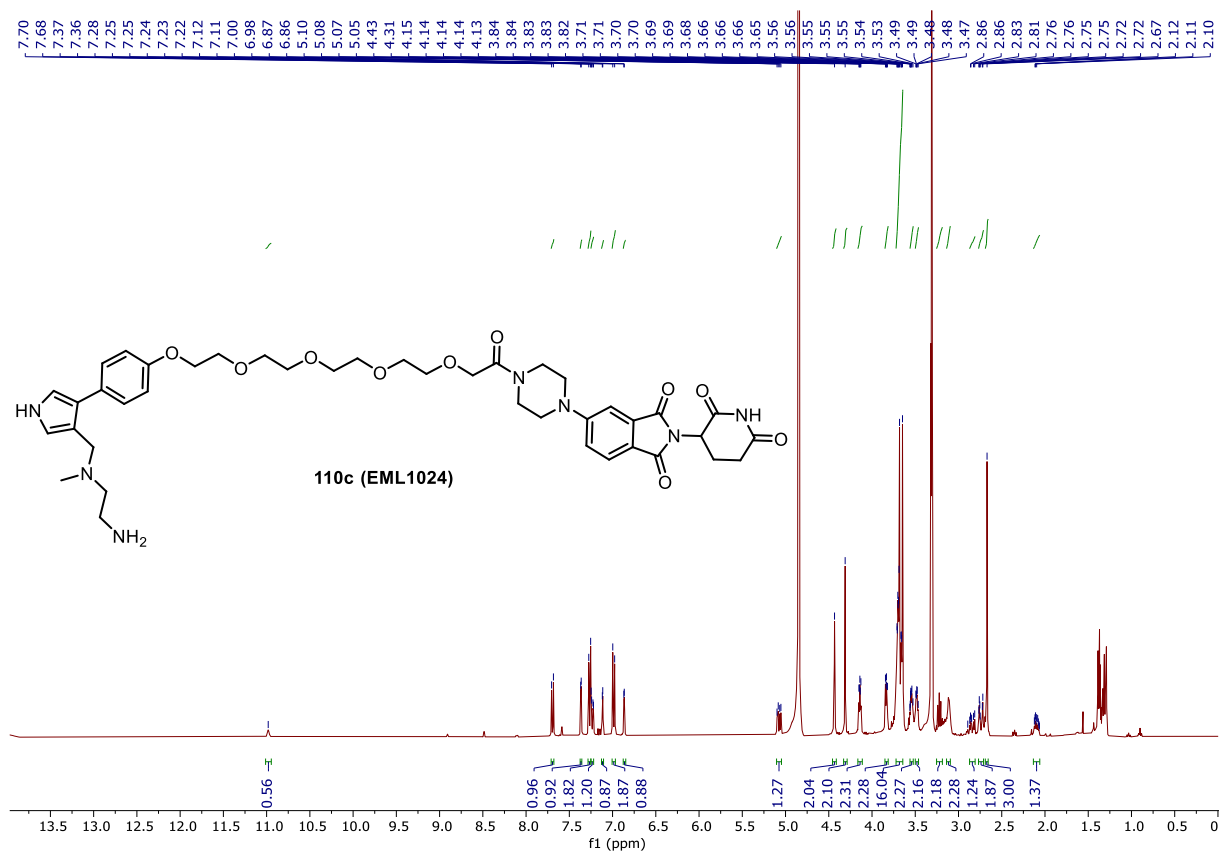


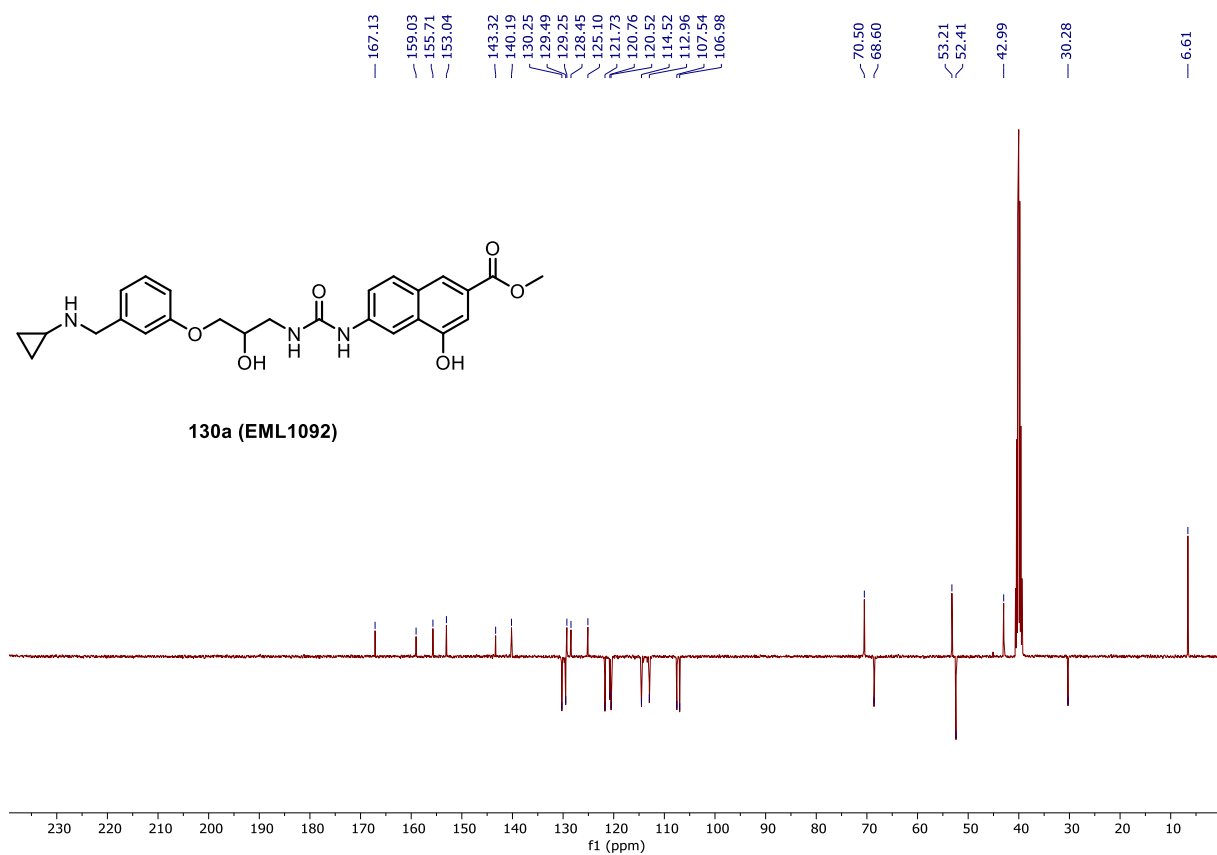
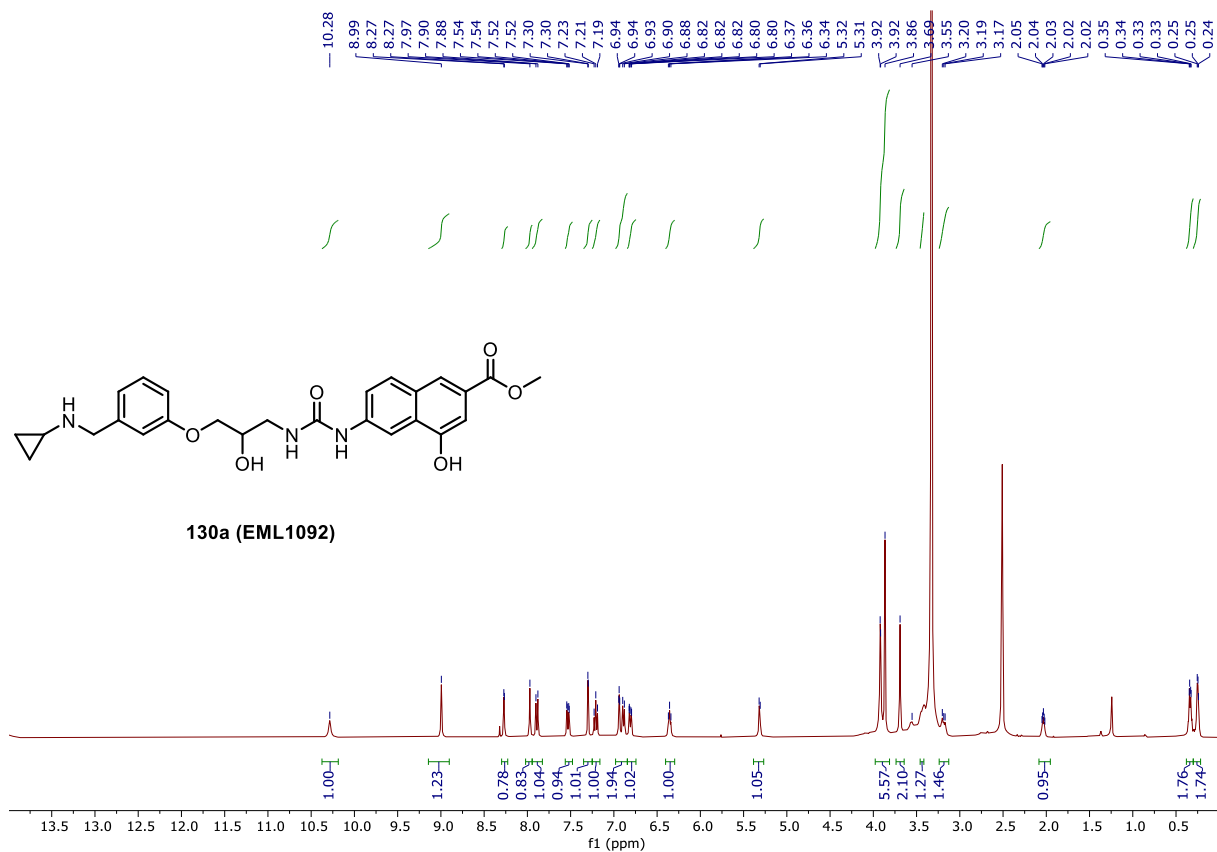


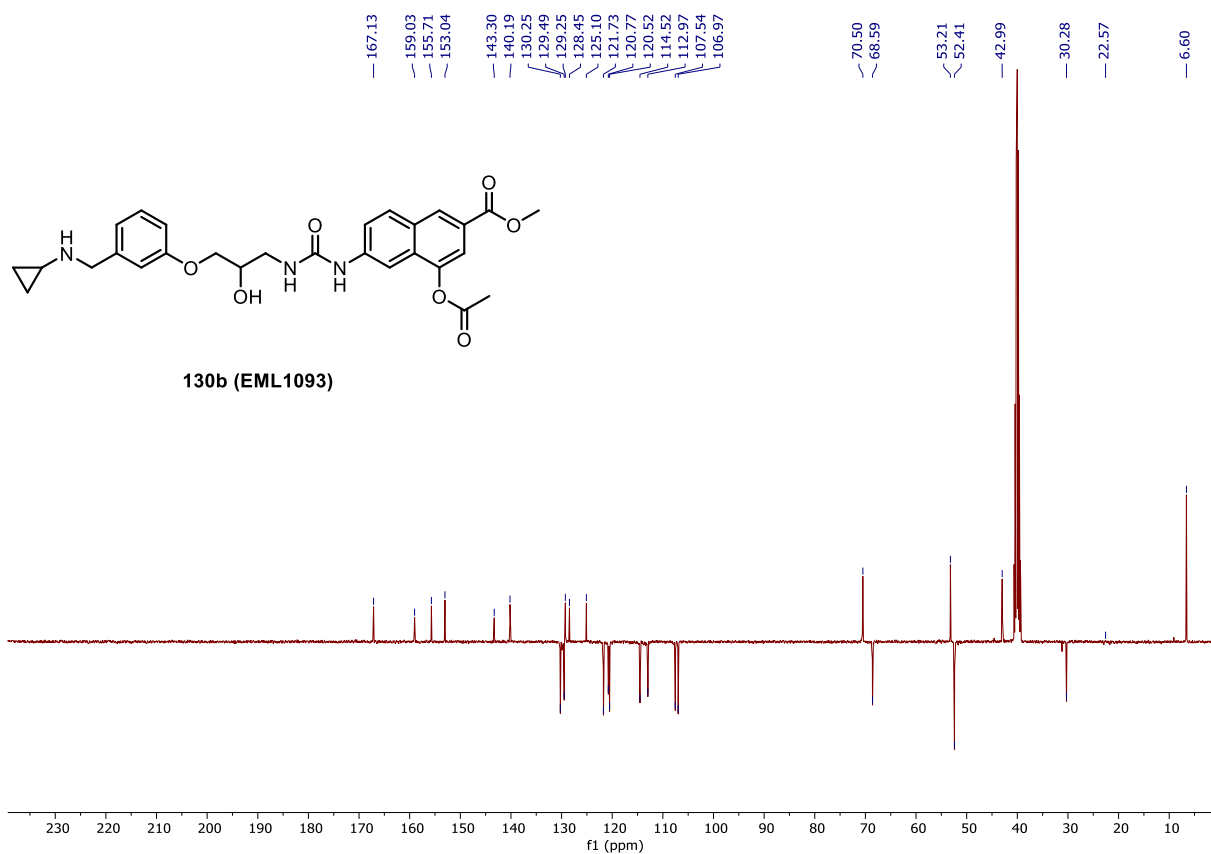
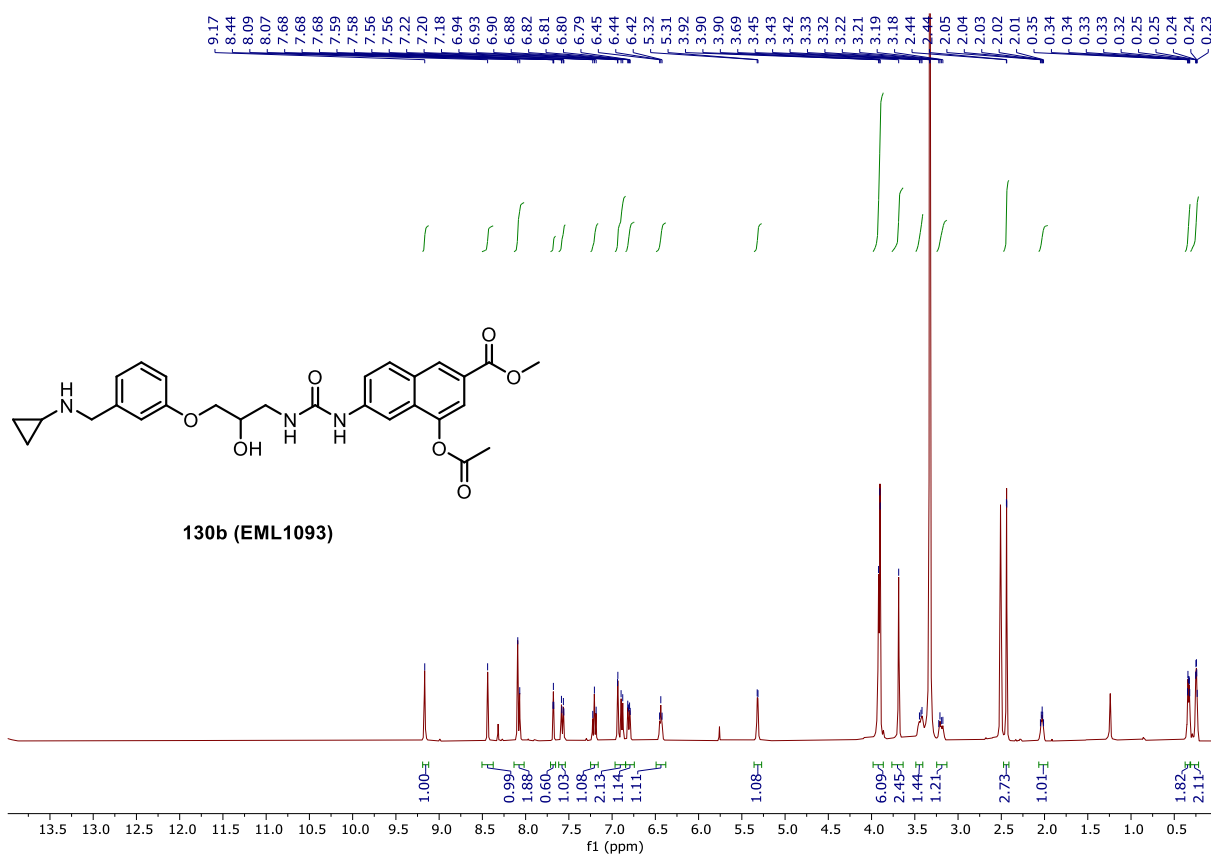


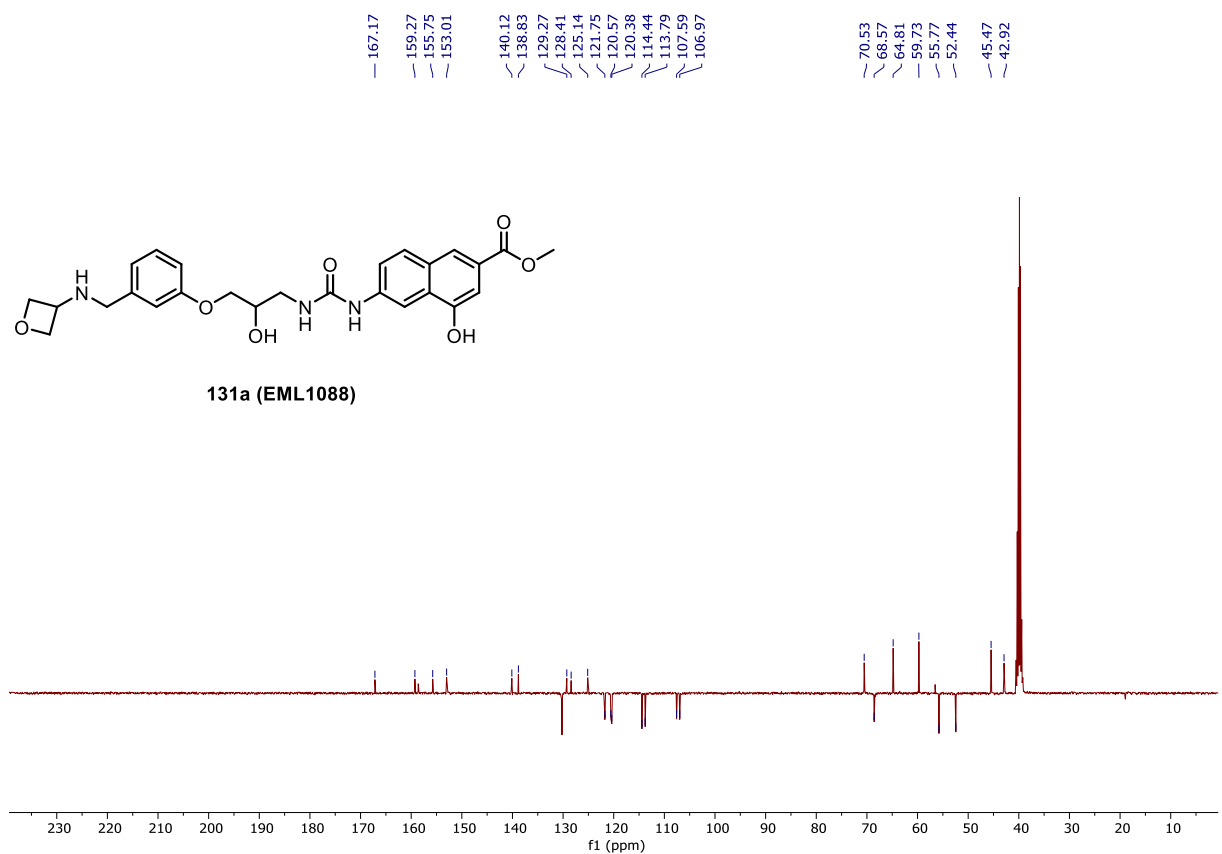
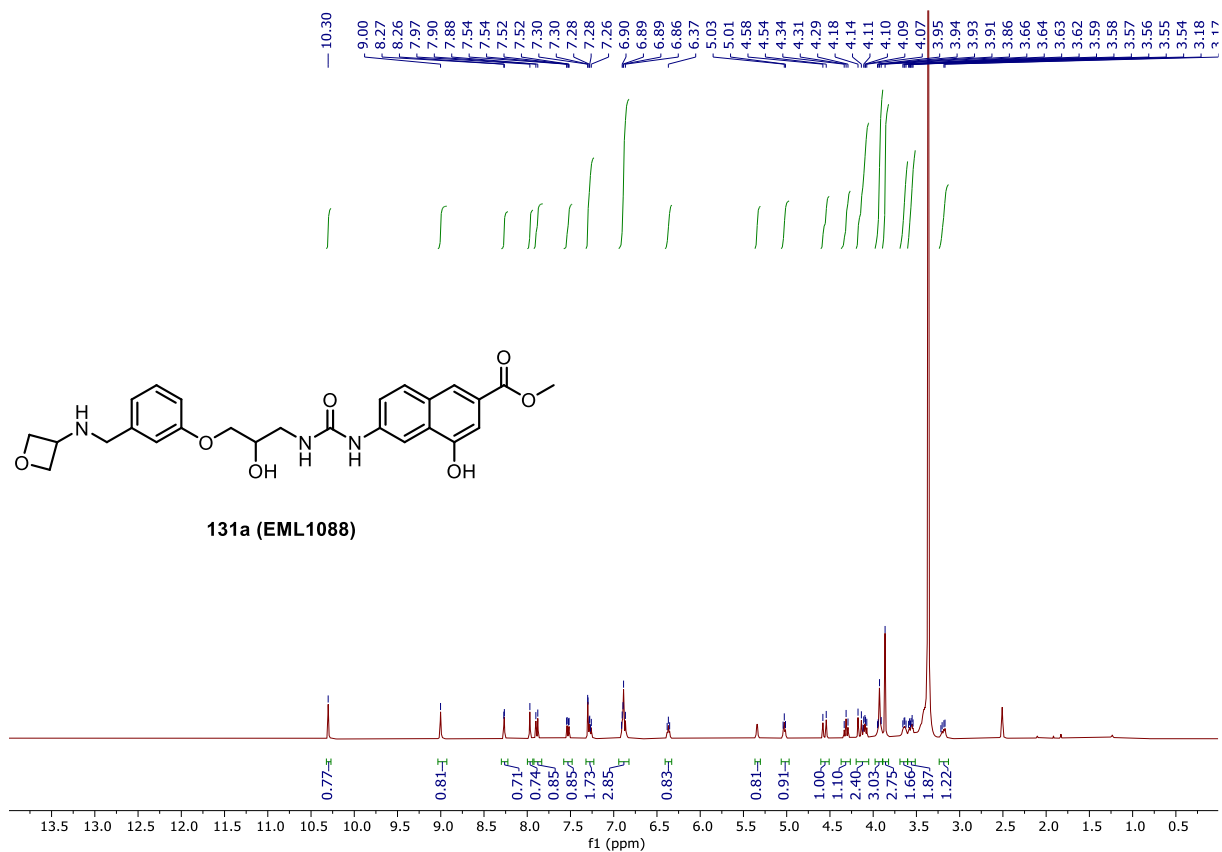


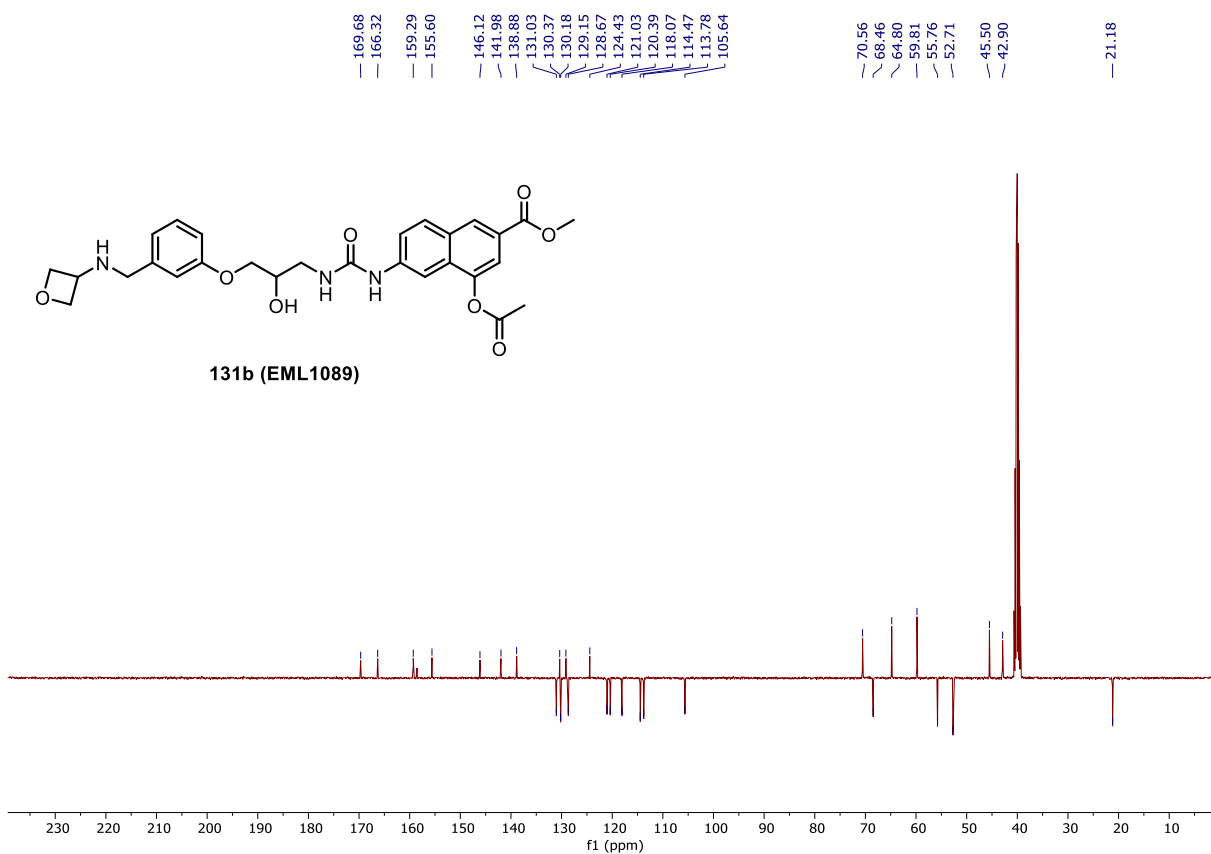
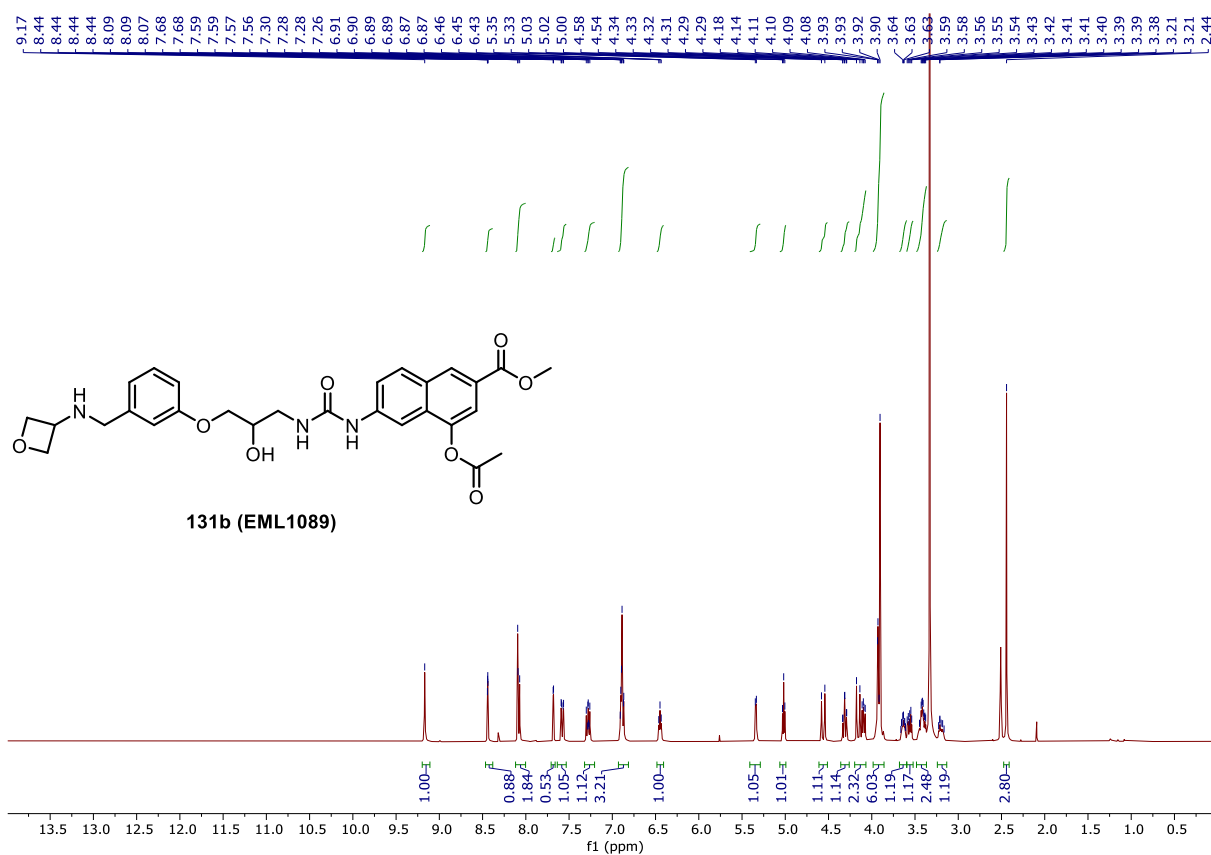


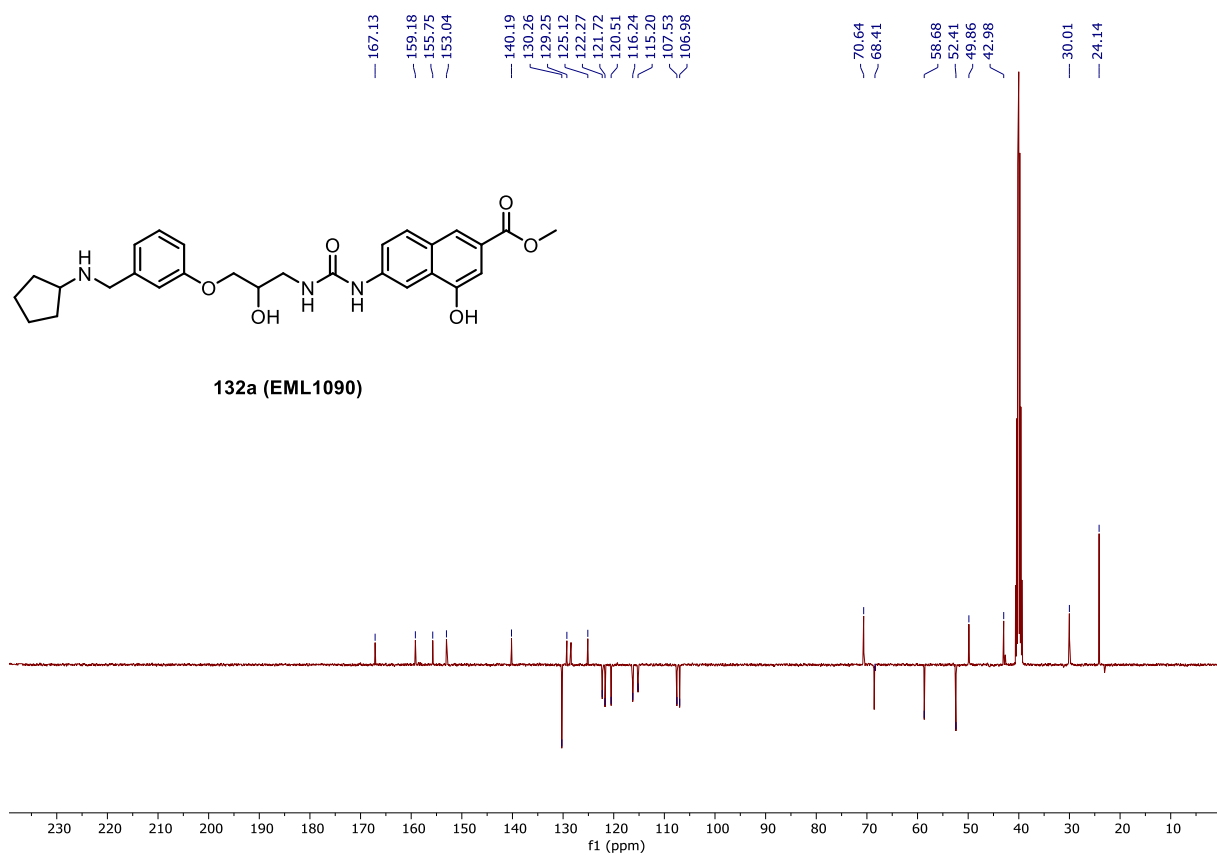
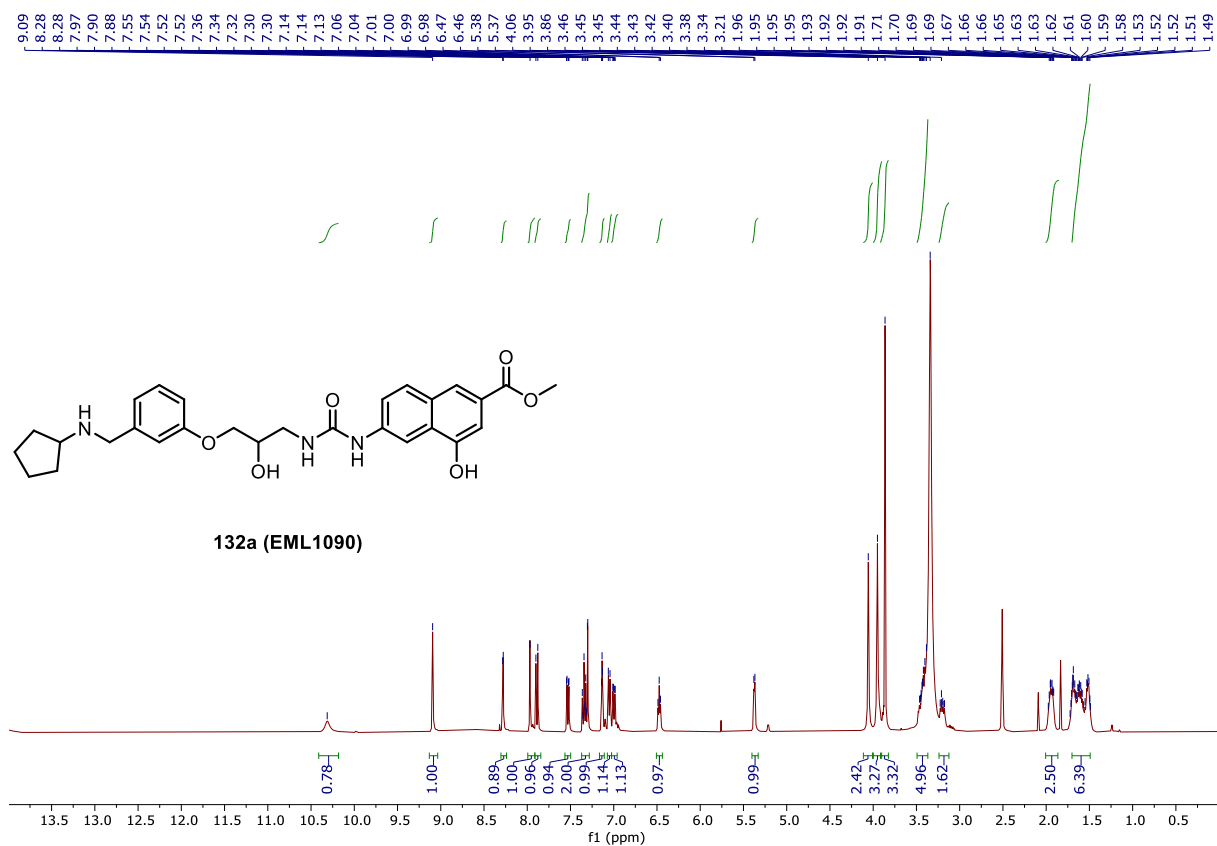


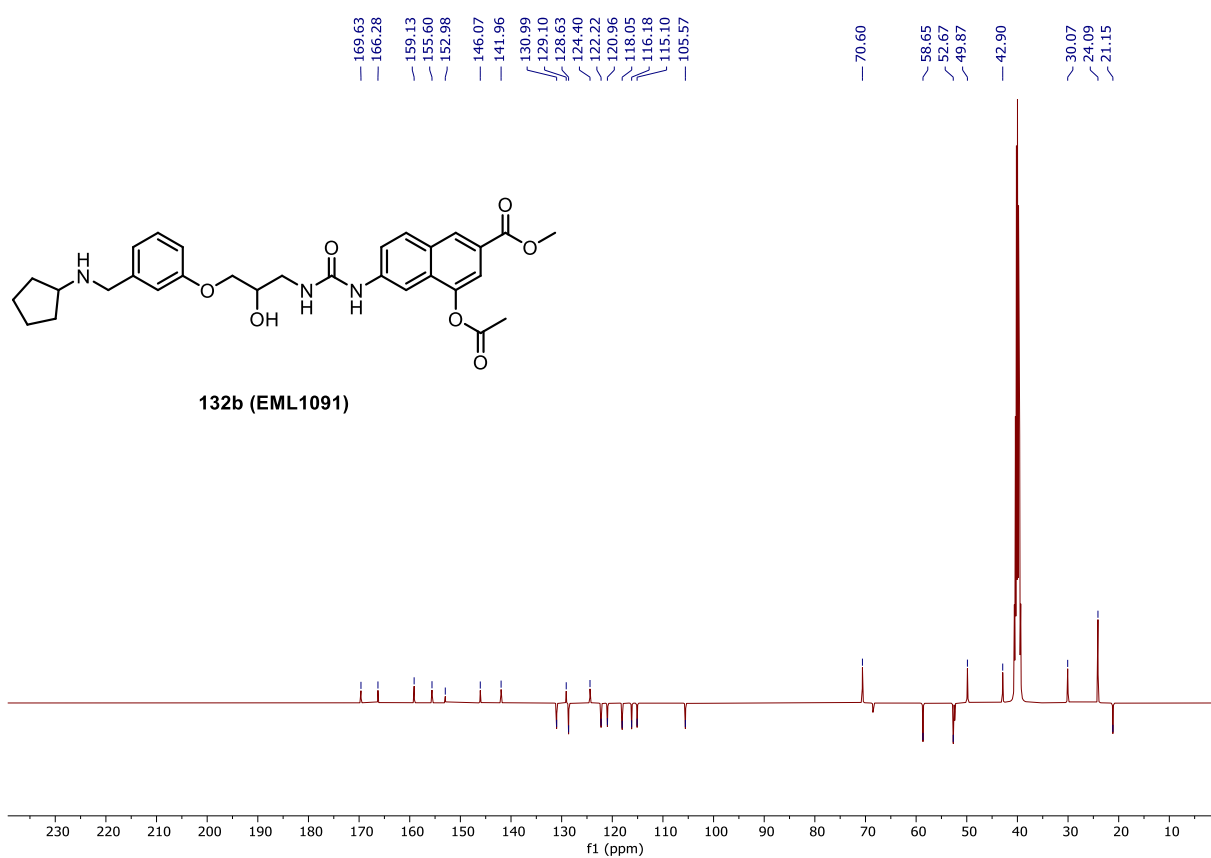
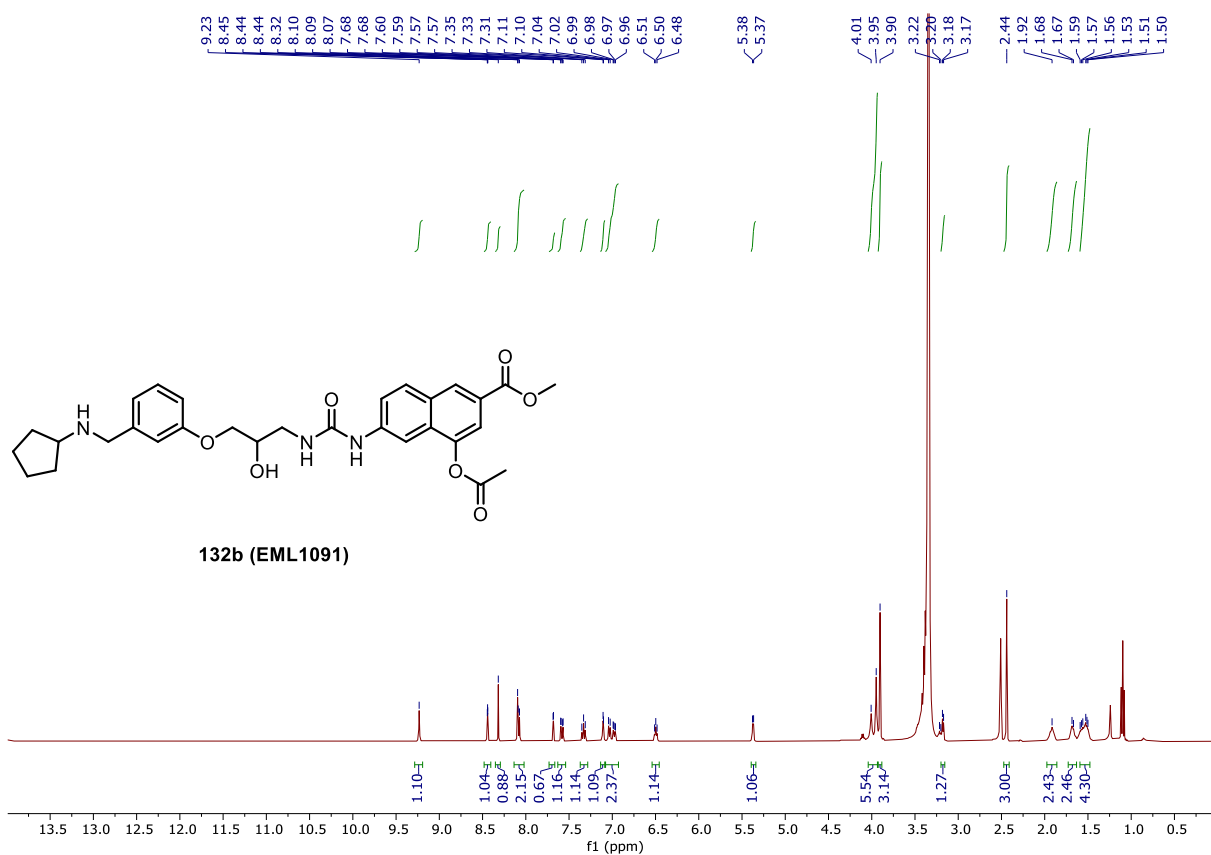












REFERENCES

1. Bird, A., Perceptions of epigenetics. *Nature (London, U. K.)* **2007**, *447* (7143), 396-398.
2. Luger, K.; Mader, A. W.; Richmond, R. K.; Sargent, D. F.; Richmond, T. J., Crystal structure of the nucleosome core particle at 2.8 Å resolution. *Nature (London)* **1997**, *389* (6648), 251-260.
3. Arrowsmith, C. H.; Bountra, C.; Fish, P. V.; Lee, K.; Schapira, M., Epigenetic protein families: a new frontier for drug discovery. *Nat. Rev. Drug Discovery* **2012**, *11* (5), 384-400.
4. Guccione, E.; Richard, S., The regulation, functions and clinical relevance of arginine methylation. *Nat. Rev. Mol. Cell Biol.* **2019**, *20* (10), 642-657.
5. Hyun, K.; Jeon, J.; Park, K.; Kim, J., Writing, erasing and reading histone lysine methylations. *Exp. Mol. Med.* **2017**, *49* (4), e324.
6. Luo, M., Current Chemical Biology Approaches to Interrogate Protein Methyltransferases. *ACS Chem. Biol.* **2012**, *7* (3), 443-463.
7. Zhou, X.; Ma, H., Evolutionary history of histone demethylase families: distinct evolutionary patterns suggest functional divergence. *BMC Evol. Biol.* **2008**, *8*, No pp. given.
8. Chang, B.; Chen, Y.; Zhao, Y.; Bruick, R. K., JMJD6 Is a Histone Arginine Demethylase. *Science (Washington, DC, U. S.)* **2007**, *318* (5849), 444-447.
9. Kwok, J.; O'Shea, M.; Hume, D. A.; Lengeling, A., Jmjd6, a JmjC dioxygenase with many interaction partners and pleiotropic functions. *Front. Genet.* **2017**, *8*, 32/1-32/19.
10. Wang, Y.; Wysocka, J.; Sayegh, J.; Lee, Y.-H.; Perlin, J. R.; Leonelli, L.; Sonbuchner, L. S.; McDonald, C. H.; Cook, R. G.; Dou, Y.; Roeder, R. G.; Clarke, S.; Stallcup, M. R.; Allis, C. D.; Coonrod, S. A., Human PAD4 regulates histone arginine methylation levels via demethyl elimination. *Science (Washington, DC, U. S.)* **2004**, *306* (5694), 279-283.
11. Yun, M.; Wu, J.; Workman, J. L.; Li, B., Readers of histone modifications. *Cell Res.* **2011**, *21* (4), 564-578.
12. Liu, K.; Chen, C.; Guo, Y.; Lam, R.; Bian, C.; Xu, C.; Zhao, D. Y.; Jin, J.; MacKenzie, F.; Pawson, T.; Min, J., Structural basis for recognition of arginine methylated Piwi proteins by the extended Tudor domain. *Proc. Natl. Acad. Sci. U. S. A., Early Ed.* **2010**, (Oct 11 2010), 1-6, 6 pp.
13. Liu, K.; Guo, Y.; Liu, H.; Bian, C.; Lam, R.; Liu, Y.; MacKenzie, F.; Rojas, L. A.; Reinberg, D.; Bedford, M. T.; Xu, R.-M.; Min, J., Crystal structure of TDRD3 and methyl-arginine binding characterization of TDRD3, SMN and SPF30. *PLoS One* **2012**, *7* (2), e30375.
14. Bedford, M. T.; Clarke, S. G., Protein arginine methylation in mammals: who, what, and why. *Mol. Cell* **2009**, *33* (1), 1-13.
15. Zhang, X.; Cheng, X., Structure of the Predominant Protein Arginine Methyltransferase PRMT1 and Analysis of Its Binding to Substrate Peptides. *Structure (Cambridge, MA, U. S.)* **2003**, *11* (5), 509-520.
16. Lee, W.-C.; Lin, W.-L.; Matsui, T.; Chen, E. S. W.; Wei, T.-Y. W.; Lin, W.-H.; Hu, H.; Zheng, Y. G.; Tsai, M.-D.; Ho, M.-C., Protein Arginine Methyltransferase 8: Tetrameric Structure and Protein Substrate Specificity. *Biochemistry* **2015**, *54* (51), 7514-7523.
17. Troffer-Charlier, N.; Cura, V.; Hassenboehler, P.; Moras, D.; Cavarelli, J., Functional insights from structures of coactivator-associated arginine methyltransferase 1 domains. *EMBO J.* **2007**, *26* (20), 4391-4401.

18. Fuhrmann, J.; Clancy, K. W.; Thompson, P. R., Chemical Biology of Protein Arginine Modifications in Epigenetic Regulation. *Chem. Rev. (Washington, DC, U. S.)* **2015**, *115* (11), 5413-5461.
19. Yang, Y.; Bedford, M. T., Protein arginine methyltransferases and cancer. *Nat. Rev. Cancer* **2013**, *13* (1), 37-50.
20. Hwang, J. W.; Cho, Y.; Bae, G.-U.; Kim, S.-N.; Kim, Y. K., Protein arginine methyltransferases: promising targets for cancer therapy. *Exp. Mol. Med.* **2021**, *53* (5), 788-808.
21. Cura, V.; Marechal, N.; Troffer-Charlier, N.; Strub, J.-M.; van Haren, M. J.; Martin, N. I.; Cianferani, S.; Bonnefond, L.; Cavarelli, J., Structural studies of protein arginine methyltransferase 2 reveal its interactions with potential substrates and inhibitors. *FEBS J.* **2017**, *284* (1), 77-96.
22. Lemmon, M. A., Pleckstrin homology (PH) domains and phosphoinositides. *Biochem. Soc. Symp.* **2007**, *74* (Signal Transduction Pathways, Part A), 81-93.
23. Antonysamy, S.; Bonday, Z.; Campbell, R. M.; Doyle, B.; Druzina, Z.; Gheyi, T.; Han, B.; Jungheim, L. N.; Qian, Y.; Rauch, C.; Russell, M.; Sauder, J. M.; Wasserman, S. R.; Wichert, K.; Willard, F. S.; Zhang, A.; Emtage, S., Crystal structure of the human PRMT5:MEP50 complex. *Proc. Natl. Acad. Sci. U. S. A.* **2012**, *109* (44), 17960-17965, S17960/1-S17960/9.
24. Tang, J.; Frankel, A.; Cook, R. J.; Kim, S.; Paik, W. K.; Williams, K. R.; Clarke, S.; Herschman, H. R., PRMT1 is the predominant type I protein arginine methyltransferase in mammalian cells. *J. Biol. Chem.* **2000**, *275* (11), 7723-7730.
25. Goulet, I.; Gauvin, G.; Boisvenue, S.; Cote, J., Alternative Splicing Yields Protein Arginine Methyltransferase 1 Isoforms with Distinct Activity, Substrate Specificity, and Subcellular Localization. *J. Biol. Chem.* **2007**, *282* (45), 33009-33021.
26. Thandapani, P.; O'Connor, T. R.; Bailey, T. L.; Richard, S., Defining the RGG/RG Motif. *Mol. Cell* **2013**, *50* (5), 613-623.
27. Cheung, N.; Fung, T. K.; Zeisig, B. B.; Holmes, K.; Rane, J. K.; Mowen, K. A.; Finn, M. G.; Lenhard, B.; Chan, L. C.; So, C. W. E., Targeting Aberrant Epigenetic Networks Mediated by PRMT1 and KDM4C in Acute Myeloid Leukemia. *Cancer Cell* **2016**, *29* (1), 32-48.
28. Li, Z.; Wang, D.; Chen, X.; Wang, W.; Wang, P.; Hou, P.; Li, M.; Chu, S.; Qiao, S.; Zheng, J.; Bai, J.; Li, Z.; Hou, P.; Li, M.; Zheng, J.; Bai, J.; Wang, D., PRMT1-mediated EZH2 methylation promotes breast cancer cell proliferation and tumorigenesis. *Cell Death Dis* **2021**, *12* (11), 1080.
29. Gou, Y.; Li, J.; Jackson-Weaver, O.; Wu, J.; Zhang, T.; Gupta, R.; Cho, I.; Ho, T. V.; Chen, Y.; Li, M.; Richard, S.; Wang, J.; Chai, Y.; Xu, J., Protein Arginine Methyltransferase PRMT1 Is Essential for Palatogenesis. *J. Dent. Res.* **2018**, *97* (13), 1510-1518.
30. Hashimoto, M.; Kumabe, A.; Kim, J.-D.; Murata, K.; Sekizar, S.; Williams, A.; Lu, W.; Ishida, J.; Nakagawa, T.; Endo, M.; Minami, Y.; Fukamizu, A., Loss of PRMT1 in the central nervous system (CNS) induces reactive astrocytes and microglia during postnatal brain development. *J. Neurochem.* **2021**, *156* (6), 834-847.
31. Zhang, L.; Tran, N.-T.; Su, H.; Wang, R.; Lu, Y.; Tang, H.; Aoyagi, S.; Guo, A.; Khodadadi-Jamayran, A.; Zhou, D.; Qian, K.; Hricik, T.; Cote, J.; Han, X.; Zhou, W.; Laha, S.; Abdel-Wahab, O.; Levine, R. L.; Raffel, G.; Liu, Y.; Chen, D.; Li, H.; Townes, T.; Wang, H.; Deng, H.; Zheng, Y. G.; Leslie, C.; Luo, M.; Zhao, X., Cross-talk between PRMT1-mediated methylation and ubiquitylation on RBM15 controls RNA splicing. *eLife* **2015**, *4*, 1-56.

32. Yu, Z.; Vogel, G.; Coulombe, Y.; Dubeau, D.; Spehalski, E.; Hebert, J.; Ferguson, D. O.; Masson, J. Y.; Richard, S., The MRE11 GAR motif regulates DNA double-strand break processing and ATR activation. *Cell Res.* **2012**, *22* (2), 305-320.
33. Boisvert, F.-M.; Rhie, A.; Richard, S.; Doherty, A. J., The GAR motif of 53BP1 is arginine methylated by PRMT1 and is necessary for 53BP1 DNA binding activity. *Cell Cycle* **2005**, *4* (12), 1834-1841.
34. Montenegro, M. F.; Gonzalez-Guerrero, R.; Sanchez-del-Campo, L.; Pinero-Madrona, A.; Cabezas-Herrera, J.; Rodriguez-Lopez, J. N., PRMT1-dependent methylation of BRCA1 contributes to the epigenetic defense of breast cancer cells against ionizing radiation. *Sci. Rep.* **2020**, *10* (1), 13275.
35. Xu, J.; Wang, A. H.; Osés-Prieto, J.; Makhijani, K.; Katsuno, Y.; Pei, M.; Yan, L.; Zheng, Y. G.; Burlingame, A.; Bruckner, K.; Derynck, R., Arginine Methylation Initiates BMP-Induced Smad Signaling. *Mol. Cell* **2013**, *51* (1), 5-19.
36. Katsuno, Y.; Qin, J.; Osés-Prieto, J.; Wang, H.; Jackson-Weaver, O.; Zhang, T.; Lamouille, S.; Wu, J.; Burlingame, A.; Xu, J.; Derynck, R., Arginine methylation of SMAD7 by PRMT1 in TGF- β -induced epithelial-mesenchymal transition and epithelial stem-cell generation. *J. Biol. Chem.* **2018**, *293* (34), 13059-13072.
37. Le Romancer, M.; Treilleux, I.; Leconte, N.; Robin-Lespinasse, Y.; Sentis, S.; Boucheikioua-Bouzaghrou, K.; Goddard, S.; Gobert-Gosse, S.; Corbo, L., Regulation of estrogen rapid signaling through arginine methylation by PRMT1. *Mol. Cell* **2008**, *31* (2), 212-221.
38. Cai, T.; Yu, Z.; Wang, Z.; Liang, C.; Richard, S., Arginine methylation of SARS-CoV-2 nucleocapsid protein regulates RNA binding, its ability to suppress stress granule formation, and viral replication. *J. Biol. Chem.* **2021**, *297* (1), 100821.
39. Wolf, S. S., The protein arginine methyltransferase family: An update about function, new perspectives and the physiological role in humans. *Cell. Mol. Life Sci.* **2009**, *66* (13), 2109-2121.
40. Lakowski, T. M.; Frankel, A., Kinetic analysis of human protein arginine N-methyltransferase 2: formation of monomethyl- and asymmetric dimethyl-arginine residues on histone H4. *Biochem. J.* **2009**, *421* (2), 253-261.
41. Dong, F.; Li, Q.; Yang, C.; Huo, D.; Wang, X.; Ai, C.; Kong, Y.; Sun, X.; Wang, W.; Zhou, Y.; Liu, X.; Li, W.; Gao, W.; Liu, W.; Kang, C.; Wu, X., PRMT2 links histone H3R8 asymmetric dimethylation to oncogenic activation and tumorigenesis of glioblastoma. *Nat. Commun.* **2018**, *9* (1), 1-14.
42. Qi, C.; Chang, J.; Zhu, Y.; Yeldandi, A. V.; Rao, S. M.; Zhu, Y.-J., Identification of protein arginine methyltransferase 2 as a coactivator for estrogen receptor α . *J. Biol. Chem.* **2002**, *277* (32), 28624-28630.
43. Yoshimoto, T.; Boehm, M.; Olive, M.; Crook, M. F.; San, H.; Langenickel, T.; Nabel, E. G., The arginine methyltransferase PRMT2 binds RB and regulates E2F function. *Exp. Cell Res.* **2006**, *312* (11), 2040-2053.
44. Vhuiyan, M. I.; Pak, M. L.; Park, M. A.; Thomas, D.; Lakowski, T. M.; Chalfant, C. E.; Frankel, A., PRMT2 interacts with splicing factors and regulates the alternative splicing of BCL-X. *J. Biochem.* **2017**, *162* (1), 17-25.
45. Zhong, J.; Cao, R. X.; Liu, J. H.; Liu, Y. B.; Wang, J.; Liu, L. P.; Chen, Y. J.; Yang, J.; Zhang, Q. H.; Wu, Y.; Ding, W. J.; Hong, T.; Xiao, X. H.; Zu, X. Y.; Wen, G. B., Nuclear loss of protein arginine N-methyltransferase 2 in breast carcinoma is associated with tumor grade and overexpression of cyclin D1 protein. *Oncogene* **2014**, *33* (48), 5546-5558.
46. Zeng, S.-Y.; Luo, J.-F.; Quan, H.-Y.; Xiao, Y.-B.; Liu, Y.-H.; Lu, H.-Q.; Qin, X.-P., Protein arginine methyltransferase 2 inhibits angiotensin II-induced proliferation and

- inflammation in vascular smooth muscle cells. *BioMed Res. Int.* **2018**, 1547452/1-1547452/8.
47. Swiercz, R.; Cheng, D.; Kim, D.; Bedford, M. T., Ribosomal Protein rpS2 Is Hypomethylated in PRMT3-deficient Mice. *J. Biol. Chem.* **2007**, 282 (23), 16917-16923.
 48. Zou, Y.; Webb, K.; Perna, A. D.; Zhang, Q.; Clarke, S.; Wang, Y., A Mass Spectrometric Study on the in Vitro Methylation of HMGA1a and HMGA1b Proteins by PRMTs: Methylation Specificity, the Effect of Binding to AT-Rich Duplex DNA, and the Effect of C-Terminal Phosphorylation. *Biochemistry* **2007**, 46 (26), 7896-7906.
 49. Fronz, K.; Otto, S.; Koelbel, K.; Kuehn, U.; Friedrich, H.; Schierhorn, A.; Beck-Sickinger, A. G.; Ostareck-Lederer, A.; Wahle, E., Promiscuous Modification of the Nuclear Poly(A)-binding Protein by Multiple Protein-arginine Methyltransferases Does Not Affect the Aggregation Behavior. *J. Biol. Chem.* **2008**, 283 (29), 20408-20420.
 50. Allali-Hassani, A.; Wasney, G. A.; Siarheyeva, A.; Hajian, T.; Arrowsmith, C. H.; Vedadi, M., Fluorescence-based methods for screening writers and readers of histone methyl marks. *J. Biomol. Screening* **2012**, 17 (1), 71-84.
 51. Singh, V.; Miranda, T. B.; Jiang, W.; Frankel, A.; Roemer, M. E.; Robb, V. A.; Gutmann, D. H.; Herschman, H. R.; Clarke, S.; Newsham, I. F., DAL-1/4.1B tumor suppressor interacts with protein arginine N-methyltransferase 3 (PRMT3) and inhibits its ability to methylate substrates in vitro and in vivo. *Oncogene* **2004**, 23 (47), 7761-7771.
 52. Domingues, P.; Lopes, M. C.; Domingues, P.; Gonzalez-Tablas, M.; Orfao, A.; Tabernero, M. D.; Otero, A.; Pascual, D.; Ruiz, L.; Miranda, D.; Sousa, P.; Goncalves, J. M.; Tabernero, M. D., Genetic/molecular alterations of meningiomas and the signaling pathways targeted. *Oncotarget* **2015**, 6 (13), 10671-88.
 53. Zhang, M.; Liu, X.; Li, Z.; Du, Y.; Liu, X.; Lv, L.; Xiao, Z.; Liu, Y.; Ping, Z.; Zhou, Y., Asymmetrical methyltransferase PRMT3 regulates human mesenchymal stem cell osteogenesis via miR-3648. *Cell Death Dis.* **2019**, 10 (8), 1-17.
 54. Jacques, S. L.; Aquino, K. P.; Gureasko, J.; Boriack-Sjodin, P. A.; Porter Scott, M.; Copeland, R. A.; Riera, T. V., CARM1 Preferentially Methylates H3R17 over H3R26 through a Random Kinetic Mechanism. *Biochemistry* **2016**, 55 (11), 1635-1644.
 55. Chen, D.; Han, M.; Hong, H.; Koh, S. S.; Huang, S.-M.; Schurter, B. T.; Aswad, D. W.; Stallcup, M. R., Regulation of transcription by a protein methyltransferase. *Science (Washington, D. C.)* **1999**, 284 (5423), 2174-2177.
 56. Lee, J.; Bedford, M. T., PABP1 identified as an arginine methyltransferase substrate using high-density protein arrays. *EMBO Rep.* **2002**, 3 (3), 268-273.
 57. Xu, Z.; Jiang, J.; Xu, C.; Wang, Y.; Sun, L.; Guo, X.; Liu, H., MicroRNA-181 regulates CARM1 and histone arginine methylation to promote differentiation of human embryonic stem cells. *PLoS One* **2013**, 8 (1), e53146.
 58. Cheng, D.; Cote, J.; Shaaban, S.; Bedford, M. T., The arginine methyltransferase CARM1 regulates the coupling of transcription and mRNA processing. *Mol. Cell* **2007**, 25 (1), 71-83.
 59. Ohkura, N.; Takahashi, M.; Yaguchi, H.; Nagamura, Y.; Tsukada, T., Coactivator-associated Arginine Methyltransferase 1, CARM1, Affects Pre-mRNA Splicing in an Isoform-specific Manner. *J. Biol. Chem.* **2005**, 280 (32), 28927-28935.
 60. Lee, Y.-H.; Stallcup, M. R., Roles of protein arginine methylation in DNA damage signaling pathways: is CARM1 a life-or-death decision point? *Cell Cycle* **2011**, 10 (9), 1343-1344.

61. Hupalowska, A.; Jedrusik, A.; Zhu, M.; Bedford, M. T.; Glover, D. M.; Zernicka-Goetz, M., CARM1 and Paraspeckles Regulate Pre-implantation Mouse Embryo Development. *Cell (Cambridge, MA, U. S.)* **2018**, *175* (7), 1902-1916.e13.
62. Zhong, X.-Y.; Yuan, X.-M.; Xu, Y.-Y.; Yin, M.; Yan, W.-W.; Zou, S.-W.; Wei, L.-M.; Lu, H.-J.; Wang, Y.-P.; Lei, Q.-Y., CARM1 Methylates GAPDH to Regulate Glucose Metabolism and Is Suppressed in Liver Cancer. *Cell Rep.* **2018**, *24* (12), 3207-3223.
63. Wang, L.; Zhao, Z.; Meyer, M. B.; Saha, S.; Yu, M.; Guo, A.; Wisinski, K. B.; Huang, W.; Cai, W.; Pike, J. W.; Yuan, M.; Ahlquist, P.; Xu, W., CARM1 Methylates Chromatin Remodeling Factor BAF155 to Enhance Tumor Progression and Metastasis. *Cancer Cell* **2016**, *30* (1), 179-180.
64. Wang, Y.-P.; Zhou, W.; Wang, J.; Huang, X.; Zuo, Y.; Wang, T.-S.; Gao, X.; Xu, Y.-Y.; Zou, S.-W.; Liu, Y.-B.; Cheng, J.-K.; Lei, Q.-Y., Arginine Methylation of MDH1 by CARM1 Inhibits Glutamine Metabolism and Suppresses Pancreatic Cancer. *Mol. Cell* **2016**, *64* (4), 673-687.
65. Veazey, K. J.; Cheng, D.; Lin, K.; Villarreal, O. D.; Gao, G.; Perez-Oquendo, M.; Van, H. T.; Stratton, S. A.; Green, M.; Xu, H.; Lu, Y.; Bedford, M. T.; Santos, M. A., CARM1 inhibition reduces histone acetyltransferase activity causing synthetic lethality in CREBBP/EP300-mutated lymphomas. *Leukemia* **2020**, *34* (12), 3269-3285.
66. Al-Dhaheeri, M.; Wu, J.; Skliris, G. P.; Li, J.; Higashimoto, K.; Wang, Y.; White, K. P.; Lambert, P.; Zhu, Y.; Murphy, L.; Xu, W., CARM1 Is an Important Determinant of ER α -Dependent Breast Cancer Cell Differentiation and Proliferation in Breast Cancer Cells. *Cancer Res.* **2011**, *71* (6), 2118-2128.
67. Wang, L.; Zeng, H.; Wang, Q.; Zhao, Z.; Boyer, T. G.; Bian, X.; Xu, W., MED12 methylation by CARM1 sensitizes human breast cancer cells to chemotherapy drugs. *Sci. Adv.* **2015**, *1* (9), e1500463/1-e1500463/11.
68. Kim, J.; Lee, J.; Yadav, N.; Wu, Q.; Carter, C.; Richard, S.; Richie, E.; Bedford, M. T., Loss of CARM1 Results in Hypomethylation of Thymocyte Cyclic AMP-regulated Phosphoprotein and Deregulated Early T Cell Development. *J. Biol. Chem.* **2004**, *279* (24), 25339-25344.
69. Wang, Y.; Ju, C.; Hu, J.; Huang, K.; Yang, L., PRMT4 overexpression aggravates cardiac remodeling following myocardial infarction by promoting cardiomyocyte apoptosis. *Biochem. Biophys. Res. Commun.* **2019**, *520* (3), 645-650.
70. Zakrzewicz, D.; Zakrzewicz, A.; Didiasova, M.; Korencak, M.; Kosanovic, D.; Schermuly, R. T.; Markart, P.; Wygrecka, M., Elevated protein arginine methyltransferase 1 expression regulates fibroblast motility in pulmonary fibrosis. *Biochim. Biophys. Acta, Mol. Basis Dis.* **2015**, *1852* (12), 2678-2688.
71. Wang, M.; Fuhrmann, J.; Thompson, P. R., Protein arginine methyltransferase 5 catalyzes substrate dimethylation in a distributive fashion. *Biochemistry* **2014**, *53* (50), 7884-7892.
72. Pal, S.; Vishwanath, S. N.; Erdjument-Bromage, H.; Tempst, P.; Sif, S., Human SWI/SNF-associated PRMT5 methylates histone H3 arginine 8 and negatively regulates expression of ST7 and NM23 tumor suppressor genes. *Mol. Cell. Biol.* **2004**, *24* (21), 9630-9645.
73. Zhao, Q.; Rank, G.; Tan, Y. T.; Li, H.; Moritz, R. L.; Simpson, R. J.; Cerruti, L.; Curtis, D. J.; Patel, D. J.; Allis, C. D.; Cunningham, J. M.; Jane, S. M., PRMT5-mediated methylation of histone H4R3 recruits DNMT3A, coupling histone and DNA methylation in gene silencing. *Nat. Struct. Mol. Biol.* **2009**, *16* (3), 304-311.

74. Chen, H.; Lorton, B.; Gupta, V.; Shechter, D., A TGF β -PRMT5-MEP50 axis regulates cancer cell invasion through histone H3 and H4 arginine methylation coupled transcriptional activation and repression. *Oncogene* **2017**, *36* (3), 373-386.
75. Liu, R.; Gao, J.; Yang, Y.; Qiu, R.; Zheng, Y.; Huang, W.; Zeng, Y.; Hou, Y.; Wang, S.; Leng, S.; Feng, D.; Yu, W.; Sun, G.; Shi, H.; Teng, X.; Wang, Y., PHD finger protein 1 (PHF1) is a novel reader for histone H4R3 symmetric dimethylation and coordinates with PRMT5-WDR77/CRL4B complex to promote tumorigenesis. *Nucleic Acids Res.* **2018**, *46* (13), 6608-6626.
76. Kota, S. K.; Roening, C.; Patel, N.; Kota, S. B.; Baron, R., PRMT5 inhibition promotes osteogenic differentiation of mesenchymal stromal cells and represses basal interferon stimulated gene expression. *Bone (N. Y., NY, U. S.)* **2018**, *117*, 37-46.
77. Dong, J.; Wang, X.; Cao, C.; Wen, Y.; Sakashita, A.; Chen, S.; Zhang, J.; Zhang, Y.; Zhou, L.; Luo, M.; Liu, M.; Liao, A.; Namekawa, S. H.; Yuan, S., UHRF1 suppresses retrotransposons and cooperates with PRMT5 and PIWI proteins in male germ cells. *Nat. Commun.* **2019**, Ahead of Print.
78. Huang, X.; Hu, H.; Webster, A.; Zou, F.; Du, J.; Patel, D. J.; Sachidanandam, R.; Toth, K. F.; Aravin, A. A.; Li, S., Binding of guide piRNA triggers methylation of the unstructured N-terminal region of Aub leading to assembly of the piRNA amplification complex. *Nat. Commun.* **2021**, *12* (1), 4061.
79. Meister, G.; Eggert, C.; Buhler, D.; Brahms, H.; Kambach, C.; Fischer, U., Methylation of Sm proteins by a complex containing PRMT5 and the putative U snRNP assembly factor pICln. *Curr. Biol.* **2001**, *11* (24), 1990-1994.
80. Cai, T.; Cinkornpumin, J. K.; Yu, Z.; Villarreal, O. D.; Pastor, W. A.; Richard, S., Deletion of RBMX RGG/RG motif in Shashi-XLID syndrome leads to aberrant p53 activation and neuronal differentiation defects. *Cell Rep.* **2021**, *36* (2), 109337.
81. Bezzi, M.; Teo, S. X.; Muller, J.; Mok, W. C.; Sahu, S. K.; Vardy, L. A.; Bonday, Z. Q.; Guccione, E., Regulation of constitutive and alternative splicing by PRMT5 reveals a role for Mdm4 pre-mRNA in sensing defects in the spliceosomal machinery. *Genes Dev.* **2013**, *27* (17), 1903-1916.
82. Gerhart, S. V.; Kellner, W. A.; Thompson, C.; Pappalardi, M. B.; Zhang, X.-P.; Montes de Oca, R.; Penebre, E.; Duncan, K.; Boriack-Sjodin, A.; Le, B.; Majer, C.; McCabe, M. T.; Carpenter, C.; Johnson, N.; Kruger, R. G.; Barbash, O., Activation of the p53-MDM4 regulatory axis defines the anti-tumour response to PRMT5 inhibition through its role in regulating cellular splicing. *Sci. Rep.* **2018**, *8* (1), 1-15.
83. Koh, C. M.; Bezzi, M.; Low, D. H. P.; Ang, W. X.; Teo, S. X.; Gay, F. P. H.; Al-Haddawi, M.; Tan, S. Y.; Osato, M.; Sabo, A.; Amati, B.; Wee, K. B.; Guccione, E., MYC regulates the core pre-mRNA splicing machinery as an essential step in lymphomagenesis. *Nature (London, U. K.)* **2015**, *523* (7558), 96-100.
84. Close, P.; East, P.; Dirac-Svejstrup, A. B.; Hartmann, H.; Heron, M.; Maslen, S.; Chariot, A.; Soeding, J.; Skehel, M.; Svejstrup, J. Q., DBIRD complex integrates alternative mRNA splicing with RNA polymerase II transcript elongation. *Nature (London, U. K.)* **2012**, *484* (7394), 386-389.
85. Rengasamy, M.; Zhang, F.; Vashisht, A.; Song, W.-M.; Aguilo, F.; Sun, Y.; Li, S.; Zhang, W.; Zhang, B.; Wohlschlegel, J. A.; Walsh, M. J., The PRMT5/WDR77 complex regulates alternative splicing through ZNF326 in breast cancer. *Nucleic Acids Res.* **2017**, *45* (19), 11106-11120.
86. Hu, D.; Gur, M.; Zhou, Z.; Gamper, A.; Hung, M.-C.; Fujita, N.; Lan, L.; Bahar, I.; Wan, Y., Interplay between arginine methylation and ubiquitylation regulates KLF4-mediated genome stability and carcinogenesis. *Nat. Commun.* **2015**, *6*, 8419.

87. Kim, H.; Kim, H.; Feng, Y.; Li, Y.; Tamiya, H.; Tocci, S.; Ronai, Z. e. A., PRMT5 control of cGAS/STING and NLRC5 pathways defines melanoma response to antitumor immunity. *Sci. Transl. Med.* **2020**, *12* (551), eaaz5683.
88. Ratovitski, T.; Arbez, N.; Stewart, J. C.; Chighladze, E.; Ross, C. A., PRMT5-mediated symmetric arginine dimethylation is attenuated by mutant huntingtin and is impaired in Huntington's disease (HD). *Cell Cycle* **2015**, *14* (11), 1716-1729.
89. Hyllus, D.; Stein, C.; Schnabel, K.; Schiltz, E.; Imhof, A.; Dou, Y.; Hsieh, J.; Bauer, U.-M., PRMT6-mediated methylation of R2 in histone H3 antagonizes H3 K4 trimethylation. *Genes Dev.* **2007**, *21* (24), 3369-3380.
90. Guccione, E.; Bassi, C.; Casadio, F.; Martinato, F.; Cesaroni, M.; Schuchlautz, H.; Luescher, B.; Amati, B., Methylation of histone H3R2 by PRMT6 and H3K4 by an MLL complex are mutually exclusive. *Nature (London, U. K.)* **2007**, *449* (7164), 933-937.
91. Waldmann, T.; Izzo, A.; Kamieniarz, K.; Richter, F.; Vogler, C.; Sarg, B.; Lindner, H.; Young, N. L.; Mittler, G.; Garcia, B. A.; Schneider, R., Methylation of H2AR29 is a novel repressive PRMT6 target. *Epigenet. Chromatin* **2011**, *4*, 11.
92. Iberg, A. N.; Espejo, A.; Cheng, D.; Kim, D.; Michaud-Levesque, J.; Richard, S.; Bedford, M. T., Arginine Methylation of the Histone H3 Tail Impedes Effector Binding. *J. Biol. Chem.* **2008**, *283* (6), 3006-3010.
93. Ma, W.-L.; Wang, L.; Liu, L.-X.; Wang, X.-L., Effect of phosphorylation and methylation on the function of the p16INK4a protein in non-small cell lung cancer A549 cells. *Oncol. Lett.* **2015**, *10* (4), 2277-2282.
94. El-Andaloussi, N.; Valovka, T.; Toueille, M.; Steinacher, R.; Focke, F.; Gehrig, P.; Covic, M.; Hassa, P. O.; Schar, P.; Hubscher, U.; Hottiger, M. O., Arginine methylation regulates DNA polymerase β . *Mol. Cell* **2006**, *22* (1), 51-62.
95. Nakakido, M.; Deng, Z.; Nakamura, Y.; Hamamoto, R.; Suzuki, T.; Dohmae, N., PRMT6 increases cytoplasmic localization of p21CDKN1A in cancer cells through arginine methylation and makes more resistant to cytotoxic agents. *Oncotarget* **2015**, *6* (31), 30957-67.
96. Han, H.-S.; Jung, C.-Y.; Yoon, Y.-S.; Choi, S.; Choi, D.; Kang, G.; Park, K.-G.; Kim, S.-T.; Koo, S.-H., Arginine methylation of CRT2 is critical in the transcriptional control of hepatic glucose metabolism. *Sci. Signaling* **2014**, *7* (314), ra19/1-ra19/10, 10 pp.
97. Yan, W.-W.; Liang, Y.-L.; Zhang, Q.-X.; Wang, D.; Lei, M.-Z.; Qu, J.; He, X.-H.; Lei, Q.-Y.; Wang, Y.-P., Arginine methylation of SIRT7 couples glucose sensing with mitochondria biogenesis. *EMBO Rep.* **2018**, *19* (12), n/a.
98. Singhroy, D. N.; Mesplede, T.; Sabbah, A.; Quashie, P. K.; Falgoutret, J.-P.; Wainberg, M. A., Automethylation of protein arginine methyltransferase 6 (PRMT6) regulates its stability and its anti-HIV-1 activity. *Retrovirology* **2013**, *10*, 73.
99. Feng, Y.; Maity, R.; Whitelegge, J. P.; Hadjikyriacou, A.; Li, Z.; Zurita-Lopez, C.; Al-Hadid, Q.; Clark, A. T.; Bedford, M. T.; Masson, J.-Y.; Clarke, S. G., Mammalian Protein Arginine Methyltransferase 7 (PRMT7) Specifically Targets RXR Sites in Lysine- and Arginine-rich Regions. *J. Biol. Chem.* **2013**, *288* (52), 37010-37025.
100. Feng, Y.; Hadjikyriacou, A.; Clarke, S. G., Substrate specificity of human protein arginine methyltransferase 7 (PRMT7): the importance of acidic residues in the double E loop. *J Biol Chem* **2014**, *289* (47), 32604-16.
101. Jain, K.; Clarke, S. G., PRMT7 as a unique member of the protein arginine methyltransferase family: A review. *Arch. Biochem. Biophys.* **2019**, *665*, 36-45.
102. Dhar, S. S.; Lee, S.-H.; Kan, P.-Y.; Voigt, P.; Ma, L.; Shi, X.; Reinberg, D.; Lee, M. G., Trans-tail regulation of MLL4-catalyzed H3K4 methylation by H4R3 symmetric

dimethylation is mediated by a tandem PHD of MLL4. *Genes Dev.* **2012**, *26* (24), 2749-2762.

103. Blanc, R. S.; Vogel, G.; Chen, T.; Crist, C.; Richard, S., PRMT7 Preserves Satellite Cell Regenerative Capacity. *Cell Rep.* **2016**, *14* (6), 1528-1539.
104. Agolini, E.; Dentici, M. L.; Bellacchio, E.; Alesi, V.; Radio, F. C.; Torella, A.; Musacchia, F.; Tartaglia, M.; Dallapiccola, B.; Nigro, V.; Digilio, M. C.; Novelli, A., Expanding the clinical and molecular spectrum of PRMT7 mutations: 3 additional patients and review. *Clin. Genet.* **2018**, *93* (3), 675-681.
105. Geng, P.; Zhang, Y.; Liu, X.; Zhang, N.; Liu, Y.; Liu, X.; Lin, C.; Yan, X.; Li, Z.; Wang, G.; Li, Y.; Tan, J.; Liu, D.-X.; Huang, B.; Lu, J., Automethylation of protein arginine methyltransferase 7 and its impact on breast cancer progression. *FASEB J.* **2017**, *31* (6), 2287-2300.
106. Cheng, D.; He, Z.; Zheng, L.; Xie, D.; Dong, S.; Zhang, P., PRMT7 contributes to the metastasis phenotype in human non-small-cell lung cancer cells possibly through the interaction with HSPA5 and EEF2. *OncoTargets Ther.* **2018**, *11*, 1-8.
107. Lee, J.; Sayegh, J.; Daniel, J.; Clarke, S.; Bedford, M. T., PRMT8, a New Membrane-bound Tissue-specific Member of the Protein Arginine Methyltransferase Family. *J. Biol. Chem.* **2005**, *280* (38), 32890-32896.
108. Penney, J.; Seo, J.; Kritskiy, O.; Elmsaouri, S.; Gao, F.; Pao, P.-C.; Su, S. C.; Tsai, L.-H., Loss of protein arginine methyltransferase 8 alters synapse composition and function, resulting in behavioral defects. *J. Neurosci.* **2017**, *37* (36), 8655-8666.
109. Lee, P. K. M.; Goh, W. W. B.; Sng, J. C. G., Network-based characterization of the synaptic proteome reveals that removal of epigenetic regulator Prmt8 restricts proteins associated with synaptic maturation. *J. Neurochem.* **2017**, *140* (4), 613-628.
110. Kim, J.-D.; Park, K.-E.; Ishida, J.; Kako, K.; Hamada, J.; Kani, S.; Takeuchi, M.; Namiki, K.; Fukui, H.; Fukuhara, S.; Hibi, M.; Kobayashi, M.; Kanaho, Y.; Kasuya, Y.; Mochizuki, N.; Fukamizu, A., PRMT8 as a phospholipase regulates Purkinje cell dendritic arborization and motor coordination. *Sci. Adv.* **2015**, *1* (11), e1500615/1-e1500615/9.
111. Simandi, Z.; Czipa, E.; Horvath, A.; Koszeghy, A.; Bordas, C.; Poliska, S.; Juhasz, I.; Imre, L.; Szabo, G.; Dezso, B.; Barta, E.; Sauer, S.; Karolyi, K.; Kovacs, I.; Hutoczk, G.; Bogнар, L.; Klekner, A.; Szucs, P.; Balint, B. L.; Nagy, L., PRMT1 and PRMT8 regulate retinoic acid-dependent neuronal differentiation with implications to neuropathology. *Stem Cells (Durham, NC, U. S.)* **2015**, *33* (3), 726-741.
112. Hernandez, S. J.; Dolivo, D. M.; Dominko, T., PRMT8 demonstrates variant-specific expression in cancer cells and correlates with patient survival in breast, ovarian and gastric cancer. *Oncol. Lett.* **2017**, *13* (3), 1983-1989.
113. Hernandez, S.; Dominko, T., Novel Protein Arginine Methyltransferase 8 Isoform Is Essential for Cell Proliferation. *J. Cell. Biochem.* **2016**, *117* (9), 2056-2066.
114. Yang, Y.; Hadjikyriacou, A.; Xia, Z.; Gayatri, S.; Kim, D.; Zurita-Lopez, C.; Kelly, R.; Guo, A.; Li, W.; Clarke, S. G.; Bedford, M. T., PRMT9 is a Type II methyltransferase that methylates the splicing factor SAP145. *Nat. Commun.* **2015**, *6*, 6428.
115. Hadjikyriacou, A.; Clarke, S. G.; Yang, Y.; Espejo, A.; Bedford, M. T., Unique Features of Human Protein Arginine Methyltransferase 9 (PRMT9) and Its Substrate RNA Splicing Factor SF3B2. *J Biol Chem* **2015**, *290* (27), 16723-43.
116. Jiang, H.; Zhou, Z.; Jin, S.; Xu, K.; Zhang, H.; Xu, J.; Sun, Q.; Wang, J.; Xu, J., PRMT9 promotes hepatocellular carcinoma invasion and metastasis via activating PI3K/Akt/GSK-3 β /Snail signaling. *Cancer Sci.* **2018**, *109* (5), 1414-1427.

117. Zhang, H.; Hu, Z.; Que, X.; Huang, W.; Li, X.; Guo, X.; Feng, X.; Wang, T.; Wang, T.; Tian, Q.; Zhu, T.; Guo, G., MiRNA-543 promotes osteosarcoma cell proliferation and glycolysis by partially suppressing PRMT9 and stabilizing HIF-1 α protein. *Oncotarget* **2017**, 8 (2), 2342-2355.
118. Wang, J.; Chen, L.; Sinha, S. H.; Liang, Z.; Chai, H.; Muniyan, S.; Chou, Y.-W.; Yang, C.; Yan, L.; Feng, Y.; Kathy Li, K.; Lin, M.-F.; Jiang, H.; George Zheng, Y.; Luo, C., Pharmacophore-Based Virtual Screening and Biological Evaluation of Small Molecule Inhibitors for Protein Arginine Methylation. *J. Med. Chem.* **2012**, 55 (18), 7978-7987.
119. Cheng, D.; Yadav, N.; King, R. W.; Swanson, M. S.; Weinstein, E. J.; Bedford, M. T., Small Molecule Regulators of Protein Arginine Methyltransferases. *J. Biol. Chem.* **2004**, 279 (23), 23892-23899.
120. Castellano, S.; Milite, C.; Ragno, R.; Simeoni, S.; Mai, A.; Limongelli, V.; Novellino, E.; Bauer, I.; Brosch, G.; Spannhoff, A.; Cheng, D.; Bedford, M. T.; Sbardella, G., Design, synthesis and biological evaluation of carboxy analogues of arginine methyltransferase inhibitor 1 (AMI-1). *ChemMedChem* **2010**, 5 (3), 398-414.
121. Spannhoff, A.; Heinke, R.; Bauer, I.; Trojer, P.; Metzger, E.; Gust, R.; Schuele, R.; Brosch, G.; Sippl, W.; Jung, M., Target-Based Approach to Inhibitors of Histone Arginine Methyltransferases. *J. Med. Chem.* **2007**, 50 (10), 2319-2325.
122. Spannhoff, A.; Machmur, R.; Heinke, R.; Trojer, P.; Bauer, I.; Brosch, G.; Schuele, R.; Hanefeld, W.; Sippl, W.; Jung, M., A novel arginine methyltransferase inhibitor with cellular activity. *Bioorg. Med. Chem. Lett.* **2007**, 17 (15), 4150-4153.
123. Bissinger, E.-M.; Heinke, R.; Spannhoff, A.; Eberlin, A.; Metzger, E.; Cura, V.; Hassenboehler, P.; Cavarelli, J.; Schuele, R.; Bedford, M. T.; Sippl, W.; Jung, M., Acyl derivatives of p-aminosulfonamides and dapsone as new inhibitors of the arginine methyltransferase hPRMT1. *Bioorg. Med. Chem.* **2011**, 19 (12), 3717-3731.
124. Eram, M. S.; Shen, Y.; Szewczyk, M. M.; Wu, H.; Senisterra, G.; Li, F.; Butler, K. V.; Kaniskan, H. U.; Speed, B. A.; dela Sena, C.; Dong, A.; Zeng, H.; Schapira, M.; Brown, P. J.; Arrowsmith, C. H.; Barsyte-Lovejoy, D.; Liu, J.; Vedadi, M.; Jin, J., A Potent, Selective, and Cell-Active Inhibitor of Human Type I Protein Arginine Methyltransferases. *ACS Chem. Biol.* **2016**, 11 (3), 772-781.
125. Sack, J. S.; Thieffine, S.; Bandiera, T.; Fasolini, M.; Duke, G. J.; Jayaraman, L.; Kish, K. F.; Klei, H. E.; Purandare, A. V.; Rosettani, P.; Troiani, S.; Xie, D.; Bertrand, J. A., Structural basis for CARM1 inhibition by indole and pyrazole inhibitors. *Biochem. J.* **2011**, 436 (2), 331-339.
126. Mitchell, L. H.; Drew, A. E.; Ribich, S. A.; Rioux, N.; Swinger, K. K.; Jacques, S. L.; Lingaraj, T.; Boriack-Sjodin, P. A.; Waters, N. J.; Wigle, T. J.; Moradei, O.; Jin, L.; Riera, T.; Porter-Scott, M.; Moyer, M. P.; Smith, J. J.; Chesworth, R.; Copeland, R. A., Aryl Pyrazoles as Potent Inhibitors of Arginine Methyltransferases: Identification of the First PRMT6 Tool Compound. *ACS Med. Chem. Lett.* **2015**, 6 (6), 655-659.
127. Ferreira de Freitas, R.; Eram, M. S.; Szewczyk, M. M.; Steuber, H.; Smil, D.; Wu, H.; Li, F.; Senisterra, G.; Dong, A.; Brown, P. J.; Hitchcock, M.; Moosmayer, D.; Stegmann, C. M.; Egner, U.; Arrowsmith, C.; Barsyte-Lovejoy, D.; Vedadi, M.; Schapira, M., Discovery of a Potent Class I Protein Arginine Methyltransferase Fragment Inhibitor. *J. Med. Chem.* **2016**, 59 (3), 1176-1183.
128. Shen, Y.; Szewczyk, M. M.; Eram, M. S.; Smil, D.; Kaniskan, H. U.; Ferreira de Freitas, R.; Senisterra, G.; Li, F.; Schapira, M.; Brown, P. J.; Arrowsmith, C. H.; Barsyte-Lovejoy, D.; Liu, J.; Vedadi, M.; Jin, J., Discovery of a Potent, Selective, and Cell-Active Dual Inhibitor of Protein Arginine Methyltransferase 4 and Protein Arginine Methyltransferase 6. *J. Med. Chem.* **2016**, 59 (19), 9124-9139.

129. Wang, C.; Jiang, H.; Jin, J.; Xie, Y.; Chen, Z.; Zhang, H.; Lian, F.; Liu, Y.-C.; Zhang, C.; Ding, H.; Chen, S.; Zhang, N.; Zhang, Y.; Jiang, H.; Chen, K.; Ye, F.; Yao, Z.; Luo, C., Development of Potent Type I Protein Arginine Methyltransferase (PRMT) Inhibitors of Leukemia Cell Proliferation. *J. Med. Chem.* **2017**, *60* (21), 8888-8905.
130. Fedoriw, A.; Rajapurkar, S. R.; O'Brien, S.; Gerhart, S. V.; Mitchell, L. H.; Adams, N. D.; Rioux, N.; Lingaraj, T.; Ribich, S. A.; Pappalardi, M. B.; Shah, N.; Laraio, J.; Liu, Y.; Butticello, M.; Carpenter, C. L.; Creasy, C.; Korenchuk, S.; McCabe, M. T.; McHugh, C. F.; Nagarajan, R.; Wagner, C.; Zappacosta, F.; Annan, R.; Concha, N. O.; Thomas, R. A.; Hart, T. K.; Smith, J. J.; Copeland, R. A.; Moyer, M. P.; Campbell, J.; Stickland, K.; Mills, J.; Jacques-O'Hagan, S.; Allain, C.; Johnston, D.; Raimondi, A.; Porter Scott, M.; Waters, N.; Swinger, K.; Boriack-Sjodin, A.; Riera, T.; Shapiro, G.; Chesworth, R.; Prinjha, R. K.; Kruger, R. G.; Barbash, O.; Mohammad, H. P., Anti-tumor Activity of the Type I PRMT Inhibitor, GSK3368715, Synergizes with PRMT5 Inhibition through MTAP Loss. *Cancer Cell* **2019**, *36* (1), 100-114.e25.
131. Kaniskan, H. U.; Szewczyk, M. M.; Yu, Z.; Eram, M. S.; Yang, X.; Schmidt, K.; Luo, X.; Dai, M.; He, F.; Zang, I.; Lin, Y.; Kennedy, S.; Li, F.; Dobrovetsky, E.; Dong, A.; Smil, D.; Min, S.-J.; Landon, M.; Lin-Jones, J.; Huang, X.-P.; Roth, B. L.; Schapira, M.; Atadja, P.; Barsyte-Lovejoy, D.; Arrowsmith, C. H.; Brown, P. J.; Zhao, K.; Jin, J.; Vedadi, M., A Potent, Selective and Cell-Active Allosteric Inhibitor of Protein Arginine Methyltransferase 3 (PRMT3). *Angew. Chem., Int. Ed.* **2015**, *54* (17), 5166-5170.
132. Kaniskan, H. U.; Eram, M. S.; Zhao, K.; Szewczyk, M. M.; Yang, X.; Schmidt, K.; Luo, X.; Xiao, S.; Dai, M.; He, F.; Zang, I.; Lin, Y.; Li, F.; Dobrovetsky, E.; Smil, D.; Min, S.-J.; Lin-Jones, J.; Schapira, M.; Atadja, P.; Li, E.; Barsyte-Lovejoy, D.; Arrowsmith, C. H.; Brown, P. J.; Liu, F.; Yu, Z.; Vedadi, M.; Jin, J., Discovery of Potent and Selective Allosteric Inhibitors of Protein Arginine Methyltransferase 3 (PRMT3). *J. Med. Chem.* **2018**, *61* (3), 1204-1217.
133. Huynh, T.; Chen, Z.; Pang, S.; Geng, J.; Bandiera, T.; Bindi, S.; Vianello, P.; Roletto, F.; Thieffine, S.; Galvani, A.; Vaccaro, W.; Poss, M. A.; Trainor, G. L.; Lorenzi, M. V.; Gottardis, M.; Jayaraman, L.; Purandare, A. V., Optimization of pyrazole inhibitors of coactivator associated arginine methyltransferase 1 (CARM1). *Bioorg. Med. Chem. Lett.* **2009**, *19* (11), 2924-2927.
134. Purandare, A. V.; Chen, Z.; Huynh, T.; Pang, S.; Geng, J.; Vaccaro, W.; Poss, M. A.; Oconnell, J.; Nowak, K.; Jayaraman, L., Pyrazole inhibitors of coactivator associated arginine methyltransferase 1 (CARM1). *Bioorg. Med. Chem. Lett.* **2008**, *18* (15), 4438-4441.
135. Wan, H.; Huynh, T.; Pang, S.; Geng, J.; Vaccaro, W.; Poss, M. A.; Trainor, G. L.; Lorenzi, M. V.; Gottardis, M.; Jayaraman, L.; Purandare, A. V., Benzo[d]imidazole inhibitors of Coactivator Associated Arginine Methyltransferase 1 (CARM1)-Hit to Lead studies. *Bioorg. Med. Chem. Lett.* **2009**, *19* (17), 5063-5066.
136. Allan, M.; Manku, S.; Therrien, E.; Nguyen, N.; Styhler, S.; Robert, M.-F.; Goulet, A.-C.; Petschner, A. J.; Rahil, G.; Robert MacLeod, A.; Deziel, R.; Besterman, J. M.; Nguyen, H.; Wahhab, A., N-Benzyl-1-heteroaryl-3-(trifluoromethyl)-1H-pyrazole-5-carboxamides as inhibitors of co-activator associated arginine methyltransferase 1 (CARM1). *Bioorg. Med. Chem. Lett.* **2009**, *19* (4), 1218-1223.
137. Ferreira de Freitas, R.; Eram, M. S.; Smil, D.; Szewczyk, M. M.; Kennedy, S.; Brown, P. J.; Santhakumar, V.; Barsyte-Lovejoy, D.; Arrowsmith, C. H.; Vedadi, M.; Schapira, M., Discovery of a Potent and Selective Coactivator Associated Arginine

- Methyltransferase 1 (CARM1) Inhibitor by Virtual Screening. *J. Med. Chem.* **2016**, *59* (14), 6838-6847.
138. Drew, A. E.; Moradei, O.; Jacques, S. L.; Rioux, N.; Boriack-Sjodin, A. P.; Allain, C.; Scott, M. P.; Jin, L.; Raimondi, A.; Handler, J. L.; Ott, H. M.; Kruger, R. G.; McCabe, M. T.; Sneeringer, C.; Riera, T.; Shapiro, G.; Waters, N. J.; Mitchell, L. H.; Duncan, K. W.; Moyer, M. P.; Copeland, R. A.; Smith, J.; Chesworth, R.; Ribich, S. A., Identification of a CARM1 Inhibitor with Potent In Vitro and In Vivo Activity in Preclinical Models of Multiple Myeloma. *Sci. Rep.* **2017**, *7* (1), 1-13.
 139. Nakayama, K.; Baba, Y.; Kunitomo, M.; Cary, D. R.; Ohashi, A.; Imaeda, Y.; Kiba, A.; Tomita, D.; Szewczyk, M. M.; Dela, S. C.; Wu, H.; Dong, A.; Zeng, H.; Li, F.; de, F. R. F.; Eram, M. S.; Schapira, M.; Vedadi, M.; Arrowsmith, C. H.; Barsyte-Lovejoy, D.; Brown, P. J.; Schapira, M.; Vedadi, M.; Tawada, M.; Saikatendu, K. S.; Grimshaw, C. E.; Arrowsmith, C. H., TP-064, a potent and selective small molecule inhibitor of PRMT4 for multiple myeloma. *Oncotarget* **2018**, *9* (26), 18480-18493.
 140. Cai, X.-C.; Jiang, M.; Wang, K.; Wang, J.; Chen, S.; Zhang, N.; Zheng, W.; Lee, J. P.; Ibanez, G.; Luo, M.; Zhang, T.; Xiang, J.; Kim, E.-J.; Xu, W.; Jiang, M.; Luo, M.; Chen, S.; Lee, J. P.; Zhang, N.; Zhang, Z.; Wu, H.; Li, F.; Dela, S. C. C.; Zeng, H.; Barsyte, D.; Szewczyk, M.; Hajian, T.; Dong, A.; Dombrowski, L.; Deng, H.; Min, J.; Arrowsmith, C. H.; Vedadi, M.; Brown, P. J.; Vivcharuk, V.; Shi, L.; Niu, X.; Mazutis, L.; Niu, X.; Chen, Y.; Deng, H.; Min, J.; Arrowsmith, C. H.; Vedadi, M.; Qin, L.-X., A chemical probe of CARM1 alters epigenetic plasticity against breast cancer cell invasion. *Elife* **2019**, *8*.
 141. Guo, Z.; Zhang, Z.; Yang, H.; Cao, D.; Xu, X.; Zheng, X.; Chen, D.; Wang, Q.; Li, Y.; Li, J.; Du, Z.; Wang, X.; Chen, L.; Ding, J.; Shen, J.; Geng, M.; Huang, X.; Xiong, B., Design and Synthesis of Potent, Selective Inhibitors of Protein Arginine Methyltransferase 4 against Acute Myeloid Leukemia. *J. Med. Chem.* **2019**, *62* (11), 5414-5433.
 142. Chan-Penebre, E.; Kuplast, K. G.; Majer, C. R.; Boriack-Sjodin, P. A.; Wigle, T. J.; Johnston, L. D.; Rioux, N.; Munchhof, M. J.; Jin, L.; Jacques, S. L.; West, K. A.; Lingaraj, T.; Stickland, K.; Ribich, S. A.; Raimondi, A.; Scott, M. P.; Waters, N. J.; Pollock, R. M.; Smith, J. J.; Barbash, O.; Pappalardi, M.; Ho, T. F.; Nurse, K.; Oza, K. P.; Gallagher, K. T.; Kruger, R.; Moyer, M. P.; Copeland, R. A.; Chesworth, R.; Duncan, K. W., A selective inhibitor of PRMT5 with in vivo and in vitro potency in MCL models. *Nat. Chem. Biol.* **2015**, *11* (6), 432-437.
 143. Duncan, K. W.; Rioux, N.; Boriack-Sjodin, P. A.; Munchhof, M. J.; Reiter, L. A.; Majer, C. R.; Jin, L.; Johnston, L. D.; Chan-Penebre, E.; Kuplast, K. G.; Porter Scott, M.; Pollock, R. M.; Waters, N. J.; Smith, J. J.; Moyer, M. P.; Copeland, R. A.; Chesworth, R., Structure and Property Guided Design in the Identification of PRMT5 Tool Compound EPZ015666. *ACS Med. Chem. Lett.* **2016**, *7* (2), 162-166.
 144. Mao, R.; Shao, J.; Zhu, K.; Zhang, Y.; Ding, H.; Zhang, C.; Shi, Z.; Jiang, H.; Sun, D.; Duan, W.; Luo, C., Potent, Selective, and Cell Active Protein Arginine Methyltransferase 5 (PRMT5) Inhibitor Developed by Structure-Based Virtual Screening and Hit Optimization. *J. Med. Chem.* **2017**, *60* (14), 6289-6304.
 145. Ye, Y.; Zhang, B.; Mao, R.; Zhang, C.; Wang, Y.; Xing, J.; Liu, Y.-C.; Luo, X.; Ding, H.; Yang, Y.; Zhou, B.; Jiang, H.; Chen, K.; Luo, C.; Zheng, M., Discovery and optimization of selective inhibitors of protein arginine methyltransferase 5 by docking-based virtual screening. *Org. Biomol. Chem.* **2017**, *15* (17), 3648-3661.
 146. Bonday, Z. Q.; Cortez, G. S.; Grogan, M. J.; Antonysamy, S.; Weichert, K.; Bocchinfuso, W. P.; Li, F.; Kennedy, S.; Li, B.; Mader, M. M.; Arrowsmith, C. H.; Brown, P. J.; Eram, M. S.; Szewczyk, M. M.; Barsyte-Lovejoy, D.; Vedadi, M.;

- Guccione, E.; Campbell, R. M., LLY-283, a Potent and Selective Inhibitor of Arginine Methyltransferase 5, PRMT5, with Antitumor Activity. *ACS Med. Chem. Lett.* **2018**, *9* (7), 612-617.
147. Lin, H.; Wang, M.; Zhang, Y. W.; Tong, S.; Leal, R. A.; Shetty, R.; Vaddi, K.; Luengo, J. I., Discovery of Potent and Selective Covalent Protein Arginine Methyltransferase 5 (PRMT5) Inhibitors. *ACS Med. Chem. Lett.* **2019**, *10* (6), 899-904.
 148. Brehmer, D.; Beke, L.; Wu, T.; Millar, H. J.; Mannens, G.; Pande, V.; Boeckx, A.; van, H. E.; Nys, T.; Gustin, E. M.; Verbist, B.; Vinken, P.; Verhulst, T.; Fiore, D.; Philippar, U.; Morschhauser, B.; De, L. D.; Keersmaekers, V.; Viellevoeye, M.; Diels, G.; Schepens, W.; Thuring, J. W.; Meerpoel, L.; Moy, C.; Sun, W.; Bhargava, V.; Safabakhsh, P.; Pastore, F.; Gu, J.; Johnson, A.; Walker, D.; Packman, K.; Lorenzi, M. V.; Laquerre, S.; Zhou, L.; Fan, Y.; Gilbert, A.; Rai, S.; Graubert, T. A., Discovery and Pharmacological Characterization of JNJ-64619178, a Novel Small-Molecule Inhibitor of PRMT5 with Potent Antitumor Activity. *Mol Cancer Ther* **2021**, *20* (12), 2317-2328.
 149. Quiroz, R. V.; Reutershan, M. H.; Schneider, S. E.; Sloman, D.; Lacey, B. M.; Swalm, B. M.; Yeung, C. S.; Gibeau, C.; Spellman, D. S.; Rankic, D. A.; Chen, D.; Witter, D.; Linn, D.; Munsell, E.; Feng, G.; Xu, H.; Hughes, J. M. E.; Lim, J.; Sauri, J.; Geddes, K.; Wan, M.; Mansueto, M. S.; Follmer, N. E.; Fier, P. S.; Siliphaivanh, P.; Daublain, P.; Palte, R. L.; Hayes, R. P.; Lee, S.; Kawamura, S.; Silverman, S.; Sanyal, S.; Henderson, T. J.; Ye, Y.; Gao, Y.; Nicholson, B.; Machacek, M. R., The Discovery of Two Novel Classes of 5,5-Bicyclic Nucleoside-Derived PRMT5 Inhibitors for the Treatment of Cancer. *J. Med. Chem.* **2021**, *64* (7), 3911-3939.
 150. Shen, Y.; Li, F.; Szewczyk, M. M.; Halabelian, L.; Chau, I.; Eram, M. S.; Dela Sena, C.; Park, K.-S.; Meng, F.; Chen, H.; Zeng, H.; McLeod, D.; Zepeda-Velazquez, C. A.; Campbell, R. M.; Mader, M. M.; Watson, B. M.; Schapira, M.; Arrowsmith, C. H.; Al-Awar, R.; Barsyte-Lovejoy, D.; Kaniskan, H. U.; Brown, P. J.; Vedadi, M.; Jin, J., A first-in-class, highly selective and cell-active allosteric inhibitor of protein arginine methyltransferase 6. *J. Med. Chem.* **2021**, *64* (7), 3697-3706.
 151. Smil, D.; Eram, M. S.; Li, F.; Kennedy, S.; Szewczyk, M. M.; Brown, P. J.; Barsyte-Lovejoy, D.; Arrowsmith, C. H.; Vedadi, M.; Schapira, M., Discovery of a Dual PRMT5-PRMT7 Inhibitor. *ACS Med. Chem. Lett.* **2015**, *6* (4), 408-412.
 152. Szewczyk, M. M.; Ishikawa, Y.; Organ, S.; Sakai, N.; Li, F.; Halabelian, L.; Ackloo, S.; Couzens, A. L.; Eram, M.; Dilworth, D.; Fukushima, H.; Harding, R.; dela Sena, C. C.; Sugo, T.; Hayashi, K.; McLeod, D.; Zepeda, C.; Aman, A.; Sanchez-Osuna, M.; Bonneil, E.; Takagi, S.; Al-Awar, R.; Tyers, M.; Richard, S.; Takizawa, M.; Gingras, A.-C.; Arrowsmith, C. H.; Vedadi, M.; Brown, P. J.; Nara, H.; Barsyte-Lovejoy, D., Pharmacological inhibition of PRMT7 links arginine monomethylation to the cellular stress response. *Nat. Commun.* **2020**, *11* (1), 2396.
 153. Ragno, R.; Simeoni, S.; Castellano, S.; Vicidomini, C.; Mai, A.; Caroli, A.; Tramontano, A.; Bonaccini, C.; Trojer, P.; Bauer, I.; Brosch, G.; Sbardella, G., Small Molecule Inhibitors of Histone Arginine Methyltransferases: Homology Modeling, Molecular Docking, Binding Mode Analysis, and Biological Evaluations. *J. Med. Chem.* **2007**, *50* (6), 1241-1253.
 154. Congreve, M.; Chessari, G.; Tisi, D.; Woodhead, A. J., Recent developments in fragment-based drug discovery. *J. Med. Chem.* **2008**, *51* (13), 3661-3680.
 155. Vieth, M.; Siegel, M. G.; Higgs, R. E.; Watson, I. A.; Robertson, D. H.; Savin, K. A.; Durst, G. L.; Hipkind, P. A., Characteristic Physical Properties and Structural Fragments of Marketed Oral Drugs. *J. Med. Chem.* **2004**, *47* (1), 224-232.

156. Ciulli, A.; Williams, G.; Smith, A. G.; Blundell, T. L.; Abell, C., Probing Hot Spots at Protein-Ligand Binding Sites: A Fragment-Based Approach Using Biophysical Methods. *J. Med. Chem.* **2006**, *49* (16), 4992-5000.
157. Daigle, S. R.; Olhava, E. J.; Therkelsen, C. A.; Majer, C. R.; Sneeringer, C. J.; Song, J.; Johnston, L. D.; Scott, M. P.; Smith, J. J.; Xiao, Y.; Jin, L.; Kuntz, K. W.; Chesworth, R.; Moyer, M. P.; Bernt, K. M.; Tseng, J.-C.; Kung, A. L.; Armstrong, S. A.; Copeland, R. A.; Richon, V. M.; Pollock, R. M., Selective Killing of Mixed Lineage Leukemia Cells by a Potent Small-Molecule DOT1L Inhibitor. *Cancer Cell* **2011**, *20* (1), 53-65.
158. Cai, X.-C.; Zhang, T.; Kim, E.-j.; Jiang, M.; Wang, K.; Wang, J.; Chen, S.; Zhang, N.; Wu, H.; Li, F.; dela Sena, C. C.; Zheng, H.; Vivcharuk, V.; Niu, X.; Zheng, W.; Lee, J. P.; Chen, Y.; Barsyte, D.; Szewczyk, M.; Hajian, T.; Ibanez, G.; Dong, A.; Dombrovsky, L.; Zhang, Z.; Deng, H.; Min, J.; Arrowsmith, C. H.; Mazutis, L.; Shi, L.; Vedadi, M.; Brown, P. J.; Xiang, J.; Qin, L.-X.; Xu, W.; Luo, M., A chemical probe of CARM1 alters epigenetic plasticity against breast cancer cell invasion. *bioRxiv* **2019**, 1-31.
159. Copeland, R. A.; Pompliano, D. L.; Meek, T. D., Drug–target residence time and its implications for lead optimization. *Nat. Rev. Drug Discovery* **2006**, *5* (9), 730-739.
160. van Haren, M.; van Ufford, L. Q.; Moret, E. E.; Martin, N. I., Synthesis and evaluation of protein arginine N-methyltransferase inhibitors designed to simultaneously occupy both substrate binding sites. *Org. Biomol. Chem.* **2015**, *13* (2), 549-560.
161. Zhang, G.; Richardson, S. L.; Mao, Y.; Huang, R., Design, synthesis, and kinetic analysis of potent protein N-terminal methyltransferase 1 inhibitors. *Org. Biomol. Chem.* **2015**, *13* (14), 4149-4154.
162. Groves, J. K., Friedel-Crafts acylation of alkenes. *Chem. Soc. Rev.* **1972**, *1* (1), 73-97.
163. Lubinskaya, O. V.; Shashkov, A. S.; Chertkov, V. A.; Smit, W. A., Facile synthesis of cyclic carboxonium salts by acylation of alkenes. *Synthesis* **1976**, (11), 742-5.
164. Lyubinskaya, O. V.; Smit, V. A.; Shashkov, A. S.; Chertkov, V. A.; Kanishchev, M. I.; Kucherov, V. F., Formation of carboxonium salts during acylation of alkenes by acylium salts and some problems of the acylation reaction mechanism. *Izv. Akad. Nauk SSSR, Ser. Khim.* **1978**, (2), 397-408.
165. Design, synthesis and biological evaluation of new small-molecule modulators of Protein Methyltransferases (PMTs). Ph. D. thesis, Agostino Cianciulli, 2016.
166. Therrien, E.; Larouche, G.; Manku, S.; Allan, M.; Nguyen, N.; Styhler, S.; Robert, M.-F.; Goulet, A.-C.; Besterman, J. M.; Nguyen, H.; Wahhab, A., 1,2-Diamines as inhibitors of co-activator associated arginine methyltransferase 1 (CARM1). *Bioorg. Med. Chem. Lett.* **2009**, *19* (23), 6725-6732.
167. Zhang, X.; Li, X.; Li, Z.; Wu, X.; Wu, Y.; You, Q.; Zhang, X., An NAD(P)H:Quinone Oxidoreductase 1 Responsive and Self-Immolative Prodrug of 5-Fluorouracil for Safe and Effective Cancer Therapy. *Org. Lett.* **2018**, *20* (12), 3635-3638.
168. Paiva, S.-L.; Crews, C. M., Targeted protein degradation: elements of PROTAC design. *Curr. Opin. Chem. Biol.* **2019**, *50*, 111-119.
169. Bekes, M.; Langley, D. R.; Crews, C. M., PROTAC targeted protein degraders: the past is prologue. *Nat. Rev. Drug Discovery* **2022**, Ahead of Print.
170. Nalawansa, D. A.; Crews, C. M., PROTACs: An Emerging Therapeutic Modality in Precision Medicine. *Cell Chem. Biol.* **2020**, *27* (8), 998-1014.
171. Bondeson, D. P.; Smith, B. E.; Burslem, G. M.; Buhimschi, A. D.; Hines, J.; Jaime-Figueroa, S.; Wang, J.; Hamman, B. D.; Ishchenko, A.; Crews, C. M., Lessons in PROTAC Design from Selective Degradation with a Promiscuous Warhead. *Cell Chem. Biol.* **2018**, *25* (1), 78-87.e5.

172. Ma, A.; Stratikopoulos, E.; Park, K.-S.; Wei, J.; Martin, T. C.; Yang, X.; Schwarz, M.; Leshchenko, V.; Rialdi, A.; Dale, B.; Lagana, A.; Guccione, E.; Parekh, S.; Parsons, R.; Jin, J., Discovery of a first-in-class EZH2 selective degrader. *Nat. Chem. Biol.* **2020**, *16* (2), 214-222.
173. Shen, Y.; Gao, G.; Yu, X.; Kim, H.; Wang, L.; Xie, L.; Schwarz, M.; Chen, X.; Guccione, E.; Liu, J.; Bedford, M. T.; Jin, J., Discovery of First-in-Class Protein Arginine Methyltransferase 5 (PRMT5) Degradere. *J. Med. Chem.* **2020**, *63* (17), 9977-9989.
174. Roy, M. J.; Winkler, S.; Hughes, S. J.; Whitworth, C.; Galant, M.; Farnaby, W.; Rumpel, K.; Ciulli, A., SPR-Measured Dissociation Kinetics of PROTAC Ternary Complexes Influence Target Degradation Rate. *ACS Chem. Biol.* **2019**, *14* (3), 361-368.
175. Bartoschik, T.; Heffern, C.; Zoephel, A.; Rumpel, K.; Ciulli, A., MST and TRIC Technology to Reliably Study PROTAC Binary and Ternary Binding in Drug Development. *Methods Mol Biol* **2021**, *2365*, 115-133.
176. Crew, A. P.; Berlin, M.; Flanagan, J. J.; Dong, H.; Ishchenko, A. Preparation of tau-protein targeting bifunctional compounds (PROTACS) as E3 ubiquitin ligase binding useful in treatment and prevention of diseases. US20180125821A1, 2018.
177. Sun, L.; Wang, M.; Lv, Z.; Yang, N.; Liu, Y.; Bao, S.; Gong, W.; Xu, R.-M., Structural insights into protein arginine symmetric dimethylation by PRMT5. *Proc. Natl. Acad. Sci. U. S. A.* **2011**, *108* (51), 20538-20543, S20538/1-S20538/3.
178. Crew, A. P.; Qian, Y.; Dong, H.; Wang, J.; Hornberger, K. R.; Crews, C. M. Tetrahydronaphthalene and tetrahydroisoquinoline derivatives as estrogen receptor degraders and their preparation. WO2018102725A1, 2018.
179. Horiuchi, K. Y.; Eason, M. M.; Ferry, J. J.; Planck, J. L.; Walsh, C. P.; Smith, R. F.; Howitz, K. T.; Ma, H., Assay Development for Histone Methyltransferases. *Assay Drug Dev. Technol.* **2013**, *11* (4), 227-236.
180. Beaudet, L.; Rodriguez-Suarez, R.; Venne, M.-H.; Caron, M.; Bedard, J.; Brechler, V.; Parent, S.; Bielefeld-Sevigny, M., AlphaLISA immunoassays: the no-wash alternative to ELISAs for research and drug discovery. *Nat. Methods* **2008**, *5* (12), an8-an9.
181. Schuck, P., Use of surface plasmon resonance to probe the equilibrium and dynamic aspects of interactions between biological macromolecules. *Annu. Rev. Biophys. Biomol. Struct.* **1997**, *26*, 541-566.
182. Faller, B., Artificial membrane assays to assess permeability. *Curr. Drug Metab.* **2008**, *9* (9), 886-892.